

# First northwestern Pacific records of the deep-sea cardinalfish *Epigonus glossodontus* (Teleostei, Epigonidae) from the Daito Islands, Japan

Mao Sato<sup>1</sup>, Shohei Ito<sup>2</sup>, Yoshihiro Fujiwara<sup>3</sup>, Keita Koeda<sup>4</sup>

<sup>1</sup> Department of Zoology, National Museum of Nature and Science, 4-1-1 Amakubo, Tsukuba, Ibaraki 305-0005, Japan

<sup>2</sup> FullDepth Co., Ltd., Industrial Liaison and Cooperative Research Center, University of Tsukuba, 1-1-1, Tennodai, Tsukuba, Ibaraki 305-0006, Japan

<sup>3</sup> Japan Agency for Marine-Earth Science and Technology (JAMSTEC), 2-15 Natsushima-cho, Yokosuka, Kanagawa 237-0061, Japan

<sup>4</sup> Faculty of Science, University of the Ryukyus, 1 Senbaru, Nishihara, Okinawa 903-0213, Japan

Corresponding author: Mao Sato ([maosato.jour@gmail.com](mailto:maosato.jour@gmail.com))

## Abstract

The deep-sea cardinalfish *Epigonus glossodontus* Gon, 1985, previously known only from the Hawaiian Islands, was observed using remotely operated vehicles (ROVs) on steep seafloors surrounding Kitadaito and Minamidaito islands, both being oceanic islands belonging to the Daito Islands, Japan in the northwestern Pacific. A total of 44 hours of ROV observations found sparse populations, each of several individuals, around or within small caves, fissures, and recesses, specifically at depths of 340–588 m within the surveyed depth of 284–1009 m. Seven individuals (36.0–114.8 mm standard length) were successfully collected during the ROV observations around the Daito Islands. A subsequent record of the species (97.5 mm standard length) from the Kyushu-Palau Ridge indicated that the species is widely distributed. A glossy bluish-green body color with black-margined scales was revealed by the field observations, the glossy color fading immediately after death.

**Key words:** Biogeography, fauna, karst, new record, oceanic islands, remotely operated vehicles, taxonomy



Academic editor: Yahui Zhao

Received: 5 September 2024

Accepted: 9 January 2025

Published: 10 March 2025

ZooBank: <https://zoobank.org/537FE5E8-77A8-494A-BEA0-6B7164FBDE0B>

**Citation:** Sato M, Ito S, Fujiwara Y, Koeda K (2025) First northwestern Pacific records of the deep-sea cardinalfish *Epigonus glossodontus* (Teleostei, Epigonidae) from the Daito Islands, Japan. ZooKeys 1231: 1–10. <https://doi.org/10.3897/zookeys.1231.136445>

Copyright: © Mao Sato et al.  
This is an open access article distributed under terms of the Creative Commons Attribution License (Attribution 4.0 International – CC BY 4.0).

## Introduction

Deep-sea cardinalfishes in the genus *Epigonus* (family Epigonidae) include 42 valid species according to Fricke et al. (2024), most having been separated into four species groups i.e., *E. oligolepis* group, *E. constanciae* group, *E. pandionis* group, and *E. telescopus* group (Abramov 1992; Okamoto 2012; Okamoto and Motomura 2013). The *E. oligolepis* group comprises seven species distributed in the central Pacific Ocean (*Epigonus glossodontus* Gon, 1985, *E. carbonarius* Okamoto & Motomura, 2011, and *E. devaneyi* Gon, 1985), Caribbean Sea (*E. oligolepis* Mayer, 1974 and *E. hexacanthus* Okamoto, Baldwin & Long, 2024), and Indian Ocean (*E. exodon* Okamoto & Motomura, 2012 and *E. indicus* Idrees Babu & Akhilesh, 2020). All are characterized by small body size (< 150 mm standard length), large scales with 33–40 pored lateral-line scales, and the absence of a strong opercular spine and ribs on the

last abdominal vertebra (Abramov 1992; Okamoto and Motomura 2011, 2012; Idrees Babu and Akhilesh 2020; Okamoto et al. 2024).

Kitadaito and Minamidaito islands, included in the Daito Islands together with Okidaito Island, are oceanic islands characterized by a karst terrain in the northwestern Pacific, about 350 km east of Okinawa Island (Ryukyu Archipelago, southwestern Japan). The respective topographies of the seafloor around Kitadaito and Minamidaito islands are significantly precipitous, each comprising steep slopes and cliffs, with depths exceeding 2000 m at 5 km offshore (Ohde and Elderfield 1992). The geology of Kitadaito Island has been confirmed by drilling as comprising almost entirely carbonate rocks, at least to a depth of 430 m which is the maximum depth sampled (Sugiyama 1934, 1936; Ohde and Elderfield 1992; Suzuki et al. 2006). The island is considered to have been formed by the accumulation of corals during its tectonic movement (accompanied by uplifts and subsidence) from its initial birth as a volcanic island near the Equator to its present location (Klein and Kobayashi 1980; Ohde and Elderfield 1992; Iryu et al. 2023). As on other karst islands, many caves and dolines have formed on land due to the erosion of limestone on both Kitadaito and Minamidaito islands (Yamauchi and Arakaki 1978; Ohde and Elderfield 1992; Knez et al. 2017; Iryu et al. 2023). Such karst features might also exist in the submerged foundations of the islands, but structural details and associated fauna below sea level are poorly understood.

During a deep-sea cave expedition called the “Deep-sea Archaic Refugia in Karst (D-ARK)” project conducted around the Daito Islands in April and May 2024, seven individuals of *E. glossodontus* were captured by three types of remotely operated vehicles (ROVs), as well as many in situ observations made of the species. Originally described from five specimens from the Hawaiian Islands, *E. glossodontus* had not been recorded from any other location to date (Gon 1985; Mundy 2005; Okamoto and Motomura 2011), the specimens from the Daito Islands therefore being the first records of *E. glossodontus* from the northwestern Pacific (including Japanese waters), together with a note on their habitats observed during the ROV surveys. A further specimen record of the species, off the Kita-Koho Seamount (Kyushu-Palau Ridge), about 400 km west of the Daito Islands, was obtained during a subsequent expedition.

## Material and methods

The specimens examined here have been deposited at NSMT-P (National Museum of Nature and Science) and URIL (University of the Ryukyus, Ichthyological Laboratory). Counts and measurements followed Gon (1985). Standard length is abbreviated as SL. Vertebrae were counted on soft X-ray photographs. Pyloric caeca were counted in three specimens (NSMT-P 149550 and URIL 1428 and 1429) by dissection. The morphological description is based on eight captured specimens (listed below; Fig. 1a, b) and associated underwater video footage, taken by three ROVs (*KM-ROV* and *Crambon* belonging to JAMSTEC; *TripodFinder2* belonging to FullDepth Co., Ltd). Identification of individuals observed in situ using the ROVs was determined based on body proportions, coloration, and the number of pored lateral-line scales (from high resolution images) matching those of the captured individuals. Three representative habitats of *E. glossodontus* near Kitadaito Island (Fig. 2a, b: 25°57.348'N, 131°20.597'E, 343 m depth,

observed on 10 May 2024) and Minamidaito Island (Figs 1c, 2c: 25°52.120'N, 131°12.726'E, 398 m depth, 9 May 2024; Fig. 2d: 25°52.531'N, 131°12.779'E, 539 m depth, 5 May 2024) were captured from ROV video footage.

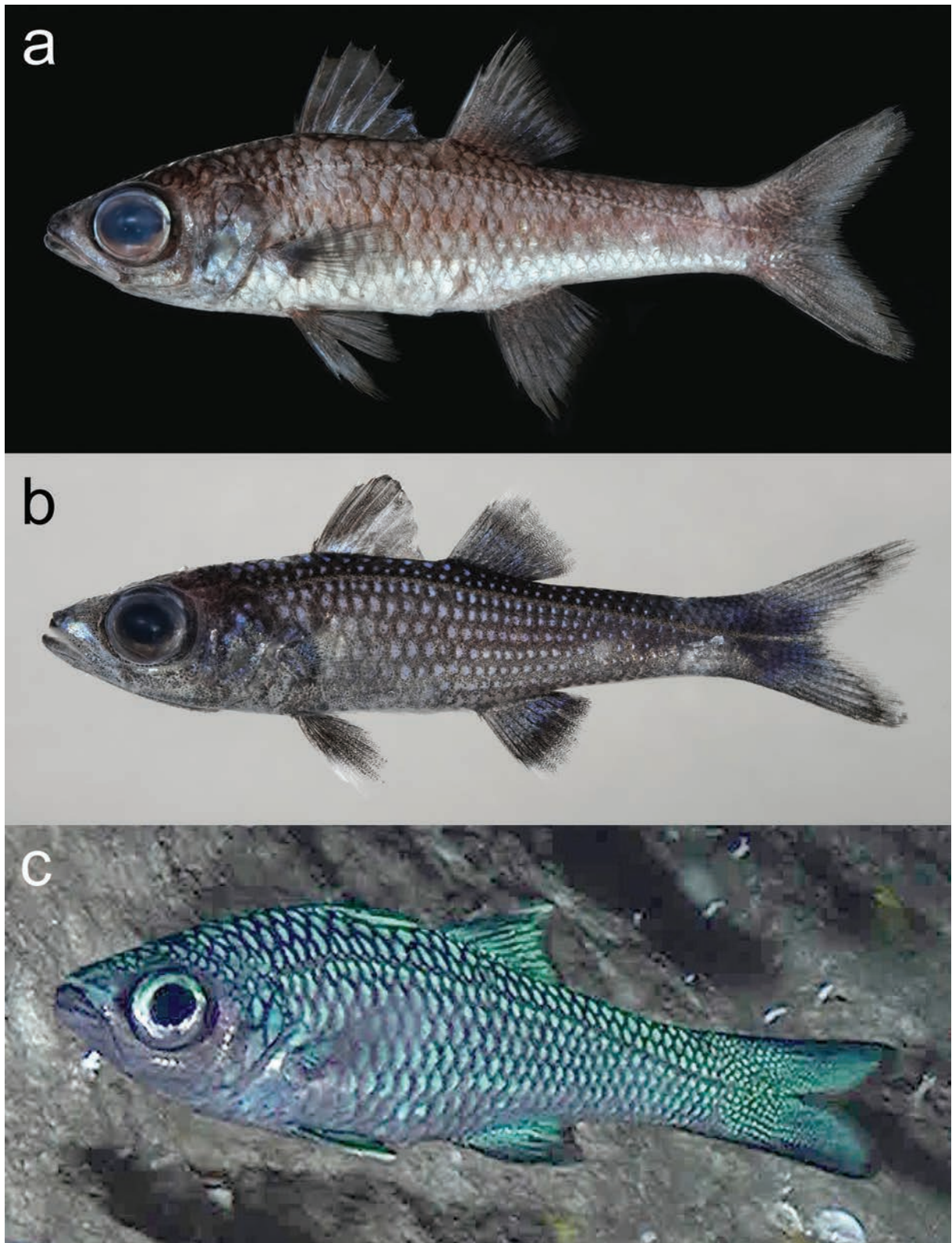


**Figure 1.** Fresh specimens (**a**, **b**) and in situ image (**c**) of *Epigonus glossodontus* **a** NSMT-P 149549, 114.8 mm SL **b** NS-MT-P149551, 54.6 mm SL **c** not collected, image rotated 90° to left.

## Results

### *Epigonus glossodontus* Gon, 1985

Figs 1, 2b, c, d

[New standard Japanese name: Horaanahisui-yasemutsu]

*Epigonus glossodontus* Gon, 1985: 222, figs 1, 2 (holotype locality: off Pearl Harbor, Mamala Bay, Oahu Island, Hawaiian Islands); Okamoto and Motomura 2011: 157–158, figs 2c, g, 4b (Oahu and Molokai islands, Hawaiian Islands).

**Material examined.** JAPAN • 1 specimen, 114.8 mm SL; northeast of Minamidaito Island; 25°50.991'N, 131°17.065'E; 537 m depth; 30 April 2024; collected using suction sampler equipped on *KM-ROV*; NSMT-P 149549 • 1, 97.7 mm SL; data as for NSMT-P 149549; URIL 1427 • 1 ♀, 98.7 mm SL; northeast of Kitadaito Island; 25°57.348'N, 131°20.597'E; 343 m depth; 10 May 2024; suction sampler equipped on *TripodFinder2*; URIL 1428 • 1, 36.0 mm SL; northeast of Kitadaito Island; 25°57.351'N, 131°20.595'E; 342 m depth; 10 May 2024; suction sampler equipped on *TripodFinder2*; NSMT-P 149550 • 1, 58.5 mm SL; south off of Minamidaito Island; 25°48.553'N, 131°15.048'E; 478 m depth; 11 May 2024; suction sampler equipped on *KM-ROV*; URIL 1429 • 1, 54.6 mm SL; data as for URIL 1429; NSMT-P 149551 • 1, 107.3 mm SL; data as for URIL 1429; NSMT-P 149552. HIGH SEA • 1 ♀, 97.5 mm SL; Kyushu-Palau Ridge, hill west of Kita-Koho Seamount; 26°43.511'N, 135°16.356'E; 562 m depth; 17 May 2024; suction sampler equipped on *Crambon*; NSMT-P 149553.

**Description.** Meristic and proportional characters are shown in Table 1. Body moderately elongated, compressed, deepest at dorsal-fin origin; nape humped; dorsal and ventral profiles gently curved, slightly concave between first and second dorsal fins. First and second dorsal-fin origins above 5<sup>th</sup> and 14<sup>th</sup> lateral-line scales, respectively. Origin of anal fin below middle of second dorsal fin. Origin of pelvic fin at level of dorsal-fin origin; upper base of pectoral fin slightly anterior to point below dorsal-fin origin. Caudal fin deeply forked, with rounded lobes. Pectoral fin rounded, reaching vertical through anus. Respective distal margins of dorsal and anal fins slightly emarginated.

Head triangular. Snout short, its tip rounded. Eye large, protruding. Pupil circular. Nostrils horizontally level with center of pupil; anterior nostril circular with a short rim directed anteriorly, midway between snout tip and anterior margin of orbit; posterior nostril a vertical slit laterally in front of eye. Mouth small, terminal. Maxillary mustache-like processes absent. Lower jaw slightly projecting; maxilla extending beyond vertical through center of pupil. Conical teeth in a line, decreasing in size posteriorly; upper jaw teeth apparent when mouth closed; two or three large conical teeth projecting anteriorly [not inclined in small specimens (NSMT-P 149550 and 149551 and URIL 1429)] on each side of mandibular symphysis, posteriorly adjacent to 3–6 mid-sized retrorse conical teeth. Mandibular symphysis sunken, toothless. Vomer spoon-shaped, with diamond-shaped head bearing small conical teeth in two (partly three) rows along midline. Palatine thin, with small conical teeth in two rows on entirety. Minute conical teeth scattered on endopterygoid. Tongue broad, with deeply-forked V-shaped teeth patch (opening rostrally) on posterior three-fourths. Posterior margin of

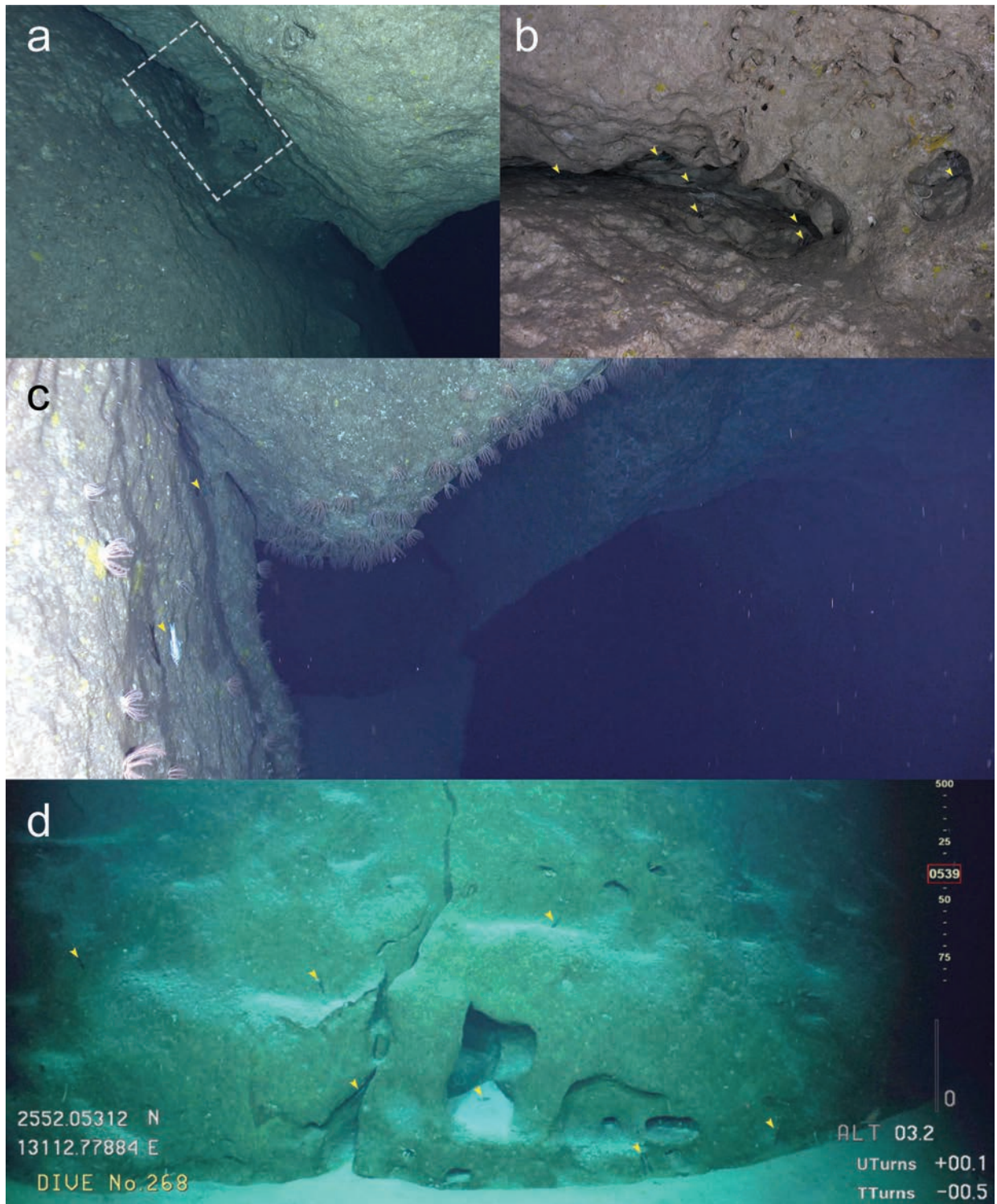


**Figure 2.** Habitats of *Epigonus glossodontus* **a** overhang on steep slope off Kitadaito Island **b** inner part of **a** (indicated by dashed box) **c** cave with branches off Minamidaito Island **d** fissure with small recesses on a wall off Minamidaito Island. Arrowheads indicate *E. glossodontus*.

preopercle smooth, membranous, covered by ctenoid scales. Opercle with weak ridge hidden under scales. Ribs absent on last abdominal vertebra.

All rays of second dorsal and anal fins branched; last anal ray bifurcating at base. Two uppermost and lowermost pectoral fin rays unbranched. Third spine of first dorsal fin longest. Lateral line generally arched, highest below middle of

**Table 1.** Counts and measurements of *Epigonus glossodontus*.

	<b>This study</b>	<b>Gon (1985)</b>
	<b>Daito Islands and Kyushu-Palau Ridge (N = 8)</b>	<b>Hawaiian Islands (N = 5)</b>
<b>Standard length (mm)</b>	<b>36.0–114.8</b>	<b>39.6–78.3</b>
<b>Counts</b>		
Dorsal fin rays	VII-I, 10	VII-I, 10
Anal fin rays	II, 9	II, 9
Principal caudal rays	9+8	9+8
Pectoral fin rays	17	17
Pelvic fin rays	I, 5	I, 5
Pored lateral-line scales	37–38	37–39
Scales above lateral line	2.5	2.5
Scales below lateral line	7	7
Predorsal scales	13–15	13–16
Branchiostegal rays	7	7
Gill rakers	5+18–19	5–6+19–21
Vertebrae	10+15	10+15
Pyloric caeca	7–8	6–8
<b>Measurements (% of standard length)</b>		
Head length	32.3–35.0	33.4–38.4
Head depth	18.7–21.9	-
Head width	15.2–17.0	-
Body depth	22.0–26.8	23.1–26.3
Body width	12.8–16.7	14.6–16.7
Orbit diameter	12.8–14.7	13.3–15.9
Interorbital width	7.9–9.7	8.2–9.5
Eye diameter	10.3–13.3	-
Snout length	7.1–8.5	6.2–8.7
Upper jaw length	12.4–15.3	13.2–15.4
Lower jaw length	14.3–16.9	14.2–17.7
Postorbital length	10.8–14.1	-
Caudal peduncle length	26.1–28.4	23.0–25.7
Caudal peduncle depth	10.3–12.5	8.3–11.4
First spine length on first dorsal fin	2.3–4.7	2.4–3.0
Second spine length on first dorsal fin	12.8–15.0	12.7–14.1
Third spine length on first dorsal fin	14.7–15.8	14.6–15.5
Second dorsal-fin spine length	10.8–13.2	11.4–12.9
Longest dorsal ray	17.6–20.0	16.1–21.0
First spine length on anal fin	1.4–3.4	1.5–2.2
Second spine length on anal fin	11.4–13.4	11.5–13.1
Longest anal ray length	16.2–19.3	17.0–18.8
Pectoral fin length	17.6–21.0	20.4–21.6
Pelvic fin spine length	11.5–13.8	12.4–13.7
Pelvic fin length	16.1–19.3	17.7–20.7
Pre-first dorsal-fin length	35.5–37.8	36.9–39.5
Pre-second dorsal-fin length	55.0–56.9	56.1–59.2
Pre-anal fin length	60.1–63.3	62.3–64.2
Pre-pectoral fin length	31.7–35.8	-
Pre-pelvic fin length	35.1–38.3	36.1–38.9
Pre-anus length	53.1–56.9	-
First dorsal-fin base length	10.6–12.5	11.0–12.6
Second dorsal-fin base length	11.0–14.1	11.0–12.6
Anal fin base length	9.2–12.8	10.1–11.5

first dorsal-fin base, anterior (rising) and posterior (lowering) portions straight; last pored lateral-line scale on end of hypural, followed by three or four pored scales and further three small tubular scales on caudal fin. Almost entire head and trunk scaled, except for around nostrils, upper and lower lips, and gular

region; all scales ctenoid, these on snout smaller than others; predorsal scales reaching to snout, level with anterior nostrils; one scale row on cheek, encircling ventral and posterior margins of eye. Small cycloid scales covering second dorsal, anal, and caudal fins, except respective distal margins; basal one-third of pectoral fin scaled; pelvic fin without scales, except for base.

**Color**—In life, head and body glossy bluish-green; all scales with black margins; ventral surface whitish. Dorsal, anal, pectoral, and caudal fin scaled areas bluish-green, respective distal margins black; scaleless part of pectoral fin translucent gray. Iris silver, dorsally bluish-green.

Fresh specimens with head and body light coppery-brown, ventrum lighter. All scale posterior margins dark brown, resulting in mottled effect on fins; infraorbital and opercular regions pale bluish. First dorsal fin brown, spines pale bluish; cycloid scales edged with brown, with mottled pattern on scaled areas of second dorsal, anal, and caudal fins. Pelvic and pectoral fins translucent, with dense melanophores.

**Distribution.** Currently known from Oahu and Molokai islands, Hawaii (Gon 1985; Okamoto and Motomura 2011), Kitadaito and Minamidaito islands in the Daito Islands, Japan, and Kita-Koho Seamount at Kyushu-Palau Ridge (this study).

**Ecological notes.** During the 44 hours of ROV observations near Kitadaito and Minamidaito islands, at least 122 *E. glossodontus* individuals were sighted at depths between 340–588 m (total depth surveyed 284–1009 m), generally forming sparse schools of several individuals within and around small caves, fissures, and recesses, and slowly swimming a few to some tens of centimeters from the bottom or walls. Swimming was sometimes directed vertically or upside down along the recess walls or ceiling (Figs 1c, 2b, c, d), while a few individuals swam horizontally above the rocky seafloor. Water temperatures in which *E. glossodontus* were observed ranged from 7.9 to 16.7 °C, the temperature range over the entire depth surveyed being 3.8 to 18.2 °C.

The body color of living individuals recorded by the ROVs was overall bluish-green with black-edged scales (Figs 1c, 2c). Although four attempts were made to bring captured individuals to the surface alive, each failed due to decompression, resulting in loss of the bluish-green coloration. Immediately after death, scales were pale blue, but quickly turned coppery-brown (Fig. 1a, b). Dissection of two captured females (NSMT-P 149553 and URIL 1428) revealed well-developed ovaries.

During a subsequent expedition centered on the Kita-Koho Seamount of the Kyushu-Palau Ridge, an ROV dive conducted on a western hill for five hours at depths of 534–778 m, with water temperatures of 5.6–9.3 °C, recorded more than 10 *E. glossodontus* individuals at a site with several recesses at 567 m depth with a temperature of 9.3 °C, where one specimen (NSMT-P 149553) was collected at a later date.

## Discussion

The present specimens were identified as *Epigonus glossodontus*, a member of the *E. oligolepis* group, based on the following characters: opercular spine weak, poorly ossified; pectoral fin rays 16 or 17; lateral-line scales to end of hypural 37 or 38; scale rows above lateral-line 2.5; gill rakers 23 or 24; two or three large anteriorly projecting teeth on each side of lower jaw symphysis; lingual teeth conical, forming V-shaped apex posteriorly; and pyloric caeca 7 or 8 (Gon 1985; Abramov

1992; Okamoto and Motomura 2011; Okamoto et al. 2024). The meristic and proportional features of the present specimens were all within or overlapped the respective ranges given in the original description of the species, except for a slight difference in caudal peduncle length (Gon 1985; Table 1). Given the overall consistency of other characters, the above difference may be due to intraspecific variation (or different measurement methods). Nevertheless, confirmation with the type series is required for verification. Within the *E. oligolepis* group, *E. glossodontus* has unique dentition i.e., two or three large rostral teeth projecting anteriorly on the lower jaw (vs. absent in other species, except *E. exodon*; Gon 1985; Okamoto and Motomura 2011; Okamoto et al. 2024), and a deep V-shaped tooth patch on a broad tongue (vs. shallow V-shaped patch on narrow tongue; Okamoto and Motomura 2012). Previously, six species of *Epigonus* have been recorded from Japanese waters (including the Daito Islands) and the Kyushu-Palau Ridge, specifically *E. atherinoides* (Gilbert, 1905), *E. ctenolepis* Mochizuki & Shirakihara, 1983, *E. denticulatus* Dieuzeide, 1950, *E. fragilis* (Jordan & Jordan, 1922), *E. pectinifer* Mayer, 1974, and *E. elongatus* Parin & Abramov, 1986, none of which are included in the *E. oligolepis* group. All have a greater number of pored lateral-line scales (minimum recorded being 46 in *E. fragilis* vs. 36–39 in *E. glossodontus*) (Okamura et al. 1982; Okamoto 2019; Okamoto and Miyamoto 2022; Okamoto et al. 2024).

Although *E. glossodontus* has been previously recorded only from the Hawaiian Islands (Gon 1985; Mundy 2005; Okamoto and Motomura 2011), the species was the most dominant benthopelagic fish observed during the Daito Islands expedition. It was also confirmed on the Kita-Koho Seamount, indicating a wide distribution in central and northwestern Pacific regions. In fact, within epigonids, *E. fragilis* shows a similar distributional pattern, occurring at depths of several hundred meters on seamounts in both Hawaiian and Japanese waters (Okamoto 2019). The parazenid *Stethopristes eos* Gilbert, 1905 (Parazenidae) is similarly distributed (Koeda et al. 2024).

The type series of *E. glossodontus* was collected by submersible from “small caves in vertical face, 366 m” off Oahu Island (Gon 1985). The Daito Islands’ habitats closely matched the original description, comprising many small caves and recesses on steep rocky slopes (Fig. 2). This underwater landscape may be related to that the islands are made of limestone being susceptible to erosion, but such argument requires further geological investigations. The fact that even the most dominant fish species during the survey period had not been accurately reported in terms of distribution suggests that such challenging environments hold a high potential for further discoveries of not only fish but also many other noteworthy species.

## Acknowledgments

We are grateful to T. Maki and other members of JAMSTEC who supported the research cruise of *R/V Kaimei*, as well as the researchers and staff involved in the cruise. We also thank the captain and crew of *R/V Kaimei* and the operation team of *KM-ROV* for ship operations and for conducting the surveys and sampling. The standard Japanese name proposed in this study (based on NSMT-P 149549) was based on suggestions from all shipboard personnel. K. Fujiwara (NSMT) aided in obtaining literature, and M. Nakae and G. Shinohara (NSMT) helped with specimen examinations. Graham S. Hardy (Ngunguru, New Zealand) grammatically improved a draft of the manuscript.

## Additional information

### Conflict of interest

The authors have declared that no competing interests exist.

### Ethical statement

No animal testing was performed during this study.

### Funding

This study was supported by the Ocean Shot Research Grant Program (to YF, SI, and KK). The Ocean Shot Research Grant Program of the Ocean Policy Research Institute of the Sasakawa Peace Foundation (OPRI-SPF) is supported by the Nippon Foundation. This study was partly supported by JSPS grants (22K15173 and 22KJ3171 to MS; 21K06313 to KK) and JST CREST (JPMJCR23J2 to KK).

### Author contributions

MS and KK coordinated data acquisition and wrote the manuscript. SI and YF promoted the ROV surveys. YF organized the research cruise. KK supervised the study. All authors approved the final version of the manuscript.

### Author ORCIDs

Yoshihiro Fujiwara  <https://orcid.org/0000-0002-1833-1866>

Keita Koeda  <https://orcid.org/0000-0003-3932-3002>

### Data availability

All data generated or analyzed during this study are included in this published article

## References

- Abramov AA (1992) Species composition and distribution of *Epigonus* (Epigonidae) in the world ocean. *Journal of Ichthyology* 32: 94–108.
- Fricke R, Eschmeyer WN, Van der Laan R (2024) Eschmeyer's Catalog of Fishes: Genera, Species, References. [Electronic version] <http://researcharchive.calacademy.org/research/ichthyology/catalog/fishcatmain.asp> [accessed 1 June 2024]
- Gon O (1985) Two new species of the deep-sea cardinalfish genus *Epigonus* (Perciformes, Apogonidae) from the Hawaiian Islands, with a key to the Hawaiian species. *Pacific Science* 39: 221–229.
- Idrees Babu KK, Akhilesh KV (2020) *Epigonus indicus*, a new species of deepwater cardinalfish (Perciformes: Epigonidae) from the Indian Ocean. *Journal of the Ocean Science Foundation* 36: 20–27. <https://doi.org/10.5281/zenodo.4243312>
- Iryu Y, Takayanagi H, Ishikawa T, Ishigaki A, Asanuma T, Teruya R, Budd DA (2023) Uplift rate of Kitadaito Jima Island on the lithospheric forebulge of the Philippine Sea Plate. *Progress in Earth and Planetary Science* 10, 4: 1–14. <https://doi.org/10.1186/s40645-023-00535-5>
- Klein GV, Kobayashi K (1980) Geological summary of the North Philippine Sea, based on deep sea drilling project leg 58 results. In: Klein GV, Kobayashi K (Eds) Initial reports of the deep sea drilling project 58. U S Government Printing Office, Washington DC, 951–961.
- Knez M, Slabe T, Urushibara-Yoshino K (2017) Lithology, rock relief and karstification of Minamidaito Island (Japan). *Acta Carsologica* 46: 47–62. <https://doi.org/10.3986/ac.v46i1.2022>

- Koeda K, Sado T, Hata H, Fujiwara Y (2024) Redescription and first Japanese seamount record of *Stethopristes eos* (Zeiformes; Parazenidae). *Zootaxa* 5399: 579–586. <https://doi.org/10.11646/zootaxa.5399.5.7>
- Mayer GF (1974) A revision of the cardinalfish genus *Epigonus* (Perciformes, Apogonidae), with descriptions of two new species. *Bulletin of the Museum of Comparative Zoology* 146: 147–203.
- Mundy BC (2005) Checklist of the fishes of the Hawaiian Archipelago. *Bishop Museum Bulletin in Zoology* 6: 1–704.
- Ohde S, Elderfield H (1992) Strontium isotope stratigraphy of Kita-daito-jima Atoll, North Philippine Sea: implications for Neogene sea-level change and tectonic history. *Earth and Planetary Science Letters* 113: 473–486. [https://doi.org/10.1016/0012-821X\(92\)90125-F](https://doi.org/10.1016/0012-821X(92)90125-F)
- Okamoto M (2012) Two new species of the genus *Epigonus* (Perciformes: Epigonidae) from the South Pacific, with a definition of the *Epigonus constanciae* group. *Ichthyological Research* 59: 242–254. <https://doi.org/10.1007/s10228-012-0284-0>
- Okamoto M (2019) Record of the epigonid fish *Epigonus fragilis* off northeast Marcus Island, western North Pacific. *The Japanese Journal of Ichthyology* 66: 79–86. [In Japanese with English abstract] <https://doi.org/10.11369/jji.19-006>
- Okamoto M, Miyamoto K (2022) First record of the epigonid fish *Epigonus elongatus* off the coast of Okinawa Island, Japan. *The Japanese Journal of Ichthyology* 69: 43–50. [In Japanese with English abstract] <https://doi.org/10.11369/jji.21-034>
- Okamoto M, Motomura H (2011) *Epigonus carbonarius*, a new species of deepwater cardinalfish (Perciformes: Epigonidae) from the Marquesas Islands, with a redefinition of the *Epigonus oligolepis* group. *Ichthyological Research* 58: 155–160. <https://doi.org/10.1007/s10228-011-0205-7>
- Okamoto M, Motomura H (2012) *Epigonus exodon*, a new species of deepwater cardinalfish (Teleostei: Perciformes: Epigonidae) from Réunion, western Indian Ocean. *Zootaxa* 3453: 84–88. <https://doi.org/10.11646/zootaxa.3453.1.6>
- Okamoto M, Motomura H (2013) Two new species of deepwater cardinalfish from the Indo-Pacific, with a definition of the *Epigonus pandionis* group (Perciformes: Epigonidae). *Ichthyological Research* 60: 301–311. <https://doi.org/10.1007/s10228-013-0352-0>
- Okamoto M, Baldwin CC, Long DJ (2024) Two new species of the deepwater cardinalfish genus *Epigonus* (Epigonidae) from deep reefs off Curaçao, southern Caribbean. *Ichthyological Research* 71: 432–441. <https://doi.org/10.1007/s10228-024-00948-2>
- Okamura O, Amaoka K, Mitani F (1982) Fishes of the Kyushu-Palau Ridge and Tosa Bay. Japan Fisheries Resource Conservation Association, Tokyo, 435 pp. [in Japanese and English]
- Sugiyama T (1934) On the drilling in Kita-Daito Island. *Contributions from the Institute of Geology and Paleontology Tohoku University* 11: 1–44. [In Japanese]
- Sugiyama T (1936) On the second drilling in Kita Daito Island. *Contributions from the Institute of Geology and Paleontology Tohoku University* 25: 1–35. [In Japanese]
- Suzuki Y, Iryu Y, Inagaki S, Yamada T, Aizawa S, Budd DA (2006) Origin of atoll dolomites distinguished by geochemistry and crystal chemistry: Kitadaito-jima, northern Philippine Sea. *Sedimentary Geology* 183: 181–202. <https://doi.org/10.1016/j.sed-geo.2005.09.016>
- Yamauchi H, Y Arakaki (1978) The fact-finding of the caves in Minami- and Kita-Daito Islands, and southern province of Okinawa Island. In: Okinawa Prefectural Board of Education (Ed.) Report of the fact-finding of the caves in Okinawa Prefecture I. Okinawa Prefectural Board of Education, Naha, 19–74. [in Japanese]

# Genomic investigation of benthic invertebrates from the Clarion-Clipperton fields of polymetallic nodules

Romain Gastineau<sup>1</sup>, Kamila Mianowicz<sup>2</sup>, Przemysław Dąbek<sup>1</sup>, Christian Otis<sup>3</sup>, Valcana Stoyanova<sup>2</sup>, Artur Krawcewicz<sup>2</sup>, Tomasz Abramowski<sup>4</sup>

<sup>1</sup> Institute of Marine and Environmental Sciences, University of Szczecin, ul. Mickiewicza 16a, Szczecin, 70-383, Poland

<sup>2</sup> Interoceanmetal Joint Organization, ul. Cyryla i Metodego 9-9A, Szczecin, 71-541, Poland

<sup>3</sup> Plateforme d'Analyse Génomique, Institut de biologie intégrative et des systèmes, Université Laval, Québec, QC, Canada

<sup>4</sup> Maritime University of Szczecin, ul. Waly Chrobrego 1-2, Szczecin, 70-500, Poland

Corresponding author: Romain Gastineau ([romain.gastineau@usz.edu.pl](mailto:romain.gastineau@usz.edu.pl))

## Abstract

The abyssal plains of the Clarion-Clipperton Zone (CCZ) are famous for their fields of polymetallic nodules, which are inhabited by benthic invertebrates. Ten specimens from the Interoceanmetal Joint Organisation (IOM) licence area in the CCZ were collected in 2014 and submitted to a short-read genome skimming sequencing. In total, mitochondrial genomes and nuclear ribosomal genes were retrieved for nine different organisms belonging to Ophiuroidea, Holothuroidea, Polychaeta, Bryozoa, Porifera, and Brachiopoda (assigned to these phyla immediately upon retrieval from the seafloor). As many of these samples were partial and physically deteriorated following their seven-year storage in IOM's collections, their morphology-based taxonomic identification could rarely be performed at the lowest possible level (species or genus) prior to preparing the samples for molecular or genomic investigations. Therefore, it was not possible to apply the reverse identification scheme recommended for such investigations. However, several of these specimens represent poorly studied groups for which few molecular references are available as of now. In two cases, the presence of introns in the mitochondrial genome questions the practicality of using the *cox1* gene for further routine molecular barcoding of these organisms. These results might be useful in future DNA primers design, molecular barcoding, and phylogeny or population genetic studies when more samples are obtained.

**Key words:** Brachiopoda, Bryozoa, genome-skimming, Holothuroidea, introns, Mitochondrial genomes, Ophiuroidea, Polychaeta, Porifera, ribosomal RNA genes

## Introduction

Located in the Pacific Ocean, the Clarion-Clipperton Zone (CCZ) spans 4.5 million km<sup>2</sup> between Hawaii and Mexico. The abyssal plain of this area has recently become a focus of attention due to the massive presence of polymetallic nodule deposits on its floor, which hold potential for exploitation. Far from being a lifeless environment, the floor of the CCZ is inhabited by benthic fauna (Rabone et al. 2023), mostly composed of invertebrates (e.g., Amon et al. 2016; Christodoulou et al. 2019) and large benthic foraminifera (e.g., Stachowska-Kamińska et al. 2022; Gooday and Wawrzyniak-Wydrowska



### Academic editor:

Didier Vanden Spiegel

Received: 22 August 2024

Accepted: 21 January 2025

Published: 10 March 2025

ZooBank: <https://zoobank.org/DF262ED4-3CC1-4E1E-B5A4-D09E88662EFD>

**Citation:** Gastineau R, Mianowicz K, Dąbek P, Otis C, Stoyanova V, Krawcewicz A, Abramowski T (2025) Genomic investigation of benthic invertebrates from the Clarion-Clipperton fields of polymetallic nodules. ZooKeys 1231: 11–44. <https://doi.org/10.3897/zookeys.1231.135347>

Copyright: © Romain Gastineau et al. This is an open access article distributed under terms of the Creative Commons Attribution License (Attribution 4.0 International – CC BY 4.0).

2023). Although the scale of environmental impacts of nodule exploitation activity (deep-sea mining) is yet to be fully understood, the retrieval of the resource from the seafloor is likely to affect benthic fauna, especially the sessile species which live attached to the nodules.

Environmental considerations have led the International Seabed Authority (ISA) to issue a certain number of recommendations in order to assess benthic biodiversity in the licence areas as part of the baseline studies. Environmental baseline studies are conducted by ISA contractors holding exploration licences with the aim to describe this benthic environment. The findings of the studies will constitute a basis (the baseline) against which exploitation impacts will be assessed, and are to be incorporated into an informed decision-making process by both ISA (e.g., while preparing standards and guidelines and defining environmental thresholds) and contractors (e.g., while preparing environmental management and monitoring plans).

Barcoding and more generally genetic studies are some of the tools used to identify and/or support taxonomic identification of fauna – in particular, key and representative species that could be used as indicator for assessing impacts – collected during exploration activities (ISBA/25/LTC/6/Rev.3 2023). This taxonomic work is of primary importance in species cataloguing and biodiversity assessment. In addition, molecular studies help to unravel the ecological functions and connectivity of species or assemblages (Danovaro et al. 2017). Although reverse taxonomy is advocated (ISBA/25/LTC/6/Rev.3 2023), this approach is not always possible when revisiting legacy data and specimen collections, as in the case in this article. Fully aware of the limitations resulting from the lack of proper morphology-based taxonomic identification of specimens retrieved from the IOM licence area in 2014, we nevertheless decided to try a genome-skimming approach on these samples.

IOM conducts exploration activities in the area located in the eastern part of the CCZ under the contract signed with ISA in 2001. Recently, IOM has developed its own protocol for the molecular study of the CCZ benthic fauna (Gastineau et al. 2023). This protocol emphasizes the use of the genome-skimming approach based on short-read sequencing whenever possible, with the aim of obtaining the largest amount of data possible within a single sequencing. In the best-case scenario, the outcome could be a complete cluster of nuclear rRNA genes and/or a complete mitochondrial genome. This is exemplified by the aforementioned article on *Abyssoprímnoa gemina* Cairns, 2015 (Gastineau et al. 2023). This deep-sea coral was collected during the IOM cruise to the CCZ in 2014, together with the specimens described in the present article. All the specimens were documented by macrophotography immediately upon retrieval but were not taxonomically identified to the species level at that time, except in a few cases, including *A. gemina*. The samples had been stored in ethanol 96% for seven years before the molecular and genomic protocol was implemented. This, in addition to the fact that several of these samples were partial, resulted in many cases in their poor physical conservation, which made it impossible to perform proper morphology-based taxonomic identification. Moreover, it has to be stressed that in the case of the CCZ fauna, there are still many species that remain undescribed (Rabone et al. 2023). Even if references exist for some of these taxa, it might still be difficult to identify them at the species level, considering the scarcity of taxonomic expertise.

When applying a basic molecular barcoding protocol to the 2014 samples to amplify the *18S* and *cox1* genes, we faced several challenges. As much as we could generally obtain positive results for the *18S* gene, we mostly failed to amplify the *cox1* gene, regardless of the phyla. This was likely a consequence of the DNA primers not being sufficiently specific rather than insufficient quality or quantity of the DNA extracted. Indeed, in several cases, the amount of DNA retrieved qualified the samples for a next-generation type of sequencing as previously performed on *A. gemina* (Gastineau et al. 2023).

In the current article, we present the results of a genome-skimming strategy applied to ten samples from the CCZ that represent two species of Ophiuroidea, one Holothuroidea, one Polychaeta, two Bryozoa, two Porifera, and one Brachiopoda. Of these samples, only the Ophiuroidea specimens could be identified at the species level (morphological identification confirmed by molecular results). It has not been possible to identify or describe the other samples at the species level so far, but our findings still hold some potential for the scientific community involved in the exploration of the CCZ. Some of these samples may represent poorly studied phyla for which few molecular references are available. Some others have mitogenomes with complex features that could not be resolved by the usual PCR and Sanger sequencing protocol, which in some cases render the amplification of their *cox1* gene impossible.

## Materials and methods

### Exploration, sampling, photographic documentation, and storage

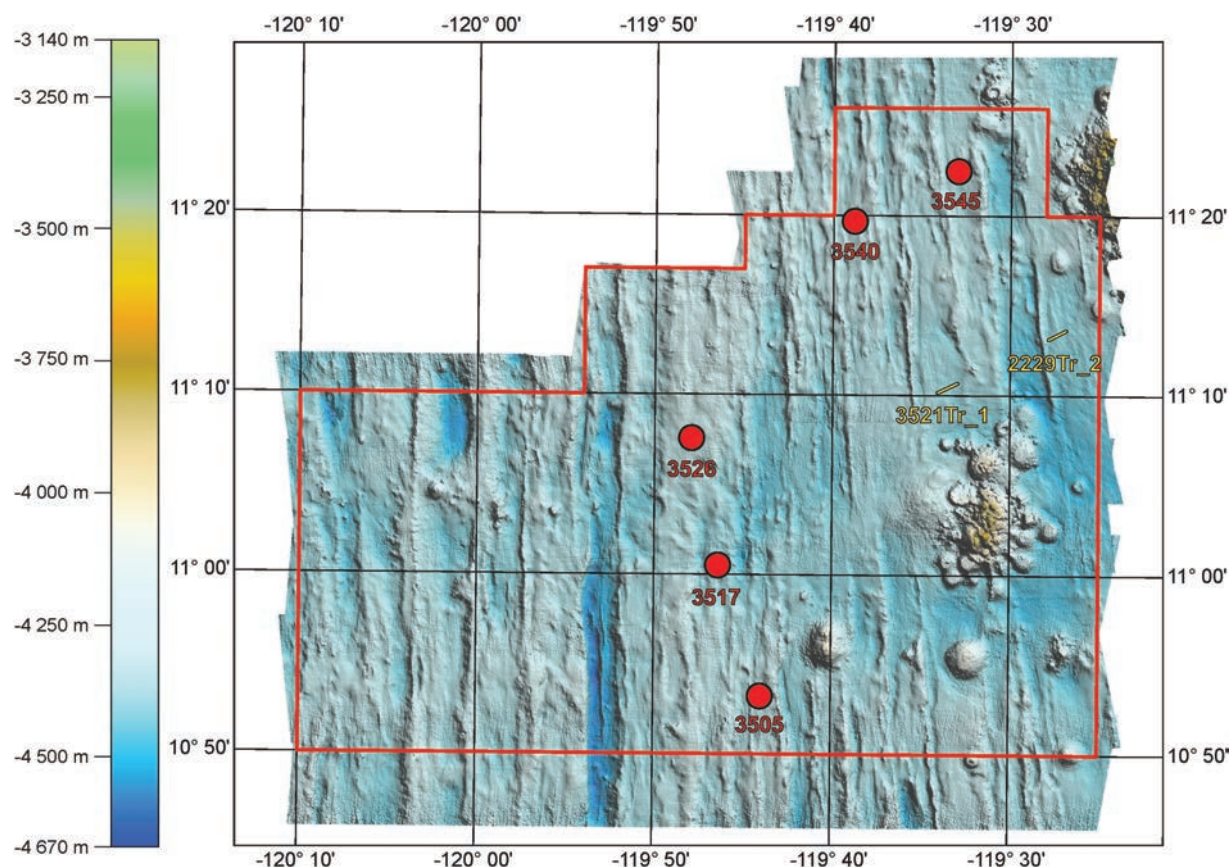
All the specimens sequenced during this study were collected during the 2014 IOM cruise. Two different sampling methods were used: point (box coring) and linear (trawling) sampling. The sample names, coordinates and depths of the sampling stations are given in Table 1, while their location is shown in Fig. 1. Polymetallic nodules and their sessile or associated fauna were retrieved from the seafloor and photographed onboard the research vessel using a Nikon D700 camera equipped with an AF-S MICRO Nikkor 105 mm 1:2.8G ED lens. All the samples were then stored in 2.0 mL Eppendorf tube filled with 96% ethanol and stored at 4 °C (the cold chain protocol was applied). They were all assigned accession numbers in the collection of IOM.

### DNA extraction, sequencing and bioinformatic analyses

DNA was extracted using the DNeasy Blood & Tissue extraction kit from Qiagen following the instructions of the manufacturer. All DNA samples were sent to the Beijing Genomics Institute in Shenzhen, China to be sequenced on a DNBSEQ platform for an average number of 60 million 100-bp paired-end reads per sample. The reads were assembled using SPAdes 3.15.5 (Bankevich et al. 2012) and a k-mer of 85. The sequences of interest (mitogenomes and rRNA nuclear clusters) were extracted from the contigs file by customized blastn queries (Camacho et al. 2009) using similar sequences from GenBank as reference. The boundaries of the rRNA nuclear genes were localized with Rfam 14 (Kalvari et al. 2021). Mitochondrial genomes were annotated using MITOS 2.1.9 (Donath et al. 2019) and uploaded to the OGDRAW server to obtain their maps (Lohse et

**Table 1.** Name, coordinates and depth of the sampling stations.

Station	Point / line (sampling method)	Coordinates	Depth
3505	point (box core)	10°53,2380'N, 119°43,9970'W	4332 m
3517	point (box core)	11°00,5100'N, 119°46,4130'W	4325 m
3526	point (box core)	11°07,5510'N, 119°47,9380'W	4241 m
3540	point (box core)	11°19,6800'N, 119°38,8230'W	4249 m
3545	point (box core)	11°22,4940'N, 119°32,9930'W	4285 m
2229Tr_2	line (trawl)	From 11°13,1495'N, 119°27,8542'W to 11°13,5805'N, 119°26,9792'W	4307–4310 m
3521Tr_1	line (trawl)	From 11°10,1623'N, 119°34,0946'W to 11°10,6813'N, 119°32,9836'W	4265–4291 m

**Figure 1.** Location of the sampling stations in the IOM claim area.

al. 2013). For the sake of clarity, all the maps are presented in a circular form, including those of the mitogenomes with no redundant endings. Megablast queries of the complete *18S* and *cox1* genes of each specimen were performed on the NCBI blast server. The specimens were given scientific names according to the World Register of Marine Species (WoRMS). When needed, maximum likelihood molecular phylogenies were performed using IQ-TREE 2.2.0 (Minh et al. 2020) with 1000 ultrafast bootstrap replicates following selection of the best model of evolution with ModelTest-NG (Darriba et al. 2020).

### Data resources

All the clean sequencing reads were deposited on SRA with accession number PRJNA1130051. All the mitochondrial genomes and the rRNA genes (complete clusters or partial) are available on GenBank with the accession numbers given in the Results section.

## Results

### Specimen IOM\_2014\_13: unidentified Demospongiae

Fig. 2.

Station ID: 3503.

Biosample: SAMN42180853.

#### Cluster of nuclear rRNA genes

The cluster is complete with a total length of 6,022 bp (GenBank: PP968935). The best 18S megablast result is *Polymastia pachymastia* voucher UCMPWC932 (GenBank: EF654528) (Kober and Nichols 2007), E-value 0.0, identity 99.93% for a length of 1,660 bp. However, it should be noted that a 100% identity was found with the shorter reference PP848924 from *Spinularia* sp. voucher RC1570, for a length of 782 bp (Lim et al. 2024). After trimming the 28S part to its variable D1/D2 region, megablast query returned a 100% identity with the 782 bp sequence of *Spinularia* sp. voucher RC1570 (GenBank: PP848924).

#### Mitochondrial genome

The mitogenome was found complete with redundant endings (GenBank: PP971517). It is 20,349 bp long and encodes 14 protein coding genes, two rRNAs and 25 tRNAs (Fig. 3, Table 2). All genes are encoded on the same strand. The nucleotide composition is A (30.89%), T (36.92%), C (12.36%) and G (19.82%). The genome is colinear with those of *Polymastia littoralis* Stephens, 1915 (GenBank: KJ129611) (del Cerro et al. 2016). The *cox1* megablast query returned a 100% identity with *Radiella sarsii* Ridley & Dendy, 1886 specimen voucher ZMBN:98039 (GenBank: HG423721) (Plotkin et al. 2017) for a length



**Figure 2.** Specimen IOM\_2014\_13 on a polymetallic nodule immediately after sampling (unscaled).

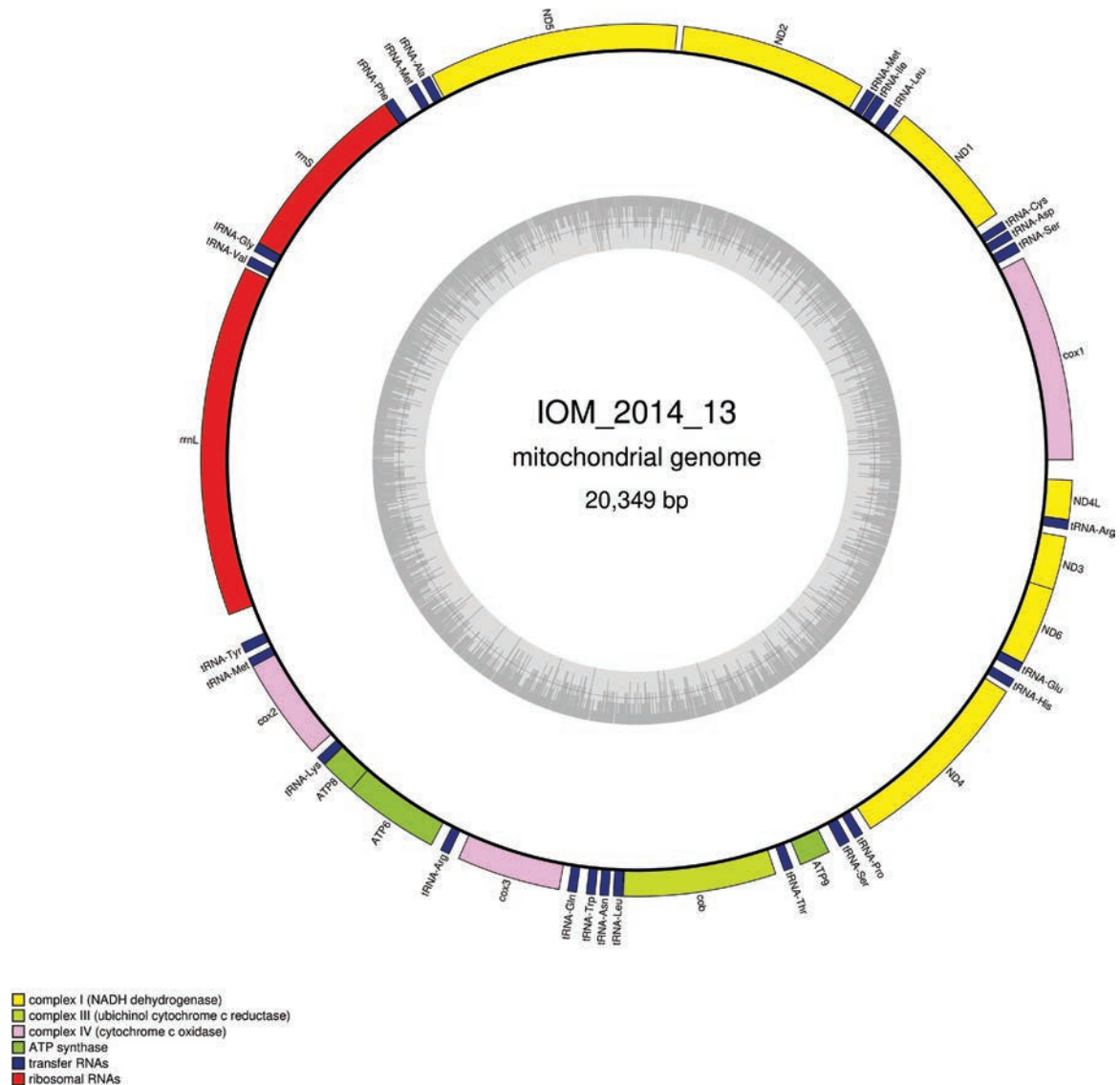


**Figure 3.** Map of the mitochondrial genome of specimen IOM\_2014\_13, with the type of genes indicated by colour boxes and the GC content indicated by the grey circle.

of 658 bp, and also with *Spinularia* sp. voucher RC1570 (GenBank: PP851905) for a length of 656 bp. The currently accepted name of *R. sarsi* is *Spinularia sarsii* Ridley & Dendy, 1886 (de Voogd et al. 2024).

### Specimen IOM\_2014\_15: unidentified Bryozoa

Fig. 4.

Station ID: 3517.

Biosample: SAMN42180854.

#### Cluster of nuclear rRNA genes

The cluster is complete with a total length of 6,768 bp (GenBank: PP968936). The best 18S megablast result is *Tubulipora lobifera* Hastings, 1963 (GenBank: JN680934) (Waeschenbach et al. 2012), E-value 0.0, identity 96.96% for a length of 1,812 bp.

**Table 2.** Characteristics of the genes encoded by the mitogenome of the unidentified Demospongiae IOM\_2014\_13.

Gene	Strand	Location	Size (bp)	Start codon	Stop codon	Anticodon
<i>cox1</i>	+	1–1563	1563	ATG	TAG	
<i>tRNA-Ser</i>	+	1613–1696	84			TGA
<i>tRNA-Asp</i>	+	1722–1793	72			GTC
<i>tRNA-Cys</i>	+	1810–1876	67			GCA
<i>ND1</i>	+	1941–2951	1011	ATG	TAG	
<i>tRNA-Leu</i>	+	3003–3086	84			TAA
<i>tRNA-Ile</i>	+	3135–3207	73			GAT
<i>tRNA-Met</i>	+	3216–3286	71			CAT
<i>ND2</i>	+	3324–4739	1416	ATG	TAA	
<i>ND5</i>	+	4782–6674	1893	ATG	TAG	
<i>tRNA-Ala</i>	+	6690–6762	73			TGC
<i>tRNA-Met</i>	+	6801–6872	72			CAT
<i>tRNA-Phe</i>	+	7009–7081	73			GAA
<i>rrnS</i>	+	7082–8486	1405			
<i>tRNA-Gly</i>	+	8487–8558	72			TCC
<i>tRNA-Val</i>	+	8602–8674	73			TAC
<i>rrnL</i>	+	8696–11349	2654			
<i>tRNA-Tyr</i>	+	11578–11657	80			GTA
<i>tRNA-Met</i>	+	11701–11772	72			CAT
<i>cox2</i>	+	11725–12543	819	ATG	TAA	
<i>tRNA-Lys</i>	+	12600–12672	73			TTT
<i>ATP8</i>	+	12674–12946	273	ATG	TAG	
<i>ATP6</i>	+	12940–13674	735	ATG	TAA	
<i>tRNA-Arg</i>	+	13748–13821	74			TCT
<i>cox3</i>	+	13895–14683	789	ATG	TAG	
<i>tRNA-Gln</i>	+	14743–14814	72			TTG
<i>tRNA-Trp</i>	+	14883–14953	71			TCA
<i>tRNA-Asn</i>	+	14984–15054	71			GTT
<i>tRNA-Leu</i>	+	15085–15158	74			TAG
<i>cob</i>	+	15160–16314	1155	ATG	TAA	
<i>tRNA-Thr</i>	+	16377–16450	74			TGT
<i>ATP9</i>	+	16506–16742	237	ATG	TAA	
<i>tRNA-Ser</i>	+	16828–16913	86			GCT
<i>tRNA-Pro</i>	+	16955–17027	73			TGG
<i>ND4</i>	+	17090–18541	1452	ATG	TAA	
<i>tRNA-His</i>	+	18576–18648	73			GTG
<i>tRNA-Glu</i>	+	18712–18783	72			TTC
<i>ND6</i>	+	18781–19380	600	ATG	TAA	
<i>ND3</i>	+	19371–19778	408	ATG	TAA	
<i>tRNA-Arg</i>	+	19832–19902	71			TCG
<i>ND4L</i>	+	19903–20202	300	ATG	TAG	

### Mitochondrial genome

The mitogenome has no redundant endings but seems to contain all conserved genes (GenBank: PP990757). For easier reading, it is represented as circular. It is 20,867 bp long and encodes 12 protein coding genes, two rRNAs and 19 tRNAs, encoded on both strands (Fig. 5, Table 3). The nucleotide composition is A (38.54%), T (39.94%), C (11.53%) and G (9.98%). No *ATP8* could be found. There are two large non-coding regions between *tRNA-Lys* and *ATP6* and between *tRNA-Pro* and *cox1*. The best *cox1* megablast result is *Tubulipora flabellaris* (O. Fabricius, 1780) (GenBank: NC\_015646) (Sun et al. 2011), E-value 0.0, identity 80.12%. This reference sequence is also a mitochondrial genome that is not colinear with those of specimen 2014\_15.



**Table 3.** Characteristics of the genes encoded by the mitogenome of the unidentified Bryozoa IOM\_2014\_15.

Gene	Strand	Location	Size (bp)	Start codon	Stop codon	Anticodon
<i>tRNA-Pro</i>	-	2198..2267	70			TGG
<i>tRNA-Lys</i>	-	2615..2674	60			TTT
<i>rrnL</i>	-	2676..3810	1135			
<i>tRNA-Leu</i>	-	3796..3852	57			TAA
<i>tRNA-Asn</i>	-	4240..4298	59			GTT
<i>tRNA-Lys</i>	-	4404..4463	60			TTT
<i>ATP6</i>	-	6981..7520	540	ATA	TAA	
<i>tRNA-Gln</i>	-	7558..7627	70			TTG
<i>rrnS</i>	-	7636..8380	745			
<i>ND2</i>	-	8438..9337	900	ATG	TAA	
<i>ND3</i>	-	9347..9622	276	ATG	TAA	
<i>tRNA-Arg</i>	-	9654..9712	59			TCG
<i>tRNA-His</i>	+	9942..9998	57			GTG
<i>ND5</i>	+	9998..11497	1500	ATG	TAG	
<i>tRNA-Ser</i>	+	11499..11548	53			TCT
<i>tRNA-Phe</i>	+	11548..11604	57			GAA
<i>tRNA-Asp</i>	-	11742..11798	57			GTC
<i>cox2</i>	-	11797..12465	669	ATG	TAA	
<i>tRNA-Glu</i>	-	12466..12525	60			TTC
<i>ND6</i>	+	12527..12985	459	ATG	TAA	
<i>ND4L</i>	+	13013..13249	237	ATG	TAA	
<i>tRNA-Ser</i>	+	13248..13303	56			TGA
<i>cob</i>	-	13302..14396	1095	ATG	TAA	
<i>tRNA-Met</i>	+	14432..14492	61			CAT
<i>tRNA-Tyr</i>	-	14495..14565	71			GTA
<i>ND1</i>	+	14617..15477	861	ATG	TAA	
<i>tRNA-Trp</i>	+	15478..15537	60			TCA
<i>cox3</i>	+	15591..16358	768	ATG	TAA	
<i>tRNA-Ala</i>	+	16364..16419	56			TGC
<i>ND4</i>	+	16420..17631	1212	ATG	TAA	
<i>tRNA-Cys</i>	+	17646..17704	59			GCA
<i>cox1</i>	+	17707..19242	1536	ATG	TAA	

### Specimen IOM\_2014\_17: unidentified Polychaeta

Fig. 6.

Station ID: 3517.

Biosample: SAMN42180855.

#### Cluster of nuclear rRNA genes

The cluster is complete with a total length of 6,365 bp (GenBank: PP970526). The best 18S megablast result is *Nicomache lumbricalis* Fabricius, 1780 isolate SPM24 (GenBank: MG975479) (Eilertsen et al. 2018), E-value 0.0, identity 99.87% for a length of 1,552 bp.

#### Mitochondrial genome

The mitogenome is complete with redundant endings (GenBank: PP990759). It is 16,265 bp long and encodes 13 protein coding genes, two rRNAs and 22 tRNAs, all on the same strand (Fig. 7, Table 4). The nucleotide composition is



**Figure 6.** Specimen IOM\_2014\_17 on a polymetallic nodule immediately after sampling (unscaled).

**Table 4.** Characteristics of the genes encoded by the mitogenome of the unidentified Polychaeta IOM\_2014\_17. T(AA) in the stop codon column indicates a premature termination with the addition of 3' A residues to the mRNA.

Gene	Strand	Location	Size (bp)	Start codon	Stop codon	Anticodon
<i>cox1</i>	+	1–1537	1537	ATG	T(AA)	
<i>tRNA-Asn</i>	+	1538–1599	62			GTT
<i>cox2</i>	+	1600–2284	685	ATG	TAA	
<i>tRNA-Asp</i>	+	2285–2348	64			GTC
<i>atp8</i>	+	2350–2512	163	ATG	TAA	
<i>tRNA-Tyr</i>	+	2513–2577	65			GTA
<i>tRNA-Gly</i>	+	2577–2641	65			TCC
<i>cox3</i>	+	2642–3421	780	ATG	TAG	
<i>tRNA-Gln</i>	+	3422–3489	68			TTG
<i>ND6</i>	+	3490–3966	477	ATG	TAA	
<i>cob</i>	+	3980–5119	1140	ATG	TAA	
<i>tRNA-Trp</i>	+	5123–5190	68			TCA
<i>ATP6</i>	+	5191–5890	700	ATG	T(AA)	
<i>tRNA-Arg</i>	+	5891–5951	61			TCG
<i>tRNA-Lys</i>	+	7374–7435	62			TTT
<i>tRNA-His</i>	+	7448–7510	63			GTG
<i>ND5</i>	+	7511–9236	1726	ATG	T(AA)	
<i>tRNA-Phe</i>	+	9237–9302	66			GAA
<i>tRNA-Glu</i>	+	9305–9368	64			TTC
<i>tRNA-Pro</i>	+	9370–9434	65			TGG
<i>tRNA-Thr</i>	+	9434–9497	64			TGT
<i>ND4L</i>	+	9498–9797	300	ATG	TAA	
<i>ND4</i>	+	9791–11158	1368	ATG	TAA	
<i>tRNA-Cys</i>	+	11161–11223	63			GCA
<i>tRNA-Met</i>	+	11224–11288	65			CAT
<i>rrnS</i>	+	11291–12131	841			
<i>tRNA-Val</i>	+	12132–12199	68			TAC
<i>rrnL</i>	+	12200–13540	1341			
<i>tRNA-Leu</i>	+	13541–13605	65			TAG
<i>tRNA-Ala</i>	+	13608–13669	62			TGC
<i>tRNA-Ser</i>	+	13670–13736	67			TGA
<i>tRNA-Leu</i>	+	13737–13799	63			TAA
<i>ND1</i>	+	13800–14733	934	ATG	T(AA)	
<i>tRNA-Ile</i>	+	14734–14802	69			GAT
<i>ND3</i>	+	14829–15182	354	ATG	TAA	
<i>tRNA-Ser</i>	+	15181–15249	69			TCT
<i>ND2</i>	+	15274–16257	984	ATG	TAA	

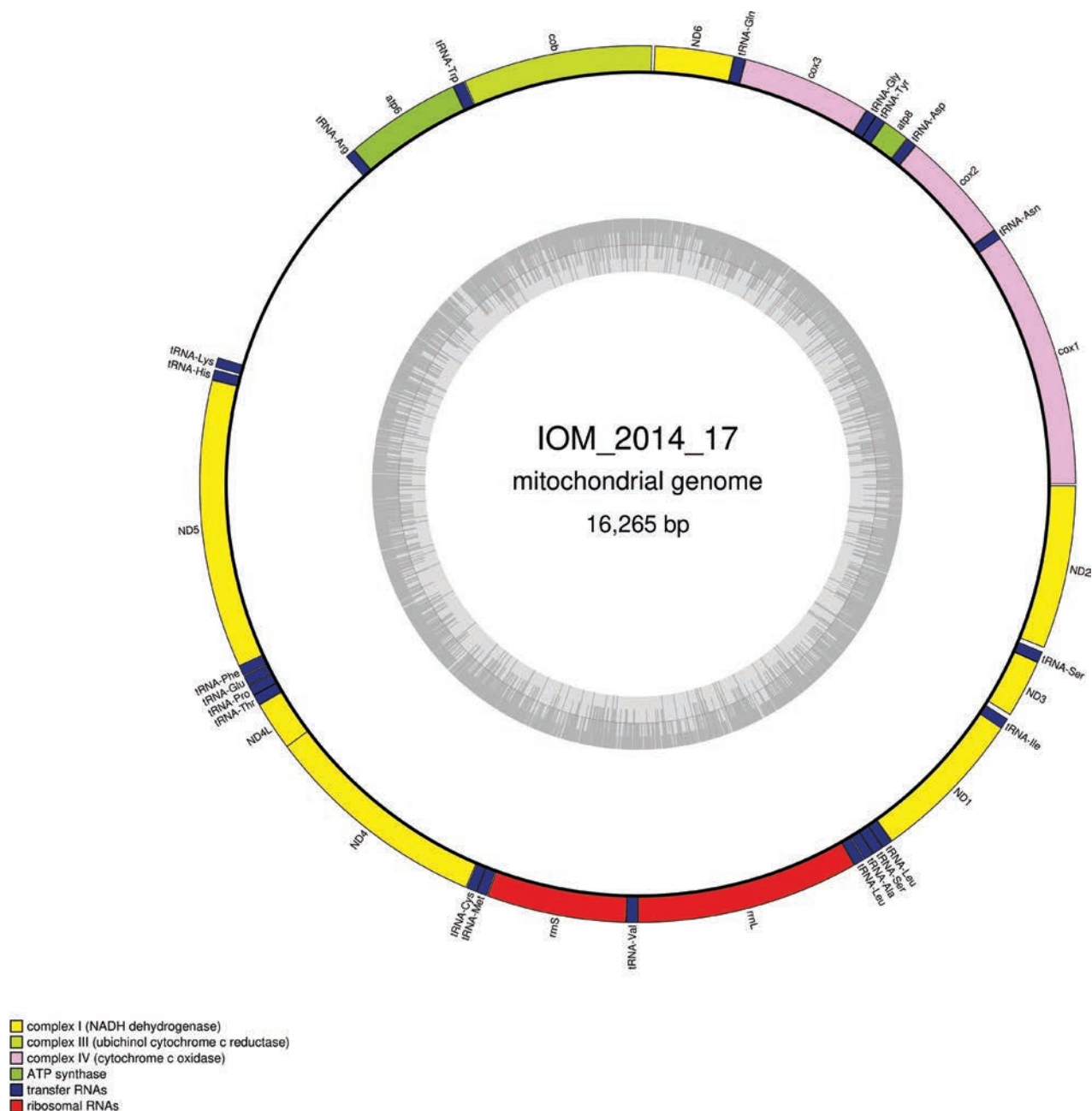


**Figure 7.** Map of the mitochondrial genome of specimen IOM\_2014\_17, with the type of genes indicated by colour boxes and the GC content indicated by the grey circle.

A (30.70%), T (32.66%), C (22.98%) and G (13.66%). The best *cox1* megablast result is *Nicomache* cf. *benthaliana* NHM\_058 (GenBank: OQ271976), which is also found in the CCZ (Stewart et al. 2023), with E-value 0.0, identity 99.28% for a length of 554 bp.

### Specimen IOM\_2014\_38: *Silax daleus* Lyman, 1879, Ophiuroidea

Fig. 8.

Station ID: 3526.

Biosample: SAMN42180856.



**Figure 8.** Specimen IOM\_2014\_38 identified as *Silax daleus* on a polymetallic nodule immediately after sampling (unscaled).

#### Cluster of nuclear rRNA genes

The cluster is complete with a total length of 6,940 bp (GenBank: PP970577). The best 18S megablast result is *Amphioplus cf. daleus* NHM\_447 (KU519529) (Glover et al. 2016), E-value 0.0, identity 100.00% for a length of 1,676 bp. *Amphioplus daleus* is a synonym of *Silax daleus* (Stöhr et al. 2024). Manual alignment of the 28S gene with the two partial sequences of *Amphioplus cf. daleus* (GenBank: MN170903 and MN170901, 993 bp and 973 bp long, respectively) (Christodoulou et al. 2019) showed a complete identity with MN170903 and three polymorphisms at the very end of the 3' part of MN170901.

#### Mitochondrial genome

The mitogenome is complete with redundant endings (GenBank: PP977505). It is 16,411 bp long and encodes 13 protein coding genes, two rRNAs and 22 tRNAs encoded on both strands (Fig. 9, Table 5). The nucleotide composition is A (34.82%), T (30.25%), C (21.54%) and G (13.39%). The best *cox1* megablast result is *Amphioplus daleus* voucher SO242\_1\_181\_D4 (GenBank: MT160448) (Christodoulou et al. 2020), E-value 0.0, identity 100% for a length of 658 bp. The mitogenome is colinear with those of *Amphiura sinicola* (GenBank: NC\_045938) (Lee et al. 2019), another representative of the Amphiuroidae family whose accepted name is currently *Amphiura (Fellaria) sinicola* Matsumoto, 1941. Both mitogenomes share identical features, including the premature ending of the protein-coding genes *cob* and *ND1* by the presence of a tRNA.

**Table 5.** Characteristics of the genes encoded by the mitogenome of *Silax daleus* specimen IOM\_2014\_38. T(AA) in the stop codon column indicates a premature termination with the addition of 3' A residues to the mRNA.

Gene	Strand	Location	Size (bp)	Start codon	Stop codon	Anticodon
<i>cox1</i>	+	1–1602	1602	ATG	TAA	
<i>tRNA-Arg</i>	+	1603–1669	67			TCG
<i>ND4L</i>	+	1670–1966	297	ATG	TAA	
<i>cox2</i>	+	1969–2655	687	ATG	TAA	
<i>tRNA-Lys</i>	+	2657–2730	74			CTT
<i>ATP8</i>	+	2732–2860	129	ATG	TAA	
<i>ATP6</i>	+	2864–3550	687	ATG	TAA	
<i>cox3</i>	+	3558–4355	798	ATG	TAG	
<i>tRNA-Ser</i>	-	4364–4435	72			TGA
<i>ND3</i>	+	4454–4813	360	ATG	TAA	
<i>ND4</i>	+	4822–6183	1362	ATG	TAA	
<i>tRNA-His</i>	+	6187–6258	72			GTG
<i>tRNA-Ser</i>	+	6260–6326	67			GCT
<i>ND5</i>	+	6328–8121	1794	ATG	TAA	
<i>ND6</i>	-	8433–8912	480	ATG	TAA	
<i>tRNA-Ala</i>	-	9481–9550	70			TGC
<i>tRNA-Glu</i>	-	9558–9625	68			TTC
<i>tRNA-Gly</i>	-	9627–9697	71			TCC
<i>rrnL</i>	-	9673–11123	1451			
<i>tRNA-Leu</i>	-	11112–11182	71			TAG
<i>tRNA-Pro</i>	-	11188–11255	68			TGG
<i>rrnS</i>	-	11250–12158	909			
<i>tRNA-Phe</i>	-	12162–12232	71			GAA
<i>tRNA-Thr</i>	-	12238–12304	67			TGT
<i>cob</i>	-	12305–13448	1144	GTG	T(AA)	
<i>tRNA-Asp</i>	-	13450–13519	70			GTC
<i>ND2</i>	-	13595–14650	1056	GTG	TAG	
<i>tRNA-Ile</i>	-	14650–14723	74			GAT
<i>tRNA-Met</i>	-	14832–14900	69			CAT
<i>ND1</i>	-	14901–15900	1000	GTG	T(AA)	
<i>tRNA-Leu</i>	-	15901–15972	72			TAA
<i>tRNA-Asn</i>	-	15973–16045	73			GTT
<i>tRNA-Gln</i>	+	16044–16115	72			TTG
<i>tRNA-Cys</i>	+	16117–16184	68			GCA
<i>tRNA-Val</i>	-	16189–16258	70			TAC
<i>tRNA-Tyr</i>	-	16260–16328	69			GTA
<i>tRNA-Trp</i>	+	16340–16410	71			TCA

### Specimen IOM\_2014\_51: Bryozoa

Fig. 10.

Station ID: 3540.

Biosample: SAMN42180857.

### Cluster of nuclear rRNA genes

The cluster is complete with a total length of 6,530 bp (GenBank: PP971152). The best 18S megablast result is *Hornera foliacea* MacGillivray, 1869 (GenBank: FJ409613) (Waeschenbach et al. 2009), E-value 0.0, identity 98.64% for a length of 1,810 bp.

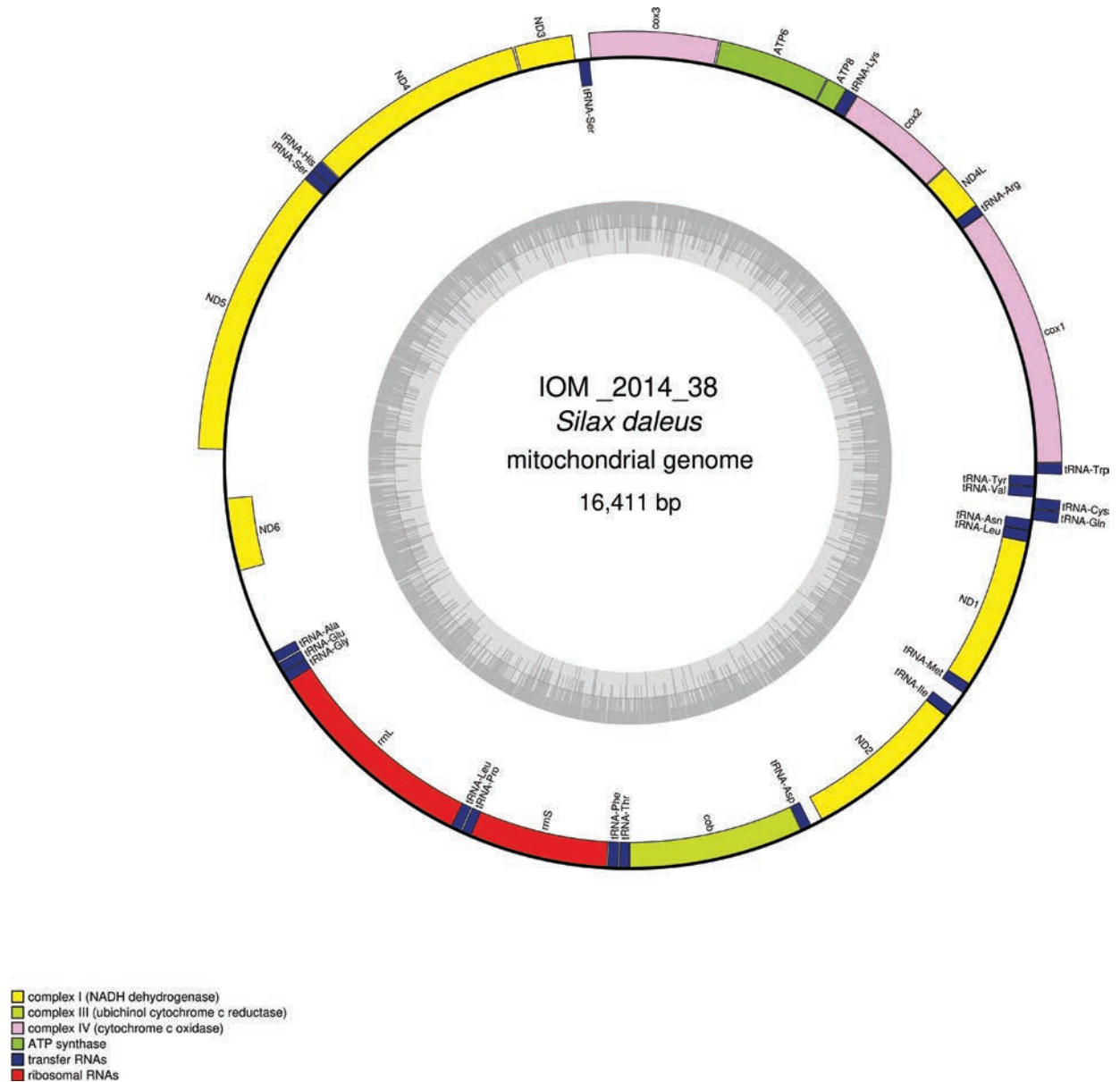


**Figure 9.** Map of the mitochondrial genome of *Silax daleus* specimen IOM\_2014\_38, with the type of genes indicated by colour boxes and the GC content indicated by the grey circle.



**Figure 10.** Specimen IOM\_2014\_51 on a polymetallic nodule immediately after sampling (unscaled).



**Table 6.** Characteristics of the genes encoded by the mitogenome the unidentified Bryozoa IOM\_2014\_51. The size of the intron-containing genes is indicated with and without the introns.

Gene	Strand	Location	Size (bp)	Start codon	Stop codon	Anticodon
<i>tRNA-Met</i>	-	450–527	78			CAT
<i>tRNA-Cys</i>	+	1291–1360	70			GCA
<i>ND6</i>	+	1482–1940	459	ATG	TAA	
<i>cox1</i>	+	1969–6242 (2 introns)	4274 (full) 1518 (CDS)	ATG	TAA	
<i>tRNA-Ser</i>	+	6251–6315	65			TCT
<i>tRNA-Pro</i>	-	6320–6377	58			TGG
<i>tRNA-Gln</i>	-	6384–6438	55			TTG
<i>tRNA-Gly</i>	+	6442–6518	77			TCC
<i>cox3</i>	+	6497–7264	768	ATG	TAA	
<i>tRNA-Tyr</i>	+	7276–7337	62			GTA
<i>tRNA-Arg</i>	+	7339–7404	66			TCG
<i>ND3</i>	+	7392–7700	309	ATG	TAG	
<i>tRNA-Thr</i>	-	7680–7746	67			TGT
<i>ND4L</i>	-	7828–8094	267	ATG	TAA	
<i>rrnL</i>	+	8353–9501	1149			
<i>tRNA-Lys</i>	+	9500–9552	53			TTT
<i>ND2</i>	-	9567–10457	891	ATG	TAA	
<i>tRNA-Phe</i>	+	10491–10547	57			GAA
<i>tRNA-Asn</i>	+	10540–10595	56			GTT
<i>ND4</i>	-	10591–11799	1209	ATG	TAA	
<i>tRNA-Val</i>	-	11802–11856	55			TAC
<i>tRNA-Trp</i>	-	11851–11906	56			TCA
<i>ND1</i>	-	11910–12770	861	ATG	TAA	
<i>ND5</i>	-	12788–14290	1503	ATG	TAA	
<i>tRNA-His</i>	-	14290–14346	57			GTG
<i>cob</i>	+	14410–17344 (3 introns)	2935 (full) 1113 (CDS)	ATG	TAA	
<i>tRNA-Glu</i>	+	17349–17413	65			TTC
<i>tRNA-Met</i>	+	17426–17489	64			CAT
<i>cox2</i>	+	17497–20172 (2 introns)	2676 (full) 666 (CDS)	ATG	TAA	
<i>tRNA-Asp</i>	+	20175–20250	76			GTC
<i>rrnS</i>	+	20336–21044	709			
<i>ATP6</i>	+	21099–21716	618	ATG	TAA	
<i>tRNA-Thr</i>	+	22313–22374	62			GGT
<i>tRNA-Glu</i>	-	23064–23121	58			TTC
<i>tRNA-Glu</i>	-	23592–23649	58			TTC

### Specimens IOM\_2014\_54 and 2014\_58: *Ophiosphalma glabrum* (Lütken & Mortensen, 1899)

Figs 12, 13.

Station ID IOM\_2014\_54: 2229Tr\_2; Station ID IOM\_2014\_58: 3521Tr\_1.

Biosample IOM\_2014\_54: SAMN46122295; Biosample IOM\_2014\_58: SAMN46122296.

### Cluster of nuclear rRNA genes

We failed at assembling the cluster of rRNA and could only retrieve the *18S* gene (GenBank: PP960805 and PP968762 for specimens IOM\_2014\_54 and IOM\_2014\_58 respectively). Both are 1816 bp long and are 100% identical with each other. The best *18S* megablast result is *Ophiomusium* cf. *glabrum*



**Figure 12.** Specimen IOM\_2014\_54 on a polymetallic nodule immediately after sampling (unscaled).

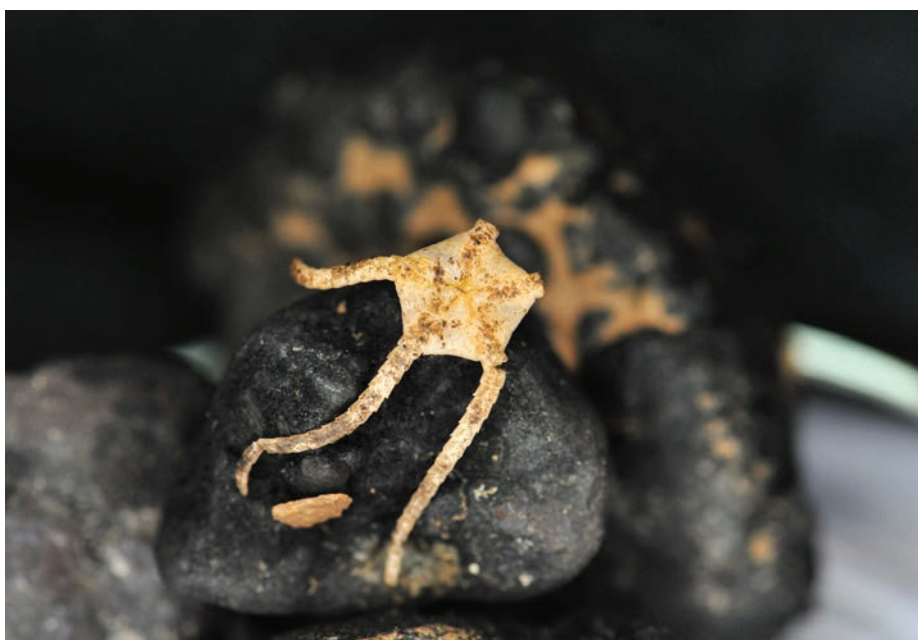


**Figure 13.** Specimen IOM\_2014\_58 on a polymetallic nodule immediately after sampling (unscaled).

NHM\_329 (GenBank: KU519536) from Glover et al. (2016), E-value 0.0, identity 99.82% for a length of 1669 bp. *Ophiomusium glabrum* is a non-accepted synonym of *Ophiosphalma glabrum*.

### Mitochondrial genome

The mitogenomes were found complete with redundant endings. They are 16,003 bp long for specimen 2014\_54 (GenBank: PP977506) and 15,994 bp long for 2014\_58 (GenBank: PP977508). The mitogenomes encode for 13 protein coding genes, two rRNA and 22 tRNA, encoded on both strands (Figs 14, 15,

Table 7). The nucleotide composition is A (35.09%/35.10%), T (33.44%/33.46%), C (19.43%/19.43%) and G (12.05%/12.01%) for IOM\_2014\_54 and IOM\_2014\_58, respectively. Both *cox2* and *cob* have premature termination by the presence of a tRNA. The best megablast results for the *cox1* gene were *Ophiosphalma glabrum* voucher DSB\_3935 (GenBank: MW770847), E-value 0.0, identity 99.70% for a length of 658 bp for IOM\_2014\_54, and *Ophiosphalma glabrum* voucher DSB\_42 (GenBank: MW770844), E-value 0.0, identity 99.85% for a length of 653 bp for IOM\_2014\_58. In Table 8, a comparison for each gene is presented. The most conserved gene was *ND6* and the most polymorph *ATP8*. It is to note that an indel was found in the *rrnS* gene. Most of the protein encoded were impacted by these mutations, except for the *cox1*, *ND4L*, and *ND6* genes.

**Table 7.** Characteristics of the genes encoded by the mitogenomes of *Ophiosphalma glabrum* specimens IOM\_2014\_54 and IOM\_2014\_58. T(AA) in the stop codon column indicates a premature termination with the addition of 3' A residues to the mRNA. When there are discrepancies in the positions of the genes, they are indicated separately for IOM\_2014\_54 and IOM\_2014\_58, respectively.

Gene	Strand	Location	Size (bp)	Start codon	Stop codon	Anticodon
<i>cox1</i>	+	1–1602	1602	ATG	TAA	
<i>tRNA-Arg</i>	+	1601–1668	68			TCG
<i>ND4L</i>	+	1675–1971	297	ATG	TAA	
<i>cox2</i>	+	1976–2666	624	ATG	T(AA)	
<i>tRNA-Lys</i>	+	2667–2734	68			CTT
<i>ATP8</i>	+	2738–2905	168	ATG	TAA	
<i>ATP6</i>	+	2893–3591	699	ATG	TAA	
<i>cox3</i>	+	3596–4393	798	ATG	TAA	
<i>tRNA-Ser</i>	-	4392–4463	72			TGA
<i>ND3</i>	+	4490–4849/4492–4851	360	ATG	TAA	
<i>ND4</i>	+	4852–6219/4854–6221	1368	ATG	TAA	
<i>tRNA-His</i>	+	6243–6314/6244–6315	72			GTG
<i>tRNA-Ser</i>	+	6317–6379/6316–6382	63			GCT
<i>ND5</i>	+	6382–8160/6383–8161	1779	ATG	TAA	
<i>ND6</i>	-	8176–8643/8177–8662	468	ATG	TAA	
<i>tRNA-Gly</i>	-	9108–9176/9099–9167	69			TCC
<i>rrnL</i>	-	9166–10549/9157–10540	1384			
<i>tRNA-Leu</i>	-	10580–10647/10571–10638	68			TAG
<i>tRNA-Ala</i>	-	10650–10716/10641–10707	67			TGC
<i>tRNA-Met</i>	-	10719–10787/10710–10778	69			CAT
<i>tRNA-Pro</i>	-	10787–10855/10778–10846	69			TGG
<i>rrnS</i>	-	10937–11841/10928–11833	905/906			
<i>tRNA-Phe</i>	-	11841–11912/11833–11904	72			GAA
<i>tRNA-Glu</i>	-	11921–11986/11913–11977	66			TTC
<i>tRNA-Thr</i>	-	12108–12173/12099–12164	66			TGT
<i>cob</i>	-	12174–13323/12165–13314	1150	ATG	T(AA)	
<i>tRNA-Asp</i>	-	13324–13391/13315–13382	68			GTC
<i>ND2</i>	-	13390–14445/13381–14436	1056	ATG	TAA	
<i>tRNA-Ile</i>	-	14445–14518/14436–14509	74			GAT
<i>ND1</i>	-	14518–15519/14509–15510	1002	ATG	TAA	
<i>tRNA-Leu</i>	-	15523–15595/15514–15586	73			TAA
<i>tRNA-Asn</i>	-	15597–15668/15588–15659	72			GTT
<i>tRNA-Gln</i>	+	15667–15736/15658–15727	70			TTG
<i>tRNA-Cys</i>	+	15735–15797/15726–15788	63			GCA
<i>tRNA-Val</i>	-	15796–15865/15787–15856	70			TAC
<i>tRNA-Tyr</i>	-	15867–15935/15858–15926	69			GTA
<i>tRNA-Trp</i>	+	15937–16003/15928–15994	67			TCA

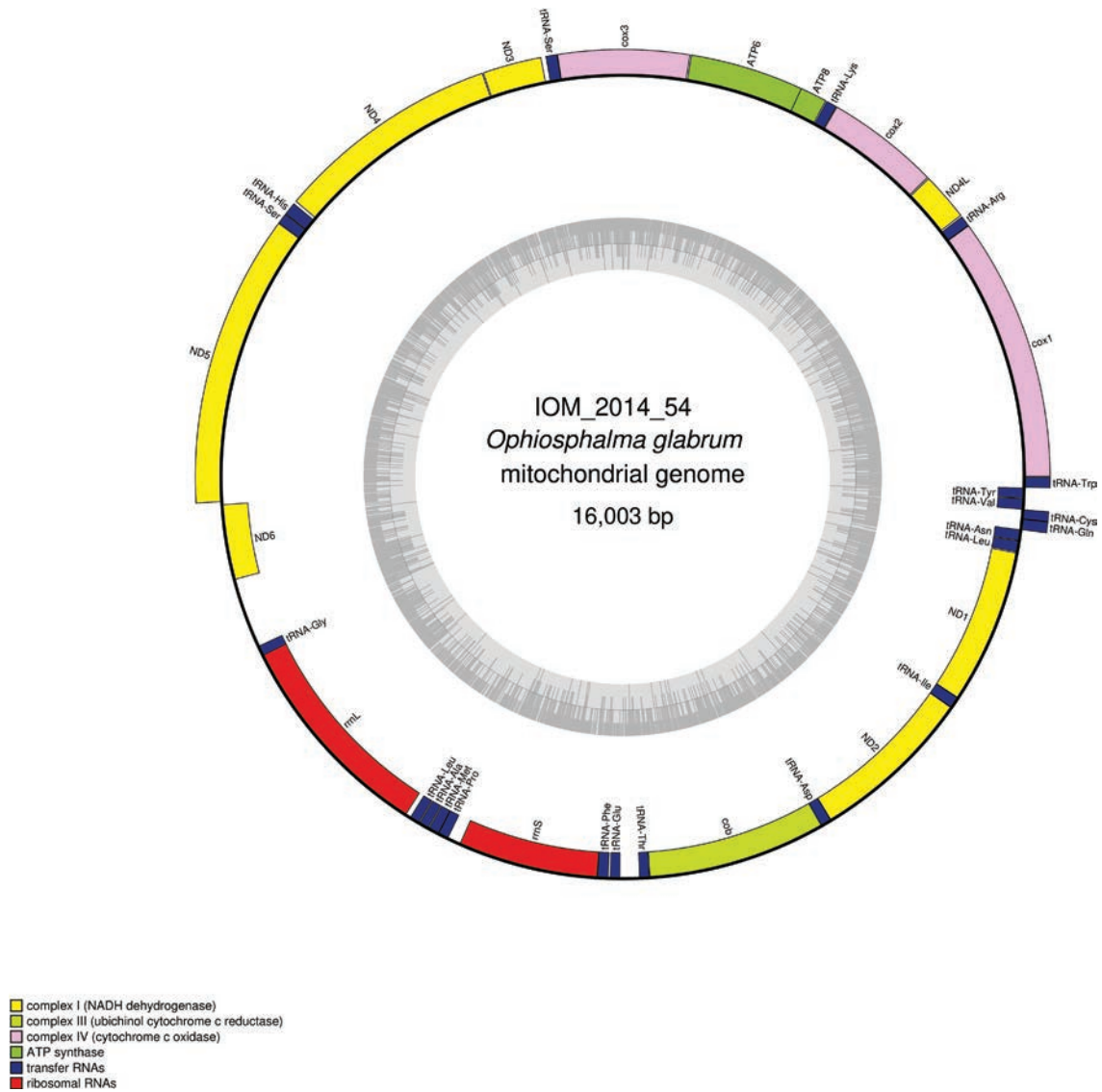


**Figure 14.** Map of the mitochondrial genome of *Ophiosphalma glabrum* specimen IOM\_2014\_54, with the type of genes indicated by colour boxes and the GC content indicated by the grey circle.

**Table 8.** Number of single nucleotide polymorphisms (SNPs) and percentage of identity between the protein-coding and rRNA genes of specimens *Ophiosphalma glabrum* 2014\_54 and 2014\_58.

Gene	SNPs/total length	Identity (%)
ATP6	9/705	98.72
ATP8	5/168	97.02
cob	12/1150	98.96
cox1	12/1602	99.25
cox2	10/691	98.55
cox3	9/798	98.75
ND1	17/1002	98.30
ND2	7/1056	99.34
ND3	4/360	98.89
ND4	16/1368	98.83
ND4L	4/297	98.65
ND5	16/1779	99.10
ND6	1/486	99.79
rrnL	5/1384	99.64
rrnS	4 SNPs + 1 indel/905–906	NA

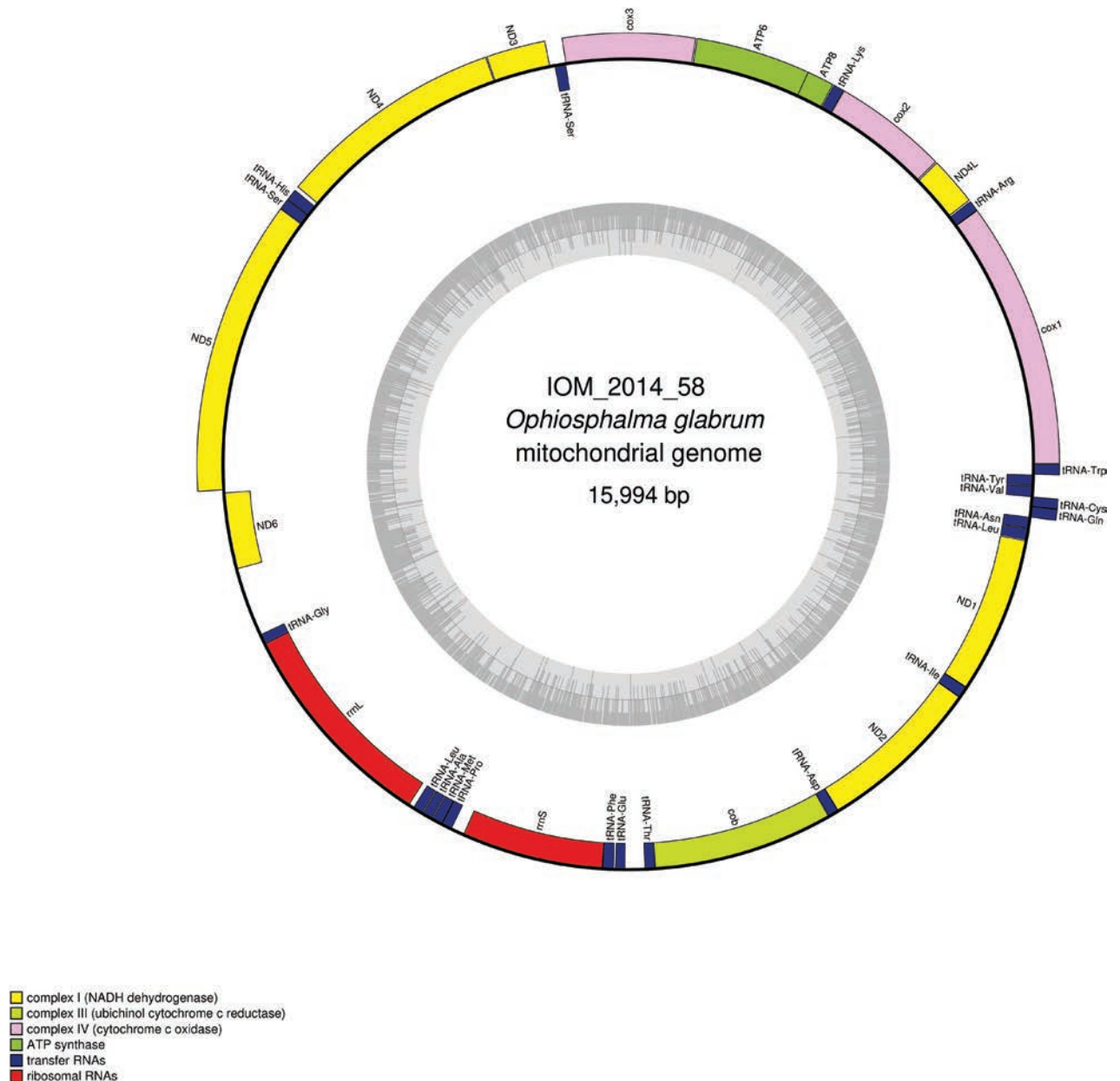


Figure 15. Map of the mitochondrial genome of *Ophiosphalma glabrum* specimen IOM\_2014\_58, with the type of genes indicated by colour boxes and the GC content indicated by the grey circle.

### Specimen IOM\_2014\_55: unidentified Holothuroidea

Fig. 16.

Station ID: 2229Tr\_2.

Biosample: SAMN42180858.

#### Cluster of nuclear rRNA genes

We failed at assembling a complete rRNA cluster. Instead, we extracted the 18S gene, which is 1,876 bp long (GenBank: PP971153). The best 18S megablast result is *Deima validum* (GenBank: KX856815), currently accepted name *Deima validum validum* Théel, 1879 (Miller et al. 2017), E-value 0.0, identity 99.34% for a length of 1,815 bp.



**Figure 16.** Specimen IOM\_2014\_55 after sampling, photo taken on a glass Petri dish after cleansing with water (unscaled).

### Mitochondrial genome

The mitogenome is complete with redundant endings (GenBank: PP977507). It is 16,097 bp long and encodes 13 protein coding genes, two rRNAs and 22 tRNAs (Fig. 17, Table 9). The nucleotide composition is A (35.23%), T (33.57%), C (17.98%) and G (13.22%). The best *cox1* megablast result is *Isostichopus badionotus* Selenka, 1867 (GenBank: MZ188901) (Drake et al. 2021), with E-value 0.0, identity 79.58% for a length of 16,318 bp (the sequence represents a complete mitochondrial genome). When aligning the *cox1* gene with sequences of various Holothuroidea from the CCZ as studied by Bribiesca-Contreras et al. (2022) and performing an ML phylogeny on them (model of evolution GTR+I+G4), the tree reveals that specimen IOM\_2014\_55 is sister to a clade containing *Oneirophanta* sp. CCZ 100 voucher CCZ\_100 (ON400706) and *Oneirophanta* cf. *mutabilis* GBC-2022 voucher CCZ\_193 (ON400724) with a 89% support at the node (tree not shown).

### Specimen IOM\_2014\_57: unidentified Porifera

Fig. 18.

Station ID: 3521Tr\_1.

Biosample: SAMN42180859.

### Cluster of nuclear rRNA genes

The cluster is complete with a total length of 5,804 bp (GenBank: PP968769). The best *18S* megablast result is again *P. pachymastia* voucher UCMPWC932 (GenBank: EF654528), E-value 0.0, identity 99.76% for a length of 1,660 bp. Megablast queries of the D1/D2 region returned a 100% identity with *Tentorium* sp. voucher NHM1404 (GenBank: PP848927) and *Tentorium* sp. voucher NHM1619 (GenBank: PP848930).

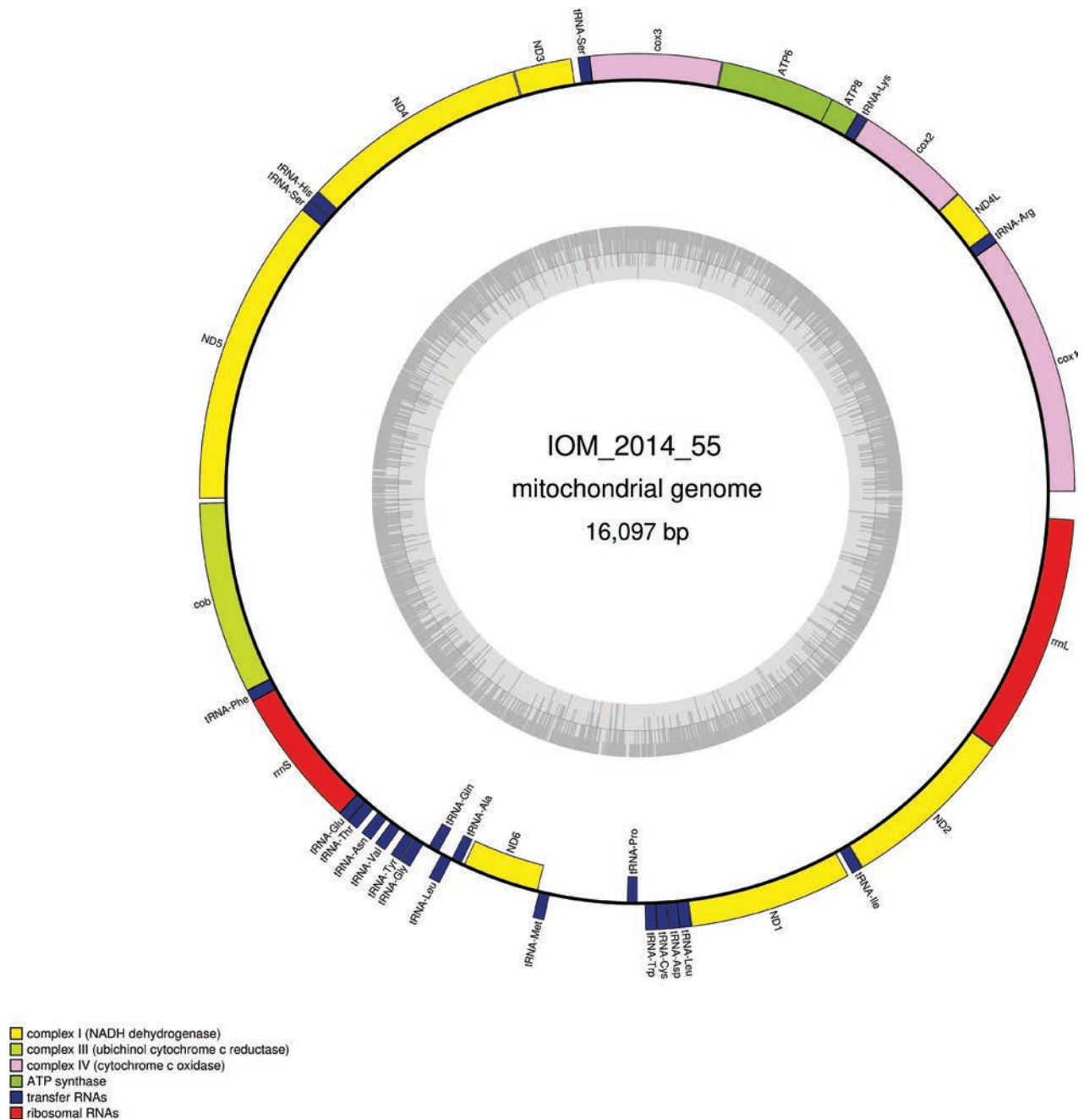


**Figure 17.** Map of the mitochondrial genome of specimen IOM\_2014\_55, with the type of genes indicated by colour boxes and the GC content indicated by the grey circle.

### Mitochondrial genome

The mitogenome is complete with redundant endings (GenBank: PP971518). It is 22,712 bp long and encodes 14 protein coding genes, two rRNAs and 25 tRNAs, all on the same strand (Fig. 19, Table 10). The nucleotide composition is A (31.35%), T (36.60%), C (12.30%) and G (19.75%). There is a group I intron in the *cox1* gene that contains a 282 amino-acid long ORF encoding a putative LAGLIDADG endonuclease. The best megablast result for the CDS of the *cox1* gene is *P. littoralis* (GenBank: KJ129611) with E-value 0.0, identity 94.81% for a length of 21,719 bp (representing a complete mitogenome).

**Table 9.** Characteristics of the genes encoded by the mitogenome the unidentified Holothuroidea IOM\_2014\_55. T(AA) in the stop codon column indicates a premature termination with the addition of 3' A residues to the mRNA.

Gene	Strand	Location	Size (bp)	Start codon	Stop codon	Anticodon
<i>cox1</i>	+	1–1554	1554	ATG	TAA	
<i>tRNA-Arg</i>	+	1553–1618	66			TCG
<i>ND4L</i>	+	1619–1915	297	ATG	TAA	
<i>cox2</i>	+	1916–2604	689	ATG	TA(A)	
<i>tRNA-Lys</i>	+	2605–2668	64			CTT
<i>ATP8</i>	+	2669–2842	174	ATG	TAA	
<i>ATP6</i>	+	2830–3519	690	ATG	TAA	
<i>cox3</i>	+	3522–4304	783	ATG	TAA	
<i>tRNA-Ser</i>	+	4303–4373	71			TGA
<i>ND3</i>	+	4412–4756	345	ATG	TAA	
<i>ND4</i>	+	4760–6116	1357	ATG	T(AA)	
<i>tRNA-His</i>	+	6118–6186	69			GTG
<i>tRNA-Ser</i>	+	6188–6254	67			GCT
<i>ND5</i>	+	6255–8090	1836	ATG	TAA	
<i>cob</i>	+	8155–9257	1103	ATG	TAA	
<i>tRNA-Phe</i>	+	9257–9327	71			GAA
<i>rrnS</i>	+	9326–10159	834			
<i>tRNA-Glu</i>	+	10158–10224	67			TTC
<i>tRNA-Thr</i>	+	10225–10294	70			TGT
<i>tRNA-Asn</i>	+	10330–10398	69			GTT
<i>tRNA-Val</i>	+	10431–10500	70			TAC
<i>tRNA-Tyr</i>	+	10543–10608	66			GTA
<i>tRNA-Gly</i>	+	10611–10675	65			TCC
<i>tRNA-Gln</i>	-	10711–10780	70			TTG
<i>tRNA-Leu</i>	+	10804–10873	70			TAG
<i>tRNA-Ala</i>	-	10873–10939	67			TGC
<i>ND6</i>	-	10958–11446	489	ATG	TAG	
<i>tRNA-Met</i>	+	11456–11524	69			CAT
<i>tRNA-Pro</i>	-	12010–12075	66			TGG
<i>tRNA-Trp</i>	+	12121–12189	69			TCA
<i>tRNA-Cys</i>	+	12190–12256	67			GCA
<i>tRNA-Asp</i>	+	12258–12325	68			GTC
<i>tRNA-Leu</i>	+	12321–12391	71			TAA
<i>ND1</i>	+	12392–13363	972	ATG	TAA	
<i>tRNA-Ile</i>	+	13389–13456	68			GAT
<i>ND2</i>	+	13457–14503	1047	ATG	TAA	
<i>rrnL</i>	+	14504–15933	1430			

**Figure 18.** Specimen IOM\_2014\_57 on a polymetallic nodule immediately after sampling (unscaled).



**Table 10.** Characteristics of the genes encoded by the mitogenome the unidentified Porifera IOM\_2014\_57. The size of the intron-containing genes is indicated with and without the introns.

Gene	Strand	Location	Size (bp)	Start codon	Stop codon	Anticodon
<i>cox1</i>	+	1–2620 (1 intron)	2620 (full) 1563 (CDS)	ATG	TAG	
<i>tRNA-Ser</i>	+	2669–2752	84			TGA
<i>tRNA-Asp</i>	+	2868–2939	72			GTC
<i>tRNA-Cys</i>	+	3467–3532	66			GCA
<i>ND1</i>	+	3571–4566	996	ATG	TAG	
<i>tRNA-Leu</i>	+	4640–4723	84			TAA
<i>tRNA-Ile</i>	+	4772–4844	73			GAT
<i>tRNA-Met</i>	+	4853–4923	71			CAT
<i>ND2</i>	+	5013–6428	1416	ATG	TAA	
<i>ND5</i>	+	6509–8401	1893	ATG	TAG	
<i>tRNA-Ala</i>	+	8470–8542	73			TGC
<i>tRNA-Met</i>	+	8640–8711	72			CAT
<i>tRNA-Phe</i>	+	8843–8915	73			GAA
<i>rrnS</i>	+	9111–10109	999			
<i>tRNA-Gly</i>	+	10393–10464	72			TCC
<i>tRNA-Val</i>	+	10478–10550	73			TAC
<i>rrnL</i>	+	11766–13180	1415			
<i>tRNA-Tyr</i>	+	13494–13564	71			GTA
<i>tRNA-Met</i>	+	13609–13680	72			CAT
<i>cox2</i>	+	13824–14555	732	ATG	TAA	
<i>tRNA-Lys</i>	+	14612–14684	73			TTT
<i>ATP8</i>	+	14686–14955	270	ATG	TAA	
<i>ATP6</i>	+	15015–15749	735	ATG	TAA	
<i>tRNA-Arg</i>	+	15912–15985	74			TCT
<i>cox3</i>	+	16062–16850	789	ATG	TAG	
<i>tRNA-Gln</i>	+	16913–16984	72			TTG
<i>tRNA-Trp</i>	+	17051–17121	72			TCA
<i>tRNA-Asn</i>	+	17238–17308	71			GTT
<i>tRNA-Leu</i>	+	17339–17413	75			TAG
<i>cob</i>	+	17415–18569	1155	ATG	TAA	
<i>tRNA-Thr</i>	+	18609–18682	74			TGT
<i>ATP9</i>	+	18799–19035	237	ATG	TAA	
<i>tRNA-Ser</i>	+	19178–19262	85			GCT
<i>tRNA-Pro</i>	+	19300–19372	73			TGG
<i>ND4</i>	+	19436–20887	1452	ATG	TAA	
<i>tRNA-His</i>	+	20939–21011	73			GTG
<i>tRNA-Glu</i>	+	21075–21146	72			TTC
<i>ND6</i>	+	21144–21740	597	ATG	TAA	
<i>ND3</i>	+	21760–22116	357	ATG	TAA	
<i>tRNA-Arg</i>	+	22194–22264	71			TCG
<i>ND4L</i>	+	22265–22564	300	ATG	TAG	

### Mitochondrial genome

The mitogenome is complete with redundant endings (GenBank: PP977509). It is 16,266 bp long and codes for 13 protein coding genes, two rRNAs and 22 tRNAs, all encoded on the same strand (Fig. 21, Table 11). The nucleotide composition is A (28.05%), T (26.52%), C (30.14%) and G (15.29%). The best *cox1* megablast result is *Hemithiris* sp. Hem1 (GenBank: AB026517) (Saito et al. 2000) with E-value 0.0, identity 81.71% for a length of 1,218 bp.



**Table 11.** Characteristics of the genes encoded by the mitogenome the unidentified Holothuroidea IOM\_2014\_62. T(AA) in the stop codon column indicates a premature termination with the addition of 3' A residues to the mRNA.

Gene	Strand	Location	Size (bp)	Start codon	Stop codon	Anticodon
<i>cox1</i>	+	1–1548	1548	ATG	TAA	
<i>cox2</i>	+	1560–2243	684	ATG	TAA	
<i>tRNA-Asp</i>	+	2242–2309	68			GTC
<i>tRNA-Met</i>	+	2368–2437	70			CAT
<i>rrnS</i>	+	2453–3298	846			
<i>rrnL</i>	+	3340–4707	1368			
<i>tRNA-Leu</i>	+	5016–5081	66			TAG
<i>tRNA-Cys</i>	+	5116–5181	66			GCA
<i>ATP8</i>	+	5205–5594	390	ATG	TAA	
<i>ATP6</i>	+	5596–6387	792	ATC	TAG	
<i>tRNA-Tyr</i>	+	6741–6806	66			GTA
<i>tRNA-Val</i>	+	6811–6875	65			TAC
<i>ND6</i>	+	6892–7384	493	ATG	T(AA)	
<i>tRNA-Pro</i>	+	7385–7451	67			TGG
<i>cob</i>	+	7543–8595	1053	ATG	TAA	
<i>tRNA-Lys</i>	+	8596–8659	64			TTT
<i>tRNA-Asn</i>	+	8660–8725	66			GTT
<i>tRNA-Ser</i>	+	8726–8792	67			TGA
<i>ND4L</i>	+	8866–9078	213	ATG	TAA	
<i>ND4</i>	+	9072–10434	1363	ATG	T(AA)	
<i>tRNA-Gln</i>	+	10435–10503	69			TTG
<i>tRNA-Trp</i>	+	10504–10567	64			TCA
<i>tRNA-His</i>	+	10567–10630	64			GTG
<i>ND5</i>	+	10676–12355	1680	ATT	TAA	
<i>tRNA-Phe</i>	+	12356–12423	68			GAA
<i>tRNA-Glu</i>	+	12425–12489	65			TTC
<i>tRNA-Gly</i>	+	12491–12556	66			TCC
<i>cox3</i>	+	12558–13340	783	ATG	TAA	
<i>tRNA-Ala</i>	+	13364–13428	65			TGC
<i>tRNA-Arg</i>	+	13429–13496	68			TCG
<i>tRNA-Ile</i>	+	13509–13580	72			GAT
<i>ND3</i>	+	13583–13933	351	GTG	TAG	
<i>tRNA-Leu</i>	+	14005–14070	66			TAA
<i>ND1</i>	+	14127–15101	975	ATA	TAA	
<i>tRNA-Ser</i>	+	15145–15210	66			TCT
<i>ND2</i>	+	15244–16194	951	ATC	TAA	
<i>tRNA-Thr</i>	+	16196–16263	68			TGT

## Discussion

It is assessed that there is a substantial gap between the CCZ biodiversity and the described metazoan species. Many species remain not only to be described, but also to be discovered (Amon et al. 2016; Christodoulou et al. 2019; Rabone et al. 2023). The gap is being slowly filled in, thanks to the increasing number of sampling efforts undertaken by scientist over the past years (including scientists working with ISA contractors), but at the same time new areas of knowledge gaps are being identified. To a certain extent, this paradox is reflected in the increasing amount of environmental data that ISA contractors are required to collect. Comparison of the LTC recommendations from previous years with the most recent ones clearly underlines the gaps in our knowledge (ISBA/25/LTC/6/Rev.3). This includes but is not limited to the application of genetic studies in assessing benthic biodiversity and population connectivity of organisms.

Although molecular studies have been making rapid progress over past years, advancing our knowledge on benthic metazoans, there are still phyla that have received limited attention from a genomic point of view. This is the case for Brachiopoda for example, which has been scarcely documented so far. Among the more than 400 known non-fossil species of Brachiopoda, fewer than ten have had their mitogenomes sequenced, with the majority of the sequences belonging to inarticulate brachiopods (Karagozlu et al. 2021; Niaison et al. 2021; Breton 2024). Only four species (and three genera) of articulate taxa, to which specimen IOM\_2014\_62 is likely to belong, have had their mitogenomes sequenced and published (Stechmann and Schlegel 1999; Helfenbein et al. 2001; Karagozlu et al. 2017; Noguchi et al. 2000). The percentage of identity of the *cox1* gene between specimen IOM\_2014\_62 and the four other species ranges between 63.27% and 72.31%. There is a practical implication of such differences: DNA primers designed using previously published reference mitogenomes may not anneal correctly on the DNA of a specimen such as IOM\_2014\_62, and possibly other Brachiopoda from the CCZ. Documenting these taxa with more mitogenome data could help solve this problem, with the subsequent possibility to design more efficient primers.

Among our specimens, half of the Porifera and Bryozoa have introns in their mitogenomes, in each case in the *cox1* gene. Although rare and nearly absent in other taxa groups, this is not the first time that introns have been found within the mitogenomes of these two phyla (Rot et al. 2006; Jenkins et al. 2022). In the case of Porifera, intron content within a single species has been proven to vary across populations (Cranston et al. 2021). Not only are these findings interesting from the evolutionary genomics point of view but, due to the unpredictable presence of introns, they also challenge the use of the *cox1* gene for routine molecular barcoding of the CCZ Bryozoa and Porifera (Neal et al. 2022, 2023). Owing to the presence of introns, amplification of this gene by PCR might fail, or at least will require adoption of a protocol for longer elongation time and possibly the use of the Taq polymerase suitable for a long PCR.

A solution to such issues might be our genome-skimming approach. However, this approach has its limitations, one of them being that obtaining the required amount of DNA could result in the destruction of the smallest samples. There could thus be a risk of not leaving a correct specimen voucher behind, which is not in line with the ISA recommendations that advocate for reverse taxonomy followed by curation of voucher specimens and molecular samples in order to maintain the link between morphology-based and molecular-based identifications (ISBA/25/LTC/6/Rev.3 2023). Otherwise, such approach might require a preliminary treatment such as whole genome amplification. Regardless of the above limitation, when specimens qualify in terms of biomass, or are expendable because of their limited further use (which was the case with some of our own material), our approach could still be applied.

Among the ten specimens in this study, five of the sequences obtained matched the sequences stored in GenBank. Sequencing confirmed that specimen IOM\_2014\_38 is *S. daleus* and that specimens IOM\_2014\_54 and IOM\_2014\_58 were *O. glabrum*. We regard as especially promising the results obtained on *O. glabrum*, for further studies in the emerging field of population genetics and connectivity in the CCZ (Taboada et al. 2018; Riehl and De Smet 2020). With 12 SNPs out of 1602 bp, the *cox1* gene would be a

useful population marker for this species, as already suggested by the works of Christodoulou et al. (2020). It could be noted that none of the sequences obtained by Christodoulou et al. (2020) were identical to the *cox1* gene of IOM\_2014\_54 and IOM\_2014\_58, which suggests a large polymorphism of this gene among this species.

The two other specimens which matched to some degree with GenBank references were identified as Demospongiae (IOM\_2014\_13) and Polychaeta (IOM\_2014\_17). Both were far more degraded, especially IOM\_2014\_17, which was torn into two pieces of ~ 1.5 cm each. Neither of the specimens was suitable for taxonomy, neither preliminary nor reverse. Megablast queries returned a 99.28% identity of IOM\_2014\_17 with *Nicomache* cf. *benthaliana* NHM\_058, an organism that has been previously found in the licence areas UK-1A and UK-1B (UK Seabed Resources Ltd.), BGR (Federal Institute for Geosciences and Natural Resources of the Federal republic of Germany) and OMS (Ocean Mineral Singapore PTE Ltd.), all of which are located to the East of IOM claim area (Stewart et al. 2023). It is also worth reminding that queries of partial *18S*, *28S*, and *cox1* returned a complete identity between IOM\_2014\_13 and *Spinularia* sp. voucher RC1570 which was also sampled in the Eastern part of the CCZ, as for the aforementioned Polychaeta.

The results of genome comparison obtained for specimen of Demospongiae IOM\_2014\_13 are more intriguing. The 100% identity with the partial *cox1* gene of *S. sarsii* poses some problems. As far as we know, this species has never been reported in the CCZ. It is mostly found in the Atlantic Ocean, and a few locations have also been reported for the South-West Pacific (de Voogd et al. 2024). If the presence of *S. sarsii* is confirmed in the CCZ, it will raise questions about its global distribution. However, no further assessment should be done for this species based on our sequencing results, as we are faced with two taxonomic issues. First, it was impossible to perform a correct morphology-based identification of a partial and degraded specimen. Second, it should be noted that the 100% identity of the *cox1* gene was returned for a 658 bp fragment deposited in GenBank, which is less than half the length of the complete *cox1* gene of Demospongiae IOM\_2014\_13, leaving room for informative polymorphisms outside this 658 bp fragment. Moreover, the differences in length between queries and the sequences registered in GenBank may lead to further difficulties. When results are sorted based on their 'Max Score' or 'Total Score', different lengths and the impact they have on the 'Query Cover' parameter affect the result returned by such query. If the reference sequence deposited in GenBank is considerably shorter than the query, it may lead to the exclusion of the reference from the sequences producing significant alignment, whose number is limited to a maximum of one hundred. This in fact could serve as an argument in favour of our genome-skimming approach: submitting complete mitogenomes to GenBank means that querying a partial gene belonging to an identical species from the CCZ will return complete sequences as top results. With this in mind, we hope that the results presented here could be used as references in future studies on phylogeny, distribution of species and possibly population genetics of benthic organisms inhabiting the CCZ. We also hope that further investigations by other teams would lead to a more formal identification or description of the unidentified taxa here studied, and that such studies will benefit from the genomic results here presented.

## Additional information

### Conflict of interest

The authors have declared that no competing interests exist.

### Ethical statement

No ethical statement was reported.

### Funding

This work was co-financed by the Minister of Science under the "Regional Excellence Initiative" Program for 2024-2027 (RID/SP/0045/2024/01).

### Author contributions

Conceptualization: RG. Funding acquisition: TA. Investigation: RG, TA, PD, KM, VS, CO. Methodology: PD, RG. Project administration: TA, KM. Visualization: AK. Writing - original draft: RG. Writing - review and editing: VS, KM, PD, TA, AK, CO.

### Author ORCIDs

Romain Gastineau  <https://orcid.org/0000-0001-8661-5118>

Kamila Mianowicz  <https://orcid.org/0000-0002-7755-3258>

Przemysław Dąbek  <https://orcid.org/0000-0002-3736-3011>

Christian Otis  <https://orcid.org/0000-0001-9680-5863>

Tomasz Abramowski  <https://orcid.org/0000-0002-9029-406X>

### Data availability

All of the data that support the findings of this study are available in the main text.

## References

- Amon DJ, Ziegler AF, Dahlgren TG, Glover AG, Goineau A, Gooday AJ, Wiklund H, Smith CR (2016) Insights into the abundance and diversity of abyssal megafauna in a poly-metallic-nodule region in the eastern Clarion-Clipperton Zone. *Scientific Reports* 6(1): 30492. <https://doi.org/10.1038/srep30492>
- Bankevich A, Nurk S, Antipov D, Gurevich AA, Dvorkin M, Kulikov AS, Lesin VM, Nikolenko SI, Pham S, Prjibelski AD, Pyshkin AV, Sirotkin AV, Vyahhi N, Tesler G, Alekseyev MA, Pevzner PA (2012) SPAdes: A new genome assembly algorithm and its applications to single-cell sequencing. *Journal of Computational Biology* 19(5): 455–477. <https://doi.org/10.1089/cmb.2012.0021>
- Breton S (2024) Comparative mitogenomics of Brachiopods reveals conservatism in articulate species and unusualness in inarticulate species. *Molecular biology reports* 51(1): 298. <https://doi.org/10.1007/s11033-024-09270-6>
- Bribiesca-Contreras G, Dahlgren TG, Amon DJ, Cairns S, Drennan R, Durden JM, Eléaume MP, Hosie AM, Kremenetskaia A, McQuaid K, O'Hara TD, Rabone M, Simon-Lledó E, Smith CR, Watling L, Wiklund H, Glover AG (2022) Benthic megafauna of the western Clarion-Clipperton Zone, Pacific Ocean. *ZooKeys* 1113: 1–110. <https://doi.org/10.3897/zookeys.1113.82172>
- Camacho C, Coulouris G, Avagyan V, Ma N, Papadopoulos J, Bealer K, Madden TL (2009) BLAST+: Architecture and applications. *BMC Bioinformatics* 10(1): 421. <https://doi.org/10.1186/1471-2105-10-421>

- Christodoulou M, O'Hara TD, Hugall AF, Arbizu PM (2019) Dark Ophiuroid Biodiversity in a Prospective Abyssal Mine Field. *Current biology* 29(22): 3909–3912.e3. <https://doi.org/10.1016/j.cub.2019.09.012>
- Christodoulou M, O'Hara T, Hugall AF, Khodami S, Rodrigues CF, Hilario A, Vink A, Martinez Arbizu P (2020) Unexpected high abyssal ophiuroid diversity in polymetallic nodule fields of the northeast Pacific Ocean and implications for conservation. *Biogeosciences* 17: 1845–1876. <https://doi.org/10.5194/bg-17-1845-2020>
- Cohen BL, Gawthrop A, Cavalier-Smith T (1998) Molecular phylogeny of brachiopods and phoronids based on nuclear-encoded small subunit ribosomal RNA gene sequences. *Philosophical Transactions of the Royal Society B: Biological Sciences* 353(1378): 2039–2061. <https://doi.org/10.1098/rstb.1998.0351>
- Cranston A, Taboada S, Koutsouveli V, Schuster A, Riesgo A (2021) A population specific mitochondrial intron from the sponge *Phakellia robusta* in the North-East Atlantic. *Deep Sea Research Part I: Oceanographic Research Papers* 172: Article 103534. <https://doi.org/10.1016/j.dsr.2021.103534>
- Danovaro R, Aguzzi J, Fanelli E, Billett D, Gjerde K, Jamieson A, Ramirez-Llodra E, Smith CR, Snelgrove PV, Thomsen L, Dover CL (2017) An ecosystem-based deep-ocean strategy. *Science (New York, N.Y.)* 355(6324): 452–454. <https://doi.org/10.1126/science.aah7178>
- Darriba D, Posada D, Kozlov AM, Stamatakis A, Morel B, Flouri T (2020) ModelTest-NG: A New and Scalable Tool for the Selection of DNA and Protein Evolutionary Models. *Molecular Biology and Evolution* 37(1): 291–294. <https://doi.org/10.1093/molbev/msz189>
- de Voogd NJ, Alvarez B, Boury-Esnault N, Cárdenas P, Díaz M-C, Dohrmann M, Downey R, Goodwin C, Hajdu E, Hooper JNA, Kelly M, Klautau M, Lim SC, Manconi R, Morrow C, Pinheiro U, Pisera AB, Ríos P, Rützler K, Schönberg C, Turner T, Vacelet J, van Soest RWM, Xavier J (2024) World Porifera Database. *Spinularia sarsii* (Ridley & Dendy, 1886). World Register of Marine Species. <https://www.marinespecies.org/aphia.php?p=taxdetails&id=989667> [accessed 10 May 2024]
- del Cerro C, Peñalver A, Cuevas C, de la Calle F, Galán B, García JL (2016) Complete mitochondrial genome of *Polymastia littoralis* (Demospongiae, Polymastiidae). *Mitochondrial DNA. Part A, DNA mapping, sequencing, and analysis* 27(1): 312–313. <https://doi.org/10.3109/19401736.2014.892092>
- Donath A, Jühling F, Al-Arab M, Bernhart SH, Reinhardt F, Stadler PF, Middendorf M, Bern M (2019) Improved annotation of protein-coding genes boundaries in metazoan mitochondrial genomes. *Nucleic acids research* 47(20): 10543–10552. <https://doi.org/10.1093/nar/gkz833>
- Drake VI, Kim E, Nigro HG, Bogantes VE, Janosik AM (2021) The complete mitochondrial genome of the chocolate chip sea cucumber *Isostichopus badionotus* (Echinodermata: Holothuroidea). *Mitochondrial DNA. Part B, Resources* 6(7): 1947–1948. <https://doi.org/10.1080/23802359.2021.1937365>
- Eilertsen MH, Georgieva MN, Kongsrud JA, Linse K, Wiklund H, Glover AG, Rapp HT (2018) Genetic connectivity from the Arctic to the Antarctic: *Sclerolinum contortum* and *Nicomache lokii* (Annelida) are both widespread in reducing environments. *Scientific Reports* 8(1): 4810. <https://doi.org/10.1038/s41598-018-23076-0>
- Gastineau R, Dąbek P, Mianowicz K, Stoyanova V, Krawcewicz A, Abramowski T (2023) Complete mitochondrial genome of the abyssal coral *Abyssoprimnoa gemina* Cairns, 2015 (Octocorallia, Primnoidae) from the Clarion-Clipperton Zone, Pacific Ocean. *ZooKeys* 1183: 81–98. <https://doi.org/10.3897/zookeys.1183.109000>
- Glover AG, Wiklund H, Rabone M, Amon DJ, Smith CR, O'Hara T, Mah CL, Dahlgren TG (2016) Abyssal fauna of the UK-1 polymetallic nodule exploration claim, Clarion-Clip-

- perion Zone, central Pacific Ocean: Echinodermata. *Biodiversity data journal* 4: e7251. <https://doi.org/10.3897/BDJ.4.e7251>
- Gooday AJ, Wawrzyniak-Wydrowska B (2023) Macrofauna-sized foraminifera in epibenthic sledge samples from five areas in the eastern Clarion-Clipperton Zone (equatorial Pacific). *Frontiers in Marine Science* 9: 1059616. <https://doi.org/10.3389/fmars.2022.1059616>
- Helfenbein KG, Brown WM, Boore JL (2001) The complete mitochondrial genome of the articulate brachiopod *Terebratalia transversa*. *Molecular biology and evolution* 18(9): 1734–1744. <https://doi.org/10.1093/oxfordjournals.molbev.a003961>
- ISBA/25/LTC/6/Rev.3 (2023) Recommendations for the guidance of contractors on the content, format and structure of annual reports. International Seabed Authority, Kingston, Jamaica. [https://www.isa.org.jm/wp-content/uploads/2022/04/ISBA\\_25\\_LTC\\_6\\_Rev.2-2211076E.pdf](https://www.isa.org.jm/wp-content/uploads/2022/04/ISBA_25_LTC_6_Rev.2-2211076E.pdf) [accessed 17 May 2024]
- Jenkins HL, Graham R, Porter JS, Vieira LM, de Almeida ACS, Hall A, O’Dea A, Coppard SE, Waeschenbach A (2022) Unprecedented frequency of mitochondrial introns in colonial bilaterians. *Scientific Reports* 12(1): 10889. <https://doi.org/10.1038/s41598-022-14477-3>
- Kalvari I, Nawrocki EP, Ontiveros-Palacios N, Argasinska J, Lamkiewicz K, Marz M, Griffiths-Jones S, Toffano-Nioche C, Gautheret D, Weinberg Z, Rivas E, Eddy SR, Finn RD, Bateman A, Petrov AI (2021) Rfam 14: Expanded coverage of metagenomic, viral and microRNA families. *Nucleic Acids Research* 49(D1): D192–D200. <https://doi.org/10.1093/nar/gkaa1047>
- Karagozlu MZ, Kim SG, Dhin TD, Kim CB (2017) Complete mitochondrial genome of *Laqueus Japonicus* (Brachiopoda, Terebratulida, Laqueidae). *Mitochondrial DNA. Part B, Resources* 2(2): 883–884. <https://doi.org/10.1080/23802359.2017.1407716>
- Karagozlu MZ, Do TD, Kim JI, Choi TJ, Kim SG, Kim CB (2021) An Investigation of the Variations in Complete Mitochondrial Genomes of *Lingula anatina* in the Western Pacific Region. *Biology* 10(5): 367. <https://doi.org/10.3390/biology10050367>
- Kober KM, Nichols SA (2007) On the phylogenetic relationships of hadromerid and poecilosclerid sponges. *Journal of the Marine Biological Association of the United Kingdom* 87(6): 1585–1598. <https://doi.org/10.1017/S0025315407058237>
- Lee T, Bae YJ, Shin S (2019) Mitochondrial gene rearrangement and phylogenetic relationships in the Amphilepidida and Ophiacanthida (Echinodermata, Ophiuroidea). *Marine Biology Research* 15(1): 26–35. <https://doi.org/10.1080/17451000.2019.1601226>
- Lim SC, Wiklund H, Bribiesca-Contreras G, Glover AG, Dahlgren TG, Tan KS (2024) Diversity and phylogeny of demosponge fauna in the abyssal nodule fields of the eastern Clarion-Clipperton Zone, Pacific Ocean. *Zoologica Scripta* 53: 880–905. <https://doi.org/10.1111/zsc.12683>
- Lohse M, Drechsel O, Kahlau S, Bock R (2013) OrganellarGenomeDRAW – A suite of tools for generating physical maps of plastid and mitochondrial genomes and visualizing expression data sets. *Nucleic Acids Research* 41(W1): W575–W581. <https://doi.org/10.1093/nar/gkt289>
- Miller AK, Kerr AM, Paulay G, Reich M, Wilson NG, Carvajal JI, Rouse GW (2017) Molecular phylogeny of extant Holothuroidea (Echinodermata). *Molecular phylogenetics and evolution* 111: 110–131. <https://doi.org/10.1016/j.ympev.2017.02.014>
- Minh BQ, Schmidt HA, Chernomor O, Schrempf D, Woodhams MD, von Haeseler A, Lanfear R (2020) IQ-TREE 2: New Models and Efficient Methods for Phylogenetic Inference in the Genomic Era. *Molecular Biology and Evolution* 37(5): 1530–1534. <https://doi.org/10.1093/molbev/msaa015>

- Neal L, Wiklund H, Gunton LM, Rabone M, Bribiesca-Contreras G, Dahlgren TG, Glover AG (2022) Abyssal fauna of polymetallic nodule exploration areas, eastern Clarion-Clipperton Zone, central Pacific Ocean: Amphinomidae and Euphosinidae (Annelida, Amphinomida). *ZooKeys* 1137: 33–74. <https://doi.org/10.3897/zookeys.1137.86150>
- Neal L, Abrahams E, Wiklund H, Rabone M, Bribiesca-Contreras G, Stewart ECD, Dahlgren TG, Glover AG (2023) Taxonomy, phylogeny, and biodiversity of Lumbrineridae (Annelida, Polychaeta) from the Central Pacific Clarion-Clipperton Zone. *ZooKeys* 1172: 61–100. <https://doi.org/10.3897/zookeys.1172.100483>
- Niaison T, Guerra D, Breton S (2021) The complete mitogenome of the inarticulate brachiopod *Glottidia pyramidata* reveals insights into gene order variation, deviant ATP8 and mtORFans in the Brachiopoda. *Mitochondrial DNA. Part B, Resources* 6(9): 2701–2703. <https://doi.org/10.1080/23802359.2021.1966342>
- Noguchi Y, Endo K, Tajima F, Ueshima R (2000) The mitochondrial genome of the brachiopod *Laqueus rubellus*. *Genetics* 155(1): 245–259. <https://doi.org/10.1093/genetics/155.1.245>
- Plotkin A, Voigt O, Willassen E, Rapp HT (2017) Molecular phylogenies challenge the classification of Polymastiidae (Porifera, Demospongiae) based on morphology. *Organisms Diversity & Evolution* 17: 45–66. <https://doi.org/10.1007/s13127-016-0301-7>
- Rabone M, Wiethase JH, Simon-Lledó E, Emery AM, Jones DO, Dahlgren TG, Bribiesca-Contreras G, Wiklund H, Horton T, Glover AG (2023) How many metazoan species live in the world's largest mineral exploration region? *Current Biology* 33: 2383–2396.e5. <https://doi.org/10.1016/j.cub.2023.04.052>
- Riehl T, De Smet B (2020) *Macrostylis metallica* spec. nov.—an isopod with geographically clustered genetic variability from a polymetallic-nodule area in the Clarion-Clipperton Fracture Zone. *PeerJ* 8: e8621. <https://doi.org/10.7717/peerj.8621>
- Rot C, Goldfarb I, Ilan M, Huchon D (2006) Putative cross-kingdom horizontal gene transfer in sponge (Porifera) mitochondria. *BMC evolutionary biology* 6: 71. <https://doi.org/10.1186/1471-2148-6-71>
- Saito M, Kojima S, Endo K (2000) Mitochondrial COI sequences of brachiopods: genetic code shared with protostomes and limits of utility for phylogenetic reconstruction. *Molecular phylogenetics and evolution* 15(3): 331–344. <https://doi.org/10.1006/mpev.2000.0773>
- Stachowska-Kamińska Z, Gooday AJ, Radziejewska T, Arbizu PM (2022) Macrofaunal foraminifera from a former benthic impact experiment site (IOM contract area) in the abyssal eastern Clarion-Clipperton Zone. *Deep-sea Research, Part I, Oceanographic Research Papers* 188: 103848. <https://doi.org/10.1016/j.dsr.2022.103848>
- Stechmann A, Schlegel M (1999) Analysis of the complete mitochondrial DNA sequence of the brachiopod *Terebratulina retusa* places Brachiopoda within the protostomes. *Proceedings of the Royal Society London B* 266(1433): 2043–2052. <https://doi.org/10.1098/rspb.1999.0885>
- Stewart ECD, Bribiesca-Contreras G, Taboada S, Wiklund H, Ravara A, Pape E, De Smet B, Neal L, Cunha MR, Jones DOB, Smith CR, Glover AG, Dahlgren TG (2023) Biodiversity, biogeography, and connectivity of polychaetes in the world's largest marine minerals exploration frontier. *Diversity and Distributions* 29: 727–747. <https://doi.org/10.1111/ddi.13690>
- Stöhr S, O'Hara T, Thuy B (Eds) (2024) World Ophiuroidea Database. *Silax daleus* (Lyman, 1879). World Register of Marine Species. <https://www.marinespecies.org/aphia.php?p=taxdetails&id=1507520> [accessed 13 May 2024]

- Sun M, Shen X, Liu H, Liu X, Wu Z, Liu B (2011) Complete mitochondrial genome of *Tubulipora flabellaris* (Bryozoa: Stenolaemata): the first representative from the class Stenolaemata with unique gene order. *Marine genomics* 4(3): 159–165. <https://doi.org/10.1016/j.margen.2011.03.006>
- Taboada S, Riesgo A, Wiklund H, Paterson GLJ, Koutsouveli V, Santodomingo N, Dale AC, Smith CR, Jones DOB, Dahlgren TG, Glover AG (2018) Implications of population connectivity studies for the design of marine protected areas in the deep sea: An example of a demosponge from the Clarion-Clipperton Zone. *Molecular Ecology* 27(23): 4657–4679. <https://doi.org/10.1111/mec.14888>
- Waeschenbach A, Cox CJ, Littlewood DT, Porter JS, Taylor PD (2009) First molecular estimate of cyclostome bryozoan phylogeny confirms extensive homoplasy among skeletal characters used in traditional taxonomy. *Molecular phylogenetics and evolution* 52(1): 241–251. <https://doi.org/10.1016/j.ympev.2009.02.002>
- Waeschenbach A, Taylor PD, Littlewood DT (2012) A molecular phylogeny of bryozoans. *Molecular phylogenetics and evolution* 62(2): 718–735. <https://doi.org/10.1016/j.ympev.2011.11.011>

# Taxonomic update of *Pycnoscelus* Scudder, 1862 (Blattodea, Blaberidae, Pycnoscelinae), with descriptions of two new species from China

Yi-Shu Wang<sup>1,2,3</sup>, Xiao-Jiao Dong<sup>1,2,3</sup>, Zong-Qing Wang<sup>1,2,3</sup>, Yan-Li Che<sup>1,2,3</sup>

<sup>1</sup> Yibin Academy of Southwest University, Yibin, Sichuan 644000, China

<sup>2</sup> College of Plant Protection, Southwest University, Beibei, Chongqing 400715, China

<sup>3</sup> Key Laboratory of Agricultural Biosafety and Green Production of Upper Yangtze River (Ministry of Education), Southwest University, Chongqing 400715, China

Corresponding author: Yan-Li Che ([shirleyche2000@126.com](mailto:shirleyche2000@126.com))

## Abstract

In this paper knowledge of the genus *Pycnoscelus* Scudder, 1862 is updated. Two new species from southern China are described: *Pycnoscelus puteus* Wang & Che, **sp. nov.** and *P. undulatus* Wang & Che, **sp. nov.** Diagnostic characters and high-definition morphological photographs are provided for five known species and two species unidentified due to limited information are reported. An updated checklist and key for *Pycnoscelus* species worldwide are provided.

**Key words:** China, cockroach, new species, *Pycnoscelus*, species group



Academic editor: Fred Legendre

Received: 7 November 2024

Accepted: 22 January 2025

Published: 10 March 2025

ZooBank: <https://zoobank.org/B49EADBB-C7AE-4C91-8536-6B9A022D63C4>

Citation: Wang Y-S, Dong X-J, Wang Z-Q, Che Y-L (2025) Taxonomic update of *Pycnoscelus* Scudder, 1862 (Blattodea, Blaberidae, Pycnoscelinae), with descriptions of two new species from China. ZooKeys 1231: 45–67. <https://doi.org/10.3897/zookeys.1231.141287>

Copyright: © Yi-Shu Wang et al.  
This is an open access article distributed under terms of the Creative Commons Attribution License (Attribution 4.0 International – CC BY 4.0).

## Introduction

The cockroach genus *Pycnoscelus* (Blattodea, Blaberidae, Pycnoscelinae) currently comprises 16 recognized species, most of which are distributed in the Oriental Region (Roth 1998; Anisyutkin 2002, 2018). Species of this genus are remarkable within Blaberidae for their shortened fore tibiae with Type C<sub>1</sub> front femur, the distinct asymmetrical subgenital plate with a relatively large right style, and a small or absent left style. Additionally, the dorsal surface of the nymph, from the fourth abdominal tergum to the supra-anal plate, is clearly rough, adorned with small tubercles (Wang et al. 2024).

The type species *Pycnoscelus surinamensis* (Linnaeus, 1758) is a widely distributed pest and notable for being exclusively parthenogenetic (Roth and Willis 1956; Roth 1974). Prior to 1967, *Pycnoscelus indicus* (Fabricius, 1775) was considered the bisexual form of *P. surinamensis*. After a series of biological experiments, Roth (1967) eventually confirmed that the bisexual relatives of *P. surinamensis* represent a separate species, *P. indicus*. Furthermore, Roth (1973, 1998) examined most type specimens in the genus, providing detailed descriptions of 12 recognized species, which serve as essential references for future taxonomic studies on *Pycnoscelus*. Since 2000, the documentation of *Pycnoscelus* species has been updated primarily by Anisyutkin (2002, 2004, 2018), who described four new species and redescribed two known ones.

Nonetheless, a revision of *Pycnoscelus* remains necessary because the species described in Roth (1998) lack detailed descriptions of male genitalia, and the drawn illustrations provided were inadequate.

In this paper, we aim to advance the taxonomic knowledge of *Pycnoscelus*, providing descriptions of two new species and additional details for five known species. We also report two unidentified species. High-definition images and diagnoses of these *Pycnoscelus* species are provided, with an updated checklist and key for the genus.

## Materials and methods

All specimens examined in this paper, including the types of new species, are deposited in College of Plant Protection, Southwest University, Chongqing, China (SWU). Dissections of male genitalia followed the protocols described in Wang et al. (2021). Photographs were taken with a Leica DFC digital microscope camera attached to a Leica M205A stereomicroscope, and all images were processed in Adobe Photoshop CS6. Descriptions of new species are based on the holotype male, with measurement ranges provided for all type material. Terminology for male genitalia sclerites follows Klass (1997) and Anisyutkin (2018).

## Taxonomic account

### Genus *Pycnoscelus* Scudder, 1862

Fig. 1A–C

*Pycnoscelus* Scudder, 1862: 421; Hebard 1917: 269; Roth 1998: 94; Anisyutkin 2018: 80. Type species: *Pycnoscelus surinamensis* (Linnaeus, 1758) = *Pycnoscelus obscurus* Scudder, 1862, nymph, adventive, by monotypy.

*Epilampria* Tepper, 1894: 174. Type species: *Pycnoscelus surinamensis* (Linnaeus, 1758) = *Epilampria tatei* Tepper, by monotypy. Synonymized by Princis 1964: 263.

**Diagnosis.** *Pycnoscelus* species can be easily recognized by the shortened fore tibiae, which is thickened distally with strong spines (Fig. 1A), as well as the right posterolateral corner of male subgenital plate angularly produced and upturned (Fig. 1C).

**Description.** Facial part of head and pronotum with distinct punctations. Pronotum with the anterior margin nearly truncate, hind margin convex medially. Anterior margin of fore femur Type C<sub>1</sub>. Hind metatarsus longer or nearly equal to the remaining segments combined; armed with large pulvilli, occupying more than half length of the segment (Fig. 1B). Claws symmetrical and unspecialized, arolium present. Subgenital plate covered by the eighth sternum; right style typically large. Male genitalia: right phallomere with R3 forked caudally, and the left branch usually wider than the right; R5 sometimes absent. Apical part of sclerite L2D well sclerotized, with the sac-like apical membrane wrapped. Sclerite L3 hooked with small, curved portion. Sclerite L4U distinct and divided into two parts.

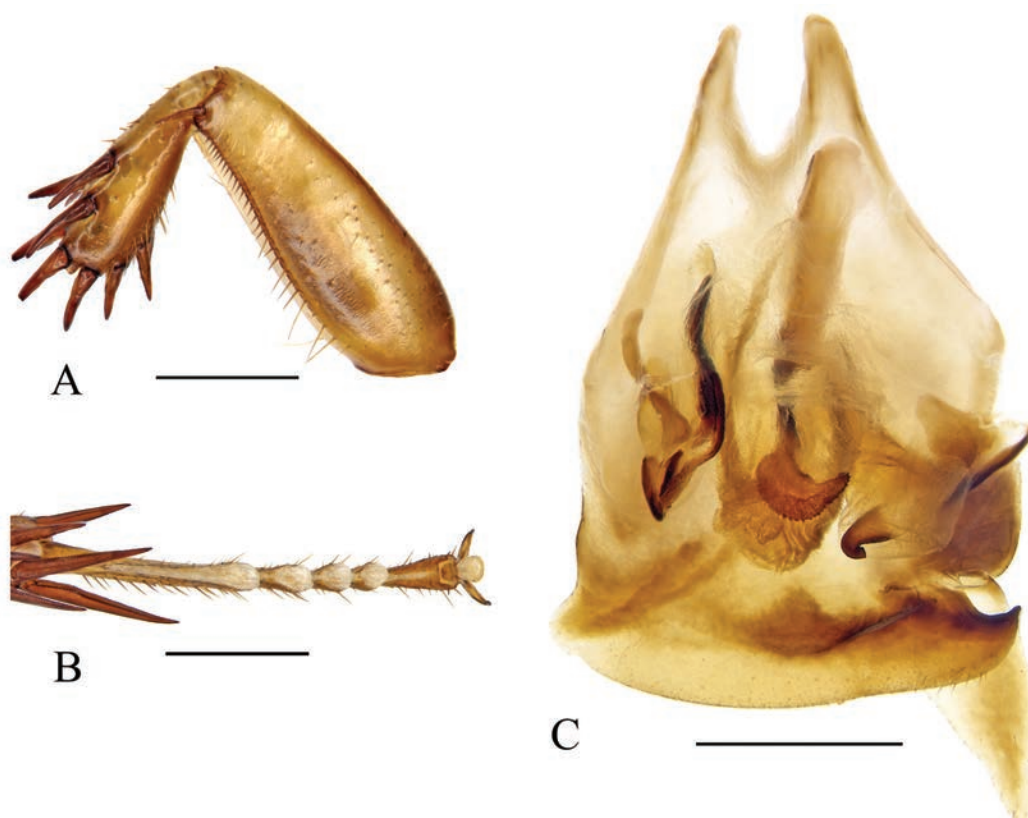


**Figure 1.** Diagnostic features of *Pycnoscelus* (*P. indicus*) **A** front femur and tibiae, ventral view **B** hind tarsi and pulvilli, ventral view **C** male genitalia and subgenital plate, dorsal view. Scale bars: 1.0 mm (**A–C**).

### Worldwide checklist and species grouping of *Pycnoscelus*

Two groups of *Pycnoscelus* species were established based on the shape of right style (Roth 1998):

1. *indicus* species group: the right style elongate with apex directed posteriorly; includes 12 species: *P. conferta* (Walker, 1869: 148); *P. femapterus* Roth, 1998: 108; *P. gorochovi* Anisyutkin, 2002: 352; *P. indicus* (Fabricius, 1775: 272); *P. janetscheki* Bey-Bienko, 1968: 60; *P. nigra* (Brunner von Wattenwyl, 1865: 280); *P. puteus* sp. nov.; *P. rothi* Anisyutkin, 2002: 355; *P. schwendingeri* Anisyutkin, 2018: 80; *P. surinamensis* (Linnaeus, 1758: 424); *P. undulatus* sp. nov.; *P. vietnamensis* Anisyutkin, 2002: 355.
2. *striatus* species group: the right style broader, plate-like, with apex directed to the left; includes five species: *P. aurantius* Hanitsch, 1935: 18; *P. rufus* Bey-Bienko, 1950: 268; *P. semivitreus* Princis, 1967: 148; *P. striatus* (Kirby, 1903: 378); *P. tenebriger* (Walker, 1868: 31).

Note: *P. micropterus* Hanitsch, 1931 has not been attributed to any group due to the lack of information on its right style. Additionally, there are six unnamed species: *Pycnoscelus* sp. A Roth, 1998: 121; *Pycnoscelus* sp. B Roth, 1998: 123; *Pycnoscelus* sp. C Roth, 1998: 123; *Pycnoscelus* sp. D Lucañas & Lit, 2016: 9; *Pycnoscelus* sp. E (Malaysia, Borneo); *Pycnoscelus* sp. F (China, Yunnan). The latter two species are included in this work.

**Key to males of the genus *Pycnoscelus* (updated from Roth 1998)**

- 1 Tegmina reaching only to the second tergum..... ***P. micropterus* Hanitsch, 1931**
- Tegmina not as above..... **2**
- 2 Right style elongate and cone-shaped..... **3**
- Right style broad and plate-like ..... **13**
- 3 Pronotum dark with a broad anterior and narrow anterolateral yellowish band..... ***P. indicus* (Fabricius, 1775) and *P. surinamensis* (Linnaeus, 1758)**
- Pronotum not as above..... **4**
- 4 Pronotum with large pale areas, and the disk with large blackish macula .... **5**
- Pronotum with or without small pale areas anteriorly and anterolaterally..... **7**
- 5 The large pale areas of pronotum scattered with dark dots ..... **6**
- The large pale areas of pronotum without scattered dark dots..... ***P. conferta* (Walker, 1869)**
- 6 The macula on pronotal disk irregular ..... ***P. schwendingeri* Anisyutkin, 2018**
- The macula on pronotal disk regular and complete ..... ***P. rothi* Anisyutkin, 2002**
- 7 Supra-anal plate with hind margin deeply concave at the right side..... **8**
- Supra-anal plate not as above ..... **10**
- 8 Head and pronotum mostly black ..... **9**
- Head and pronotum reddish brown; right style more bulky..... ***P. undulatus* sp. nov.**
- 9 Subgenital plate with distinct projection on left posterolateral angle ..... ***P. gorochovi* Anisyutkin, 2002**
- Subgenital plate without distinct projection on left posterolateral angle.... ***P. vietnamensis* Anisyutkin, 2002**
- 10 General color shiny, black or dark brown ..... **11**
- Pronotum mostly black, tegmina yellowish brown with anal field and proximal region of the posterior field darker..... ***P. femapterus* Roth, 1998**
- 11 Interocular space nearly equal to or narrower than the distance between ocellar spots, hind margin of supra-anal plate with a shallow medial excavation..... ***P. nigra* (Brunner, 1865)**
- Interocular space wider than the distance between inner margins of ocellar spots ..... **12**
- 12 Pronotum with moderately broad yellow areas anterolaterally, tegmina and wings extending beyond the apex of the abdomen by just over half the length of the pronotum ..... ***P. janetscheki* Bey-Bienko, 1968**
- Pronotum with two indistinct and narrow yellow borders anterolaterally, tegmina and wings extending well beyond end of abdomen ..... ***P. puteus* sp. nov.**
- 13 Right style huge, extends to the left posterolateral angle of subgenital plate..... ***P. semivitreus* Princis, 1967**
- Right style not as above..... **14**
- 14 Tegmina and wings reduced, reaching to approximately the seventh tergum ..... ***P. striatus* (Kirby, 1903)**
- Tegmina and wings well developed, extending beyond end of abdomen... **15**

- 15 General color yellowish brown; tegmina bicolored with proximal parts reddish brown; right style as in Anisytukin (2004: fig. 5) .....***P. rufus* Bey-Bienko, 1950**
  - General color darker, reddish brown or orangish..... **16**
- 16 Tegmina distinctly bicolored, with proximal parts reddish brown and remaining part pale yellowish (Fig. 8G).....***P. striatus* (Kirby, 1903)**
  - Tegmina coloration not as above..... **17**
- 17 Right style relatively small, with the apex directed to the left and rounded (Fig. 7G) .....***P. aurantius* Hanitsch, 1935**
  - Right style relatively large, with the apex directed to the left and sharp, as in Roth (1998: fig. 37, 38)..... ***P. tenebriger* (Walker, 1868)**

### ***Pycnoscelus indicus* (Fabricius, 1775)**

Fig. 2

*Blatta indica* Fabricius, 1775: 272.

*Pycnoscelus indicus*: Roth 1967: 774; Roth 1998: 99.

**Material examined.** CHINA • 5 males & 3 females; Fujian Prov., Putian City, Meizhou Island; 22–23 July 2013; Shun-Hua Gui & Yan Shi leg. • 2 males; Guangdong Prov., Zhongshan City, Zimaling Park, 11 Oct. 2018; Ke-Liang Wu leg. • 1 female; Guangxi Prov., Baise City, Renzhuang Township, Tengmao Village, Nongli tun; 9–13 July 2015; Jian-Yue Qiu leg. • 1 male; Guangxi Prov., Longzhou County; Nonggang Nature Reserve; 29–30 June 2015; Lu Qiu & Qi-Kun Bai leg. • 11 males & 2 females; Yunnan Prov., Yuxi City, Yuanjiang County; 533m; 22 May 2018; Lu Qiu, Wen-Bo Deng & Zhi-Wei Dong leg. JAPAN • 2 males & 5 females; Okinawa, Mt. Yonahadake; 222m; 10 Aug. 2016; Jian-Yue Qiu & Hao Xu leg.

**Diagnosis.** This species is characterized by its pronotum with a broad anterior and narrow anterolateral yellowish band (Fig. 2E), a feature also presents in *P. surinamensis*. The two species are difficult to distinguish in appearance. The key distinction between *P. indicus* and *P. surinamensis* lies in their reproductive modes: *P. indicus* reproduces bisexually, while *P. surinamensis* reproduces parthenogenetically (Roth 1967).

**Supplementary description of male.** Hind margin of supra-anal plate variable, weakly incised medially, or entire and convexly rounded (Fig. 2G). Sclerotized level and shape of subgenital plate variable: the inner plate nearly symmetrical or strongly asymmetrical, lateral projection on left posterolateral angle distinct or not (Fig. 2H–J). Male genitalia: Right phallomere with caudal part of sclerite R1T widened; R2 slightly curved; the projection arising from the junction of R1T and R2 elongate; R3 forked caudally; R4 plate-like, close to the caudal part of R1; R5 absent (Fig. 2K, L). Sclerite L2D divided into basal and apical parts: the basal part straight; the apical part croissant-shaped with outer margin toothed; apical membrane covered with heavy chaetae (Fig. 2M). Sclerite L3 with hook short and robust, sclerite L4U divided into two parts (Fig. 2N).

**Measurements (mm).** Body length including tegmen: male 15.8–17.2, female 16.4–18.6; pronotum length × width: male 4.0–4.4 × 5.4–5.9, female 4.3–5.1 × 6.0–6.7; tegmen length: male 13.8–15.3, female 12.7–15.0.

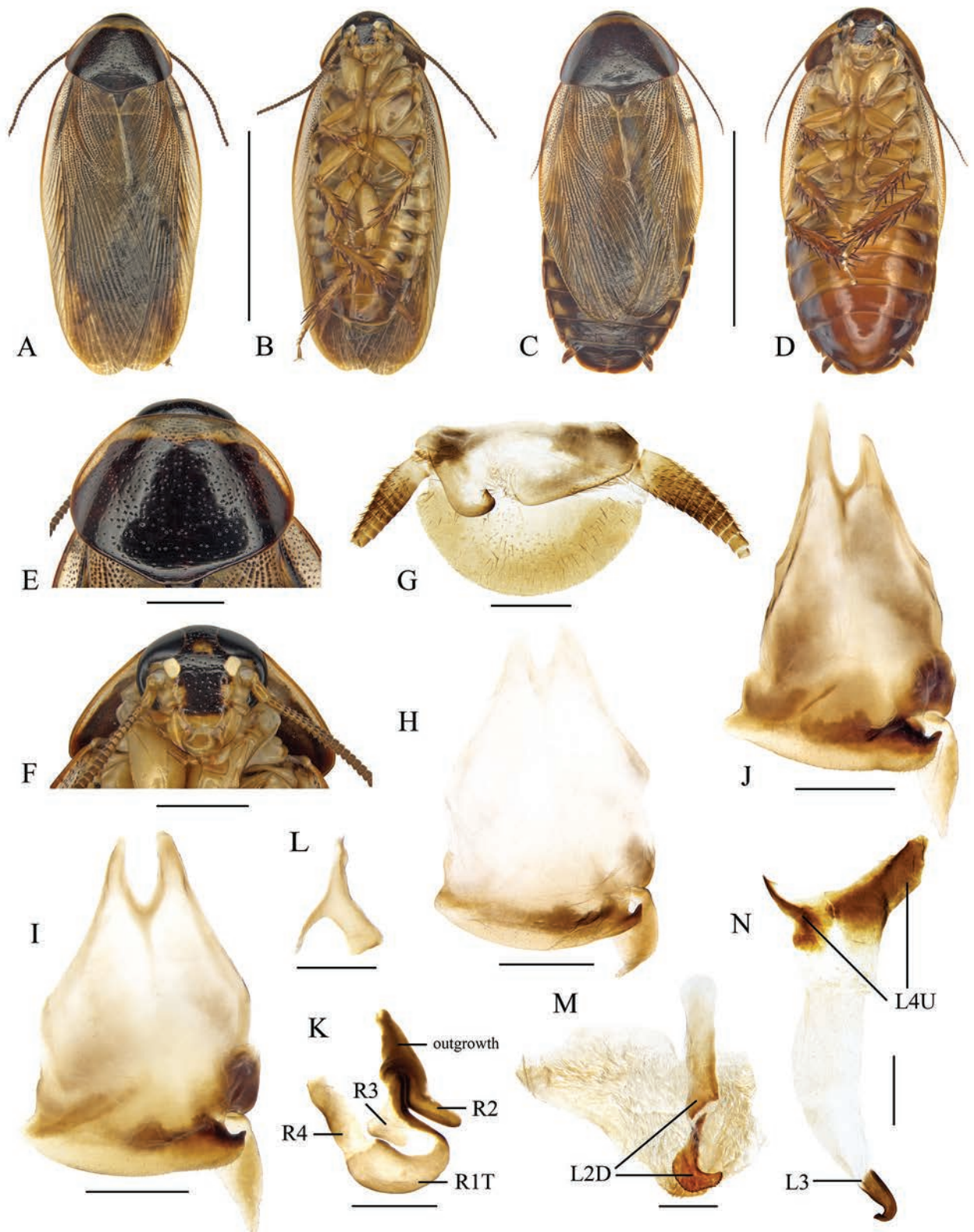


**Figure 2.** *Pycnoscelus indicus* (Fabricius, 1775) **A, B, E–M** male **C, D** female **A, C** dorsal view **B, D** ventral view **E** pronotum, dorsal view **F** head, ventral view **G** supra-anal plate, ventral view **H** subgenital plate, dorsal view (from Yuxi, Yunnan) **I** subgenital plate, dorsal view (from Zimaling, Guangdong) **J** subgenital plate, dorsal view (from Longzhou, Guangxi) **K** right phallosome, dorsal view **L** sclerite R3 of right phallosome, ventral view **M** median phallosome, dorsal view **N** left phallosome, dorsal view. Scale bars: 1.0 cm (**A–D**); 2.0 mm (**E, F**); 1.0 mm (**G–J**); 0.5 mm (**K–N**).

***Pycnoscelus nigra* (Brunner von Wattenwyl, 1865)**

Fig. 3

*Panchlora nigra* Brunner von Wattenwyl, 1865: 280.

*Pycnoscelis* [sic] *nigra*: Princis 1964: 274.

*Pycnoscelus nigra*: Princis 1967: 709; Roth, 1998: 103.

**Material examined.** CHINA • 1 female; Guangdong Prov., Zhongshan City, Mt. Wuguishan; 5 May 2018; Ke-Liang Wu leg. • 5 males; Yunnan Prov., Xishuangbanna, Mengla County, Menglun Town; 25 May 2016; Lu Qiu & Zhi-Wei Qiu leg. • 1 female; Hainan Prov., Mt. Diaoluo shan; 275 m; 24–25 May 2014; Shun-Hua Gui & Xin-Ran Li leg. • 1 male; Chongqing City, Hechuan District, Dashi Town; 18 July 2013; Zong-Qing Wang leg. • 2 males & 4 females; Sichuan Prov., Panzhihua City, Xinzhuang Village; 1306 m; 15 Oct. 2014; Li He leg. • 6 males; Yunnan Prov., Menglun Town, Xishuangbanna Tropical Botanical Garden, Lvshilin (Green stone forest); 25 May 2016; Lu Qiu & Zhi-Wei Qiu leg. • 1 male; Yunnan Prov., Baoshan City, Mt. Gaoligongshan, Baihualing, Hanlong Zhai; 1400–1900 m; 20–23 June 2020; Lu Qiu & Jin-Lin Liu leg.

**Diagnosis.** This species is characterized by the generally dark coloration (Fig. 3A–D) and pronotum with narrow yellow area anterolaterally (Fig. 3E).

**Supplementary description of male.** Male genitalia: Right phallomere with caudal part of sclerite R1T widened distinctly; R2 nearly straight; the outgrowth arising from the junction of R1T and R2 broad, plate-like; R3 forked caudally; R4 plate-like; R5 absent (Fig. 3I, J). Sclerite L2D with the apical part bifurcated basally; apical membrane covered with heavy chaetae (Fig. 3K). Sclerite L3 with hook comparatively slender, sclerite L4U divided into two parts (Fig. 3L).

**Measurements (mm).** Body length including tegmen: male 19.5–23.8, female 20.3–24.1; pronotum length × width: male 4.5–4.9 × 5.4–6.9, female 5.0–6.0 × 7.5–8.1; tegmen length: male 15.9–19.6, female 16.5–20.8.

**Remarks.** Roth (1998) recorded a male of *P. nigra* from Jingdong (= Kintung), Yunnan, and found its left style present. However, the left style is absent in all our new material from Yunnan (Fig. 3H).

***Pycnoscelus puteus* Wang & Che, sp. nov.**

<https://zoobank.org/D2D97057-9C9B-40AD-8DFD-63B12C1EB69C>

Fig. 4

**Type material. Holotype.** CHINA • male; Yunnan Prov., Xishuangbanna, Mengla County, Menglun Town, Xishuangbanna Tropical Botanical Garden; 25 May 2016; Lu Qiu & Zhi-Wei Qiu leg.; SWU-B-BB120101. **Paratypes.** CHINA • 2 males; same collection data as holotype; SWU-B-BB120102 and 120103 • 1 male; same collection data as holotype; 27 May 2016; SWU-B-BB120104 • 4 males; Yunnan Prov., Pu'er City, Meizihu Lake; Lu Qiu & Zhi-Wei Qiu leg.; 20–21 May 2016; SWU-B-BB120105 to 120109 • 1 male; Yunnan Prov., Xishuangbanna, Jinghong City, Dadugang; 5 May 2013; Zong-Qing Wang leg.; SWU-B-BB120110.

**Differential diagnosis.** *Pycnoscelus puteus* sp. nov. is very similar to *P. nigra* in general appearance and coloration but differs strongly from the later in interocular distance and male genitalia, especially the sclerotized part associated

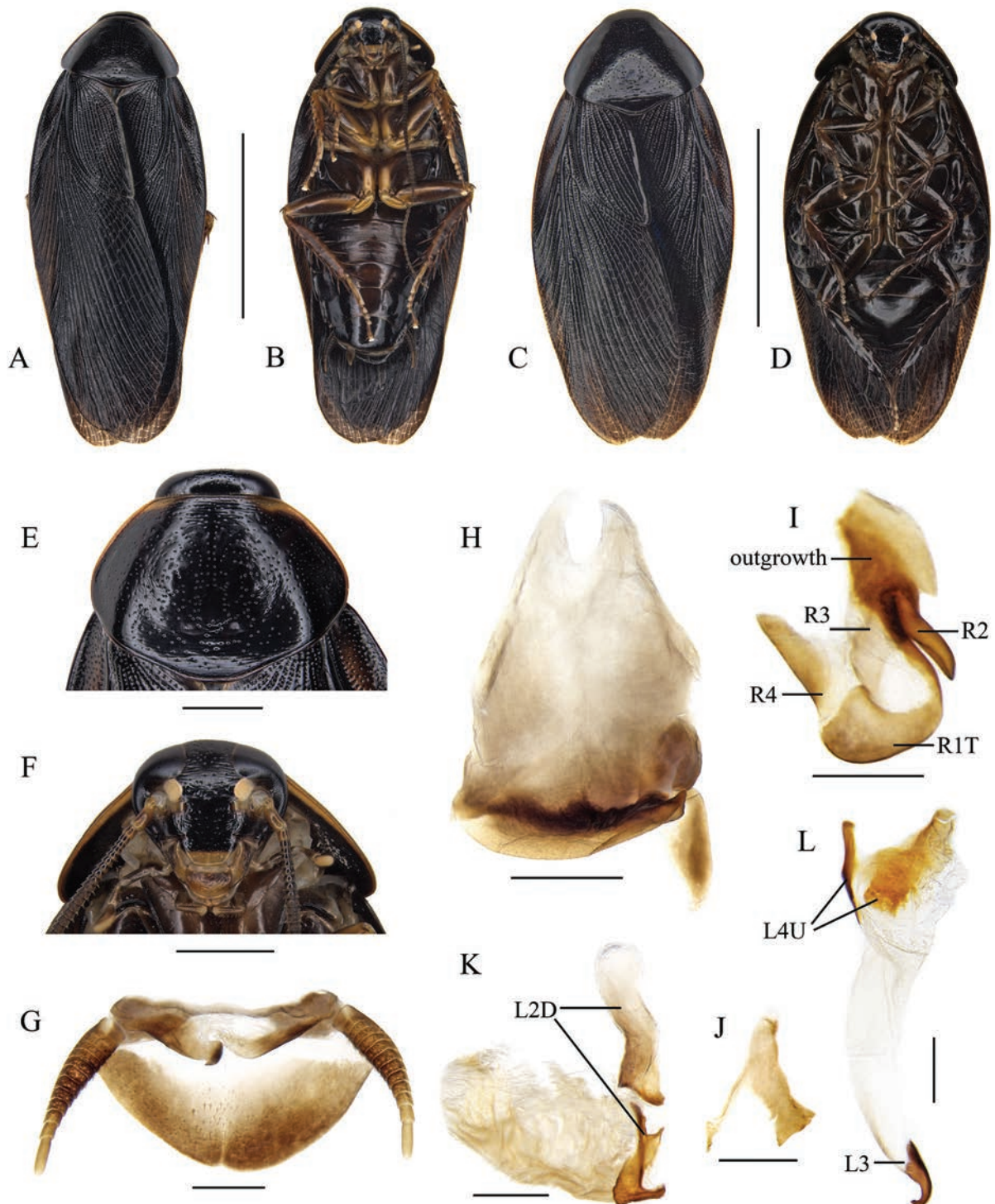


**Figure 3.** *Pycnoscelus nigra* (Brunner von Wattenwyl, 1865) **A, B, E–K** male **C, D** female **A, C** dorsal view **B, D** ventral view **E** pronotum, dorsal view **F** head, ventral view **G** supra-anal plate, ventral view **H** subgenital plate, dorsal view **I** right phallosome, dorsal view **J** sclerite R3 of right phallosome, ventral view **K** median phallosome, dorsal view **L** left phallosome, dorsal view. Scale bars: 1.0 cm (**A–D**); 2.0 mm (**E, F**); 1.0 mm (**G, H**); 0.5 mm (**I–L**).

with sclerite R1T and R2 (compare Fig. 3F, I and Fig. 4F, J in present paper). Furthermore, the male genitalia distinguish this new species from all other known species of genus *Pycnoscelus* except *P. rothi*, but the coloration of the pronotum could separate them easily (compare Fig. 4E with Anisytukin 2002: fig. 1).

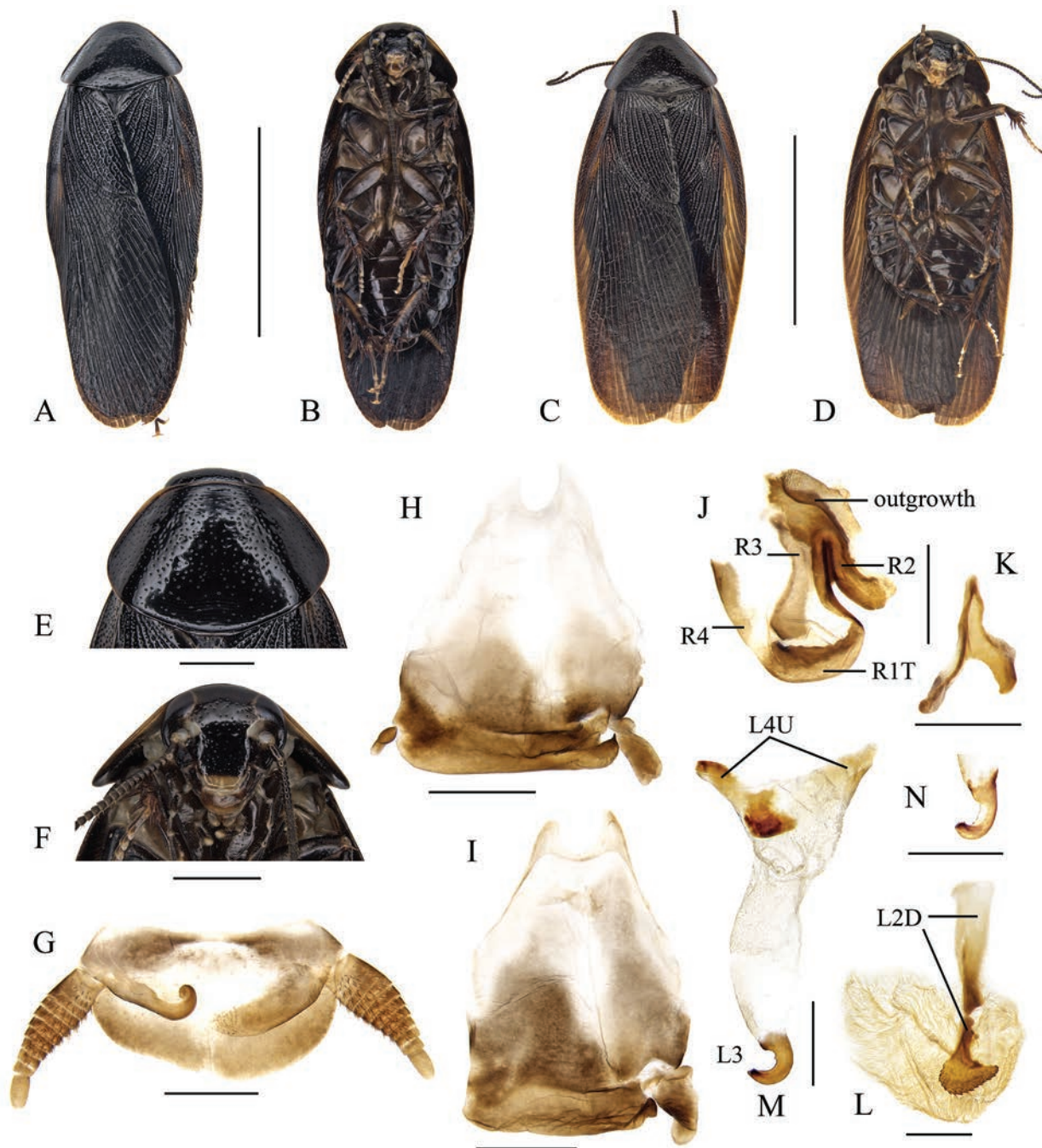


**Figure 4.** *Pycnoscelus puteus* sp. nov., male **A, B, E–H, J–L** holotype SWU-B-BB120101 **C, D, I, M** paratype SWU-B-BB120105 **A** dorsal view **B** ventral view **C** dorsal view **D** ventral view **E** pronotum, dorsal view **F** head, ventral view **G** supra-anal plate, ventral view **H** subgenital plate, dorsal view (from Xishuangbanna, Yunnan) **I** subgenital plate, dorsal view (from Pu'er, Yunnan) **J** right phallosome, dorsal view **K** sclerite R3 of right phallosome, ventral view **L** median phallosome, dorsal view **M** left phallosome, dorsal view (from Xishuangbanna, Yunnan) **N** left phallosome, lateral view (from Pu'er, Yunnan). Scale bars: 1.0 cm (**A–D**); 2.0 mm (**E, F**); 1.0 mm (**G–I**); 0.5 mm (**J–N**).

**Description. Male (holotype).** General color black (Fig. 4A, B). Head black except for yellowish brown clypeo-labral area; maxillary palps and antennae brownish black; eyes black, ocellar spots whitish. Pronotum shining black, with two indistinct, narrow yellow borders anterolaterally (Fig. 4E). Tegmina similar to those of *P. nigra*, dark when folded. Abdomen and legs brownish black. Cerci slightly lighter.

Body slender. Head slightly exposed. Eyes comparatively small; outer margin of ocelli obscure; interocular space wider than the distance between the inner margin of ocellar spots, and smaller than distance between antennal sockets (Fig. 4F). Pronotum subpentagonal, densely punctured (Fig. 4E). Tegmina and wings extending beyond the end of abdomen. Front femur Type C<sub>1</sub>. Hind metatarsus distinctly longer than other segments combined; four proximal tarsomeres with well-developed pulvilli, the one on the first tarsomere occupying almost the complete length of the segment; claws symmetrical and simple; arolium large. Supra-anal plate transverse, slightly asymmetrical, hind margin with a small medial incision (Fig. 4G). Paraprocts of blaberid type, asymmetrical. Subgenital plate asymmetrical, with the right posterolateral corner acute and upturned. Left style minute, right one large and robust (Fig. 4H).

**Male genitalia.** Right phallomere with caudal part of sclerite R1T rounded; R2 curved; an outgrowth arising from the junction of R1T and R2, with an additional heavily sclerotized part whose surface is pitted; R3 forked caudally, R4 plate-like, R5 absent (Fig. 4J, K). Sclerite L2D divided into basal and apical parts: the basal part short, apically widened; the apical part strongly sclerotized with posterior margin distinctly toothed; apical membrane well developed, with surface covered by microtrichia (Fig. 4L). Sclerite L3 hook with apical incision, inner curved margin with a small tooth; sclerite L4U present and divided into two parts (Fig. 4M, N).

**Variation.** Body broader, brownish black (Fig. 4C, D); some individuals lack left style (probably missing, Fig. 4I); inner curved margin of hook of sclerite L3 with two small projections (Fig. 4N).

**Measurements (mm).** Male, body length including tegmina: 20.1–20.9; pronotum length × width: 3.7–4.0 × 5.0–5.6; tegmen length: 16.1–18.0.

**Etymology.** Derived from the Latin word *puteus*, referring to the pitted surface of the sclerotized enlargement associated with sclerites R1T and R2.

### ***Pycnoscelus undulatus* Wang & Che, sp. nov.**

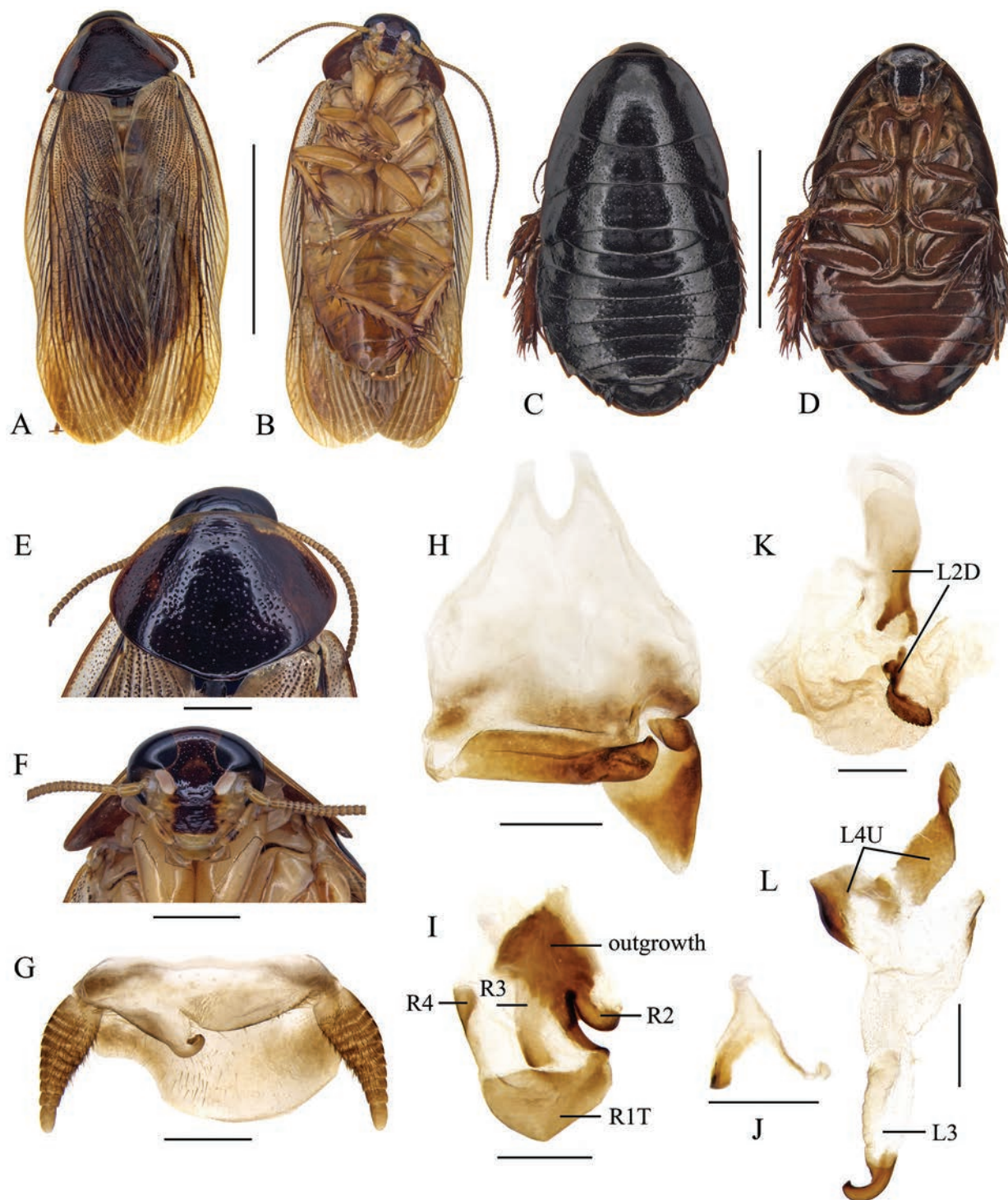
<https://zoobank.org/ECA45FFD-3DAE-4200-9FB3-5E2714DC7AEB>

Fig. 5

**Type material. Holotype.** CHINA • male; Guangdong Prov., Guangzhou City, Longyandong Forest Park; 28 June 2015; Zhi-Wei Qiu & Yong-Quan Zhao leg.; SWU-B-BB120201. **Paratypes.** CHINA • 1 male; same collection data as holotype; SWU-B-BB120202 • 1 male; Guangxi Prov., Hepu County, Shiwan Town; 14 May 2016; Yi-Zhou Liu leg.; SWU-B-BB120203 • 2 females & 1 nymph; Guangxi Prov., Hepu County, Shiwan Town; 14 May 2016; Yi-Zhou Liu leg.; SWU-B-BB120204 to 120206.

**Differential diagnosis.** The male of this species is similar to *P. vietnamensis* Anisutkin, 2002 and *P. gorochovi* Anisutkin, 2002 in the shape of supra-anal plate, which has a deep emargination at the right posterolateral side, but *P. undulatus* sp. nov. differs strongly from these two species by its dark reddish brown pronotum, light marking on facial part between eyes, and the bulky right style (compare Fig. 5H with Anisutkin 2002: figs 15, 16).

**Description. Male (holotype).** General color brownish yellow (Fig. 5A, B). Facial part of head dark reddish brown, with an indistinct three-radial stripe between eyes; other part of head, clypeus, labrum and antennae brownish yellow;



**Figure 5.** *Pycnoscelus undulatus* sp. nov. **A, B, E–K** holotype, male SWU-B-BB120201 **C, D** paratype, female SWU-B-BB120204 **A** dorsal view **B** ventral view **C** dorsal view **D** ventral view **E** pronotum, dorsal view **F** head, ventral view **G** supra-anal plate, ventral view **H** subgenital plate, dorsal view **I** right phallomere, dorsal view **J** sclerite R3 of right phallomere, ventral view **K** median phallomere, dorsal view **L** left phallomere, dorsal view. Scale bars: 1.0 cm (**A–D**); 2.0 mm (**E, F**); 1.0 mm (**G, H**); 0.5 mm (**I–L**).

maxillary palps brownish yellow with reddish brown maculae; eyes black, ocellar spots whitish. Pronotum reddish brown, with two yellow areas anterolaterally (Fig. 5E). Tegmina brownish yellow. Abdomen yellowish brown to reddish brown. Legs and cerci yellowish brown.

Head slightly exposed. Ocelli subrectangular; interocular space distinctly less than the distance between ocellar spots and antennal sockets (Fig. 5F). Pronotum subpentagonal, densely punctured. Tegmina and wings fully developed, exceeding the end of abdomen. Front femur Type C<sub>1</sub>. Hind metatarsus not quite as long as other segments combined; four proximal tarsomeres with well-developed pulvilli, the one on the first tarsomere occupying almost the whole length of the segment; claws symmetrical and simple; arolium large. Supra-anal plate asymmetrical with hind margin deeply concave at the right side. Paraprocts of blaberid type, asymmetrical. Cerci stout at base (Fig. 5G). Subgenital plate asymmetrical, with the right posterolateral corner slightly obtuse and upturned. Left style absent, right style broadly trigonal (Fig. 5H).

**Male genitalia.** Right phallomere with caudal part of sclerite R1T irregular and widened; R2 short and curved; a well-developed projection arising from the junction of R1T and R2; R3 forked caudally, R4 plate-like, R5 absent (Fig. 5I, J). Sclerite L2D divided into basal and apical parts: the basal part forked caudally with the inner margin indented; the apical part well sclerotized and more uniform in width than in other *Pycnoscelus* species, posterior margin toothed; apical membrane covered with microtrichia (Fig. 5K). Sclerite L3 hook without an apical incision, inner curved margin with a sharp convexity at apex; sclerite L4U present and divided into two parts (Fig. 5L).

**Females.** Thoracic segments and abdominal tergum black with minute punctures, abdominal sterna and legs reddish brown. Tegmina and wings absent.

**Measurements (mm).** Male, body length including tegmen: 22.2–23.0; pronotum length × width: 4.3–4.5 × 6.3–7.1; tegmen length: 17.0–20.1. Female, body length: 16.1–20.6; pronotum length × width: 4.35–4.44 × 7.36–7.37.

**Etymology.** The species epithet is derived from the Latin word *undulatus*, which refers to the caudal edge of basal part of sclerite L2D undulated.

### ***Pycnoscelus semivitreus* Princis, 1967**

Fig. 6

*Pycnoscelus semivitreus* Princis, 1967: 148; Princis 1971: 1141; Roth 1998: 112.

**Material examined.** MALAYSIA • 1 male; Borneo, Mt. Trus Madi, Jungle Girl Camp; 2–5 Oct. 2015; Ye-Jie Lin leg. • 1 male; Borneo, Mt. Trus Madi, Jungle Girl Camp; 3 May 2023; Cai-Xia Yuan leg.

**Diagnosis.** This species can be easily distinguished from all its congeners by its huge right style, which extends to the left posterolateral angle of subgenital plate (Fig. 6G).

**Supplementary description of male.** Male genitalia: right phallomere with caudal part of sclerite R1T irregular, inner margin produced at middle; R2 nearly straight, R3 forked, R4 plate-like; R5 elongated, lying above R2 (Fig. 6H). Apical part of sclerite L2D elongated, the right side with several sharp teeth; apical membrane well developed, covered with microtrichia (Fig. 6I, J). Sclerite L3 hook subquadrate apically, inner margin with a tooth at apex; sclerite L4U divided into two parts (Fig. 6K).

**Measurements (mm).** Body length including tegmen: 20.7; pronotum length × width: 4.7 × 6.2; tegmen length: 17.0.

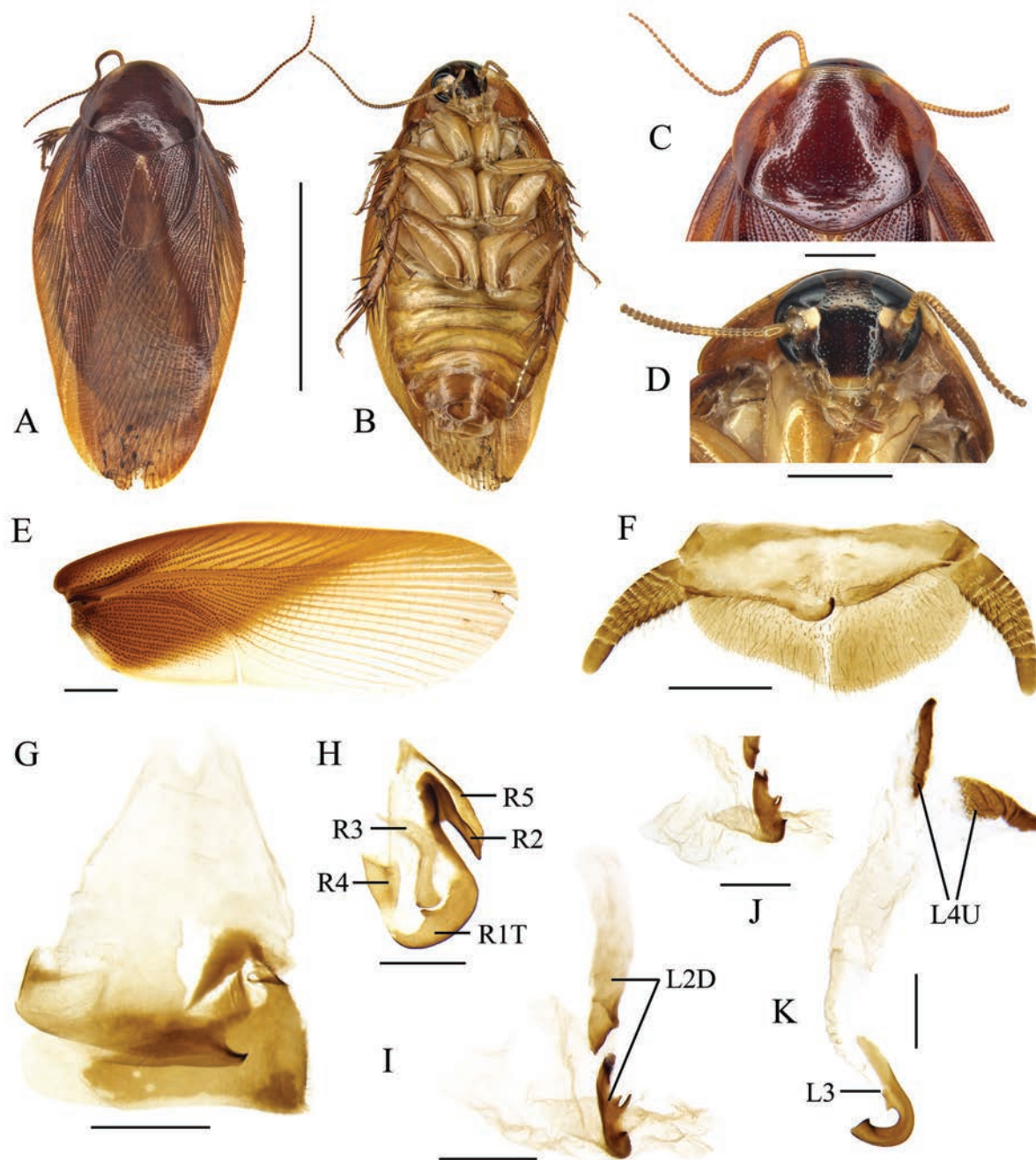


**Figure 6.** *Pycnoscelus semivitreus* Princis, 1967, male **A** dorsal view **B** ventral view **C** pronotum, dorsal view **D** head, ventral view **E** tegmen, dorsal view **F** supra-anal plate, ventral view **G** subgenital plate, dorsal view **H** right phallomere, dorsal view **I** median phallomere, dorsal view **J** median phallomere, lateral view **K** left phallomere, dorsal view. Scale bars: 1.0 cm (**A**, **B**); 2.0 mm (**C**–**E**); 1.0 mm (**F**, **G**); 0.5 mm (**H**–**K**).

***Pycnoscelus aurantius* Hanitsch, 1935**

Fig. 7

*Pycnoscelus aurantius* Hanitsch, 1935: 18; Bruijning 1947: 210; Roth 1998: 125.  
*Pycnoscelis* [sic] *aurantia*: Princis 1964: 275.

**Material examined.** MALAYSIA • 1 male; Sabah, Mt. Trus Madi; 1121m; 5 Oct. 2015; Gui-Qiang Huang leg.

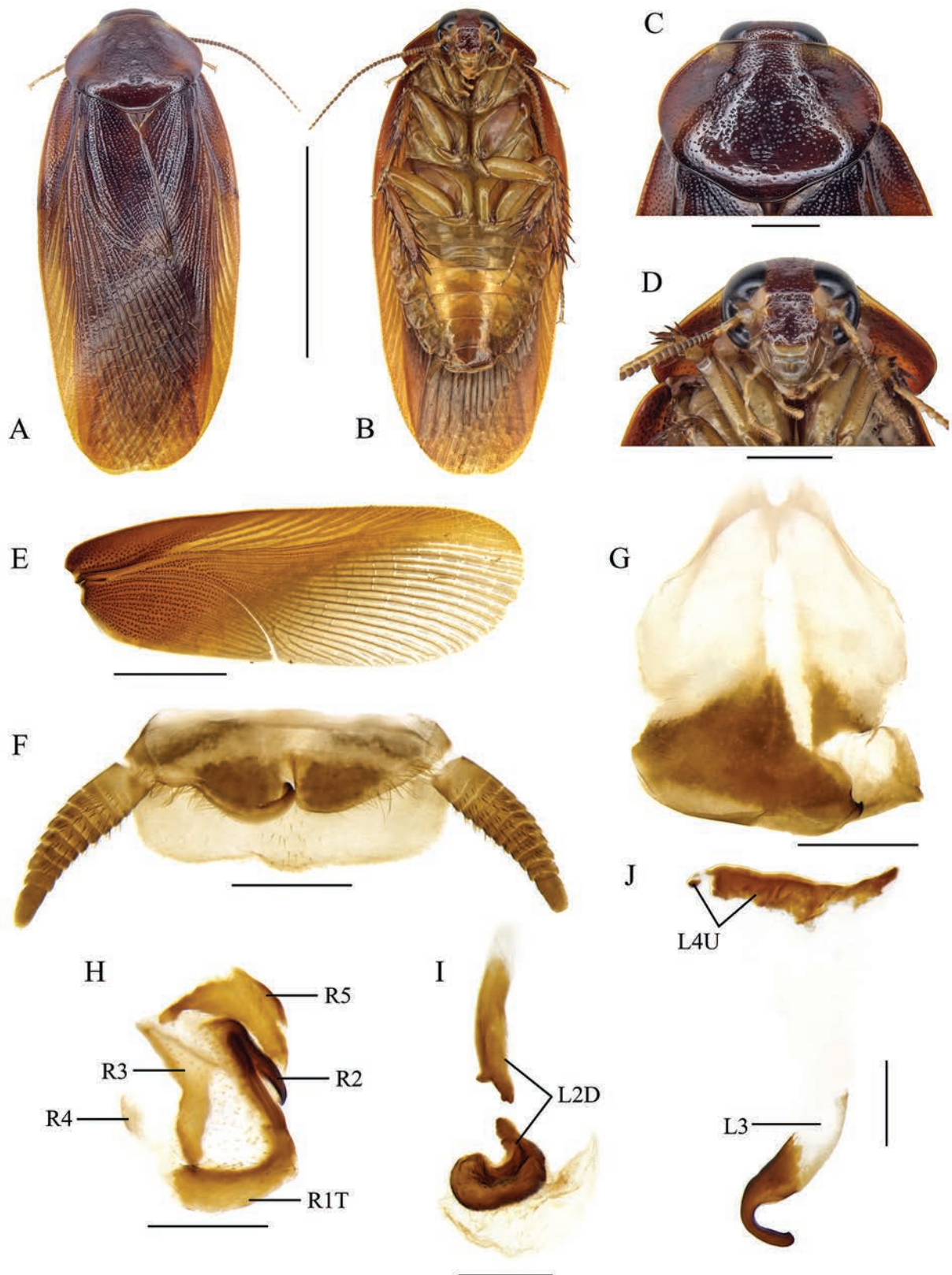


**Figure 7.** *Pycnoscelus aurantius* Hanitsch, 1935, male **A** dorsal view **B** ventral view **C** pronotum, dorsal view **D** head, ventral view **E** tegmen, dorsal view **F** supra-anal plate, ventral view **G** subgenital plate, dorsal view **H** right phallomere, dorsal view **I** median phallomere, dorsal view **J** left phallomere, dorsal view. Scale bars: 1.0 cm (**A**, **B**); 2.0 mm (**C**, **D**); 5.0 mm (**E**); 1.0 mm (**F**, **G**); 0.5 mm (**H**–**J**).

**Diagnosis.** General color dark orange, similar to *P. semivitreus*, but *P. aurantius* can be readily distinguished from *P. semivitreus* by its smaller right style and the apical part of sclerite L2D blunt without any process.

**Supplementary description of male.** Tegmina is somewhat bicolored as *P. semivitreus*, from proximally orange to distally yellowish, with the boundary indistinct (Fig. 7E). Male genitalia: right phallomere with distinct bristles, caudal part of sclerite R1T nearly rectangular, R2 curved, R3 forked, R4 small; R5 lies above R2, irregular, prolonged (Fig. 7H). The basal part of sclerite L2D strongly sclerotized with apical portion less sclerotized and nearly transparent; the apical part of sclerite L2D C-shaped, outer margin without any tooth; apical membrane less developed, covered with microtrichia (Fig. 7I). Sclerite L3 hook slender, inner curved margin with a tooth at apex; sclerite L4U divided into two parts (Fig. 7J).

**Measurements (mm).** Body length including tegmen: 21.9; pronotum length × width: 4.6 × 6.5; tegmen length: 19.8.

**Remarks.** The specimen we examined is generally identical to the description of *P. aurantius* provided by Roth (1998). However, Roth (1998) examined the type of *P. aurantius* and found its left style present, whereas this structure is absent in the specimen we examined (Fig. 7G). As only a single specimen is available in our study, it is difficult to determine whether the style is missing or naturally absent. More specimens will be needed in the future to clarify this question, and for now, we have tentatively identified the specimen as *P. aurantius*.

### ***Pycnoscelus striatus* (Kirby, 1903)**

Fig. 8

*Leucophaea striata* Kirby, 1903: 378; Kirby 1904: 151; Hanitsch 1915: 122; Chopard 1919: 358.

*Pycnoscelis* [sic] *striata*: Princis 1964: 274.

*Pycnoscelus striatus*: Roth, 1998: 117; Lucañas and Lit 2016: 7; Anisyutkin 2018: 83.

**Material examined.** MALAYSIA • 5 males & 1 female; Borneo, Sandakan, Goman-tong cave; 19 Apr. 2024; Wei-Wei Zhang leg. • 1 male; Borneo, Mt. Trus Madi, Jungle Girl Camp; 19–25 July 2016; Ren-Zhi Zhang leg. • 1 male; Borneo, Mt. Trus Madi, Jungle Girl Camp; 4 May 2023; Cai-Xia Yuan leg.

**Diagnosis.** This species is close to *P. semivitreus* in the structure of male genitalia, but the shape of the right style could distinguish them easily: extending over the middle of subgenital plate in *P. striatus* (vs more elongate and extending to the left posterolateral angle of subgenital plate in *P. semivitreus*).

**Measurements (mm).** Macropterous, male, body length including tegmen: 23.6; pronotum length × width: 5.7 × 7.0; tegmen length: 20.8. Brachypterous, body length (from vertex to tip of abdomen): male 14.0–15.0, female 15.0; pronotum length × width: male 3.7–4.1 × 5.4, female 4.2 × 5.6; tegmen length: male 7.4–7.5, female 7.1.

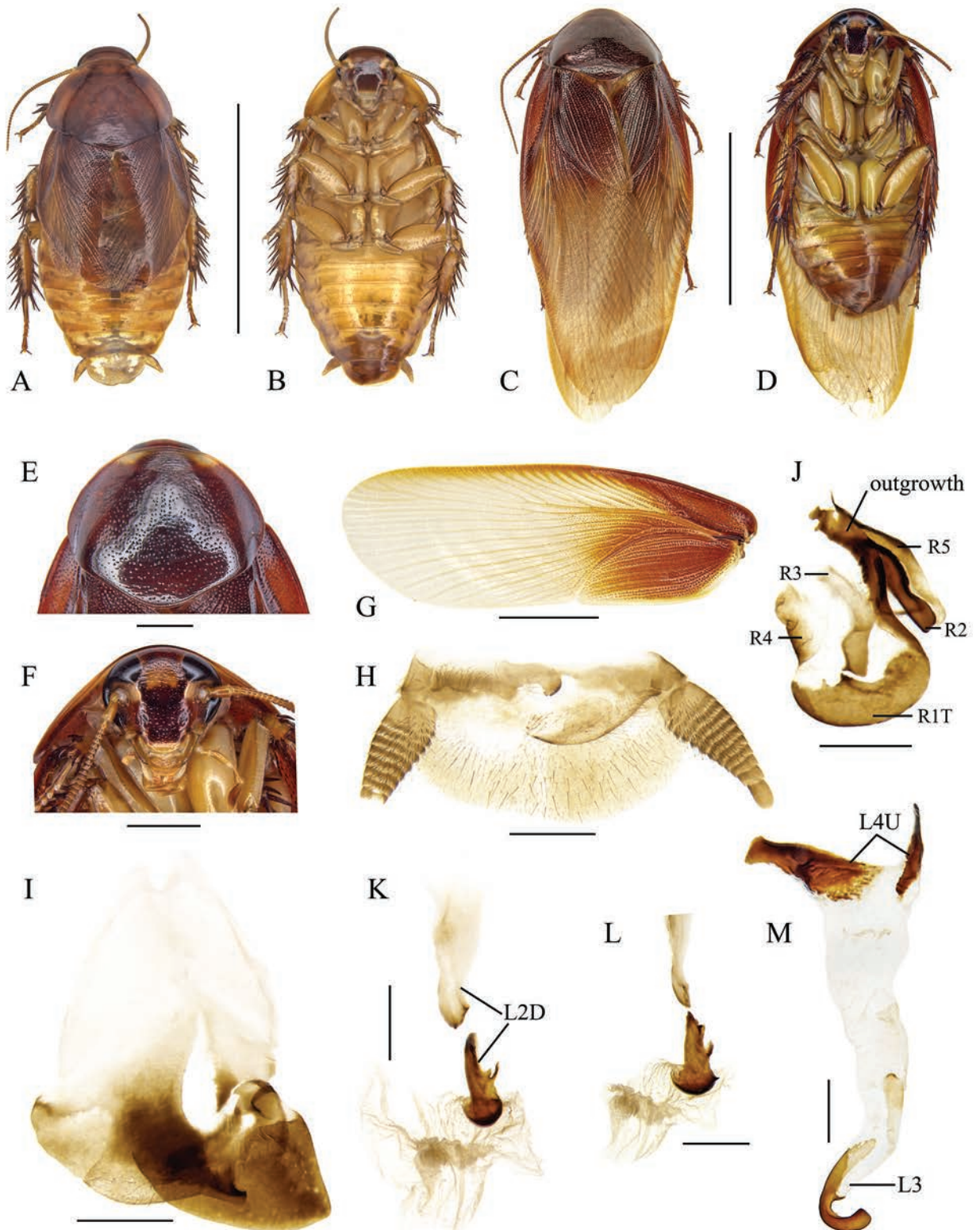


**Figure 8.** *Pycnoscelus striatus* (Kirby, 1903), male **A, B** brachypterous **C, D** macropterous **A, C** dorsal view **B, D** ventral view **E** pronotum, dorsal view **F** head, ventral view **G** tegmen, dorsal view **H** supra-anal plate, ventral view **I** subgenital plate, dorsal view **J** right phallomere, dorsal view **K** median phallomere, dorsal view **L** median phallomere, lateral view **M** left phallomere, dorsal view. Scale bars: 1.0 cm (**A–D**); 2.0 mm (**E, F**); 5.0 mm (**G**); 1.0 mm (**H, I**); 0.5 mm (**J–M**).

### ***Pycnoscelus* sp. E**

Fig. 9

**Material examined.** MALAYSIA • 1 male; Borneo, Mt. Trus Madi, Jungle Girl Camp; 2–5 Oct. 2015; Ye-Jie Lin leg. • 1 male; Borneo, Mt. Trus Madi, Jungle Girl Camp; 3 May 2023; Cai-Xia Yuan leg.

**Diagnosis.** This species can be readily distinguished from other *Pycnoscelus* species by the color pattern of pronotum and tegmina. The apical part of sclerite L2D of this species is also peculiar in this genus (see description below for details).

**Description.** General color yellowish brown, with pronotum, tegmina, and abdominal sternites partly reddish brown (Fig. 9A, B). Facial part of head dark brownish, with a three-radial stripe between eyes; other part of head, clypeus, labrum and antennae yellowish brown; eyes black, ocellar spots yellow white. Pronotum dark reddish brown, with a yellow stripe along the anterior margin (Fig. 9C). Tegmina bicolored, the dark part, principally half anal field reddish brown, remainder yellowish hyaline; the boundary between the two regions extends obliquely from the left posterolateral side of the anal field to half of the radial field; in the dark region, dark brown spots scattered along veins (Fig. 9E). Abdomen yellowish, with last sternites reddish brown. Legs yellowish brown except for reddish brown tibia and tarsomere. Cerci reddish brown.

Head slightly exposed. Interocular space narrower than the distance between ocellar spots and antennal sockets (Fig. 9D). Pronotum subpentagonal, densely punctured. Tegmina and wings fully developed, exceeding the end of abdomen. Front femur Type C<sub>1</sub>. Hind metatarsus slightly longer than other segments combined; four proximal tarsomeres with well-developed pulvilli, the one on the first tarsomere occupying almost the whole length of the segment; claws symmetrical and simple; arolium large. Supra-anal plate weakly asymmetrical, covered with bristles; paraprocts of blaberid type, asymmetrical (Fig. 9F). Subgenital plate asymmetrical, with the right posterolateral corner sharp and upturned. Left style absent, right style plate-like, broadly trigonal (Fig. 9H).

**Male genitalia.** Right phallomere with caudal part of sclerite R1T rounded, inner margin produced apically; R2 nearly straight; R3 forked caudally, with left branch projected at apex; R4 plate-like; R5 lies above R2 and fused with its distal part (Fig. 9H). Sclerite L2D divided into basal and apical parts, the apical part well sclerotized, irregular, with distal part hairy instead of toothed; apical membrane less developed (Fig. 9I). Sclerite L3 hook very short, with the apex widened; sclerite L4U present and divided into two parts (Fig. 9J).

**Measurements (mm).** Body length including tegmen: 17.7–18.0; pronotum length × width: 3.8–4.0 × 4.4–4.8; tegmen length: 14.7.

**Remarks.** According to the description of *P. rufus* given by Anisyutkin (2004), *Pycnoscelus* sp. E closely resembles this species in general color pattern, the shape of right style and right phallomere, but differs in features of pronotum and the apical part of sclerite L2D. We refrain from defining *Pycnoscelus* sp. E as a new species until we examine the type specimen of *P. rufus*.

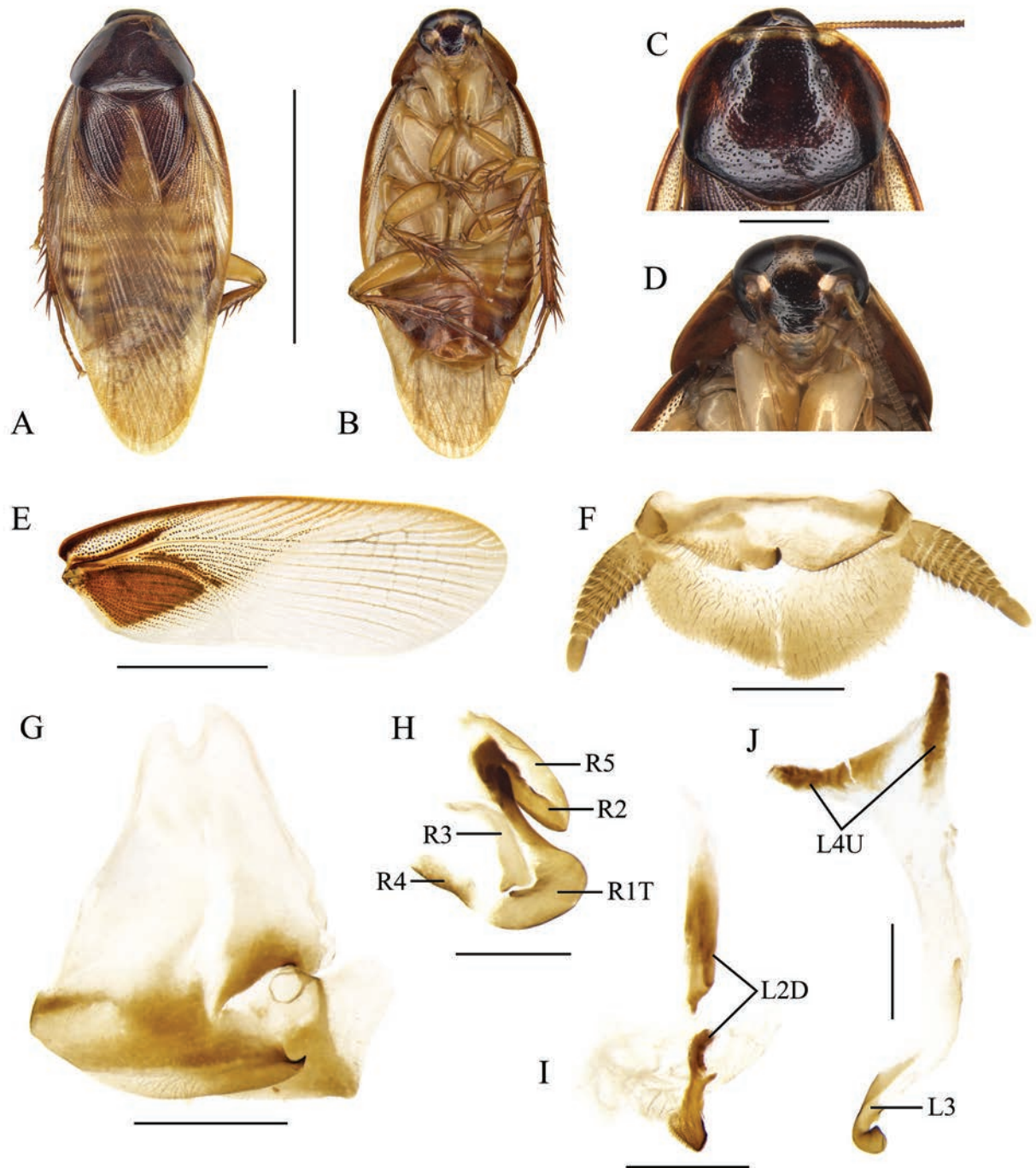


**Figure 9.** *Pycnoscelus* sp. E, male **A** dorsal view **B** ventral view **C** pronotum, dorsal view **D** head, ventral view **E** tegmen, dorsal view **F** supra-anal plate, ventral view **G** subgenital plate, dorsal view **H** right phallomere, dorsal view **I** median phallomere, dorsal view **J** left phallomere, dorsal view. Scale bars: 1.0 cm (**A**, **B**); 2.0 mm (**C**, **D**); 5.0 mm (**E**); 1.0 mm (**F**, **G**); 0.5 mm (**H**–**K**).

***Pycnoscelus* sp. F**

Fig. 10

**Material examined.** CHINA • 1 female; Yunnan Prov., Mengla County, Menglun Town, Manbian Cun; 30 July 2009; Zong-Qing Wang leg.

**Measurements (mm).** Body length: 17.4; pronotum length × width: 4.3 × 7.8; tegmen length: 2.5.

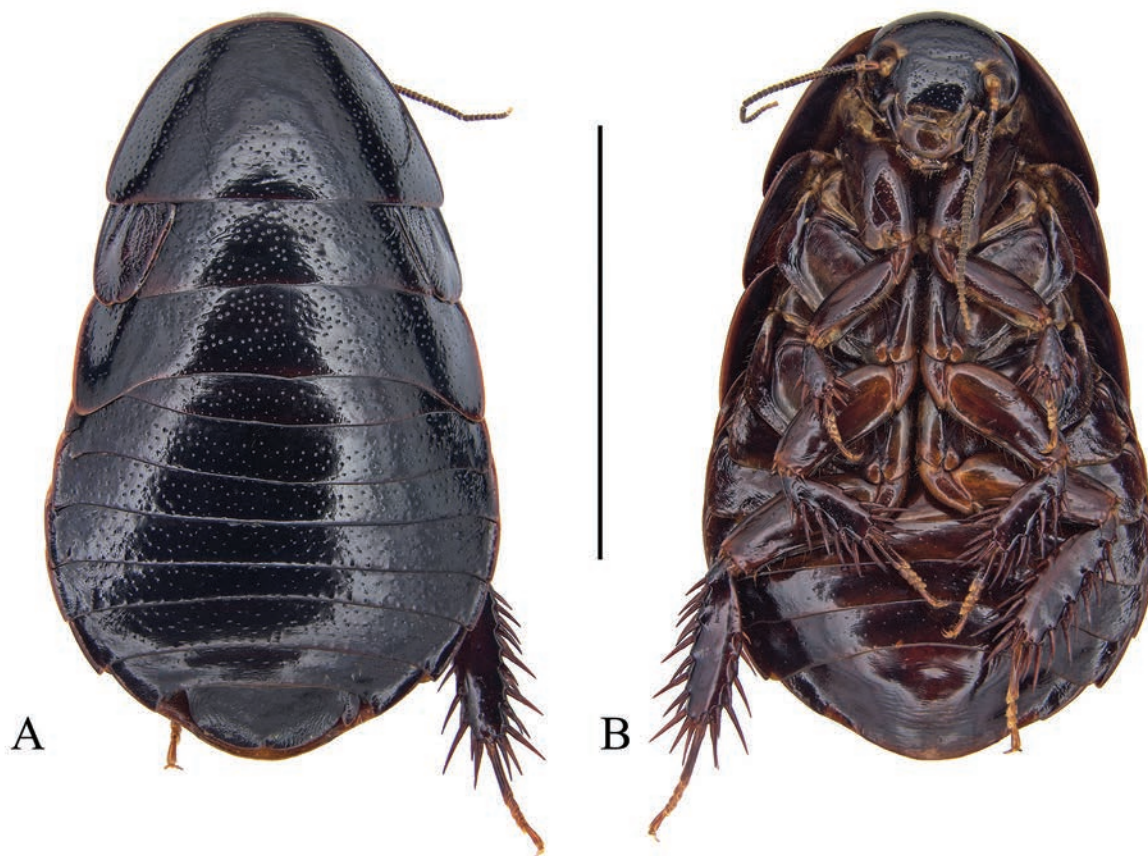


Figure 10. *Pycnoscelus* sp. F, female **A** dorsal view **B** ventral view. Scale bar: 1.0 cm.

**Remarks.** *Pycnoscelus* sp. F is currently represented by a single female specimen. This specimen is characterized by its strongly reduced tegmina (lobiform and lateral) and the complete absence of hind wings. Wing reduction is also observed in the females of *P. micropterus* Hanitsch, 1931, *P. striatus* (Kirby, 1903), *P. femapterus* Roth, 1998, and *P. undulatus* sp. nov. However, *P. micropterus* and *P. striatus* differ from *Pycnoscelus* sp. F by the tegmina reaching the abdominal terga, and the presence of hind wings. Furthermore, *P. femapterus* and *P. undulatus* sp. nov. can be distinguished from *Pycnoscelus* sp. F by the complete lack of both tegmina and wings.

It is worth noting that no female specimens of *P. puteus* sp. nov. have been recorded, and both *P. puteus* sp. nov. and *Pycnoscelus* sp. F were collected from Menglun Town, Mengla County, Yunnan Province. It is plausible that *Pycnoscelus* sp. F represents the female form of *P. puteus* but it needs further study.

## Discussion

Classifying species into groups is essential for understanding their putative phylogenetic relationships and for rapid identification. Anisyutkin (2003) previously noted that male genitalia structures, particularly sclerite L2D, often show similarities between closely related species; he used this feature as the primary criterion to divide the genus *Rhabdoblatta* into groups. Similarly, Roth (1989) suggested that sclerite L2D could effectively indicate relationships among *Paranauphoeta* species.

**Table 1.** Characters of *Pycnoscelus* species (characters of *P. gorochovi* Anisyutkin, 2002, *P. rothi* Anisyutkin, 2002, *P. vietnamensis* Anisyutkin, 2002, *P. rufus* Bey-Bienko, 1950 and *P. schwendingeri* Anisyutkin, 2018 were gathered from literature). I – right style elongate and cone-shaped (0), broader and plate-like (1); II – apical part of sclerite L2D with caudal margin toothed (0), smooth (1), covered with chaetae (2); III – R5 present (0), absent (1); IV – outgrowth arising from the junction of sclerite R1T and R2 absent (0), present (1).

Species	Characters			
	I	II	III	IV
<i>P. indicus</i> (Fabricius, 1775)	0	0	1	1
<i>P. nigra</i> (Brunner von Wattenwyl)	0	0	1	1
<i>P. puteus</i> sp. nov.	0	0	1	1
<i>P. undulatus</i> sp. nov.	0	0	1	1
<i>P. gorochovi</i> Anisyutkin, 2002	0	0	1	1
<i>P. rothi</i> Anisyutkin, 2002	0	0	1	1
<i>P. vietnamensis</i> Anisyutkin, 2002	0	0	1	1
<i>P. schwendingeri</i> Anisyutkin, 2018	0	0	1	1
<i>P. rufus</i> Bey-Bienko, 1950	1	1	0	0
<i>P. semivitreus</i> Princis, 1967	1	1	0	0
<i>P. aurantius</i> Hanitsch, 1935	1	1	0	0
<i>P. striatus</i> (Kirby, 1903)	1	1	0	1
<i>Pycnoscelus</i> sp. E	1	2	0	0

For the genus *Pycnoscelus*, Roth (1998) proposed two species groups based solely on the shape of the right style: the *indicus* species group and the *striatus* species group. In this study, we examined eight *Pycnoscelus* species, for which male genitalia characters were obtained. Combining the data from Anisyutkin (2002, 2004, 2018), we found distinct differences between the species of the *indicus* group and those of the *striatus* group (summarized in Table 1). Specifically, species in the *indicus* group, including *P. indicus*, *P. nigra*, *P. puteus* sp. nov., *P. undulatus* sp. nov., *P. gorochovi*, *P. rothi*, *P. vietnamensis*, and *P. schwendingeri*, share the absence of sclerite R5 and the apical part of sclerite L2D with its caudal margin toothed. In contrast, species in the *striatus* group, comprising *P. aurantius*, *P. rufus*, *P. striatus*, and *P. semivitreus*, have sclerite R5 present, and the apical part of sclerite L2D with untoothed caudal margin. These differences in male genitalia characters can be used to further distinguish the two groups. The remaining species, *Pycnoscelus* sp. E, differs from all other species by the feature of sclerite L2D, whose apical part is neither toothed nor smooth but covered with chaetae. Thus, the position of *Pycnoscelus* sp. E within the species groups remains unclear.

Furthermore, the outgrowth arising from the junction of sclerites R1 and R2 is likely an apomorphy of the genus *Pycnoscelus*, as such a structure is quite rare in other Blaberidae taxa. In this case, the absence of this outgrowth in *P. aurantius*, *P. rufus*, and *P. semivitreus* is possibly a plesiomorphic condition, also suggesting a close relationship between them. On the other hand, the simultaneous presence of the outgrowth and sclerite R5 in *P. striatus* may represent an autapomorphy within *Pycnoscelus*.

Although we proposed additional male genitalia characters to further distinguish and delineate the two species groups of *Pycnoscelus*, these are based only on species with known male genitalia data; information on the male

genitalia of 15 species is still lacking. Describing the male genitalia of these species and acquiring molecular data in future studies would validate the proposed characters and greatly enhance our understanding of the systematics of *Pycnoscelus*, thereby enabling a more comprehensive classification.

## Acknowledgements

We extend our sincere gratitude to all the collectors of the specimens examined in this study, with special thanks to Cai-Xia Yuan, Gui-Qiang Huang, Hao Xu, Ji-an-Yue Qiu, Li He, Ren-Zhi Zhang, Ye-Jie Lin, Yi-Zhou Liu and Wei-Wei Zhang. We also appreciate Frédéric Legendre, Leonid Anisutkin, and Zuzana Varadínová for their valuable suggestions on our manuscript.

## Additional information

### Conflict of interest

The authors have declared that no competing interests exist.

### Ethical statement

No ethical statement was reported.

### Funding

This work was supported by Shuangcheng cooperative agreement research grant of Yibin, China (YBSCXY2023020012), the National Natural Sciences Foundation of China (no. 32070468) and by a Program of the Ministry of Science and Technology of the People's Republic of China (2022FY202100).

### Author contributions

Funding acquisition: ZQW. Supervision: YLC. Validation: XJD. Writing – original draft: YSW.

### Author ORCIDs

Yi-Shu Wang  <https://orcid.org/0009-0008-5507-760X>

Zong-Qing Wang  <https://orcid.org/0000-0001-9413-1105>

Yan-Li Che  <https://orcid.org/0000-0003-3214-9494>

### Data availability

All of the data that support the findings of this study are available in the main text.

## References

- Anisutkin LN (2002) Notes on the cockroaches of the subfamily Pycnoscelinae and Diplopterinae from South-East Asia (Blaberidae: Dictyoptera). *Zoosystematica Rossica* 10(2): 351–359. <https://doi.org/10.31610/zsr/2001.10.2.351>
- Anisutkin LN (2003) New and little known cockroaches of the genus *Rhabdoblatta* Kirby (Dictyoptera, Blaberidae) from Vietnam and Southern China. II. *Entomological Review* 83(5): 540–556.
- Anisutkin LN (2004) Redescription of *Pycnoscelus rufus* Bey-Bienko, *Heminauphoeta picea* Shelford and *Eutheganopteryx mirabilis* Shelford (Dictyoptera: Blattina). *Zoosystematica Rossica* 12(2): 177–183. <https://doi.org/10.31610/zsr/2003.12.2.177>

- Anisyutkin LN (2018) New data on the genus *Pycnoscelus* Scudder, 1862 with the description of *P. schwendingeri* sp. nov. (Blaberidae: Pycnoscelinae). *Revue suisse de Zoologie* 125(1): 79–86. <https://doi.org/10.5281/ZENODO.1196021>
- Bey-Bienko GY (1950) Cockroach insects. *Fauna USSR (New Series)* 40: 1–343.
- Bey-Bienko GY (1968) On the orthopteroid insects (Orthopteroidea) from Eastern Nepal. *Entomologicheskoe Obozrenie* 48(1): 106–130.
- Bruijning CFA (1947) An account of the Blattidae (Orthoptera) from Celebes, the Moluccas, and New Guinea. *Zoologische Mededelingen, Leiden* 27: 205–252.
- Brunner von Wattenwyl C (1865) *Nouveau système des Blattaires*. Charles Ueberreuter, Wien, 426 pp. <https://doi.org/10.5962/bhl.title.8507>
- Fabricius JC (1775) *Systema entomologiae, sistens insectorum classes, ordines, genera, species, adiectis synonymis, locis, descriptionibus, observationibus*. Korte, Flensburgi et Lipsiae, 832 pp. <https://doi.org/10.5962/bhl.title.36510>
- Hanitsch R (1931) On a collection of Malayan Blattidae from the British Museum (Natural History). *Annals and Magazine of Natural History (Series 10)* 7: 385–408. <https://doi.org/10.1080/00222933108673325>
- Hanitsch R (1935) On further Blattids (Orth.) from Celebes. *Stylops* 4: 14–19. <https://doi.org/10.1111/j.1365-3113.1935.tb01292.x>
- Kirby WF (1903) Notes on Blattidae & c., with descriptions of new genera and species in the collection of the British Museum, South Kensington. III. *Annals and Magazine of Natural History (Series 7)* 12: 373–381. <https://doi.org/10.1080/00222930308678873>
- Kirby WF (1904) A synonymic catalogue of Orthoptera. Vol. I. Orthoptera Euplexoptera, Cursoria, et. Gressoria. (Forficulidae, Hemimeridae, Blattidae, Mantidae, Phasmidae). British Museum, London, 501 pp.
- Klass KD (1997) The external male genitalia and the phylogeny of Blattaria and Mantodea. *Bonner Zoologische Monographien* 42: 1–341.
- Linnaeus C (1758) *Systema naturæ per regna tria naturæ, secundum classes, ordines, genera, species, cum characteribus, differentiis, synonymis, locis*. Tomus I. Editio X, reformata. Salvius, Holmiae, 824 pp. <https://doi.org/10.5962/bhl.title.542>
- Lucañas CC, Lit IL (2016) Cockroaches (Insecta, Blattodea) from caves of Polillo Island (Philippines), with description of a new species. *Subterranean Biology* 19(1): 51–64. <https://doi.org/10.3897/subtbiol.19.9804>
- Princis K (1964) Blattariae: Subordo Blaberoidea. Fam.: Panchloridae, Gynopeltidae, Derocalymmidae, Perisphaeriidae, Pycnoscelidae. *Orthopterorum Catalogus* 6: 174–281.
- Princis K (1967) Kleine Beiträge zur Kenntnis der Blattarien und ihrer Verbreitung. X. *Opuscula entomologica* 32: 141–151.
- Princis K (1971) Blattariae: Subordo Epilamproidea, Family Ectobiidae. Pt. 14 in *Orthopterorum Catalogus*. Dr. W. Junk N.V., The Hague, pars 14: 1039–1224.
- Roth LM (1967) Sexual isolation in parthenogenetic *Pycnoscelus surinamensis* and application of the name *Pycnoscelus indicus* to its bisexual relative (Dictyoptera: Blattaria: Blaberidae: Pycnoscelinae). *Annals of the Entomological society of America* 60(4): 774–779. <https://doi.org/10.1093/aesa/60.4.774>
- Roth LM (1973) The male genitalia of Blattaria. X. Blaberidae. *Pycnoscelus*, *Stilpnoblata*, *Proscratea* (Pycnoscelinae) and *Diploptera* (Diplopterinae). *Psyche* 80: 249–264. <https://doi.org/10.1155/1973/32467>
- Roth LM (1974) Reproductive potential of bisexual *Pycnoscelus indicus* and clones of its parthenogenetic relative, *Pycnoscelus surinamensis*. *Annals of the Entomological Society of America* 67(2): 215–223. <https://doi.org/10.1093/aesa/67.2.215>

- Roth LM (1989) *Paranauphoeta rufipes* Brunner in Queensland, and a description of the female *Cololompra elegans* Roth and Princis (Dictyoptera: Blattaria: Blaberidae). *Memoirs of the Queensland Museum* 27: 589–597.
- Roth LM (1998) The cockroach genus *Pycnoscelus* Scudder, with a description of *Pycnoscelus femapterus*, sp. nov. (Blattaria: Blaberidae: Pycnoscelinae). *Oriental Insects* 32: 93–130. <https://doi.org/10.1080/00305316.1998.10433770>
- Roth LM, Willis ER (1956) Parthenogenesis in Cockroaches. *Annals of The Entomological Society of America* 49: 195–204. <https://doi.org/10.1093/aesa/49.3.195>
- Scudder SH (1862) Materials for a monograph of the North American Orthoptera, including a catalogue of the known New England species. *Boston Journal of Natural History* 7: 409–480. <https://doi.org/10.5962/bhl.part.11211>
- Walker F (1869) Catalogue of the specimens of Dermaptera, Saltatoria and supplement to the Blattariae in the collection of the British Museum. British Museum, London, 224 pp.
- Wang YS, Chen R, Jin DT, Che YL, Wang ZQ (2021) New record of *Cyrtonotula* Uvarov, 1939 (Blaberidae, Epilamprinae) from China, with three new species based on morphological and COI data. *ZooKeys* 1021: 127–143. <https://doi.org/10.3897/zookeys.1021.59526>
- Wang ZQ, Qiu L, Che YL (2024) *Cockroaches of China*. Chongqing University Press, Chongqing, 370 pp.



# Mating and egg-laying behaviour of the Southeast Asian apple snail *Pila pesmei* (Morlet, 1889) (Caenogastropoda, Ampullariidae)

Supunya Annate<sup>1</sup>, Ting Hui Ng<sup>2</sup>, Chirasak Sutcharit<sup>1</sup>, Somsak Panha<sup>1,3</sup>

<sup>1</sup> Animal Systematics Research Unit, Department of Biology, Faculty of Science, Chulalongkorn University, 254 Phayathai Road, Pathumwan, Bangkok 10330, Thailand

<sup>2</sup> Institute for Tropical Biology and Conservation, Universiti Malaysia Sabah, Jalan UMS, 88450 Kota Kinabalu, Sabah, Malaysia

<sup>3</sup> Academy of Science, The Royal Society of Thailand, Bangkok 10300, Thailand

Corresponding author: Somsak Panha ([somsak.pan@chula.ac.th](mailto:somsak.pan@chula.ac.th))

## Abstract

The apple snail *Pila pesmei* is an economically valuable freshwater snail in mainland Southeast Asia whose populations have recently dramatically declined. Although conservation concerns have been rising in the region, the lack of basic knowledge of its reproductive biology remains an obstacle to its conservation. This study describes the mating and egg-laying behaviours of *P. pesmei* under laboratory conditions using continuous video recordings. Fifteen mating behaviours were recorded in four mating phases: pre-courtship, courtship, copulation, and post-copulation. Mating sequences were variable, especially in the courtship phase. However, many males performed a common courtship sequence of mate probing, mounting, shell circling, and positioning. When a female performed a variety of actions against the male's approach, males then performed various alternative courtship sequences. The egg-laying process was similar among different females. They burrowed into the soil substrate to lay eggs. A total of six behaviours were recorded in the egg-laying process: crawling, resting, withdrawal, burrowing, egg depositing, and aestivating. Females did not return to the water after laying eggs but remained in the egg-laying cavity with their egg masses. This behaviour has not been reported in any other *Pila* species to date. Overall, our examination revealed the previously unknown mating and egg-laying processes in *P. pesmei*, which included some distinct behaviours and increased the basic knowledge of its reproductive biology.

**Key words:** Copulation, female resistance, freshwater snail, oviposition, reproduction, reproductive behaviour, spawning, video recording



Academic editor: Frank Köhler

Received: 1 October 2024

Accepted: 31 January 2025

Published: 10 March 2025

ZooBank: <https://zoobank.org/D195BC1E-89A2-41FB-A67C-C0DE3A27B9CF>

**Citation:** Annate S, Ng TH, Sutcharit C, Panha S (2025) Mating and egg-laying behaviour of the Southeast Asian apple snail *Pila pesmei* (Morlet, 1889) (Caenogastropoda, Ampullariidae). ZooKeys 1231: 69–83. <https://doi.org/10.3897/zookeys.1231.138263>

Copyright: © Supunya Annate et al.  
This is an open access article distributed under terms of the Creative Commons Attribution License (Attribution 4.0 International – CC BY 4.0).

## Introduction

The Southeast Asian apple snail, *Pila pesmei* (Morlet, 1889), is a freshwater snail belonging to the family Ampullariidae. *Pila pesmei* has been reported in all the mainland Southeast Asian countries: Cambodia, Laos, Myanmar, Thailand, and Vietnam (Keawjam 1986, 1990; Cowie 2015; Ng et al. 2020a, 2020b). It is one of the economically valuable freshwater snails in the region. Natural populations of *P. pesmei* have been exploited for food acquisition and trading (Ngor et al. 2018; Ng et al. 2020b). Recently, populations of *P. pesmei*, like other Southeast Asian apple snails have decreased due to several likely factors,

including habitat degradation, overexploitation, and introduction of the South American apple snails *Pomacea canaliculata* (Lamarck, 1822) and *Pomacea maculata* Perry, 1810 (Ngor et al. 2018; Marwoto et al. 2020; Ng et al. 2020a). Although concern for the conservation of these species has been rising in the last few years, effective conservation action is still hard to enact because of the lack of knowledge regarding their reproductive biology (Annate et al. 2023).

There is no study of the reproductive biology of *P. pesmei* to date. A few details of its reproductive biology have been scattered in reports of taxonomic or ecological studies (Keawjam 1987; Lamkom and Phosri 2017; Ng et al. 2020a). *Pila pesmei* is dioicous. Male and female snails are indistinguishable by external morphology. Shell sizes of mature snails range from 30 to 60 mm long and from 27 to 50 mm wide (Keawjam 1986; Ng et al. 2020a). However, the mating process in this species is unknown and remains to be described.

The egg-laying behaviour of *P. pesmei* has been briefly mentioned by Lamkom and Phosri (2017) and Ng et al. (2020a), but these two studies reported slightly different egg-laying behaviours. Based on casual observation, the species was reported to lay approximately 100 white spherical eggs in a shallow cavity away from water in the wild (Ng et al. 2020a), whereas the ex-situ study (Lamkom and Phosri 2017) reported that it lays 107–301 white eggs on the soil.

Because of these scattered and confusing details, it is necessary to investigate the reproductive behaviour of *P. pesmei*. Building on previous research documenting the behaviours of *Pila* species (Annate et al. 2023), herein we report the mating and egg-laying behaviours of *P. pesmei*.

## Methods

### Materials

We collected 70 mature snails (shell length over 30 mm) from a population inhabiting a paddy field in Mukdahan province, Thailand (16°42'46"N, 104°42'36"E) on 25 May 2023 when they had first emerged from aestivation following the first flood after the dry season. Snails were transported to the laboratory on the same day and sexed according to the presence of the penis sheath. From the 33 males and 37 females collected, eight males and eight females were used in the first egg-laying behaviour trial (video recorded). The other 25 males and 29 females were maintained separately in 0.45 m<sup>2</sup> circular concrete containers, each containing 80 l of tap water, at a maximum density of 10 snails/container for 30 days. They were then used in mating behaviour trials (video recorded) and the second and third egg-laying behaviour trials (also video recorded). Snails were fed with lettuce *ad libitum*. Water was changed and maintenance containers were cleaned monthly.

### Mating behaviour: (i) video recording

Prior to video recording the mating behaviour, snails were transferred from the maintenance containers to a 17.5-l glass aquarium containing 10 l of tap water for acclimatisation. Males and females were kept in separate aquaria at a stocking density of two snails/aquarium at ambient temperature (29 ± 1 °C) under a 12:12 h photoperiod. They were acclimatised for 24 h and were fed with lettuce *ad libitum* during this period.

To video record the mating behaviour, one male and one female were randomly transferred to a 17.5-l glass aquarium containing 10 l of tap water. Five pairs were recorded concurrently in each of a total of 10 trials in July and August 2023. Snail behaviour was recorded for 24 h from when they were paired using an infrared digital video camera (5 MP HD IP Camera, Model YM500L) installed in front of the aquarium (one per aquarium).

After video recording, females that had mated were transferred to an egg-laying aquarium where they were kept to screen for oviposition. Males that had mated were transferred to new maintaining containers. Snails that had not mated were returned to their maintaining containers and reused for subsequent mating behaviour video recording trials after 24 h.

### Mating behaviour: analysis of video recordings

Video records of the mating behaviour of *P. pesmei* were first thoroughly scanned for the presence of an insemination posture (Fig. 1). The video record of each pair was then analysed by watching at 1–8× of the normal speed rate. Behaviour of each mating pair was analysed from the beginning of the video record, when the pairs were released into the mating aquaria, until one hour after they had dismounted from each other. Behaviour of non-mating pairs was analysed for 4 h from their initial release into the mating aquarium.

Mating behaviours of *P. pesmei* were classified based on the descriptions for *P. virescens* (Deshayes, 1824) (Annate et al. 2023) and *Pomacea canaliculata* (Burela and Martín 2009). The mating process was divided into the four phases,

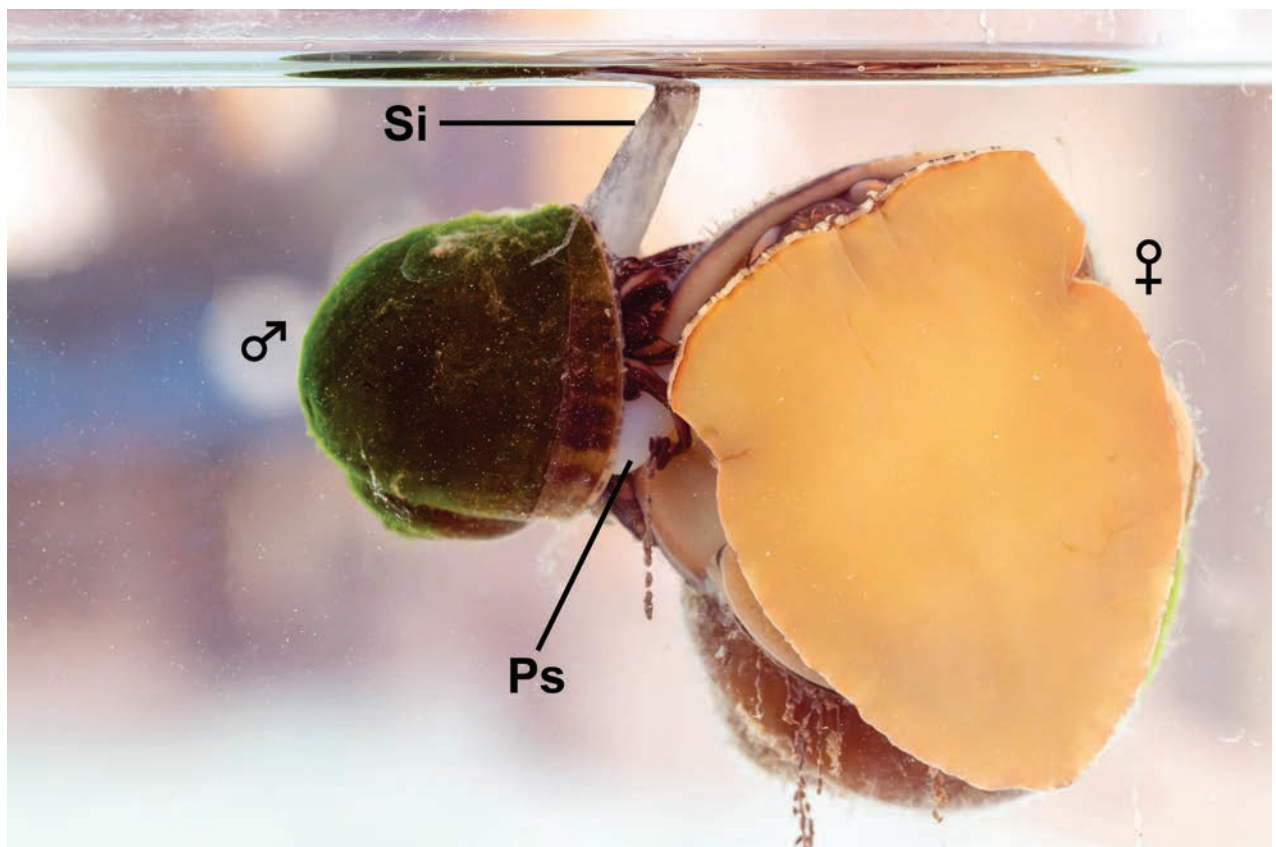


**Figure 1.** Insemination posture of *Pila pesmei*. Abbreviations: Ps, penis sheath; Si, siphon.

following Burela and Martín (2009): 1. Pre-courtship phase, the period from the beginning to the first contact between two snails; 2. Courtship phase, the period from the first contact between two snails to the time point that the male inserts the penis sheath into the female genital pore; 3. Copulation phase, the period from penis insertion to penis withdrawal; and 4. Post-copulation, the period from penis withdrawal to the time point that the two snails separated from each other.

All the observed behaviours that may be related to mating were then described with a diagram of the mating sequences. The duration of the entire mating process and each of the behavioural phases were recorded in hours and presented as the mean  $\pm$  one standard deviation (SD).

### **Egg-laying behaviour: (i) video recording**

Each egg-laying arena was a 0.45 m<sup>2</sup> circular concrete container housing the water body (40 l of tap water) and the soil area for oviposition. Snail behaviour was recorded for 30 days using one infrared digital video camera installed 1.5 m above each of the two arenas in each of three trials.

Four males and four females were randomly selected and transferred from the maintenance concrete containers to an egg-laying arena. Before releasing the snails into the egg-laying arenas, the shell width and shell length were measured using digital Vernier calipers to the nearest millimeter. Snails were marked using nail polish for sex identification in the subsequent video examination. The first trial was conducted between 25 May and 25 June 2023, the second between 28 June and 28 July 2023, and the third between 30 July and 30 Aug 2023. At the end of each trial, snails were removed from the arenas. The soil areas were searched for egg masses. Each arena was cleaned before conducting the next trial.

### **Egg-laying behaviour: (ii) video examination**

Video records were scanned for the presence of females in the soil areas away from the water body or for any burrowing behaviour every 10 min. When the females showed a burrowing behaviour, we re-examined the video records by continuously watching at 1–8 $\times$  of the normal speed from the time point that the female started crawling out of the water until the female finished egg laying or returned to the water.

All the observed behaviours in the egg-laying process were then described with a diagram of the egg-laying sequences. The duration of each behaviour in the egg-laying process was recorded in hours and presented as the mean  $\pm$  SD.

## **Results**

### **Mating behaviour**

Among the 50 recorded pairs, six pairs mated, and the other 44 pairs did not mate. Among the 44 non-mating pairs, eight did not show any visible behavioural interaction in the first 4 h, while the other 36 non-mating pairs showed some behavioural interactions. Therefore, a total of 42 pairs (six mating pairs and 36 non-mating pairs) were included in the mating behaviour analysis.

Paired snails showed 15 distinguishable behaviours in the mating process. Names and descriptions of each behaviour are provided in Table 1. The mating process included four phases within which the behavioural interactions and sequences were variable (Fig. 2). The pre-courtship phase included breathing, resting, withdrawal, and walking behaviours. When each pair was released into the aquarium, they withdrew their body into the shell and the operculum completely closed the aperture. Then, they extruded their tentacles and cephalopodium while opening the operculum slightly. The first contact between the male and female occurred while they moved around in the aquarium. In 29 out of the 42 pairs, males contacted females first, whereas females contacted males first in the other 13 pairs. After the first contact, four pairs showed no further behavioural interaction in the 4 h; thus, these pairs did not enter the courtship phase. The other 38 pairs entered the courtship phase performing various behavioural interactions.

In 16 of the 38 pairs, the male immediately courted the female by pushing, mounting, and circling on the female's shell following the first contact. In contrast, the other 22 pairs did not perform any immediate subsequent courtship behaviour following the first contact. Rather, they began courting after later contacts. Among the 38 pairs that entered the courtship phase, 17 pairs performed only one courtship behaviour, which was mate probing. The other 21 pairs performed variable sequences of courtship behaviours, such as mate probing and shell pushing or mate probing and mounting (Fig. 2). However, the courtship sequences that led to copulation were almost the same. A total of six pairs that courted then entered the copulation phase. Five of these six pairs performed the same courtship sequence of four behaviours: mate probing, mounting, shell circling, and positioning. For the other pair, the male did not perform shell circling but mounted on the female shell near the aperture above the gonopore.

**Table 1.** Descriptions of the mating behaviour of *Pila pesmei* (applied from Annate et al. 2023).

Behavioural type	Behaviour	Description
<b>Mating behaviour</b>		
	Mate probing	Contact with cephalic tentacles, labial palps, or foot.
	Shell pushing	Push another snail by moving its shell towards another snail, generally performed by males in response to a female resistance behaviour especially retracting.
	Mounting	Mount on another snail with the foot having completely lost its hold on the aquarium.
	Shell circling	Crawl on another snail's shell and move over it in either a clockwise or counterclockwise direction.
	Positioning	Male adheres on the female's last whorl at the right side of the shell rim above the opening of the female gonopore.
	Insemination posture	Male adheres to the right side of the female's last whorl with coiled tentacles. Female usually motionless, but occasionally moves around.
	Sheath withdrawal	Male withdraws penis sheath from female gonopore.
	Post-copulation mounting	Male continues mounting on the female shell after sheath withdrawal.
	Dismounting	Male detaches from the female's shell.
	Passive	Motionless, while copulation with coiled tentacles; male tightly adheres to the female's shell, female tightly adheres to or detaches from the aquarium.
<b>Resistance behaviour</b>		
	Jerking	Contraction and release cephalopodium into- and out of the shell several times.
	Operculum closing	Quickly close the aperture with their operculum in response to any contacts from another snail.
	Retracting	Contraction of cephalopodium into the shell and tightly adhere to or completely detach from the aquarium.
	Swinging	Rotate the shell several times in a counter- and clockwise directions.
	Withdrawal-wrestling	Female pushes the male's shell with her operculum at the rim of the male aperture.

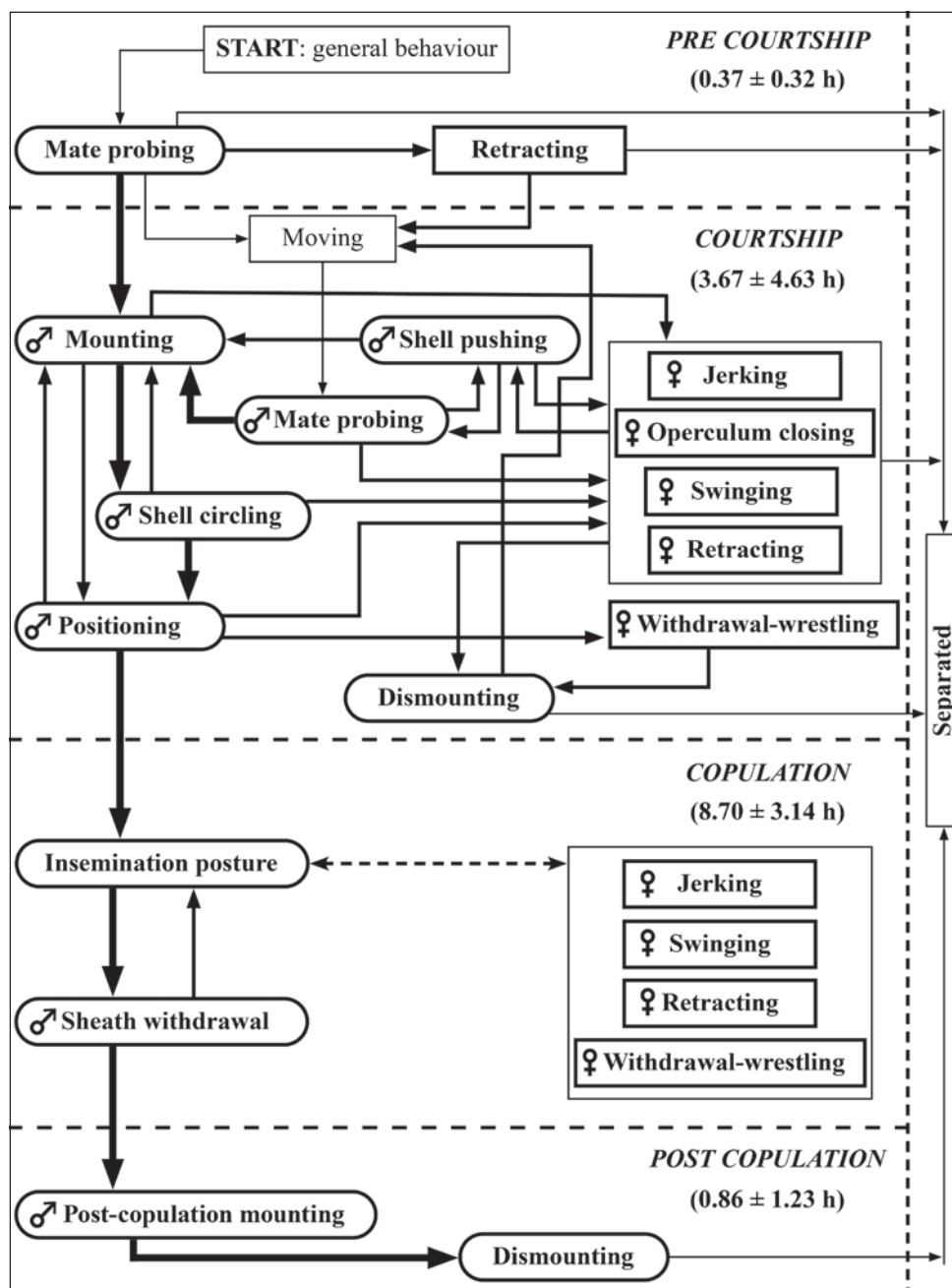


**Figure 2.** Mating sequences of *Pila pesmei*. Thick-rounded boxes represent mating behaviour. Thick-straight boxes represent female resistance behaviour. Solid arrows indicate behavioural transitions of the main mating sequences. Moderate arrows indicate behavioural transitions of the alternative mating behavioural sequences. Thin arrows indicate behavioural transitions between general and mating behaviours. The hatched arrow indicates the co-occurrence of the insemination posture and female resistance behaviour. Durations of each phase are provided in brackets (mean ± SD).

In 14 pairs, the female did not show a distinctive behaviour after being approached or courted by a male. In the other 24 pairs, the female performed five types of resistance behaviours: jerking, operculum closing, retracting, swinging, and withdrawal-wrestling (see description in Table 1).

The copulation phase began after the male positioned himself on the right side of the rim of the female's last whorl above her gonopore. The male then inserted a penis sheath into the female pallial cavity, and the pair stayed still. The process of penis sheath insertion was not recorded in this study because all penis sheath

insertion happened when mating pairs were on the side of the aquarium with no camera facing. However, the beginning of the copulation phase was judged based on the combination of male and female behaviours: the male had a coiled tentacle and tightly adhered to the rim of the female's last whorl above the gonopore, while the female suddenly ceased all moving and withdrew the soft body staying on the aquarium wall. After that, the mating pairs remained in the insemination posture (Fig. 1) for several hours. During this period, the mating pairs were generally in a passive state, staying still in the same position. Sometimes, copulating females crawled around, mainly to the water surface for gas exchange. In addition, five of the six copulating females performed some resistance behaviours simultaneously with being passive or crawling. Four resistance behaviours: jerking, retracting, swinging, and withdrawal-wrestling were recorded in this phase. The male's posture was consistent since the beginning of copulation. Males moved only their siphons for gas exchange when the mating pairs were near the water surface. When the copulating females crawled on the aquarium wall in front of the camera, the male's penis sheath was seen clearly (Fig. 1).

At the end of the copulation phase, males withdrew the penis sheath from the female pallial cavity. At the same time, males started uncoiling their tentacles and moving. In response, females retracted their soft bodies strongly but did not close the operculum. After copulation, five of the six mating pairs entered the post-copulation phase. The other pair copulated again and then entered the post-copulation phase.

In the post-copulation phase, the male stayed on the female's shell after penial separation from the female's pallial cavity. They either adhered to the female's shell without movement or crawled over the female's shell for several rounds. At the end of the post-copulation phase, the male dismounted from the female's shell, and moved to the water surface for gas exchange, after which they remained adhered to the aquarium wall, entering the resting stage for over one hour with only a few slight movements. In contrast, females moved around in the mating aquaria and often climbed out of the water on the aquarium wall.

### Egg-laying behaviour

A total of 11 females laid eggs in the egg-laying observation containers. They burrowed into the soil and laid eggs within the burrow. Five females burrowed deep into the soil and remained out of view (Fig. 3A). Consequently, six egg-laying occasions were recorded and examined in this study. In the three phases of the egg-laying process, females performed six different behaviours (Table 2).

Egg-laying sequences were simple and similar among the females (Fig. 4). Females crawled out of the water body in the nighttime onto the soil area and

**Table 2.** Descriptions of the egg-laying behaviour of *Pila pesmei*.

Stage	Behaviour	Description
Pre-egg depositing	Crawling	Crawling out of water onto land and moving around on land.
	Resting	Stop crawling or digging and stay motionless while still extruding the soft body out of the shell.
	Withdrawal	Complete withdrawal of the soft parts into the shell and closing of the aperture with the operculum.
	Burrowing	Digging into the soil to make an egg-laying cavity.
Egg depositing	Egg depositing	Laying eggs to form an egg mass within an egg-laying cavity.
Post-egg depositing	Aestivating	Complete closing of the aperture with the operculum and staying inside the egg-laying cavity.

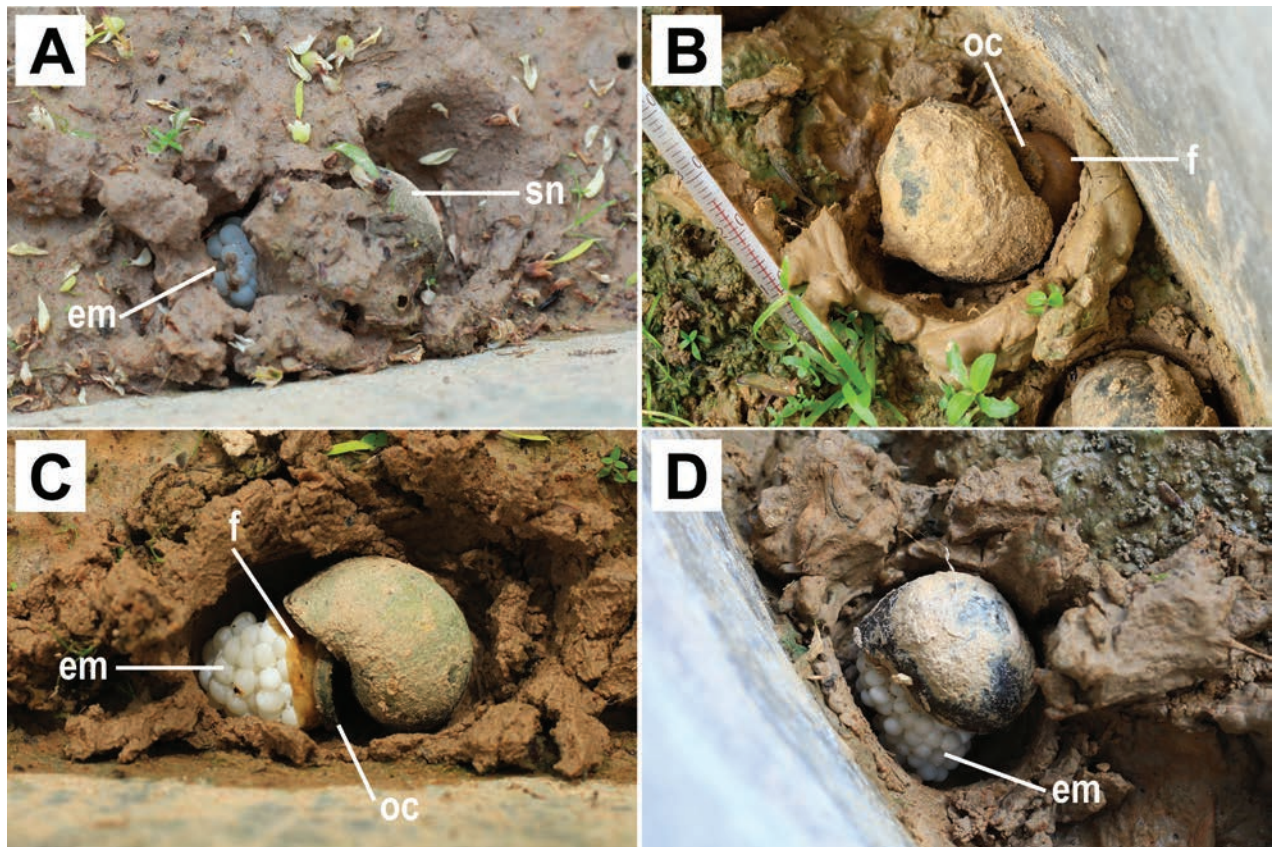


Figure 3. Egg-laying behaviour of *Pila pesmei*. **A** female lays eggs in an egg-laying cavity that is obscured by soil **B** female's foot becomes a dome shape **C** egg mass exceeds the foot coverage and can be seen clearly **D** female stays on top of the egg mass after finishing egg laying. Abbreviations: em, egg mass; f, foot; oc, operculum; sn, snail.

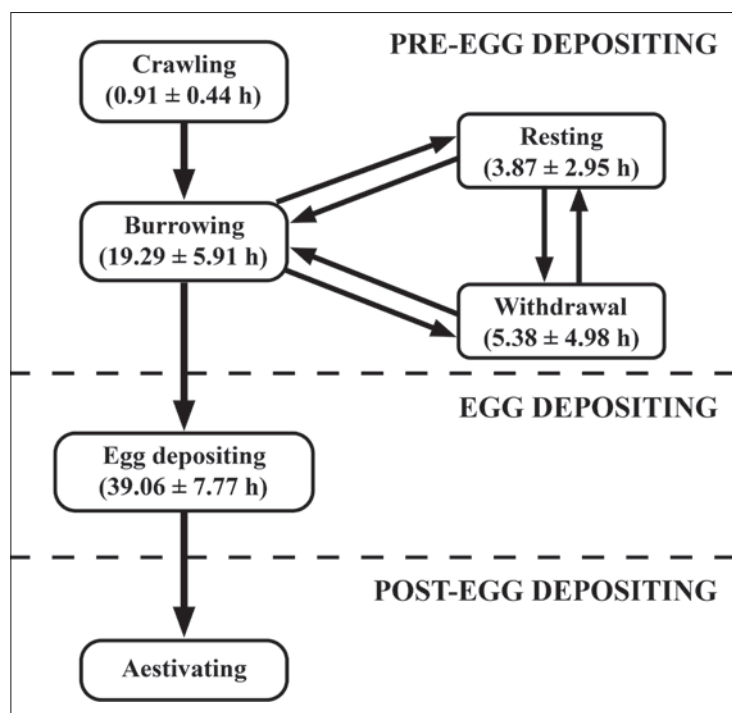


Figure 4. Egg-laying sequences of *Pila pesmei*. Thick-rounded boxes represent each egg-laying behaviour with the duration of the behaviour provided in brackets (mean  $\pm$  SD). Arrows indicate behavioural transitions of the egg-laying sequences.

then moved around on the soil surface. After that, females burrowed into the soil making a cavity. While making a cavity, they sometimes stopped burrowing and stayed motionless while extruding their soft body or withdrawing it inside the shell and closing the aperture with an operculum. Females took 10–24 h to make the egg-laying cavity.

The depth of the egg-laying cavity ranged from 3 to 5 cm. After the egg-laying cavity was completed, females expanded their feet roundly. After a few hours, the female's foot became dome-shaped (Fig. 3B), under which eggs were sometimes visible through a thin area of the female's foot. After several hours, the egg mass exceeded the foot coverage (Fig. 3C). At the end of egg laying, females closed the aperture with the operculum and stayed in the egg-laying cavity beside or on top of their egg masses (Fig. 3D). Until the end of the video recording period, they did not return to the water in the containers. When transferred into the water, they began to move around.

## Discussion

This study provides the first description of the mating and egg-laying behaviours of *P. pesmei* under laboratory conditions. Male and female pairs performed 15 different behaviours in four mating phases. Females performed six egg-laying behaviours in three egg-laying phases.

In general, the mating process of *P. pesmei* is similar to the common mating pattern of other apple snails: male mounts on the female's shell, crawls on the female's shell, positions himself on the right side of the female's last whorl above her gonopore, inserts the penis sheath into the female's pallial cavity, and mates for several hours (Albrecht et al. 1996; Burela and Martín 2007, 2009; Tiecher et al. 2014; Gurovich et al. 2017; Annate et al. 2023). However, the behavioural interactions between males and females and the behavioural transitions between different behaviours in the courtship phase of *P. pesmei* are variable (Fig. 2). Courtship variations mainly occurred in the mating pairs in which the females performed resistance behaviour. A clear example of consistent courtship variation is the performing of shell pushing. In courtship bouts without female resistance, the male performed mate probing and mounting. In some of the courtship bouts with female resistance, the male sequentially performed mate probing, shell pushing, and mounting. Such variation is possibly an alternative male reproductive tactic that is influenced by female mate choice (Oliveira et al. 2008).

Female resistance has previously been reported in two apple snails: *Pomacea canaliculata* (Burela and Martín 2009) and *P. virescens* (Annate et al. 2023). Burela and Martín (2009) reported three types of female resistance: operculum closing, swinging, and withdrawal-wrestling and suggested these behaviours are mate-rejection actions because these behaviours can cease mating. In our previous study on the mating behaviour of *P. virescens* (Annate et al. 2023), two more female resistance behaviours that can cease the mating process of *P. virescens* were identified: jerking and retracting. In addition, these five female resistance behaviours have been suggested as mate-rejection behaviours in several freshwater snails (Barraud 1957; DeWitt 1991; Facon et al. 2006; Tiecher et al. 2014). In *P. pesmei*, five types of female resistance behaviour, which have previously been reported in other apple snails, were recorded. Female resistance can cease some courtship bouts of *P. pesmei*. Therefore, it is possibly

a mate-rejection behaviour as suggested in previous studies on other snail species (Burela and Martín 2009; Annate et al. 2023).

Nevertheless, it is unknown why several females rejected their given partner in this study. Immaturity is unlikely to be the reason because some of these females mated and laid eggs when reused in the egg-laying behaviour video recording. Two possible reasons for females to avoid copulation are (1) they are ready to lay eggs and (2) they prefer to mate with a suitable male. Snails used in this study were collected from nature, and so they may have mated before being collected. Although they were maintained separately for 30 days before use in the video recording, it is possible that females can store sperm for over 30 days. Sperm-storing ability of over 30 days has been reported in some apple snails (Albrecht et al. 1996; Estebenet and Martín 2002; Tiecher et al. 2014). If female *P. pesmei* can store sperm, they may then avoid excessive mating with the given experimental male.

Female mate choice has never been reported in apple snails but cannot be ruled out because some females that did not mate in the video recorded mating behaviour trials mated when they were kept in the collective container where several males were present. Presumably, they rejected the given partner but accepted the suitable mate in the collective container.

Should female mate choice exist in this species, it is possible that female resistance is also related to their assessment of the male because five of the six copulating females performed a clear resistance behaviour in the courtship and copulation phases but finally entered the passive stage of the insemination posture. These females may perform resistance behaviour to screen for a suitable mate, for example, rotating their shells to evaluate male size and weight. One potential evidence for this assumption is that four of the six copulating females performed three types of resistance behaviour—jerking, retracting, and swinging—that resulted in shell rotation or movement in different directions. Although these behaviours were performed several times, none of them interrupted the copulation.

There was one mating pair in which the copulation was interrupted. The most noticeable difference in the mating process of this pair compared to the other mating pairs was the withdrawal-wrestling behaviour. The female performed withdrawal-wrestling in the early copulation phase. Although the pair entered the passive stage of the insemination posture at first, the male withdrew the penis sheath from the female pallial cavity after being in the passive stage for 2 h and then reinserted the penis sheath and entered the insemination posture again. Penis sheath withdrawal in the early stage of the insemination posture has previously been reported in *Pomacea canaliculata*. It was assumed that the male withdrew the penis sheath because it could not find the female gonopore or the female closed the gonopore as a last mate-rejection mechanism (Burela and Martín 2009). Following these assumptions, withdrawal-wrestling may play a part in disturbing the penis sheath intromission of *P. pesmei* and, as such, it would be a clear mate-rejection behaviour.

At the end of the mating process, the male dismounted from the female's shell, and the mating pair separated (Burela and Martín 2009; Annate et al. 2023). We followed the behaviour of the snails for one hour after dismounting. All the males spent most of the time resting, and none performed courtship again during this period. It is possible that they need to recover after the energy expenditure during mating. In contrast to males, females spent most of their time moving around in the water and frequently crawling above water. Presumably, they moved above water to find an area for laying eggs.

Apple snails in the genus *Pila* exhibit various aerial egg-laying behaviours, such as *P. globosa* (Swainson, 1822) lays eggs in a hollow on a pond bank (Bahl 1928), *P. virescens* lays eggs on soil near a water line or floating plants (Ng et al. 2020a; Annate et al. 2023), and *P. celebensis* (Quoy & Gaimard, 1834) lays eggs on hard vertical substrates above water (Djajasasmita 1987; Ng et al. 2020a). Most of the apple snails in the genus *Pomacea* lay eggs on hard vertical substrates above water (Hayes et al. 2009, 2015; Burks et al. 2010; Gurovich et al. 2017) except for one species, *Pomacea urceus* (Müller, 1774), which burrows into the soil, then lays eggs in its shell, and aestivates with its eggs over the dry season (Burky et al. 1972). Previously, it was unclear whether *P. pesmei* lays eggs on the soil (Lamkom and Phosri 2017) or in a shallow cavity (Ng et al. 2020a). Here, our results agree with Ng et al. (2020a).

The egg-laying process of *P. pesmei* can be divided into three phases: pre-egg depositing, egg depositing, and post-egg depositing phases. The pre-egg depositing phase started at night when the females first crawled out of the water, which follows the general nighttime oviposition reported for other apple snails (Albrecht et al. 1996; Heiler et al. 2008; Gilal et al. 2015; Gurovich et al. 2017). However, since the egg-laying process of *P. pesmei* lasted over 24 h, then the full egg-laying process occurred during both the day and night.

Prior to laying eggs, *P. pesmei* burrows into the soil, at a depth of 3–5 cm to make an egg-laying cavity. The egg-laying cavity seems important for *P. pesmei* because the female took 10–24 h to make it. In addition, some females performed resting and withdrawal behaviours alternately with burrowing. This could represent the high energy expenditure of the female to burrow the cavity. Laying eggs in a cavity has been previously reported only in *P. globosa*, where the cavity was suggested to be a shelter to protect the eggs from predators, sunlight, and desiccation (Bahl 1928).

The egg-depositing process occurred in-between the ventral foot surface and the soil. Therefore, it was not recorded from the top view camera of the present experimental design. From the top view, the female posture was consistent between all the females and is similar to that reported for *P. globosa*: females protruded their feet roundly with their head parts moderately withdrawn and later their feet became dome shaped for holding and arranging the eggs into egg masses (Bahl 1928). Presumably, the egg-depositing process occurring in between the ventral foot surface and the soil is also similar between the two species.

After depositing eggs, most of the previously studied apple snail species returned to the water immediately or within a short period (Bahl 1928; Albrecht et al. 1996; Annate et al. 2023) except for one species, *Pomacea urceus*, which incubates its eggs and aestivates over the dry season (Burky et al. 1972). In this study, *P. pesmei* did not return to the water, but then stayed in the egg-laying cavities with completely closed apertures. None of the females left their egg masses even after the eggs hatched 20–23 days later. Therefore, it is possible that females of *P. pesmei* may aestivate after laying eggs or that they protect and incubate their eggs, similar to that previously reported in *Pomacea urceus*. However, oviposition in *Pomacea urceus* mostly occurs at the beginning of the dry season and their hatchlings then aestivated until the next rainy season (Burky et al. 1972). In contrast, we found that the oviposition of *P. pesmei* was mainly observed during the first and second observation trials that were conducted between May and July, in the early part of the rainy season. In addition,

some hatchlings of *P. pesmei* emerged from the egg-laying cavity and went into the water before the end of the video recording period. Thus, *P. pesmei* hatchlings may not need to aestivate immediately after hatching as they still have time over the remaining two months of the wet season to grow before the beginning of the dry season. However, for the females, it is questionable why females of *P. pesmei* did not return to the water after egg laying, since they laid eggs in the early rainy season and so do not need to immediately aestivate. We observed that some females in the collective containers, exposed to natural weather conditions, left their egg-laying cavity 7–10 days after laying the eggs following rain. Therefore, it can be assumed that they are more likely to stay in the egg-laying cavity to protect or incubate their eggs than to aestivate. Rain may be a key trigger inducing females to return to the water, explaining why females in the collective containers returned to the water when exposed to rain but those in the egg-laying observation containers, which were under roof cover, never returned to the water because they were never exposed to rain.

In conclusion, our examination into the details of the reproductive behaviour of the Southeast Asian apple snail, *P. pesmei*, revealed its previously unknown mating and egg-laying processes and confirmed the oviposition location of *P. pesmei* in a shallow cavity, as reported by Ng et al. (2020a). Since the oviposition location is a significant character for understanding apple snail evolutionary history (Hayes et al. 2009), confirming the oviposition location of *P. pesmei* contributes to a better understanding of the biology and evolution of the genus *Pila* and the family Ampullariidae. However, confirming the oviposition location of *P. pesmei* from different populations is still needed because the oviposition location of *P. pesmei* in the present study is contradictory to that which was previously reported by Lamkom and Phosri (2017). These contrary reports may reflect a variation in this species between different populations or habitats. Furthermore, Lamkom and Phosri (2017) identified their species as *P. ampullacea* (Linnaeus, 1758) instead, although the image provided, and the distribution and size reported indicated that the species is *P. pesmei*. Thus, it is also possible that the species studied by Lamkom and Phosri (2017) is a different species that shows a similar shell morphology to *P. pesmei*. Based on molecular data, Ng et al. (2020a) suggested the possibility of cryptic species within *P. pesmei* in Thailand. Owing to this uncertainty, we have not compared our data to the previous study by Lamkom and Phosri (2017). Rather, we recommend future research to explore the egg-laying behaviour of *P. pesmei* from different populations, combined with molecular species confirmation of each studied population, to broadly understand the behavioural variation patterns.

## Acknowledgements

We thank Mrs Thevee Khullasood for locality information, permission to collect specimens on her private land and for help in the field sampling; Mr Sangkhom Annate and members of Animal Systematics Research Unit of Chulalongkorn University for assistance in the laboratory; and reviewers for useful suggestions that improved the manuscript. The authors also thank Dr Robert Butcher for helpful English suggestions and grammar corrections.

## Additional information

### Conflict of interest

The authors have declared that no competing interests exist.

### Ethical statement

This study did not require human or animal ethical approval.

### Funding

The main funding support for the project was from The Centre of Excellence on Biodiversity and National Research Council of Thailand (NRCT) (BDC-N34670115). We also acknowledge the Thailand Research Fund for financial support through the Royal Golden Jubilee Ph.D. Program (grant no. PHD/0206/2559) to SA and SP.

### Author contributions

Conceptualization, S.P. and S.A.; Field work, S.A., S.P., T.H.N. and C.S.; Methodology and Investigation, S.A. and S.P.; Writing original draft, S.A. and S.P.; Editing, S.A., S.P., T.H.N. and C.S.; Supervision, S.P., T.H.N. and C.S.

### Author ORCIDs

Supunya Annate  <https://orcid.org/0009-0001-6359-7954>

Ting Hui Ng  <https://orcid.org/0000-0002-5123-0039>

Chirasak Sutcharit  <https://orcid.org/0000-0001-7670-9540>

Somsak Panha  <https://orcid.org/0000-0002-4431-2458>

### Data availability

All of the data that support the findings of this study are available in the main text.

## References

- Albrecht EA, Carreñ NB, Castro-Vazquez A (1996) A quantitative study of copulation and spawning in the South American apple snail, *Pomacea canaliculata* (Prosobranchia: Ampullariidae). *The Veliger* 39(2): 142–147.
- Annate S, Ng TH, Sutcharit C, Panha S (2023) Ethogram and classification of the mating and egg-laying behaviour of the Southeast Asian apple snail *Pila virescens* (De-shayes, 1824) (Mollusca, Gastropoda, Caenogastropoda, Ampullariidae). *ZooKeys* 1180: 295–316. <https://doi.org/10.3897/zookeys.1180.106498>
- Bahl KN (1928) On the reproductive processes and development of *Pila globosa* (Swaison). *Memoirs of the Indian Museum* 9: 1–11.
- Barraud E (1957) The copulatory behaviour of the freshwater snail (*Lymnaea stagnalis* L.). *The British Journal of Animal Behaviour* 5(2): 55–59. [https://doi.org/10.1016/S0950-5601\(57\)80027-6](https://doi.org/10.1016/S0950-5601(57)80027-6)
- Burela S, Martín PR (2007) Nuptial feeding in the freshwater snail *Pomacea canaliculata* (Gastropoda: Ampullariidae). *Malacologia* 49(2): 465–470. <https://doi.org/10.4002/0076-2997-49.2.465>
- Burela S, Martín PR (2009) Sequential pathways in the mating behavior of the apple snail *Pomacea canaliculata* (Caenogastropoda: Ampullariidae). *Malacologia* 51(1): 157–164. <https://doi.org/10.4002/040.051.0111>

- Burks RL, Kyle CH, Trawick MK (2010) Pink eggs and snails: field oviposition patterns of an invasive snail, *Pomacea insularum*, indicate a preference for an invasive macrophyte. *Hydrobiologia* 646: 243–251. <https://doi.org/10.1007/s10750-010-0167-1>
- Burky AJ, Pacheco J, Pereyra E (1972) Temperature, water, and respiratory regimes of an amphibious snail, *Pomacea urceus* (Müller), from the Venezuelan Savannah. *Biological Bulletin* 143(2): 304–316. <https://doi.org/10.2307/1540055>
- Cowie RH (2015) The Recent apple snails of Africa and Asia (Mollusca: Gastropoda: Ampullariidae: *Afropomus*, *Forbesopomus*, *Lanistes*, *Pila*, *Saulea*): a nomenclatural and type catalogue. The apple snails of the Americas: addenda and corrigenda. *Zootaxa* 3940(1): 1–92. <https://doi.org/10.11646/zootaxa.3940.1.1>
- DeWitt TJ (1991) Mating behavior of the freshwater pulmonate snail, *Physa gyrina*. *American Malacological Bulletin* 9(1): 81–84.
- Djajasmita M (1987) The apple snail *Pila ampullacea*: food and reproduction (Gastropoda: Ampullariidae). *Berita Biologi* 3(7): 342–346.
- Estebenet AL, Martín PR (2002) *Pomacea canaliculata* (Gastropoda: Ampullariidae): life-history traits and their plasticity. *Biocell* 26(1): 83–89.
- Facon B, Ravigné V, Goudet J (2006) Experimental evidence of inbreeding avoidance in the hermaphroditic snail *Physa acuta*. *Evolutionary Ecology* 20(5): 395–406. <https://doi.org/10.1007/s10682-006-0009-9>
- Gilal AA, Muhamad R, Omar D, Aziz N, Gnanasegaram M (2015) Effectiveness of an automated digital infrared CCTV multi-camera system in investigating mating and oviposition behavior of apple snails, *Pomacea* spp. *Journal of Entomology and Zoology Studies* 3(4): 254–259.
- Gurovich FM, Burela S, Martín P.R (2017) First description of egg mass, oviposition and copulation of a neglected apple snail endemic to the Iguazú and Alto Paraná Rivers. *Molluscan Research* 37(4): 242–251. <https://doi.org/10.1080/13235818.2017.1357090>
- Hayes KA, Cowie RH, Jørgensen A, Schultheiß R, Albrecht C, Thiengo SC (2009) Molluscan models in evolutionary biology: apple snails (Gastropoda: Ampullariidae) as a system for addressing fundamental questions. *American Malacological Bulletin* 27(1/2): 47–58. <https://doi.org/10.4003/006.027.0204>
- Hayes KA, Burks RL, Castro-Vazquez A, Darby PC, Heras H, Martín PR, Qiu JW, Thiengo SC, Vega IA, Wada T, Yusa Y, Burela S, Cadierno MP, Cueto JA, Dellagnola FA, Dreon MS, Frassa MV, Giraud-Billoud M, Godoy MS, Ituarte S, Koch E, Matsukura K, Pasquevich MY, Rodriguez C, Saveanu L, Seuffert ME, Strong EE, Sun J, Tamburi NE, Tiecher MJ, Turner RL, Valentine-Darby PL, Cowie RH (2015) Insights from an integrated view of the biology of apple snails (Caenogastropoda: Ampullariidae). *Malacologia* 58(1–2): 245–302. <https://doi.org/10.4002/040.058.0209>
- Heiler KCM, Von Oheimb PV, Ekschmitt K, Albrecht C (2008) Studies on the temperature dependence of activity and on the diurnal activity rhythm of the invasive *Pomacea canaliculata* (Gastropoda: Ampullariidae). *Mollusca* 26(1): 73–81.
- Keawjam RS (1986) The apple snails of Thailand: distribution, habitats and shell morphology. *Malacological Review* 19(1–2): 61–81.
- Keawjam RS (1987) The apple snails of Thailand: aspects of comparative anatomy. *Malacological Review* 20(1–2): 60–89.
- Keawjam RS (1990) The apple snails of Thailand: molecular genetics. *Journal of Medical and Applied Malacology* 2: 1–44.
- Lamkom T, Phosri D (2017) Study on gonadosomatic index of Thai native apple snail (*Pila ampullacea* Linnaeus, 1758) in the rice fields of Sriruamng-mai district, Ubon

- Ratchathani and effect of diet on the growth of juveniles. *Journal of Fisheries and Environment* 41(1): 27–36.
- Marwoto RM, Heryanto H, Joshi RC (2020) The invasive apple snail *Pomacea canaliculata* in Indonesia: a case study in Lake Rawa Pening, Central Jawa. *BIO Web of Conferences* 19: 1–5. <https://doi.org/10.1051/bioconf/20201900014>
- Ng TH, Annate S, Jeratthitikul E, Sutcharit C, Limpanont Y, Panha S (2020a) Disappearing apple snails (Caenogastropoda: Ampullariidae) of Thailand: a comprehensive update of their taxonomic status and distribution. *Journal of Molluscan Studies* 86(4): 290–305. <https://doi.org/10.1093/mollus/eyaa015>
- Ng TH, Jeratthitikul E, Sutcharit C, Chhuoy S, Pin K, Pholyotha A, Siriwut W, Srisonchai R, Hogan ZS, Ngor PB (2020b) Annotated checklist of Freshwater molluscs from the largest freshwater lake in Southeast Asia. *ZooKeys* 958: 107–141. <https://doi.org/10.3897/zookeys.958.53865>
- Ngor PB, Sor R, Prak LH, So N, Horgan ZS, Lek S (2018) Mollusc fisheries and length-weight relationship in Tonle Sap flood pulse system, Cambodia. *International Journal of Limnology* 54: 34. <https://doi.org/10.1051/limn/2018026>
- Oliveira RF, Taborsky M, Brockmann HJ (2008) *Alternative Reproductive Tactics: an Integrative Approach*. Cambridge University Press, Cambridge, 507 pp. <https://doi.org/10.1017/CBO9780511542602>
- Tiecher MJ, Burela S, Martín PR (2014) Mating behavior, egg laying and embryonic development in the South American apple snail *Asolene pulchella* (Ampullariidae: Caenogastropoda). *Invertebrate Reproduction and Development* 58(1): 13–22. <https://doi.org/10.1080/07924259.2013.793624>



# Topotypes of the millipede species *Kronopolites swinhoei* (Pocock, 1895) reveal a new synonym with revalidation of *Kronopolites svenhedini* (Verhoeff, 1934) (Diplopoda, Polydesmida, Paradoxosomatidae)

Yuan Xiong<sup>1</sup>, Huiming Chen<sup>2</sup>, Xuankong Jiang<sup>2</sup>, Chao Jiang<sup>1</sup>

1 State Key Laboratory for Quality Ensurance and Sustainable Use of Dao-di Herbs, National Resource Center for Chinese Materia Medica, China Academy of Chinese Medical Sciences, 100700, Beijing, China

2 Institute of Biology, Guizhou Academy of Sciences, Guiyang 550009, China

Corresponding authors: Xuankong Jiang ([antoma93@gmail.com](mailto:antoma93@gmail.com)); Chao Jiang ([jiangchao0411@126.com](mailto:jiangchao0411@126.com))



Academic editor: Michelle Hamer

Received: 24 September 2024

Accepted: 12 February 2025

Published: 10 March 2025

ZooBank: <https://zoobank.org/8447554B-8E25-447E-8C05-2D823F66C8DD>

Citation: Xiong Y, Chen H, Jiang X, Jiang C (2025) Topotypes of the millipede species *Kronopolites swinhoei* (Pocock, 1895) reveal a new synonym with revalidation of *Kronopolites svenhedini* (Verhoeff, 1934) (Diplopoda, Polydesmida, Paradoxosomatidae). ZooKeys 1231: 85–98. <https://doi.org/10.3897/zookeys.1231.137769>

Copyright: © Yuan Xiong et al.  
This is an open access article distributed under terms of the Creative Commons Attribution License (Attribution 4.0 International – CC BY 4.0).

## Abstract

The millipede genus *Kronopolites* Attems, 1914 was originally described by monotypy with *Strongylosoma swinhoei* Pocock, 1895 as the type species, which was based on a single female specimen. Although this species has been believed to be widespread in China, there have been no confirmed reports of it from its type locality, leading to uncertainty about its taxonomic status. To address this issue, we newly sampled specimens from its type locality in Zhifu, Shandong Province, China. Our morphological analysis suggests that *Kronopolites swinhoei* (Pocock, 1895) should be reclassified as *Nedyopus swinhoei* (Pocock, 1895) **comb. nov.** and is a senior synonym of *Nedyopus patrioticus* Attems, 1898, **syn. nov.** The results also support the recovery of the name *Kronopolites svenhedini* (Verhoeff, 1934) **sp. reval.**, which was previously misidentified as a junior synonym under *K. swinhoei*. The former is now the genus type of *Kronopolites*.

**Key words:** New combination, revalidation, revision, taxonomy, topotypes

## Introduction

Pocock (1895) described Chilopoda and Diplopoda from the coastal regions of China and Japan and treated 18 millipede species, including 17 species new to science. These are some of the earliest millipede findings documented in China. *Strongylosoma swinhoei* Pocock, 1895 was initially described based on exclusively a female specimen from Zhifu (= Chee Foo) Island in Yantai, Shandong Province. In 1914, Attems established the genus *Kronopolites* by monotypy with this species. However, subsequent identification by Brölemann (1896) of specimens from Zhoushan Island, Zhejiang Province as *K. swinhoei*, without examination of the gonopods, led to the premature acceptance of its wider distribution. To date, *K. swinhoei* has been documented in Chongqing, Gansu, Guizhou, Qinghai, Shaanxi, Shandong, Sichuan, Yunnan, and Zhejiang provinces (Golovatch 2019; Chen et al. 2023); all of these are geographically

distant from Zhifu Island, Shandong Province. This casted further doubt on the validity of the identification of this species.

Attems (1914) established the genus *Kronopolites* by monotypy with *Strongylosoma swinhoei* (Pocock, 1895), based on the wide tibia of the gonopod. The genus *Kronopolites* has since undergone two revisions, first by Hoffman (1962) and later by Likhitrakarn et al. (2015), and currently comprises 12 species, which are mainly distributed in China, Kashmir Himalaya, Laos, Nepal, Thailand, and Vietnam, with five species found in China (Golovatch 2020; Golovatch and Semenyuk 2021). However, the male of *K. swinhoei* has never been verified from its type locality, which poses challenges to the comprehensive understanding of this species and the genus (Hoffman 1962).

To address this issue, millipedes closely matching Pocock's description were collected on Zhifu Island and identified as topotypic *K. swinhoei*. Subsequent morphological studies indicate that Brölemann's identification of *K. swinhoei* was incorrect. Consequently, it is determined that *K. swinhoei* belongs to the genus *Nedyopus* and is a senior synonym of *Nedyopus patrioticus* (Attems, 1898), which is widely distributed in East Asia. This removal of *K. swinhoei* from *Kronopolites* leads to the revalidation and reassignment of *Kronopolites svenhedini* (Verhoeff, 1934), instead, as the type species of the genus *Kronopolites*.

## Materials and methods

Specimens were collected by tweezers and preserved in 75% ethanol for morphological studies. Live animals were photographed with a Sony A7R4A camera with a Sony FE 90 mm macro lens. Specimens are deposited in National Resource Center for Chinese Materia Medica, China Academy of Chinese Medical Sciences, Beijing, China (**CMMI**) and the Institute of Biology, Guizhou Academy of Sciences, Guiyang, China (**IBGAS**). All specimens deposited in CMMI are numbered and stored according to the collection date (year/month/day) plus an auto-incrementing serial number. If the dates are the same for the same collection site, only the numbers will be retained (e.g. 20230922044 and 20230922045 will be changed into 20230922044 and -45).

Specimens were examined, photographed, and measured using a Leica M205 MCA microscope equipped with a Leica DMC 6200 camera and LAS software v. 4.1 (Leica, Germany). Photos were converted into hand-drawn illustrations using SKETCHBOOK v. 6.0.6. Maps were generated with ArcMap v. 10.7.1 software (Figs 4,7). Grammarly was used to polish English in the manuscript. Terminology is from Hoffman (1962), Chen et al. (2006b), and Likhitrakarn et al. (2015).

## Results

### Taxonomy

**Family Paradoxosomatidae Daday, 1889**

**Subfamily Paradoxosomatinae Daday, 1889**

**Tribe Nedyopodini Attems, 1898**

**Genus *Nedyopus* Attems, 1914**

**Type species.** *Orthomorpha cingulata* Attems, 1898, by original designation.

***Nedyopus swinhoei* (Pocock, 1895), comb. nov.**

Figs 1A, 2–4

*Stronglosoma Swinhoei* Pocock, 1895: 354–355. Type specimen: holotype female, collected from Chee Foo (= Zhifu), Yantai, Shandong Province of China, deposited at the British Museum of Natural History (Hoffman 1962), not examined.

*Kronopolites swinhoei*: Attems 1914.

*Strongylosoma patrioticum* Attems, 1898: 300, figs 12, 13. Type locality: Japan. New synonymy.

*Nedyopus patrioticus*: Attems 1914: 201; Attems 1937: 138–139; Takashima 1949:17; Takakuwa 1954: 47; Takashima and Haga 1956: 332; Miyosi 1959: 49, 71; Wang 1964: 71; Wang 1996: 87; Mikhaljova et al. 2000: 119; Korsós 2004: 23; Chen et al. 2006b: 3998–4000; Nguyen and Sierwald 2013: 1231. New synonymy.

**Diagnosis.** Differs from other species of the genus by the following combination of characters. The metaterga have strong contrasting colors, which are not circularly patterned as in other *Nedyopus* species, and the gonopod femur suddenly widens at the base, with I' and I'' not jagged.

**Material examined. CHINA – Anhui Province:** • 1 ♂, Fuyang, 30.I.2020, Yihao Ge leg. (IBGAS). • **Jiangxi Province:** 1 ♂ and 1 ♀, Ji'an, (27.1439°N, 115.0426°E), 50 m a.s.l., 19.V.2017, Xuankong Jiang leg. (IBGAS). • **Shandong Province:** 1 ♂ and 1 ♀ (20231025001), Yantai, Zhifu District, Zhifu Island, (37.6100°N, 121.3716°E), 40 m a.s.l., 25.X.2023, Xuankong Jiang, Tian Lu and Chongwu Lu leg. (CMMI); • 16 ♂♂ and 12 ♀♀, same data, (IBGAS); • 15 ♂♂ and 13 ♀♀, Yantai, Zhifu District, Tashan Park, (37.5056°N, 121.3972°E), 290 m a.s.l., 24.X.2023, Xuankong Jiang, Tian Lu and Chongwu Lu leg. (IBGAS).

**Description.** Length ca 17.5–25.1 mm (♂), 18.2–32.7 mm (♀) with 20 segments. Live color variable (Fig. 1A). Posterior half of each metazonae with transverse band, pale yellow to orange. Antennomere 1–6 dark brown, antennomere 7 whitish. Legs light yellow (Fig. 2A–H).

Clypeolabral region and vertex densely setose. Epicranial suture distinct. Width of body gradually expanded from head to 5<sup>th</sup> segment, approximately equal in width from 5<sup>th</sup> to 16<sup>th</sup> segments, and tapering from 16<sup>th</sup> to telson. Caudal corner of collum broadly rounded, declined ventrad, produced behind rear tergal margin (Fig. 2A, B).

Cuticle shining (Fig. 2A, C, F); surface below paranota finely microgranulate (Fig. 2B, D, G). Paranota strongly developed (Fig. 2A, B, C, F), slightly upturned, lying rather high (at upper 1/3 of body) but below dorsum; anterior edge broadly rounded and narrowly bordered; posterior edge nearly straight. Ozopores evident, lying on paranota at its posterior margin, in segments 5, 7, 9, 10, 12, 13, 15–19. Transverse sulcus usually distinct (Fig. 2A, C, F), complete on metaterga 5–18 (♂), narrow, linear, shallow, reaching bases of paranota, faintly ribbed at bottom. Stricture between pro- and metazonae evident, broad and deep, ribbed at dorsal side down to base of paranota (Fig. 2A–F). Pleurosternal carinae with a sharp caudal tooth on segments 3–6. Epiproct (Fig. 2G, H) conical, flattened dorsoventrally; tip subtruncate; pre-apical papillae small, lying close to tip. Hypoproct roundly subtriangular, spinnerets at caudal edge small and well separated (Fig. 2H). Sterna densely setose, without modifications, but with two small, rounded, fully separated, setose cones between ♂ coxae 4 (Fig. 2E).

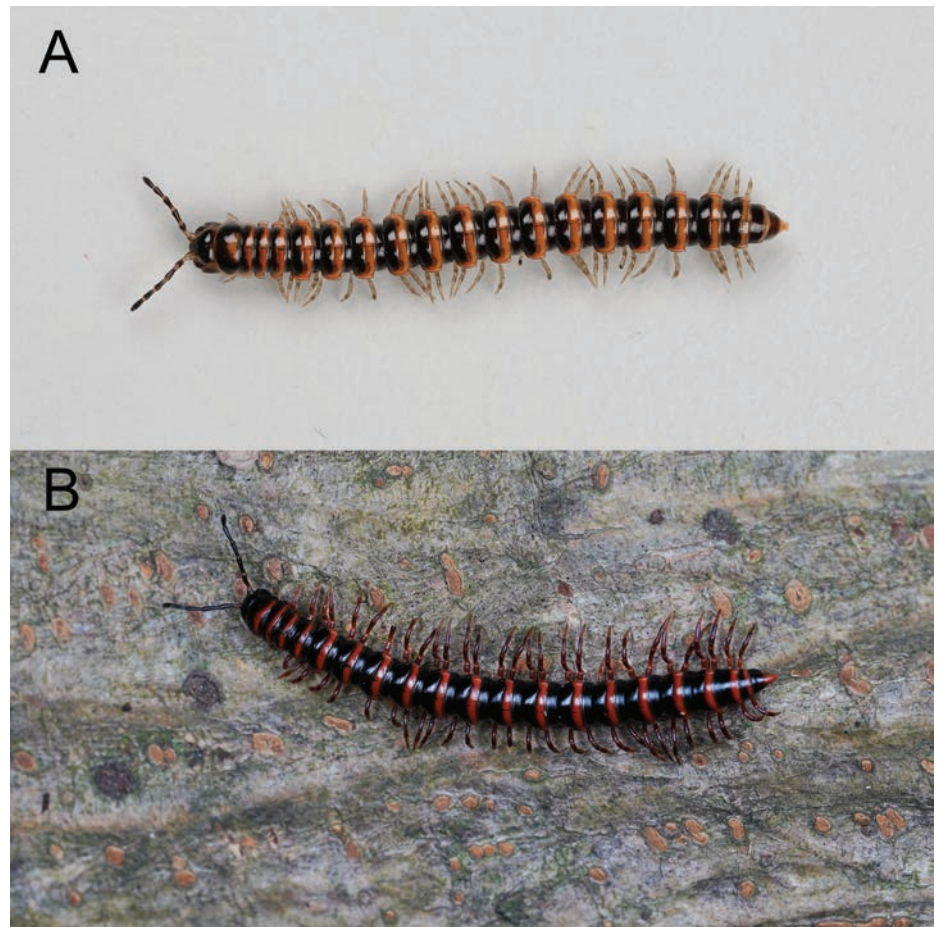


**Figure 1.** Live specimens **A** *Nedyopus swinhoei* (Pocock, 1895) comb. nov. from Zhifu Island, Shandong, China **B** *Kronopolites svenhedini* (Verhoeff, 1934) sp. reval. from Xinyang, Henan, China. Not to scale. Photographs by Xuankong Jiang.

Gonopods (Fig. 3) intricate. Coxite elongate, subcylindrical, strongly setose distoventrally. Prefemoral part nearly half femoral length. Femorite short and bulge out at one end like a belly, distal portion carrying two lobes (I' and I''). I' parallel to solenophore. Solenophore lamelliform, twisted distally. Solenomere short and flagelliform.

**Distribution.** China: Anhui (New record), Jiangsu, Jiangxi (New record), Shandong, Taiwan (Pocock 1895; Chen et al. 2006b; Zhang et al. 2024); Indonesia, Japan, Korea (Nguyen and Sierwald 2013).

**Remarks.** The specimens from Zhoushan Island were initially identified as *K. swinhoei* by Brölemann in 1896, without providing a justification. However, our investigation reveals a distinct divergence from the original description. For instance, the specimens from Zhoushan are notably larger (47 mm vs 35 mm) and have more vivid in color on the metazonites (orange-red vs yellow).

During our research in Zhifu, we found a species that closely matches Pocock's description, leading us to confidently identify it as *K. swinhoei*. On examination of the topotypes, we observed significant differences in the gonopods compared to Brölemann's illustrations (1896). These differences, including the femorite (strongly twisted and expanded in *Nedyopus* vs straight in *Kronopolites*), the postfemoral sulcus (missing in *Nedyopus* vs existed in *Kronopolites*) and the solenophore (lamelliform in *Nedyopus* vs tubuliform

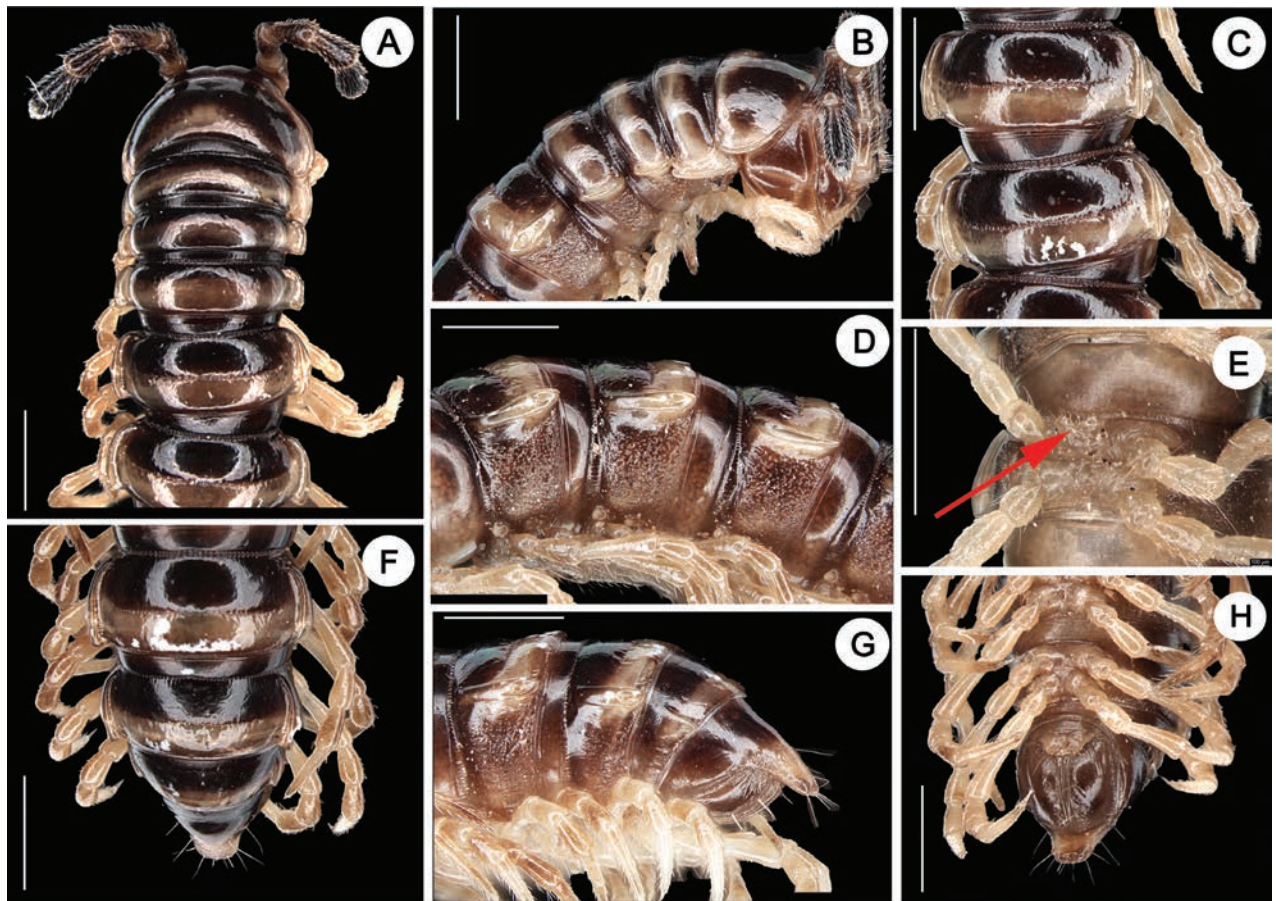


**Figure 2.** *Nedyopus swinhoi* comb. nov. **A** anterior part of body, dorsal view **B** anterior part of body, lateral view **C** segments 10 and 11, dorsal view **D** segments 9–11, lateral view **E** sternal cones between coxae 4, anterior view **F–H** posterior part of body, dorsal, lateral, and ventral view, respectively. Scale bar: 1 mm.

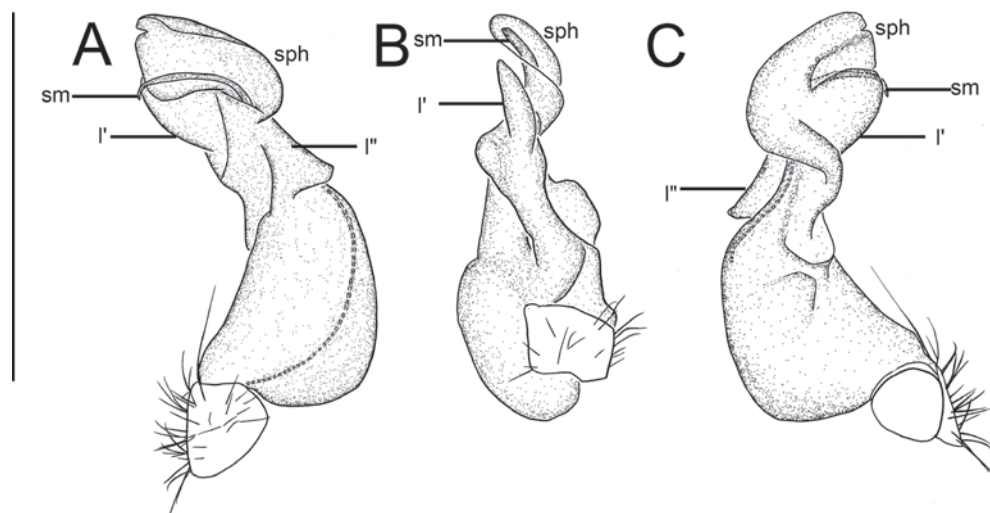


**Figure 3.** *Nedyopus swinhoi* comb. nov., left gonopod **A** lateral view **B** dorsal view **C** mesal view. sm, solenomere; sph, solenophore; l', l''. Scale bar: 1 mm.

in *Kronopolites*), indicate that this species belongs to *Nedyopus* rather than *Kronopolites*, and is identical to the widespread species *Nedyopus patrioticus* (Attems, 1898). Consequently, *K. swinhoi* is formally transferred to *Nedyopus*,

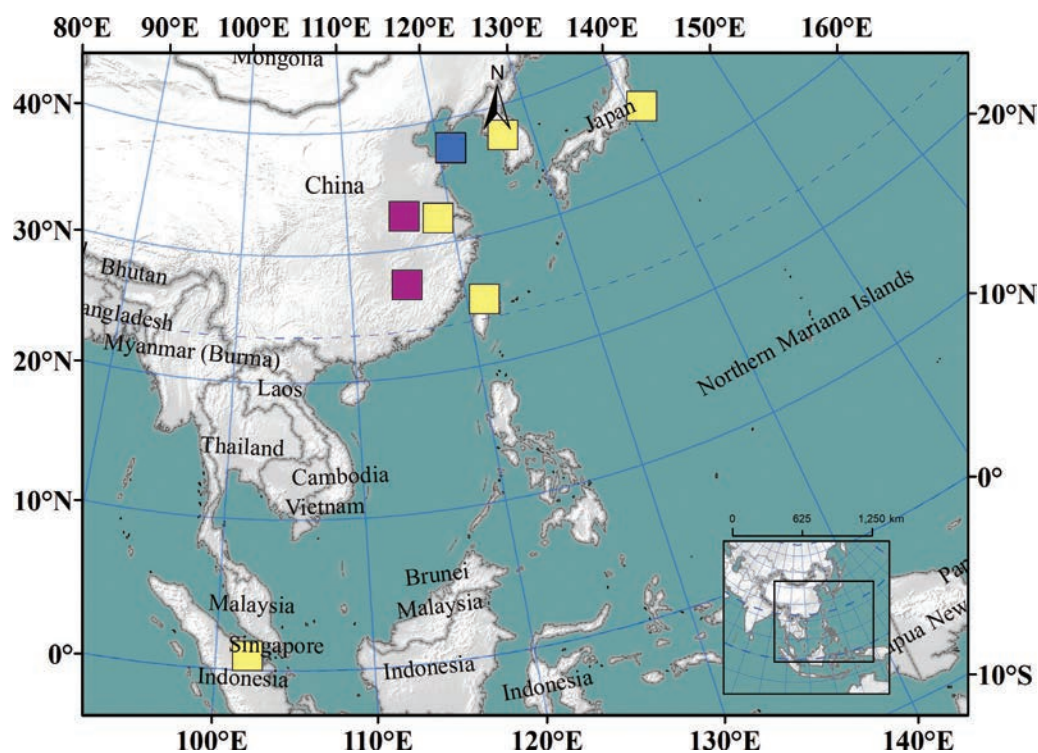


Figure 4. Distribution of *Nedyopus swinhoi* comb. nov. Yellow: literature records; purple: specimens collected in this article; blue: type locality.

and *Nedyopus patrioticus* is considered a junior synonym of *Nedyopus swinhoi* (Pocock, 1895) comb. nov. Additionally, *N. patrioticus* consists of two subspecies *Nedyopus patrioticus patrioticus* (Attems, 1898) from Japan and *Nedyopus patrioticus unicolor* (Carl, 1902) from Indonesia. Therefore, the subspecies *unicolor* should be treated as *Nedyopus swinhoi unicolor* (Carl, 1902) comb. nov.

*Nedyopus swinhoi* (Pocock, 1895) comb. nov. has a wide distribution across Asia, from Indonesia to China, Korea, and Japan (Wang 1955; Nguyen and Sierwald 2013). This species is often found near human habitation and may spread through human activities. In China, documented records of this species were limited to Jiangsu, Shandong, and Taiwan provinces (Pocock 1895; Wang 1955; Zhang et al. 2024), possibly due to limited investigation. Our study identified additional distribution locations in Anhui and Jiangxi, suggesting that the species might be found in other regions across China in the future.

### Tribe Sulciferini Attems, 1898

#### Genus *Kronopolites* Attems, 1914

*Kronopolites* Attems 1914: 219.

*Kronopolites*: Attems 1929: 272; 1931: 113; 1936: 225; 1937: 49; Verhoeff 1939: 274; Takashima 1950: 38; Takakuwa 1954: 30; Hoffman 1962: 579; 1980: 169; Jeekel 1971: 225; 1982: 243; 1988: 98; Chen et al. 2006a: 252; Golovatch 2009: 121; 2013: 12; Nguyen and Sierwald 2013: 1286; Likhitrakarn et al. 2015: 32; Golovatch 2015: 135; Golovatch 2016: 1; Golovatch 2019: 348; Golovatch and Liu 2020: 170; Golovatch and Semenyuk 2021: 479.

*Kansupus* Verhoeff 1934: 17, synonymized by Attems (1936: 233).

*Kansupus*: Jeekel 1971: 225; Hoffman 1980: 169.

*Parakansupus* Verhoeff 1939: 273, synonymized by Hoffman (1962: 579).

*Parakansupus*: Jeekel 1971: 230; Hoffman 1980: 169.

**Type species.** *Kronopolites svenhedini* (Verhoeff, 1934) sp. reval., by present designation.

**Diagnosis.** See Likhitrakarn et al. (2015: 29).

**Remarks.** Attems (1914) established the genus and designated *Strongylosoma swinhoei* Pocock, 1895 as the type species by monotypy. However, due to the misidentification of this species, which was later transferred to *Nedyopus*, the correct designation by Attems, *Kronopolites svenhedini* (Verhoeff, 1934) sp. reval., has now been reclassified as the type species of the genus.

***Kronopolites svenhedini* (Verhoeff, 1934) sp. reval.**

Figs 1B, 5–7

*Strongylosoma Swinhoei*: Brölemann 1896: 354–357, fig. 9–11; Attems 1898: 304 (misidentified).

*Kansupus svenhedini* Verhoeff, 1934: 17, figs.4–8, synonymized by Hoffman 1962: 581. Type locality: N. O. Szetschuan (= northeastern Sichuan Province), China; ♂ and Süd-Kansu (= Longnan, Gansu Province, China; ♀).

*Kronopolites swinhoei*: Attems 1914: 219; Attems 1936: 226, fig. 44; Attems 1937: 50–51, fig. 64; Chamberlin and Wang 1953: 5; Hoffman 1962: 581–583, figs 1, 2; Golovatch 1978: 678; 1982: 298; Wang 1996: 86; Geoffroy and Golovatch 2004: 20; Korsós 2004: 23; Chen et al. 2006a: 252; Golovatch 2009: 121; 2013: 2, figs 1–4; Nguyen and Sierwald 2013: 1286; Likhitrakarn et al. 2015: 32; Golovatch 2016: 1; 2019: 348, figs 4, 5; 2020: 166; Golovatch and Liu 2020: 170; Golovatch and Semenyuk 2021: 479, figs 28–30 (misidentified).

*Kronopolites svenhedini*: Attems 1936: 233; 1937: 53, fig. 66; Zhang and Li 1978: 12; Wang 1996: 86.

*Kansupus svenhedini* var. *dentiger* Verhoeff, 1934: 19, fig. 9; Attems 1936: 233; Attems 1937: 54, synonymized with *Kronopolites swinhoei* by Hoffman 1962: 581. Type locality: Pei-shui-ho (= Baishuijiang National Nature Reserve), Wen County, Gansu Province, China).

**Material examined. CHINA – • Gansu Province:** 5 ♂♂ and 40 ♀♀ (20230922044, -45, -46, 20230922048–20230922051, 20230922054–20230922057, -60, -61, -63, -66, -67, -68, -70, -72, -73, -75, -76, 20230922078–20230922090, 20230922092–20230922098, -101, -102, -104), Lintao County, Fenghuangshan Forest Park (35.4009°N, 103.8901°E), 1960 m a.s.l., 22.IX.2023, Tianyun Chen, Jiabo Fan & Yiyang Zhao leg., (CMMI); • 2 ♂♂ and 2 ♀♀, Dingxi City, Anding District, Guanying Town, Yawan Village, 27.VI.2008, Zhiyong Di leg., (IBGAS). • **Henan Province:** 1 ♂ and 2 ♀♀, Xinyang City, Dabieshan station (32.1252°N, 114.0118°E), 110 m a.s.l., 10.VIII.2023, Xuankong Jiang & Leilei Shi leg., (IBGAS); • 1 ♂ and 1 ♀ 5J, Xinyang City, Shihe district, Bailongtan Reservoir (31.9987°N, 113.9105°E), 230 m a.s.l., 10.VIII.2023, Xuankong Jiang & Leilei Shi leg., (IBGAS); • 17 ♂♂ and 5 ♀♀ 3J, Xinyang, Nanwan Reservoir (32.1252°N, 114.0118°E), 110 m a.s.l., 9.VIII.2023,

Xuankong Jiang & Leilei Shi leg., (IBGAS). • **Qinghai Province**: 3 ♂♂ and 10 ♀♀, Huangnan Tibetan Autonomous Prefecture, Jianzha County, Zhiyong Di leg., (IBGAS). • **Shaanxi Province**: 1 ♂ (20190907029), Mei County, Honghegu National Forest Park (34.0533°N, 107.7836°E), 1730 m a.s.l., 7.IX.2019, Chao Jiang leg., (CMMI); • 3 ♂♂ and 4 ♀♀ (20200905117, -118, 20230802001, -02), Xi'an, Hui District, Taiping National Forest Park (33.9951°N, 108.7163°E), 540 m a.s.l., 2.VIII.2023, Tianyun Chen & Yuan Xiong leg., (CMMI). • **Zhejiang Province**: 3 ♂♂ and 3 ♀♀, Anji County, Longwangshan Scenic Area, 22.VII.2018, Rong Fu leg., (IBGAS).

**Diagnosis.** Differs from other species of the genus by the following combination of characters: metazonae have two shapes, either as a transverse band or a median oval spot, and also have two color variations, ranging from pale yellow to orange-red; paraterga relatively poorly developed, set lower (mostly at about 1/3 height of segments), caudal corners usually not surpassing rear tergal contours, at most narrowly rounded; ♂ sternal cones present; processes *a* and *b* of gonopod on a broad common stem, neither slender nor long (Golovatch 2009).

**Description.** Length ca 26.0–50.0 mm (♂), 27.0–60.0 mm (♀) with 20 segments. Live color variable (Fig. 1B). Head, prozonae, anterior part of collum, and metazonae black; posterior part of collum and each metazonite with transverse band or oval spot, pale yellow to orange-red. If the patches not covering ozopores, then the ozopores exhibit the same color of the patches. Telson black with color of tip identical to the patches. Antennae black; legs black to reddish brown (Fig. 5A–H).

Head densely setose. Antennae moderately long (Fig. 5A), extending behind body segment 3 when stretched dorsally. Width gradually widened from collum to 5<sup>th</sup> segment, roughly equal in 5<sup>th</sup>–16<sup>th</sup> segments, and tapering from 16<sup>th</sup> to telson.

Collum of different specimens with one or two transverse rows of setae, one row with 1+1 anterior, two rows with 1+1 at both anterior and intermediate. Caudal corner of collum very broadly rounded, declined ventrad, produced behind rear tergal margin (Fig. 5A, B).

Cuticle shining, prozonae finely shagreened, metaterga finely rugulose (Fig. 5A, C, F), surface below paranota finely microgranulate (Fig. 5B, D). Post-collum metaterga with one transverse row of setae: 4+4 or 3+3 in anterior (pre-sulcus). Tergal setae long and slender, mostly abraded. Paranota well developed (Fig. 5A–F), lying rather high (at upper 1/2 of body), arched. Ozopores evident, lateral, lying in an ovoid groove at about 1/4 in front of posterior edge of metaterga, in segments 5, 7, 9, 10, 12, 13, 15–19. Transverse sulcus usually distinct (Fig. 5A, C, F), slightly incomplete on segment 18, complete on metaterga 3–18 (♂), narrow, linear, shallow, reaching bases of paranota, faintly ribbed at bottom. Stricture between pro- and metazonae evident, broad and deep, ribbed at bottom down to base of paranota (Fig. 5A, B, D, G). Pleurosternal carinae with a sharp caudal tooth on segments 2–7, thereafter increasingly strongly reduced until 18<sup>th</sup> segment (♂). Epiproct (Fig. 5G, H) conical, flattened dorsoventrally, with two small apical papillae; tip subtruncate; pre-apical papillae small, lying close to tip. Hypoproct roundly subtriangular, spinnerets at caudal edge small and well separated (Fig. 5H). Sterna densely setose with a long tongue-shaped process on ♂ coxae 4 (Fig. 5E). Legs rather long and slender (Fig. 5A, B, D, G).

Coxite of gonopods (Fig. 6) thick, pressing inwards on the spermathecal fossa in the prefemur. Prefemur short, with numerous slender setae. Femorite rather stout, with an evident mesal groove and a strong distolateral sulcus demarcating a postfemoral part; the latter well developed, with very prominent

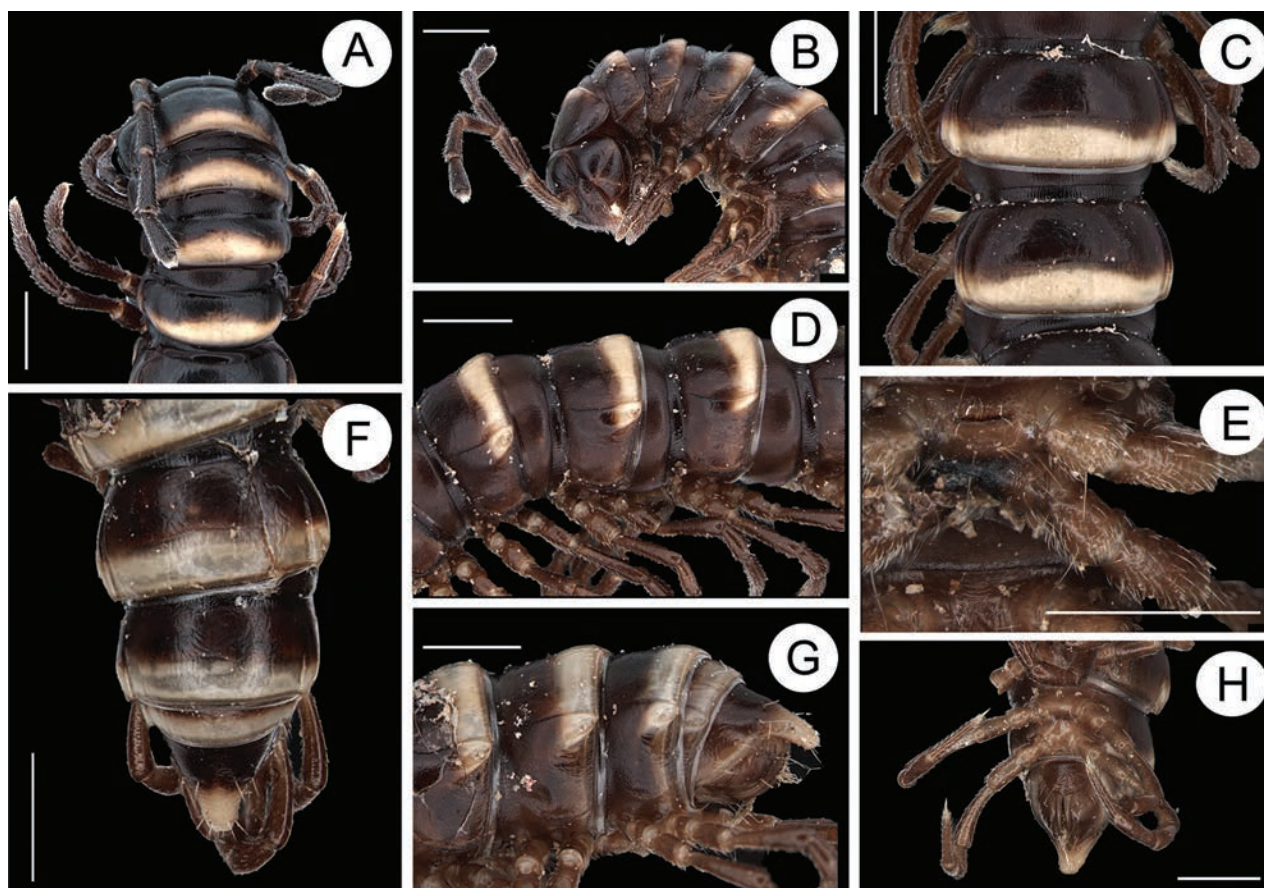


**Figure 5.** *Kronopolites svenhedini* sp. reval. **A** anterior part of body, dorsal view **B** anterior part of body, lateral view **C** segments 10 and 11, dorsal view **D** segments 9–11, lateral view **E** sternal cones between coxae 4, ventral view **F–H** posterior part of body, dorsal, lateral and ventral views, respectively. Scale bars: 1 mm.

bipartite, crescent-shaped, lateral processes: process *a* rather long and broad; process *b* short, broad and pointed. Solenophore in the form of a long, tubular branch. Solenomere flagelliform.

**Distribution.** China: Chongqing, Qinghai, Gansu, Guizhou, Henan (new record), Shaanxi, Sichuan, Yunnan and Zhejiang (Golovatch 2019; Chen et al. 2023).

**Remarks.** Verhoeff (1934) described a new monotypic genus and species, *Kansupus svenhedini*, based on specimens from Gansu, China. Later, Attems (1936) and Hoffman (1962) synonymized the name with *Kronopolites* and *K. swinhoei* respectively, relying on Brölemann's (1896) description. However, our research shows that Brölemann (1896) misidentified this species. Thus, *K. svenhedini* sp. reval. should be resurrected. To maintain the stability of the taxonomic name *Kronopolites*, the type species of *Kronopolites* now fixed (under Article 70.3 of the International Code of Zoological Nomenclature 1999) as *Kronopolites svenhedini* (Verhoeff, 1934), which was misidentified as *Kronopolites swinhoei* (Pocock, 1895) in the original designation by Attems (1914). Furthermore, the publications mentioning this species did not state where the type specimen is preserved, rendering the location of its storage unknown (Verhoeff 1934; Attems 1936, 1937; Hoffman 1962; Zhang and Li 1978; Wang 1996).

*Kronopolites svenhedini* (Verhoeff, 1934) sp. reval. is widely distributed in China, with the westernmost occurrence in Qinghai, the easternmost in Zhejiang, the southernmost in Yunnan and the northernmost in Gansu. It shows variation in

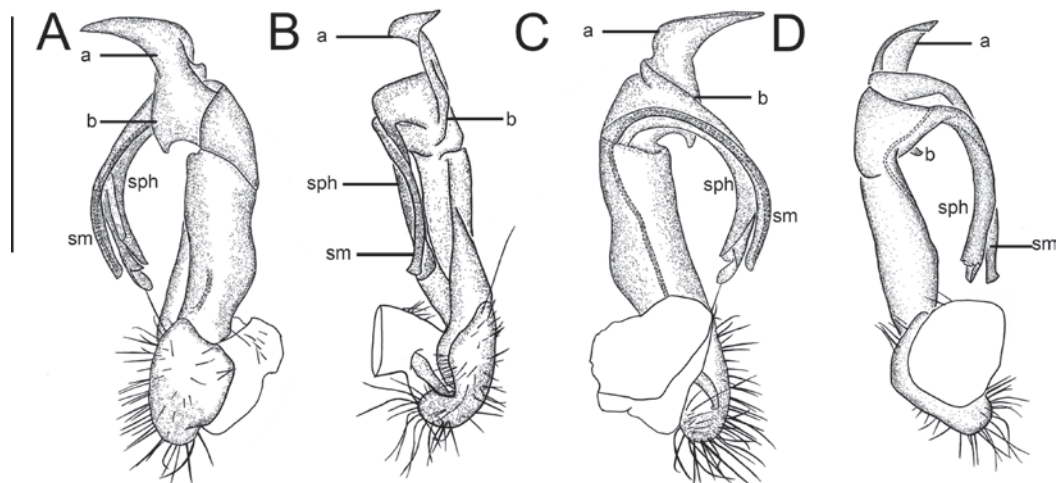


**Figure 6.** *Kronopolites svenhedini* sp. reval, left gonopod **A** ventral view **B** mesal view **C** dorsal view **D** lateral view. sm, solenomere; sph, solenophore; a, b. Scale bar: 1 mm.

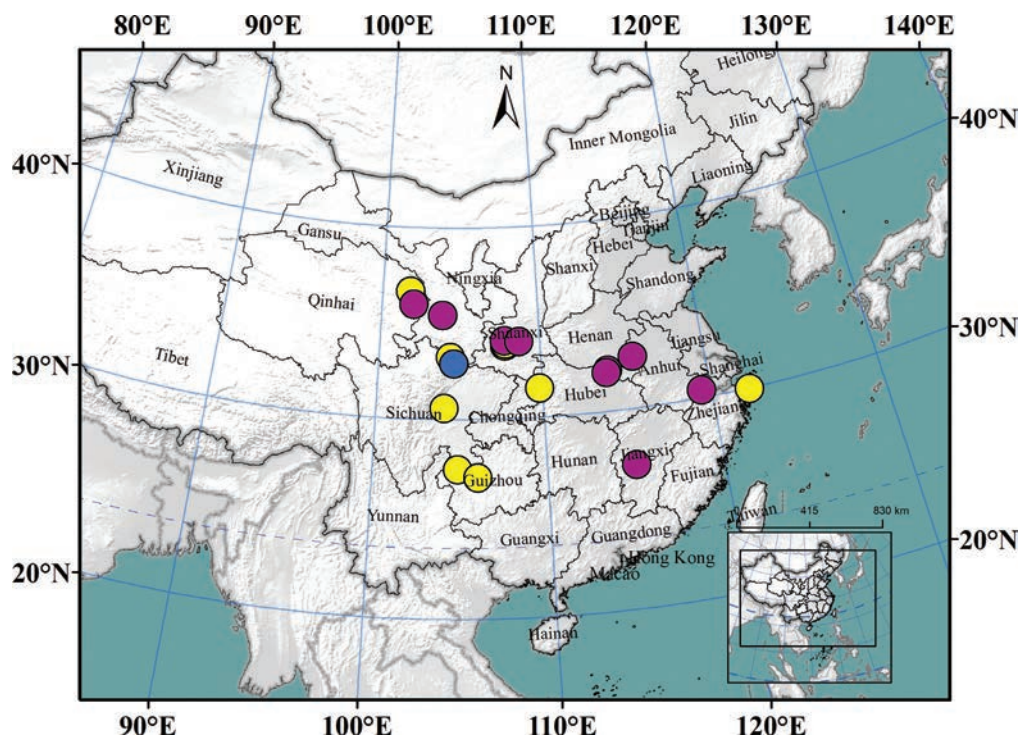


**Figure 7.** Distribution of *Kronopolites svenhedini* sp. reval. Yellow: literature records; purple: specimens collected in this article. blue: type locality.

color, body size, and subtle differences in gonopod shape among different populations (Golovatch 2013). These differences may be attributed to geographic isolation or varying habitats, suggesting the potential presence of cryptic species. This hypothesis could be explored in future research using molecular methods.

### Additional information

#### Conflict of interest

The authors have declared that no competing interests exist.

## Ethical statement

No ethical statement was reported.

## Funding

This research was supported by grants from the CACMS Innovation Fund (nos. CI2023E002), the National Natural Science Foundation of China (32100365), the Doctoral Foundation of Guizhou Academy of Sciences (R [2021]1) and the Forestry and Grassland Ecological Protection and Restoration Fund of Guizhou Province (2022-2024) and Key project at central government level: The ability establishment of sustainable use for valuable Chinese medicine resources (nos. 2060302).

## Author contributions

Yuan Xiong: Resources, Methodology, Software, Data Curation, Writing – Original Draft, Writing – Review & Editing. Huiming Chen: Resources, Supervision, Writing – Review & Editing, Project administration. Xuankong Jiang: Conceptualization, Resources, Methodology, Supervision, Writing – Review & Editing, Project administration, Funding acquisition. Chao Jiang: Conceptualization, Resources, Methodology, Supervision, Writing – Review & Editing, Project administration, Funding acquisition.

## Author ORCIDs

Yuan Xiong  <https://orcid.org/0009-0000-3812-9932>

Huiming Chen  <https://orcid.org/0000-0002-2449-3036>

Xuankong Jiang  <https://orcid.org/0000-0003-3506-5894>

Chao Jiang  <https://orcid.org/0000-0003-1841-1169>

## Data availability

All of the data that support the findings of this study are available in the main text.

## Acknowledgements

We sincerely thank Paul Marek (Virginia Polytechnic Institute and State University, USA), Dr Cathy Car for reviewing the manuscript and offering critical comments. We appreciate the help of Dr Sergei I. Golovatch (Institute for Problems of Ecology and Evolution, Russian), Petra Sierwald, and Dr Peter Decker for providing important references and their generous help. We thank Dr Lu Tian (Shandong Jianzhu University, China), Shi Leilei (Henan University, China) and Mr Lu Chongwei (Guizhou Institute of Biology, China) for the assistance during fieldwork. We are grateful to Di Zhiyong (Hebei University, China), Dr Ge Yihao (Anhui Normal University, China) and Ms Fu Rong for providing the valuable specimens.

## References

- Attems C (1898) System der Polydesmiden I. Theil. Denkschriften der Mathematisch-Naturwissenschaftlichen Class der Kaiserlichen Akademie der Wissenschaften. Classe 67: 221–482.
- Attems C (1914) Die indo-australischen Myriapoden. Archiv für Naturgeschichte Berlin 80A: 1–398.

- Attems C (1929) Diplopoden des Belgischen Congo. I. Polydesmoidea. *Revue de Zoologie et de Botanique Africaines* 17(3): 253–378.
- Attems C (1931) Die Familie Leptodesmidae und andere Polydesmiden. *Zoologica (Stuttgart)* 79: 1–150.
- Attems C (1936) Diplopoda of India. *Memoirs of the Indian Museum* 11(4): 133–353.
- Attems C (1937) Myriapoda 3. Polydesmoidea I. Fam. Strongylosomidae. *Das Tierreich* 68: 1–300. <https://doi.org/10.1515/9783111567099>
- Brölemann HW (1896) Sur quelques myriapodes de Chine. *Mémoires de la Société zoologique de France* 9: 349–362.
- Carl J (1902) Exotische Polydesmiden. *Revue Suisse de Zoologie* 10: 563–679. <https://doi.org/10.5962/bhl.part.13794>
- Chamberlin RV, Wang YM (1953) Records of millipeds (Diplopoda) from Japan and other Oriental areas, with descriptions of new genera and species. *American Museum Novitates* 1621: 1–13.
- Chen CC, Golovatch SI, Chang HW (2006a) The millipede tribe Sulciferini in Taiwan (Diplopoda: Polydesmida: Paradoxosomatidae). In: Meidell N, Hansen LO, Sømme L (Eds) *Proceedings of the 13<sup>th</sup> International Congress of Myriapodology*, Bergen, Norway, 15–29 July 2005. *Norwegian Journal of Entomology* 53(2): 249–270.
- Chen CC, Golovatch SI, Chang HW (2006b) The millipede tribe Nedyopodini, with special reference to the fauna of Taiwan (Diplopoda: Polydesmida: Paradoxosomatidae). *Journal of Natural History* 39(47): 3997–4030. <https://doi.org/10.1080/00222930600556112>
- Chen HM, Zheng CB, Jiang XK (2023) The millipedes (Diplopoda) in Yintiaoling National Natural Reserve, southwest China. *Zootaxa* 5257(1): 49–81. <https://doi.org/10.11646/zootaxa.5257.1.6>
- Geoffroy JJ, Golovatch SI (2004) Some polydesmidan millipedes from caves in southern China (Diplopoda: Polydesmida), with descriptions of four new species. *Arthropoda Selecta* 13(1–2): 19–28.
- Golovatch SI (1978) Some east Asian millipedes (Diplopoda) in the collection of the Zoological Institute, USSR Academy of Science. *Entomologeskoe Obozrenie* 57: 677–681.
- Golovatch SI (1982) Two Paradoxosomatidae from the Kashmir Himalayas (Diplopoda). *Senckenbergiana Biologica* 63(3–4): 297–302.
- Golovatch SI (2009) On several new or poorly-known Oriental Paradoxosomatidae (Diplopoda: Polydesmida), IX. *Arthropoda Selecta* 18(3–4): 119–124.
- Golovatch SI (2013) On several new or poorly-known oriental paradoxosomatidae (Diplopoda: Polyclesmicla), XIII. *Arthropoda Selecta* 22(1): 1–31. <https://doi.org/10.15298/arthsel.22.1.01>
- Golovatch SI (2015) On several new or poorly-known Oriental Paradoxosomatidae (Diplopoda: Polydesmida), XVII. *Arthropoda Selecta* 24(2): 127–168. <https://doi.org/10.15298/arthsel.24.2.01>
- Golovatch SI (2016) On several new or poorly-known Oriental Paradoxosomatidae (Diplopoda: Polydesmida), XVIII. *Arthropoda Selecta* 25(1): 1–18. <https://doi.org/10.15298/arthsel.25.1.01>
- Golovatch SI (2019) On several new or poorly-known Oriental Paradoxosomatidae (Diplopoda: Polydesmida), XXVI. *Arthropoda Selecta* 28(3): 347–367. <https://doi.org/10.15298/arthsel.28.3.01>
- Golovatch SI (2020) On several new or poorly-known Oriental Paradoxosomatidae (Diplopoda: Polydesmida), XXVIII. *Arthropoda Selecta* 29(2): 161–172. <https://doi.org/10.15298/arthsel.29.2.01>

- Golovatch SI, Liu W (2020) Diversity, distribution patterns, and faunogenesis of the millipedes (Diplopoda) of mainland China. *ZooKeys* 930: 153–198. <https://doi.org/10.3897/zookeys.930.47513>
- Golovatch SI, Semenyuk II (2021) On several new or poorly-known Oriental Paradoxosomatidae (Diplopoda: Polydesmida), XXX. *Arthropoda Selecta* 30(4): 473–496. <https://doi.org/10.15298/arthsel.30.4.04>
- Hoffman RL (1962) A contribution to the knowledge of Asiatic Strongylosomoid diplopoda (Polydesmida: Strongylosomatidae). *Annals and Magazine of Natural History Series, Series 13* 5(58): 577–593. <https://doi.org/10.1080/00222936208651289>
- Hoffman RL (1980) Classification of the Diplopoda. *Muséum d'Histoire naturelle, Genève*, 237 pp.
- International Commission on Zoological Nomenclature (1999) International code of zoological nomenclature. 4<sup>th</sup> edn. The International Trust for Zoological Nomenclature, London.
- Jeekel CAW (1971) Nomenclator generum et familiarum Diplopodorum: a list of the genus and family-group names in the class Diplopoda from the 10<sup>th</sup> edn. of Linnaeus, 1758, to the end of 1957. *Monografieën van de Nederlandse Entomologische Vereniging* 5: I–XII, 1–412.
- Jeekel CAW (1982) New records and descriptions of southeast Asian Paradoxosomatidae (Diplopoda, Polydesmida). *Bollettino del Museo civico di Storia naturale di Verona* 9: 225–253.
- Jeekel CAW (1988) The generic position of *Orthomorpha bucharensis* Lohmander and *O. muminabadensis* Gulicka, and the taxonomic status of *Hedinomorpha* Verhoeff (Diplopoda, Polydesmida, Paradoxosomatidae). *Bulletin Zoölogisch Museum, Universiteit van Amsterdam* 11(11): 97–104.
- Korsós Z (2004) Checklist and bibliography of millipedes (Diplopoda) of Taiwan. *Collection and Research* 17: 11–32.
- Likhitrakarn N, Golovatch SI, Panha S (2015) Review of the millipede genus *Kronopolites* Attems, 1914 (Diplopoda, Polydesmida, Paradoxosomatidae), with the description of a new species from Laos. *ZooKeys* (472): 27–41. <https://doi.org/10.3897/zookeys.472.9001>
- Mikhailjova EV, Golovatch SI and Wytwer J (2000) On some new or poorly-known millipedes (Diplopoda) from North Korea. *Fragmenta Faunistica* 43(10): 109–122. <https://doi.org/10.3161/00159301FF2000.43.10.109>
- Miyosi Y (1959) Über japanische Diplopoden. *Arachnological Society of East Asia, Osaka*, 223 pp.
- Nguyen AD, Sierwald P (2013) A worldwide catalog of the family Paradoxosomatidae Daday, 1889 (Diplopoda: Polydesmida). *Check List* 9(6): 1132–1353. <https://doi.org/10.15560/9.6.1132>
- Pocock RI (1895) Report upon the Chilopoda and Diplopoda obtained by PW Bassett-Smith, Esq., Surgeon RN, and JJ Wallcer, Esq., RN, during the cruise in the Chinese Seas of HMS 'Penguin,' Commander W.U. Moore commanding. *Journal of Natural History, Series 6* 15(88): 346–369. <https://doi.org/10.1080/00222939508677895>
- Takakuwa Y (1954) Diplopoden aus Japan und ihn angrenzenden Gebieten. *Japan Society for the Promotion of Science, Tokyo*, 241 pp. [in Japanese, with a German summary].
- Takashima H (1949) The general view of Japanese Myriapods. *Acta Arachnologica* 11(1–2): 8–25. <https://doi.org/10.2476/asjaa.11.8>
- Takashima H (1950) A general view of Japanese myriapods (II). *Acta Arachnologica* 11(1): 36–38. [in Japanese] <https://doi.org/10.2476/asjaa.12.36>

- Takashima H, Haga A (1956) A contribution towards the Japanese cave-dwelling species of the class Diplopoda. *Journal of the Yamashina Institute for Ornithology*, 8: 329–343. <https://doi.org/10.3312/jyio1952.1.329>
- Verhoeff KW (1934) Schwedisch-chinesische wissenschaftliche Expedition nach den nordwestli Geoffroy Provinzen Chinas unter Leitung von Dr. Sven Hedin und Prof. Sü Ping-Chang. Myriapoda gesammelt vom schwedischen Arzt der Expedition Dr. David Hummel 1927–1930. *Arkiv för Zoologi* 26A (10): 1–41.
- Verhoeff KW (1939) Zur Kenntnis ostasiatischer Diplopoden IV. *Zoologischer Anzeiger* 127(11–12): 273–285.
- Wang YHM (1955) Serica 1a: records of myriapods on Formosa with description of new species. *Quarterly Journal of the Taiwan Museum* 8: 13–16.
- Wang YHM (1964) Serica 1 op: Wallacea and insular fauna of millipedes. *Quarterly Journal of the Taiwan Museum* 17(1–2): 67–76.
- Wang D (1996) Review and perspective of study on myriapodology of China. *Acta Myriapodologica*, 81–99.
- Zhang CZ, Li ZY (1978) On medical *Kronotpolites svenhedini* (Verhoeff) (Diplopoda: Paradoxosomatidae). *Chinese Journal of Zoology* 3: 12–13. [in Chinese]
- Zhang G, Xu T, Chen Y, Xu W, Wang Y, Li Y, Zhu F, Liu H, Ruan H (2024) Complete Mitochondrial Genomes of *Nedyopus patrioticus*: new Insights into the Color Polymorphism of Millipedes. *Current Issues in Molecular Biology* 46(3): 2514–2527. <https://doi.org/10.3390/cimb46030159>

# Two new species of the genus *Viscosia* de Man, 1890 (Nematoda, Enoplea, Enoplida, Oncholaimidae) from the intertidal zone of the Yellow Sea, China

Lingyun Sun<sup>1</sup>, Huimin Gu<sup>1</sup>, Yong Huang<sup>1</sup>

<sup>1</sup> College of Agriculture and Biology, Liaocheng University, Liaocheng 252059, China  
Corresponding author: Yong Huang ([huangy@lcu.edu.cn](mailto:huangy@lcu.edu.cn))

## Abstract

Two new species of *Viscosia* from the intertidal zone along the Yellow Sea are described and illustrated. *Viscosia media* **sp. nov.** is characterized by a heavily cuticularized and relatively shallow buccal cavity with stubby teeth; cephalic setae 7–8  $\mu\text{m}$  long; amphidial fovea invisible; slender spicules almost straight, cephalated proximally and conical distally; and tail conical, straight in males and slightly bent ventrally in females. *Viscosia sinica* **sp. nov.** is characterized by a relatively large amphidial fovea, conico-cylindrical tail with swollen horseshoe-shaped tip, spicules slightly curved ventrally, and 10–12 setae surrounding the cloaca, each 3–4  $\mu\text{m}$  long. The basic morphological data of males of 26 valid species in *Viscosia* with a body length of 1–2.9 mm are presented.

**Key words:** Biodiversity, free-living marine nematodes, Huangdao coast, Qingdao, Rizhao coast, Shandong Province, taxonomy



Academic editor: Alexei Tchesunov  
Received: 18 November 2024  
Accepted: 8 February 2025  
Published: 11 March 2025

ZooBank: <https://zoobank.org/A65EAA36-BA3E-4B4B-9EF2-93041E5F621A>

**Citation:** Sun L, Gu H, Huang Y (2025) Two new species of the genus *Viscosia* de Man, 1890 (Nematoda, Enoplea, Enoplida, Oncholaimidae) from the intertidal zone of the Yellow Sea, China. ZooKeys 1231: 99–117. <https://doi.org/10.3897/zookeys.1231.142078>

Copyright: © Lingyun Sun et al.  
This is an open access article distributed under terms of the Creative Commons Attribution License (Attribution 4.0 International – CC BY 4.0).

## Introduction

Free-living marine nematodes are the most widespread and abundant meiofaunal group in marine benthic habitats (Heip et al. 1982). They play a significant role in marine environment and are widely used as pollution indicators in biological monitoring (Lamshead 2004). However, many species of nematodes are still unknown. At present, less than 600 species of free-living marine nematodes have been identified in the Chinese sea area, which is estimated to be less than half of the total species (Sun et al. 2024).

The Yellow Sea is located on the edge of the western Pacific Ocean, between China and the Korean Peninsula. It is a semi-enclosed inland shallow sea basin. Biodiversity surveys and taxonomical studies on nematodes in the Yellow Sea have been carried out in recent years (Huang and Sui 2024; Huang and Zhai 2024; Li et al. 2024). More than 390 species of nematodes have been identified, of which 117 species were new to science (Sun et al. 2024). The new species accounted for 30% of the total known species. However, the total number of nematodes in this sea area is unknown, and new species are routinely found. It is, therefore, important to continue investigating the taxonomy of nematodes in the region. Here, the present paper

describes two new species of the genus *Viscosia* de Man, 1890 that were discovered in the intertidal zone of Qingdao and Rizhao, Yellow Sea.

*Viscosia* is a large genus with many species. It occurs in marine, brackish, and freshwater sediments (Smol et al. 2014; Leduc and Zhao 2023). The genus was established by de Man in 1890 as a subgenus of *Oncholaimus* Dujardin, 1845. Later, it was raised to genus by Filipjev in 1918. Wieser and Hopper (1967), Gerlach and Riemann (1974), Filipjev (1918), Smol and Sharma (1984), Smol et al. (2014), and Leduc and Zhao (2023) successively reviewed the genus. Wieser and Hopper (1967) stressed the importance of certain characteristics in species identification, such as the size of amphids, the shape of the buccal cavity and teeth, the arrangement of the male circumanal organs like papillae and bursa, and the shape of the tail. Gagarin (2020) provided the basic morphological features of males of 24 valid species with body length of 1–2 mm within the genus *Viscosia*. Currently, the World Database of Nematodes (Nemys eds. 2024) makes a list of 92 valid species including four freshwater species (*Viscosia nicaraguensis* Gerlach, 1957, *V. orientalis* Gagarin, 2020, *V. timmi* Gagarin & Nguyen Thi Thu, 2008 and *V. uipii* Coomans, Vincx & Decraemer, 1985). But in fact, many species were described only based on juveniles or females, and lack the characters of males. In the Chinese sea area, only seven species within *Viscosia* were recorded. They are *Viscosia bandaensis* Kreis, 1932, *V. elegans* (Kreis, 1924) Lorenzen, 1981, *V. franzii* Boucher, 1977, *V. glabra* (Bastian, 1865) de Man, 1890, *V. heterolaima* Smol & Sharma, 1984, *V. longicaudatoides* Nguyen Vu Thanh & Gagarin, 2013 and *V. nuda* Kreis, 1932.

## Material and methods

The meiofauna samples were collected from the top sediment layer (0–8 cm deep) using a 2.9 cm diameter sawn-off syringe. The samples were fixed with an equal amount of 10% formalin solution. In the laboratory, samples were stained with 0.1% Rose Bengal for 24 hours. The stained samples were poured through two sieves (500 and 42 µm mesh sizes), and washed with tap water to remove silt and separate macrofauna from meiofauna. The intercepted material in the 42 µm mesh was centrifuged in Ludox-TM (50% colloidal silica, suspension in water; product of Sigma Aldrich Co., USA) with a specific gravity of 1.15 g/ml (de Jonge and Bouwman 1977) to separate meiofauna from the heavier sediment particles. The supernatant obtained after three rounds of centrifugation was poured into the 42 µm mesh to filter Ludox-TM. The sample in the 42 µm mesh was washed into a Petri dish with distilled water and meiofauna was sorted out under a stereoscopic microscope.

Nematodes were transferred into a cavity block containing a solution of 5% glycerol, 5% pure ethanol, and 90% distilled water in volume (McIntyre and Warwick 1984). After ethanol was slowly evaporated, the specimens were mounted in glycerin on permanent slides. The descriptions were made using a differential interference contrast microscope (Leica DM 2500). The photos were taken with a Leica DMC 5400 digital camera. Line drawings were made with the aid of a camera lucida. All measurements were taken using Leica software of LAS X version 3.3.3, and all curved structures were measured along the curved median line. All measurements are in µm. Type specimens were deposited in the Marine Biological Museum of the Chinese Academy of Sciences, Qingdao.

## Results and discussion

### Taxonomy

**Class Enoplea Inglis, 1983**

**Order Enoplida Filipjev, 1929**

**Family Oncholaimidae Filipjev, 1916**

**Genus *Viscosia* de Man, 1890**

**Diagnosis (according to Smol et al. 2014).** Buccal cavity large, barrel-shaped with three unequal immovable teeth, of which the right subventral tooth largest. Females didelphic-amphidelphic with reflexed ovaries. Spicules short, straight or slightly curved. Gubernaculum absent. Demanian system present and simple, consisting of prolongation of the ovary at the reflexed point that connects it with the intestine through the osmosium.

### List of valid species (64 species)

- V. abyssorum* (Allgén, 1933) Wieser, 1953.  
syn. *Oncholaimus abyssorum* Allgén, 1933.
- V. angustata* (Cobb, 1890) Kreis, 1934.  
syn. *Oncholaimus angustatus* Cobb, 1890.
- V. antarctica* Allgén, 1959.
- V. bandaensis* Lorenzen, 1981.  
syn. *Mononcholaimus bandaensis* Kreis, 1932.
- V. bandaensis* Kreis, 1932.  
syn. *Mononcholaimus bandaensis* Kreis, 1932.
- V. bayensis* Keppner, 1987.
- V. brachylaima* Filipjev, 1927.
- V. brevicaudata* Mawson, 1958.
- V. brevilaima* Allgén, 1959.
- V. cobbi* Filipjev, 1918.
- V. coomansi* Smol & Sharma, 1984.
- V. dossena* Leduc & Zhao, 2023.
- V. elegans* (Kreis, 1924) Lorenzen, 1981.  
syn. *Mononcholaimus elegans* Kreis, 1924.
- V. elongata* Filipjev, 1922.
- V. epapillosa* Platonova, 1971.
- V. erasmi* Furstenberg & Vincx, 1989.
- V. falklandiae* Allgén, 1959.
- V. filiformis* (Kreis, 1932) Lorenzen, 1981.  
syn. *Mononcholaimus filiformis* Kreis, 1932.
- V. floridana* Keppner, 1987.
- V. franzii* Boucher, 1977.
- V. glabra* (Bastian, 1865) de Man, 1890.  
syn. *Oncholaimus glaber* Bastian, 1865.  
syn. *Viscosia micoletzkyi* Chitwood, 1951.
- V. grahami* Allgén, 1959.
- V. hanstroemi* Wieser, 1953.

- V. heterolaima* Smol & Sharma, 1984.  
*V. keiensilis* Lorenzen, 1981.  
syn. *Mononcholaimus keiensis* Kreis, 1932.  
*V. keiensis* Kreis, 1932.  
syn. *Mononcholaimus keiensis* Kreis, 1932.  
*V. langrunensis* (de Man, 1890) Filipjev, 1918.  
syn. *Oncholaimus langrunensis* de Man, 1890.  
*V. longicaudatoides* Nguyen Vu Thanh & Gagarin, 2013.  
*V. macramphida* Chitwood, 1951.  
*V. macrobursata* Keppner, 1987.  
*V. megalaima* (Ditlevsen, 1928) Hope & Murphy, 1972.  
syn. *Steineria megalaima* Ditlevsen, 1928.  
*V. meridionalis* Kreis, 1932.  
*V. microseta* Wieser, 1953.  
*V. nicaraguensis* Gerlach, 1957.  
syn. *Viscosia papillata nicaraguensis* Gerlach, 1957.  
*V. nona* Filipjev, 1946.  
*V. norvegica* (Allgén, 1946) Lorenzen, 1981.  
syn. *Mononcholaimus norvegicus* Allgén, 1946.  
*V. nuda* Kreis, 1932.  
*V. oncholaimelloides* Wieser & Hopper, 1967.  
*V. orientalis* Gagarin, 2020.  
*V. papillata* Chitwood, 1951.  
*V. papillatoides* Chitwood, 1960.  
*V. papillatula* Lorenzen, 1981.  
syn. *Mononcholaimus papillatus* Kreis, 1932.  
*V. parafalklandiae* Allgén, 1959.  
*V. parapellucida* (Allgén, 1959) Gerlach & Riemann, 1974.  
syn. *Viscosia pellucida* Allgén, 1959.  
*V. parasetosa* (Kreis, 1932) Lorenzen, 1981.  
syn. *Mononcholaimus parasetosus* Kreis, 1932.  
*V. pedroensis* Allgén, 1947.  
*V. profunda* (Vitiello, 1970) Lorenzen, 1981.  
syn. *Mononcholaimus profundus* Vitiello, 1970.  
*V. propinqua* Allgén, 1959.  
*V. pseudoglabra* Kreis, 1932.  
*V. pygmaea* Nguyen Vu Thanh & Gagarin, 2013.  
*V. rectangulata* Wieser, 1953.  
*V. rustica* (Kreis, 1929) Lorenzen, 1974.  
syn. *Mononcholaimus rusticus* Kreis, 1929.  
*V. sedata* Gagarin & Nguyen Vu Thanh, 2007.  
*V. separabilis* (Wieser, 1953) Lorenzen, 1981.  
syn. *Mononcholaimus separabilis* Wieser, 1953.  
*V. setosa* (Kreis, 1932) Lorenzen, 1981.  
syn. *Mononcholaimus setosus* Kreis, 1932.  
*V. similis* Allgén, 1959.  
*V. stenolaima* Filipjev, 1927.  
*V. tenuissima* Allgén, 1959.  
*V. timmi* Gagarin & Nguyen Thi Thu, 2008.

- V. tumidula* Wieser, 1959.
- V. uipii* Coomans, Vincx & Decraemer, 1985.
- V. viscosa* (Bastian, 1865) de Man, 1890.
  - syn. *Mononcholaimus viscosus* Allgén, 1930.
  - syn. *Oncholaimus viscosus* Bastian, 1865.
- V. viscosula* Lorenzen, 1981.
  - syn. *Mononcholaimus viscosus* Allgén, 1930.
- V. wieseri* Mawson, 1958.

#### Species *inquirendae* (38 species)

- V. brachydonta* Allgén, 1959.
- V. brachylaimoides* Chitwood, 1937.
- V. brevidentata* (Vitiello, 1967) Lorenzen, 1981.
  - syn. *Mononcholaimus brevidentatus* Vitiello, 1967.
- V. conicaudata* (Kreis, 1932) Lorenzen, 1981.
  - syn. *Mononcholaimus conicaudatus* Kreis, 1932.
- V. crassa* Kreis, 1932.
- V. cryptodentata* Allgén, 1959.
- V. diodon* (Wieser, 1951) Lorenzen, 1981.
  - syn. *Mononcholaimus diodon* (Wieser, 1951) Wieser, 1953.
  - syn. *Oncholaimellus diodon* Wieser, 1951.
- V. dubiosa* Kreis, 1932.
- V. fatigans* Filipjev, 1946.
- V. filipjevi* Paramonov, 1929.
- V. gabriolae* (Allgén, 1951) Lorenzen, 1981.
  - syn. *Mononcholaimus gabriolae* Allgén, 1951.
- V. glaberoides* (Allgén, 1932) Lorenzen, 1981.
  - syn. *Mononcholaimus glaberoides* Allgén, 1932.
- V. isotonchula* Kreis, 1932.
- V. klatti* (Allgén, 1941) Lorenzen, 1981.
  - syn. *Mononcholaimus klatti* Allgén, 1941.
- V. leptolaima* Kreis, 1932.
- V. linstowi* (de Man, 1904) Filipjev, 1918.
  - syn. *Oncholaimus linstowi* de Man, 1904.
- V. longicaudata* (Kreis, 1932) Lorenzen, 1981.
  - syn. *Meroviscosia longicaudata* Kreis, 1932.
- V. longidentata* (Schuurmans Stekhoven, 1931) Lorenzen, 1981.
  - syn. *Mononcholaimus longidentatus* (Schuurmans Stekhoven & Adam in Schuurmans Stekhoven, 1931) Kreis, 1934.
  - syn. *Oncholaimus longidentatus* Schuurmans Stekhoven & Adam in Schuurmans Stekhoven, 1931.
- V. longissima* Filipjev, 1946.
- V. macrorhopalocerca* Kreis, 1932.
- V. minor* Filipjev, 1918.
- V. minudonta* Vitiello, 1970.
- V. nijhoffi* Allgén, 1935.
- V. nordgaardi* Allgén, 1940.
- V. palmae* Schuurmans Stekhoven, 1942.

- V. papillosa* (Eberth, 1863) Kreis, 1934.  
syn. *Oncholaimus papillosus* Eberth, 1863.
- V. paralinstowi* Chitwood, 1937.
- V. parapedroensis* Allgén, 1947.
- V. paridentata* Kreis, 1932.
- V. parva* Kreis, 1929.
- V. pellucida* (Cobb, 1898) Filipjev, 1918.  
syn. *Oncholaimus pellucidus* Cobb, 1898.
- V. poseidonica* Belogurov & Belogurova, 1977.
- V. pseudosegmentata* Allgén, 1947.
- V. stenostoma* Platonova, 1971.
- V. strandi* Allgén, 1935.
- V. subantarctica* Allgén, 1959.
- V. tasmaniensis* (Allgén, 1927) Lorenzen, 1981.  
syn. *Mononcholaimus tasmaniensis* Allgén, 1927.
- V. tenuilaima* Allgén, 1959.

#### Invalid species

- V. aegyptica* (Steiner, 1921) Schuurmans Stekhoven 1943 = *Oncholaimus aegypticus* Steiner, 1921.
- V. carnleyensis* (Ditlevsen, 1921) Kreis, 1932 = *Viscosia glabra* (Bastian, 1865) de Man, 1890.
- V. carnleyensis tropica* Kreis, 1932 = *V. carnleyensis* (Ditlevsen, 1921) Kreis, 1932.
- V. donsi* Allgén, 1947 = *Oncholaimus donsi* (Allgén, 1947) Wieser, 1953.
- V. micoletzkyi* Chitwood, 1951 = *Viscosia glabra* (Bastian, 1865) de Man, 1890.
- V. pacifica* Allgén, 1951 = *Oncholaimus rapax* Kreis, 1932.
- V. papillata nicaraguensis* Gerlach, 1957 = *Viscosia nicaraguensis* Gerlach, 1957.
- V. paralangrunensis* Allgén, 1947 = *Oncholaimus paralangrunensis* (Allgén, 1947) Allgén, 1959.
- V. pellucida* Allgén, 1959 = *V. parapellucida* (Allgén, 1959) Gerlach & Riemann, 1974.
- V. scanica* Allgén, 1935 = *Oncholaimus scanicus* (Allgén, 1935) Wieser, 1953.
- V. taboguillensis* Allgén, 1947 = *Adoncholaimus taboguillensis* (Allgén, 1947) Wieser, 1953.

**Remarks.** According to the relevant literature, there are 27 species described only from juveniles or females (five species, *V. brachydonta*, *V. conicaudata*, *V. leptolaima*, *V. macrorhopalocerca* and *V. palmae*, were described only from juveniles; 18 species, *V. brevidentata*, *V. cryptodentata*, *V. fatigans*, *V. filipjevi*, *V. isotonchula*, *V. linstowi*, *V. longidentata*, *V. minor*, *V. papillosa*, *V. paralinstowi*, *V. paridentata*, *V. parva*, *V. pellucida*, *V. poseidonica*, *V. stenostoma*, *V. subantarctica*, *V. tasmaniensis* and *V. tenuilaima*, were described only from females; four species, *V. crassa*, *V. diodon*, *V. longissimi* and *V. minudonta*, were described from females and juveniles). These species should be considered as *inquirendae*. According to the original description of *V. brachylaimoides* by Chitwood (1937) and the opinion of Leduc and Zhao (2023), this species has a large left ventrosublateral tooth instead of large right ventrosublateral tooth, indicating that the species does not belong to *Viscosia*. Here, *V. brachylaimoides* is treated as species *inquirendum*. Based on the

observation and analysis by Smol and Sharma (1984), the largest ventro-sublateral tooth of *V. franzii* is situated on the right side instead of the left as described by Boucher (1977). The species is consistent with the diagnosis of *Viscosia*, and it is a valid species of the genus. Meanwhile, Smol and Sharma considered *V. carnleyensis* as a synonym of *V. glabra*.

***Viscosia media* sp. nov.**

<https://zoobank.org/EE875370-C9F8-4025-A4D0-519431DC0893>

Figs 1–3, Table 1

**Diagnosis.** Body slender, medium size in the genus. Heavily cuticularized and relatively shallow buccal cavity with three stubby teeth, and a right ventro-sublateral tooth massive. Cephalic setae 7–8 µm long. Amphidial fovea invisible. Spicules slender, almost straight, cephalated proximally and conical distally. Tail conical, straight in males, slightly bent ventrally in females.

**Holotype and paratype material.** Four males and two females were measured. **Holotype** male 1 on slide RZ080312-9. **Paratype** 1 (male 2) on slide RZ080310-3, both **paratype** 2 (male 3) and **paratype** 3 (male 4) on slide RZ0803123-4, **paratype** 4 (female 1) on slide RZ080312-9, and **paratype** 5 (female 2) on slide RZ0803123-4.

**Type locality and habitat.** Holotype and paratypes were all collected from the surface layer of fine sand sediment on an intertidal beach along the Rizhao coast of the Yellow Sea, China (35°34'21"N, 119°39'29"E).

**Etymology.** Species epithet *media* refers to the medium body size of this species within the genus.

**Measurements.** All measurement data are given in Table 1.

**Descriptions. Males.** Body medium in size, and slender, tapering slightly towards both extremities. Cuticle smooth. Cervical setae 4–6 µm long, sparse, present only in the anterior portion of pharyngeal region. Cephalic region truncated, continuing with body contour. Six lips, each bearing a single inner labial papilla. Six outer labial setae and four slightly longer cephalic setae in a single circle. Outer labial setae 6–7 µm long, cephalic setae 7–8 µm long. Amphidial fovea invisible. Buccal cavity heavily cuticularized, relatively shallow, 15–18 µm deep and 7–9 µm wide, with three stubby teeth. Right ventro-sublateral tooth massive and larger than left ventro-sublateral tooth and dorsal tooth. The tip of right ventro-sublateral tooth at the same level with outer labial and cephalic setae. The height of left ventro-sublateral tooth and dorsal tooth are almost equal. Pharynx cylindrical, widening slightly towards posterior extremity. Cardia conical, surrounded by intestinal tissue. Nerve ring located pre-mid of length of pharynx. Secretory-excretory system present; excretory pore located slightly posterior to nerve ring, 160–170 µm from anterior end. Ventral gland located at anterior part of the intestine.

Reproductive system with two opposed and outstretched testes located to the right of intestine. Sperm cells oval or irregularly square, 12–16 µm long and 8–10 µm wide. Spicules slender, almost straight, cephalated proximally and conical distally. Gubernaculum absent. Tail conical, narrowing abruptly immediately posterior to cloaca and directed slightly dorsally, without caudal setae. Three caudal glands extending anteriorly to tail region. Spinneret present.

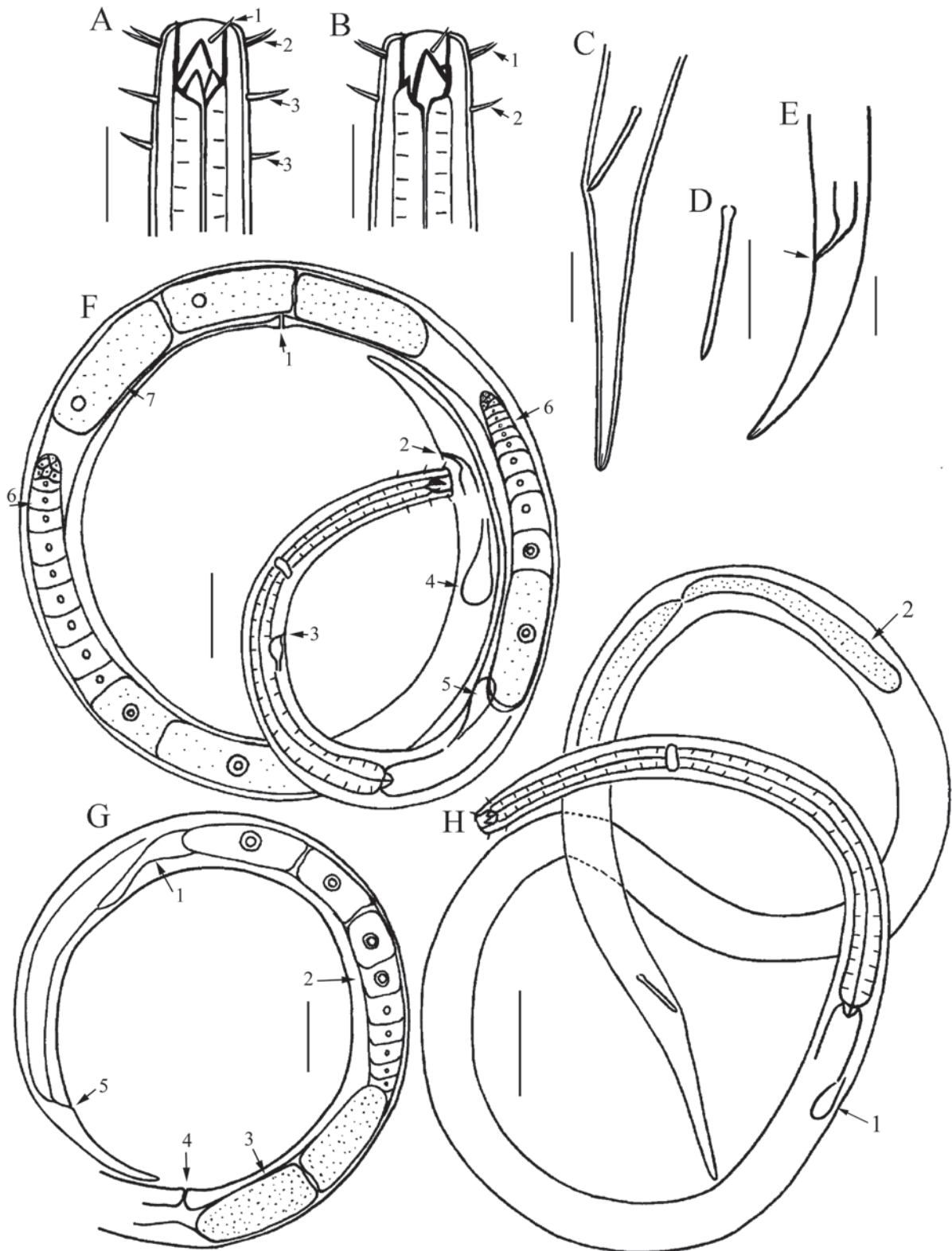


**Figure 1.** Drawings of *Viscosia media* sp. nov. **A** anterior end of holotype, showing outer labial seta (arrow 1), outer labial and cephalic setae (arrow 2), buccal cavity with three teeth, and cervical setae (arrow 3) **B** anterior end of female, showing large right subventral tooth, small dorsal tooth, outer labial and cephalic setae (arrow 1) and cervical setae (arrow 2) **C** posterior end of holotype, showing spicule and tail **D** spicule **E** posterior end of female, showing anus (arrow) and tail **F** entire view of female (arrow 1, vulva; 2, anus; 3, excretory pore; 4, caudal gland; 5, ventral gland; 6, ovary) **G** posterior part of female (arrow 1, Demanian system; 2, ovary; 3, egg; 4, vulva; 5, anus) **H** entire view of male (arrow 1, ventral gland; arrow 2, testis). Scale bars: 20  $\mu\text{m}$  (**A–E**); 50  $\mu\text{m}$  (**F–H**).

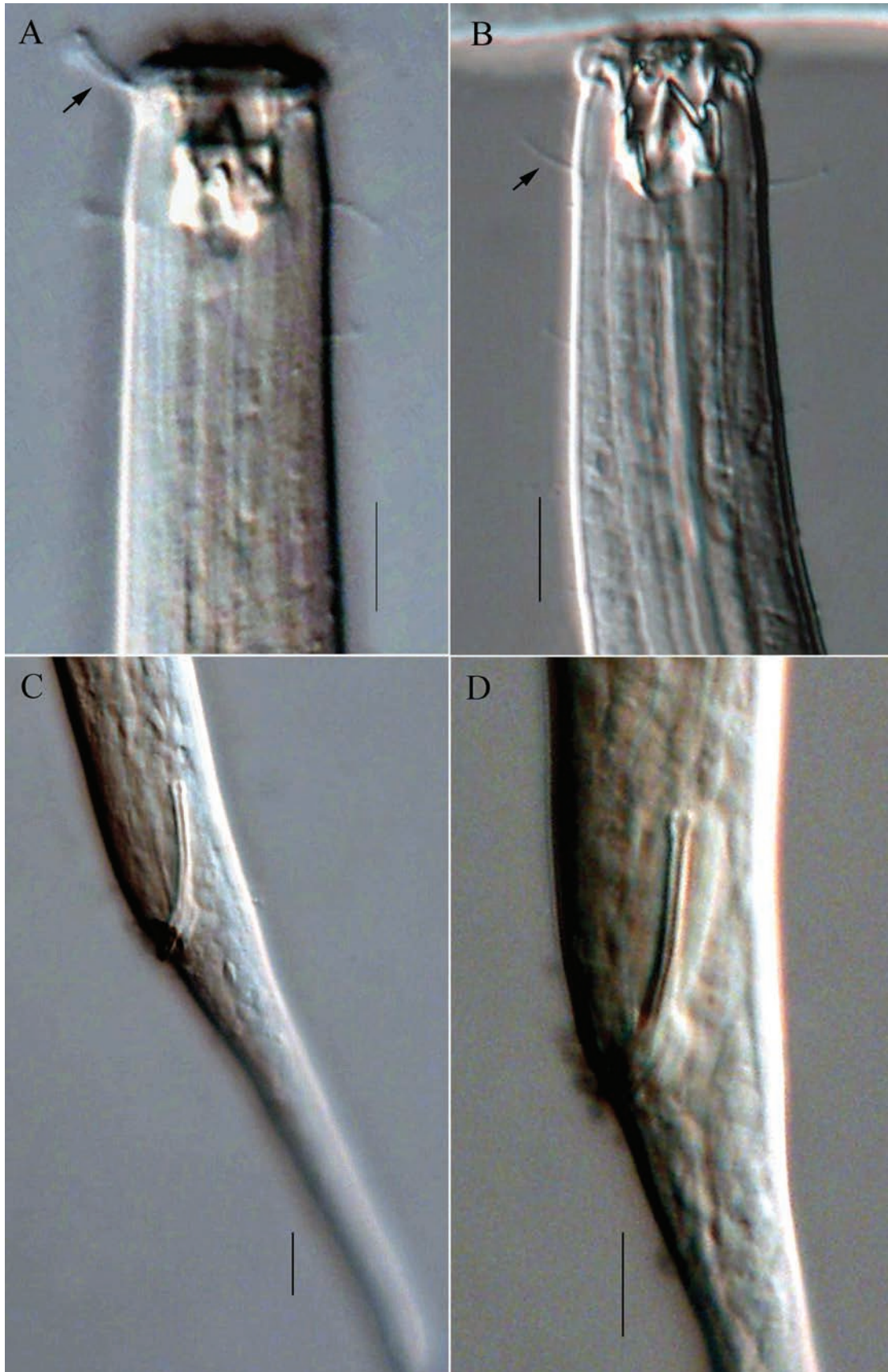


**Figure 2.** Micrographs of *Viscosia media* sp. nov. **A** anterior end of holotype, showing outer labial and cephalic setae (arrow); buccal cavity with three teeth **B** anterior end of female, showing right subventral tooth and cervical setae (arrow) **C** posterior end of holotype, showing spicule and tail **D** cloacal region of male, showing spicule. Scale bars: 10  $\mu$ m.

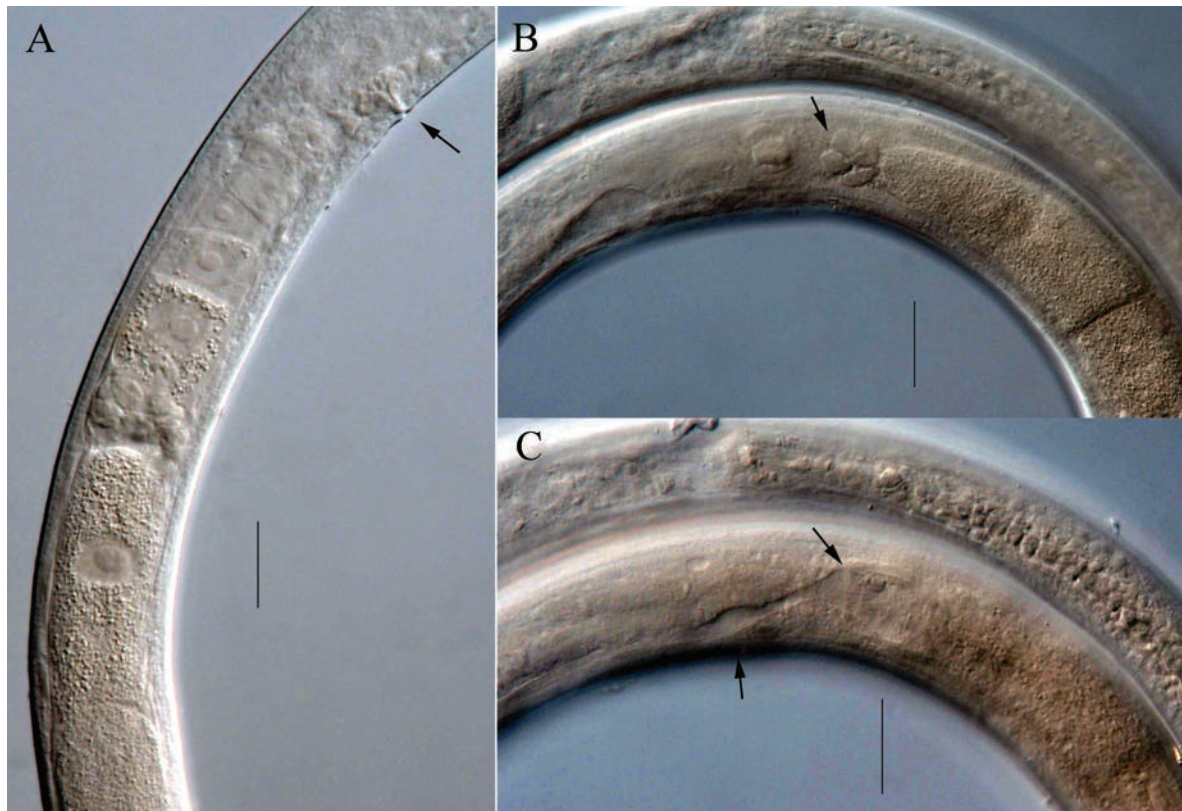


**Figure 3.** Micrographs of *Viscosia media* sp. nov. **A** middle region of female body, showing vulva (arrow), ovary and eggs **B** showing gland cells (arrow) at the reflexed point of ovary **C** showing sac-like structure and osmosium of Demanian system (arrows).

**Table 1.** Individual measurements of *Viscosia media* sp. nov. and *Viscosia sinica* sp. nov. (in  $\mu\text{m}$  except a, b, c, c' and V%) a, ratio of body length to maximum body diameter; b, ratio of body length to pharynx length; c, ratio of body length to tail length; c', ratio of tail length to cloacal or anus body diameter; V%, position of vulva from anterior end expressed as a percentage of total body length; -, no data.

Characters	<i>Viscosia media</i> sp. nov.						<i>Viscosia sinica</i> sp. nov.					
	♂1	♂2	♂3	♂4	♀1	♀2	♂1	♂2	♂3	♂4	♀1	♀2
Total body length	1620	1534	1615	1522	1539	1458	1733	1885	1840	1821	1457	1653
Maximum body diameter	32	33	33	26	41	35	28	26	26	25	31	28
Head diameter	17	16	17	16	18	17	13	14	14	14	13	15
Length of outer labial setae	6	7	7	6	6	6	5	7	7	5	5	6
Length of cephalic setae	7	8	7	7	7	6	5	7	7	5	5	6
Depth of buccal cavity	18	15	16	17	16	17	29	22	21	26	16	16
Width of buccal cavity	9	8	8	7	9	9	10	8	8	8	8	9
Height of amphidial fovea	-	-	-	-	-	-	5	5	6	5	4	5
Width of amphidial fovea	-	-	-	-	-	-	10	11	11	9	8	8
Length of pharynx	317	310	320	307	305	312	278	298	287	304	260	304
Body diameter at pharyngeal base	26	27	27	24	32	31	24	23	24	24	31	26
Spicules length along arc	29	24	30	32	-	-	20	21	22	19	-	-
Vulva from anterior end	-	-	-	-	732	690	-	-	-	-	720	820
V%	-	-	-	-	47.6	47.3	-	-	-	-	49.4	49.6
Body diameter at cloaca or anus	17	16	17	15	16	15	16	16	16	16	19	15
Tail length	86	75	85	80	75	83	81	104	106	98	88	97
a	50.6	46.5	48.9	58.5	37.5	41.7	61.9	72.5	70.8	72.8	47.0	59.0
b	5.1	4.9	5.1	5.0	5.0	4.7	6.2	6.3	6.4	6.1	5.6	5.4
c	18.8	20.4	19.0	19.0	20.5	17.6	21.4	18.1	17.4	18.6	16.6	17.0
c'	5.1	4.7	5.0	5.3	4.7	5.5	5.1	6.5	6.6	6.1	4.4	6.5

**Females.** Similar to males in most morphological characteristics but there are less cervical setae, and tail slightly bent ventrally. Reproductive system with two opposed and reflexed ovaries both located to the right of intestine. Eggs very long, can be up to 220  $\mu\text{m}$  long. Demanian system simple, consisting of a sac-like prolongation of the ovary at the reflexed point of the ovary and a duct-shaped osmosium. Vulva located at mid-body.

**Differential diagnosis and discussion.** *Viscosia media* sp. nov. is characterized by heavily cuticularized and relatively shallow buccal cavity with three stubby teeth, right ventrosublateral tooth massive, cephalic setae 7–8  $\mu\text{m}$  long, amphidial fovea invisible, spicules slender, almost straight, cephalated proximally and conical distally, tail conical, straight in males, slightly bent ventrally in females. The new species is similar to *V. epapillosa* Platonova, 1971 in the deep of buccal cavity and length of cephalic setae, but differs by the wider head diameter (16–18  $\mu\text{m}$  versus 11–13  $\mu\text{m}$ ), buccal cavity with heavily cuticularized parallel walls (versus buccal cavity wider in the middle and narrower at the ends), having cervical setae (versus absent in the latter species), spicules enlarged proximally (versus not enlarged), and a conical tail almost straight in the males (versus conico-cylindrical tail bent in the latter species). The new species is also similar to *Viscosia pygmaea* Nguyen Vu Thanh & Gagarin, 2013 in the tail shape, but differs from *V. pygmaea* by the longer body length (1458–1620  $\mu\text{m}$  versus 838–992  $\mu\text{m}$ ), longer cephalic setae (7–8  $\mu\text{m}$  versus 3–3.5  $\mu\text{m}$ ), shallower buccal cavity with stubby teeth (1 head diameter versus 1.5 head diameters in depth with slender teeth), amphidial fovea invisible (versus obvious and located close to the base of buccal cavity), and the different spicule shape (slender with cephalated proximal end and tapering distally end versus conical and tapering off). *Viscosia media* sp. nov. can be differentiated from all other species of the genus by its heavily cuticularized and relatively shallow buccal cavity with stubby teeth, 7–8  $\mu\text{m}$  cephalic setae, and a conical tail. The basic morphological characteristics of the valid species with similar size to the new species in the genus are compared in Table 2.

***Viscosia sinica* sp. nov.**

<https://zoobank.org/1EB9C0EF-BDC5-484C-8932-4CFBA8F1D88D>

Figs 4, 5, Table 1

**Dianosis.** Relatively large amphidial fovea, about 80% corresponding body diameter wider in males and 53–62% in females. Cephalic setae 5–7  $\mu\text{m}$  long. Tail conico-cylindrical with swollen horseshoe-shaped tip. Spicules slender, slightly curved ventrally, not cephalate proximally. 10–12 setae surrounding the cloaca, each 3–4  $\mu\text{m}$  long.

**Holotype and paratype material.** Four males and two females were measured. **Holotype** male 1 on slide RZ080123-4. **Paratype** 1 (male 2) on slide YST24251-2, paratype 2 (male 3) on slide YST24381-11, paratype 3 (male 4) on slide YST24253-1, paratype 4 (female 1) on slide RZ0803123-4, paratype 5 (female 2) on slide YST2418-12.

**Type locality and habitat.** Holotype and paratype 4 (female 1) were collected from the surface layer of fine sand sediment on an intertidal beach along the Rizhao coast of the Yellow Sea (35°34'21"N, 119°39'29"E). The other paratypes

were all collected from the surface layer of silt sediment on an intertidal beach of Huangdao along the Yellow Sea (31°44'53"N, 121°55'43"E).

**Etymology.** The species epithet refers to the country of origin, China.

**Measurements.** All measurement data are given in Table 1.

**Descriptions. Males.** Body relatively slender. Cuticle smooth, without somatic setae. Labial region spherical, demarcated by slight constriction. Six lips, each bearing a single internal labial papilla. Six outer labial setae and four cephalic

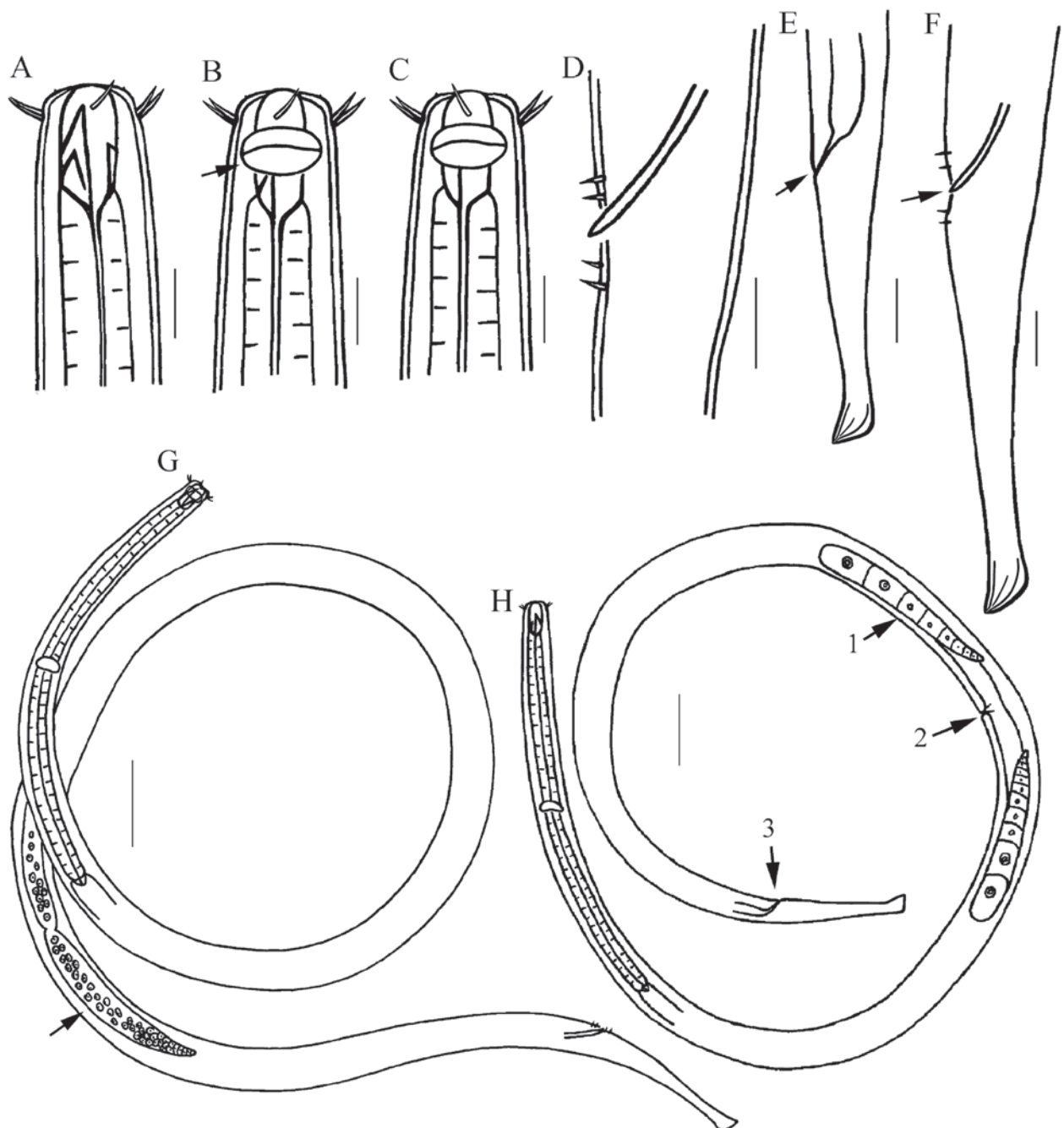


**Figure 4.** Drawings of *Viscosia sinica* sp. nov. **A** anterior end of holotype, showing outer labial and cephalic setae, buccal cavity with three teeth **B** anterior end of male, showing amphidial fovea (arrow) **C** anterior end of female **D** spicule and setae surrounding the cloaca **E** posterior end of female, showing anus (arrow) and tail **F** posterior end of holotype, showing cloaca (arrow), spicule and tail **G** entire view of male (arrow showing testis) **H** entire view of female (arrow 1, ovary; 2, vulva; 3, anus). Scale bars: 10  $\mu$ m (**A–D, F**); 20  $\mu$ m (**E**); 50  $\mu$ m (**G, H**).

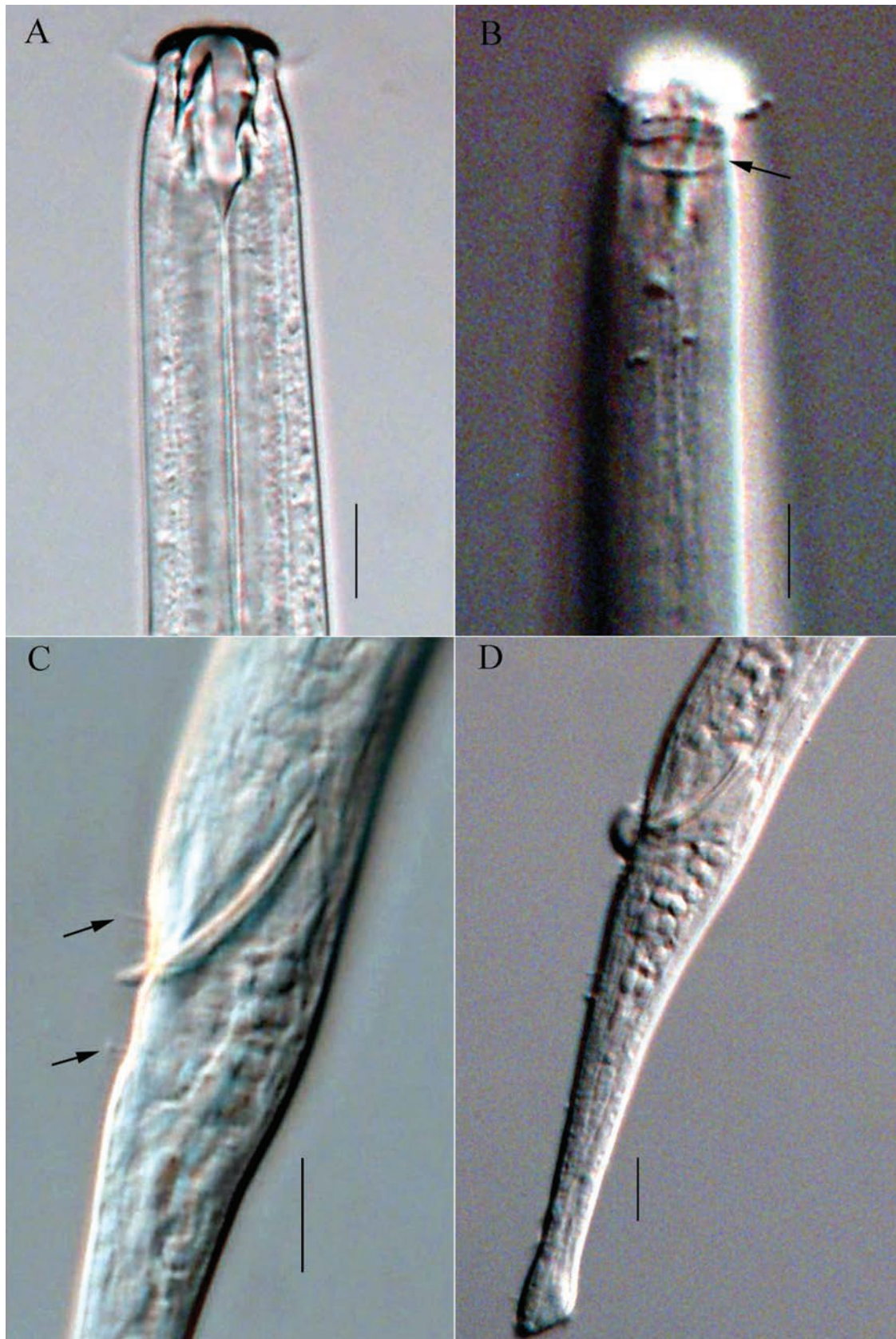


**Figure 5.** Micrographs of *Viscosia sinica* sp. nov. **A** anterior end of holotype, showing buccal cavity with large right subventral and dorsal teeth **B** anterior end of male 1, showing outer labial and cephalic setae, amphidial fovea (arrow) **C** cloacal region of male 2, showing spicule and setae surrounding cloaca (arrows) **D** posterior end of holotype, showing spicule and tail. Scale bars: 10  $\mu$ m.

setae in a single circle, equal in length. Amphidial fovea relatively large, pocket-shaped, 9–11  $\mu\text{m}$  wide, about 80% corresponding body diameter, and 5–6  $\mu\text{m}$  deep, located at level of the middle of buccal cavity. Buccal cavity 16–29  $\mu\text{m}$  deep and 8–10  $\mu\text{m}$  wide, with three teeth. Right ventrosublateral tooth larger than left ventrosublateral tooth and dorsal tooth. The tip of right ventrosublateral tooth at the same level with outer labial and cephalic setae. The height of left ventrosublateral tooth and dorsal tooth are almost equal. Pharynx cylindrical, widening slightly towards posterior extremity. Cardia conical, about 15  $\mu\text{m}$  long, surrounded by intestinal tissue. Nerve ring located approximately halfway down length of pharynx. Secretory-excretory system and excretory pore not observed.

Reproductive system with two opposed and outstretched testes located to the right of intestine. Spicules slender, slightly curved ventrally, not cephalate proximally. Gubernaculum absent. 10–12 setae surrounding the cloaca, each 3–4  $\mu\text{m}$  long. Tail conico-cylindrical, with swollen horseshoe-shaped tip. Caudal setae absent. Three caudal glands extending anteriorly to tail region. Spinneret present.

**Females.** Similar to males in the most morphological characteristics but amphidial fovea slightly smaller, 53–62% corresponding body diameter wider, and buccal cavity slightly shallower (21–29  $\mu\text{m}$  versus 16  $\mu\text{m}$  deep). Reproductive system with two opposed and reflexed ovaries both located to the right of intestine. Demanian system indistinct. Vulva located at mid-body.

**Table 2.** Basic morphological features of males of the valid species in *Viscosia* with body length of 1000–2900  $\mu\text{m}$  (according to Gagarin 2020) (in  $\mu\text{m}$  except a, b, c and c') L, body length; a, ratio of body length to maximum body diameter; b, ratio of body length to pharynx length; c, ratio of body length to tail length; c', ratio of tail length to cloacal or anus body diameter.

Species	L	a	b	c	c'	Cephalic sensilla length	Buccal cavity depth	Spicules length
<i>V. bandaensis</i>	1389–1715	41–48	4.8–5.1	12.8–13.8	6.0–6.5	papilla	23	18–20
<i>V. bayensis</i>	1630–1820	41–48	5.2	17.3	5.6	9–11	25–29	43–50
<i>V. dossena</i>	1759–2048	23–25	5–6	19–20	3.0	4–6	31–35	27–33
<i>V. epapillosa</i>	1750	51	5.3	20.7	4.9	6	16	29
<i>V. erasmi</i>	1905	60	5.7	15.9	5.0	5	23	32
<i>V. glabra</i>	1600–2100	42–70	5.3–6.3	7.5–11.0	10–13.0	papilla	23–25	27
<i>V. longicaudatoides</i>	1348–1432	53–54	4.8–5.4	8.3–9.0	10.1–10.8	2.3–3	17–18	27
<i>V. macramphida</i>	1400	39	5.6	7.9	9.6	papilla	15	18–19
<i>V. macrobursata</i>	1680–2200	50–53	5.7	13.2	8.6	10–12	23–29	20
<i>V. meridionalis</i>	1415–1743	30–43	5.3–6.9	8.2–9.6	7.3–9.8	papilla	18–25	32–40
<i>V. media</i> sp. nov.	1522–1620	46.5–58.5	4.9–5.1	18.8–20.4	4.7–5.5	7–8	16–18	24–30
<i>V. microseta</i>	1850	44	6.1	16.5	4.3	1.5–2.0 $\mu\text{m}$	20–22	33
<i>V. nuda</i>	1625–1931	45–54	5.2–6.0	7.3–8.0	13.0–13.5	papilla	18–22	18
<i>V. oncholaimelloides</i>	1950	89	6.5	13.9	9.1	papilla	13	17
<i>V. orientalis</i>	991–1122	17–20	4.7–5.1	15.7–19.9	2.8–3.0	2.0 $\mu\text{m}$	18–20	34–36
<i>V. papillatoides</i>	1520–2200	40–51	5.5–5.6	19.1–23.0	3.4–4.6	papilla	24–32	26–29
<i>V. papillate</i>	1520	31	5.0	11.0	6.0	papilla	18	24
<i>V. parasetosa</i>	1721–1748	52–55	5.7–5.9	11.6–12.0	8.2–8.3	2.7 $\mu\text{m}$	18–20	24
<i>V. profunda</i>	1311–1501	47–50	5.0–5.6	14.8–15.4	4.5–5.2	2.0–2.5 $\mu\text{m}$	17.5–18	17.5
<i>V. separabilis</i>	1320–2200	32–78	4.8–7.8	12.9–16.6	5.0–8.0	7.5 $\mu\text{m}$	20–26	19–26
<i>V. setosus</i>	1784–1857	51–57	6.0–6.1	11.9–12.1	8.0–9.0	5.0 $\mu\text{m}$	20–21	22
<i>V. sinica</i> sp. nov.	1733–1885	62–73	6.1–6.4	17.4–21.4	5.1–6.6	5–7 $\mu\text{m}$	26–29	19–22
<i>V. stenolaimus</i>	1870	37	4.5	12.6	4.6	papilla	25–27	37
<i>V. timmi</i>	1016–1509	22–37	4.1–5.1	16.0–25.6	2.0–3.5	2.5–3.0 $\mu\text{m}$	21–28	24–28
<i>V. viscosa</i>	1700–2600	52–60	5.0–6.5	12.0–16.0	6.0–7.5	4.0 $\mu\text{m}$	22–30	27–30
<i>V. weiseri</i>	1600–2900	29–46	4.3–5.2	13.3–17.7	4.5	5.0 $\mu\text{m}$	28–30	42

**Differential diagnosis and discussion.** *Viscosia sinica* sp. nov. is characterized by relatively large amphidial fovea, conico-cylindrical tail with horse-shoe-shaped tip, spicules slender, slightly curved ventrally, not cephalate proximally, 10–12 setae surrounding the cloaca, each 3–4  $\mu\text{m}$  long. The new species resembles *V. brachylaima* Filipjev, 1927 and *V. filipjevi* Paramonov, 1929 in tail shape, but differs from *V. brachylaima* by larger amphidial fovea (80% versus 30% corresponding body diameter) and higher value of de Man ratio *a* in males (61.9–72.8 versus 42.5). The new species differs from *V. filipjevi* which description is based only in females by larger amphidial fovea (wider than width of buccal cavity versus narrower than width of buccal cavity), and smaller body size (1.46–1.65 mm in body length and 28–31  $\mu\text{m}$  maximum body diameter in females versus 2.17–2.20 mm in length and 40.5–48.6  $\mu\text{m}$  maximum body diameter in *V. filipjevi*). The new species is also similar to *V. elegans* (Kreis, 1924) Lorenzen, 1981 in body size and shape, but differs by larger amphidial fovea (80% versus 33% corresponding body diameter) and horseshoe-shaped tail tip. The new species differs from *V. media* sp. nov. in having deeper buccal cavity with slender teeth in males (21–29  $\mu\text{m}$  deep versus 15–18  $\mu\text{m}$  with stubby teeth), larger amphidial fovea (versus invisible), and different tail shape (conico-cylindrical with swollen horseshoe-shaped end versus conical). *Viscosia sinica* sp. nov. is distinguished from all other known species of the genus by its relatively large amphidial fovea, 5–7  $\mu\text{m}$  cephalic setae, and conico-cylindrical tail with swollen horseshoe-shaped end.

## Acknowledgments

This work was supported by the National Natural Science Foundation of China (No. 41176107). Authors are very thankful to Prof. Dr Virag Venekey (the famous nematologist from Brazil) for constructive suggestions and for improving English writing of this article. We are sincerely grateful to anonymous referees for reviewing and improving the manuscript.

## Additional information

### Conflict of interest

The authors have declared that no competing interests exist.

### Ethical statement

No ethical statement was reported.

### Funding

This research was funded by the National Natural Science Foundation of China (grant number 41676146) and the Natural Science Foundation of Shandong Province (grant number ZR2022QC218).

### Author contributions

Project management, work program and taxonomy: Y.H.; methodology, experiment, and data collection: L.Y.S. and H.M.G; writing and editing of paper: Y.H. and L.Y.S. All authors have read and agreed to the submitted version of the manuscript.

## Author ORCIDs

Lingyun Sun  <https://orcid.org/0009-0005-3553-3645>

Huimin Gu  <https://orcid.org/0009-0008-5820-4678>

Yong Huang  <https://orcid.org/0000-0002-1846-8088>

## Data availability

All of the data that support the findings of this study are available in the main text.

## References

- Allgén CA (1927) Freilebende marine Nematoden von der Küste Tasmaniens. *Zoologischer Anzeiger* 9(10): 197–217.
- Allgén CA (1930) Über einige neue oder wenig bekannte Brachwasser-Nematoden von der Litoralzone des Öresunds. *Zoologischer Anzeiger* 85: 58–72.
- Allgén CA (1932) Weitere Beiträge zur Kenntnis der marinen nematodenfauna der Campbellinsel. *Nyt Magazin for Naturvidenskaberne* 70: 97–198.
- Allgén CA (1933) Freilebende Nematoden aus dem Trondhjemsfjord. *Capita Zoologica* 4(2): 1–162.
- Allgén CA (1935) Die freilebenden Nematoden des Öresunds. *Capita Zoologica* 6(3): 1–192.
- Allgén CA (1940) Über einige neue freilebende Nematoden von der Nordwest- und Nordküste Norwegens. *Folia Zoologica et Hydrobiologica* 10: 443–449.
- Allgén CA (1941) Über einige freilebende Nematoden aus Bandirma an der Nordküste Kleinasiens (Marmarameer, Türkei). *Zoologischer Anzeiger* 135: 281–294.
- Allgén CA (1946) Zur Kenntnis norwegischer Nematoden VI. Neue freilebende marine Nematoden von der Insel Frøya. *Kongelige Norske Videnskabers Selskab Forhandlingar* 18(38): 160–162.
- Allgén CA (1947) Die Nematoden-Familie Tripyloididae, ihre Arten und Verwandtschaft. *Arkiv for Zoologi* 39: 1–35.
- Allgén CA (1951) Pacific Freelifving Marine Nematodes. (Papers from Dr. Th. Mortensen's Pacific Expedition 1914–1916. LXXVI). *Videnskabelige Meddelelser fra Dansk naturhistorisk Forening* 113: 263–411.
- Allgén CA (1959) Freelifving marine nematodes. Further zoological results of the Swedish Antarctic expedition, 1901–1903 under the direction of Dr. Otto Nordenskjöld. 5(2) P.A. Norstedt & Söner, Stockholm, 293 pp.
- Bastian HC (1865) Monograph of the Anguillulidae, or Free Nematoids, Marine, Land, and Freshwater; with Descriptions of 100 New Species. *The Transactions of the Linnean Society of London* 25(2): 73–184. <https://doi.org/10.1111/j.1096-3642.1865.tb00179.x>
- Belogurov OI, Belogurova LS (1977) The morphology of *Viscosia poseidonica* n. sp. and *V. stenostoma* Platonova, 1971 (Nematoda, Oncholaimidae) free-living nematodes from the neighbourhood of the island of Furugel'ma Islands (Translated from Russian). *Nauchnye Doklady Vyssei Shkoly, Biologicheskie Nauki* 6: 44–47.
- Boucher G (1977) Nématodes des sables fins infralittoraux de la Pierre Noire (Manche occidentale). IV. Enoplida. *Bulletin du Muséum National d'Histoire Naturelle* 468: 733–752. <https://doi.org/10.5962/p.282054>
- Chitwood BG (1937) A new genus and ten new species of marine nematodes from North Carolina. *Proceedings of the Helminthological Society of Washington* 4: 54–59.
- Chitwood BG (1951) North American nematodes. *The Texas Journal of Science* 4: 617–672.

- Chitwood BG (1960) A preliminary contribution on the marine nemas (Adenophorea) of Northern California. *Transactions of the American Microscopical Society* 79: 347–384. <https://doi.org/10.2307/3224119>
- Cobb NA (1890) Arabian Nematodes. *Proceedings of the Linnean Society of New South Wales* 5: 449–468. <https://doi.org/10.5962/bhl.part.18647>
- Cobb NA (1898) Australian free-living marine nematodes. *Proceedings of the Linnean Society of New South Wales* 23(3): 383–407.
- Coomans AV, Vincx M, Decraemer W (1985) Nematodes from a fresh-water pool on a coral island in the Solomon Islands. *Hydrobiologia* 123(3): 265–281. <https://doi.org/10.1007/BF00034389>
- de Jonge VN, Bouwman LA (1977) A simple density separation technique for quantitative isolation of meiobenthos using the colloidal silica Ludox-TM. *Marine Biology* 42: 143–148. <https://doi.org/10.1007/BF00391564>
- de Man JG (1890) Quatrième note sur les nématodes libres de la mer du Nord et de la Manche. *Mémoires de la Société Zoologique de France* 3: 169–194.
- de Man, JG (1904) Nématodes libres (Expédition. Antarctique Belge). *Résultats du Voyage S. Y. Belgica*, 1–51.
- Ditlevsen H (1921) Papers from Dr. Th. Mortensens Pacific Expedition 1914–1916. III Marine free-living Nematodes from the Auckland and Campbell Islands. *Videnskabelige Meddelelser fra Dansk naturhistorisk Forening i Kjøbenhavn* 73: 1–39.
- Ditlevsen H (1928) Free-living marine nematodes from Greenland waters. *Meddelelser om Grønland* 23: 199–250.
- Dujardin F (1845) *Histoire naturelle des helminthes ou vers intestinaux*. Librairie Encyclopedique de Roret. Paris, 654 pp. <https://doi.org/10.5962/bhl.title.10123>
- Eberth CJ (1863) *Untersuchungen über Nematoden*. Leipzig, Verlag von Wilhelm Engelmann, 77 pp.
- Filipjev IN (1916) Les nematodes libres contenus dans les collections du musee Zoologique de l'Academie Imperiale des Sciences de Petrograd. *Annales du Museum Zoologique de Academie des Sciences Petrograd* 21: 59–116.
- Filipjev IN (1918) Free-living marine Nematodes from the vicinity of Sevastopol. Part 1. *Trudy Osoboï Zoologicheskoi Laboratorii Sebastopolskoi Stantsii Rossiïkoi, Series 2* 4: 1–614.
- Filipjev IN (1922) New data on free nematodes of the Black Sea (Novye Dannye o Svobodnykh Nematodakh Chernogo Moria.). *Trudy Stavropolskogo Selskokhoziaistvennogo Instituta* 1: 13–184.
- Filipjev IN (1927) Les Nématodes libres des mers septentrionales appartenant a la famille des Enoplidae. *Archiv für Naturgeschichte* 91: 1–216.
- Filipjev IN (1929) Classification of freelifing Nematoda and relations to parasitic forms. *Journal of Parasitology* 15: 281–282.
- Filipjev IN (1946) Nématodes libres du bassin polaire. *Trudy Dreifuiushchiae Ekspeditsiia Glavsevmorputi na Ledokol'nom Parokhode G. Sedov 1937–1940* 3: 158–184.
- Furstenberg JP, Vincx M (1989) Two oncholaimid species from a South African estuary (Nematoda, Oncholaimidae). *Hydrobiologia* 184: 43–50. <https://doi.org/10.1007/BF00014300>
- Gagarin VG, Nguyen Vu Thanh (2007) *Ingenia communis* sp. n., *Adoncholaimus longispiculatus* sp. n. and *Viscosia sedata* sp. n. (Nematoda: Enoplida) from Mekong River Delta, Vietnam. *International Journal of Nematology* 17(2): 205–212.
- Gagarin VG (2020) *Halalaimus borealis* sp. nov. and *Viscosia orientalis* sp. nov. (Nematoda, Enoplida) from the mouth of the Cam River in Vietnam. *Amurian Zoological Journal* 12: 26–42. <https://doi.org/10.33910/2686-9519-2020-12-1-26-42>

- Gagarin VG, Nguyen TT (2008). Free-living nematodes from the Red River delta, Vietnam. *Inland Water Biology* 1(4): 320–325. <https://doi.org/10.1134/S1995082908040020>
- Gerlach SA (1957) Die Nematodenfauna des Sandstrandes an der Küste von Mittelbrasilien (Brasilianische Meerese-Nematoden IV). *Mitteilungen aus dem Zoologischen Museum Berlin* 33: 411–459. <https://doi.org/10.1002/mmz.19570330206>
- Gerlach SA, Riemann F (1974) The Bremerhaven Checklist of Aquatic Nematodes. A catalogue of Nematoda Adenophorea, excluding the Doryaimida. Part 2. Veröffentlichungen des Instituts für Meeresforschung in Bremerhaven Supplement 4(2): 404–735.
- Heip C, Smol N, Vranken G (1982) The systematics and ecology of free-living marine nematodes. *Helminthological Abstracts Series B* 51(1): 1–31.
- Hope WD, Murphy DG (1972) A taxonomic hierarchy and checklist of the genera and higher taxa of marine nematodes. *Smithsonian Contributions to Zoology* 137: 1–101. <https://doi.org/10.5479/si.00810282.137>
- Huang M, Sui XX (2024) Description of *Amphimonhystrella sinica* sp. nov. and *Cobbia zhangii* sp. nov. of the family Xyalidae (Nematoda: Monhysterida) from the Yellow Sea, China *Zootaxa* 5471(3): 343–354. <https://doi.org/10.11646/zootaxa.5471.3.4>
- Huang M, Zhai HX (2024) Two new species of the genus *Halichoanolaimus* (Nematoda, Selachinematidae) from the intertidal zone of the Yellow Sea, China. *Zookeys* 1208: 259–274. <https://doi.org/10.3897/zookeys.1208.124047>
- Inglis WG (1983) An outline classification of the phylum Nematoda. *Australian Journal of Zoology* 31: 243–255. <https://doi.org/10.1071/ZO9830243>
- Keppner EJ (1987) Five new and one known species of free-living marine nematodes of the family Oncholaimidae (Nematoda: Enoplida) from Northwest Florida, U.S.A. *Transactions of the American Microscopical Society* 106(3): 214–231. <https://doi.org/10.2307/3226251>
- Kreis HA (1924) Zur Kenntnis der freilebenden marinen Nematoden. *Schriften für Süßwasser und Meereskunde, Büsum* 2: 157–170.
- Kreis HA (1929) Freilebende marine Nematoden von der Nordwest-Küste Frankreichs (Trébeurden Côtes du Nord). *Capita Zoologica* II 7: 1–98.
- Kreis HA (1932) Freilebende marine Nematoden von den Sunda-Inseln II. Oncholaiminae. *Videnskabelige Meddelelser fra Dansk naturhistorisk Forening* 93: 23–69.
- Kreis HA (1934) Oncholaiminae Filipjev 1916. Eine monographische Studie. *Capita Zoologica* 4(5): 1–271.
- Lambshhead PJD (2004) Marine nematode biodiversity. In: Chen ZX, Chen SY, Dickson DW (Eds) *Nematology: Advances and Perspectives*, Vol. 1. Nematode Morphology, Physiology and Ecology. CABI, Wallingford, 438–468. <https://doi.org/10.1079/9780851996455.0438>
- Leduc D, Zhao ZQ (2023) The Marine Biota of Aotearoa New Zealand. Ngā toke o Parumoana: Common free-living Nematoda of Pāuatahanui Inlet, Te-Awarua-o-Porirua Harbour, Wellington. *NIWA Biodiversity Memoir*, 135, 212 pp. <https://niwa.co.nz/oceans/niwa-biodiversity-memoirs>
- Li T, Huang Y, Huang M (2024) Two new species of the order Monhysterida (Nematoda) from the sea of China, *Zookeys* 1193: 63–79. <https://doi.org/10.3897/zookeys.1193.110188>
- Lorenzen S (1974) Die Nematodenfauna der sublitoralen Region der Deutschen Bucht, insbesondere im Titan-Abwassergebiet bei Helgoland. *Veröffentlichungen des Instituts für Meeresforschung in Bremerhaven* 14: 305–327.

- Lorenzen S (1981) Entwurf eines phylogenetischen System der freilebenden Nematoden. Veröffentlichungen des Instituts für Meeresforschung in Bremerhaven 7: 1–472.
- Mawson PM (1958) Free-living nematodes. Section 3: Enoploidea from subantarctic stations. B.A.N.Z. Antarctic Research Expedition Reports, Series B 6(14): 307–358.
- McIntyre AD, Warwick RM (1984) Meiofauna techniques. In: Holme NA, McIntyre AD (Eds) Methods for the study of marine benthos. Blackwell Scientific Publications, Oxford, 217–244.
- Nemys eds (2024) Nemys: World Database of Nematodes. [accessed 1 December 2024] <https://doi.org/10.14284/366>
- Nguyen Vu Thanh, Gagarin VG (2013) Three new species of nematodes (Nematoda: Enoplida) from coastal waters of Vietnam. Russian Journal of Marine Biology 39(6): 420–428. <https://doi.org/10.1134/S1063074013060060>
- Paramonov AA (1929) Die freilebenden Nematoden der Kinburnsenge und der angrenzenden Gewässer. Trudy Gosudarstvennoi Ikhtologicheskoi Opytnoi Stantsii 4(1): 59–129.
- Platonova TA (1971) Exploration of the fauna of the seas VIII (XVI). Fauna and flora of the Possjet Bay of the Sea of Japan. Zoological Institute Academy of Sciences of the USSR 8(41): 72–108.
- Schuermans Stekhoven Jr JH (1931) Ökologische und morphologische Notizen über Zuiderseenematoden. I. Die westliche Hälfte der Zuidersee. Zeitschrift für Morphologie Ökologie der Tiere 20 (4): 613–678. <https://doi.org/10.1007/BF00407681>
- Schuermans Stekhoven Jr JH (1942) The free living nematodes of the Mediterranean. III. The Balearic Islands. Zoologische Mededeelingen 23: 229–262.
- Schuermans Stekhoven Jr JH (1943) Freilebende marine Nematoden des Mittelmeeres. IV. Freilebende marine Nematoden der Fischereigründe bei Alexandrien. Zoologische Jahrbücher (Systematik) 76(4): 267–396.
- Smol N, Sharma J (1984) Two new and three redescribed species of *Viscosia* (Nematoda, Oncholaimidea). Hydrobiologia 114: 123–147. <https://doi.org/10.1007/BF00018110>
- Smol N, Muthumbi A, Sharma J (2014) Order Enoplida In: Schmidt-Rhaesa A (Ed.) Handbook of Zoology: Gastrotricha, Cycloneuralia and Gnathifera, Vol. 2: Nematoda. De Gruyter, Berlin, 193–249. <https://doi.org/10.1515/9783110274257.193>
- Steiner G (1921) Beiträge zur Kenntnis mariner Nematoden. Zoologische Jahrbücher (Systematik) 44: 1–68.
- Sun X Y, Bai RB, Zhai HX, Huang Y (2024) Species list of free-living marine nematodes in the Yellow Sea, China. Journal of Liaocheng University (Natural Science Edition) 37(6): 34–52. <https://doi.org/10.19728/j.issn1672-6634.2024050010>
- Vitiello P (1967) Nématodes libres marins de Roscoff. I. Description de cinq espèces nouvelles. Cahiers de Biologie Marine 8: 403–416.
- Vitiello P (1970) Nématodes libres marins des vases profondes du Golfe du Lion. I. Enoplida. Téthys 2: 139–210.
- Wieser W (1951) Untersuchungen über die algenbewohnende Mikrofauna mariner Hartböden. I. Zur Ökologie und Systematik der Nematodenfauna von Plymouth. Österreichische Zoologische Zeitschrift 3: 425–480.
- Wieser W (1953) Reports of the Lund University Chile expedition 1948–1949: 1. Enoploidea. Lunds Universitets Årsskrift, N. F. 49(6): 1–155.
- Wieser W (1959) Free-living nematodes and other small invertebrates of Puget Sound beaches. University of Washington Publications in Biology 19: 1–179.
- Wieser W, Hopper B (1967) Marine nematodes of the east coast of North America. I. Florida. Bulletin of the Museum of Comparative Zoology 135: 239–344.



# Notes on the genus *Diestramima* Storozhenko, 1990 (Orthoptera, Rhaphidophoridae) with description of three new species from China

Qidi Zhu<sup>1,2</sup>, Hao Xu<sup>1</sup>, Ruigang Yang<sup>3</sup>, Fuming Shi<sup>1</sup>

<sup>1</sup> College of Life Sciences, Hebei University, Baoding 071002, China

<sup>2</sup> College of Agronomy, Jiangxi Agricultural University, Nanchang 330045, China

<sup>3</sup> Scientific Research Academy of Guangxi Environmental Protection, Nanning 530022, China

Corresponding author: Fuming Shi ([shif\\_m@126.com](mailto:shif_m@126.com))

## Abstract

Three new species of the genus *Diestramima* are described from China: *Diestramima ligula* Zhu & Shi, **sp. nov.**, *Diestramima longzhouensis* Zhu & Shi, **sp. nov.**, and *Diestramima napoensis* Zhu & Shi, **sp. nov.** Moreover, the females of *Diestramima parabispinosa* Qin, Wang, Liu & Li, 2016 and *Diestramima distincta* Gorochov, 2010 are described for the first time. Images illustrating the morphology of these species are provided.

**Key words:** China, *Diestramima*, morphology, new species, taxonomy



Academic editor: Jun-Jie Gu

Received: 29 November 2024

Accepted: 3 February 2025

Published: 11 March 2025

ZooBank: <https://zoobank.org/AD0AFB1C-B2B9-4508-91D5-D93B7BB6D871>

Citation: Zhu Q, Xu H, Yang R, Shi F (2025) Notes on the genus *Diestramima* Storozhenko, 1990 (Orthoptera, Rhaphidophoridae) with description of three new species from China. ZooKeys 1231: 119–132. <https://doi.org/10.3897/zookeys.1231.143063>

Copyright: © Qidi Zhu et al.

This is an open access article distributed under terms of the Creative Commons Attribution License (Attribution 4.0 International – CC BY 4.0).

## Introduction

Storozhenko (1990) established the genus *Diestramima* and assigned *Diestrammena palpata* Rehn, 1906 as the type species. Subsequently, 34 species have been described in or transferred to the genus *Diestramima* based on morphological characters (Storozhenko 1990; Gorochov and Storozhenko 1992, 2015; Gorochov 1994, 1998, 2002, 2010; Liu and Zhang 2001; Storozhenko and Dawwrueng 2014; Qin et al. 2016; Zhu and Shi 2018; Wang et al. 2019; Cigliano et al. 2024). Gorochov and Storozhenko (2019) classified *Diestramima* into three subgenera, and Zhu et al. (2022) described six new species based on morphological and molecular evidence. Recently, Zhu et al.'s (2022) phylogenetic analysis did not support this three-subgenera classification system. He et al. (2023) reconstructed the phylogeny of *Diestramima* based on three mitochondrial genes and found that the topology was consistent with Zhu et al. (2022); He et al. (2023) published two new species and a junior synonym.

The genus *Diestramima* is mainly distributed across China, Vietnam, Laos, Myanmar, and the Indian Subcontinent. These insects prefer dark, moist habitats and are typically nocturnal, active at night, but hiding under leaves or loose bark during the day. Until now, the genus *Diestramima* has included 41 species, 31 species of which are recorded from China.

## Materials and methods

Specimens were collected by hand at night. The genitalia were dissected with an insect needle. Images were taken with a Zeiss AxioCam ICc5 digital camera attached to a Zeiss Stereo Discovery V12 microscope and edited with ADOBE PHOTOSHOP 2022. The measurements follow Zhu and Shi (2018). The type specimens of the new species are deposited in the Museum of Hebei University, Baoding, China (HBU).

## Results

### Genus *Diestramima* Storozhenko, 1990

#### *Diestramima ligula* Zhu & Shi, sp. nov.

<https://zoobank.org/69B04028-7993-490B-8338-6B6A27CB6EE7>

Fig. 1

**Material examined. Holotype:** CHINA • ♂, Yunnan Province, Wenshan Zhuang and Miao Autonomous Prefecture, Maguan County, 22.8576°N, 104.0042°E, alt. 1790 m, 19.VI.2024, Hao Xu leg. **Paratypes:** 1♂1♀, same data as for holotype.

**Diagnosis.** The new species is similar to *Diestramima major* Gorochov, 1998, but it can be easily distinguished from the latter by the shape of the seventh abdominal tergite and the paraproct of male. Posteromedian process of the seventh abdominal tergite of male rather long, surpassing apex of paraproct, basal half slender, paralleled on both sides, apical half slightly wider, apical area with a notch. Male paraproct digitiform, basal half broad, apical half slender, pointing upwards.

**Description. Male.** Body medium-sized. Fastigium verticis with 2 conical tubercles, apices separated, obtusely rounded, pointing forwards. Eyes ovoid, protruding forwards; median ocellus oval, located between antennal sockets, lateral ocelli nearly circular, situated on lateral surface of basal rostral tubercles. Apical segment of maxillary palp obviously longer than subapical one, apex truncated. Pronotum broad, anterior margin of disc straight, posterior margin arcuate; lateral lobe longer than high, ventral margin arched. Mesonotum and metanotum short, posterior margin of mesonotum arcuate, posterior margin of metanotum straight. Fore coxa with 1 small spine; femur unarmed on ventral surface, internal genicular lobe with 1 small spine, external genicular lobe with 1 long spine; tibia with 2 inner spines and 2 outer spines on ventral surface, apex with 1 outer spine on dorsal surface and 1 pair of spines on ventral surface, between the paired ventral spines with 1 small spine. Middle femur unarmed on ventral surface, internal and external genicular lobes with 1 long spine respectively; tibia with 2 inner spines and 2 outer spines on ventral surface, apex with 1 pair of dorsal spines and 1 pair of ventral spines, between the paired ventral spines with 1 small spine. Hind femur with 12 inner spines on ventral surface, internal genicular lobe with 1 small spine, external genicular lobe unarmed; tibia with 22–25 inner spines and 26 or 27 outer spines on dorsal surface, subapex with 1 pair of dorsal spines, apex with 1 pair of dorsal spines and 2 pairs of ventral spines, intero-dorsal spine obviously shorter than hind



**Figure 1.** *Diestramima ligula* Zhu & Shi, sp. nov. **A–F, I** ♂ **A–C** head and pronotum **A** frontal view **B** lateral view **C** dorsal view **D–F** apex of abdomen **D** lateral view **E** dorsal view **F** ventral view **I** hind tarsus in lateral view **G, H** ♀ **G** subgenital plate **H** ovipositor in lateral view.

basitarsus; hind basitarsus with 1 dorsal spine. Posterior margin of sixth abdominal tergite straight. Posteromedian process of seventh abdominal tergite rather long, surpassing apex of paraproct, basal half slender, paralleled on both sides, apical half slightly wider, apical area with a notch. Paraproct digitiform, basal half broad, apical half slender, pointing upwards. Cercus narrow, conical, apex acute. Genitalia with 8 membranous lobes, apical area of dorso-median lobe with a distinct notch, dorso-lateral lobes shorter than dorso-median lobe, ventro-lateral lobes divided into 2 lobes, ventro-median lobe short, apical area with a notch. Subgenital plate transverse and broad, posterior margin rounded.

**Female.** Appearance is similar to male. Posterior margin of seventh abdominal

tergite with a small process. Ovipositor narrow and long, slightly curved upwards, dorsal margin smooth, apical areas of ventral margin denticulate. Subgenital plate ligulate, apex rounded.

**Coloration.** Body light brown. Apical area of fastigium verticis and eyes yellow. Face with 4 longitudinal black stripes. All tibia with ring-like yellowish-brown stripes, basal half of hind femur with penniform yellowish-brown stripes.

**Measurements (mm).** Body length: ♂23.74, ♀20.46–22.02; length of pronotum: ♂5.18, ♀5.10–5.38; length of fore femur: ♂13.60, ♀13.66–14.04; length of hind femur: ♂22.16, ♀23.42; length of hind tibia: ♂26.28, ♀26.66; length of hind basitarsus: ♂4.04, ♀4.32; length of ovipositor: 23.56–26.82.

**Etymology.** The name of the new species refers to the ligulate subgenital plate of female. Latin “*ligul-*” referring to ligulate.

**Distribution.** Yunnan (Maguan County).

***Diestramima longzhouensis* Zhu & Shi, sp. nov.**

<https://zoobank.org/2BE2A27A-E72B-4A86-A9FD-677A920DC40E>

Figs 2, 3A, B

**Material examined. Holotype:** CHINA • ♂, Guangxi Zhuang Autonomous Region, Longzhou County, Zhubu Town, 16.VII.2021, Meng An leg. **Paratype:** CHINA • 1 ♀, Guangxi Zhuang Autonomous Region, Longzhou County, Nonggang, 22.4649°N, 106.9591°E, alt. 260 m, 16.VI.2024, Hao Xu leg.

**Other material.** CHINA • 1 ♂, Guangxi Zhuang Autonomous Region, Dahua County, Yalong Town, Hongri Village, 23.9918°N, 107.7900°E, alt. 700 m, 20.VII.2024, Yueting Duan leg.

**Diagnosis.** The new species can be easily distinguished from congeneric known species by the shape of the seventh abdominal tergite and the paraproct of male. Posteromedian process of the seventh abdominal tergite of male long, paralleled on both sides, apical half slightly curved downwards, apical area with a notch. Male paraproct digitiform, apex obtusely rounded.

**Description. Male.** Body larger than congeneric known species. Fastigium verticis with 2 conical tubercles, apices drawn together, obtusely rounded, pointing forwards. Eyes ovoid, protruding forwards; median ocellus oval, located between antennal sockets, lateral ocelli nearly circular, situated on lateral surface of basal rostral tubercles. Apical segment of maxillary palp obviously longer than subapical one, apex inflated, globular. Pronotum broad, anterior margin of disc straight, posterior margin arcuate; lateral lobe longer than high, ventral margin arc-shaped. Mesonotum and metanotum short, posterior margin of mesonotum arcuate, posterior margin of metanotum straight. Fore coxa with 1 small spine; femur unarmed on ventral surface, internal genicular lobe with 1 small spine, external genicular lobe with 1 long spine; tibia with 2 inner spines and 2 outer spines on ventral surface, apex with 1 outer spine on dorsal surface and 1 pair of spines on ventral surface, between the paired ventral spines with 1 small spine. Middle femur unarmed on ventral surface, internal and external genicular lobes with 1 long spine respectively; tibia with 2 inner spines and 2 outer spines on ventral surface, apex with 1 pair of dorsal spines and 1 pair of ventral spines, between the paired ventral spines with 1 small spine. Hind femur with 15–17 inner spines

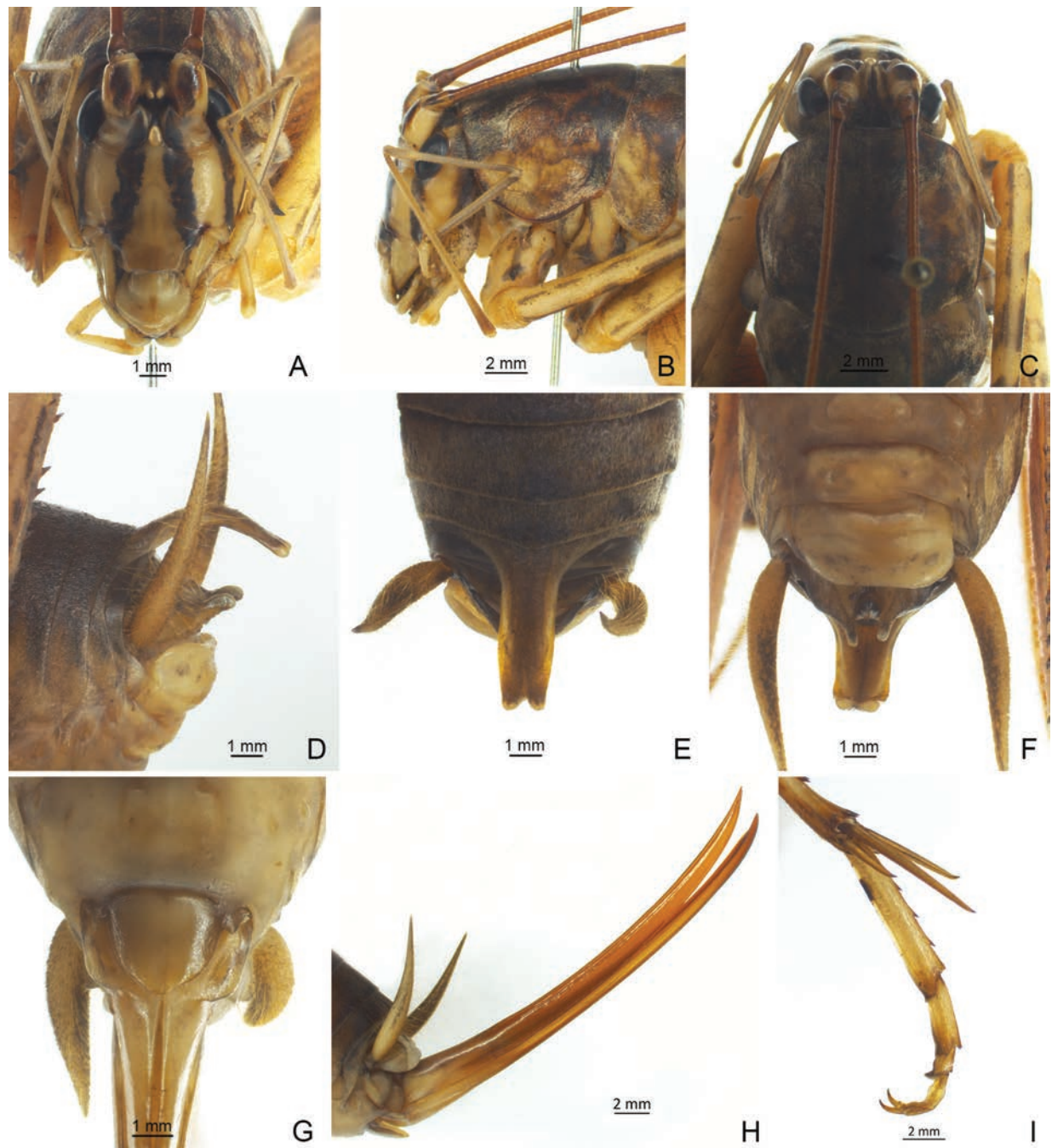


**Figure 2.** *Diestramima longzhouensis* Zhu & Shi, sp. nov. **A–F, I** ♂ **A–C** head and pronotum **A** frontal view **B** lateral view **C** dorsal view **D–F** apex of abdomen **D** lateral view **E** dorsal view **F** ventral view **I** hind tarsus in lateral view **G, H** ♀ **G** subgenital plate **H** ovipositor in lateral view.

and 6–9 outer spines on ventral surface, internal genicular lobe with 1 small spine, external genicular lobe unarmed; tibia with 38 or 39 inner spines and 39–41 outer spines on dorsal surface, subapex with 1 pair of dorsal spines, apex with 1 pair of dorsal spines and 2 pairs of ventral spines, intero-dorsal spine slightly shorter than hind basitarsus; hind basitarsus with 4 dorsal spines. Posterior margin of sixth abdominal tergite straight. Posteromedian process of seventh abdominal tergite long, paralleled on both sides, apical half slightly curved downwards, apical area with a notch. Paraproct digitiform, apex obtusely rounded. Cercus narrow, conical, apex acute.

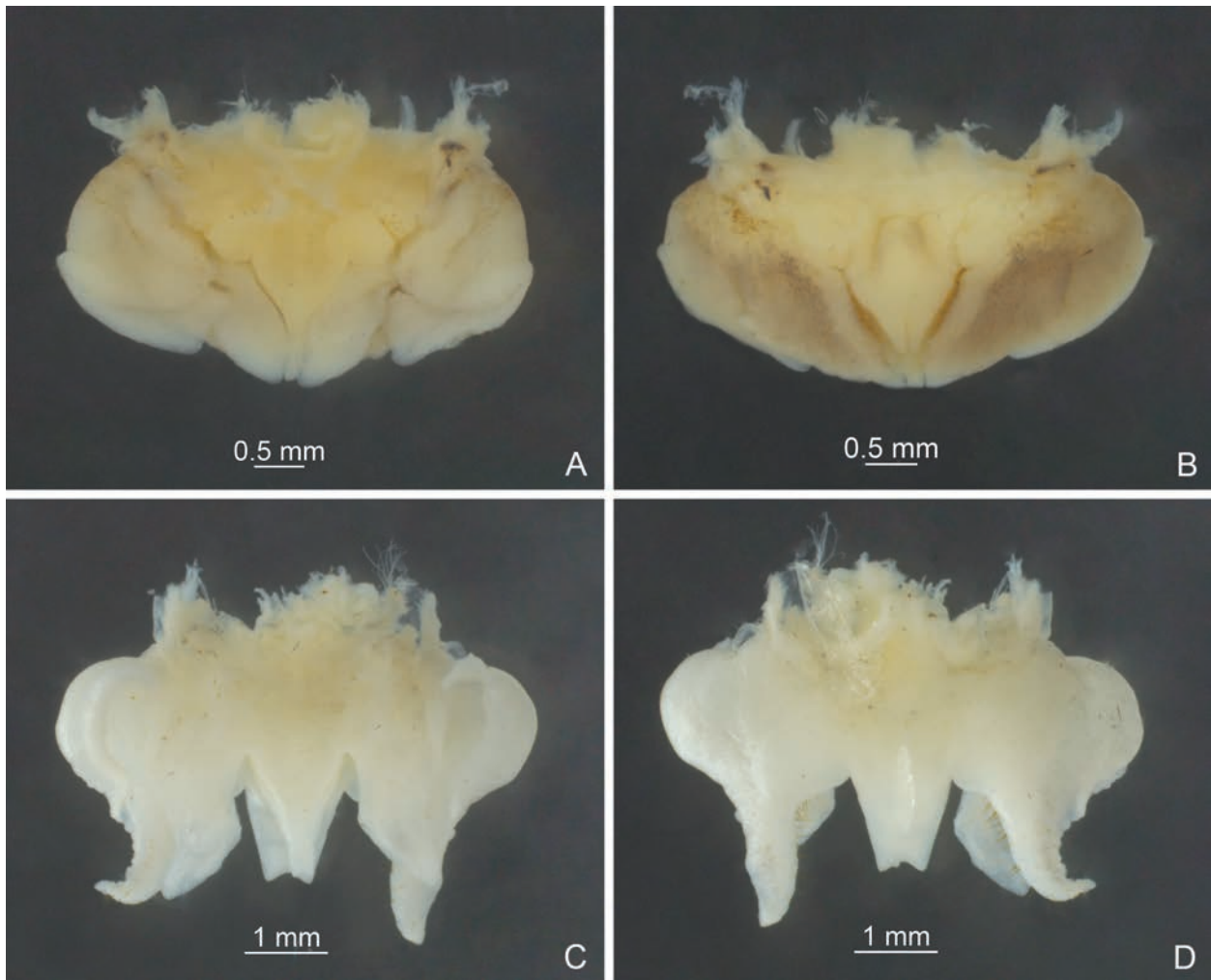


**Figure 3.** Male genitalia of *Diestramima* spp. **A, C** dorsal view **B, D** ventral view **A, B** *Diestramima longzhouensis* Zhu & Shi, sp. nov. **C, D** *Diestramima napoensis* Zhu & Shi, sp. nov.

Genitalia with 8 membranous lobes, apical area of dorso-median narrower than basal area, dorso-lateral lobes nearly equal to dorso-median lobe, ventro-lateral lobes divided into 2 lobes, ventro-median lobe short, apical area with a notch. Subgenital plate transverse and broad, posterior margin truncated. **Female.** Appearance is similar to male. Posterior margin of seventh abdominal tergite with a small process. Ovipositor narrow and long, slightly curved upwards, dorsal margin smooth, apical areas of ventral margin denticulate. Subgenital plate triangular, apex rounded.

**Coloration.** Body yellowish-brown. Face with 4 longitudinal black stripes. Fore and mid femora with ring-like black stripes, basal half of hind femur with penniform brown stripes.

**Measurements (mm).** Body length: ♂31.04–31.34, ♀34.92; length of pronotum: ♂8.30–8.70, ♀9.54; length of fore femur: ♂21.24–21.38, ♀22.50; length of hind femur: ♂41.04–43.82, ♀44.12; length of hind tibia: ♂47.36–48.82, ♀51.3; length of hind basitarsus: ♂8.54–8.80, ♀9.56; length of ovipositor: 30.24.

**Etymology.** The name of the new species derives from the type locality.

**Distribution.** Guangxi (Longzhou County, Dahua County).

***Diestramima napoensis* Zhu & Shi, sp. nov.**

<https://zoobank.org/35C9A27B-F64C-4F5C-8B6A-590A852A4C2C>

Figs 3C, D, 4, 5

**Material examined. Holotype:** CHINA • ♂, Guangxi Zhuang Autonomous Region, Napo County, Defu village, 23.2943°N, 105.8023°E, alt. 1330 m, 13.VIII.2024, Hao Xu leg. **Paratypes:** CHINA • 4♂4♀, Guangxi Zhuang Autonomous Region, Napo County, Defu village, 23.2943°N, 105.8023°E, alt. 1330 m, 11–14.VIII.2024, Hao Xu leg.

**Other material.** CHINA – Guangxi Zhuang Autonomous Region • 7♂2♀, Napo County, Defu village, 23.2943°N, 105.8023°E, alt. 1330 m, 11–14.VIII.2024, Hao Xu leg.; • 5♂6♀, Napo County, Baisheng Town, 23.0863°N, 105.5711°E, alt. 1310 m, 15.VIII.2024, Hao Xu leg.

**Diagnosis.** The new species is similar to *Diestramima austrosinensis* Go-rochov, 1998, but it can be easily distinguished by the shape of the seventh abdominal tergite and the paraproct of male. Posteromedian process of the seventh abdominal tergite of male long, basal 1/3 curved backwards and downwards, apical area divided into 2 branches, each with 2 small processes. Male paraproct platelike, pointing upwards, apex rounded.

**Description. Male.** Body medium-sized. Fastigium verticis with 2 conical tubercles, apices drawn together, obtusely rounded, pointing forwards. Eyes ovoid, protruding forwards; median ocellus oval, located between antennal sockets, lateral ocelli nearly circular, situated on lateral surface of basal rostral tubercles. Apical segment of maxillary palp obviously longer than subapical one, apex inflated, globular. Pronotum broad, anterior margin of disc straight, posterior margin arcuate; lateral lobe longer than high, ventral margin arch-shaped. Mesonotum and metanotum short, posterior margin of mesonotum arcuate, posterior margin of metanotum straight. Fore coxa with 1 small spine; femur unarmed on ventral surface, internal genicular lobe with 1 small spine, external genicular lobe with 1 long spine; tibia with 2 inner spines and 2 outer spines on ventral surface, apex with 1 outer spine on dorsal surface and 1 pair of spines on ventral surface, between the paired ventral spines with 1 small spine. Middle femur unarmed on ventral surface, internal and external genicular lobes with 1 long spine respectively; tibia with 2 inner spines and 2 outer spines on ventral surface, apex with 1 pair of dorsal spines and 1 pair of ventral spines, between the paired ventral spines with 1 small spine. Hind femur with 5–7 inner spines on ventral surface, internal genicular lobe with 1 small spine, external genicular lobe unarmed; tibia with 27–33 inner spines and 33 or 34 outer spines on dorsal surface, subapex with 1 pair of dorsal spines, apex with 1 pair of dorsal spines and 2 pairs of ventral spines, intero-dorsal spine slightly shorter than hind basitarsus; hind basitarsus with 2 dorsal spines. Posterior margin of sixth abdominal tergite straight. Posteromedian process of seventh abdominal tergite long, basal 1/3 curved backwards and downwards, apical area divided into 2 branches, each with 2 small processes. Paraproct platelike, pointing upwards and backwards, apex rounded. Cercus narrow, conical, apex acute. Genitalia with 8 membranous lobes, dorso-median lobe narrower, apical area with a notch, dorso-lateral lobes slightly longer than dorso-median lobe, ventro-lateral lobes divided into 2 lobes, ventro-median lobe broad, nearly equal to dorso-median lobe, apical area with a notch. Subgenital plate transverse

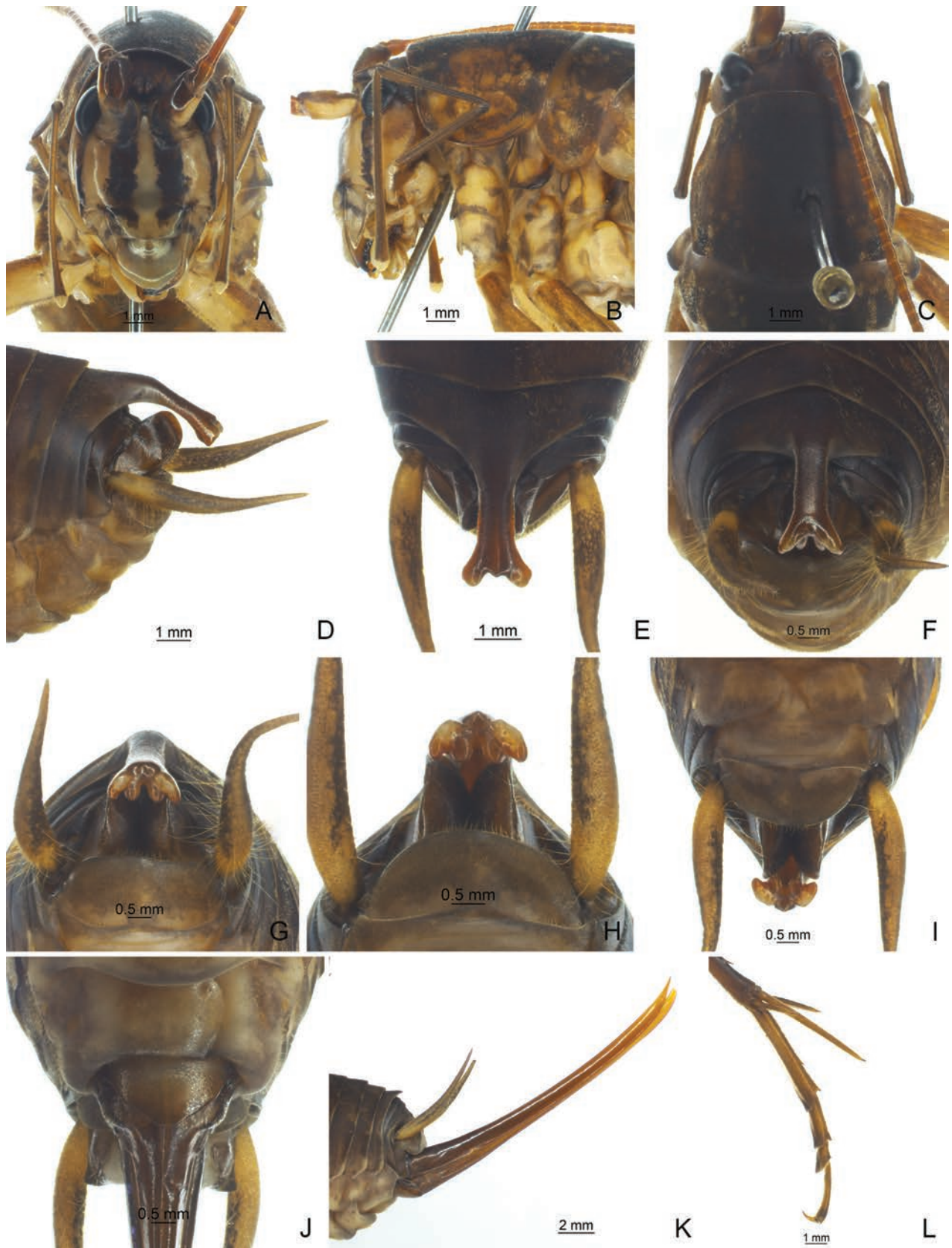


**Figure 4.** *Diestramima napoensis* Zhu & Shi, sp. nov. **A–I, L** ♂ **A–C** head and pronotum **A** frontal view **B** lateral view **C** dorsal view **D–I** apex of abdomen **D** lateral view **E** dorsal view **F** dorso-apical view **G, H** apical view **I** ventral view **L** hind tarsus in lateral view **J, K** ♀ **J** subgenital plate **K** ovipositor in lateral view.



Figure 5. Habitats of *Diestramima napoensis* Zhu & Shi, sp. nov. Photograph by Qianle Lu.

and broad, posterior margin truncated. **Female.** Appearance is similar to male. Posterior margin of seventh abdominal tergite with a small process. Ovipositor narrow and long, slightly curved upwards, dorsal margin smooth, apical areas of ventral margin denticulate. Subgenital plate triangular, apex rounded.

**Coloration.** Body light brown. Ocelli yellow. Face with 4 longitudinal black stripes. All femora with ring-like brown stripes, basal half of hind femur with penniform yellowish-brown stripes.

**Measurements (mm).** Body length: ♂19.32–22.56, ♀20.50–21.82; length of pronotum: ♂5.80–5.90, ♀5.78–6.08; length of fore femur: ♂13.80–14.72, ♀13.22–14.16; length of hind femur: ♂26.88–29.78, ♀27.34–28.04; length of hind tibia: ♂29.24–31.36, ♀28.54–30.24; length of hind basitarsus: ♂5.00–5.90, ♀5.70–5.90; length of ovipositor: 18.64–18.96.

**Etymology.** The name of the new species derives from the type locality.

**Distribution.** Guangxi (Napo County).

***Diestramima parabispinosa* Qin, Wang, Liu & Li, 2016**

Figs 6, 7A, B

*Diestramima parabispinosa* Qin, Wang, Liu & Li, 2016: 518.

**Material examined. Holotype:** CHINA • ♂, Guangxi Zhuang Autonomous Region, Huanjiang County, Mulun nature reserve, 18–22.VII.2015, alt. 300 m, Meiling Sun leg. **Paratype:** 1♀, same data as for holotype.

**Other material.** CHINA – Guangxi Zhuang Autonomous Region • 2♂2♀, Huanjiang County, Mulun, 25.1332°N, 107.9730°E, alt. 560 m, 28.VII.2024, Yueting

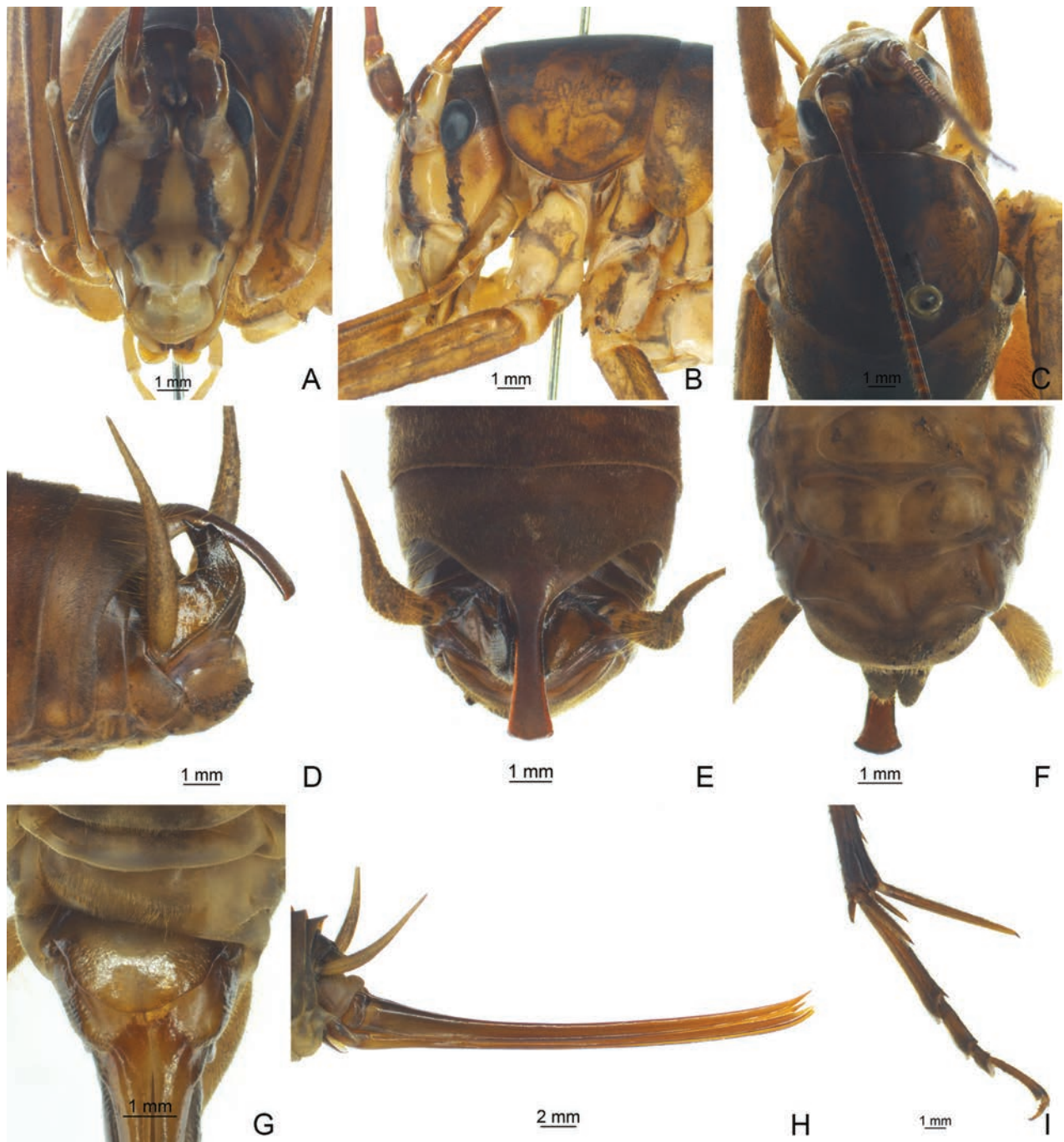


**Figure 6.** *Diestramima parabispinosa* Qin, Wang, Liu & Li, 2016. **A–F, I** ♂ **A–C** head and pronotum **A** frontal view **B** lateral view **C** dorsal view **D–F** apex of abdomen **D** lateral view **E** dorsal view **F** ventral view **I** hind tarsus in lateral view **G, H** ♀ **G** subgenital plate **H** ovipositor in lateral view.

Duan leg.; • 2♂1♀, Huanjiang County, Baidan Village, 25.1196°N, 108.0275°E, alt. 430 m, 4.VIII.2024, Yueting Duan leg.; • 1♂, Nandan County, Dongjia Village, 25.1131°N, 107.7472°E, alt. 840 m, 28.VII.2024, Yueting Duan leg.

**Description. Female.** Appearance is similar to male. Posterior margin of seventh abdominal tergite with a small process. Ovipositor narrow and long, dorsal margin smooth, apical areas of ventral margin denticulate. Subgenital plate semi-rounded.

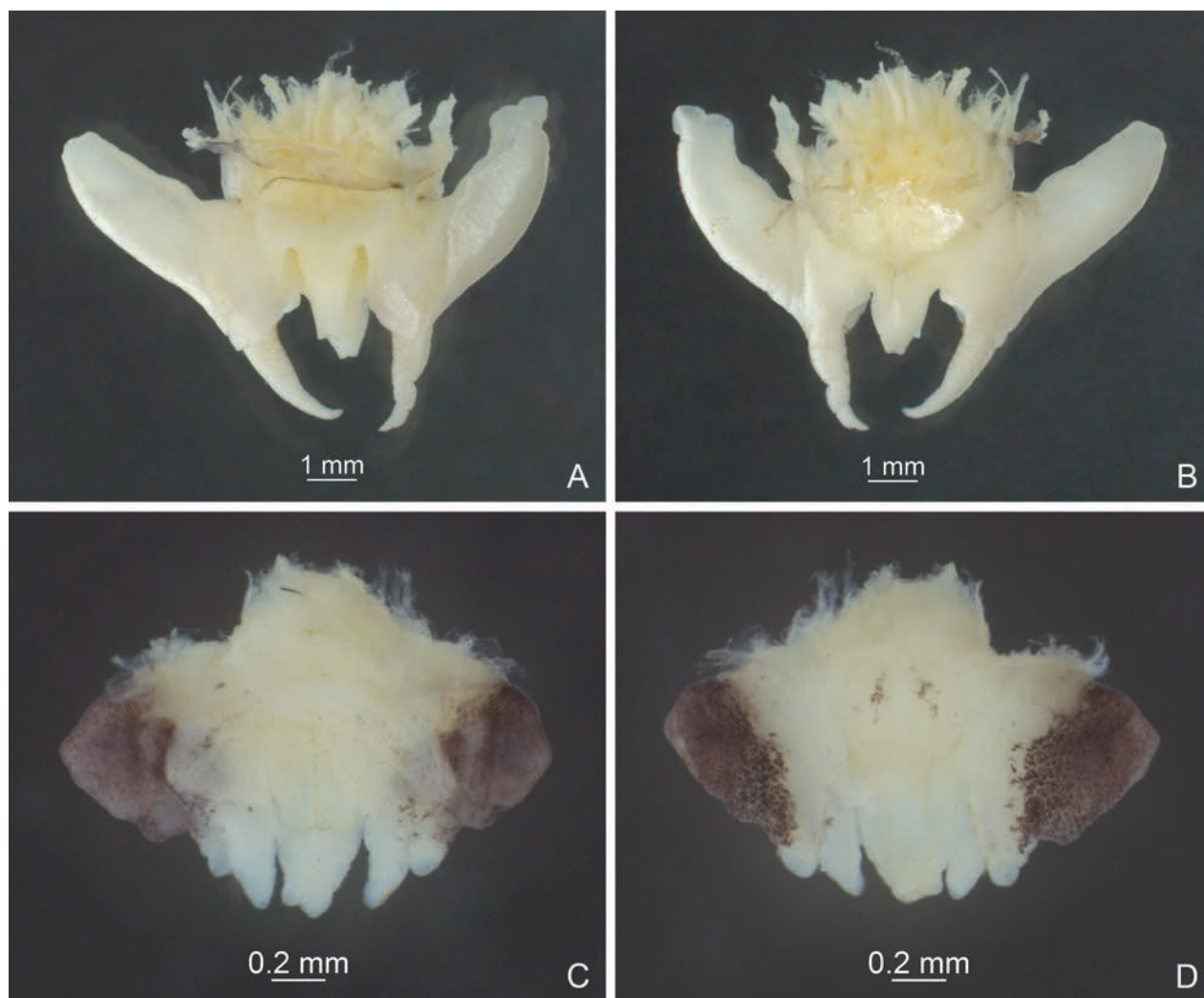


**Figure 7.** Male genitalia of *Diestramima* spp. **A, C** dorsal view **B, D** ventral view **A, B** *Diestramima parabispinosa* Qin, Wang, Liu & Li, 2016 **C, D** *Diestramima distincta* Gorochov, 2010.

**Distribution.** Guangxi (Huanjiang County, Nandan County).

**Remarks.** The female of *Diestramima parabispinosa* Qin, Wang, Liu & Li, 2016 is described for the first time.

***Diestramima distincta* Gorochov, 2010**

Figs 7C, D, 8

*Diestramima distincta* Gorochov 2010: 14.

**Material examined.** CHINA • 28♂46♀, Xizang Autonomous Region, Cuona County, Senmuzha, 27.8246°N, 91.7468°E, alt. 2630 m, 15–16.VII.2024, Qidi Zhu leg.

**Description. Female.** Appearance is similar to male. Posterior margin of seventh abdominal tergite with a small process. Ovipositor curved upwards, dorsal margin smooth, apical areas of ventral margin denticulate. Subgenital plate semi-rounded.

**Distribution.** Xizang (Cuona County).

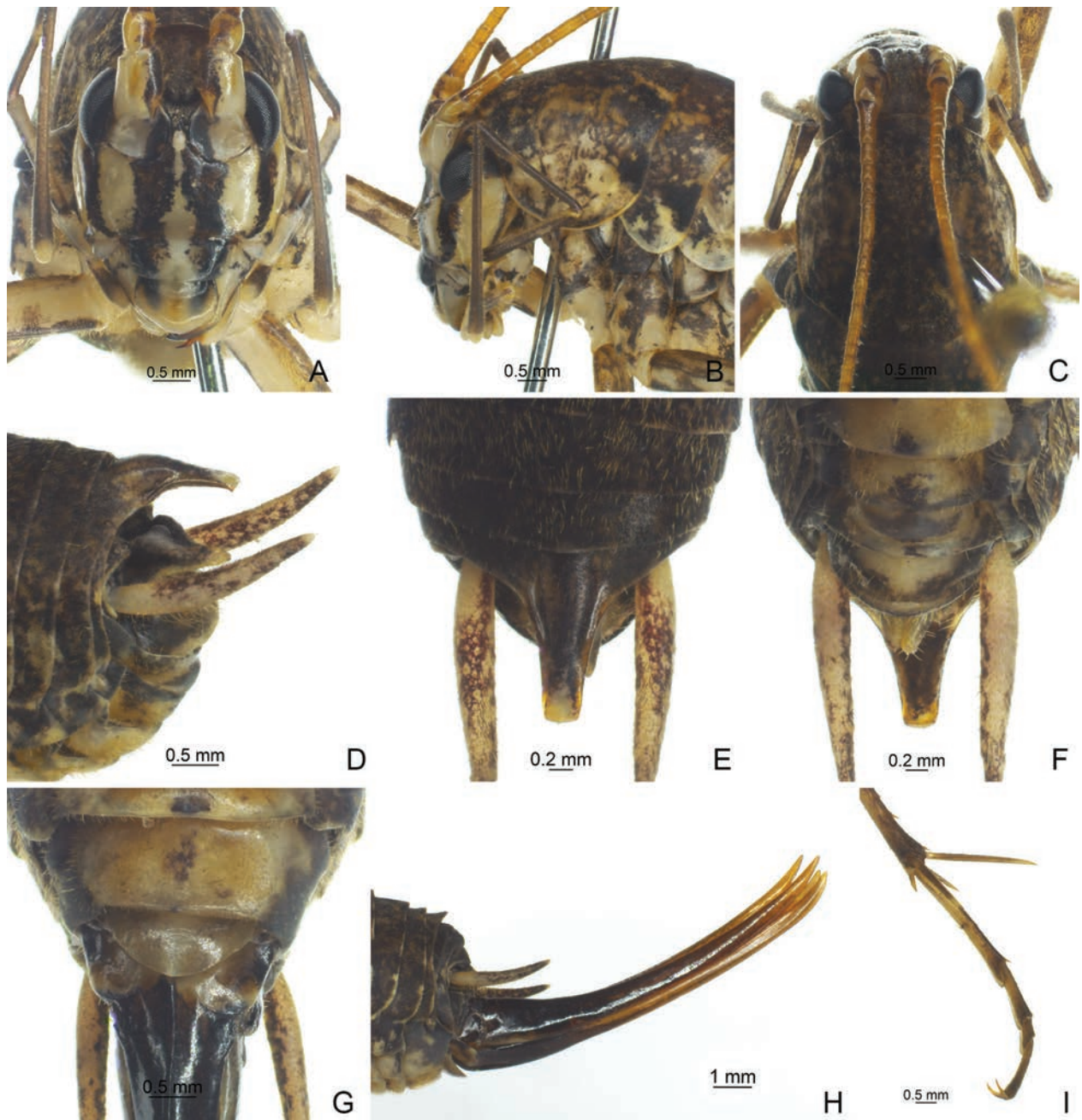


**Figure 8.** *Diestramima distincta* Gorochov, 2010. **A–F, I** ♂ **A–C** head and pronotum **A** frontal view **B** lateral view **C** dorsal view **D–F** apex of abdomen **D** lateral view **E** dorsal view **F** ventral view **I** hind tarsus in lateral view **G, H** ♀ **G** subgenital plate **H** ovipositor in lateral view.

**Remarks.** The female of *Diestramima distincta* Gorochov, 2010 is described for the first time.

### Acknowledgements

We are grateful to all the collectors for collecting the specimens and Mr Qianle Lu for providing the habitats of *Diestramima napoensis*. Special thanks are given to subject editor Junjie Gu and anonymous reviewers for their insightful comments and suggestions on the manuscript.

## Additional information

### Conflict of interest

The authors have declared that no competing interests exist.

### Ethical statement

No ethical statement was reported.

### Funding

This research was supported by the National Natural Science Foundation of China (No. 32400365, 31872268), the Survey of Wildlife Resources in Key Areas of Xizang (Phase II) (No. ZL202303601) and the Survey and Assessment of Priority Areas for Terrestrial Biodiversity Conservation in Guangxi (2024).

### Author contributions

Investigation: QZ, HX, RY. Writing-original draft: QZ. Writing-review and editing: QZ, FS.

### Author ORCIDs

Qidi Zhu  <https://orcid.org/0000-0001-8187-1286>

Hao Xu  <https://orcid.org/0009-0004-2497-1458>

Ruigang Yang  <https://orcid.org/0009-0009-4375-8798>

Fuming Shi  <https://orcid.org/0000-0002-4885-9012>

### Data availability

All of the data that support the findings of this study are available in the main text.

## References

- Cigliano MM, Braun H, Eades DC, Otte D (2024) Orthoptera Species File Online. Version 5.0/5.0. <http://Orthoptera.SpeciesFile.org> [Accessed on 22 November 2024]
- Gorochov AV (1994) New orthopterans of the infraorder Tettigoniidea (Orthoptera) from Vietnam and China. *Proceedings of the Zoological Institute of the Russian Academy of Sciences* 257: 18–50.
- Gorochov AV (1998) Data on fauna and taxonomy of Stenopelmatoidea (Orthoptera) from Indochina and some other territories: I. *Entomological Review* 78(1): 26–53.
- Gorochov AV (2002) Data on fauna and taxonomy of Stenopelmatoidea (Orthoptera) from Indochina and other territories: III. *Entomological Review* 82(7): 765–781.
- Gorochov AV (2010) New species of the families Anostostomatidae and Rhaphidophoridae (Orthoptera: Stenopelmatoidea) from China. *Far Eastern Entomologist* 206: 1–16.
- Gorochov AV, Storozhenko SY (1992) On the fauna of the subfamily Aemodogryllinae (Orthoptera, Rhaphidophoridae) in Vietnam. In *Proceedings of the Zoological Institute of the Russian Academy of Sciences* 245: 17–34.
- Gorochov AV, Storozhenko SY (2015) New and little-known taxa of the tribe Diestramimini (Orthoptera: Rhaphidophoridae: Aemodogryllinae) from Southeast Asia. Part 1. *Zoosystematica Rossica* 24(1): 48–84. <https://doi.org/10.31610/zsr/2015.24.1.48>
- Gorochov AV, Storozhenko SY (2019) New and little-known taxa of the tribe Diestramimini (Orthoptera: Rhaphidophoridae: Aemodogryllinae) from Southeast Asia.

- Part 2. Zoosystematica Rossica 28(1): 132–154. <https://doi.org/10.31610/zsr/2019.28.1.132>
- He ZQ, Yu ZY, Zong JS, Di M, Shen ZH, Liu YJ, Qin YY, Li K (2023) Two new species of the genus *Diestramima* from China (Orthoptera: Rhaphidophoridae: Aemodogryllinae). *Zootaxa* 5343(3): 281–295. <https://doi.org/10.11646/zootaxa.5343.3.4>
- Liu XW, Zhang WN (2001) Orthoptera: Tettigonioidae, Rhaphidophoroidea and Gryllacridoidea. In: Wu H, Pan CW (Eds) *Insects of Tianmushan National Nature Reserve*. Science Press Beijing: 90–102.
- Qin YY, Wang HQ, Liu XW, Li K (2016) A taxonomic study on the species of the genus *Diestramima* Storozhenko (Orthoptera: Rhaphidophoridae: Aemodogryllinae). *Zootaxa* 4126(4): 514–532. <https://doi.org/10.11646/zootaxa.4126.4.4>
- Storozhenko SY (1990) Review of the orthopteran subfamily Aemodogryllinae (Orthoptera, Rhaphidophoridae). *Entomologicheskoe Obozrenie* 69(4): 835–849.
- Storozhenko SY, Dawwrueng P (2014) New genus of the tribe Diestramimini (Orthoptera: Rhaphidophoridae) from Thailand. *Zootaxa* 3765(3): 288–294. <https://doi.org/10.11646/zootaxa.3765.3.5>
- Wang P, Zhu QD, Shi FM (2019) Supplement of the genus *Diestramima* Storozhenko, 1990 (Orthoptera: Rhaphidophoridae: Aemodogryllinae) from China. *Zootaxa* 4615(3): 577–584. <https://doi.org/10.11646/zootaxa.4615.3.10>
- Zhu QD, Shi FM (2018) Review of the genus *Diestramima* Storozhenko, 1990 (Orthoptera: Rhaphidophoridae: Aemodogryllinae) from China. *Zootaxa* 4450(2): 249–274. <https://doi.org/10.11646/zootaxa.4450.2.5>
- Zhu QD, Zhou ZJ, Zheng X, Wang T, Ma L, Shi FM (2022) Phylogeny and phylogeography of *Diestramima* cave crickets (Orthoptera: Rhaphidophoridae): speciation driven by multiple dispersal and vicariance events. *Systematic Entomology* 47: 179–201. <https://doi.org/10.1111/syen.12524>

# First report of subfamily Scydmaeninae (Coleoptera, Staphylinidae) from Shanghai, with description of two new species

Zi-Wei Yin<sup>1</sup>, Ting Feng<sup>2</sup>, De-Yao Zhou<sup>3</sup>

<sup>1</sup> Laboratory of Systematic Entomology, College of Life Sciences, Shanghai Normal University, Xuhui District, Shanghai 200234, China

<sup>2</sup> Shanghai Zoo, 2381 Hongqiao Road, Changning District, Shanghai 200335, China

<sup>3</sup> Jiading Agriculture Technology Extension Service Center, Jiading District, Shanghai 201403, China

Corresponding author: De-Yao Zhou ([scydmaeninae@163.com](mailto:scydmaeninae@163.com))

## Abstract

The subfamily Scydmaeninae (Coleoptera: Staphylinidae) is reported from Shanghai, China for the first time. Three species of the genus *Euconnus* Thomson were recognized: *E. (s. str.) dulcis* Sharp, 1886, *E. (s. str.) imparitus* **sp. nov.** (type locality: Waigang Town, Jiading District), and *E. (s. str.) magnoculus* **sp. nov.** (type locality: Shanghai Zoo, Hongqiao District). The new species are described, and diagnoses and illustrations of the habitus and important diagnostic features for all taxa are provided for ready identification. Furthermore, *Euconnus cerastiventris* Vit, 2006, **syn. nov.** is placed as a junior synonym of *E. dulcis*. A key to *Euconnus* species that occur in Shanghai is provided.

**Key words:** Ant-like stone beetles, East Asia, *Euconnus*, identification key, new record, new synonym, new taxa, Stenichnini, taxonomy, urban ecosystems



Academic editor: Jan Klimaszewski

Received: 23 November 2024

Accepted: 14 February 2025

Published: 11 March 2025

ZooBank: <https://zoobank.org/0AB2C080-BD9F-41C2-B480-8B7F94E84222>

**Citation:** Yin Z-W, Feng T, Zhou D-Y (2025) First report of subfamily Scydmaeninae (Coleoptera, Staphylinidae) from Shanghai, with description of two new species. ZooKeys 1231: 133–143. <https://doi.org/10.3897/zookeys.1231.142538>

Copyright: © Zi-Wei Yin et al.  
This is an open access article distributed under terms of the Creative Commons Attribution License (Attribution 4.0 International – CC BY 4.0).

## Introduction

The potential role of Shanghai, a mega-international metropolis in China, as a habitat for undescribed insect species has been consistently demonstrated over the past decade. A number of novel species, predominantly from the order Coleoptera (beetles), have been documented (Wang et al. 2017; Yin et al. 2017; Song et al. 2018, 2019). A continued survey of the rove beetle fauna in Shanghai, conducted primarily by a group of researchers affiliated with Shanghai Normal University, has resulted in the discovery of a small number of specimens belonging to the subfamily Scydmaeninae (Coleoptera: Staphylinidae), a large taxonomic group previously unreported in the city (O’Keefe and Li J-K 1998; Schülke and Smetana 2015). This study focuses on the genus *Euconnus* Thomson and reports findings on three species. The first two species, each represented by a single male specimen collected from Jiading and Hongqiao districts, respectively, are described herein as new to science. The third one, represented by both sexes collected from Minhang and Songjiang districts, has been identified as conspecific with a previously known species that exhibits a broad distributional range across East Asia. Although at least two additional potentially distinct species were observed, these are represented solely by females and are not presented in detail. This paper marks the first scientific

record of the subfamily Scydmaeninae in Shanghai and highlights the significance of fragmented habitats for preserving previously undocumented biodiversity within urban ecosystems.

## Material and methods

All specimens examined in this study are housed in the Insect Collection of Shanghai Normal University, Shanghai, China (SNUC). The label data for these specimens are quoted verbatim. Dissected parts were mounted in Euparal on plastic slides pinned with the specimen. Habitus images of the beetles were captured using a Canon EOS R5 camera equipped with a 10 × Mitutoyo M Plan Apo lens, with three 10W LED bulbs (5500 K) serving as the light source. Images of morphological details were taken using a Canon G9 camera mounted on an Olympus CX31 microscope under reflected or transmitted light. Image stacking was performed using Helicon Focus v. 8.2.0 Pro, and all images were edited and compiled into plates using Adobe Photoshop CC 2020.

Measurements were conducted as follows: head length was measured from the anterior margin of the clypeus to the head base, excluding the cervical constriction; head width was measured across the eyes; pronotum length was measured along the midline, and pronotum width was measured at its maximum width; elytra length was measured along the suture, while elytra width was measured at its maximum width across both elytra; total body length was measured from the apex of clypeus to the apex of elytra. In descriptions, paired appendages are treated as singular. Following Chandler (2001) and Yin (2022), the abdominal segments are numbered in Arabic (starting from the first visible segment) and Roman (reflecting true morphological position) numerals, e.g., sternite 1 (III).

## Taxonomy

**Family Staphylinidae Latreille, 1802**

**Subfamily Scydmaeninae Leach, 1815**

**Supertribe Scydmaenitae Leach, 1815**

**Tribe Stenichnini Fauvel, 1885**

**Genus *Euconnus* Thomson, 1859**

***Euconnus* (*s. str.*) *dulcis* Sharp, 1886**

Chinese common name: 雅宽突苔甲

Figs 1, 4

*Euconnus dulcis* Sharp, 1886: 47; Hoshina 2019: 201. Type locality: Nagasaki.

*Euconnus* (*s. str.*) *dulcis* Sharp; Jałoszyński 2022: 3; Byeon et al. 2023: 321.

*Euconnus chinensis* Li, J.-K. & Wang, Z.-Y., 1993: 163 (*nec. E. chinensis* Franz, 1985: 114). Type locality: Ningguo. Syn. nov.

*Euconnus cerastiventrif* Vit, 2006: 75 (replacement name for *E. chinensis* Li, J.-K. & Wang, Z.-Y.). Syn. nov.

**Material examined (5 exx.).** • 1 ♂: 'China: Shanghai City, Minhang Dist., 31°01'N, 121°28'E, alt. 4 m, 6.iv.2014, Xiao-Bin Song leg.'; • 2 ♀♀: 'China: Shanghai City,

Songjiang Dist., East Sheshan, 9.iv.2021, Xiao-Bin Song leg.'; • 3 ♀♀: 'China: Shanghai City, Jiading Dist., Liudao, 31°29'38"N, 121°14'3"E, alt. 3 m, 3.x.2023, Yin & Zhou leg.'. (all in SNUC).

**Diagnosis. Male.** Body length 1.4–1.7 mm. Dorsum of body finely punctate. Thick bristles present on tempora and sides of pronotum, especially dense on tempora. Anterior margin of clypeus (Fig. 1B) angularly prominent at middle. Antenna elongate, club loosely formed by apical four moderately enlarged antennomeres, occupying about half of antennal length. Pronotum bell-shaped, with two asetose basolateral pits connected by shallow transverse impression. Each elytron with two closely-placed basal pits. Abdomen greatly modified (Fig. 1C), sternite 4 (VI) and 5 (VII) each with two posterolateral nodules directed posteromedially, area between nodules on sternite 4 filled with peg-like granules distributed roughly in two transverse rows. Aedeagus (Fig. 1D, E) with apical projection much longer than parameres; endophallus armature composed of group of symmetric sclerites; parameres each greatly broadened, bearing two long setae near apex and three similar setae along lateral margin. **Female** (Fig. 1A). External morphology similar to male. Abdomen unmodified. Spermatheca (Fig. 1F) spherical; spermathecal duct broadened at base.

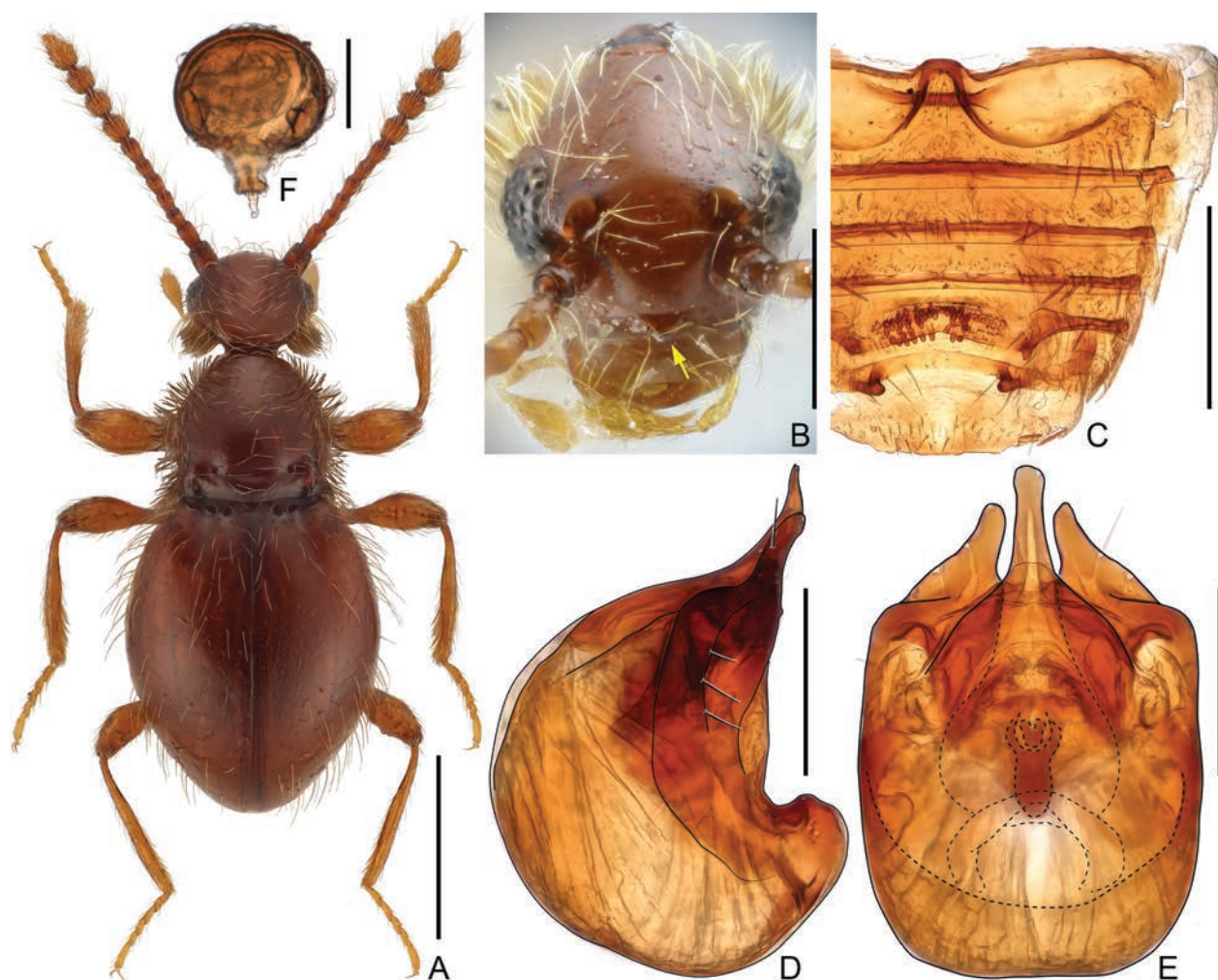


**Figure 1.** *Euconnus* (*s. str.*) *dulcis* (B–E male, F female) A dorsal habitus B head, in anterior view, showing clypeal angulation C sternites, showing modification on 4 (VI) and 5 (VII) D, E aedeagus, lateral (D) and ventral (E) F spermatheca, lateral. Scale bars: 0.5 mm (A); 0.2 mm (B, C); 0.1 mm (D, E); 0.05 mm (F).

**Description.** See Vit (2006) and Jałoszyński (2022). Measurement for Shanghai population: male body length 1.48 mm; length/width of head 0.35 mm/0.34 mm, pronotum 0.38 mm/0.37 mm, elytra 0.78 mm/0.63 mm, length of antenna 0.81 mm, club 0.42 mm, length of aedeagus 0.27 mm; female body length 1.49–1.53 mm; length/width of head 0.37–0.39 mm/0.34–0.38 mm, pronotum 0.41–0.43 mm/0.39–0.41 mm, elytra 0.86–0.88 mm/0.67–0.71 mm, length of antenna 0.77–0.80 mm, club 0.36–0.38 mm, maximum diameter of spermatheca 0.27 mm.

**Distribution.** East China: Anhui, Shanghai (Minhang, Songjiang, Jiading) (Fig. 4A); Japan: Honshu, Kyushu; South Korea: Jeju. New record for Shanghai.

**Biology.** Adult specimens were obtained by sifting grass roots, and mixed bush and bamboo leaf litter (Fig. 4B–D).

**Remarks.** This species exhibits a wide distribution across East Asia and is readily distinguishable by an angulate clypeus in both sexes, a sexually dimorphic abdomen in the male, and a distinctive morphology of the aedeagus. The descriptions and illustrations presented by Vit (2006) and Jałoszyński (2022) offer compelling evidence supporting the proposed synonymy. The spermatheca (Fig. 1F) of this species is illustrated for the first time.

***Euconnus (s. str.) imparitus* Zi-Wei Yin, Ting Feng & De-Yao Zhou, sp. nov.**

<https://zoobank.org/E0AF44E1-5C56-4F4A-996E-DCD68A6448AB>

Chinese common name: 异跗宽突苔甲

Figs 2, 4

**Type material (1 ex.). Holotype:** CHINA: ♂: 'China: Shanghai, Jiading, Waigang To., Quanjing Vill., 31°22'29"N, 121°8'22"E, late vii.2018, light trap, D-Y Zhou leg., 嘉定外冈泉泾村测报灯周德尧' (SNUC).

**Diagnosis. Male.** Habitus elongate; body length approximately 1.7 mm. Head and elytra finely punctate, subglabrous, with sparse long setae; punctation and setae of pronotal disc similar to those of head and elytra, lateral margins densely setose and with numerous thick bristles. Head subspherical, eyes anteriorly situated, tempora much longer than eyes. Antennae elongate, antennomeres elongate, clubs loosely formed by apical four enlarged antennomeres. Pronotum lacking antebasal pits, transverse impression, or sublateral carinae; broadest slightly posterior to middle. Tarsomere 1 of protarsus modified, ventrally protruding to form apically truncate projection. Aedeagus moderately elongate, dorso-ventrally symmetric; compressor plate in ventral view with two lateral lobes; apical projection of median lobe broad at base and narrowing apically; parameres broadened before apices, each paramere with three macrosetae at apex. **Female.** Unknown.

**Description. Male.** Body (Fig. 2A) length 1.66 mm; body uniformly reddish-brown, mouthparts and tarsi paler in color. Setae long and suberect, sparse on head and pronotal and elytral discs, sides of pronotum with dense, thick bristles. Dorsum of body finely and sparsely punctate, almost glabrous.

Head subrounded, as long as wide, broadest at eyes, length and width 0.36 mm; vertex and frons confluent, weakly convex; supraantennal tubercles barely prominent; eyes relatively small, barely convex and finely faceted. Punctures on vertex and frons fine; setae long and sparse, suberect, tempora much

longer than eyes, lacking bristles. Antenna elongate, length 0.93 mm, club 0.48 mm; antennomeres 1–7 each elongate, 2 and 7 longest, 8–11 broader than 2–7, enlarged, form loose club.

Pronotum in dorsal view slightly longer than wide, subglobose, broadest slightly posterior to middle and narrowing anteriorly and posteriorly, length 0.4 width 0.41 mm; lacking lateral antebasal pits, transverse antebasal groove and sublateral carinae. Punctures on pronotal disc rather fine, almost glabrous; setae sparse and long, laterally obscured by dense, long and thick bristles.

Elytra suboval and slightly flattened, broadest approximately at middle, length 0.94 mm, width 0.73 mm, length/width 1.29; basal impressions shallow, with four small, asetose basal pits, humeral calli weak; apices of elytra separately rounded. Punctures on elytral disc fine and shallow; sparse setae long and suberect. Metathoracic wings fully developed, functional.

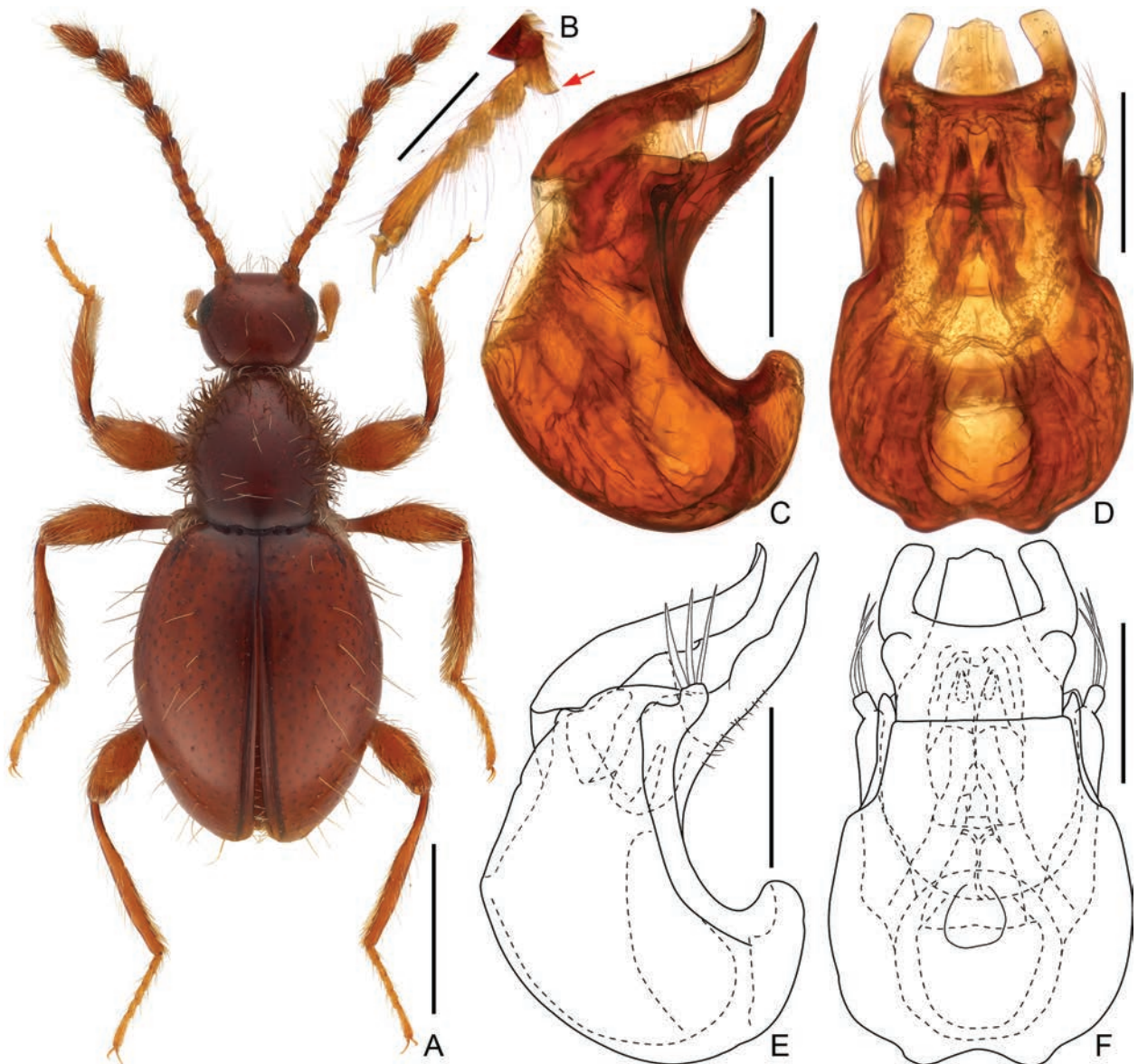


**Figure 2.** *Euconnus* (s. str.) *imparitus* sp. nov., male **A** dorsal habitus **B** protarsus **C–F** aedeagus, lateral (**C**, **E**) and ventral (**D**, **F**). Scale bars: 0.5 mm in (**A**); 0.1 mm (**B–F**).

Meso- and metaventrite fused. Mesoventral intercoxal process posteriorly extending far beyond level of posterior margin of mesocoxae. Metaventral intercoxal process broad, emarginate at middle.

Legs long and slender; protarsus with tarsomere 1 projecting ventrally, forming short, apically truncate lobe (Fig. 2B).

Aedeagus (Fig. 2C–F) moderately elongate, dorso-ventrally almost symmetric, length 0.34 mm, in ventral view median lobe with long, apically narrowing projection greatly curved dorsally, with two rows of fine setae along dorsal wall of projection; compressor plate broadened in dorso-ventral view, with pair of short and broad lateral lobes, plate inclined to apically-projected median lobe in lateral view and curved dorsally; endophallus armature composed of pairs of elongate and sclerotized plates and membranous structures; parameres elongate, narrow, extending just beyond base of apical projection of median lobe, areas before apices greatly broadened and then abruptly narrowing apically, each paramere with three long macrosetae at apex.

**Female.** Unknown.

**Comparative notes.** This species is closely related to *Euconnus impar* Sharp, distributed in Japan and South Korea, due to similar morphological features (elongate habitus, subglabrous head and elytra, dense bristles on pronotum sides, loosely assembled tetramerous antennal clubs), and particularly the modified male protarsi. However, *E. imparitus* is clearly distinguishable by its significantly different aedeagal structure. The aedeagus of the new species comprises a compressor plate with two short, blunt lateral lobes (vs. with two long, rod-like lobes in *E. impar*), a dorso-apical projection of the median lobe that narrows apically in ventral view (vs. apical projection broad and blunt in *E. impar*), and parameres broadening near the apices, each bearing three apical macrosetae (vs. parameres slender throughout, each with two long apical setae in *E. impar*). Additionally, the apical four antennomeres forming the club of this species appear relatively more elongate than those of *E. impar*.

**Distribution.** East China: Shanghai (Jiading) (Fig. 4A).

**Biology.** The male was taken from a mixed light trap sample deployed in an agricultural setting (Fig. 4E).

**Etymology.** The specific epithet is derived from a combination of *E. impar*, a closely related species, and the Latin suffix “-itus (-a, -um)”, denoting an affinity between these two species.

***Euconnus* (s. str.) *magnoculus* Zi-Wei Yin, Ting Feng & De-Yao Zhou, sp. nov.**

<https://zoobank.org/5A02E349-93CC-44C7-97F3-A3012053D692>

Chinese common name: 大眼宽突苔甲

Figs 3, 4

**Type material (1 ex.). Holotype: CHINA:** • ♂: ‘China: Shanghai, Hongqiao Dist., Shanghai Zoo, 31.198056°N, 121.354964°E, alt. 10 m, 07.vi.2023, Ting Feng leg., 上海动物园封婷采’ (SNUC).

**Diagnosis. Male.** Body length approximately 1.5 mm. Eyes greatly prominent, approximately 1.4 × as long as tempora. Terminal four antennomeres greatly enlarged and forming distinct club, occupying approximately 5.5/10 of antennal length. Sides of elytra distinctly narrowing posteriorly from broadest point.

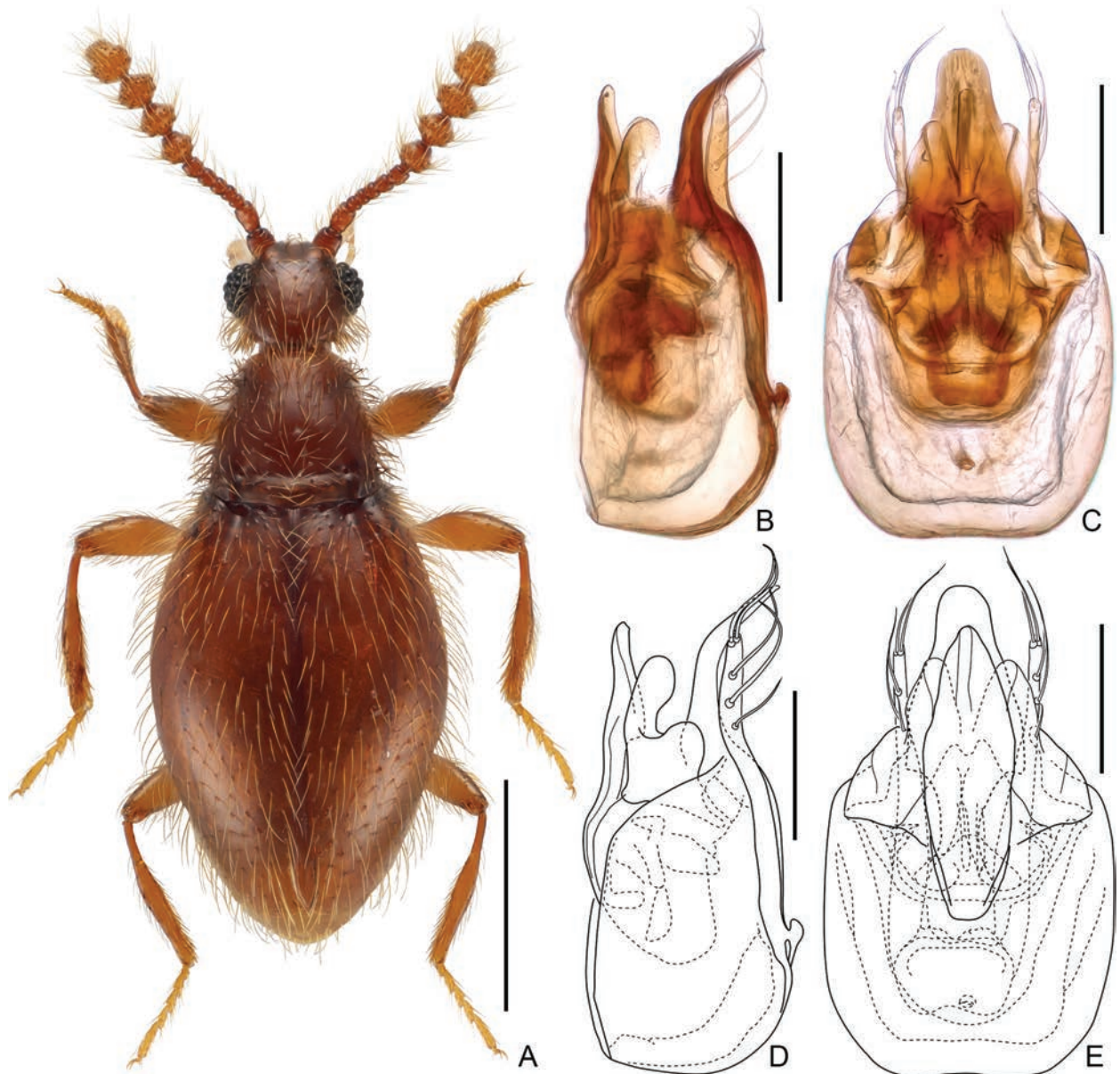


**Figure 3.** *Euconnus* (s. str.) *magnoculus* sp. nov., male **A** dorsal habitus **B–E** aedeagus, lateral (**B, D**) and ventral (**C, E**). Scale bars: 0.5 mm (**A**); 0.1 mm (**B–E**).

Aedeagus with compressor plate elongate and subfusiform in ventral view; apical projection of median lobe rounded and greatly protruding in ventral view, curved dorsally in apical portion in lateral view; median lobe with pair of apically rounded lateral projections, and transversely rhomboidal plate on ventral wall; broad and elongate parameres narrowing from bases toward apices, each with two long setae at apex and three similar long setae along apical 2/5. **Female.** Unknown.

**Description. Male.** Body (Fig. 3A) length 1.52 mm; body uniformly reddish-brown, mouthparts and tarsi paler in color. Setae long and suberect, tempora of head and sides of pronotum with dense, thick bristles. Dorsum of body finely and sparsely punctate.

Head roundly rhomboidal, as long as wide, broadest at eyes, length and width 0.31 mm; vertex and frons confluent, weakly convex; supraantennal tubercles barely prominent; eyes large, strongly convex and coarsely faceted. Punctures on vertex



**Figure 4.** Distribution and collecting circumstances of *Euconnus* species in Shanghai **A** distribution of the three species **B–D** collecting circumstance of *E. dulcis* at Minhang (**B**), Sheshan (**C**), and Liudao (**D**), *E. imparitus* sp. nov. at Quanjing Village (**E**), and *E. magnoculus* sp. nov. at Shanghai Zoo (**F**).

and frons fine; setae long and sparse, suberect, additionally tempora with long bristles directed posteriorly. Antenna moderately short, length 0.56 mm, club 0.31 mm; antennomeres 1 and 2 subcylindrical, elongate, 3–7 compact, gradually larger, 8–11 greatly enlarged, conical, 11 largest, distinctly shorter than 9 and 10 combined.

Pronotum in dorsal view subtrapezoidal, broadest at base and strongly narrowing anteriorly, length 0.35 mm, width 0.38 mm; lateral antebasal pits small but distinct, asetose, connected by transverse antebasal groove.

Punctures on pronotal disc fine; setae long, obscured by dense, long and thick bristles especially on sides.

Elytra suboval and slightly flattened, broadest approximately at middle, length 0.89 mm, width 0.63 mm, length/width 1.39; basal impressions shallow but distinct, with four small, aetose basal pits, humeral calli elongate; apices of elytra separately rounded. Punctures on elytral disc fine and shallow; setae long, sparse and suberect. Metathoracic wings fully developed, functional.

Meso- and metaventrite fused. Sides of mesoventral intercoxal process posteriorly divergent, form pair of ridges, similar to condition in *E. maklinii* (Mannerheim) (Jałoszyński 2021: fig. 8). Metaventral intercoxal process relatively narrow.

Legs long and slender; unmodified.

Aedeagus (Fig. 3B–E) moderately elongate, dorso-ventrally almost symmetric, length 0.31 mm, in ventral view median lobe with abruptly delimited and long, broad apical projection greatly curved dorsally, rounded at apex; compressor plate relatively narrow and subfusiform in dorso-ventral view, with narrowed anterior and posterior margins, connected in parallel to median lobe in lateral view; lateral projections broad and partially sclerotized, curved dorsally, with round apices; endophallus armature composed of pairs of complex, symmetric sclerotized plates and large, transversely rhomboidal plate, its apical margin with two admesal roundly acute projections; parameres broad and elongate, narrowing from bases toward apices, each with two long setae at apex, and three similar long setae along apical 2/5.

**Female.** Unknown.

**Comparative notes.** Among the East Asian *Euconnus* fauna, several species exhibit a similar general shape of the aedeagus. These include *E. efferus* Franz from China (Taiwan) (Franz 1985), *E. deprecator* Kurbatov from the Russian Far East (Kurbatov 1993), and *E. akane* Hoshina from Japan (Hoshina 2020). Despite the similarities, these species are distinctly differentiated by their endophallus armature, which comprises asymmetric sclerites. In contrast, the new species possesses an aedeagus that is almost symmetric both externally and internally. Additionally, similarly symmetric aedeagi are found in *E. kelantanensis* Franz from West Malaysia and *E. parakelantanensis* Franz from north-central Thailand; however, these species are considerably smaller, measuring only 1.20 mm and 1.10 mm in length, respectively (Franz 1970, 1985).

**Distribution.** East China: Shanghai (Hongqiao) (Fig. 4A).

**Biology.** The specimen was collected from a leaf litter sample taken in a secondary mixed forest within Shanghai Zoo (Fig. 4F).

**Etymology.** The name is a combination of the Latin adjective “*magnus* (great, large)” and noun “*oculus* (eye)”, referring to the large eyes of this species.

### Key to *Euconnus* species occurring in Shanghai (male)

- 1 Head lacking thick bristles on tempora (Fig. 2A); antennal clubs comprising elongate antennomeres (Fig. 2A); male protarsomere 1 modified, ventrally expanded to form blunt projection (Fig. 2A, B) ..... ***E. imparitus* sp. nov.**
- Head with thick bristles on tempora; antennal clubs formed by cornicle or submoniliform antennomeres; male protarsomere 1 simple, lacking modifications ..... **2**
- 2 Eyes greatly convex, much longer than tempora (Fig. 3A); antennomeres 8–10 conical (Fig. 3A); anterior margin of clypeus smooth, lacking tuber-

- cle at middle; sternites 4 (VI) and 5 (VII) simple, lacking modifications ..... *E. magnoculus* sp. nov.
- Eyes moderately convex, distinctly shorter than tempora (Fig. 1A); antennomeres 8–10 submoniliform; anterior margin of clypeus with angulate tubercle at middle (Fig. 1B); sternites 4 (VI) and 5 (VII) modified, each with pair of lateral tubercles on posterior margin (Fig. 1C)..... *E. dulcis* Sharp

## Acknowledgments

An anonymous reviewer and Sergey Kurbatov (All-Russian Plant Quarantine Center, Moscow, Russia) commented on the draft manuscript which improved the manuscript. Xiao-Bin Song (Big City Small Bug Studio, Shanghai, China) gifted specimens collected in Minhang and Songjiang districts as well as habitat pictures.

## Additional information

### Conflict of interest

The authors have declared that no competing interests exist.

### Ethical statement

No ethical statement was reported.

### Funding

Financial support was provided by the National Natural Science Foundation of China (No. 32370465), and Minhang District Biodiversity Survey and Assessment Project.

### Author contributions

ZWY prepared the illustrations, drafted the manuscript, and secured the funding. TF collected and examined the specimens and revised the manuscript. DYZ conceptualized the study, collected and examined the specimens, and revised the manuscript. All authors read and approved the final manuscript.

### Author ORCIDs

Zi-Wei Yin  <https://orcid.org/0000-0001-6659-9448>

Ting Feng  <https://orcid.org/0009-0007-0869-6654>

De-Yao Zhou  <https://orcid.org/0000-0002-2014-9967>

### Data availability

All of the data that support the findings of this study are available in the main text.

## References

- Byeon U-J, Song M-H, Park J-S (2023) Two species of the genus *Euconus* Thomson (Coleoptera: Staphylinidae: Scydmaeninae) new to Korea. *Journal of Asia-Pacific Biodiversity* 16: 317–323. <https://doi.org/10.1016/j.japb.2022.12.002>
- Chandler DS (2001) Biology, morphology, and systematics of the ant-like litter beetles of Australia (Coleoptera: Staphylinidae: Pselaphinae). *Memoirs on Entomology International* 15: 1–560.

- Franz H (1970) Zur Kenntnis der Scydmaeniden-Fauna von Singapore, Malakka und Indonesien (Coleoptera: Scydmaenidae). *Beiträge zur Entomologie* 20(5–6): 535–578. <https://doi.org/10.21248/contrib.entomol.20.5-6.535-578>
- Franz H (1985) Neue und ungenügend bekannte Scydmaeniden (Coleoptera) aus Taiwan, Fukien und Thailand. *Mitteilungen der Münchner Entomologischen Gesellschaft* (1984) 74: 91–128.
- Hoshina H (2019) Taxonomic note on the genus *Euconnus* (Coleoptera: Staphylinidae: Scydmaeninae) from Japan (III). *Japanese Journal of Systematic Entomology* 25(2): 201–202.
- Hoshina H (2020) Three new species of the genus *Euconnus* (Coleoptera: Staphylinidae: Scydmaeninae) from Shikoku, Japan. *Memories of the Faculty of Education, Humanities and Social Sciences, University of Fukui* 4: 67–75.
- Jałoszyński P (2021) Taxonomy of ‘*Euconnus* complex’. Part XXIII. Status of *Napochus* Thomson, *Pycnophus* Casey, and *Filonapochus* Franz revisited (Coleoptera, Staphylinidae, Scydmaeninae). *Zootaxa* 5026(2): 255–270. <https://doi.org/10.11646/zootaxa.5026.2.6>
- Jałoszyński P (2022) *Euconnus* Thomson of Japan: redescriptions of species established by Reitter, Sharp and Franz, new synonyms, and summary of current state of knowledge (Coleoptera, Staphylinidae, Scydmaeninae). *Zootaxa* 5093(1): 1–37. <https://doi.org/10.11646/zootaxa.5093.1.1>
- Kurbatov SA (1993) Scydmaenid beetles of the genera *Stenichnus* Thoms. and *Euconnus* Thoms. (Coleoptera, Scydmaenidae) of Russian Far East. *Entomologicheskoe Obozrenie* 72(3): 591–596. [in Russian]
- Li J-K, Wang Z-Y (1993) The Soil Beetles in Anhui Province. In: Li J-K, Chen P (Eds) *Studies on fauna and ecogeography of soil animal*. Northeast Normal University Press, Changchun, 151–167. [in Chinese]
- O’Keefe ST, Li J-K (1998) Review of the Scydmaenidae (Coleoptera) of eastern Asia, with particular reference to *Scydmaenus*, and description of the first scydmaenid from Hainan Island, China. *Journal of the New York Entomological Society* 106: 150–162.
- Schülke M, Smetana A (2015) Family Staphylinidae Latreille, 1802. In: Löbl I, Löbl D (Eds) *Catalogue of Palaearctic Coleoptera. Hydrophiloidea-Staphylinoidea*. Vol. 2. Revised and updated edition, Brill, Leiden/Boston, 304–1134.
- Sharp D (1886) The Scydmaenidae of Japan. *Entomologist’s Monthly Magazine* 23: 46–51.
- Song X-B, Tang L, Peng Z (2018) Flanged Bombardier beetles from Shanghai, China, with description of a new species in the genus *Eustra* Schmidt-Goebel (Coleoptera, Carabidae, Paussinae). *ZooKeys* 740: 45–57. <https://doi.org/10.3897/zookeys.740.20458>
- Song X-B, Zhou D-Y, Chen Z-B, Lin M-Z, Zhu J-Q (2019) First record of tribe Laenini (Coleoptera, Tenebrionidae, Lagriinae) from Shanghai, with description of a new species of the genus *Laena* Dejean. *Zootaxa* 4712(1): 90–100. <https://doi.org/10.11646/zootaxa.4712.1.6>
- Vit S (2006) On *Euconnus cerastiventr*is nom. nov. for *Euconnus chinensis* (Coleoptera: Staphylinoidea: Scydmaenidae). *Entomological Problems* 36(1): 75–78.
- Wang C-B, Perreau M, Růžička J, Song X-B (2017) Revision of the genus *Sinobathyscia* Perreau (Coleoptera, Leiodidae, Cholevinae) from China, with description of a new species. *Zootaxa* 4303(3): 350–360. <https://doi.org/10.11646/zootaxa.4303.3.2>
- Yin Z-W (2022) The Batrisini of Tibet: unveiling an enigmatic ant-loving beetle diversity on Earth’s Third Pole (Coleoptera, Staphylinidae, Pselaphinae). *Zootaxa* 5111(1): 1–211. <https://doi.org/10.11646/zootaxa.5111.1.1>
- Yin Z-W, Jiang R-X, Chen Z-B (2017) Notes on the Pselaphinae (Coleoptera: Staphylinidae) in Shanghai, China. *Zootaxa* 4238(3): 433–439. <https://doi.org/10.11646/zootaxa.4238.3.10>



# Plume moths (Lepidoptera, Pterophoridae) of a recently discovered lepidopteran diversity hotspot in the Mount Cameroon area, with descriptions of four new species

Peter Ustjuzhanin<sup>1,2</sup>, Vasily N. Kovtunovich<sup>3</sup>, Sylvain Delabye<sup>4,5</sup>, Vincent Maicher<sup>5,6</sup>, Szabolcs Sáfian<sup>7</sup>, Eric B. Fokam<sup>8</sup>, Robert Tropek<sup>4,5</sup>

1 *Altai State University, Lenina 61, Barnaul, RU-656049, Russia*

2 *Biological Institute, Tomsk State University, Lenina Prospekt 36, Tomsk 634050, Russia*

3 *University of the Free State (UFS), 205 Nelson Mandela Dr., Park West, Bloemfontein, Free State, South Africa*

4 *Department of Ecology, Faculty of Science, Charles University, Viničná 7, CZ-12843 Prague, Czech Republic*

5 *Institute of Entomology, Biology Centre of the Czech Academy of Sciences, Branišovská 31, CZ-37005 České Budějovice, Czech Republic*

6 *The Nature Conservancy Gabon, Impasse Edouard, Libreville, Gabon*

7 *Hungarian Natural History Museum, Department of Zoology, Baross utca 13, H-1088 Budapest, Hungary*

8 *Department of Animal Biology and Conservation, Faculty of Science, University of Buea, P.O. Box 63, Buea, Cameroon*

Corresponding author: Robert Tropek ([robert.tropek@gmail.com](mailto:robert.tropek@gmail.com))



Academic editor: Kevin Keegan

Received: 19 October 2024

Accepted: 4 February 2025

Published: 11 March 2025

ZooBank: <https://zoobank.org/DF0C00D9-04D3-4C2C-8CA0-DCD81ED76D73>

**Citation:** Ustjuzhanin P, Kovtunovich VN, Delabye S, Maicher V, Sáfian S, Fokam EB, Tropek R (2025) Plume moths (Lepidoptera, Pterophoridae) of a recently discovered lepidopteran diversity hotspot in the Mount Cameroon area, with descriptions of four new species. ZooKeys 1231: 145–168. <https://doi.org/10.3897/zookeys.1231.139530>

Copyright: © Peter Ustjuzhanin et al.  
This is an open access article distributed under terms of the Creative Commons Attribution License (Attribution 4.0 International – CC BY 4.0).

## Abstract

Moth diversity on Mount Cameroon, a critical biodiversity hotspot in the Afrotropics, remains understudied despite the region's rich and unique ecosystems. In this study, 34 species of plume moths (Pterophoridae) were recorded from the Mount Cameroon region, including four species new to science: *Titanoptilus bigoti* Ustjuzhanin & Kovtunovich, **sp. nov.**, *Titanoptilus murkwe* Ustjuzhanin & Kovtunovich, **sp. nov.**, *Hellinsia ekonjo* Ustjuzhanin & Kovtunovich, **sp. nov.**, and *Hellinsia mapanja* Ustjuzhanin & Kovtunovich, **sp. nov.** Images of the adult type specimen and male genitalia for *Titanoptilus melanodonta* Hampson, 1905 are published for the first time. In addition, 25 species are reported as new records for the Cameroonian fauna, raising the number of known Pterophoridae species in the country from 19 to 48. The results significantly expand our understanding of plume moth diversity in the region and extend the known distribution range of several species. These findings emphasise the importance of Mount Cameroon as a biodiversity hotspot within the Afrotropics. Enhanced conservation efforts are essential to preserve the unique biodiversity of Mount Cameroon, especially considering threats such as ongoing habitat degradation in some parts of the region and climate change.

**Key words:** Afrotropics, biodiversity, Cameroon, microlepidoptera, new species, Pterophoridae, taxonomy, tropical rainforest

## Introduction

Mount Cameroon (4,040 m a.s.l.), an active volcano in southwestern Cameroon, is recognised as one of the key centres of insect diversity within the Afrotropics, particularly for lepidopterans (Ustjuzhanin et al. 2018, 2020a, 2024; Larsen 2005). Its position within the biodiversity-rich Guineo-Congolian forest zone,

combined with its gradients in elevation (ranging from sea level to 4,040 metres) and precipitation (from its southwestern foothills, which rank among the three rainiest places in the world, to relatively dry savannahs in rain shadows on its northeastern slopes; Cable and Cheek 1998; Maicher et al. 2020a), supports highly heterogeneous habitats that accommodate large numbers of both widespread and endemic species of insects and other taxa (e.g., Ustjuzhanin et al. 2018; Delabye et al. 2020). Moreover, due to its inaccessibility and, later, its legal protection as part of the Mount Cameroon National Park, large portions of Mount Cameroon's ecosystems have remained relatively well-preserved from the negative effects of human activity (Cable and Cheek 1998).

Several lepidopteran groups, including butterflies (e.g., Sáfián and Tropek 2016; Maicher et al. 2018, 2020a, b; Delabye et al. 2021), various microlepidopterans (Ustjuzhanin et al. 2018, 2020a, 2024), and other moth groups (e.g., Maicher et al. 2016, 2020a, b; Yakovlev and Sáfián 2016; Przybyłowicz et al. 2019a, b; Delabye et al. 2020; Mertens et al. 2021), have been the focus of recent studies on Mount Cameroon, revealing the exceptional diversity of these taxa on the mountain. Notably, prior research has identified Mount Cameroon as a hotspot for many-plumed moths (Alucitidae), significantly advancing our understanding of their Afrotropical biodiversity (Ustjuzhanin et al. 2018, 2020a, 2024). Despite this progress, many lepidopteran groups remain understudied in the Mount Cameroon region, highlighting the need for further exploration of its insect diversity.

Pterophoridae, commonly referred to as plume moths, represent one such understudied family in the region. Characterised by their often deeply cleft wings, which give them their distinctive “plume-like” appearance, this group has a global distribution but remains insufficiently documented in the Afrotropics (De Prins and De Prins 2025). Knowledge of plume moths in Cameroon is still very limited, as no comprehensive studies on this family have been conducted in the country. To date, only 19 species have been recorded from Cameroon (De Prins and De Prins 2025). By summarising plume moth material sampled over several years of ecological studies of moth communities in the Mount Cameroon region, including descriptions of new species and numerous new country records, this study provides the first comprehensive survey of Pterophoridae on Mount Cameroon.

## Materials and methods

We sampled plume moths on Mount Cameroon using standardised light trapping methods over multiple field seasons between 2014 and 2018, at localities spanning elevations from 30 to 2,400 m a.s.l. across the mountain's southwestern, southern, and northern slopes. Light traps equipped with white and ultraviolet (UV) emitting bulbs were operated from dusk until dawn to attract moths. Specimens were collected manually from white sheets, euthanised using ammonium vapour, pinned, and preliminarily spread directly in the field for easier later processing, and stored dried with silica gel for transportation. The collected moths were identified based on external morphology and genitalia dissections; dissection and preparation of genitalia followed the standard lepidopteran taxonomic protocols described in Ustjuzhanin et al. (2018). The genitalia were mounted on permanent microscopic slides for further study, with unique identification codes assigned to each specimen for reference in taxonomic work. Holotypes will be

deposited in the Nature Education Centre, Jagiellonian University, Kraków, Poland (**NECJU**), while paratypes and other specimens will be split between NECJU and the personal collections of P. Ustjuzhanin and V. Kovtunovich, located in Novosibirsk and Moscow, Russia (**CUK**). Morphological terminology follows Zagulajev (1986) and the distribution of individual species follows the Afromoths database (De Prins and De Prins 2025), unless specified otherwise.

The sampling localities are listed below in an alphabetical order:

- Bamboo Camp, 350 m a.s.l., Mount Cameroon (SW slope), 4.0879°N, 9.0505°E; a lowland rainforest with historical disturbances from selective logging.
- Bimbia-Bonadikombo, 30 m a.s.l., Bimbia-Bonadikombo Community Forest, Mexico Camp, 3.9818°N, 9.2625°E; littoral forest in the part of the community forest that is officially disturbance-free, but with intensive ongoing illegal logging (Ferenc et al. 2018).
- Crater Lake, 1,500 m a.s.l., Mount Cameroon (SW slope), 4.1443°N, 9.0717°E; submontane rainforest with a sparse canopy layer as a consequence of local disturbances by forest elephants (Maicher et al 2020b).
- Drink Gari, 650 m a.s.l., Mount Cameroon (SW slope), Drink Gari camp (also known as “Drinking Gari”), 4.1014°N, 9.0610°E; lowland rainforest with a dense canopy layer.
- Ekonjo, 1,500 m a.s.l., Mount Cameroon (S slope), 4.0881°N, 9.1168°E; upland closed-canopy rainforest belonging to the Ekonjo village.
- Ekonjo farmland, 800 m a.s.l., Mount Cameroon (S slope), 4.0687°N, 9.1311°E; farmlands and secondary growths surrounding the Ekonjo village.
- Elephant Camp, 1,850 m a.s.l., Mount Cameroon (SW slope), 4.1170°N, 9.0729°E; montane rainforest with a sparse canopy layer as a consequence of local disturbances by forest elephants (Maicher et al 2020b).
- Mann’s Spring, 2,200 m a.s.l., Mount Cameroon (SW slope), 4.1428°N, 9.1225°E; montane forest at the natural timberline.
- Mapanja, Mapanja camp, 1,850 m a.s.l., Mount Cameroon (S slope), 4.1157°N, 9.1315°E; montane forest with a mostly closed canopy layer, supplemented by small openings after fallen trees on a steep slope.
- PlanteCam, 1,100 m a.s.l., Mount Cameroon (SW slope), PlanteCam camp (also misspelled as “PlantCamp” or “PlanteCamp”), 4.1175°N, 9.0709°E; upland rainforest in the transition between lowland and montane zones, with a sparse canopy layer as a consequence of local disturbances by forest elephants (Maicher et al 2020b).
- P&T antenna station, an area surrounding an antenna station of the Ministry of Post and Communications (P&T; sometimes misspelled as “PNT” by foreigners), 2,400 m a.s.l., Mount Cameroon (N slope), 4.21556°N, 9.2725°E; transition between montane forests and subalpine grasslands.

## Results

Altogether, we recorded 34 plume moth species in the Mount Cameroon area, four of which are described here as new to science. Additionally, we report 25 species (marked with \*) as new records for Cameroon, as only five of the recorded species had been previously known from the country.

## Descriptions of the new species

### *Titanoptilus bigoti* Ustjuzhanin & Kovtunovich, sp. nov.

<https://zoobank.org/8EA59C5A-694E-49B9-9B85-2004189371BE>

Figs 1, 2

**Type material examined.** *Holotype* ♂ (NECJU No. 241015), CAMEROON, Bamboo Camp, 350 m a.s.l., Mount Cameroon, 4.0879°N, 9.0505°E, 14–23.II.2016, Sz. Sáfián, R. Tropek, V. Maicher leg.

**External characters.** The wingspan is 31 mm. The head and tegulae are pale brown. The thorax is interspersed with dark-brown filiform scales. The labial palpi are thin, straight, and equal in length to the eye diameter, basally brown, and noticeably paler apically. The antennae are thin and dark brown. The forewings are pale brown, with a small elongated brown discal spot at the base. There is a distinct brown spot at the cleft base. The fringe inside the cleft is yellowish brown. The hindwings are yellowish brown. The hindwing fringes are dark, with the third lobe interspersed with evenly distributed dark spatulate scales on the costal margin and forming three distinct patches on the anal margin, a small cluster at the tip, two triangular patches along the middle, and a cluster at the base. The abdomen is long and pale brown, with creamy scales at the base of the thorax extending to the first abdominal segment. The hind legs are long and pale brown with noticeable darkening at the bases of the spurs.

**Description. Male genitalia.** The genitalia are symmetrical. The valves each comprise two lobes: the basal lobes arise beyond the sacculus are relatively wide and subquadrate, and narrow apically. The distal lobes are narrower, and longer, and  $\sim 2 \times$  the length of the basal lobes. Narrow sclerotized processes extend from the distal lobes and are only slightly shorter than those lobes. The uncus is robust, equal in length to the distal lobes of the valves, basally wide, and apically narrow and rounded. The saccus is wide and triangular. Sternum VIII is forked, with sclerotised distal margins. The aedeagus is long and thin in its distal 2/3, bent at a right angle  $\sim 1/3$  along its length. The basal part is noticeably thicker up to the bend.

**Diagnosis.** In terms of size and wings colour, the new species is similar to *Titanoptilus melanodonta* Hampson, 1905 (Figs 3, 4) but differs in the absence of fringe bundles along the lower margin of the second lobe of the forewing



Figures 1, 2. *Titanoptilus bigoti* Ustjuzhanin & Kovtunovich, sp. nov. 1 adult male, holotype, NECJU 2 male genitalia, holotype, NECJU, preparation slide no. 241015. Scale bar: 10 mm.



**Figures 3, 4.** *Titanoptilus melanodonta* Hampson, 1905 **3** adult male, holotype, NHMUK, locality: [Kenya], British East Africa, N'dimiy, Uganda Railway, mile 469, leg. C. S. Betton **4** male genitalia, holotype, NHMUK, gen.pr. no.21811. Scale bar: 10 mm.

and at the base of the third lobe of the hindwing. In the male genitalia, the new species is similar to *Titanoptilus procerus* Bigot, 1969 (male genitalia described and illustrated in Bigot 1969), in having bilobed valves and the narrow, long, and bent aedeagus. However, in the new species, the valves are basally wide, and the aedeagus is bent at a right angle, while in *T. procerus*, the valves are basally narrow, and the aedeagus is arched.

**Distribution.** Cameroon, Democratic Republic of Congo.

**Flight period.** On Mount Cameroon, the species was collected in February.

**Etymology.** The species is named in honour of Louis Bigot, the first researcher who worked on African plume moths, as a token of gratitude for his significant contributions.

**Note.** In Bigot (1969), this species was misidentified and illustrated as *T. melanodonta* (collected in the Democratic Republic of Congo, d'Eala et de Bokuma, Equateur, leg. L. Bigot), because L. Bigot did not have an opportunity to study the *T. melanodonta* type specimen, and the species' genitalia were not known at that time. Upon examining the male genitalia of *T. melanodonta* type specimen, collected in Kenya (Kenya, British East Africa, N'dimiy, Uganda Railway, mile 469, leg. C.S. Betton; Figs 3, 4) and stored in the Natural History Museum in London, UK (NHMUK), PU and VK found that the male image in Bigot (1969) does not correspond to the type specimen. Therefore, we have illustrated the *T. melanodonta* holotype in this study (Figs 3, 4). Instead, the male genitalia image in Bigot (1969) exactly matches the newly described species. Although we do not have access to the specimens, we expect they belong to *T. bigoti*, described in this study, based on Bigot's illustrations.

***Titanoptilus murkwe* Ustjuzhanin & Kovtunovich, sp. nov.**

<https://zoobank.org/ACF340B5-2310-4B02-8D4D-321652E6AFE9>

Figs 5, 6

**Type material examined. Holotype** ♀ (NECJU no. 241016), CAMEROON, Crater Lake, 1,500 m a.s.l., Mt. Cameroon, 4.1443°N, 9.0717°E, 23–29.IV.2017, V. Maicher, P. Potocký, S. Delabye leg.

**External characters.** The wingspan is 36 mm. The head and thorax are dark brown, while the tegulae are pale brown. The labial palpi are thin, straight, and

apically acute, with a length equal to the eye diameter. The antennae are thin and dark brown. The forewings are brown, with a narrow oblique yellowish stripe across the base of the first lobe. The first lobe is distally lightened with white scales, while the second lobe is mottled with brown and pale scales. The fringe inside the cleft is dark brown. Along the outer margin of the second lobe, the fringe is narrow and brownish grey but it widens and becomes darker in its distal part. The hindwings are brown, slightly paler than the forewings (unfortunately, not clearly visible in the specimen picture; Fig. 5). The fringe of the third lobe anal margin features a row of short dark spatulate scales on the basal half. These scales narrow further towards the middle before lengthening into a long, rounded scale bundle, which narrows again towards the apical fringe bundle, forming a rounded scale tooth at the lobe terminus. The hind legs are long and pale brown, with noticeable darkening at the bases of the spurs.

**Description. Female genitalia.** The papillae anales are elongated and oval. The antrum is narrow, tubular, and sclerotized, with the ostium slightly extended. The ductus is thin, long, and membranous. The bursa copulatrix is long and oval, 2 × as long as the ductus, and contains paired robust sclerotized signa in its distal portion, each ~0.24 × the length of the bursa.

**Differential diagnosis.** In size and wing colour, the new species is similar to *T. melanodonta*, but it differs in the absence of the wide portion of dark spatulate scales along the fringe of the outer margin under the cleft on the second lobe and the narrow basal row of spatulate scales among the fringes of the third lobe. In *T. melanodonta*, a wide scale tooth within the fringe of the anal margin is present under the forewing cleft, and the basal fringe of the third lobe of the hindwing forms a wide triangular scale tooth. In the female genitalia, the presence of signa in the bursa copulatrix distinguishes *T. murkwe* from other large species of the genus.

**Distribution.** The species is only known from Cameroon.

**Flight period.** The species was collected in April.



Figures 5, 6. *Titanoptilus murkwe* Ustjuzhanin & Kovtunovich, sp. nov. 5 adult female, holotype, NECJU 6 female genitalia, holotype, NECJU, preparation slide no. 241016. Scale bar: 10 mm.

**Etymology.** The species name is a noun in apposition, given in honour of the young and talented Cameroonian entomologist, Mercy Murkwe, who accompanied us during sampling of most specimens reported in this study.

***Hellinsia ekonjo* Ustjuzhanin & Kovtunovich, sp. nov.**

<https://zoobank.org/65DE0D2E-884E-46CE-84DE-83E609AC0572>

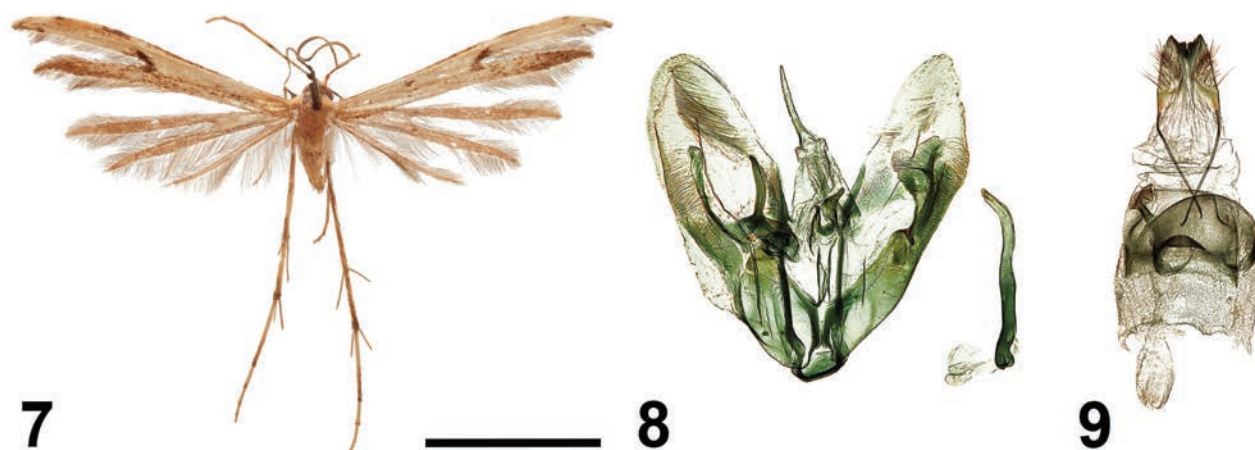
Figs 7–9

**Type material examined.** *Holotype* • ♂ (NECJU no. 241017), CAMEROON, Plante-Cam, 1,100 m a.s.l., Mount Cameroon, 4.1175000°N, 9.0709440°E, 09–14.IV.2015, V. Maicher, Sz. Sáfián, S. Janeček, R. Tropek leg.; *Paratypes* • 1♂, CAMEROON, Buea, Mount Cameroon (SE slope), 09.XI.1986, G. Bassi leg. • 1♀, CAMEROON, Crater Lake, 21.XI.2016, V. Maicher, Sz. Sáfián, S. Janeček, R. Tropek leg.; 3♀, 17–18.II.2017, P. Potocký, Sz. Sáfián, R. Tropek, J. Mertens, S. Janeček leg.; 1♂, 2♀, 23–29.IV.2017, V. Maicher, P. Potocký, S. Delabye leg. • 1♂, 1♀, CAMEROON, Ekonjo, 24.X.2017, V. Maicher, S. Delabye leg. • 2♀, CAMEROON, Elephant Camp, 19–24.XI.2014, V. Maicher, Sz. Sáfián, S. Janeček, R. Tropek leg.; 4♂, 2♀, 17–22.II.2017, P. Potocký, Sz. Sáfián, R. Tropek, J. Mertens, S. Janeček leg.; 1♀, 18–26.IV.2017, V. Maicher, P. Potocký, S. Delabye leg. • 1♀, CAMEROON, Mapanja, 14.V.2017, V. Maicher, P. Potocký, S. Delabye leg.; 2♂, 1♀, 23–28.X.2017, V. Maicher, S. Delabye leg.; 1♀, 23.X.2017, V. Maicher, S. Delabye leg. • 3♀, same data as the holotype; 1♂, 2♀, CAMEROON, PlanteCam, 11–18.XII.2014, V. Maicher, Sz. Sáfián, S. Janeček, R. Tropek leg.; 1♂, 3♀, 29.I.–07.II.2016, Sz. Sáfián, R. Tropek, V. Maicher leg. (CUK, NECJU).

**External characters.** The wingspan ranges from 15 to 19 mm, with the holotype measuring 17 mm. The thorax and tegulae are yellow. The head is covered with clinging yellow scales between the antennae. The collar is brown. The labial palpi are straight, short, and half the length of the eye diameter. The antennae are yellowish grey. The forewings are greyish brown, with the costal margin distally darkened with brown scales. A distinct oblique brown stroke is present at the base of the cleft, not extending as far as the costa. The fringes inside the cleft include a mix of yellow and dark-grey sections. The second lobe has dark-brown filiform scales on the dorsum, with narrow white patches near the apex, and an apical part darkened with brown scales. The hindwings are grey, noticeably darker than the forewings, with a pale brown fringe. The hind legs are yellowish brown.

**Description. Male genitalia.** The valves are oval and asymmetric. The sacculus on the left valve is relatively narrow and slightly wider apically, and barely extends beyond the middle of the valve. The harpe on the same valve is slightly shorter than the sacculus, slightly bent, and narrows apically. The right sacculus has a plate extending from a bifurcate sclerotised arm. The uncus is straight, acute, and bent slightly along its length. The saccus is slightly moderately rounded. The anellus arms are asymmetric, with the left arm being slightly shorter. Both arms are apically acute. The aedeagus is thin, apically slightly bent, and 2/3 the length of the right valve.

**Female genitalia.** The papillae anales are narrow and tapered. The posterior apophyses are thin. The distal margin of sternum VII is convex and rounded. The ostium is funnel-shaped, and the antrum is short, tubular, and shifted to the left. The ductus is as thick as the antrum, but membranous and relatively long. The bursa copulatrix is oval and lacks signa.



Figures 7–9. *Hellinsia ekonjo* Ustjuzhanin & Kovtunovich, sp. nov. 7 adult male, holotype, NECJU 8 male genitalia, holotype, NEJCU, preparation slide no. 241017 9 female genitalia, paratype. Scale bar: 5 mm.

**Differential diagnosis.** The male genitalia of the new species are similar to *Hellinsia adumbratus* (Walsingham, 1881), but the latter differs in the absence of the tapered harpe on the right valve, having a narrower uncus, and an apically curved aedeagus. In the female genitalia, the convex sternum VII and the left-shifted antrum resemble *Hellinsia madecasseus* (Bigot, 1964), but the new species differs by having a narrower ductus and lacking signa in the bursa copulatrix.

**Distribution.** The species is only known from Cameroon.

**Flight period.** The species was collected from February to May, and from October to December.

**Etymology.** The species is named after Ekonjo, a village on the southern slope of Mount Cameroon, where it was collected. Several villagers contributed as field assistants and supported the project in various ways. This dedication aims to support the protection of Mount Cameroon unique biodiversity.

***Hellinsia mapanja* Ustjuzhanin & Kovtunovich, sp. nov.**

<https://zoobank.org/AA56663D-6C2E-463F-B718-2D41DA942DAB>

Figs 10–12

**Type material examined.** *Holotype* • ♂, (NECJU No. 241019), CAMEROON, Crater Lake, 1,500 m a.s.l., Mount Cameroon, 4.1443°N, 9.0717°E, 21.XI.2016, V. Maicher, Sz. Sáfián, S. Janeček, R. Tropek leg.; *Paratypes* • 1♂, 1♀, and 3 other ex. CAMEROON, Crater Lake, 23–29.IV.2017, V. Maicher, P. Potocký, S. Delabye leg.; 3♂, 1♀, 17–25.II.2017, P. Potocký, Sz. Sáfián, R. Tropek, J. Mertens, S. Janeček leg. • 3♂, CAMEROON, Elephant camp, 17–22.II.2017, P. Potocký, Sz. Sáfián, R. Tropek, J. Mertens, S. Janeček leg.; 5 ex., 18–26.IV.2017, V. Maicher, P. Potocký, S. Delabye leg. • 2♂, 1♀, and 7 other ex., Cameroon, Mapanja, 10–15.V.2017, V. Maicher, P. Potocký, S. Delabye leg.; 2♂, 2♀, and 3 other ex., 23–28.X.2017, V. Maicher, S. Delabye leg. (CUK, NECJU).

**External characters.** The wingspan ranges from 17 to 19 mm, with the holotype measuring 19 mm. The head is brown, while the thorax and tegulae are pale yellow. The labial palpi are brown, thin, and short, being half the length of the eye diameter. The antennae are yellow, interspersed with brown scales. The forewings are pale yellow, with an oblique elongated brown streak at the cleft base, reaching the cos-



Figures 10–12. *Hellinsia mapanja* Ustjuzhanin & Kovtunovich, sp. nov. **10** adult male, holotype, NECJU **11** male genitalia, holotype, NEJCU, preparation slide no. 241019 **12** female genitalia, paratype. Scale bar: 5 mm.

tal margin of the first lobe. A more or less round brown discal spot is present near middle of the forewing. The costal margin of the forewing, up to the cleft, is mixed with tiny brown scales. A brown spot is situated medially along the costal margin on the first lobe. The fringe inside the cleft is yellow, with brown filiform scales distally. The second lobe is apically darkened with brown scales. The fringe along the outer edge of the forewing is pale yellow, except for a patch of pale brown filiform scales in its distal part under cleft. The hindwings are yellow and lack any pattern. The fringe on the hindwings is pale yellow, with alternating pale brown portions. The hind legs are pale yellow, interspersed with tiny brown scales.

**Description. Male genitalia.** The valves are asymmetric, with the left valve narrower and longer than the right valve. The saccular process on the left valve is well-developed and strongly sclerotised, extending far beyond the middle of the valve, and is widened and curved distally. The harpe is shaped like a short, slightly curved spike. The right valve is wide and slightly shorter than the left valve. The sacculus in the distal portion has a well-expressed sclerotized plate with processes on the sides. The uncus is narrow, slightly curved, and apically acute. The saccus is slightly rounded. The anellus arms are short and wide, with the left arm slightly shorter than the right. Both arms are apically narrow and acute. The aedeagus is thin, straight, and less than half as long as the right valve.

**Female genitalia.** The papillae anales are short and triangular. The posterior apophyses are thin and long. The distal margin of sternum VII is convex and rounded, with a notch on the inner edge. The ostium is funnel-shaped, and the antrum is short, tubular, and shifted to the left. The ductus is short and membranous, smoothly transitioning into the narrow, elongated bursa copulatrix. Small, narrow, elongated signa are present laterally on the bursa.

**Differential diagnosis.** Externally and in the genital structure, the species is similar to *Hellinsia ekonjo*. The wings are characterised by a pale yellowish tint and an oblique elongated brown streak that reaches the costal edge of the forewing, whereas in *H. ekonjo*, the wings are greyish brown and the elongated streak does not reach the costal edge of the forewing. In the male genitalia, the new species is distinguished by the valves of unequal length and width, the shape and size of the sacculus on the left valve, the shorter harpe, and the shorter, apically straight aedeagus. In the female genitalia, it is characterised by the signa in the bursa copulatrix and the small triangular papillae anales.

**Distribution.** The species is only known from Cameroon.

**Flight period.** The species was collected from February to May, and from October to November.

**Etymology.** The species is named after Mapanja, a village on the southern slope of Mount Cameroon, where it was collected. Several villagers contributed as field assistants and supported the project in various ways. We strongly believe this dedication will also help protect the unique biodiversity of the region.

### Other species recorded on Mount Cameroon

#### **\**Agdistis clara* Arenberger, 1986**

*Agdistis clara* Arenberger, 1986: 189. (Type locality: Botswana).

**Material examined.** 2♂, 1♀ (CUK, NECJU), Cameroon, Ekonjo farmland, 19.II.2017, P. Potocký leg.

**Distribution.** Botswana, Namibia, Republic of South Africa, and Cameroon.

**Note.** New species for Cameroon.

#### **\**Deuterocopus socotranus* Rebel, 1907**

*Deuterocopus socotranus* Rebel, 1907: 115. (Type locality: Yemen, Socotra).

*Deuterocopus deltoptilus* Meyrick, 1930: 565. (Type locality: Uganda).

*Deuterocopus henrioti* Bigot & Boireau, 2006: 16–17. (Type locality: Cote d'Ivoire).

**Material examined.** 1♀ (CUK), Cameroon, PlanteCam, 09–14.IV.2015, V. Maicher, Sz. Sáfián, S. Janeček, R. Tropek leg.

**Distribution.** Widely distributed species, besides several Afrotropical countries, it occurs also in Australasian, Oriental, and Palaeartic regions.

**Note.** New species for Cameroon.

#### **\**Titanoptilus procerus* Bigot, 1969**

*Titanoptilus procerus* Bigot, 1969: 182. (Type locality: West Kasai, Sankuru, Dimbelenge, Democratic Republic of Congo).

**Material examined.** 1♀ (CUK), Cameroon, PlanteCam, 09–14.IV.2015, V. Maicher, Sz. Sáfián, S. Janeček, R. Tropek leg.

**Distribution.** Congo and Cameroon.

**Note.** New species for Cameroon.

#### **\**Walsinghamiella prolai* (Gibeaux, 1994)**

*Titanoptilus prolai* Gibeaux, 1994: 82. (Type locality: Comoros).

**Material examined.** 2♂ (CUK, NECJU), Cameroon, Bamboo Camp, 17–23.IV.2015, V. Maicher, Sz. Sáfián, S. Janeček, R. Tropek leg.

**Distribution.** Comoros, Republic of South Africa, Eswatini, Zimbabwe, Tanzania, and Cameroon.

**Note.** New species for Cameroon.

### ***Platyptilia benitensis* Strand, 1913**

*Platyptilia benitensis* Strand, 1913: 64. (Type locality: Alén, Equatorial Guinea).

**Material examined.** 1♀, Cameroon, Crater Lake, 17–25.II.2017, P. Potocký, Sz. Sáfián, J. Mertens, Š. Janeček, R. Tropek leg.; 2♂, 1♀, 23–29.IV.2017, V. Maicher, P. Potocký, S. Delabye leg. • 1♀, Cameroon, PlanteCam, 09–14.IV.2015, V. Maicher, Sz. Sáfián, S. Janeček, R. Tropek leg. • 1♀, Cameroon, Mapanja, 25.X.2017, V. Maicher, S. Delabye leg. (CUK, NECJUK).

**Distribution.** Equatorial Guinea, Democratic Republic of Congo, Cote d'Ivoire, Cameroon, Kenya, Nigeria, Republic of South Africa, Sao Tome and Principe, Tanzania, and Uganda.

### **\**Platyptilia daemonica* Meyrick, 1932**

*Platyptilia daemonica* Meyrick, 1932: 109. (Type locality: Jem-Jem Forest, Ethiopia).

**Material examined.** 1♂, Cameroon, Crater Lake, 24.XI.2016, V. Maicher, Sz. Sáfián, S. Janeček, R. Tropek leg.; 2♂, 17–25.II.2017, P. Potocký, Sz. Sáfián, R. Tropek, J. Mertens, S. Janeček leg.; 1♂, 23–29.IV.2017, V. Maicher, P. Potocký, S. Delabye leg. • 1♂, 1♀, Cameroon, Elephant Camp, 19–24.XI.2014; 3♂, 18–26.IV.2017, V. Maicher, P. Potocký, S. Delabye leg.; 2♂, 17–22.II.2017, P. Potocký, Sz. Sáfián, R. Tropek, J. Mertens, S. Janeček leg. • 3♂, Cameroon, Mann's spring, 07–09.XI.2016, V. Maicher, Sz. Sáfián, S. Janeček, R. Tropek leg.; 1♂, 31.I.2017, P. Potocký, Sz. Sáfián, R. Tropek, J. Mertens, S. Janeček leg.; 1 ex., 13.VIII.2017, P. Potocký leg. • 2♂, Cameroon, Mapanja, 22.X.2017, V. Maicher, S. Delabye leg. (CUK, NECJU).

**Distribution.** Ethiopia, Rwanda, and Cameroon.

**Note.** New species for Cameroon.

### **\**Platyptilia fletcheri* Ustjuzhanin & Kovtunovich, 2016**

*Platyptilia fletcheri* Ustjuzhanin & Kovtunovich, 2016: 2. (Type locality: Ruwenzori Range, Lake Mahoma, Uganda).

**Material examined.** 4♂, 1♀, Cameroon, Mann's spring, 8–12.XI.2016, V. Maicher, Sz. Sáfián, S. Janeček, R. Tropek leg.; 4♂, 1♀, 31.I–04.II.2017, P. Potocký, Sz. Sáfián, R. Tropek, J. Mertens, S. Janeček leg. (CUK, NECJU).

**Distribution.** Uganda, Rwanda (Ustjuzhanin et al. 2016), and Cameroon.

**Note.** New species for Cameroon.

**\**Platyptilia gondarensis* Gibeaux, 1994**

*Platyptilia gondarensis* Gibeaux, 1994: 424. (Type locality: Gondar Province, Ethiopia).

**Material examined.** 1♀ (CUK), Cameroon, P&T antenna station, 28.III.2015, Sz. Sáfián leg.

**Distribution.** Ethiopia, Kenya, Uganda, and Cameroon.

**Note.** New species for Cameroon.

**\**Platyptilia morophaea* Meyrick, 1920**

*Platyptilia morophaea* Meyrick, 1920: 38. (Type locality: station 39, Kenya).

**Material examined.** 3♂, Cameroon, Mann's spring, 08–11.XI.2016, V. Maicher, Sz. Sáfián, S. Janeček, R. Tropek leg.; 35 ex., 28.I–04.II.2017, P. Potocký, Sz. Sáfián, R. Tropek, J. Mertens, S. Janeček leg.; 3 ex., 16–21.IV.2017, V. Maicher, P. Potocký, S. Delabye leg. • 4 ex., Cameroon, Mapanja, 22–23.X.2017, V. Maicher, S. Delabye leg. (CUK, NECJU).

**Distribution.** Kenya, Burundi, Democratic Republic of Congo, Ethiopia, Malawi, Tanzania, and Cameroon.

**Note.** New species for Cameroon.

**\**Platyptilia mugesse* Kovtunovich & Ustjuzhanin, 2014**

*Platyptilia mugesse* Kovtunovich & Ustjuzhanin, 2014: 459. (Type locality: Mugesse Forest, Malawi).

**Material examined.** 2♀, Cameroon, Crater Lake, 17–25.II.2017, P. Potocký, Sz. Sáfián, R. Tropek, J. Mertens, S. Janeček leg. • 1♀, Cameroon, Mann's spring, 31.I.2017 • 1♀, Cameroon, Mapanja, 23.X.2017, V. Maicher, S. Delabye leg. (CUK, NECJU).

**Distribution.** The species was found in Malawi (Kovtunovich et al. 2014) and Cameroon.

**Note.** New species for Cameroon.

**\**Platyptilia sciophaea* Meyrick, 1920**

*Platyptilia sciophaea* Meyrick, 1920: 40. (Type locality: Kenya).

**Material examined.** 1♀, Cameroon, Mann's spring, 31.I.2017, P. Potocký, Sz. Sáfián, R. Tropek, J. Mertens, S. Janeček leg. (CUK, NEJCU).

**Distribution.** Kenya, Uganda, and Cameroon.

**Note.** New species for Cameroon.

**\**Platyptiliodes albisignatula* Strand, 1913**

*Platyptiliodes albisignatula* Strand, 1913: 65. (Type locality: Alén, Equatorial Guinea).

**Material examined.** 2♂, Cameroon, Bimbia-Bonadikombo, 27–28.XII.2014, V. Maicher, Sz. Sáfián, R. Tropek, S. Janeček, leg. • 1♂, Cameroon, Crater Lake, 17–25.II.2017, P. Potocký, Sz. Sáfián, R. Tropek, J. Mertens, S. Janeček leg. (CUK, NECJU).

**Distribution.** Equatorial Guinea and Cameroon.

**Note.** New species for Cameroon.

**\**Amblyptilia direptalis* (Walker, 1864)**

*Oxyptilus direptalis* Walker, 1864: 934. (Type locality: Cape Province, Republic of South Africa).

*Platyptilia amblydectis* Meyrick, 1932: 108. (Type locality: Jem-Jem Forest, Ethiopia).

**Material examined.** 1♂, Cameroon, Crater Lake, 23–29.IV.2017, V. Maicher, P. Potocký, S. Delabye leg. 1♂, Cameroon, Elephant camp, 17–22.II.2017, P. Potocký, Sz. Sáfián, R. Tropek, J. Mertens, S. Janeček leg. • 2♂, Cameroon, Mann's spring, 30.I.2017 • (CUK, NECJU).

**Distribution.** Republic of South Africa, Burundi, Democratic Republic of the Congo, Malawi, Tanzania, Zimbabwe, Kenya, Ethiopia; India, Sri Lanka, Cameroon, and China (Ustjuzhanin et al. 2021).

**Note.** New species for Cameroon.

**\**Stenoptilia natalensis* Ustjuzhanin & Kovtunovich, 2010**

*Stenoptilia natalensis* Ustjuzhanin & Kovtunovich, 2010: 695. (Type locality: Howick, KwaZulu Natal, Republic of South Africa).

**Material examined.** 1♂, Cameroon, Crater Lake, 02–17.II.2017, P. Potocký, Sz. Sáfián, R. Tropek, J. Mertens, S. Janeček leg. • 1♂, Cameroon, Mann's spring, 12.XI.2016, V. Maicher, Sz. Sáfián, S. Janeček, R. Tropek leg.; 9 ex., 28–31.I.2017, P. Potocký, Sz. Sáfián, R. Tropek, J. Mertens, S. Janeček leg.; 1♂, 02.IV.2017, V. Maicher, P. Potocký, S. Delabye leg. • 1♂, 1♀, Cameroon, 22–23.X.2017, V. Maicher, S. Delabye leg. • 1♂, 2♀, Cameroon, P&T antenna station, 28.III.2015, Sz. Sáfián leg. (CUK, NECJU).

**Distribution.** Republic of South Africa, Lesotho, Malawi, and Cameroon.

**Note.** New species for Cameroon.

**\**Vietteilus borbonica* (Viette, 1957)**

*Platyptilia borbonica* Viette, 1957: 170. (Type locality: Reunion Island).

**Material examined.** 1♂, 1♀, Cameroon, Crater Lake, 23–29.IV.2017, V. Maicher, P. Potocký, S. Delabye leg. • 1♂, 1♀, Cameroon, Mann's spring, 13–16.VIII. 2017, P. Potocký leg.; 2♀, Cameroon, Mapanja, 23–29.X.2017. V. Maicher, P. Potocký, S. Delabye leg.; 1♂, 11.XI.2016, V. Maicher, Sz. Sáfián, S. Janeček, R. Tropek leg. • 1♀, Cameroon, Mapanja, 14.V.2017, V. Maicher, P. Potocký, S. Delabye leg.; (CUK, NECJU).

**Distribution.** Reunion Island, Tanzania, and Cameroon.

**Note.** New species for Cameroon.

**\**Bipunctiphorus dimorpha* (Fletcher, 1910)**

*Platyptilia dimorpha* Fletcher, 1910: 401. (Type locality: Morne Blanc, Mahé, Seychelles).

*Platyptilia patriarcha* Meyrick, 1912: 54. (Type locality: Mfongosi, Zululand, Republic of South Africa).

*Bipunctiphorus etiennei* Gibeaux, 1994: 57. (Type locality: above Cialos, Piton Bleu Forest, Réunion).

**Material examined.** 1♀, Cameroon, Crater Lake, 23–29.IV.2017, V. Maicher, P. Potocký, S. Delabye leg. • 1♂, 1♀, Cameroon, Mapanja, 11–12.V.2017, V. Maicher, P. Potocký, S. Delabye leg. (CUK, NECJU).

**Distribution.** Seychelles, Republic of South Africa, Reunion Island, Tanzania, Uganda, Zimbabwe, Kenya, Madagascar, Malawi, Sierra Leone, and Cameroon.

**Note.** New species for Cameroon.

**\**Stenoptilodes taprobanes* (Felder & Rogenhofer, 1875)**

*Amblyptilia taprobanes* Felder & Rogenhofer, 1875: plate 140, fig. 54. (Type locality: Ceylon [Sri Lanka]).

*Platyptilia legrandi* Bigot, 1962b: 86. (Type locality: Beau Vallon, Mahé, Seychelles).

*Stenoptilodes vittata* Service, 1966: 11. (Type locality: Nigeria).

**Material examined.** 1♂, Cameroon, Bamboo Camp, 17–23.IV.2015, V. Maicher, Sz. Sáfián, S. Janeček, R. Tropek leg. • 2♀, Cameroon, PlanteCam, 11–20. XII.2014, V. Maicher, Sz. Sáfián, S. Janeček, R. Tropek leg.; 4 ex., 29.I.–07. II.2016, Sz. Sáfián, R. Tropek, V. Maicher leg. (CUK, NECJU).

**Distribution.** Widespread throughout tropical and subtropical regions.

**Note.** New species for Cameroon.

***Sphenarches anisodactylus* (Walker, 1864)**

*Sphenarches anisodactylus* Walker, 1864: 934. (Type locality: Ceylon [Sri Lanka]).

*Platyptilia pygmaeana* Strand, 1913: 64. (Type locality: Cameroon).

**Material examined.** 1♂, Cameroon, Crater Lake, 25.XI.2016, V. Maicher, Sz. Sáfián, S. Janeček, R. Tropek leg. • 1♀, Cameroon, Ekonjo, 21.X.2017, V. Maicher, S. Delabye leg. • 1♂, 2♀, Cameroon, PlanteCam, 11–18.XII.2014, V. Maicher, Sz. Sáfián, S. Janeček, R. Tropek leg.; 2 ex., 29.I.–07.II.2016, Sz. Sáfián, R. Tropek, V. Maicher leg. (CUK, NECJU).

**Distribution.** Widely distributed in tropical and subtropical regions.

**\**Procapperia insomnis* (Townsend, 1956)**

*Capperia insomnis* Townsend, 1956: 93. (Type locality: Nakuru, Kenya).

*Procapperia hackeri* Arenberger, 2002: 74. (Type locality: Yemen).

**Material examined.** 1♀ (CUK), Cameroon, PlanteCam, 11–18.XII.2014, V. Maicher, Sz. Sáfián, S. Janeček, R. Tropek leg.

**Distribution.** Kenya, Democratic Republic of the Congo, Yemen, Namibia, Zimbabwe, Republic of South Africa, Malawi, and Cameroon.

**Note.** New species for Cameroon.

***Megalorhipida leucodactylus* (Fabricius, 1794)**

*Pterophorus leucodactylus* Fabricius, 1794: 346. (Type locality: Virgin Islands).

*Pterophorus defectalis* Walker, 1864: 943. (Type locality: Sierra Leone).

**Material examined.** 1♂ (CUK), Cameroon, Bamboo Camp, 14–23. II.2016, Sz. Sáfián leg.

**Distribution.** Widespread throughout tropical and subtropical regions.

**\**Inferuncus strictiformis* (Meyrick, 1932)**

*Platyptilia strictiformis* Meyrick, 1932: 251. (Type locality: Kampala, Uganda).

*Platyptilia spiculivalva* Gielis, 1990: 120. (Type locality: E Usambara Mts, Amani, Tanzania).

**Material examined.** 1♂ (CUK), Cameroon, PlanteCam, 09–14.IV.2015, V. Maicher, Sz. Sáfián, S. Janeček, R. Tropek leg.

**Distribution.** Uganda, Tanzania, Congo, and Cameroon.

**Note.** New species for Cameroon.

**\**Inferuncus toxochorda* (Meyrick, 1934)**

*Platyptilia toxochorda* Meyrick, 1934: 402. (Type locality: Sao Tome).

*Platyptilia pentheres* Bigot, 1969: 191. (Type locality: Equateur, Bokuma, Democratic Republic of Congo).

**Material examined.** 1 ♀ (CUK), Cameroon, Mann's spring, 12.VIII.2017, P. Potocký, S. Janeček leg.

**Distribution.** Sao Tome and Principe, Congo, Democratic Republic of Congo, Tanzania, Ghana, Liberia, and Cameroon.

**Note.** New species for Cameroon.

**\**Exelastis pumilio* (Zeller, 1873)**

*Mimeseoptilus pumilio* Zeller, 1873 (Type locality: Texas, Dallas, U.S.A.).

*Mimaeseoptilus gilvidorsis* Hedemann, 1896 (Type locality: Saint Croix, American Virgin Islands).

*Exelastis gilvidorsis* (Hedemann, 1896).

*Marasmarcha liophanes* Meyrick, 1886 (Type locality: Saint-Denis, Réunion).

*Exelastis liophanes* (Meyrick, 1886).

*Marasmarcha tenax* Meyrick, 1913 (Type locality: Barberton, Mpumalanga, Republic of South Africa).

*Exelastis tenax* (Meyrick, 1913).

*Exelastis bergeri* Bigot, 1969: 176. (Type locality: Democratic Republic of Congo).

**Material examined.** 1 ♂ (CUK), Cameroon, PlanteCam, 11–18.XII. 2014, V. Maicher, Sz. Sáfián, S. Janeček, R. Tropek leg.

**Distribution.** Democratic Republic of Congo, Republic of South Africa, Sierra Leone, Uganda, and Cameroon.

**Note.** New species for Cameroon. Ustjuzhanin et al. (2020b) mentioned *E. bergeri* and *E. tenax* as separate species. Nevertheless, these changes have never been formalised, and until a detailed revision, they remain synonyms of *E. pumilio*.

**\**Hellinsia ambo* Ustjuzhanin & Kovtunovich, 2011**

*Hellinsia ambo* Ustjuzhanin & Kovtunovich, 2011: 356. (Type locality: West Shewa, Ethiopia).

*Hellinsia ruhuruinia* Gielis, 2011: 51. (Type locality: Aberdare N.P., Ruhuruini Gates, Kenya).

**Material examined.** 1 ♂, Cameroon, Crater Lake, 17.II.2017, P. Potocký, Sz. Sáfián, R. Tropek, J. Mertens, S. Janeček leg. • 1 ♀, Cameroon, Ekonjo, 21.X.2017, V. Maicher, S. Delabye leg. • 1 ♂, Cameroon, Elephant Camp, 19–24.XI.2014, V. Maicher, Sz. Sáfián, S. Janeček, R. Tropek leg.; 1 ♂, 18–26.IV. 2017, V. Maicher, P. Potocký, S. Delabye leg.; 1 ex., 17–22.II.2017, P. Potocký, Sz. Sáfián, R. Tropek, J. Mertens, S. Janeček leg. • 1 ♂, Cameroon, Mann's spring, 13.VIII.2017, P. Potocký leg.; 1 ♂, 30.I.2017, P. Potocký, Sz. Sáfián, S. Janeček, R. Tropek, leg.; 1 ♂, 15.VIII.2017, P. Potocký leg. • 1 ♂, 1 ♀, Cameroon, Mapanja, 22–23.X.2017, V. Maicher, S. Delabye leg. (CUK, NECJU).

**Distribution.** Ethiopia, Kenya, Rwanda, Uganda, Ghana, and Cameroon.

**Note.** New species for Cameroon.

**\**Picardia eparches* (Meyrick, 1931)**

*Pterophorus eparches* Meyrick, 1931: 176. (Type locality: Butandiga, Uganda).

**Material examined.** 5 ex., Cameroon, Crater Lake, 17.II.2017, V. Maicher, Sz. Sáfián, S. Janeček, R. Tropek leg.; 10 ex., 23–29.IV.2017, V. Maicher, P. Potocký, S. Delabye leg. • 3 ex., Cameroon, Elephant camp, 18–26.IV.2017 • 3 ex., Cameroon, Mann's spring, 16–21.IV.2016, leg.; 1 ex., 04.II.2017, P. Potocký, Sz. Sáfián, R. Tropek, J. Mertens, S. Janeček leg.; 1 ♀, 15.VIII.2017. P. Potocký leg. • 7 ex., Cameroon, Mapanja, 10–15.V.2017, V. Maicher, P. Potocký, S. Delabye leg.; 1 ♂, 23.X.2017, V. Maicher, S. Delabye leg. • 1 ♂, Cameroon, PlanteCam, 09–14.IV.2015, V. Maicher, Sz. Sáfián, S. Janeček, R. Tropek leg. (CUK, NECJU).

**Distribution.** Uganda, Kenya, Malawi, Zimbabwe, Tanzania (Kovtunovich et al. 2014), Zambia (Ustjuzhanin et al. 2022), and Cameroon.

**Note.** New species for Cameroon.

***Picardia tropeki* Ustjuzhanin & Kovtunovich, 2022**

**Material examined.** 1 ♂ (NECJU), Cameroon, PlanteCam, 09–14.IV.2015, V. Maicher, Sz. Sáfián, S. Janeček, R. Tropek leg.

**Distribution.** Cameroon.

**Note.** This species was previously described from the same material sampled on Mount Cameroon in a separate global overview of the genus *Picardia* (Ustjuzhanin et al. 2022).

**\**Pselnophorus busoroensis* Gielis, 2011**

*Pselnophorus busoroensis* Gielis, 2011: 51. (Type locality: Nyungwe NP, Busoro, Rwanda).

**Material examined.** 1 ♂, 1 ♀, Cameroon, Crater Lake, 23–29. IV. 2017, V. Maicher, P. Potocký, S. Delabye leg. • 1 ♂, 1 ♀, Cameroon, Elephant camp, 17–22. II.2017, P. Potocký, Sz. Sáfián, R. Tropek, J. Mertens, S. Janeček leg. • 1 ♀, Cameroon, Mann's spring, 28.I.2017, P. Potocký, Sz. Sáfián, R. Tropek, J. Mertens, S. Janeček leg. (CUK, NECJU).

**Distribution.** Rwanda and Cameroon.

**Note.** New species for Cameroon.

**\**Adaina microdactyla* (Hübner, [1813])**

*Alucita microdactyla* Hübner, [1813]: pl. 5, figs 26, 27. (Type locality: Europe).

*Oidaematophorus madecasseus* Gibeaux, 1994: 130. (Type locality: Madagascar).

**Material examined.** 1 ♀ (CUK), Cameroon, Mapanja, 12.V.2017, V. Maicher, P. Potocký, S. Delabye leg.

**Distribution.** Madagascar, Democratic Republic of Congo, Tanzania, Malawi, and Cameroon, together with parts of Palaearctic and Palaeotropical regions, and New Guinea.

**Note.** New species for Cameroon.

**\**Pterophorus cleronoma* (Meyrick, 1920)**

*Alucita cleronoma* Meyrick, 1920: 41. (Type locality: Mt Kenya, Kenya).

**Material examined.** 1♀, Cameroon, Crater Lake, 24.XI.2016, V. Maicher, Sz. Sáfián, S. Janeček, R. Tropek leg.; 8 ex., 17–25.II.2017, P. Potocký, Sz. Sáfián, R. Tropek, J. Mertens, S. Janeček leg.; 1♂, 23–29.IV.2017, V. Maicher, P. Potocký, S. Delabye leg. • 2♂, Cameroon, Elephant camp, 17–22.II.2017, P. Potocký, Sz. Sáfián, R. Tropek, J. Mertens, S. Janeček leg.; 1♂, 18–26.IV.2017, V. Maicher, P. Potocký, S. Delabye leg. • 2♂, Cameroon, Mann's spring, 8–12.XI.2016, P. Potocký, Sz. Sáfián, S. Janeček, R. Tropek leg. • 2♂, Cameroon, Mapanja, 22.X.2017, V. Maicher, S. Delabye leg. (CUK, NECJU).

**Distribution.** Kenya and Cameroon.

**Note.** New species for Cameroon.

***Cosmoclostis schouteni* Gielis, 1990**

*Cosmoclostis schouteni* Gielis, 1990: 123. (Type locality: Daloa, Cote d'Ivoire).

*Pterophorus ashanti* Arenberger, 1995: 250. (Type locality: Kumasi, Ghana).

**Material examined.** 1♂, 1♀ (CUK), Cameroon, Drink Gari, 06–15.II.2016, V. Maicher, Sz. Sáfián, R. Tropek leg.

**Distribution.** Cote d'Ivoire, Cameroon, Liberia, Nigeria, Ghana.

## Discussion

In this study, we report 34 species of Pterophoridae from Mount Cameroon, including four species new to science, and 25 species recorded in the country for the first time. These species also represent 14 genera not recorded in Cameroon previously: *Adaina*, *Agditis*, *Amblyptilia*, *Bipunctiphorus*, *Deuterocopus*, *Inferuncus*, *Platyptiloides*, *Procapperia*, *Pselnophorus*, *Stenoptilia*, *Stenoptilodes*, *Titanoptilus*, *Vietteilus*, and *Walsinghmiella*. These records highlight Mount Cameroon as a significant locality for plume moth diversity. Beyond the newly described species, the addition of numerous new records for Cameroon confirms the importance of Mount Cameroon as a previously overlooked site for studying Afrotropical moths (Maicher et al. 2016; Ustjuzhanin et al. 2018, 2020a, 2024; Delabye et al. 2020).

This study substantially increased the documented diversity of plume moths in this underexplored region, raising the number of Pterophoridae species known from Cameroon from 19 (De Prins and De Prins 2025) to 48. Consequently, Cameroon is now known to host more than 10% of the 429 known species from the Afrotropics (based on De Prins and De Prins 2025, plus the new

species described here). This significant contribution emphasises the need for further surveys in understudied areas, such as Cameroon, to fully elucidate the diversity of Afrotropical Pterophoridae.

In addition to the new species descriptions, this study significantly expands the known distribution of several plume moth species. While some of the recorded species also occur in neighbouring countries, nine species (*P. daemonica*, *P. fletcheri*, *P. gondarensis*, *P. mugesse*, *P. sciophaea*, *V. borbonica*, *P. eparches*, *P. busoroensis*, and *P. cleronoma*) were previously known only from East Africa, *A. clara* was known only from South Africa, and two species (*W. prolai* and *S. natalensis*) were previously recorded from both of these distant regions. Although such scattered distributional patterns are documented in other moth groups (Maicher et al. 2016; Delabye et al. 2020) and better-studied taxa like butterflies (Larsen 2005), these range extensions more likely reflect the insufficient knowledge of plume moth distribution in Sub-Saharan Africa. Mount Cameroon is now the easternmost point in the known distribution for the West African species *C. schouteni*, and the westernmost point for the Central African species *T. procerus* and *P. albisignatula*, reflecting Cameroon's position as a biogeographical crossroads between West and Central Africa. Nevertheless, for any biogeographical conclusions and interpretations, much better faunistic and taxonomic knowledge of the Pterophoridae Afrotropical diversity is needed.

Mount Cameroon continues to demonstrate its status as a critical biodiversity hotspot within the Afrotropics. Although the diversity at the site is not as exceptional for Pterophoridae as for Alucitidae (Ustjuzhanin et al. 2018, 2020a, 2024), the number of endemic plume moth species and the biogeographically significant records align with patterns seen in butterflies (Larsen 2005), other moths (Yakovlev and Sáfián 2016), and some other non-lepidopteran taxa (Cable and Cheek 1998; Damaška et al. 2022; Hlaváč et al. 2023; Janeček and Janečková 2025). This can be attributed to the mountain's wide range of habitats, from littoral forests and lowland rainforests to montane cloud forests and subalpine grasslands, with large areas under minimal anthropogenic pressure. Its position at the border of two biogeographic regions, along with its isolation from other montane ranges, further contributes to the area's high level of endemism.

Our findings confirm the critical need to protect the ecosystems of Mount Cameroon. While parts of the region remain relatively well-preserved inside Mount Cameroon National Park, ongoing threats from habitat degradation and deforestation persist, particularly in lowland areas (Cable and Cheek 1998; Ferenc et al. 2018; Dongmo et al. 2023) and on the more densely populated eastern and southeastern slopes, where the regional capital, Buea, is located (Cable and Cheek 1998). Additionally, climate change poses significant risks to high-elevation species uniquely adapted to cooler, more stable environments (e.g., Ivory et al. 2016; Linck et al. 2021). Continued conservation efforts, particularly in the form of habitat protection within the national park and sustainable land-use practices in its buffer zones, will be key to preserving the biodiversity of this globally important site. We hope that dedicating some of the newly described species to local communities will foster greater appreciation for the biodiversity of their ecosystems. Our findings reinforce the urgent need to prioritise the conservation of the Mount Cameroon region to ensure the long-term survival of its unique ecosystems and the species they harbour.

## Acknowledgements

We are grateful to Francis E. Luma, Štěpán Janeček, Pavel Potocký jr., Jan E.J. Mertens, Jennifer T. Kimbeng, Mercy Murkwe, Ishmeal N. Kobe, Congo S. Kulu, and several other assistants for their help in the field, and to the MCNP staff for all their assistance. We used the ChatGPT 4o language model for English proofreading. This study was performed under several authorisations from the Ministries of the Republic of Cameroon for Forestry and Wildlife, and for Research and Innovations.

## Additional information

### Conflict of interest

The authors have declared that no competing interests exist.

### Ethical statement

No ethical statement was reported.

### Funding

R. Tropek and S. Delabye were funded by the Czech Science Foundation (project no. 20-16499S).

### Author contributions

RT conceived the study ideas and supervised the project; RT, SD, VM, SzS, and EBF sampled the material; PU and VK identified and compared the material, and prepared the species descriptions; RT, PU, and SD wrote the first draft; all authors contributed to writing and approved the final text.

### Author ORCIDs

Peter Ustjuzhanin  <https://orcid.org/0000-0002-5222-2241>

Vasily N. Kovtunovich  <https://orcid.org/0000-0001-5091-4263>

Sylvain Delabye  <https://orcid.org/0000-0003-0911-9721>

Vincent Maicher  <https://orcid.org/0000-0002-9147-3529>

Szabolcs Sáfián  <https://orcid.org/0000-0002-0614-4203>

Eric B. Fokam  <https://orcid.org/0000-0003-4531-3580>

Robert Tropek  <https://orcid.org/0000-0001-7499-6259>

### Data availability

All of the data that support the findings of this study are available in the main text.

## References

- Bigot L (1969) Les Lépidoptères Pterophoridae du musée royal de l'Afrique centrale, à Tervuren. *Revue de Zoologie et de Botanique Africaines* 79: 165–206.
- Cable S, Cheek M (1998) The plants of Mount Cameroon: A conservation checklist. Royal Botanic Gardens, Kew, 198 pp.
- Damaška AF, Konstantinov A, Fikáček M (2022) Multiple origins of moss-inhabiting flea beetles (Coleoptera: Chrysomelidae): molecular phylogeny, overview of genera and a new genus from Africa. *Zoological Journal of the Linnean Society* 196: 647–676. <https://doi.org/10.1093/zoolinnean/zlab112>

- De Prins J, De Prins W (2025) AfroMoths. Online database of Afrotropical moth species (Lepidoptera). <http://www.afromoths.net> [accessed 22 January 2025]
- Delabye S, Maicher V, Sáfián S, Potocký P, Mertens J, Przybyłowicz Ł, Murkwe M, Kobe I, Fokam E, Janeček Š, Tropek R (2020) First records of 31 species of butterflies and moths (Lepidoptera) in Cameroon, with remarks on their elevational ranges. *Biodiversity Data Journal* 8: e50543. <https://doi.org/10.3897/BDJ.8.e50543>
- Delabye S, Maicher V, Sáfián S, Doležal J, Altman J, Janeček Š, Kobe IN, Murkwe M, Šebek P, Tropek R (2021) Butterfly and moth communities differ in their response to habitat structure in rainforests of Mount Cameroon. *Biotropica* 53: 567–580. <https://doi.org/10.1111/btp.12900>
- Dongmo MA, Hanna R, Bonebrake TC (2023) Enhancing scientific and community capacity to conserve Central African Lepidoptera. *Biological Conservation* 279: 109938. <https://doi.org/10.1016/j.biocon.2023.109938>
- Ferenc M, Sedláček O, Tropek R, Albrecht T, Altman J, Dančák M, Doležal J, Janeček Š, Maicher V, Majeský L, Motombi FN, Murkwe M, Sáfián S, Svoboda M, Hořák D (2018) Something is missing at the bottom: Importance of coastal rainforests for conservation of trees, birds and butterflies in the Mount Cameroon area. *African Journal of Ecology* 56: 679–683. <https://doi.org/10.1111/aje.12506>
- Hlaváč P, Baňář P, Fokam EB (2023) Pselaphinae of the Cameroon Volcanic Line. Part 3. A new genus of Goniacerini (Coleoptera: Staphylinidae: Goniaceritae) from Mount Cameroon. *Zootaxa* 5323: 255–267. <https://doi.org/10.11646/zootaxa.5323.2.5>
- Ivory SJ, Early R, Sax DF, Russell J (2016) Niche expansion and temperature sensitivity of tropical African montane forests. *Global Ecology and Biogeography* 25: 693–703. <https://doi.org/10.1111/geb.12446>
- Janeček Š, Janečková P (2025) Field Guide to Plants of Mount Cameroon 1. Flowering plants above the forest line. Janečkovi, Třeboň, 159 pp.
- Kovtunovich VN, Ustjuzhanin PY, Murphy RJ (2014) Plume moths of Malawi (Lepidoptera: Pterophoridae). *Zootaxa* 3847: 451–494. <https://doi.org/10.11646/zootaxa.3847.4.1>
- Larsen TB (2005) Butterflies of West Africa. Apollo Books, Stenstrup, 865 pp. <https://doi.org/10.1163/9789004531093>
- Linck EB, Freeman BG, Cadena CD, Ghalambor CK (2021) Evolutionary conservatism will limit responses to climate change in the tropics. *Biology Letters* 17: 20210363. <https://doi.org/10.1098/rsbl.2021.0363>
- Maicher V, Sáfián S, Ishmeal KN, Murkwe M, Kimbeng TJ, Janeček Š, Tropek R (2016) Two genera and nineteen species of fruit-feeding erbid moths (Lepidoptera: Erebidae) recorded in Cameroon for the first time. *Entomological News* 126: 64–70. <https://doi.org/10.3157/021.126.0108>
- Maicher V, Sáfián S, Murkwe M, Przybyłowicz L, Janeček Š, Fokam EB, Pycrz T, Tropek R (2018) Flying between raindrops: Strong seasonal turnover of several Lepidoptera groups in lowland rainforests of Mount Cameroon. *Ecology and Evolution* 8: 12761–12772. <https://doi.org/10.1002/ece3.4704>
- Maicher V, Sáfián S, Murkwe M, Delabye S, Przybyłowicz Ł, Potocký P, Kobe IN, Janeček Š, Mertens J, Fokam EB, Pycrz T, Doležal J, Altman J, Hořák D, Fiedler K, Tropek R (2020a) Seasonal shifts of biodiversity patterns and species' elevation ranges of butterflies and moths along a complete rainforest elevational gradient on Mount Cameroon. *Journal of Biogeography* 47: 342–354. <https://doi.org/10.1111/jbi.13740>

- Maicher V, Delabye S, Murkwe M, Doležal J, Altman J, Kobe IN, Desmist, J, Fokam EB, Pycrz T, Tropek R (2020b) Effects of disturbances by forest elephants on diversity of trees and insects in tropical rainforests on Mount Cameroon. *Scientific Reports* 10: 21618. <https://doi.org/10.1038/s41598-020-78659-7>
- Mertens JEJ, Brisson L, Janeček Š, Klomberg Y, Maicher V, Sáfián S, Delabye S, Po-tocký P, Kobe IN, Pycrz T, Tropek R (2021) Elevational and seasonal patterns of butterflies and hawkmoths in plant-pollinator networks in tropical rainforests of Mount Cameroon. *Scientific Reports* 11: 9710. <https://doi.org/10.1038/s41598-021-89012-x>
- Przybyłowicz L, Maicher V, László GM, Sáfián S, Tropek R (2019a) *Amerila* (Lepidoptera: Erebidae: Arctiinae) of Cameroon with morphological remarks on male and female genitalia. *Zootaxa* 4674: 283–295. <https://doi.org/10.11646/zootaxa.4674.2.8>
- Przybyłowicz L, Tarcz S, László GM, Sáfián S, Zilli A (2019b) Revision of the *Amerila syntomina* species complex with description of a new species from West Africa (Lepidoptera: Erebidae: Arctiinae). *Annales Zoologici* 69: 703–717. <https://doi.org/10.3161/00034541ANZ2019.69.4.006>
- Ustjuzhanin P, Kovtunovich V, Sáfián S, Maicher V, Tropek R (2018) A newly discovered biodiversity hotspot of many-plumed moths (Lepidoptera, Alucitidae) in the Mount Cameroon area: first report on species diversity, with description of nine new species. *Zookeys* 777: 119–139. <https://doi.org/10.3897/zookeys.777.24729>
- Ustjuzhanin PY, Kovtunovich VN, Ustjuzhanina AK (2016) New species of “giant” plume moths of the genus *Platyptilia* (Lepidoptera, Pterophoridae) from Uganda. *European Journal of Taxonomy* 172: 1–6. <https://doi.org/10.5852/ejt.2016.172>
- Ustjuzhanin P, Kovtunovich V, Maicher V, Sáfián S, Delabye S, Streltsov A, Tropek R. (2020a) Even hotter hotspot: Description of seven new species of many-plumed moths (Lepidoptera, Alucitidae) from Mount Cameroon. *Zookeys* 935: 103–119. <https://doi.org/10.3897/zookeys.935.49843>
- Ustjuzhanin P, Kovtunovich V, Udovichenko P, Armstrong A, Streltsov A (2020b) Plume moths in the protected areas of KwaZulu Natal province, Republic of South Africa. *Ecologica Montenegrina* 27: 11–21. <https://doi.org/10.37828/em.2020.27.2>
- Ustjuzhanin PY, Kovtunovich VN, Saldaitis A, Streltsov AN (2021) New species of plume moths (Lepidoptera: Pterophoridae) from China, Sichuan Province. *Russian Entomological Journal* 30: 323–327. <https://doi.org/10.15298/rusentj.30.3.10>
- Ustjuzhanin PY, Kovtunovich VN, Streltsov AN (2022) Overview of the species of the genus *Picardia* Gibeaux, 1994 (Lepidoptera: Pterophoridae) in the world fauna, with description of new species. *Ecologica Montenegrina* 52: 12–23. <https://doi.org/10.37828/em.2022.52.2>
- Ustjuzhanin P, Kovtunovich V, Delabye S, Maicher V, Sáfián Sz, Streltsov A, Tropek R (2024) Magnifying the hotspot: Description of nine new species of many-plumed moths (Lepidoptera, Alucitidae), with an identification key to all species known from Cameroon. *Zookeys* 1193: 25–48. <https://doi.org/10.3897/zookeys.1193.111544>
- Yakovlev RV, Sáfián S (2016) *Geraldocossus* gen. nov. (Lepidoptera, Cossidae) from Mount Cameroon (West Africa). *Zootaxa* 4114: 595–599. <https://doi.org/10.11646/zootaxa.4114.5.8>
- Zagulajev AK (1986) Pterophoridae. In: *Opredelitel Nasekomykh Evropeyskoi Chasti SSSR*. Vol. 4. Cheshuekrylye, Part 3. Nauka, Leningrad, pp. 26–215.

## Appendix 1

### List of all species of Pterophoridae recorded in Cameroon

The list follows the AfroMoths online database (de Prins and de Prins 2025), with the addition of the species included in this paper (new country records are marked by an asterisk).

*\*Adaina microdactyla* (Hübner, [1813])  
*\*Agdistis clara* Arenberger, 1986  
*\*Amblyptilia direptalis* (Walker, 1864)  
*Antarches tessmanni* (Strand, 1913)  
*\*Bipunctiphorus dimorpha* (Fletcher, 1910)  
*Cosmoclostis schouteni* Gielis, 1990  
*\*Deuterocopus socotranus* Rebel, 1907  
*Exelastis crudipennis* (Meyrick, 1932)  
*\*Exelastis pumilio* (Meyrick, 1913)  
*Fletcherella niphadarcha* (Meyrick, 1930)  
*\*Hellinsia ambo* Ustjuzhanin & Kovtunovich, 2011  
*\*Hellinsia ekonjo* Ustjuzhanin & Kovtunovich, sp. nov.  
*Hellinsia lienigianus* (Zeller, 1852)  
*\*Hellinsia mapanja* Ustjuzhanin & Kovtunovich sp. nov.  
*\*Inferuncus strictiformis* (Meyrick, 1932)  
*\*Inferuncus toxochorda* (Meyrick, 1934)  
*Marasmarcha sisyrodes* Meyrick, 1921  
*Megalorhipida leucodactylus* (Fabricius, 1794)  
*\*Picardia eparches* (Meyrick, 1931)  
*Picardia tropeki* Ustjuzhanin & Kovtunovich, 2022  
*Platyptilia benitensis* Strand, 1913  
*\*Platyptilia daemonica* Meyrick, 1932  
*Platyptilia farfarellus* (Zeller, 1867)  
*\*Platyptilia fletcheri* Ustjuzhanin & Kovtunovich, 2016  
*\*Platyptilia gondarensis* Gibeaux, 1994  
*\*Platyptilia morophaea* Meyrick, 1920  
*\*Platyptilia mugesse* Kovtunovich & Ustjuzhanin, 2014  
*\*Platyptilia sciophaea* Meyrick, 1920  
*\*Platyptiliodes albisignatula* Strand, 1913  
*\*Procapperia insomnis* (Townsend, 1956)  
*\*Pselnophorus busoroensis* Gielis, 2011  
*Pterophorus albidus* (Zeller, 1852)  
*Pterophorus candidalis* (Walker, 1864)  
*\*Pterophorus cleronoma* (Meyrick, 1920)  
*Pterophorus ceraunia* (Bigot, 1969)  
*Pterophorus lampra* (Bigot, 1969)  
*Pterophorus rhyparias* (Meyrick, 1908)  
*Pterophorus spissa* (Bigot, 1969)  
*Pterophorus virgo* (Strand, 1913)  
*Sphenarches anisodactylus* (Walker, 1864)

*Stenodacma wahlbergi* (Zeller, 1852)

\**Stenoptilia natalensis* Ustjuzhanin & Kovtunovich, 2010

\**Stenoptilodes taprobanes* (Felder & Rogenhofer, 1875)

\**Titanoptilus bigoti* Ustjuzhanin & Kovtunovich, sp. nov.

\**Titanoptilus murkwe* Ustjuzhanin & Kovtunovich, sp. nov.

\**Titanoptilus procerus* Bigot, 1969

\**Vietteilus borbonica* (Viette, 1957)

\**Walsinghmiella prolai* (Gibeaux, 1994)

# An updated checklist of *Anopheles* (Diptera, Culicidae) of Colombia with new records and distribution data

Nelson Naranjo-Díaz<sup>1</sup>, Margarita M. Correa<sup>1</sup> 

<sup>1</sup> Grupo Microbiología Molecular, Escuela de Microbiología, Universidad de Antioquia, Calle 70 No. 52-21, Medellín, Colombia  
Corresponding author: Margarita M. Correa ([margarita.correa@udea.edu.co](mailto:margarita.correa@udea.edu.co))

## Abstract

Several species of *Anopheles* mosquitoes (Arthropoda, Insecta, Diptera, Culicidae) are important in public health due to their role in malaria transmission. Of the more than 500 *Anopheles* species worldwide, 47 have been reported in Colombia, but only nine are known to transmit malaria. Taxonomic classification of these mosquitoes is complicated by the existence of species complexes and groups of closely related species that are difficult to distinguish based on morphological characteristics. However, molecular techniques have contributed to resolving taxonomic uncertainties, definition of molecular variants and facilitated the correction of erroneous taxonomic assignments. This study aimed to update the list of *Anopheles* species reported for Colombia. A species checklist was compiled by reviewing catalogs, publications, databases, and unpublished data. Only formally characterized species were included, along with their geographic range and ecological distribution. The final list includes 44 formally characterized *Anopheles* species belonging to five subgenera. The *Nyssorhynchus* subgenus constituted the largest group with 17 species and the widest distribution, occurring in 18 ecoregions. The *Anopheles* subgenus was the second largest group with 16 species and occurrences in 16 ecoregions. Sixty-six new presence records were added to the checklist. The updated *Anopheles* checklist, encompassing presence records and ecological distributions, enhances our understanding of *Anopheles* mosquito biodiversity. Furthermore, it contributes to improved public health by providing a foundation for targeted vector control interventions.

**Key words:** *Anopheles*, biodiversity, Colombia, ecological distribution, inventory, malaria vectors



Academic editor: John Soghigian  
Received: 2 August 2024  
Accepted: 16 January 2025  
Published: 12 March 2025

ZooBank: <https://zoobank.org/3D134FAA-6E53-44C7-90FE-1DD02C3B1B46>

**Citation:** Naranjo-Díaz N, Correa MM (2025) An updated checklist of *Anopheles* (Diptera, Culicidae) of Colombia with new records and distribution data. ZooKeys 1231: 169–189. <https://doi.org/10.3897/zookeys.1231.133711>

Copyright: ©  
Nelson Naranjo-Díaz & Margarita M. Correa.  
This is an open access article distributed under  
terms of the Creative Commons Attribution  
License (Attribution 4.0 International – CC BY 4.0).

## Introduction

The *Anopheles* genus is highly diverse, with 511 formally recognized species belonging to eight subgenera, including various species complexes. Some of these complexes still contain unnamed members (Harbach 2023). *Anopheles* mosquitoes thrive in a wide range of ecosystems, contributing to their broad geographical distribution. Additionally, some species have adapted to anthropically modified habitats (Hiwat and Bretas 2011; Harbach 2023). The primary importance of this genus lies in its role as a vector of human and animal pathogens, particularly, *Plasmodium* parasites, the causative agents of malaria (WHO 2022). Some *Anopheles* species also transmit *Wuchereria bancrofti*, the nematode that

causes filariasis in Africa and Asia (Manguin et al. 2010), and O'nyong-nyong virus, which produces polyarthritis and fever in Africa (Brault et al. 2004).

Most of Colombia has ecological conditions that favor the widespread distribution of *Anopheles* mosquitoes (Olano et al. 2001; IGAC 2002; Hernández-Valencia et al. 2020). In the country, 47 species have been identified (Montoya-Lerma et al. 2011; Gómez et al. 2015), and nine of these are considered malaria vectors. Three species from the *Nyssorhynchus* subgenus play a significant role in malaria transmission: *Anopheles darlingi*, *An. nuneztovari*, and *An. albimanus* (Olano et al. 2001; Gutiérrez et al. 2008). *Anopheles darlingi* is the primary malaria vector in Latin America (Hiwat and Bretas 2011) and is predominantly found in the northwest, east and Amazon regions of Colombia. *Anopheles nuneztovari* is more common in the northwest, northeast and east, while *An. albimanus* is primarily present in coastal areas (Olano et al. 2001; Naranjo-Díaz et al. 2016a, b).

Knowledge of *Anopheles* species in Colombia is based primarily on catalogs published in the mid-20<sup>th</sup> century (Gast 1943; Barreto-Reyes 1955; Stone et al. 1959; Knight and Stone 1977) and older reports from the former government malaria control program "Servicio Nacional de Erradicación de la Malaria-SEM" (SEM 1957). Subsequent contributions by Carrejo and González (1992) and González and Carrejo (2007, 2009), focusing on the taxonomy and control of medically important insects, with an emphasis on population and taxonomic studies, have significantly improved our understanding of *Anopheles* in Colombia. While the number of reports on *Anopheles* species occurrence and distribution has increased, information remains scattered and, in some cases, inaccessible to the public.

Molecular tools have significantly improved the resolution of taxonomic ambiguities, particularly within species complexes and among closely related species; they have also facilitated the correction of erroneous taxonomic assignments (Brochero et al. 2007; Ruiz-Lopez et al. 2012; Escovar et al. 2014; Gómez et al. 2015). These findings underscore the need for an updated list of species occurrence. A comprehensive checklist of *Anopheles* species in Colombia, incorporating current ecological and geographical data, is essential for advancing medical entomological research and biodiversity assessment.

## Materials and methods

To update the *Anopheles* species checklist, we reviewed various sources, including mosquito catalogs (Gast 1943; Barreto-Reyes 1955; Knight and Stone 1977; Heinemann and Belkin 1978; Faran 1980; Carrejo and Gonzalez 1992), taxonomic keys (Faran and Linthicum 1981; Gonzalez and Carrejo 2009), and government reports (SEM 1957). Additionally, we obtained data on *Anopheles* species occurrence, including geographical coordinates, from databases (Gaffigan et al. 2014; SIB Database 2020; GBIF 2024), scientific articles, and unpublished new records of specimens collected by members of our research group (named "new occurrence data"). The identities of the new records were previously verified using molecular methods, e.g., COI barcoding or ITS2 analysis (Zapata et al. 2007; Cienfuegos et al. 2011; Gómez et al. 2015) (Suppl. material 1).

To be included in the checklist, an *Anopheles* species was required to have a formal description and validation (Harbach 2023; ITIS 2024). Species variants originally described using only molecular methods were excluded. The checklist includes species listed in alphabetic order. Each entry contains

the genus, subgenus, authorship, and year of description; (new occurrence data): This designation is used to indicate that the records are the result of previous work by our research group. Geographical distribution is presented at the level of Colombian administrative departments. An asterisk (\*) indicates species occurrences with associated geographical coordinates.

Notes provide information on the sources of the data, changes in the taxonomic classification of species, molecular species designations, and new occurrence data, including the municipalities where specimens were collected. The checklist is accompanied by a map illustrating the distribution of *Anopheles* species with associated geographical coordinates (Figs 1, 2, Suppl. material 1).

In addition to the list, a summary table of the *Anopheles* records by administrative departments is included (Table 1), and also, a table of species distribution per ecoregion (WWF 2015) (Table 2), which includes the following: Amazon-Ori-noco-Southern Caribbean mangroves, Apure-Villavicencio dry forests, Caquetá moist forests, Catatumbo moist forests, Cauca Valley dry forests, Cauca Valley montane forests, Chocó-Darién moist forests, Cordillera Oriental montane forests, Eastern Cordillera Real montane forests, Guajira-Barranquilla xeric scrub, Llanos, Magdalena Valley montane forests, Magdalena-Urabá moist forests, Napo moist forests, Negro-Branco moist forests, Northwestern Andean montane forests, Sinú Valley dry forests, Solimões–Japurá moist forests, South American Pacific mangroves, Southwest Amazon moist forests, and Western Ecuador moist forests.

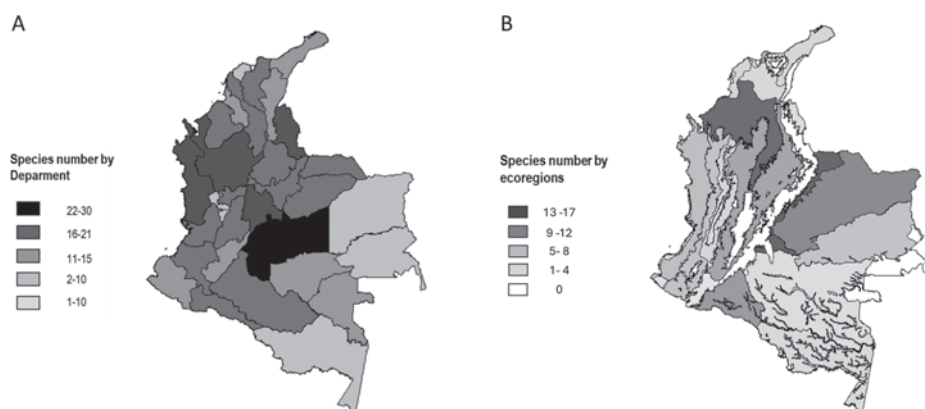


**Figure 1.** Maps depicting the number of *Anopheles* species reported in Colombia **A** by administrative area (Department) **B** by ecological region.

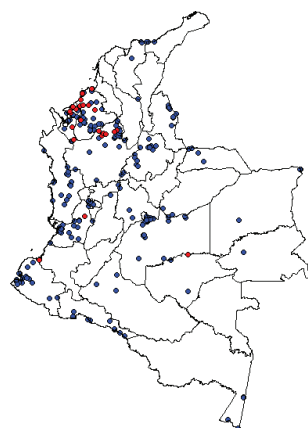


**Figure 2.** Map indicating the location of species records, according to geographic coordinates. Blue: previously reported records; red: new occurrence data.

**Table 1.** Summary of *Anopheles* records by Colombian administrative departments.

Department	Subgenera	Species	New geographic coordinate registers*	Total geographic coordinate registers <sup>‡</sup>
Amazonas	3	8	-	11
Antioquia	3	22	40	155
Arauca	2	16	-	6
Atlántico	2	10	-	1
Bolívar	3	17	-	-
Boyacá	3	17	-	4
Caldas	3	17	-	1
Caquetá	4	18	-	6
Casanare	2	16	-	2
Cauca	4	18	1	42
Cesar	2	15	-	-
Chocó	4	23	-	31
Córdoba	2	18	21	80
Cundinamarca	5	23	-	2
Guainía	2	7	-	-
Guaviare	3	13	3	5
Huila	3	13	-	-
La Guajira	2	15	-	4
Magdalena	3	17	-	6
Meta	5	30	-	60
Nariño	4	15	-	35
Norte de Santander	4	24	-	14
Putumayo	3	18	-	36
Quindío	2	7	-	-
Risaralda	2	7	-	3
San Andres y Providencia	1	1	-	-
Santander	2	19	-	33
Sucre	2	13	-	-
Tolima	3	18	-	1
Valle del Cauca	4	19	1	33
Vaupés	5	15	-	-
Vichada	2	10	-	9

\* Number of new geographic coordinate records described during this study; <sup>‡</sup> Total number of geographic coordinate records, including both previous and new occurrence data.

**Table 2.** List of *Anopheles* recorded in Colombia by ecoregion.

Ecoregions*	Species
Amazon-Orinoco-Southern Caribbean mangroves	<i>An. (Ano.) apicimacula</i> , <i>An. (Ano.) punctimacula</i> , <i>An. (Ano.) pseudopunctipennis</i> <sup>‡</sup>
Apure-Villavicencio dry forests	<i>An. (Ano.) costai</i> , <i>An. (Ano.) apicimacula</i> , <i>An. (Ano.) pseudopunctipennis</i> <sup>‡</sup> , <i>An. (Ker) bambusicolus</i> , <i>An. (Ker) homunculus</i> , <i>An. (Ker) pholidotus</i> <sup>‡</sup> , <i>An. (Nys.) albitarsis</i> , <i>An. (Nys.) argyritarsis</i> , <i>An. (Nys.) benarrochi</i> <sup>‡</sup> , <i>An. (Nys.) braziliensis</i> , <i>An. (Nys.) darlingi</i> <sup>‡</sup> , <i>An. (Nys.) marajoara</i> , <i>An. (Nys.) nuneztovari</i> <sup>‡</sup> , <i>An. (Nys.) rangeli</i> , <i>An. (Nys.) triannulatus</i> , <i>An. (Ste.) nimbus</i>
Caquetá moist forests	<i>An. (Nys.) darlingi</i> <sup>‡</sup> , <i>An. (Nys.) braziliensis</i>
Catatumbo moist forests	<i>An. (Ano.) malefactor</i> , <i>An. (Ano.) neomaculipalpus</i> , <i>An. (Nys.) albitarsis</i> , <i>An. (Nys.) marajoara</i> , <i>An. (Nys.) nuneztovari</i> <sup>‡</sup>
Cauca Valley dry forests	<i>An. (Ano.) calderoni</i> <sup>‡</sup> , <i>An. (Ano.) punctimacula</i> <sup>‡</sup> , <i>An. (Ano.) pseudopunctipennis</i> <sup>‡</sup> , <i>An. (Ker) neivai</i> <sup>‡</sup> , <i>An. (Nys.) albimanus</i> <sup>‡</sup>
Cauca Valley montane forests	<i>An. (Ano.) apicimacula</i> , <i>An. (Ano.) calderoni</i> <sup>‡</sup> , <i>An. (Ano.) pseudopunctipennis</i> <sup>‡</sup> , <i>An. (Nys.) albimanus</i> <sup>‡</sup> , <i>An. (Nys.) albitarsis</i> , <i>An. (Nys.) nuneztovari</i> <sup>‡</sup> , <i>An. (Nys.) triannulatus</i>

Ecoregions*	Species
Chocó-Darién moist forests	<i>An. (Ano.) apicimacula</i> , <i>An. (Ano.) calderoni</i> <sup>‡</sup> , <i>An. (Ano.) costai/forattinii</i> , <i>An. (Ano.) malefactor</i> , <i>An. (Ano.) punctimacula</i> <sup>‡</sup> , <i>An. (Ker) neivai</i> <sup>‡</sup> , <i>An. (Nys.) albimanus</i> <sup>¥</sup> , <i>An. (Nys.) darlingi</i> <sup>¥</sup> , <i>An. (Nys.) eiseni</i> , <i>An. (Nys.) nuneztovari</i> <sup>¥</sup> , <i>An. (Nys.) triannulatus</i>
Cordillera Oriental montane forests	<i>An. (Ker) homunculus</i> , <i>An. (Nys.) darlingi</i> <sup>¥</sup> , <i>An. (Nys.) rangeli</i>
Eastern Cordillera Real montane forests	<i>An. (Nys.) argyritarsis</i>
Guajira-Barranquilla xeric scrub	<i>An. (Ano.) neomaculipalpus</i> , <i>An. (Ano.) punctimacula</i> <sup>‡</sup>
Llanos	<i>An. (Ano.) costai</i> , <i>An. (Ano.) peryassui</i> , <i>An. (Ano.) pseudopunctipennis</i> <sup>‡</sup> , <i>An. (Ano.) shannoni</i> , <i>An. (Ker) bambusicolus</i> , <i>An. (Nys.) albitarsis</i> , <i>An. (Nys.) argyritarsis</i> , <i>An. (Nys.) braziliensis</i> , <i>An. (Nys.) darlingi</i> <sup>¥</sup> , <i>An. (Nys.) marajoara</i> , <i>An. (Nys.) nuneztovari</i> <sup>¥</sup> , <i>An. (Nys.) oswaldoi</i> , <i>An. (Nys.) rangeli</i> , <i>An. (Nys.) triannulatus</i>
Magdalena Valley montane forests	<i>An. (Ano.) apicimacula</i> , <i>An. (Ano.) neomaculipalpus</i> , <i>An. (Ano.) pseudopunctipennis</i> <sup>‡</sup> , <i>An. (Nys.) argyritarsis</i> , <i>An. (Nys.) darlingi</i> <sup>¥</sup> , <i>An. (Nys.) nuneztovari</i> <sup>¥</sup> , <i>An. (Nys.) parvus</i> , <i>An. (Nys.) rangeli</i> , <i>An. (Nys.) triannulatus</i>
Magdalena-Urabá moist forests	<i>An. (Ano.) apicimacula</i> , <i>An. (Ano.) malefactor</i> , <i>An. (Ano.) mattogrossensis</i> , <i>An. (Ano.) neomaculipalpus</i> , <i>An. (Ano.) peryassui</i> , <i>An. (Ano.) pseudopunctipennis</i> <sup>‡</sup> , <i>An. (Ano.) punctimacula</i> <sup>‡</sup> , <i>An. (Ker) neivai</i> <sup>‡</sup> , <i>An. (Lop) squamifemur</i> , <i>An. (Nys.) albimanus</i> <sup>¥</sup> , <i>An. (Nys.) albitarsis</i> , <i>An. (Nys.) aquasalis</i> , <i>An. (Nys.) argyritarsis</i> , <i>An. (Nys.) benarrochi</i> <sup>‡</sup> , <i>An. (Nys.) braziliensis</i> , <i>An. (Nys.) darlingi</i> <sup>¥</sup> , <i>An. (Nys.) evansae</i> , <i>An. (Nys.) marajoara</i> , <i>An. (Nys.) nuneztovari</i> <sup>¥</sup> , <i>An. (Nys.) oswaldoi</i> , <i>An. (Nys.) rangeli</i> , <i>An. (Nys.) strodei</i> , <i>An. (Nys.) triannulatus</i> , <i>An. (Ste.) nimbus</i>
Napo moist forests	<i>An. (Ano.) costai</i> , <i>An. (Ano.) mattogrossensis</i> , <i>An. (Ano.) neomaculipalpus</i> , <i>An. (Ano.) punctimacula</i> <sup>‡</sup> , <i>An. (Nys.) albitarsis</i> , <i>An. (Nys.) bellator</i> , <i>An. (Nys.) benarrochi</i> <sup>‡</sup> , <i>An. (Nys.) braziliensis</i> , <i>An. (Nys.) darlingi</i> <sup>¥</sup> , <i>An. (Nys.) marajoara</i> , <i>An. (Nys.) oswaldoi</i> , <i>An. (Nys.) rangeli</i> , <i>An. (Nys.) strode</i> , <i>An. (Nys.) triannulatus</i>
Negro-Branco moist forests	<i>An. (Ano.) mattogrossensis</i> , <i>An. (Ano.) peryassui</i> , <i>An. (Nys.) braziliensis</i> , <i>An. (Nys.) darlingi</i> <sup>¥</sup> , <i>An. (Nys.) oswaldoi</i>
Northwestern Andean montane forests	<i>An. (Ano.) calderoni</i> <sup>‡</sup> , <i>An. (Ano.) pseudopunctipennis</i> <sup>‡</sup> , <i>An. (Nys.) albimanus</i> <sup>¥</sup> , <i>An. (Nys.) argyritarsis</i> , <i>An. (Nys.) darlingi</i> <sup>¥</sup> , <i>An. (Nys.) nuneztovari</i> <sup>¥</sup> , <i>An. (Nys.) triannulatus</i>
Sinú Valley dry forests	<i>An. (Ano.) punctimacula</i> <sup>‡</sup>
Solimões–Japurá moist forests	<i>An. (Ano.) costai</i> , <i>An. (Ano.) peryassui</i> , <i>An. (Nys.) darlingi</i> <sup>¥</sup> , <i>An. (Nys.) dunhami</i>
South American Pacific mangroves	<i>An. (Ano.) apicimacula</i> , <i>An. (Ano.) calderoni</i> <sup>‡</sup> , <i>An. (Ker) neivai</i> <sup>‡</sup> , <i>An. (Nys.) albimanus</i> <sup>¥</sup>
Southwest Amazon moist forests	<i>An. (Nys.) darlingi</i> <sup>¥</sup>
Western Ecuador moist forests	<i>An. (Ano.) calderoni</i> <sup>‡</sup> , <i>An. (Nys.) albimanus</i> <sup>¥</sup>

\* Ecoregions according to WWF (2015). Subgenera *Ano*: *Anopheles*, *Ker*: *Kerteszia*, *Lop*: *Lophopodomomyia*, *Nys*: *Nyssorhynchus*, *Ste*: *Stethomyia*. <sup>¥</sup> Primary malaria vector; <sup>‡</sup> Local malaria vector.

## Checklist of *Anopheles* mosquitos in Colombia

Order Diptera Linnaeus, 1758

Infraorder Culicomorpha Hennig, 1948

Superfamily Culicoidea Meigen, 1818

Family Culicidae Meigen, 1818

Subfamily Anophelinae Grassi, 1900

Genus *Anopheles* Meigen, 1818

Subgenus *Anopheles* Meigen, 1818

***Anopheles (Anopheles) apicimacula* Dyar & Knab, 1906**

**Distribution.** Antioquia\*, Arauca, Bolívar, Boyacá, Caldas, Casanare, Cauca, Cesar, Chocó\*, Córdoba\*, Cundinamarca, Guaviare, Huila, La Guajira, Magdalena, Meta\*, Nariño\*, Norte de Santander, Putumayo, Risaralda, Santander\*, Sucre, Tolima, Valle del Cauca\*.

**Notes.** Reported by Barreto-Reyes (1955), Knight and Stone (1977), Brochero et al. (2005), González and Carrejo (2009), Parra-Henao et al. (2012), Montoya et al. (2017), SIB (2020), Zuleta-Ruiz et al. (2022).

***Anopheles (Anopheles) calderoni* Wilkerson, 1991**

**Distribution.** Antioquia, Caldas, Chocó\*, Huila, La Guajira, Magdalena, Nariño\*, Norte de Santander, Quindio, Risaralda\*, Tolima, Valle del Cauca\*.

**Notes.** Local malaria vector. Reported by González and Carrejo (2009), González et al. (2010), Lucumi-Aragón et al. (2011), Orjuela et al. (2015), Montoya et al. (2017), Galeano-Castañeda et al. (2019), SIB Database (2020).

***Anopheles (Anopheles) costai* Da Fonseca & Ramos, 1939**

**Distribution.** Amazonas\*, Antioquia, Arauca, Bolívar, Boyacá, Caldas, Caquetá, Cesar, Chocó, Córdoba, Cundinamarca, Guainía, Guaviare, Huila, Meta\*, Nariño, Putumayo\*, Santander, Sucre, Valle del Cauca, Vaupés.

**Notes.** Reported by González and Carrejo (2009), Gutiérrez et al. (2009), Ahumada et al. (2013), Orjuela et al. (2013), SIB (2020). *Anopheles costai* was resurrected from synonymy with *Anopheles mediopunctatus* (Sallum et al. 1999), and it was previously erroneously reported in Colombia as *An. mediopunctatus*, as pointed out by Sallum et al. (1999) and Quiñones et al. (2001).

***Anopheles (Anopheles) eiseni* Coquillett, 1902**

**Distribution.** Antioquia, Boyacá, Caldas, Casanare, Cauca, Chocó\*, Cundinamarca, Huila, La Guajira, Magdalena, Meta, Nariño, Norte de Santander, Quindío, Risaralda, Santander, Tolima, Valle del Cauca\*.

**Notes.** Reported by Barreto-Reyes (1955), Knight and Stone (1977), SIB (2020).

***Anopheles (Anopheles) fluminensis* Root, 1927**

**Distribution.** Norte de Santander.

**Notes.** Reported by González and Carrejo (2009).

***Anopheles (Anopheles) forattinii* Wilkerson & Sallum, 1999**

**Distribution.** Meta, Vaupés.

**Notes.** Reported by Wilkerson and Sallum (1999). It was indicated that *An. forattinii* was previously reported in Colombia as *An. mediopunctatus* (Sallum et al. 1999; Quiñones et al. 2001).

***Anopheles (Anopheles) malefactor* Dyar & Knab, 1907**

**Distribution.** Antioquia\*, Chocó\*, Córdoba\*, Meta, Norte de Santander\*.

**Notes.** Reported by Wilkerson (1990), Álvarez et al. (2018), SIB Database (2020). New occurrence data from Monteria municipality, Córdoba Department.

***Anopheles (Anopheles) mattogrossensis* Lutz & Neiva, 1911**

**Distribution.** Amazonas\*, Arauca, Caquetá\*, Cauca, Guainía, Guaviare, Meta, Norte de Santander, Putumayo, Vaupés, Vichada\*.

**Notes.** Reported by Barreto-Reyes (1955), Knight and Stone (1977), Brochero et al. (2006), Orjuela et al. (2013), Brochero and Conn (2015), Álvarez et al. (2018), Prado et al. (2019).

***Anopheles (Anopheles) neomaculipalpus* Curry, 1931**

**Distribution.** Amazonas, Antioquia\*, Arauca, Atlántico, Bolívar, Boyacá, Caldas, Casanare, Caquetá, Cauca, Cesar, Chocó, Córdoba\*, Cundinamarca, Guaviare, Huila, La Guajira\*, Magdalena, Meta, Nariño, Norte de Santander\*, Putumayo\*, Santander\*, Sucre, Tolima, Valle del Cauca, Vaupés.

**Notes.** Reported by Barreto-Reyes (1955), Knight and Stone (1977), Brochero et al. (2006), Parra-Henao and Alarcón (2008), González and Carrejo (2009), Parra-Henao et al. (2012), Orjuela et al. (2013), Álvarez et al. (2018). New occurrence data from Cáceres Municipality, Antioquia Department, and Montería and Valencia municipalities, Córdoba Department.

***Anopheles (Anopheles) peryassui* Dyar & Knab, 1908**

**Distribution.** Amazonas\*, Antioquia\*, Caldas, Caquetá, Casanare, Cundinamarca, Guainía, Guaviare, Meta\*, Putumayo, Santander\*, Sucre, Vaupés, Vichada\*.

**Notes.** Reported by Barreto-Reyes (1955), Knight and Stone (1977), González and Carrejo (2009), Brochero and Conn (2015), Álvarez et al. (2018), SIB (2020).

***Anopheles (Anopheles) pseudopunctipennis* Theobald, 1901**

**Distribution.** Antioquia\*, Arauca, Atlántico, Bolívar, Boyacá, Caldas, Caquetá, Casanare, Cauca, Cesar, Chocó, Córdoba\*, Cundinamarca, Guaviare, Huila, La Guajira, Magdalena\*, Meta\*, Nariño, Norte de Santander, Putumayo, Quindío, Risaralda, Santander\*, Sucre, Tolima, Valle del Cauca\*.

**Notes.** Local malaria vector. Reported by Barreto-Reyes (1955), Knight and Stone (1977), Brochero et al. (2006), Parra-Henao and Alarcón (2008), González and Carrejo (2009), Parra-Henao et al. (2012), Naranjo-Díaz et al. (2013), Montoya et al. (2017), SIB (2020). New occurrence data from Apartadó, Arboletes, Cáceres, Necoclí, San Juan de Urabá and Tarazá Municipalities in Antioquia Department, and Canalete Municipality in Córdoba Department.

***Anopheles (Anopheles) punctimacula* Dyar & Knab, 1906**

**Distribution.** Antioquia\*, Arauca, Atlántico, Bolívar, Boyacá\*, Caldas, Caquetá, Casanare, Cauca, Cesar, Chocó\*, Córdoba\*, Cundinamarca, Guaviare, Huila, La Guajira\*, Magdalena\*, Meta, Nariño\*, Norte de Santander, Putumayo\*, Quindío, Risaralda, Santander, Sucre, Tolima, Valle del Cauca\*, Vaupés, Vichada.

**Notes.** Local malaria vector. Reported by Barreto-Reyes (1955), Knight and Stone (1977), González and Carrejo (2009), Gutiérrez et al. (2009), Orjuela et al. (2013), Naranjo-Díaz et al. (2013, 2014), Montoya et al. (2017), Álvarez et al. (2018), Galeano-Castañeda et al. (2019), SIB (2020). New occurrence data from Apartadó, Caucasia and Necoclí Municipalities in Antioquia Department, and Canalete Municipality in Córdoba Department.

***Anopheles (Anopheles) shannoni* Davis, 1931**

**Distribution.** Vaupés, Vichada\*.

**Notes.** Reported by González and Carrejo (2009), Brochero and Conn (2015).

***Anopheles (Anopheles) vestitipennis* Dyar & Knab, 1906**

**Distribution.** Cesar, Valle del Cauca.

**Notes.** Reported by Barreto-Reyes (1955), Knight and Stone (1977).

**Subgenus *Kerteszia* Theobald, 1905**

***Anopheles (Kerteszia) bambusicolus* Komp, 1937**

**Distribution.** Caquetá, Meta\*.

**Notes.** Reported by Gast (1943), Barreto-Reyes (1955), Knight and Stone (1977), SIB Database (2020).

***Anopheles (Kerteszia) bellator* Dyar & Knab, 1906**

**Distribution.** Putumayo\*.

**Notes.** Reported by Barreto-Reyes (1955), Knight and Stone (1977), SIB Database (2020).

***Anopheles (Kerteszia) boliviensis* (Theobald, 1905)**

**Distribution.** Caldas, Cauca, Chocó, Cundinamarca, Huila, Meta, Nariño, Tolima.

**Notes.** Reported by Barreto-Reyes (1955), Knight and Stone (1977), González and Carrejo (2009).

***Anopheles (Kerteszia) homunculus* Komp, 1937**

**Distribution.** Boyacá, Cauca, Chocó, Cundinamarca, Meta\*, Norte de Santander, Tolima.

**Notes.** Reported by Barreto-Reyes (1955), Knight and Stone (1977), González and Carrejo (2009), SIB Database (2020).

***Anopheles (Kerteszia) neivai* Howard, Dyar & Knab, 1913**

**Distribution.** Antioquia, Bolívar, Boyacá, Cauca, Chocó\*, Cundinamarca, Nariño\*, Norte de Santander, Tolima, Valle del Cauca\*, Vaupés.

**Notes.** Local malaria vector. Reported by Barreto-Reyes (1955), Knight and Stone (1977), Solarte et al. (1996), Gutiérrez et al. (2008, 2009), González and Carrejo (2009), Naranjo-Díaz et al. (2014, 2023), SIB (2020).

***Anopheles (Kerteszia) pholidotus* Zavortink, 1973**

**Distribution.** Caquetá, Cundinamarca, Magdalena, Meta\*, Norte de Santander, Putumayo\*, Tolima\*, Valle del Cauca.

**Notes.** Local malaria vector. Reported by González and Carrejo (2009), Escovar et al. (2014), SIB (2020). Previously reported as *Anopheles lepidotus* (Escovar et al. 2014), a species that is not present in the country.

#### **Subgenus *Lophopodomyia* Antunes, 1937**

##### ***Anopheles (Lophopodomyia) gilesi* (Peryassú, 1908)**

**Distribution.** Meta.

**Notes.** Reported by Barreto-Reyes (1955), Knight and Stone (1977).

##### ***Anopheles (Lophopodomyia) oiketorakras* Osorno-Mesa, 1947**

**Distribution.** Cundinamarca, Nariño.

**Notes.** Reported by Barreto-Reyes (1955), Knight and Stone (1977).

##### ***Anopheles (Lophopodomyia) squamifemur* Antunes, 1937**

**Distribution.** Antioquia\*, Cauca, Chocó, Norte de Santander, Valle del Cauca, Vaupés.

**Notes.** Reported by Barreto-Reyes (1955), Knight and Stone (1977). New occurrence data from Cáceres Municipality in Antioquia Department.

#### **Subgenus *Nyssorhynchus* Blanchard, 1902**

##### ***Anopheles (Nyssorhynchus) albimanus* Wiedemann, 1820**

**Distribution.** Antioquia\*, Atlántico, Bolívar, Cauca\*, Cesar, Chocó\*, Córdoba\*, La Guajira, Magdalena, Nariño\*, Risaralda\*, Sucre, San Andrés y Providencia, Valle del Cauca\*.

**Notes.** Primary malaria vector. Reported by Barreto-Reyes (1955), Knight and Stone (1977), Faran (1980), Gutierrez et al. (Gutiérrez et al. 2008, 2009), Calle et al. (2008), González and Carrejo (2009), Naranjo-Díaz et al. (2013, 2014, 2023), Montoya et al. (2017), Galeano-Castañeda et al. (2019), Altamiranda-Saavedra et al. (2023), SIB (2020). New occurrence data from Apartadó, Mutatá, Necoclí, San Juan de Urabá and Tarazá Municipalities in Antioquia Department, Guapi Municipality in Cauca Department, Canalete, Monteria and Puerto Escondido Municipalities in Córdoba Department, and El Zarzal Municipality in Valle del Cauca.

##### ***Anopheles (Nyssorhynchus) albitarsis* Lynch Arribálzaga, 1878**

**Distribution.** Antioquia\*, Meta\*, Norte de Santander\*, Putumayo\*, Vichada\*.

**Notes.** Reported by Calle et al. (2008), Gutiérrez et al. (2009), González and Carrejo (2009), Jiménez et al. (2012), Ahumada et al. (2013), Orjuela et al. (2013), Montoya et al. (2017), Galeano-Castañeda et al. (2019), SIB (2020). In Colombia, *Anopheles albitarsis* was previously reported as *An. albitarsis* s.l. or *An. marajonara*, both are part of the Albitaris Complex, which potentially comprises at least ten species, only five have been formally described (Bourke et al. 2021). Only the molecular variants *An. albitarsis* F and *An. albitarsis* I are reported in the country,

*An. marajoara* could not be confirmed (Ruiz-Lopez et al. 2012). New occurrence data from Arboletes and Cauca Municipality in Antioquia Department, Moñitos and San Antero Municipalities in Córdoba Department.

***Anopheles (Nyssorhynchus) aquasalis* Curry, 1932**

**Distribution.** Atlántico, Bolívar, Chocó, Córdoba\*, La Guajira\*, Magdalena

**Notes.** Reported by Barreto-Reyes (1955), Knight and Stone (1977), Calle et al. (2008). New occurrence data from San Antero Municipality in Córdoba Department.

***Anopheles (Nyssorhynchus) argyritarsis* Robineau-Desvoidy, 1827**

**Distribution.** Antioquia\*, Arauca, Atlántico, Bolívar, Boyacá, Caldas, Caquetá, Casanare, Cauca, Cesar, Chocó, Córdoba\*, Cundinamarca, Huila, La Guajira, Magdalena, Meta\*, Nariño\*, Norte de Santander, Putumayo, Quindío, Risaralda, Santander\*, Tolima, Valle del Cauca, Vaupés, Vichada\*.

**Notes.** Reported by Barreto-Reyes (1955), Knight and Stone (1977), González and Carrejo (2009), Jiménez et al. (2012), Parra-Henao et al. (2012) Naranjo-Díaz et al. (2013), SIB (2020). New occurrence data from Cáceres Municipality in Antioquia Department.

***Anopheles (Nyssorhynchus) benarrochi* Gabaldón, Cova García & Lopez, 1941**

**Distribution.** Meta\*, Putumayo\*, Santander\*.

**Notes.** Local malaria vector. Reported by Barreto-Reyes (1955), Knight and Stone (1977), Quiñones et al. (2001), Calle et al. (2008), González and Carrejo (2009), Parra-Henao et al. (2012), Orjuela et al. (2013). In Colombia, a molecular variant denominated *An. benarrochi* B was reported, distributed in the south of the country (Ruiz et al. 2005).

***Anopheles (Nyssorhynchus) braziliensis* Chagas, 1907**

**Distribution.** Amazonas, Antioquia\*, Arauca, Bolívar, Boyacá, Caldas, Caquetá, Casanare, Cesar, Chocó, Córdoba, Cundinamarca, Guainía, Guaviare\*, Huila, La Guajira, Magdalena, Meta\*, Norte de Santander, Putumayo\*, Santander, Tolima, Valle del Cauca, Vaupés, Vichada\*.

**Notes.** Reported by Barreto-Reyes (1955), Brochero et al. (2005), Calle et al. (2008), González and Carrejo (2009), Naranjo-Díaz et al. (2013, 2023), Jiménez et al. (2012, 2014), Ahumada et al. (2013), SIB (2020). New occurrence data from Arboletes, Cáceres, Cauca and Tarazá Municipalities in Antioquia Department, San Jose del Guaviare Municipality in Guaviare Department.

***Anopheles (Nyssorhynchus) darlingi* Root, 1926**

**Distribution.** Amazonas\*, Antioquia\*, Arauca, Bolívar, Boyacá, Caldas, Caquetá, Casanare, Cesar, Chocó\*, Córdoba\*, Cundinamarca, Guainía, Guaviare\*, La Guajira, Magdalena, Meta\*, Norte de Santander, Putumayo\*, Santander, Sucre, Vaupés, Vichada\*.

**Notes.** Primary malaria vector. Reported by Barreto-Reyes (1955), Knight and Stone (1977), Brochero et al. (2005), Calle et al. (2008), González and Carrejo (2009), Jiménez et al. (2012, 2014), Ahumada et al. (2013), Orjuela et al. (2013), Naranjo-Díaz et al. (2013, 2014, 2016a, 2019), Montoya et al. (2017), Pacheco et al. (2017), Galeano-Castañeda et al. (2019), SIB (2020). New occurrence data from Apartadó, Cáceres, Caucasia and Necoclí Municipalities in Antioquia Department, San Carlos and Valencia Municipalities in Córdoba Department, San Jose del Guaviare Municipality in Guaviare Department.

***Anopheles (Nyssorhynchus) dunhami* Causey, 1945**

**Distribution.** Amazonas\*.

**Notes.** Reported by Ruiz et al. (2010).

***Anopheles (Nyssorhynchus) evansae* Brèthes, 1926**

**Distribution.** Córdoba\*.

**Notes.** Reported by Knight and Stone (1977), Parra-Henao and Alarcon (2008).

***Anopheles (Nyssorhynchus) marajoara* Galvão & Damasceno, 1942**

**Distribution.** Antioquia\*, Arauca, Atlántico, Bolívar, Boyacá, Caldas, Caquetá\*, Casanare, Cauca, Cesar, Chocó, Córdoba, Cundinamarca, Guaviare, Huila, La Guajira, Magdalena\*, Meta\*, Norte de Santander\*, Putumayo, Santander, Sucre, Tolima, Vaupés, Vichada\*.

**Notes.** Reported by Knight and Stone (1977), González and Carrejo (2009), Brochero et al. (2010), Jiménez et al. (2012).

***Anopheles (Nyssorhynchus) nuneztovari* Gabaldón, 1940**

**Distribution.** Antioquia\*, Arauca\*, Bolívar, Boyacá, Caldas, Caquetá, Casanare\*, Cauca, Cesar, Chocó\*, Córdoba\*, Cundinamarca, Huila, Magdalena, Meta, Norte de Santander\*, Putumayo, Santander\*, Sucre, Tolima, Valle del Cauca\*.

**Notes.** Primary malaria vector. Reported by Barreto-Reyes (1955), Knight and Stone (1977), Calle et al. (2002, 2008), Brochero et al. (2006), Fajardo et al. (2008), Parra-Henao and Alarcón (2008), González and Carrejo (2009), Fonseca-González et al. (2009), Ruiz et al. (2010), Parra-Henao et al. (2012), Naranjo-Díaz et al. (2013, 2014, 2016b, 2023), Montoya et al. (2017), Galeano-Castañeda et al. (2019), Altamiranda-Saavedra et al. (2023), SIB (2020). New occurrence data from Apartadó, Caucasia, Necoclí and Tarazá Municipalities in Antioquia Department, Monteria and Moñitos Municipalities in Córdoba Department.

***Anopheles (Nyssorhynchus) oswaldoi* Peryassú, 1922**

**Distribution.** Amazonas, Antioquia\*, Arauca, Atlántico, Bolívar, Boyacá, Caldas, Caquetá, Casanare, Cauca, Cesar, Chocó, Córdoba, Cundinamarca, Guainía, Guaviare\*, Magdalena, Meta, Nariño, Norte de Santander, Putumayo\*, Santander\*, Sucre, Tolima, Valle del Cauca, Vaupés, Vichada\*.

**Notes.** Reported by Barreto-Reyes (1955), González and Carrejo (2009), Ruiz et al. (2010), Parra-Henao et al. (2012), Jiménez et al. (2012, 2014), Orjuela et al. (2013). New occurrence data from Caucasia Municipality in Antioquia Department, San Jose del Guaviare Municipality in Guaviare Department.

***Anopheles (Nyssorhynchus) parvus* Chagas, 1907**

**Distribution.** Arauca, Casanare, Meta, Santander\*, Vichada.

**Notes.** Reported by Barreto-Reyes (1955), Knight and Stone (1977), Parra-Henao et al. (2012), SIB (2020).

***Anopheles (Nyssorhynchus) rangeli* Gabaldón, Cova García & Lopez, 1940**

**Distribution.** Antioquia\*, Arauca\*, Bolívar, Boyacá\*, Caldas\*, Caquetá\*, Casanare, Cauca, Cesar, Chocó, Córdoba\*, Cundinamarca\*, Guainía, Guaviare\*, La Guajira, Magdalena, Meta\*, Nariño, Norte de Santander, Putumayo\*, Santander\*, Tolima, Valle del Cauca.

**Notes.** Reported by Barreto-Reyes (1955), Knight and Stone (1977), Brochero et al. (2005, 2006), Calle et al. (2008), González and Carrejo (2009), Jiménez et al. (2012), Parra-Henao et al. (2012), Orjuela et al. (2013), SIB (2020). New occurrence data from Arboletes and Caucasia Municipalities in Antioquia Department, Moñitos Municipality in Córdoba Department.

***Anopheles (Nyssorhynchus) strodei* Root, 1926**

**Distribution.** Antioquia, Arauca\*, Bolívar, Boyacá, Caquetá, Casanare, Chocó, Córdoba, Cundinamarca, La Guajira, Meta\*, Norte de Santander, Putumayo\*, Santander\*, Valle del Cauca.

**Notes.** Reported by Barreto-Reyes (1955), Calle et al. (2008), González and Carrejo (2009), Parra-Henao et al. (2012), SIB Database (2020).

***Anopheles (Nyssorhynchus) triannulatus* Neiva & Pinto, 1922**

**Distribution.** Amazonas, Antioquia\*, Arauca, Atlántico, Bolívar, Boyacá, Caldas, Caquetá, Casanare, Cauca, Cesar, Chocó\*, Córdoba\*, Cundinamarca, Guaviare, Huila, La Guajira, Magdalena\*, Meta\*, Nariño, Norte de Santander, Putumayo\*, Quindío, Santander\*, Sucre, Tolima, Valle del Cauca.

**Notes.** Reported by Barreto-Reyes (1955), Knight and Stone (1977), Brochero et al. (2006), Calle et al. (2008), González and Carrejo (2009), Parra-Henao et al. (2012), Ahumada et al. (2013), Naranjo-Díaz et al. (2013, 2023), Orjuela et al. (2013), Montoya et al. (2017), Atencia-Pineda et al. (2018), SIB (2020). New occurrence data from Apartadó, Arboletes, Caucasia, Necoclí, and San Juan de Urabá Municipalities in Antioquia Department, Canalete, Monteria, Moñitos, San Antero, and Valencia Municipalities in Córdoba Department.

***Anopheles (Nyssorhynchus) trinkae* Faran, 1979**

**Distribution.** Meta\*.

**Notes.** Reported by González and Carrejo (2009), SIB Database (2020).

### **Subgenus *Stethomyia* Theobald, 1902**

#### ***Anopheles (Stethomyia) kompi* Edwards, 1930**

**Distribution.** Caquetá.

**Notes.** Reported by Barreto-Reyes (1955), Knight and Stone (1977).

#### ***Anopheles (Stethomyia) nimbus* (Theobald, 1902)**

**Distribution.** Cundinamarca, Guaviare, Meta, Vaupés, Valle del Cauca.

**Notes.** Reported by Barreto-Reyes (1955), Knight and Stone (1977), González and Carrejo (2009).

#### ***Anopheles (Stethomyia) thomasi* Shannon, 1933**

**Notes.** Reported by Barreto-Reyes (1955), Knight and Stone (1977).

## **Discussion**

The genus *Anopheles* contains eight subgenera, five of which are present in the Neotropical region (*Anopheles*, *Kerteszia*, *Lophopodomys*, *Nyssorhynchus*, and *Stethomyia*; Harbach 2023). All five subgenera are present in Colombia. The current checklist only includes formally described species and excludes molecularly identified variants. Therefore, a total of 44 species are listed as present in Colombia. Species of the subgenera *Nyssorhynchus* and *Anopheles* are the most widely distributed in the country, occurring in 32 and 31 Colombian departments, respectively. *Nyssorhynchus* is the subgenus with the highest species richness, comprising 17 species. *Stethomyia* has a limited distribution, being found in only three departments. *Stethomyia* and *Lophopodomys* subgenera are represented by three species each. The highest species richness was detected in Meta Department, with a total of 30 species, followed by Norte de Santander with 24. San Andres and Providencia Department exhibited the lowest species richness, with only the main Colombian malaria vector, *An. albimanus*, being recorded in this insular region (Table 1) (Fig. 1).

It is well known that factors such as temperature, rainfall, and humidity affect the geographical distribution of *Anopheles* species (Abiodun et al. 2016). Colombia exhibits a wide variety of ecological conditions, and 34 ecoregions are described (WWF 2015). The current checklist reports the presence of *Anopheles* species in 21 of those ecoregions (Table 2). The Magdalena-Urabá moist forests ecoregion exhibits the highest richness with 23 species, dominated by the species of the subgenera *Nyssorhynchus* and *Anopheles*, 14 and 7 species, respectively. The characteristics of this ecoregion include consistently high temperatures exceeding 28 °C and average annual rainfall within the range of 2,000–4,000 millimeters (WWF 2015). This ecoregion forms part of the important Tumbes-Chocó-Magdalena biodiversity hotspot, which spans southern Panamá to northern Perú and encompasses coastal and lowland areas of the Magdalena River basin and the Urabá region in northwest Colombia. The diverse ecological requirements of *Anopheles* species, which thrive on a variety of landscapes ranging from mosaic tropical rainforests to wetlands, mangrove swamps, and coastal plains, contribute to the high species richness detected in these Colombian regions.

Several members of the genus *Anopheles* are important in public health due to their role as malaria vectors. In Colombia, the annual number of malaria cases has exceeded 70,000 in recent years (INS 2021, 2022, 2023). Of the nine *Anopheles* species implicated in malaria transmission (Olano et al. 2001; Gutiérrez et al. 2008; Orjuela et al. 2013; Naranjo-Díaz et al. 2013), at least one malaria vector species was registered in each of the 21 ecoregions with occurrence data, except for the Eastern Cordillera Real montane forests (Table 1). As the Magdalena-Urabá moist forests ecoregion exhibited the highest species richness, it is not surprising that it also contained most of the malaria vectors, including the three primary vectors (*An. albimanus*, *An. darlingi*, and *An. nuneztovari*) and four local vectors (*An. pseudopunctipennis*, *An. punctimacula*, *An. neivai*, and *An. benarrochi*). The Chocó-Darién moist forests ecoregion was second in the number of vectors present, including the three primary vectors and three local vectors (*An. calderoni*, *An. punctimacula*, and *An. neivai*). These two ecoregions encompass the most important Colombian malaria regions, the Urabá, Bajo Cauca, Alto Sinú, and Pacific regions, which report the highest annual number of malaria cases (INS 2023).

Several factors contribute to the discrepancies between previous catalogs and the current checklist. For example, *An. mediopunctatus* may be restricted to Brazil, and in Colombia, it was likely misidentified as *An. costai* or *An. forattinii* (Sallum et al. 1999; Quiñones et al. 2001). Additionally, *Anopheles cruzii*, although reported from Costa Rica to Argentina, has not been confirmed in Colombia (Wilkerson and Peyton 1991). Furthermore, *Anopheles vargasi* has been registered in neighboring Venezuela (Del Ventura et al. 2013), but there is no evidence of its presence in Colombia (Osorno-Mesa 1947). Mistaken taxonomic assignments, often due to the existence of cryptic species, have led to erroneous reports. For instance, *An. pholidotus* was previously reported as *An. lepidotus* (Escovar et al. 2014).

## Conclusions

In recent decades, numerous studies and surveys conducted in the country have provided valuable data on the presence and distribution of *Anopheles* species. The current checklist attempts to compile the available information. The current list includes 44 formally characterized *Anopheles* species from five subgenera, with the subgenera *Nyssorhynchus* and *Anopheles* being the largest and most widely distributed species groups. Information for 66 new occurrence data is also provided. The incorporation of presence records and ecological distributions is essential for accurately estimating the *Anopheles* species diversity and assessing the malaria vectors. This is fundamental for the design and implementation of effective control interventions.

An interesting finding is that most of the new species records are concentrated in specific regions, likely reflecting research interest in the most malaria-endemic regions of Colombia. It is noteworthy that after 47 species had been recorded in the country, the current checklist only includes 44 species. For an *Anopheles* species to be included in the list, it was required to have a formal description and validation; species variants originally described using only molecular methods were excluded. Among the factors contributing to the discrepancies between previous catalogs and the current checklist are the existence of problematic species, or in some cases damaged specimens, which can lead to

misidentifications; also, mistaken taxonomic assignments can occur due to the existence of cryptic species. In addition, for some species, there was no evidence of their presence in Colombia. Finally, while the use of molecular techniques has helped to clarify the taxonomic status of several problematic species, this has led to an increase in the number of molecular variants reported. However, it has also facilitated the correction of erroneous taxonomic assignments, which in turn, may lead to a decrease in the number of species formally described.

## Additional information

### Conflict of interest

The authors have declared that no competing interests exist.

### Ethical statement

No ethical statement was reported.

### Funding

This work received support from Escuela de Microbiología, Universidad de Antioquia, project code No. 2023-66350.

### Author contributions

Nelson Naranjo-Díaz: specimen identification, data analysis, writing, review & editing. Margarita M. Correa: data analysis, project coordinator, critical revisions and editing of manuscript drafts.

### Author ORCIDs

Margarita M. Correa  <https://orcid.org/0000-0003-2419-7269>

### Data availability

The dataset containing the information on *Anopheles* species occurrence in Colombia is available in: <https://doi.org/10.5281/zenodo.13527884>. (Data will be available upon publication).

## References

- Abiodun GJ, Maharaj R, Witbooi P, Okosun KO (2016) Modelling the influence of temperature and rainfall on the population dynamics of *Anopheles arabiensis*. *Malaria Journal* 15: 1–15. <https://doi.org/10.1186/s12936-016-1411-6>
- Ahumada ML, Pareja PX, Buitrago LS, Quiñones ML (2013) Biting behavior of *Anopheles darlingi* Root, 1926 (Diptera: Culicidae) and its association with malaria transmission in Villavicencio (Meta, Colombia). *Biomédica* 33: 241–250. [PMID: 24652134] <https://doi.org/10.7705/biomedica.v33i2.1492>
- Altamiranda-Saavedra M, Naranjo-Díaz N, Conn JE, Correa MM (2023) Entomological parameters and population structure at a microgeographic scale of the main Colombian malaria vectors *Anopheles albimanus* and *Anopheles nuneztovari*. *PLoS ONE* 18: e0280066. <https://doi.org/10.1371/journal.pone.0280066>
- Álvarez N, Gómez GF, Naranjo-Díaz N, Correa MM (2018) Discrimination of *Anopheles* species of the Arribalzagia Series in Colombia using a multilocus approach. *Infection, Genetics and Evolution* 64: 76–84. <https://doi.org/10.1016/j.meegid.2018.06.018>

- Atencia-Pineda M, Toro-Cantillo A, Hoyos-López RO (2018) Diversidad genética y estructura poblacional de *Anopheles triannulatus* s.l. en Córdoba, Colombia, determinadas mediante el método de región de código de barras de ADN. *Biomédica* 38: 117–126. <https://doi.org/10.7705/biomedica.v38i0.4055>
- Barreto-Reyes P (1955) Lista de Mosquitos de Colombia, S. A. (Diptera: Culicidae). *Anales de la Sociedad de Biología de Bogotá* 7: 46–94.
- Bourke BP, Justi SA, Caicedo-Quiroga L, Pecor DB, Wilkerson RC, Linton YM (2021) Phylogenetic analysis of the Neotropical *Albitarsis* Complex based on mitogenome data. *Parasites and Vectors* 14: 1–18. <https://doi.org/10.1186/s13071-021-05090-w>
- Brault AC, Foy BD, Myles KM, Kelly CLH, Higgs S, Weaver SC, Olson KE, Miller BR, Powers AM (2004) Infection patterns of o'nyong nyong virus in the malaria-transmitting mosquito, *Anopheles gambiae*. *Insect molecular biology* 13: 625–635. <https://doi.org/10.1111/j.0962-1075.2004.00521.x>
- Brochero H, Conn JE (2015) New records of *Anopheles* (Diptera: Culicidae) in Puerto Carreño, Vichada, Colombia. *Check List* 11(1): 1518. <https://doi.org/10.15560/11.1.1518>
- Brochero HL, Rey G, Buitrago LS, Olano VA (2005) Biting activity and breeding sites of *Anopheles* species in the municipality Villavicencio, Meta, Colombia. *Journal of the American Mosquito Control Association* 21: 182–186. [https://doi.org/10.2987/8756-971X\(2005\)21\[182:BAABSO\]2.0.CO;2](https://doi.org/10.2987/8756-971X(2005)21[182:BAABSO]2.0.CO;2)
- Brochero H, Pareja P, Ortiz G, Olano V (2006) Breeding places and biting activity of *Anopheles* species in the municipality of Cimitarra, Santander, Colombia. *Biomédica* 26: 269–277. [PMID: 16925099] <https://doi.org/10.7705/biomedica.v26i2.1416>
- Brochero HL, Li C, Wilkerson RC (2007) A newly recognized species in the *Anopheles* (*Nyssorhynchus*) *albitarsis* complex (Diptera: Culicidae) from Puerto Carreño, Colombia. *The American journal of tropical medicine and hygiene* 76: 1113–1117. [PMID: 17556620] <https://doi.org/10.4269/ajtmh.2007.76.1113>
- Brochero H, Li C, Wilkerson R, Conn JE, Ruiz-García M (2010) Genetic structure of *Anopheles* (*Nyssorhynchus*) *marajoara* (Diptera: Culicidae) in Colombia. *The American journal of tropical medicine and hygiene* 83: 585–595. <https://doi.org/10.4269/ajtmh.2010.09-0482>
- Calle L DA, Quiñones ML, Erazo HF, Jaramillo O N (2002) Morphometric discrimination of females of five species of *Anopheles* of the subgenus *Nyssorhynchus* from Southern and Northwest Colombia. *Memórias do Instituto Oswaldo Cruz* 97: 1191–1195. <https://doi.org/10.1590/S0074-02762002000800021>
- Calle DA, Quiñones ML, Erazo HF, Jaramillo N (2008) Discriminación por morfometría geométrica de once especies de *Anopheles* (*Nyssorhynchus*) presentes en Colombia. *Biomédica* 28: 371–385. <https://doi.org/10.7705/biomedica.v28i3.75>
- Carrejo NS, Gonzalez R (1992) Introducción al conocimiento de los Diptera. Centro Editorial Universidad del Valle, Cali, 197 pp.
- Cienfuegos A, Rosero DA, Naranjo N, Luckhart S, Conn JE, Correa MM (2011) Evaluation of a PCR-RFLP-ITS2 assay for discrimination of *Anopheles* species in northern and western Colombia. *Acta tropica* 118: 128–135. <https://doi.org/10.1016/j.actatropica.2011.02.004>
- Del Ventura F, Liria J, Navarro JC (2013) Determinación de áreas de endemismo en mosquitos (Diptera: Culicidae) en Venezuela, mediante criterios explícitos de optimización. *Boletín de Malaria y Salud Ambiental* 53: 165–182.
- Escovar JE, González R, Quiñones ML, Wilkerson RC, Ruiz F, Harrison BA (2014) Morphology of the larvae, male genitalia and DNA sequences of *Anopheles* (*Kerteszia*) *pholidotus* (Diptera: Culicidae) from Colombia. *Memórias do Instituto Oswaldo Cruz* 109: 1–7. <https://doi.org/10.1590/0074-0276130596>

- Fajardo Ramos M, González Obando R, Fidel Suárez M, López D, Wilkerson R, Sallum MAM (2008) Morphological analysis of three populations of *Anopheles* (*Nyssorhynchus*) *nuneztovari* Gabaldón (Diptera: Culicidae) from Colombia. *Memórias do Instituto Oswaldo Cruz* 103: 85–92. <https://doi.org/10.1590/S0074-02762008000100013>
- Faran M (1980) Mosquitos Studies (Diptera, Culicidae) XXXIV. A revision of the *Albimanus* Section of the subgenus *Nyssorhynchus* of *Anopheles*. *Contributions of the American Entomological Institute* 15: 1–215.
- Faran M, Linthicum L (1981) handbook of the Amazonian species of *Anopheles* (*Nyssorhynchus*) (Diptera: Culicidae). *Mosquito Systematics* 13: 1–81.
- Fonseca-González I, Cárdenas R, Quiñones ML, McAllister J, Brogdon WG (2009) Pyrethroid and organophosphates resistance in *Anopheles* (*N.*) *nuneztovari* Gabaldón populations from malaria endemic areas in Colombia. *Parasitology Research* 105: 1399–1409. <https://doi.org/10.1007/s00436-009-1570-2>
- Gaffigan TV, Wilkerson RC, Pecor JE, Stoffer JA, Anderson T (2014) Systematic Catalog of Culicidae - Walter Reed Biosystematics Unit - Home. <http://www.mosquitocatalog.org/> [October 5, 2023]
- Galeano-Castañeda Y, Urrea-Aguirre P, Piedrahita S, Bascuñán P, Correa MM (2019) Composition and structure of the culturable gut bacterial communities in *Anopheles albimanus* from Colombia. *PLoS ONE* 14. <https://doi.org/10.1371/journal.pone.0225833>
- Gast A (1943) Biología y distribución de los anophelinos en Colombia. *Revista de la Facultad de Medicina* 12: 1–55.
- GBIF (2024) GBIF Occurrence Download. <https://doi.org/10.15468/dl.wp8yjf/> [accessed 08 May 2024]
- Gómez GF, Bickersmith SA, González R, Conn JE, Correa MM (2015) Molecular taxonomy provides new insights into *Anopheles* species of the neotropical arribalzagia series. *PLoS ONE* 10: e0119488. <https://doi.org/10.1371/journal.pone.0119488>
- González R, Carrejo N (2007) Introducción al estudio taxonomico de *Anopheles* de Colombia Claves y notas de distribución. Universidad del Valle, Cali, 237 pp.
- González R, Carrejo N (2009) Introducción al estudio taxonomico de *Anopheles* de Colombia Claves y notas de distribución. 2<sup>nd</sup> edn. Universidad del Valle, Cali, 260 pp.
- González R, Carrejo N, Wilkerson RC, Alarcon J, Alarcon-Ormasa J, Ruiz F, Bhatia R, Loaiza J, Linton Y-M (2010) Confirmation of *Anopheles* (*Anopheles*) *calderoni* Wilkerson, 1991 (Diptera: Culicidae) in Colombia and Ecuador through molecular and morphological correlation with topotypic material. *Memórias do Instituto Oswaldo Cruz* 105: 1001–1009. <https://doi.org/10.1590/S0074-02762010000800009>
- Gutiérrez LA, Naranjo N, Jaramillo LM, Muskus C, Luckhart S, Conn JE, Correa MM (2008) Natural infectivity of *Anopheles* species from the Pacific and Atlantic Regions of Colombia. *Acta tropica* 107: 99–105. <https://doi.org/10.1016/j.actatropica.2008.04.019>
- Gutiérrez LA, González JJ, Gómez GF, Castro MI, Rosero DA, Luckhart S, Conn JE, Correa MM (2009) Species composition and natural infectivity of anthropophilic *Anopheles* (Diptera: Culicidae) in the states of Córdoba and Antioquia, Northwestern Colombia. *Memórias do Instituto Oswaldo Cruz* 104: 1117–1124. <https://doi.org/10.1590/S0074-02762009000800008>
- Harbach RE (2023) Culicidae Classification. Mosquito Taxonomic Inventory. <http://mosquito-taxonomic-inventory.info/simpletaxonomy/term/6223> [July 21, 2023]
- Heinemann SJ, Belkin JN (1978) Collection records of the project "Mosquitoes of Middle America" 12. Colombia (COA, COB, COL, COM). *Mosquito Systematics* 10: 493–540.
- Hernández-Valencia JC, Rincón DS, Marín A, Naranjo-Díaz N, Correa MM (2020) Effect of land cover and landscape fragmentation on anopheline mosquito abundance and

- diversity in an important Colombian malaria endemic region. PLoS ONE 15. <https://doi.org/10.1371/journal.pone.0240207>
- Hiwat H, Bretas G (2011) Ecology of *Anopheles darlingi* Root with respect to vector importance: a review. Parasites & Vectors 4: 177. <https://doi.org/10.1186/1756-3305-4-177>
- IGAC (2002) Atlas de Colombia. 5<sup>th</sup> edn. Imprenta Nacional de Colombia, Bogota, 167 pp.
- INS (2021) Instituto Nacional de Salud, Boletín epidemiológico Semanal. Estadísticas del sistema de vigilancia en salud pública- SIVIGILA, Casos totales en la Semana Epidemiológica 52 y acumulados del año, Subdirección de Vigilancia y Control en Salud Pública. <https://portalsivigila.ins.gov.co/Paginas/Vigilancia-Rutinaria.aspx> [May 4, 2024]
- INS (2022) Instituto Nacional de Salud, Boletín epidemiológico Semanal. Estadísticas del sistema de vigilancia en salud pública- SIVIGILA, Casos totales en la Semana Epidemiológica 52 y acumulados del año, Subdirección de Vigilancia y Control en Salud Pública. <https://portalsivigila.ins.gov.co/Paginas/Vigilancia-Rutinaria.aspx> [May 5, 2024]
- INS (2023) Instituto Nacional de Salud, Boletín epidemiológico Semanal. Estadísticas del sistema de vigilancia en salud pública- SIVIGILA, Casos totales en la Semana Epidemiológica 52 y acumulados del año, Subdirección de Vigilancia y Control en Salud Pública. <https://portalsivigila.ins.gov.co/Paginas/Vigilancia-Rutinaria.aspx> [May 7, 2024]
- ITIS (2024) Integrated Taxonomic Information System. <https://www.itis.gov/> [June 6, 2024]
- Jiménez P, Conn JE, Wirtz R, Brochero H (2012) *Anopheles* (Diptera: Culicidae) vectors of malaria in Puerto Carreño municipality, Vichada, Colombia. Biomedica 32: 13. <https://doi.org/10.7705/biomedica.v32i0.414>
- Jiménez P, Conn JE, Brochero H (2014) Malaria vectors in San José del Guaviare, Orinoquia, Colombia. Journal of the American Mosquito Control Association 30(2): 91–98. <https://doi.org/10.2987/13-6382.1>
- Knight KL, Stone A (1977) A catalog of the mosquitoes in the world. (Diptera: Culicidae). Entomological Society of America, Maryland, 611 pp. <https://doi.org/10.4182/FXDZ6899>
- Lucumi-Aragón D, González RO, Salas-Quinchucua C (2011) Actividad de picadura de *Anopheles calderoni* (Diptera: Culicidae) en dos localidades del Valle del Cauca, Colombia. Revista Colombiana de Entomología 37: 256–261. <https://doi.org/10.25100/socolen.v37i2.9086>
- Manguin S, Bangs MJ, Pothikasikorn J, Chareonviriyaphap T (2010) Review on global co-transmission of human *Plasmodium* species and *Wuchereria bancrofti* by *Anopheles* mosquitoes. Infection, Genetics and Evolution 10: 159–177. <https://doi.org/10.1016/j.meegid.2009.11.014>
- Montoya C, Bascuñán P, Rodríguez-Zabala J, Correa MM (2017) Abundance, composition and natural infection of *Anopheles* mosquitoes from two malaria-endemic regions of Colombia. Biomedica 37: 98–105. <https://doi.org/10.7705/biomedica.v37i0.3553>
- Montoya-Lerma J, Solarte YA, Giraldo-Calderón GI, Quiñones ML, Ruiz-López F, Wilkerson RC, González R (2011) Malaria vector species in Colombia: a review. Memórias do Instituto Oswaldo Cruz 106(Suppl): 223–238. <https://doi.org/10.1590/S0074-02762011000900028>
- Naranjo-Díaz N, Rosero DA, Rua-Urbe G, Luckhart S, Correa MM (2013) Abundance, behavior and entomological inoculation rates of anthropophilic anophelines from

- a primary Colombian malaria endemic area. *Parasites & Vectors* 6: 61. <https://doi.org/10.1186/1756-3305-6-61>
- Naranjo-Díaz N, Altamiranda M, Luckhart S, Conn JE, Correa MM (2014) Malaria vectors in ecologically heterogeneous localities of the Colombian Pacific region. *PLoS ONE* 9: e103769. <https://doi.org/10.1371/journal.pone.0103769>
- Naranjo-Díaz N, Conn JE, Correa MM (2016a) Behavior and population structure of *Anopheles darlingi* in Colombia. *Infection, genetics and evolution* 39: 64–73. <https://doi.org/10.1016/j.meegid.2016.01.004>
- Naranjo-Díaz N, Sallum MAM, Correa MM (2016b) Population dynamics of *Anopheles nuneztovari* in Colombia. *Infection, Genetics and Evolution* 45: 56–65. <https://doi.org/10.1016/j.meegid.2016.08.019>
- Naranjo-Díaz N, Altamiranda-Saavedra M, Correa MM (2019) *Anopheles* species composition and entomological parameters in malaria endemic localities of North West Colombia. *Acta Tropica* 190: 13–21. <https://doi.org/10.1016/j.actatropica.2018.10.011>
- Naranjo-Díaz N, Hernandez-Valencia JC, Gomez GF, Correa MM (2023) Spatial and Temporal Diversity Variation in the *Anopheles* Communities in Malaria-Endemic Regions of Colombia. *The American Journal of Tropical Medicine and Hygiene* 108: 744–754. <https://doi.org/10.4269/ajtmh.22-0569>
- Olano V, Brochero H, Sáenz R, Quiñones M, Molina J (2001) Mapas preliminares de la distribución de especies de *Anopheles* vectores de malaria en Colombia. *Biomédica* 21: 402–408.
- Orjuela LI, Herrera M, Erazo H, Quiñones ML (2013) Especies de *Anopheles* presentes en el departamento del Putumayo y su infección natural con *Plasmodium*. *Biomédica* 33: 42–52. <https://doi.org/10.7705/biomedica.v33i1.619>
- Orjuela LI, Ahumada ML, Avila I, Herrera S, Beier JC, Quiñones ML (2015) Human biting activity, spatial-temporal distribution and malaria vector role of *Anopheles calderoni* in the southwest of Colombia. *Malaria Journal* 14: 1–9. <https://doi.org/10.1186/s12936-015-0764-6>
- Osorno-Mesa E (1947) Una nueva especie de *Anopheles* de Bogotá, Colombia. *Caldasia* 4(20): 431–446.
- Pacheco MA, González R, Brochero HL (2017) *Anopheles darlingi* (Diptera: Culicidae) Rood 1926: Morphometric variations in wings and legs of populations from Colombia. *Biomedica* 37: 124–134. <https://doi.org/10.7705/biomedica.v37i0.3492>
- Parra-Henao G, Alarcón EP (2008) Observaciones sobre la bionomía de *Anopheles* spp. (Diptera: Culicidae) en el municipio Valencia, departamento Córdoba, Colombia. *Boletín de Malariología y Salud Ambiental XLVIII*: 95–98.
- Parra-Henao G, Delgado D, Alarcón EP (2012) Especies de *Anopheles* en el Canón del Río Sogamoso, Santander, Colombia, al inicio de la puesta en marcha del proyecto hidroeléctrico. *Boletín de Malariología y Salud Ambiental* 52: 287–294.
- Prado CC, Alvarado-Cabrera LA, Camargo-Ayala PA, Garzón-Ospina D, Camargo M, Soto-De León SC, Cubides JR, Celis-Giraldo CT, Patarroyo ME, Patarroyo MA (2019) Behavior and abundance of *Anopheles darlingi* in communities living in the Colombian Amazon riverside. *PLoS ONE* 14(3): e0213335. <https://doi.org/10.1371/journal.pone.0213335>
- Quiñones ML, Harbach RE, Calle DA, Ruiz F, Erazo HF, Linton YM (2001) Variante morfológica de adultos hembras de *Anopheles benarrochi* (Diptera: Culicidae) en Putumayo, Colombia. *Biomédica* 21: 351. <https://doi.org/10.7705/biomedica.v21i4.1128>
- Ruiz F, Quiñones ML, Erazo HF, Calle DA, Alzate JF, Linton YM (2005) Molecular differentiation of *Anopheles* (*Nyssorhynchus*) *benarrochi* and *An. (N.) oswaldoi* from

- southern Colombia. *Memorias do Instituto Oswaldo Cruz* 100: 155–160. <https://doi.org/10.1590/S0074-02762005000200008>
- Ruiz F, Linton YM, Ponsonby DJ, Conn JE, Herrera M, Quiñones ML, Vélez ID, Wilkerson RC (2010) Molecular comparison of topotypic specimens confirms *Anopheles* (*Nyssorhynchus*) *dunhami* Causey (Diptera: Culicidae) in the Colombian Amazon. *Memorias do Instituto Oswaldo Cruz* 105: 899. <https://doi.org/10.1590/S0074-02762010000700010>
- Ruiz-Lopez F, Wilkerson RC, Conn JE, McKeon SN, Levin DM, Quiñones ML, Póvoa MM, Linton Y-M (2012) DNA barcoding reveals both known and novel taxa in the Albitarsis Group (*Anopheles*: *Nyssorhynchus*) of Neotropical malaria vectors. *Parasites & vectors* 5: 44. <https://doi.org/10.1186/1756-3305-5-44>
- Sallum MA, Wilkerson RC, Forattini OP (1999) Taxonomic study of species formerly identified as *Anopheles mediopunctatus* and resurrection of *An. costai* (Diptera: Culicidae). *Journal of medical entomology* 36: 282–300. <https://doi.org/10.1093/jmedent/36.3.282>
- SEM Servicio Nacional de Erradicación de la Malaria (1957) Plan para la erradicación de la malaria en Colombia. Volumen II. Ministerio de Salud Pública y Oficina Sanitaria Panamericana, Bogotá, 365 pp.
- SIB Colombia (2020) Sistema de Información sobre Biodiversidad de Colombia. <https://sibcolombia.net/> [accessed 30 May 2024]
- Solarte Y, Hurtado C, Gonzalez R, Alexander B (1996) Man-biting activity of *Anopheles* (*Nyssorhynchus*) *albimanus* and *An. (Kerteszia) neivai* (Diptera: Culicidae) in the Pacific lowlands of Colombia. *Memórias do Instituto Oswaldo Cruz* 91: 141–146. <https://doi.org/10.1590/S0074-02761996000200002>
- Stone A, Knight KL, Starcke H (1959) A synoptic catalog of the mosquitoes of the world (Diptera, Culicidae). *Entomological Society of America*, 358 pp. <https://doi.org/10.4182/UMJB2446>
- WHO (2022) World Malaria Report 2022. World Health Organization: 293. [https://reliefweb.int/report/world/world-malaria-report-2022?gclid=CjwKCAiAzp6eBhByEiwA\\_gGq5NTTnODwucx32cIn1jrven6oy0qHvmQAoWLOEotgDzgzvcTKsdJrPRoCrbkQAvD\\_BwE](https://reliefweb.int/report/world/world-malaria-report-2022?gclid=CjwKCAiAzp6eBhByEiwA_gGq5NTTnODwucx32cIn1jrven6oy0qHvmQAoWLOEotgDzgzvcTKsdJrPRoCrbkQAvD_BwE) [accessed 18 January 2023]
- Wilkerson RC (1990) Redescriptions of *Anopheles punctimacula* and *An. malefactor* (Diptera: Culicidae). *Journal of medical entomology* 27: 225–247. <https://doi.org/10.1093/jmedent/27.2.225>
- Wilkerson R, Peyton E (1991) The Brazilian malaria vector *Anopheles* (*Kerteszia*) *cruzii*: life stages and biology (Diptera: Culicidae). *Mosquito Systematics* 23: 110–122.
- Wilkerson RC, Sallum MA (1999) *Anopheles* (*Anopheles*) *forattinii*: a new species in Series Arribalzagia (Diptera: Culicidae). *Journal of medical entomology* 36: 345–354. <https://doi.org/10.1093/jmedent/36.3.345>
- WWF (2015) List of Ecoregions. World Wildlife Fund. [http://wwf.panda.org/about\\_our\\_earth/ecoregions/ecoregion\\_list/](http://wwf.panda.org/about_our_earth/ecoregions/ecoregion_list/)
- Zapata MA, Cienfuegos A V, Quirós OI, Quiñones ML, Luckhart S, Correa MM (2007) Discrimination of seven *Anopheles* species from San Pedro de Urabá, Antioquia, Colombia, by polymerase chain reaction-restriction fragment length polymorphism analysis of its sequences. *The American journal of tropical medicine and hygiene* 77: 67–72. <https://doi.org/10.4269/ajtmh.2007.77.67>
- Zuleta-Ruiz BR, Gómez-Vargas W, Ortiz-Reyes A, Ruiz-López F (2022) Identificación de *Anopheles* spp. (Diptera: Culicidae) presentes en áreas endémicas de transmisión de malaria en Turbo, Antioquia y su infección con *Plasmodium* spp. *Actualidades Biológicas* 44(116): e5. <https://doi.org/10.17533/udea.acbi.v44n116a05>

## Supplementary material 1

### Data on *Anopheles* species occurrence in Colombia

Authors: Nelson Naranjo-Díaz, Margarita M. Correa

Data type: xlsx

Explanation note: Geographic coordinates are shown in decimal degrees and were taken from database portals, scientific articles, and the research group unpublished new occurrence data.

Copyright notice: This dataset is made available under the Open Database License (<http://opendatacommons.org/licenses/odbl/1.0/>). The Open Database License (ODbL) is a license agreement intended to allow users to freely share, modify, and use this Dataset while maintaining this same freedom for others, provided that the original source and author(s) are credited.

Link: <https://doi.org/10.3897/zookeys.1231.133711.suppl1>



# Review of the millipede genus *Xystodesmus* (Diplopoda, Polydesmida), with seven new species from the southwestern part of Japan

Zoltán Korsós<sup>1,2,3</sup>, Yasuyuki Nakamura<sup>3,4</sup>

1 Department of Zoology, Hungarian Natural History Museum, Baross u. 13, H-1088 Budapest, Hungary

2 Department of Zoology, University of Veterinary Medicine Budapest, Rottenbiller u. 50, H-1077 Budapest, Hungary

3 Tropical Biosphere Research Center, University of the Ryukyus, Senbaru 1, Nishihara, Okinawa 903-0213, Japan

4 Fujukan, The Museum of the University of the Ryukyus, Senbaru 1, Nishihara, Okinawa 903-0129, Japan

Corresponding author: Zoltán Korsós ([zkorsos@gmail.com](mailto:zkorsos@gmail.com))

## Abstract

The genus *Xystodesmus* Cook, 1895 (most closely related to *Riukiaria* Attems, 1938) is retained as a taxon of xystodesmine millipedes with a relatively small body length (25–35 mm), male gonopods more complicated than just a forceps-like conformation, and with live colouration of grey-brown tergites with red, orange, or yellow paranotal spots. Seven new species of the genus (*Xystodesmus fasciatus* sp. nov., *X. keramae* sp. nov., *X. kumamotoensis* sp. nov., *X. kumeensis* sp. nov., *X. parvus* sp. nov., *X. rebekae* sp. nov., *X. sesokoensis* sp. nov.) are described from the islands of Kyushu, Okinawa-jima, Kume-jima, Okinoerabu-jima, Aka-jima, Amami-O-shima, and Sesoko-jima, southwestern Japan. *Koreoaria* Verhoeff, 1937, **syn. nov.** is synonymised with *Xystodesmus* Cook, 1895, so *X. pallidus* (Verhoeff, 1937), **comb. nov.** (ex *Koreoaria pallida*), and *X. amoenus* (Takakuwa, 1942), **comb. nov.** (ex *K. amoena*) are established. Furthermore, *X. variatus* (Pocock, 1895), **comb. nov.** (ex *Fontaria variata*), and *X. saltuosus* (Haga, 1968), **comb. nov.** (ex *Rhysodesmus saltuosus*) are re-evaluated and redescribed, based on re-examination of types and of freshly collected material (*X. variatus* only). All new species, as well as *X. martensii* (Peters, 1864), *X. nikkoensis* (Chamberlin & Wang, 1953), and *X. variatus* are illustrated with colour habitus photographs taken of live specimens, to facilitate field identification.

**Key words:** Island geography, millipede colouration, new combinations, new species, Ryukyu Archipelago, Xystodesmidae



Academic editor: Nesrine Akkari

Received: 10 November 2024

Accepted: 3 February 2025

Published: 12 March 2025

ZooBank: <https://zoobank.org/94B32AD5-4D03-4ECA-8B73-DB157E8AAF3E>

**Citation:** Korsós Z, Nakamura Y (2025) Review of the millipede genus *Xystodesmus* (Diplopoda, Polydesmida), with seven new species from the southwestern part of Japan. ZooKeys 1231: 191–232. <https://doi.org/10.3897/zookeys.1231.141443>

**Copyright:** © Zoltán Korsós & Yasuyuki Nakamura. This is an open access article distributed under terms of the Creative Commons Attribution License (Attribution 4.0 International – CC BY 4.0).

## Introduction

The millipede genus *Xystodesmus* Cook, 1895 belongs in the tribe Xystodesmini, subfamily Xystodesminae, family Xystodesmidae (Marek et al. 2014; Means et al. 2021b). As it was defined by Tanabe and Shinohara (1996) who had considered Harpaphini and Xystodesmini together, the tribe Xystodesmini – in addition to the four North American genera (*Harpaphe* Cook, 1904, *Isaphe* Cook, 1904, *Tabaphe* Causey, 1954, and *Thrinaphe* Shelley, 1993) – also consists of

four more Far Eastern genera: *Levizonus* Attems, 1898, *Koreoaria* Verhoeff, 1937, *Riukiaria* Attems, 1938, and *Yaetakaria* Hoffman, 1949. The *Xystodesmini* also includes species formerly included in the North American tribes Chonaphini and Orophini based on the molecular phylogenetics of Means et al. (2021b). Of the four Far Eastern genera, *Levizonus* was previously revised by Tanabe (1994), and restricted only to two species: *L. montanus* (Takakuwa, 1941) and *L. takakuwai* (Verhoeff, 1941). *Koreoaria* is herewith synonymised with *Xystodesmus*, based on the examination of its type species *K. pallida* Verhoeff, 1937. The genus *Yaetakaria* is likely best considered as a synonym of *Riukiaria* (Shinohara 1977; Means et al. 2021b).

Tanabe and Shinohara (1996), when revising *Xystodesmus*, concluded that its closest relative is *Riukiaria*, and attempted to identify the synapomorphic characters of the two genera. This evolutionary sister-group relationship of *Riukiaria* and *Xystodesmus* was supported by the analysis by Means et al. (2021b). Tanabe and Shinohara (1996) recognised six species in *Xystodesmus*: *X. martensii* (Peters, 1864), *X. shirozui* (Takakuwa, 1942), *X. gracilipes* (Takakuwa, 1943), *X. serrulatus* (Miyosi, 1952), *X. nikkoensis* (Chamberlin & Wang, 1953), and *X. tokaiensis* Tanabe & Shinohara, 1996. However, during their analysis of several other populations, and also considering literature data, at the end they listed a number of “uncategorised populations” and possible synonyms, hence hypothesising several undescribed species of the genus. Masuda (2001) described *Xystodesmus yamamiensis* Masuda, 2001 from Honshu, Chita Peninsula, Aichi Prefecture, Japan. The description is not fully detailed, but the gonopod sketches clearly show a valid species of the genus.

In this paper we provide descriptions of seven new *Xystodesmus* species, two from Kyushu (Kagoshima, Kumamoto, and Oita prefectures) and five from the Central Ryukyu Archipelago (Kagoshima and Okinawa prefectures). The latter records considerably extend the distribution range of the genus to the south. In addition, we also provide redescriptions of four old and poorly known species: *Fontaria variata* Pocock, 1895, *Koreoaria pallida* Verhoeff, 1937, *K. amoena* Takakuwa, 1942, and *Rhysodesmus saltuosus* Haga, 1968. With the re-examination of their types (except *K. amoena*, which is considered lost), and in the case of *F. variata* also with freshly collected material at hand, we assign them to *Xystodesmus*, thus increasing the known number of species in the genus to 18. The relationship between *Xystodesmus* and *Riukiaria* is also briefly reassessed.

## Materials and methods

Samples were collected by the authors on various occasions, in the framework of a comprehensive survey to investigate the millipede fauna of the Ryukyu Archipelago in the southwestern part of Japan. Denomination and writing style of the Japanese island names throughout the present paper follow Nakamura and Korsós (2010).

Type specimens of *Fontaria variata*, *Koreoaria pallida*, *Rhysodesmus saltuosus*, and *Xystodesmus yamamiensis* were borrowed from the Natural History Museum, London (**NHMUK**), the Bavarian State Collection of Zoology (Zoologische Staatssammlung), München (**ZSMC**), and the National Museum of Nature and Science, Tokyo (**NSMT**).

Specimens were observed and drawn by the first author (ZK) with a Leica M125 stereomicroscope at the University of the Ryukyus. Terminology of xystodesmid gonopods follows Tanabe and Shinohara (1996) and Shelley and Smith (2018), with additional advice by R. L. Hoffman, W. A. Shear, and R. M. Shelley (in litt.). Total length of specimens was measured with a string, and midbody width on the 10<sup>th</sup> segment under the microscope with an eyepiece reticule. Live photographs of specimens were taken in the field with a Nikon D90 digital camera, fitted with 60 mm Micro Nikkor lens and R1C1 macroflash system.

Type material of new species and other specimens are deposited in the Department of Zoology, Division of Terrestrial Invertebrates, National Museum of Nature and Science, Tokyo (**NSMT**), in Fujukan, the Museum of the University of the Ryukyus, Okinawa (**RUMF**), in the Myriapoda Collection of the Hungarian Natural History Museum, Budapest (**HNHM**), in the Natural History Museum of Denmark, Copenhagen (**NHMD**), and in the Virginia Museum of Natural History, Martinsville, USA (**VMNH**).

### Abbreviations (institute acronyms follow Sierwald and Reft 2004)

<b>NHMUK</b>	Natural History Museum, London, United Kingdom
<b>HNHM</b>	Myriapoda Collection of the Hungarian Natural History Museum, Budapest, Hungary
<b>NHMD</b>	(formerly ZMUC) – Natural History Museum of Denmark, Copenhagen, Denmark
<b>NCSM</b>	North Carolina State Museum of Natural Sciences, Raleigh, USA
<b>NSMT</b>	Department of Zoology, Division of Terrestrial Invertebrates, National Museum of Nature and Science, Tokyo, Japan
<b>RUMF</b>	Fujukan, the Museum of the University of the Ryukyus, Okinawa, Japan
<b>VMNH</b>	Virginia Museum of Natural History, Martinsville, USA
<b>ZSMC</b>	Bavaria State Collection of Zoology, München, Germany

### Taxonomy

**Family Xystodesmidae Cook, 1895**

**Subfamily Xystodesminae Hoffman, 1978**

**Tribe Xystodesmini Hoffman, 1980**

**Genus *Xystodesmus* Cook, 1895**

*Takakuwaia* Verhoeff, 1936 (with the type species *T. furculigera* Verhoeff, 1936): synonymised by Hoffman (1956)

*Cyphonaria* Verhoeff, 1936 (with the type species *C. scabra* Verhoeff, 1936): synonymised by Hoffman (1980)

*Phruodesmus* Takakuwa, 1943 (with the type species *P. gracilipes* Takakuwa, 1943): synonymised by Tanabe and Shinohara (1996)

*Nikkonus* Chamberlin & Wang, 1953 (with the type species *N. nikkoensis* Chamberlin & Wang, 1953): synonymised by Tanabe and Shinohara (1996)

*Koreoaria* Verhoeff, 1937, syn. nov.

**Type species by original designation.** *Polydesmus* (*Fontaria*) *martensii* Peters, 1864.

**Diagnosis.** The genus *Xystodesmus*, as a member of the tribe Xystodesmini, is characterised by the followings: small body size (less than 40 mm), posteriolateral corners of paranota usually acute, extending posteriorly beyond medial metatergal margin, presence of paranotal spots (red, orange, or yellow), and gonopods composed of coxa with prefemur and acropodite fused into a simple telopodite. In East Asia the tribe Xystodesmini is represented by five genera: *Koreoaria* Verhoeff, 1937 (herewith synonymised with *Xystodesmus*), *Levizonus* Attems, 1938, *Riukiaria* Attems, 1938, *Xystodesmus*, and *Yaetakaria* Hoffman, 1949. From these, based on gonopods, the most similar genus to *Xystodesmus* is *Riukiaria*, which share a common male gonopodal plan, usually with two well-developed processes (Tanabe and Shinohara 1996; Korsós et al. 2011). *Xystodesmus*, however, has various additional gonopodal appendages, while those of *Riukiaria* have none or only a few (its gonopod is more-or-less forceps-like). We also consider that colouration of live specimens is distinctive, with respect to their bright paranotal spots. All xystodesmids are strongly fluorescent when illuminated with ultraviolet light. Although traditional taxonomy is primarily based on gonopod morphology (Marek et al. 2014), the separation of the two genera is also supported by molecular phylogeny (Means et al. 2021b).

*Koreoaria* was introduced by Verhoeff (1937) with the South Korean species *K. pallida* (Verhoeff, 1937). He compared the new genus to *Pachydesmus* Cook, 1895, based on the superficially similar gonopod conformation (Verhoeff 1937). *Pachydesmus*, however, proved to be a strictly North American genus (Hoffman 1958) in its own tribe Pachydesmini (Hoffman 1980), and *Koreoaria* was considered belonging to the East Asian members of Xystodesmini (Tanabe and Shinohara 1996; Korsós et al. 2011). A second species, *Koreoaria amoena* (Takakuwa, 1942) was described, also from South Korea, and both species were proposed as “species possibly belonging to *Xystodesmus*” (Tanabe and Shinohara 1996: 1487). Observing the overall similarity of the type material of the type species of *Koreoaria*, here we take the opportunity to formalise the synonymy under *Xystodesmus*.

**Species and distribution of *Xystodesmus*** (in order of date of description):

*X. martensii* (Peters, 1864): Kanto and Chubu regions, Honshu, Japan (Peters 1864: 3 as *Polydesmus martensii*; Cook 1895: 5; Hoffman 1956: 97–99, figs 1–4; Tanabe and Shinohara 1996: 1480–1482, figs 2–9, 10A–E, 11A–E, 12A, B, 14, 17A–F)

*X. variatus* (Pocock, 1895), comb. nov.: Okinawa-jima Isl., Okinawa Pref., Japan (Pocock 1895: 361, figs 15, 15a as *Fontaria variata*)

*X. pallidus* (Verhoeff, 1937), comb. nov.: South Korea (Verhoeff, 1937: 319–320, fig. 8 as *Koreoaria pallida*)

*X. shirozui* (Takakuwa, 1942): Tsushima and Iki Isl., also Danjo Isl. (Oshima, Meshima), Nagasaki Pref., Japan (Takakuwa 1942a: 239, fig. 5 as *Rhysodesmus shirozui*; Takakuwa 1954: 63–64, fig. 65; Miyosi 1959: 80, fig. 55; Minato 1973: 127–128, fig. A; Tanabe and Shinohara 1996: 1485–1487, figs 11M, N, 13C, D, 16C, D, 17O, P)

*X. amoenus* (Takakuwa, 1942), comb. nov.: Daegu, South Korea (Takakuwa 1942b: 362–363, fig. 5 as *Koreoaria amoena*)

*X. gracilipes* (Takakuwa, 1943): Ehime Pref., Shikoku, Japan (Takakuwa 1943: 604–605, fig. 2 as *Phruodesmus gracilipes*; Takakuwa 1954: 84–85, figs 93,

94; Murakami 1965: 165, figs 1, 2; Tanabe and Shinohara 1996: 1484–1485, figs 11L, 13B, 16B, 17K)

*X. serrulatus* (Miyosi, 1952): Central part of Honshu and Shikoku (Tokushima Pref.), Japan (Miyosi 1952: 281, fig. 1 as *Rhysodesmus serrulatus*; Tanabe and Shinohara 1996: 1483–1484, figs 10G, 11H, I, 12D, 15D–I, 17I, J)

*X. nikkoensis* (Chamberlin & Wang, 1953): Yaku-shima Isl., Kagoshima Pref., Japan (the two type specimens from Honshu: Tochigi Pref., Nikko, are probably mislabeled) (Chamberlin and Wang 1953: 9, fig. 3 as *Nikkonus nikkoensis*; Tanabe and Shinohara 1996: 1484, figs 11J, K, 13A, 16A, 17L, M)

*X. saltuosus* (Haga, 1968), comb. nov.: Fukuoka Pref., Kyushu, Japan (Haga 1968 8, fig. 6a–e as *Rhysodesmus saltuosus*)

*X. tokaiensis* Tanabe & Shinohara, 1996: Shizuoka Pref., Honshu, Japan (Tanabe and Shinohara 1996: 1482–1483, figs 1, 10F, 11F, G, 12C, 15A–C, 17G, H)

*X. yamamiensis* Masuda, 2001: Aichi Pref., Honshu, Japan (Masuda 2001: 635–636, fig. 1A–H)

*X. fasciatus* sp. nov.: Satsuma Peninsula, Kagoshima Pref., Kyushu, Japan

*X. keramae* sp. nov.: Aka-jima Isl. (possibly also Tokashiki-jima Isl.), Okinawa Pref., Japan

*X. kumamotoensis* sp. nov.: Kumamoto and Oita Pref., Kyushu, Japan

*X. kumeensis* sp. nov.: Kume-jima Isl., Okinawa Pref., Japan

*X. parvus* sp. nov.: Okinoerabu-jima Isl., Kagoshima Pref., Japan

*X. rebekae* sp. nov.: Okinawa-jima Isl., Okinawa Pref., Japan

*X. sesokoensis* sp. nov.: Sesoko-jima Isl., Okinawa Pref., Japan

From the species list above, we did not have the opportunity to examine specimens of four species, *X. shirozui*, *X. gracilipes*, *X. serrulatus*, and *X. tokaiensis*, all occurring on the main islands of Japan (Honshu, Shikoku, and Kyushu) and adjacent islands, because of the loss of type material and/or the lack of fresh specimens. *Xystodesmus martensii* and *X. yamamiensis* are also distributed in Honshu, but since we had freshly collected material and the type specimens, respectively, we could compare them to the other species and include them in our descriptions. For the former Korean genus *Koreoaria*, type material of *K. pallida* was available for comparison and redescription, but unfortunately the types of *K. amoena* could not be found; the majority of Y. Takakuwa's material, kept after his death in 1960 by Y. Miyosi, is believed to have been lost after Miyosi's death in 1995 (Tanabe and Shinohara 1996; Chao and Chang 2008). All the other *Xystodesmus* species in our review, including the new ones, occur in the southwestern part of Japan (Kagoshima and Okinawa prefectures).

#### ***Xystodesmus fasciatus* sp. nov.**

<https://zoobank.org/DAAF356A-CB47-4987-A534-9E3CAA3285FD>

Figs 1A–F, 16A

**Type material. Holotype:** • male, Japan, Kyushu, Kagoshima Pref., Satsuma Peninsula, Hioki City, Fukiage Town, Yokura, *Cryptomeria japonica* plantation, 15 m a.s.l., 31°30'46.4"N, 130°22'31.1"E, 14 October 2009, leg. Z. Korsós and Y. Nakamura (NSMT-My 534). **Paratypes:** • 1 male, and 1 juv. male, same locality and date as holotype (HNHM diplo-04540). 2 males, same locality and data as holotype (RUMF-ZD-00952 and 00953).

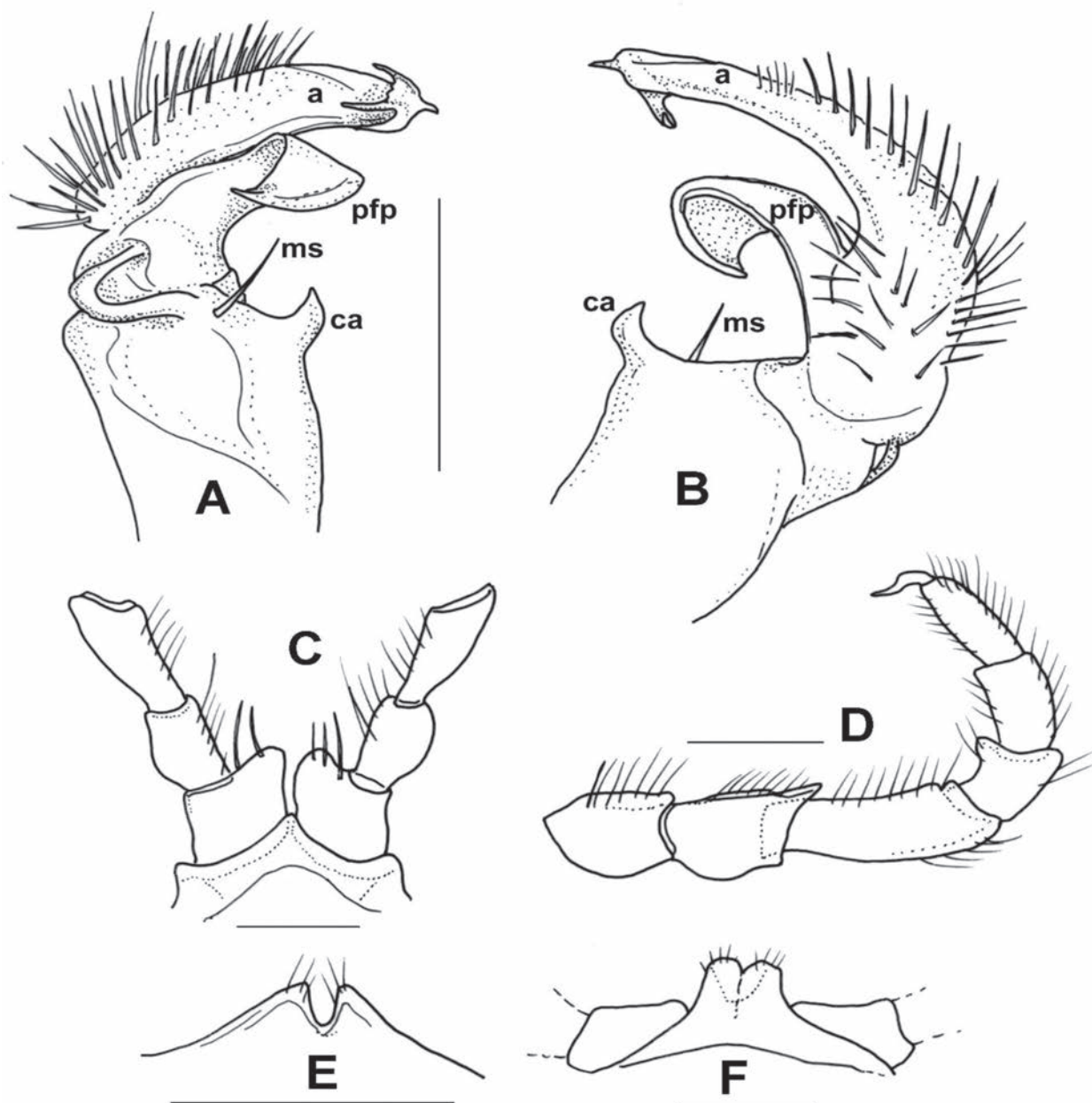


**Figure 1.** *Xystodesmus fasciatus* sp. nov., male paratype from Fukiage, Kagoshima Pref. **A, B** right gonopod, ventromesal and dorsolateral views, respectively **C** 2<sup>nd</sup> legpair, anterior view **D** left 6<sup>th</sup> leg, posterior view **E** sterna of 3<sup>rd</sup> segment, anterior view **F** sterna of 4<sup>th</sup> segment, anterior view. Abbreviations: a = acropodite, ca = coxal apophysis, ms = macroseta, pfp = prefemoral process. Scale bars: 1 mm.

**Diagnosis.** Medium-sized *Xystodesmus* species showing the general colour pattern plus a dark dorsal transversely banded appearance. Metatergites are smooth, shine, in contrast to that of *X. martensii* where they are conspicuously tuberculate. In terms of gonopods, the most similar species is *X. martensii* which also has a strong coxal apophysis, but in *X. fasciatus* sp. nov. it is almost hook-like; prefemoral process flat and wide, curving backwards, in *X. martensii* it is slender and straight. Acropodite with three small teeth at tip, whereas in *X. martensii* it has a cup-shaped process. *X. yamamiensis* has also a strong coxal apophysis, but its acropodite is strongly bifurcated and its prefemoral process is slender and tapering.

**Description** (based on the two adult male specimens). Length 32–33 mm, midbody width with paranota 5.8 mm, metatergal length 1.9 mm, collum width 4.9 mm, median collum length 3.1 mm. Body sides between segments 5–13 parallel. Head smooth, with 1+1 frontal setae, epicranial suture distinct. Antennae straight, slender, first article globose, articles 2–4 subequal in length, 5 and 6 increasingly longer, 7 small, with length equal to width. Proterga completely smooth, metaterga very weakly wrinkled, each with a transverse depression in the middle. No trace of tubercles or punctation on metaterga. Collum subtrapezoid-shape, convex, its length double of metatergum 2, lateral edges directed ventrad, anteriolateral margin with weak ridge. Posteriolateral edge of paranota 2 and 3 rounded, of 4 slightly pointed, from 5 onwards triangular shaped, with strong half-circle excavation on the posterior edge of each metaterga. Pore formula normal, pores on segments 5, 7, 9, 10, 12, 13, 15, 16, 17, and 18, in lateral position on slightly swollen paranota.

Segments 14–19 gradually tapering, posteriolateral projections becoming more pointed, with strong excavations along their mesal side. Epiproct protruding, in lateral view distinctly curved, with two pairs of setae on small side tubercles, and with two setae apically; paraprocts (anal valves) smooth, with a pair of setae on obvious median ridges; hypoproct semicircular.

Bases of midbody leg pairs well separated (by 1.6 mm), sterna smooth and wide, pro- and metasterna well separated. Prefemur with well-developed ventral spine, increasingly larger from midbody legs onwards, femur ~ 2× as long as prefemur, almost straight, postfemur short and incrassate, tibia slender, long, nearly as long as tarsus, claw on pregonopodal legs flattened and curved, leaf-like, becoming normal on other legs towards the end of body.

Colour of living specimens on dorsal side vividly banded as a result of alternating pale greyish prozona and dark chocolate-brown metazona (Fig. 16A). Collum pale greyish in the middle and bordered with dark brown. Dark brown median stripe on dorsum from 4<sup>th</sup> segments onward. Paranota bright reddish orange. Clypeus light brownish, underside of head, antennae, legs, epiproct, and whole ventral side pale, almost whitish. Colour in alcohol quickly bleaches, only the dorsal dark banded pattern remains visible.

**Male sexual characters.** Sterna of segments 3 and 4 (Fig. 1E, F) with a pair of protruding processes, on segment 3 small, widely separated from each other, with long apical setae; on segment 4 nearly as high as width of coxae, closely packed to each other, with short setae. Second leg pair with low but definite, blunt coxal processes (Fig. 1C). Other legs and sterna without extra modifications. Gonopods (Fig. 1A, B): Basically composed of two conspicuous processes, one considered as prefemoral process (*pfp*), and one as acropodite (*a*). Coxa strong, stout, nearly as long as wide, with well-developed, hook-like apophysis (*ca*) on its anteriomesal shoulder, and a large single apophyseal seta (*ms*). Prefemur stout, bent dorsad, densely setose, prefemoral process broad and flat, like a lamella, abruptly tapering to its tip which is pointed and curved backwards, in the direction of the coxal apophysis. Acropodite setose up to 2/3 of its length, gradually tapering towards its tip which is bent mesad, and terminates in two pointed branches connected to each other by a transparent, thin plate. At approximately the separation point of the two tips on the lateral side a small, there is a pointed process like a spur. Prostatic groove runs along the dorsomesal edge of the acropodite.

Female unknown.

**Remarks.** The specimens were found in planted and managed *Cryptomeria japonica* forest, in the deeper layers of mulch, in association with another xystodesmine millipede, *Riukiaria cornuta* (Haga, 1968).

**Etymology.** To emphasise the transversely banded appearance (= *fasciatus*, in Latin). Adjective, masculine.

***Xystodesmus keramae* sp. nov.**

<https://zoobank.org/029BA6FC-846B-4834-B32C-7D0F47AEB664>

Figs 2A–D, 16B

**Type material. Holotype:** • male, Japan, Central Ryukyus, Okinawa Pref., Okinawa Group, Aka-jima Isl., Mt. Ootake, shrine, 120 m a.s.l., mixed forest, 26°12'08.6"N, 127°16'32.5"E, 24 September 2010, leg. Z. Korsós (NSMT-My 535). **Paratypes:** •1 male, 2 females (NSMT-My 536), 1 male, 2 females (RUMF-ZD-00945), 1 male, 1 female (HNHM diplo-04541) same locality and date.

**Diagnosis.** *Xystodesmus keramae* sp. nov. is a medium-sized *Xystodesmus* with typical colour pattern similar to *X. parvus* sp. nov. but differs from it by the well-developed coxal apophysis and the long, backwardly curved prefemoral process. It is also different from *X. serrulatus* where acropodite and prefemoral process are subequal in length, entirely straight, and very slender.

**Description.** Length 26–32 mm, midbody width with paraterga 5.5–6.5 mm, midbody metatergal length 1.2–1.6 mm, collum width 4.4–4.8 mm, median collum length 1.9–2.4 mm. Body sides between segments 7–15 subparallel.

Head smooth, with 1+1 frontal setae, epicranial suture distinct. First antennal article sub-globose, 2<sup>nd</sup> slightly clavate, otherwise subequal in length to straight articles 3–6, article 7 small, as long as wide, slightly tapering to its tip.

Pro- and metaterga completely smooth, transverse depression in metaterga clearly noticeable. Collum smooth, in dorsal view almost semicircular, posterior edge straight, slightly wavy, no marginal ridges, lateral corners triangular, directed posterior. Anterio-lateral edges of all paranota rounded, postero-lateral corners of segment 2–4 in obtuse angle, posterior margins laterally bent forward. Small triangular projection starts from metaterga 5, only weakly increasing from segment 6 onwards, sublateral excavations lacking or only very shallow. Lateral sides of paranota slightly arched, outline of segments clearly delimited. Pore formula normal, pores in lateral central position on narrow paranota.

Segments 16–19 gradually tapering, caudal corners becoming strong and blunt. Epiproct in dorsal view triangular, in lateral view slightly curved downward, with four large setae on each lateral side on tubercles, projection with 2+2 setae apically; paraprocts slightly wrinkled, with two pairs of setae, upper ones on strong margin, lower ones on sides; hypoproct semicircular with two setae on tubercles.

Bases of midbody leg pairs clearly separated (by 1.2–1.6 mm in males, 1.5–1.7 mm in females), sterna smooth and wide, pro- and metasterna also clearly separated. Coxa short, as long as wide; prefemur ~ 1.8× longer than coxa, on male postgonopodal legs and on all female legs with well-developed ventral spine; femur strongly incrassate, only ~ 1.5× longer than prefemur; post-femur short, sub-globose, tibia and tarsus subequal in length, ~ 2× as long as wide; claw normal on all legs.

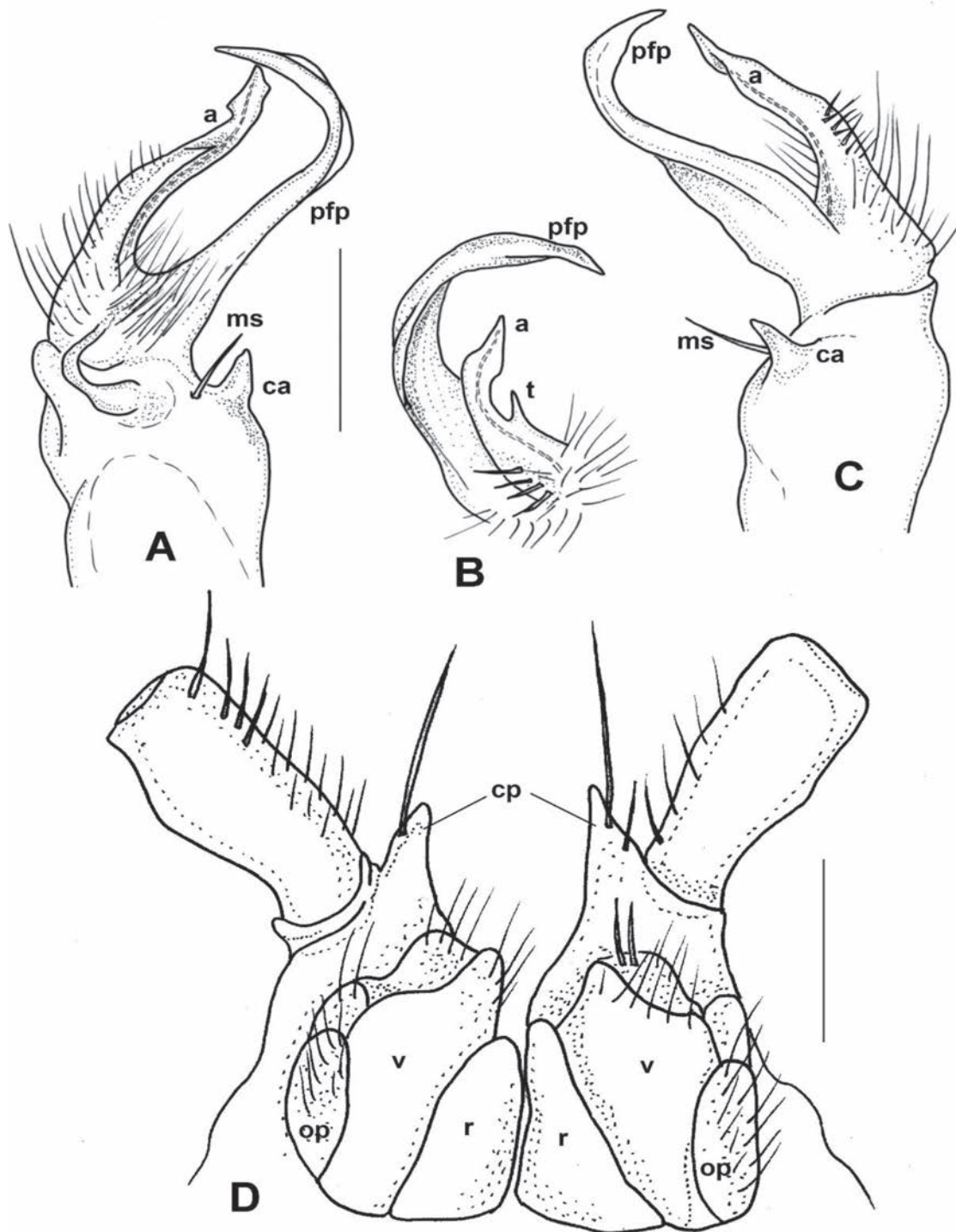


**Figure 2.** *Xystodesmus keramae* sp. nov., Aka-jima Island, Okinawa Pref. **A–C** right gonopod of male paratype, mesal, lateral, and ventral (**B**, telopodite only) views, respectively **D** cyphopods with 2<sup>nd</sup> leg pair of female paratype, posterior view. Abbreviations: a = acropodite, ca = coxal apophysis, cp = coxal projections, ms = macroseta, op = operculum, pfp = prefemoral process, r = receptacle, t = tooth, v = valve. Scale bars: 0.5 mm.

Colour of living specimens (Fig. 16B) pale brown, collum with dark margins, segments 2–4 with dark brown posterior margin, from 5 onwards medial part of metaterga with dark brown posterior margin; epiproct lighter. Head pale brown, antennae, legs, all paranota, and whole ventral side pale brown. Paranotal spots faded, hardly visible.

**Male sexual characters.** Second leg pair with strong, tubular coxal processes (as of *X. kumamotoensis* sp. nov., Fig. 3D) provided with numerous apical setae, sterna, and coxae of segments 4–6 and further legs without any modifications. Gonopods (Fig. 2A–C): Coxa stout, ~ 1.2× longer than wide, with strong but slender coxal apophysis, and a single macroseta (*ms*) next to it. Prefemur short, thick, densely setose on ventral side; prefemoral process (*pf*) strong, longer than and parallel to acropodite, but its pointed tip bent ventrad and almost touching tip of acropodite; acropodite (*a*) short, more slender than prefemoral process, gradually tapering towards the somewhat broader, leaf-like tip, and with a small triangular tooth (*t*) on half way of its mesal side (Fig. 2B). Prostatic groove runs along the dorsomesal edge of acropodite.

**Female characters** (Fig. 2D). 2<sup>nd</sup> leg pair with pointed coxal projections (*cp*); cyphopods behind closely packed in small aperture, very close to each other. Receptacula (*r*) on postero-mesal side small, triangular, hardly setose; operculum (*op*) elongated with 3 several small setae; bursal valves (*v*) large, setose, with high mesal apices.

**Remarks.** The type locality, Aka-jima Island is a member of the Kerama Islands, ~ 25 km west from the southern part of Okinawa-jima Island. Another member of the Kerama Islands is Tokashiki-jima Island, where a number of female *Xystodesmus* specimens were also found (see unidentified female at the end of the paper), probably the same as *X. keramae* sp. nov.

**Etymology.** Named after the type locality which belongs in the Kerama Islands (a subgroup of the Okinawa Group), west of Okinawa-jima Isl., Okinawa Pref., Japan. Genitive, from *kerama*.

***Xystodesmus kumamotoensis* sp. nov.**

<https://zoobank.org/5003BCBE-F05C-4FB2-BE92-F1FB906D1DD7>

Figs 3A–D, 4A–C

**Type material. Holotype:** • male, Japan, Kyushu, Kumamoto Pref., Yatsushiro City, Toyo Town, Kawamata, Kaerizaka, along prefectural road No. 25, 32°30'31.4"N, 130°45'42.5"E, 230 m a.s.l., 17 November 2008, leg. M. Nakano (NSMT-My 537).

**Paratypes:** • 1 male, 2 females, same locality and date (NSMT-My 538); • 1 male, Japan, Kyushu, Kumamoto Pref., Yatsushiro City, Toyo Town, Kawamata, Tsurukoba, along prefectural road No. 25, 32°28'45.9"N, 130°45'11.2"E, *Cryptomeria japonica* forest, 700 m a.s.l., 18 September 2009, leg. T. Iihoshi (RUMF-ZD-00940); • 2 males, Japan, Kyushu, Oita Pref., Hita City, Kamitsue Town, Kawahara, 33°06'58.8"N, 130°57'50.9"E, along National Road No. 387, *Cryptomeria japonica* forest, 14 November 2008, leg. T. Menda (HNHM diplo-04542, NHMD 1184732).

**Diagnosis.** Relatively small *Xystodesmus* with colour pattern faded from preservation in ethanol but still typical for the genus. (Unfortunately, this is the only species of which we did not have live colour photo.) Gonopod completely lacks coxal apophysis as in the most similar species *X. shirozui* (Takakuwa, 1942), but differs from it by the widely bifurcated acropodite and the laminate, tongue-like prefemoral process.

**Description.** Length 26–27 mm, midbody width with paraterga 4.8–5.0 mm, midbody metatergal length 1.2–1.3 mm, collum width 3.8–3.9 mm, median collum length 1.9 mm. Body sides between segments 5–16 subparallel.

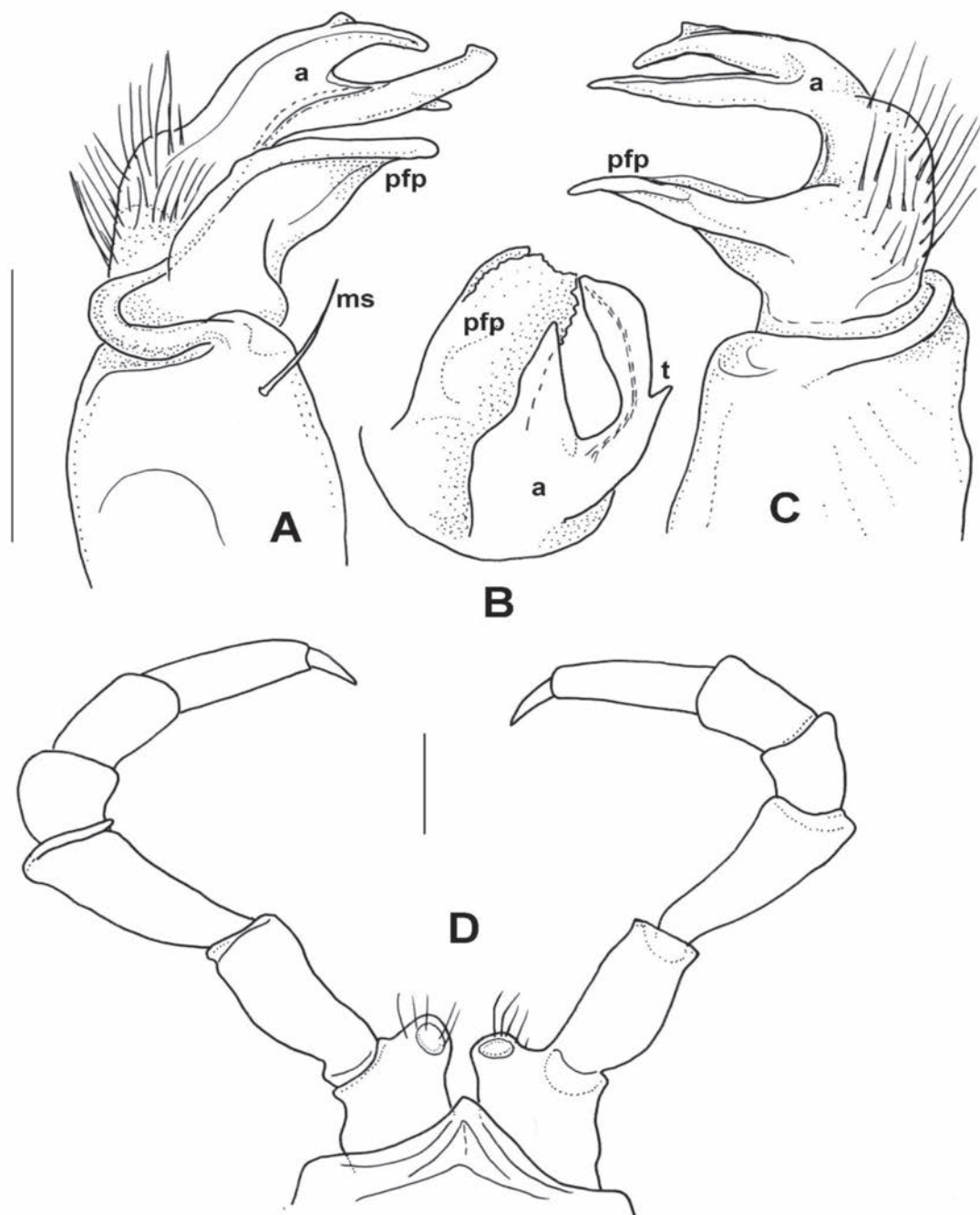


**Figure 3.** *Xystodesmus kumamotoensis* sp. nov., male paratype from Yatsushiro, Kumamoto Pref. **A–C** right gonopod, mesal, lateral, and acropodite (**B**) in ventral views, respectively. **D** 2<sup>nd</sup> leg pair, posterior view. Abbreviations: a = acropodite, ms = macroseta, pfp = prefemoral process, t = tooth. Scale bars: 0.5 mm (**B**), 1 mm (**D**).

Head smooth, with two frontal setae, epicranial suture distinct. Antennal articles straight, slender, first article short, 1.5× longer than wide, articles 2–6 subequal in length, 7 small, with length equal to width.

Proterga completely smooth, metaterga weakly wrinkled, each with a shallow transverse depression in the middle. Collum subtrapezoid-shape, arched, 1.5× longer than metatergum 2, lateral edges directed posteroventrad, anteriolateral

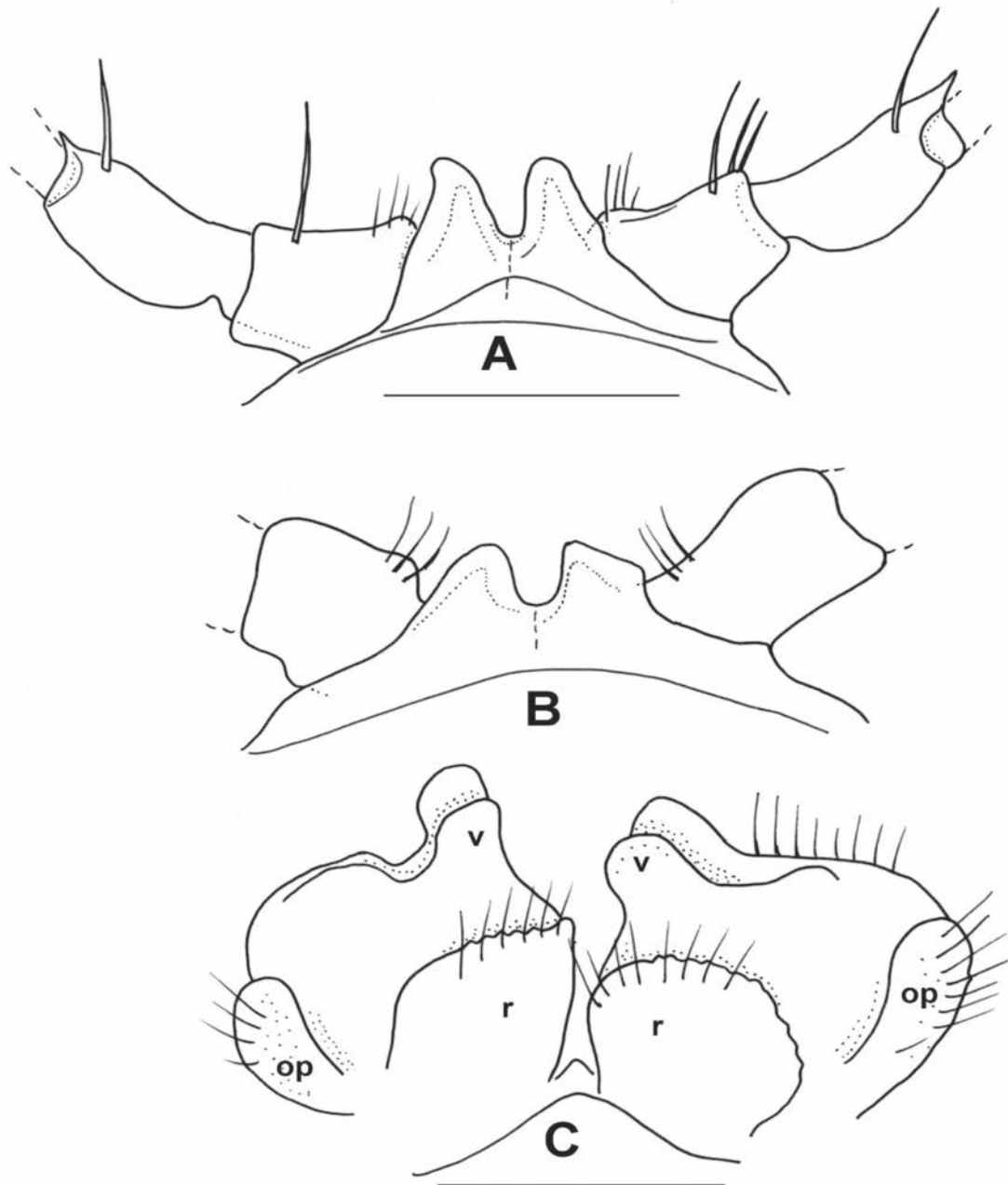


**Figure 4.** *Xystodesmus kumamotoensis* sp. nov. **A, B** male paratype from Yatsushiro, Kumamoto Pref. **A** sterna of 4<sup>th</sup> segment, anterior view **B** sterna of 5<sup>th</sup> segment, anterior view **C** cyphopods of female paratype from Yatsushiro, Kumamoto Pref., posterior view. Abbreviations: op = operculum, r = receptacle, v = valve. Scale bars: 1 mm (**A, B**); 0.5 mm (**C**).

margin with well visible ridge. Posterior edge of paranota 2–5 rounded, triangular projection only starts from segment 6 onwards, posterior margin of each metaterga straight, sublateral excavations hardly detectable. Lateral sides of paranota straight, almost giving a parallel straight outline to the body. Pore formula normal, pores in lateral position on narrow paranota.

Segments 17–19 gradually tapering, posteriolateral corners becoming more pointed. Epiproct protruding, in lateral view slightly curved, with two pairs of setae on small side tubercles, and with two setae apically; paraprocts smooth, with two pair of setae on obvious median ridges; hypoproct subtriangular.

Bases of midbody leg pairs clearly separated (by 1.1 mm), sterna smooth and wide, pro- and metasterna also clearly separated. Postgonopodal prefemora with well-developed ventral spine, increasingly larger from midbody legs onwards, femur 1.5× longer than prefemur, slightly bent proximad, postfemur short and curved, tibia slender, tarsus 1.5× longer than tibia, claws normal on all legs.

Colour of living specimens unknown. Preserved specimens show faded pattern typical for *Xystodesmus*: metaterga slightly darker, proterga paler, paranota with pale orangish/ yellowish spot. Clypeus light brownish, underside of head, antennae, legs, epiproct, and whole ventral side light pale white.

**Male sexual characters.** Second leg pair with tubulous coxal processes (Fig. 3D), densely setose. Sterna of segments 4 and 5 (Fig. 4A, B) with a pair of protruding processes, on segment 4 longer, pointed, without setae, on segment 5 lower, widely separated from each other, without setae. Other legs and sterna without modifications. Gonopods (Fig. 3A–C): Coxa short and thick, almost as wide as long, no trace of apophyseal process, only a strong single seta (*ms*) on the anteriomesal side. Prefemur stout, nearly straight, densely setose, prefemoral process (*pfp*) broad and flat, lamellate, ~ 2× as long as wide, subrectangular from ventral view, distal margin slightly serrated (Fig. 3B). Acropodite (*a*) delimited from prefemur by a weak constriction, its length only a little longer than prefemoral process, and soon divided into two branches subequal in length, directed anteriorly and gradually tapering to their pointed tips. Prostatic groove runs to the tip of the branch situated laterad, which is also provided with a small tooth (Fig. 3B, *t*) on its lateral side, best visible in situ from direct ventral view.

**Female sexual characters.** Cyphopods (Fig. 4C) situated in deep, joint excavation behind leg pair 2, loosely encapsulated in vulval sacs, well separated from each other. Receptacles (*r*) both on anterior and posterior side, densely setose; operculum (*op*) situated laterally, small, rounded, with numerous short setae; valves (*v*) hairless, mesally with conspicuous pointed apices, closely parallel to each other.

**Remarks.** In the type locality and Toyo Town, 700 m a.s.l., *Riukiaria semicircularis semicircularis* (Takakuwa, 1941) and *R. cornuta* (Haga, 1968) were also found. In Hita City, *R. semicircularis semicircularis* and *Parafontaria tonominea* (Attems, 1899) were also found together with the new species.

**Etymology.** Named after the locality, Kumamoto Pref., Kyushu, Japan. Adjective, masculine.

***Xystodesmus kumeensis* sp. nov.**

<https://zoobank.org/2E374500-FA16-4E0D-85A8-56694CE56BEC>

Figs 5A–F, 16C

**Type material. Holotype:** • male, Japan, Central Ryukyus, Okinawa Pref., Okinawa Group, Kume-jima Isl., Kanegusuku–Self Defense Force base, 2.2 km from pref. road, 90 m a.s.l., 23 February 1992, leg. T. Tanabe (NSMT-My 539). **Paratypes:** • 4 females (NSMT-My 540) same locality and date; • 1 male, 1 female, Japan, Central Ryukyus, Okinawa Pref., Okinawa Group, Kume-jima Isl., Uegusuku shrine, 26°22'35"N, 126°46'20"E, 235 m a.s.l., from roots of *Ficus* tree, 7 November 2011, leg. A. and Z. Korsós (RUMF-ZD-00946 [male] and -00947 [female]); • 2 males, Japan, Central Ryukyus, Okinawa Pref., Okinawa Group, Kume-jima

Isl., Daruma-yama forest road, 26°22'07"N, 126°45'50"E, 204 m a.s.l., 9 November 2011, leg. A. and Z. Korsós (HNHM diplo-04543).

**Other non-type material.** 18 juveniles, same locality and date as holotype (NSMT-My 541).

**Diagnosis.** Medium-sized *Xystodesmus*, male with essentially simple, two-branched gonopod, and a small, isolated coxal apophysis. Most similar to *X. rebekae* sp. nov., *X. gracilipes*, and *X. nikkoensis*, but differs from them by the presence of a coxal apophysis and by the configuration of the prefemoral and tibiotarsal processes. Prefemoral process is strongly twisted, longer than acropodite, at approximately midpoint with a small tooth, whereas in all the three others it is straight, slender, and subequal to acropodite, without tooth. In *X. nikkoensis*, acropodite has ventrally a small triangular process which is missing in *X. kumeensis* sp. nov.

**Description.** Length 30–32 mm, midbody width with paraterga 5.5–6.2 mm, midbody metatergal length 1.4–1.8 mm, collum width 4.2–4.9 mm, median collum length 1.9–2.4 mm. Body sides between segments 5–14 subparallel.

Head smooth, epicranial suture distinct. Antennal articles slightly clavate, first article sub-globose, articles 2–6 subequal in length, 2 and 3 are most clavate, 4–6 almost straight, article 7 small, as long as wide, slightly tapering to its tip.

Pro- and metaterga completely smooth, transverse depression in metaterga hardly noticeable. Collum in dorsal view almost oval, edges rounded, with only very weak ridges, lateral corners directed ventrad, length along median line ~ 2× as long as metatergum 2. Anterior edge of paranota 2–4 rounded, posterior edge rounded, lacking projection. Posteriolateral triangular projection starts on metaterga 5, from 6 onwards increasingly pointed, sublateral excavations on caudal margin of midbody segments strong, semicircular. Lateral sides of paranota arched, outline of segments clearly delimited. Pore formula normal, pores in lateral central position on narrow paranota.

Segments 15–19 gradually tapering, caudal corners becoming more pointed. Epiproct protruding, in lateral view slightly curved, thick, with 2+2 large setae on each lateral side on tubercles, projection with 2+2 setae apically (i.e., 6 pairs of setae altogether); paraprocts smooth, with two pair of setae on strong median ridges; hypoproct semicircular with two setae on small tubercles.

Bases of midbody leg pairs well separated (by 1.2 mm in male, 1.6–1.8 mm in females), sterna smooth and wide, pro- and metasterna well separated. Coxa short, just a little bit longer than wide; prefemur ~ 1.2× longer, on postgonopodal legs with well-developed ventral spine; femur 2× as long as coxa, incrassate; postfemur short again like coxa, tibia, and tarsus subequal in length, both ~ ½ as long as femur; claws normal on all legs.

Colour of living specimens pale brown, almost yellowish, paranotal spots hardly visible (Fig. 16C). Preserved specimens show faded pattern typical for *Xystodesmus*: metaterga slightly darker, proterga paler, clypeus light brownish, underside of head, antennae, legs, epiproct, and whole ventral side yellowish white.

**Male sexual characters.** Second leg pair with tubulose coxal processes, sterna of segments 4–6 and further legs without any modifications. Gonopods (Fig. 5A–C): Coxa stout, ~ 1.5× longer than wide, coxal apophysis (*ca*) present in form of a small bump emerging from a circular field, next to a short, thick apophyseal macroseta (*ms*). Prefemur stout, subparallel-sided, densely setose only on ventral side; prefemoral process (*pfp*) slender, longer than acropodite,

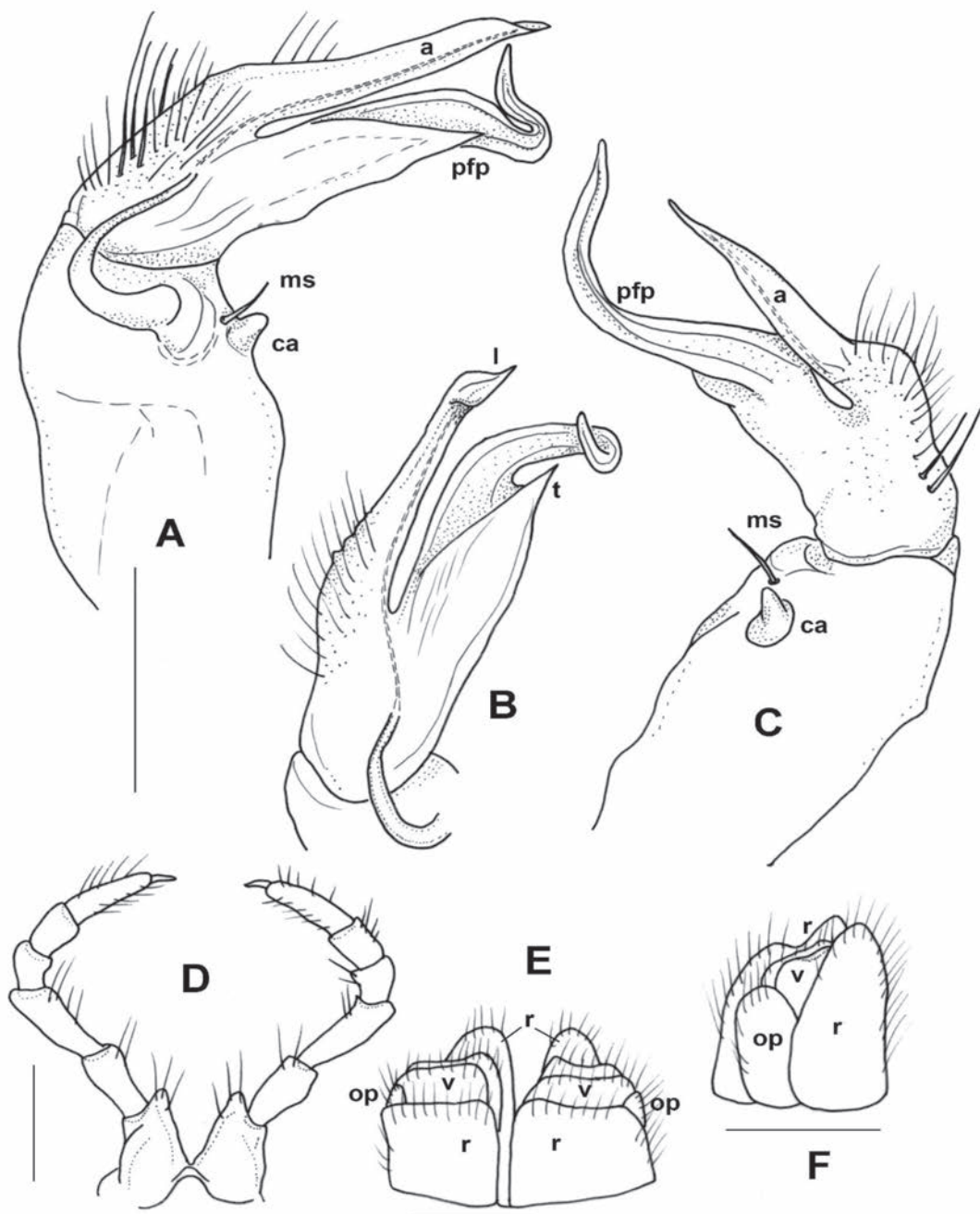


**Figure 5.** *Xystodesmus kumeensis* sp. nov., paratypes from Kume-jima Island, Okinawa Pref. **A–C** right gonopod of male paratype, mesal, lateral, and ventromesal (**B**, telopodite only) views, respectively **D** 2<sup>nd</sup> legpair of female paratype, anterior view **E** cyphopods, posterior view **F** left cyphopod, anteriolateral view. Abbreviations: a = acropodite, ca = coxal apophysis, l = lamella, ms = macroseta, op = operculum, pfp = prefemoral process, r = receptacle, t = tooth, v = valve. Scale bars: 0.5 mm (**A–C**, **F**); 1 mm (**D**); 0.4 mm (**E**).

strongly curved into a sharp, pointed tip, at approximately midpoint with a widely based, triangular side tooth (Fig. 5B, t); acropodite (a) slim, more slender than prefemoral process, only ~ 2/3 of its length, almost straight, gradually tapering towards tip, slightly broadening before pointed tip into a leaf-like lamella (Fig. 5B, l). Prostatic groove runs straight on the mesal side of acropodite.

**Female sexual characters.** Coxae of 2<sup>nd</sup> leg pair with a pair of small, pointed, setose projections (Fig. 5D). Cyphopods (Fig. 5E, F) situated in deep, joint

aperture behind leg pair 2, loosely encapsulated in vulval sacs, well separated from each other. Receptacula (*r*) both on anterior and posterior side, densely setose; anterior receptaculum low, broad, posterior one high, slender, higher than bursal valves; operculum (*op*) small, rounded, situated laterad, in anterior view hardly visible; bursal valves (*v*) equal shaped, broad, rectangular, with short setae, without pointed apices.

**Remarks.** The species was treated as an uncategorised population under *Xystodesmus* in Tanabe and Shinohara (1996: Cluster I, figs 7, 11Q, 16H, 17R). The individuals were found on Kume-jima Island in mixed *Pinus luchuensis* and broad-leaved evergreen forest.

**Etymology.** Named after the collecting locality, Kume-jima Island, west of Okinawa-jima Isl., where the species is probably endemic to. Adjective, masculine.

***Xystodesmus parvus* sp. nov.**

<https://zoobank.org/3BE0CB3D-3C8A-41B4-9C7F-871361BF3C2B>

Figs 6A–E, 16D

**Type material. Holotype:** • male, Japan, Central Ryukyus, Kagoshima Pref., Amami Group, Okinoerabu-jima Isl., Oyama botanical garden, 27°21'56.4"N, 128°34'00.0"E, 240 m a.s.l., 13 June 2010, leg. Z. Korsós and Y. Nakamura (NS-MT-My 542). **Paratypes:** • 4 females (NSMT-My 543), 1 male (RUMF-ZD-00941), 3 females (RUMF-ZD-00942), same locality and date as holotype.

**Diagnosis.** Differs from its congeners by the small body size (length under 23 mm), and by the male gonopods lacking coxal apophysis and having two simple branches (prefemoral process and acropodite) subequal in length and bent parallel together. The closest species is the similarly small *X. sesokoensis* sp. nov., but its prefemoral process has two small branches at tip, and its acropodite is longer, the end is thicker with a small tooth.

**Description.** Length 19–22 mm, midbody width with paraterga 4.1–4.2 mm, midbody metatergal length 0.9–1.1 mm, collum width 3.1–3.2 mm, median collum length 1.3–1.4 mm. Body sides between segments 5–15 subparallel.

Head smooth, with two frontal setae, epicranial suture distinct. Antennal articles slightly clavate, first article sub-globose, articles 2–6 subequal in length, article 7 small, as long as wide.

Collum in dorsal view oval, edges rounded, with well-developed anterior ridge, laterally even stronger like paranotum, corners rounded. Pro- and metaterga completely smooth, transverse depression in metaterga short but noticeable. Anterio-lateral edge of paranota rounded, postero-lateral corner of segments 2 and 3 rounded, lacking projection; on 4 with small projection, from 5 increasingly pointed, triangular, sublateral excavations on posterior margin becoming stronger. Lateral sides of paranota straight, outline of segments clearly delimited. Pore formula normal, pores in lateral central position on narrow paranota.

Segments 16–19 gradually tapering, posterior corners becoming obtuse, sublateral excavations disappearing. Epiproct in dorsal view triangular, in lateral view slightly curved ventrad, with 4+4 large setae on tubercles on lateral sides, projection with 2+2 apical setae; paraprocts smooth, with two pairs of setae, upper ones on margin, lower ones on side; hypoproct semicircular with two setae on small tubercles.

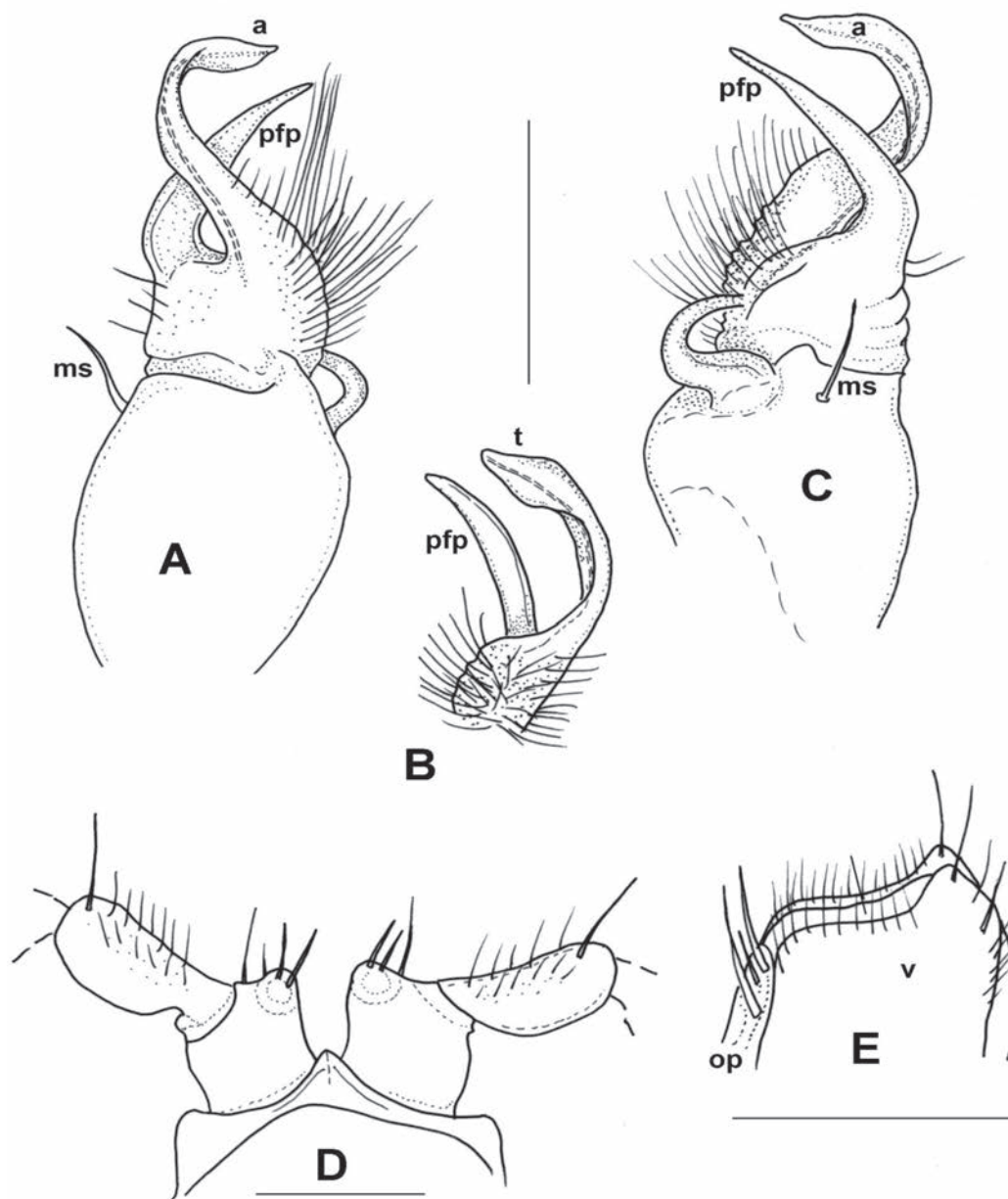


**Figure 6.** *Xystodesmus parvus* sp. nov., paratypes from Okinoerabu-jima Island, Kagoshima Pref. **A–C** right gonopod of male paratype, lateral, mesal, and ventral (**B**, telopodite only) views, respectively **D** 2<sup>nd</sup> leg pair (from femur omitted) of male paratype, anterior view **E** left cyphopod of female paratype (receptaculum omitted), anterior view. Abbreviations: a = acropodite, ms = macroseta, op = operculum, pfp = prefemoral process, t = tip of acropodite, v = valve. Scale bars: 0.5 mm.

Bases of midbody leg pairs well separated (by 1.2 mm in male, 1.6–1.8 mm in females), sterna smooth and wide, pro- and metasterna fused. Coxa short, rectangular; prefemur ~ 2× as long as wide, with well-developed ventral spine; femur 1.5× longer than prefemur, incassate; postfemur small, sub-globose, tibia slender, approximately same length as postfemur, tarsus 2× as long as tibia, slender, tapering towards small, curved claw.

Colour of living specimens (Fig. 16D) pale brown, collum, segments 2, 18, 19, and epiproct darker, all metaterga with dark posterior margin. Underside of head, antennae, legs, and whole ventral side pale white. Sides of collum and all paranota (except segment 19) with faint, pinkish-orange spots.

**Male sexual characters.** Second leg pair with small coxal processes provided with three or four strong setae (Fig. 6D), sterna of segments 4–6 and further legs without any modifications. Gonopods (Fig. 6A–C): Coxa stout, ~ 1.2× longer than wide, coxal apophysis completely lacking, apophyseal macroseta (*ms*) relatively small. Prefemur short, stout, parallel-sided, densely setose on ventral side, with a few setae on dorsal side; prefemoral process (*pfp*) slender, shorter than acropodite, bent ventrad and ending in a long, pointed tip; acropodite (*a*) slightly broader and longer, bending subparallel to prefemoral process, gradually tapering towards somewhat broader, leaf-like tip (*t*) (Fig. 6B). Prostatic groove runs along mesal side of acropodite.

**Female sexual characters.** Cyphopods (Fig. 6E) situated in deep, joint aperture behind leg pair 2, loosely encapsulated in vulval sacs, well separated from each other. Receptacula (not shown in figure) on both anterior and posterior side, setose only along margins, with pointed mesal tips; operculum (*op*) elongated with three strong setae; bursal valves (*v*) hidden between high receptacula, with short setae only.

**Remarks.** The new species was found in a protected botanical garden on the top of the central hill on the 93 km<sup>2</sup> Okinoerabu-jima Island. The vegetation cover is subtropical broad-leaved evergreen forest, and the specimens were collected in the deep, humid, top-soil litter layer. No sympatric species of millipede were found.

**Etymology.** Named after its small size (*parvus*, in Latin). Adjective, masculine.

***Xystodesmus rebekae* sp. nov.**

<https://zoobank.org/204CFBCA-2A67-4E13-A922-AE529E4A1E71>

Figs 7A–D, 16E

**Type material. Holotype:** • male, Japan, Central Ryukyus, Okinawa Pref., Okinawa Group, Okinawa-jima Isl., Motobu Peninsula, Mt. Yae-dake, 26°38'17.5"N, 127°55'37.9"E, 390 m a.s.l., 30 December 2009, leg. R. Korsós, Z. Korsós and Y. Nakamura (NSMT-My 544). **Paratypes:** • 6 males and 2 females, same locality and date (1 male, 1 female NSMT-My 545; 1 male, 1 female RUMF-ZD-00943, RUMF-ZD-00944; • 1 male HNHM diplo-04544; • 1 male VMNH112447, 1 male NHMD 1184733); • 1 juv. male, same locality, 8 November 2010, leg. Z. Korsós and Y. Nakamura (No. 285) (HNHM diplo-04545).

**Diagnosis.** Medium to relatively large *Xystodesmus* with typical colour pattern, dark brown terga and bright orange paranotal spots. With its simple, two-branched male gonopod completely lacking coxal apophysis and sternal modifications on pregonopodal legs *X. rebekae* sp. nov. differs from all its congeners. Most similar species are *X. variatus* and *X. gracilipes* which also have only two gonopodal processes, but *X. rebekae* sp. nov. has a longer, S-shaped femoral process and a shorter, slimmer acropodite.

**Description.** Length 29–33 mm, midbody width with paraterga 6.6–7.3 mm, midbody metatergal length 1.5–1.8 mm, collum width 5.3–5.8 mm, median collum length 2.5–2.7 mm. Body sides between segments 5–14 subparallel.

Head smooth, with two frontal setae, epicranial suture distinct. Antennal articles more-or-less straight, slender, first article sub-globose, articles 2 and 3 subequal in length, 4–6 also subequal but slightly longer than 2 and 3, 7 small, little wider than long.

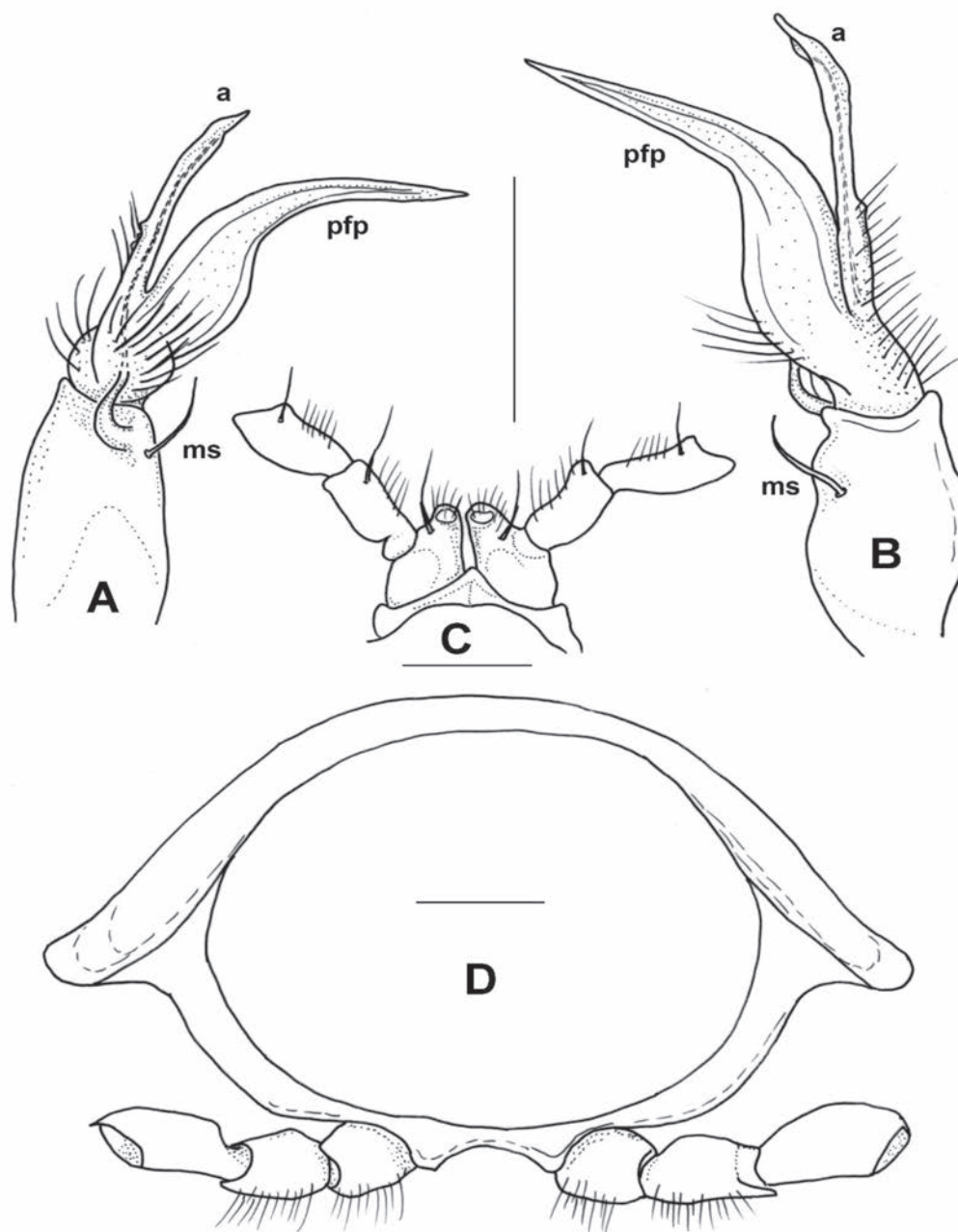


**Figure 7.** *Xystodesmus rebekae* sp. nov., male paratype from Mt. Yae-dake, Okinawa-jima Island, Okinawa Pref. **A, B** right gonopod, ventromesal and dorsolateral views, respectively **C** 2<sup>nd</sup> legpair (from tibia omitted), anterior view **D** body cross section, 6<sup>th</sup> segment, anterior view. Abbreviations: a = acropodite, ms = macroseta, pfp = prefemoral process. Scale bars: 1 mm.

Pro- and metaterga completely smooth, transverse depression in metaterga hardly noticeable, but on midbody segments with two weak lateral swellings. Collum subtrapezoidal, arched,  $\leq 2\times$  longer than metatergum 2, lateral edges directed posteroventrad, anteriolateral margin with well visible ridge. Anterior edge of paranota 2–4 slightly rounded, almost right-angled, posterior edge rounded, without projection. Triangular projection behind on metaterga 5, from 6 onwards increasingly pointed, sublateral excavations on posterior margin of midbody segments already strong, semicircular. Lateral sides of paranota arched, outline of segments clearly delimited. Pore formula normal, pores in lateral central position on narrow paranota.

Segments 15–19 gradually tapering, posterior corners becoming more pointed. Epiproct protruding, in lateral view slightly curved, with two large setae on each lateral side on tubercles, projection with two pairs of setae on small side tubercles, two pairs in dorsolateral position, and 2+2 setae apically (8 pairs of setae altogether); paraprocts smooth, with two pair of setae on obvious median ridges; hypoproct subtrapezoidal with two setae on small tubercles.

Bases of midbody leg pairs well separated (by 1.3–1.5 mm), sterna smooth and wide, pro- and metasterna well separated. Coxa short, almost as wide as long; prefemur 1.2× longer, on postgonopodal legs with well-developed ventral spine; femur 1.2× longer than prefemur, slightly bent proximad; postfemur, tibia, and tarsus subequal in length, all ~ ½ as long as femur; claws normal on all legs.

Colour of living specimens (Fig. 16E) generally dark brown appearance with bright orange paranotal spots. Proterga slightly paler, metaterga with two circular lateral spots. Preserved specimens paler, but the circular markings and the yellowish paranotal spots still noticeable. Clypeus pale brownish, underside of head, antennae, epiproct, and whole ventral side pale whitish, legs pale brown.

**Male sexual characters.** Second leg pair (Fig. 7C) with small tubulous coxal processes, ~ 1/3 length of prefemora, sterna of segments 4–6 without any modifications (Fig. 7D). Gonopods (Fig. 7A, B): Coxa long and slender, ~ 2× as long as wide, coxal apophysis completely lacking, only a single apophyseal macroseta (*ms*) on anteriomesal side. Prefemur slender, bottle-shaped, densely setose; prefemoral process (*pfp*) long, longer than acropodite, drawn S-shaped, smooth, without spines or spurs, gradually tapering and ending in a pointed tip. Acropodite (*a*) slim, subparallel-sided, ~ 2/3 in length of prefemoral process, slightly spatulate before pointed tip where prostatic groove opens. In situ both branches (acropodite and prefemoral process) directed ventromesad, and those of the two gonopods crossing each other.

**Female sexual characters.** Cyphopods deeply embedded in joint aperture closely behind leg pair 2, encapsulated in separate vulval sacs. Receptacula on both anterior and posterior side, subtriangular, setose on entire surface; operculum oval, narrow; valves round, without projected tips, with short setae along margins.

**Remarks.** The individuals were collected in broad-leaved forest ground, always under loose stones. In the same habitat, but in the litter, *Riukiaria holstii* (Pocock, 1895) and *Riukiaria neptuna* (Pocock, 1895) were also found. *X. rebe-kae* sp. nov. seems to be confined to the single locality which is a limestone hill with medium altitude (350–400 m) (relatively high for Okinawa-jima Isl.).

**Etymology.** Named after Rebeka Korsós, daughter of ZK, who found the first specimen in the type locality. Genitive noun derived as a matronym.

***Xystodesmus sesokoensis* sp. nov.**

<https://zoobank.org/4777B6CE-6F41-4F35-B67F-B2ABF3922444>

Figs 8A–C, 16F

**Type material. Holotype:** • male, Japan, Central Ryukyus, Okinawa Pref., Okinawa Group, Sesoko-jima Isl., Ominebaru, 26°38'36.7"N, 127°52'4.7"E, 11 March 2012, leg. Z. Korsós and K. Watanabe (NSMT-My 546). **Paratypes:** • 1 male and 1 juvenile, same locality and date as holotype (HNHM diplo-04546).

**Diagnosis.** A small-sized *Xystodesmus*, with typical colour pattern, pale brown with orange paranotal spots. In its adult size, the most similar species is *X. parvus* sp. nov. that has two simple branches whereas *X. sesokoensis* sp. nov. has a prefemoral process with two small branches at tip, and a long, bending acropodite with a thickened end and a small tooth. Gonopods are somewhat similar to those of *X. fasciatus* sp. nov. but are larger, with a strong coxal apophysis, and its prefemoral process is much wider.

**Description.** Total body length 19–20 mm, midbody paratergal width 3.7 mm, length 0.8 mm, collum width 2.9–3.0 mm, length 1.3 mm. Body sides between segments 5–15 subparallel.

Head smooth, with two frontal setae, epicranial suture distinct. Antennal articles slightly clavate, first article sub-globose, articles 2–6 subequal in length, article 7 small, as long as wide.

Collum in dorsal view oval, edges rounded, with small anterior ridge, corners rounded. Pro- and metaterga completely smooth, transverse depression not visible. Segments 2 and 3 rectangular, both anterior- and posterior-lateral edge of paranota rounded, lacking projection; small projection starts on segment 4, then from 5 increasingly pointed, triangular, sublateral excavations on posterior margin becoming stronger. Lateral sides of paranota straight, outline of segments clearly delimited. Pore formula normal, pores in lateral central position on narrow paranota.

Segments 16–19 gradually tapering, posterior corners becoming obtuse, sublateral excavations disappear. Epiproct in dorsal view triangular, blunt, in lateral view slightly curved ventrad, with 4+4 large setae on tubercles on lateral sides, projection with 2+2 apical setae; paraprocts smooth, with two pairs of setae, upper ones on margin, lower ones on side; hypoproct semicircular with two setae on small tubercles.

Bases of midbody leg pairs weakly separated, sterna smooth and wide, pro- and metasterna fused. Coxa short, rectangular; prefemur ~ 2× as long as wide, with well-developed ventral spine; femur 1.5× longer than prefemur, incrassate; postfemur small, sub-globose; tibia slender, approximately same length as postfemur, tarsus 2× as long as tibia, slender, tapering towards small, curved claw.

Colour of living specimens (Fig. 16F) uniformly yellowish brown, only epiproct darker. Head, antennae, legs, and whole ventral side pale yellowish-greyish. Sides of collum and all paranota (except segment 19) with strong, pinkish-orangish spots.

**Male characters.** Second leg pair with small coxal processes provided with three or four strong setae (as in *X. parvus* sp. nov., Fig. 6D), sterna and coxae of further legs without any modifications. Gonopods (Fig. 8A–C): Coxa stout, sub-globose, approximately as long as wide, instead of coxal apophysis only a small bump, with strong apophyseal macroseta (*ms*) above. Prefemur short, rectangular, densely setose on ventral side, with a few setae on dorsal side; prefemoral process (*pfp*) slender, shorter than acropodite, bent ventrad and ending in two small projections; acropodite (*a*) slightly broader, longer, only slightly bending subparallel to prefemoral process, gradually thickening towards tip, ending in two small projections: one broader, leaf-like, strongly curved ventrad, the other one like a small tooth (*t*) (Fig. 8C). Prostatic groove runs along medio-ventral side of acropodite.

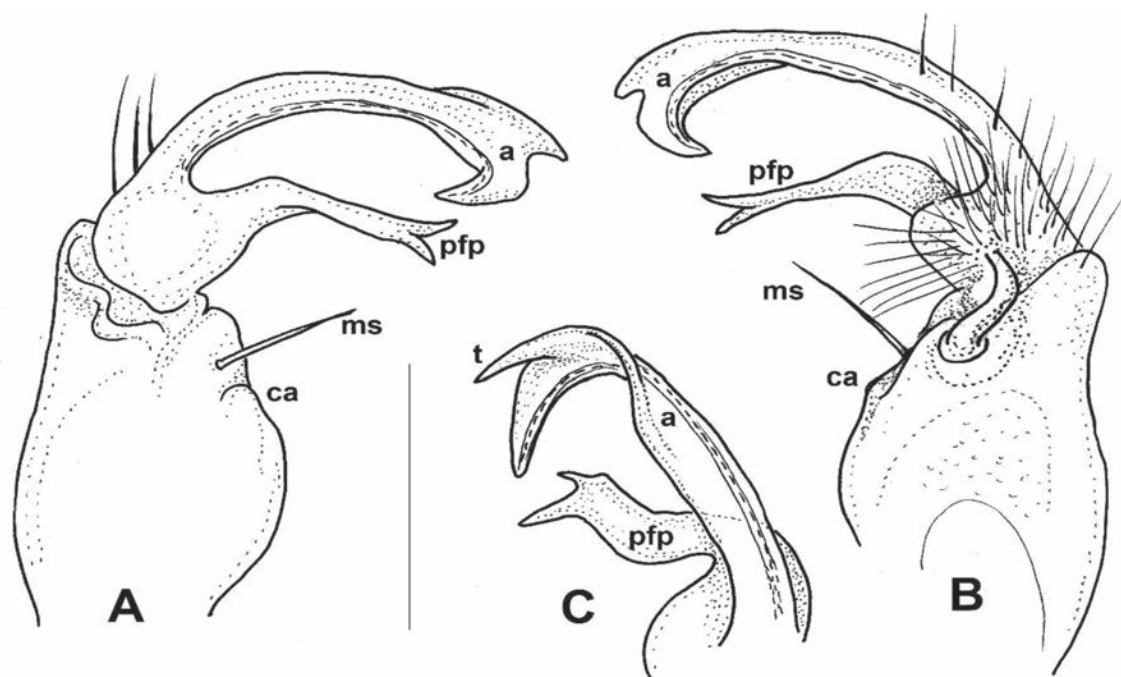


**Figure 8.** *Xystodesmus sesokoensis* sp. nov., left gonopod of male paratype from Sesoko-jima Isl., Okinawa Pref. **A** lateral view **B** mesal view **C** Tip of telopodite, ventral view. Abbreviations: a = acropodite, ca = coxal apophysis, ms = macroseta, pfp = prefemoral process, t = tooth. Scale bar: 0.5 mm.

Female unknown.

**Remarks.** Sesoko-jima is a small island (area less than 3 km<sup>2</sup>) very close to Okinawa-jima Isl., and it is somewhat surprising that it holds an endemic species of millipede. The species seems to be restricted to a small forest on the island.

**Etymology.** Named after the type locality, Sesoko-jima Island, connected by bridge to the island of Okinawa-jima Isl.. Adjective, masculine.

***Xystodesmus variatus* (Pocock, 1895), comb. nov.**

Figs 9A–4D, 17A, B

*Fontaria variata* Pocock, 1895: 361, figs 15, 15a; “Great Loo-Choo (Holst Coll.)” (= Okinawa)

*Rhysodesmus variatus*: Takakuwa 1954: 62

*Riukiaria variata*: Hoffman 1949: 5; Shinohara 1977: 118 (listed)

*Riukiaria variata*: Tanabe and Shinohara 1996: 1487 (“species possibly belonging to *Xystodesmus*”)

*Riukiaria variata*: Marek et al. 2014: 78

**Type material examined.** *Holotype* (Fig. 9D 39): • male, labeled as: “1892.10.10.51, Gr. Loo-Choo, purchased of H. Seebom” (NHMUK).

**Additional material examined.** • 1 male, Japan, Central Ryukyus, Okinawa Pref., Okinawa-jima Isl., Nakijin-son, Nakijin Village, 30 January 1996, leg. K. Yahata (NS-MT-My 547); • 2 males, Japan, Central Ryukyus, Okinawa Pref., Okinawa Group, Okinawa-jima Isl., Ogimi Village, limestone hill near Mt. Nekumachiji-dake, 26°41.0'N, 128°08.1'E, 250 m a.s.l., 24 January 2009, leg. R., P., and Z. Korsós (HNHM)

diplo-04547); • 1 male, 4 females, Japan, Central Ryukyus, Okinawa Pref., Okinawa Group, Kouri-jima Isl., limestone hill, 26°42'08.6"N, 128°00'38.5"E, 40 m a.s.l., 30 January 2010, leg. R., P., and Z. Korsós (RUMF-ZD-00937); • 2 males, 3 females, Japan, Central Ryukyus, Okinawa Pref., Okinawa Group, Kouri-jima Isl., limestone hill, 26°42'08.6"N, 128°00'38.5"E, 50 m a.s.l., 18 April 2010, leg. Z. Korsós (1 female HNHM diplo-04548; 1 male, 1 female VMNH; 1 male, 1 female NHMD 1184734).

**Diagnosis.** Small *Xystodesmus* with typical colour pattern still visible on preserved specimens, metaterga darker, proterga and paranota paler. Gonopod has only two branches, similar to *X. parvus* sp. nov. and *X. rebekae* sp. nov., but *X. parvus* sp. nov. is much smaller, and in *X. rebekae* sp. nov. both prefemoral process and acropodite are slender and straight, whereas in *X. variatus* comb. nov. they are strongly pointed and sickle-shaped in mesal view.

**Description.** Measurements: length 29 mm, midbody segment width: 6.2 mm, metatergal length 2 mm; collum width 4.7 mm, median collum length 2.2 mm. Measurements of new material: length 24–29 mm, midbody segment width: 5.4–6.0 mm, metatergal length 1.2–1.4 mm; collum width 4.2–4.7 mm, median collum length 1.6–1.9 mm. Body sides between segments 5–15 parallel.

Head smooth, epicranial suture distinct. Antennal articles slightly clavate, first article sub-globose, articles 2–6 subequal in length, article 7 as long as wide.

Pro- and metaterga smooth, transverse depression on metaterga hardly noticeable. Collum in dorsal view elongated sub-hexagonal, with weak marginal ridges all around, lateral corners directed postero-ventrad, weakly pointed, posterior margin wavy. Anterior edges of all paranota rounded, postero-lateral corners increasingly pointed caudad, from segment 5 onwards with a concave posterior excision. Lateral sides of paranota arched, those bearing pores depressed, pore formula normal.

Segments 15–19 gradually tapering, caudal corners becoming more pointed. Epiproct protruding, in lateral view slightly curved, slender, with 2+2 apical and 4+4 lateral setae all on strong tubercles; paraprocts smooth, with two pairs of setae, upper ones on margins, lower ones on sides; hypoproct semicircular with 1+1 setae on small tubercles.

Bases of midbody leg pairs well separated (by 1.0–1.2 mm in male, 1.5–1.7 mm in females), sterna smooth and wide, pro- and metasterna fused together. Coxa ~ 2× as long as wide; prefemur ~ 1.5× longer, with well-developed ventral spine; femur 1.5× longer than coxa, clavate; postfemur shorter than coxa, approximately as long as wide, tibia and tarsus slender, tarsus ~ 1.5× longer than tibia; claw small, slightly curved ventrad.

Colour of newly collected living specimens (Fig. 17A, B) generally greyish, blueish brown with orange or yellowish paranotal spots. These are less conspicuous than in other *Xystodesmus* species (e.g., in *X. kumamotoensis* sp. nov. or *X. rebekae* sp. nov.). Proterga and sides of metaterga paler, more greyish, and in most cases a dark dorsomedial line also traceable, at least in midbody region. Preserved specimens lost colouration, but differences between pro- and metaterga, and the metatergal side spots still visible. Clypeus and epiproct pale brownish, underside of head, antennae, legs, and whole ventral side pale whitish.

**Male sexual characters.** Second leg pair with small coxal processes provided with three or four strong setae (as in *X. parvus* sp. nov., Fig. 6D), sterna of segments 4–6 and further legs without any modifications. Gonopods (Fig. 9A–C): Coxa stout, approximately as long as wide, coxal apophysis completely

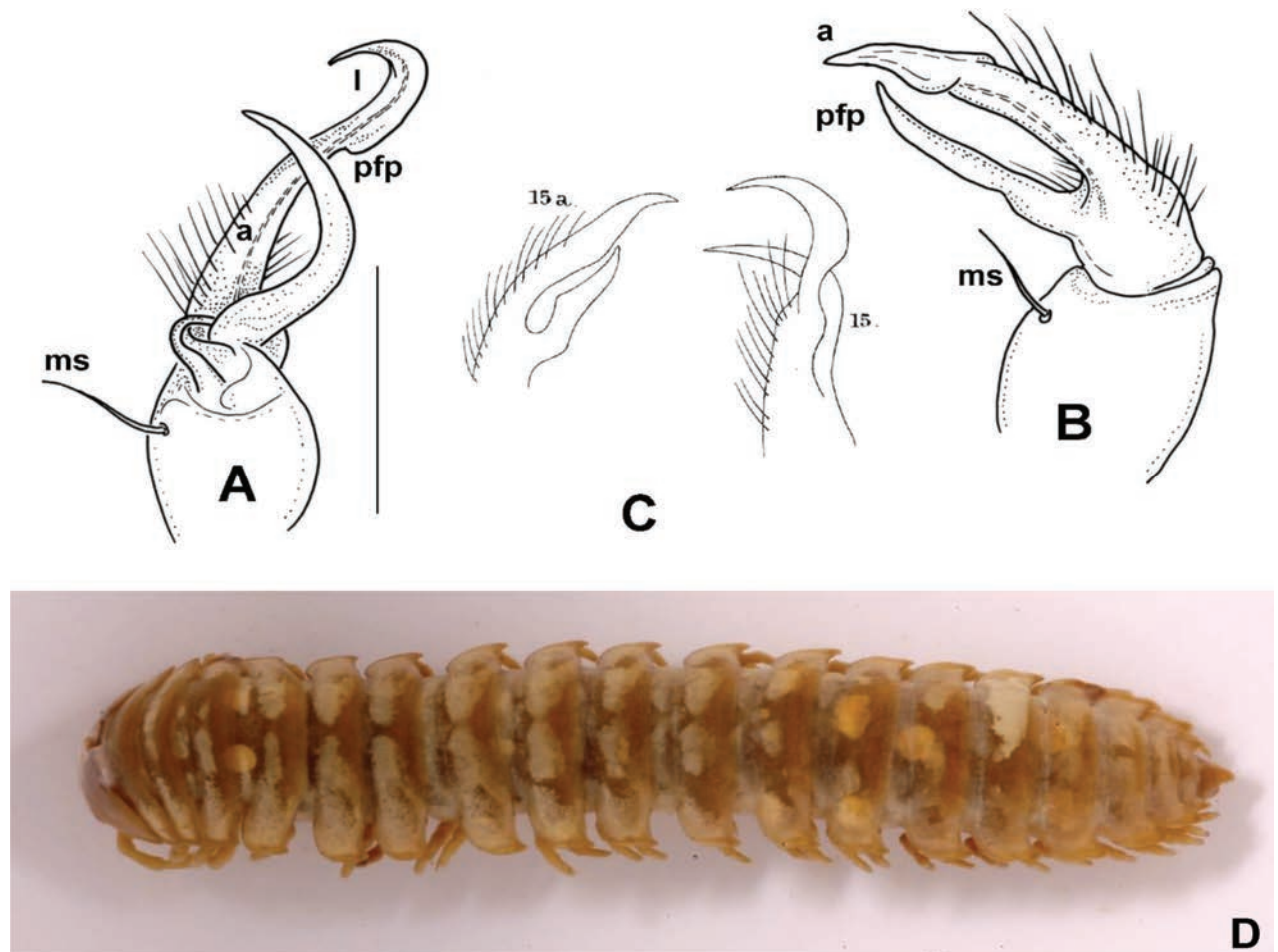


**Figure 9.** *Xystodesmus variatus* (Pocock, 1895) comb. nov. **A, B** right gonopod of male from Kouri-jima Isl., Okinawa Pref., mesal and lateral views, respectively. **C** original figures by Pocock (1895), “fig. 15. *Fontaria variata*. Left copulatory foot from below, fig. 15a. Ditto, outer view.” **D** *Fontaria variata* Pocock, 1895, holotype male specimen (BMNH, Reg. Nr. 1892.10.10.51). Abbreviations: a = acropodite, ms = macroseta, l = lobe, pfp = prefemoral process. Scale bar: 1 mm (**A, B**).

lacking, apophyseal macroseta (*ms*) relatively small. Prefemur short, sub-globose, densely setose on ventral side, setosity goes on to halfway of acropodite; prefemoral process (*pfp*) slender, curved ventrad,  $\sim \frac{3}{4}$  as long as acropodite, ending in a long, pointed tip; acropodite (*a*) slightly broader at base, gradually tapering towards pointed tip, but subapically with a leaf-like broadening (*l*), in mesal view similar to an eagle’s claw (Fig. 9A). Prostatic groove runs along the mesal side of acropodite to the pointed tip.

**Female sexual characters.** Cyphopods (Fig. 10) deeply embedded in joint aperture closely behind leg pair 2, encapsulated in separate vulval sacs. Receptacula (*r*) on both anterior and posterior side, low, subtriangular, setose on entire surface; operculum (*op*) narrow,  $\sim \frac{3}{4}$  as high as bursal valves; valves (*v*) rectangular, laterally with small projected tips, with several row of short setae along margins.

**Remarks.** With the re-examination and the side-by-side comparison of the type specimens of *Fontaria variata* Pocock, 1895 and the freshly acquired specimens it became clear that they were conspecific. In the original description the colour, obviously based on preserved specimens, is described as “upper surface rather thickly clouded with fuscous, with a clearer spot on each side above the keels” (Pocock 1895: 361); and those spots correspond to the

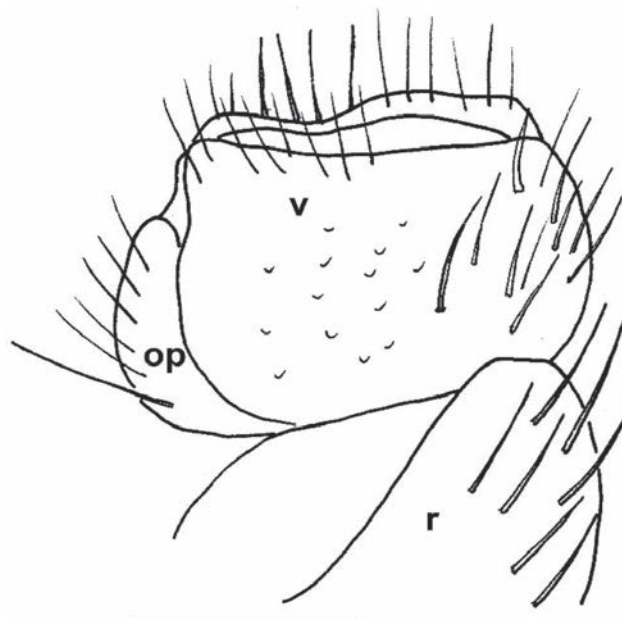


**Figure 10.** *Xystodesmus variatus* (Pocock, 1895), comb. nov. Left cyphopod of female from Kouri-jima Isl., Okinawa Pref., anterior view. Abbreviations: op = operculum, r = receptacle, v = valve. Scale bar 0.5 mm.

orange paranotal spots observed on the living specimens. The body size, the shape and structure of metaterga and paranota, and especially the gonopods are in complete agreement in both samples, so the assignment of *F. variata* to *Xystodesmus* is justified.

Hoffman (1949) placed *F. variata* in *Riukiaria* together with *F. holstii* Pocock, 1895, but Tanabe and Shinohara (1996) tentatively separated them in different genera, assigning *variatus* “possibly” to *Xystodesmus*. In the last part of their paragraph, Tanabe and Shinohara (1996: 1487), perhaps due to a typographical error, referred to *variatus* together with other species described by Takakuwa, saying that “*Rhysodesmus spinosissimus* (recte *spinosissimus*), *Riukiaria geniculata*, *Ri. spiralipes*, *Ri. variata*, *K. amoeba* (recte *amoena*), and *Pachydesmus bazanensis*, their types, which had been deposited in Y. Miyosi’s private collection, were destroyed in 1945”. However, *R. variata* was actually described by Pocock (1895), not Takakuwa, and its type has never been in Miyosi’s private collection, but has been stored and was recently found in the Natural History Museum, London, and is redescribed. The newly collected specimens were found in association with *Riukiaria holstii* (Pocock, 1895), a widespread species on the central and northern part of Okinawa-jima Island. This long-known species has also been recorded from more southwestern and remote islands in the Ryukyu Archipelago, such as Ishigaki-jima and Iriomote-jima in the Yaeyama Group and Uotsuri-jima in the Senkaku Group (Nakamura and Korsós 2010). However, from our extensive myriapodological surveys conducted in the archipelago, we can say with near certainty that these records should be regarded as misidentifications. There are superficially similar species such as *Riukiaria chelifera* (Takakuwa, 1941), endemic to the Yaeyama Group. The “*Rhysodesmus variatus*” found on Uotsuri-jima Island (Ikehara and Shimojana 1971) may be an undescribed species due to the biogeographic peculiarities of the terrestrial faunas in the Senkaku Group among Japanese islands (Ota 1998; Kurita et al. 2017).

***Xystodesmus pallidus* (Verhoeff, 1937), comb. nov.**

Figs 11A–E, 12A–D, 13A, B

*Koreoaria pallida* Verhoeff, 1937: South Korea (Verhoeff 1937: 319–320, fig. 8)

*Koreoaria pallida*: Tanabe and Shinohara 1996: 1487 (“species possibly belonging to *Xystodesmus*”)

*Koreoaria pallida*: Tanabe and Shinohara 1996: 1487

*Koreoaria pallida*: Marek et al. 2014: 71

**Type material examined. Holotype:** • male (ZSMC, Reg. Nr. A20060019): in 2 fragments, gonopods and legs are on separate slide (ZSMC, Reg. Nr. A20033594) (Fig. 11). **Paratypes:** • 4 females (ZSMC, Reg. Nr. A20060019).

**Description of holotype.** Male total body length ~ 21 mm; collum length 1.5 mm, width 3.3 mm; 10<sup>th</sup> segment width 4.2 mm, metazonal length 1.1 mm. Paranotal processes from segment 6 onwards projected caudad, anterior margin broadly rounded, male 2<sup>nd</sup> leg pair with long, slender coxal projection, 3<sup>rd</sup> with nothing, 4<sup>th</sup> and 5<sup>th</sup> with small, triangular coxal processes; postgonopodal prefemoral spines strong and long, half as long as length of prefemur, sternal plate broad, coxal distance 1.2 mm, anterior-posterior sterna fused.



Figure 11. *Xystodesmus pallidus* (Verhoeff, 1937), comb. nov. **A–C** Slide of male gonopods and 6–8<sup>th</sup> leg pairs of holotype from “Süd-Korea” (ZSMC, Reg. Nr. A20033594) **B** right gonopod in slide, lateral view **C** back of slide with comment by R. L. Hoffman, 28 June 1960 **D, E** male holotype in 2 pieces (ZSMC, Reg. Nr. A20060019). Scale bar: 10 mm (**E**).

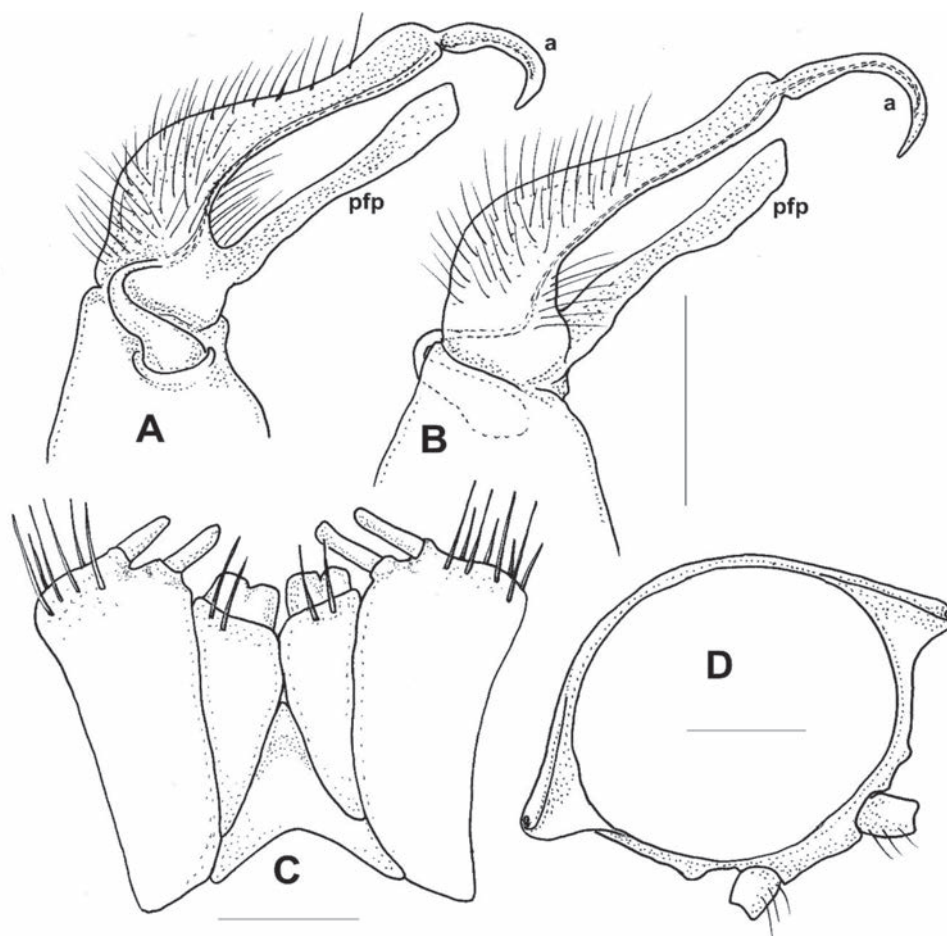


**Figure 12.** *Xystodesmus pallidus* (Verhoeff, 1937), comb. nov. **A, B** right and left gonopods of holotype male, drawn from slide (Fig. 11B), mesal and lateral views, respectively **C** gnathochilarium of male holotype, ventral view **D** cross section of broken female paratype, 5<sup>th</sup> segment, posterior view. Abbreviations: a = acropodite, pfp = prefemoral process. Scale bars: 0.5 mm (**A–C**); 1 mm (**D**).

**Male gonopods** (Figs 11A–C, 12A, B) fits well to the original description and drawing.

**Female paratypes.** Total body length 22–26 mm; collum length 1.6–1.8 mm, width 3.5–3.8 mm; 10<sup>th</sup> segment paranotal width 4.4–5.1 mm, metazonal length 1.1–1.2 mm, coxal distance 1.1–1.5 mm. Gnathochilarium (Figs 12C, 13A) and cyphopods (Fig. 13B) are here illustrated for the first time.

**Colouration** (Fig. 11D–E). Type material in alcohol completely faded. Verhoeff (1937: 319), however, provided a description which is in total agreement of *Xystodesmus* characters: “braune Metatergite und rötlichgelben Längswisch auf den Seitenflügeln” [metatergites brown, and paranota with reddish yellow longitudinal spots].

**Remarks.** The flat gonopodal prefemoral process (*pfp*, Fig. 12A, B) was called by Verhoeff (1937: 317, fig. 8) as “abgespaltener Tibiotarsus”, and in the generic comparison of *Koreoaria* he had set it against the prefemoral process of *Pachydesmus* Cook, 1895. According to Verhoeff, the longer process made of two parts, the “praefemorofemur” and its disjunct ending, the solenomere (Verhoeff 1937: fig. 8, *sl*). In our opinion this is a misunderstanding, as the longer process corresponds to the acropodite (Fig. 12A, B, *a*), and the other one is the prefemoral process (correctly interpreted by Takakuwa 1942b for *Koreoaria amoena*).

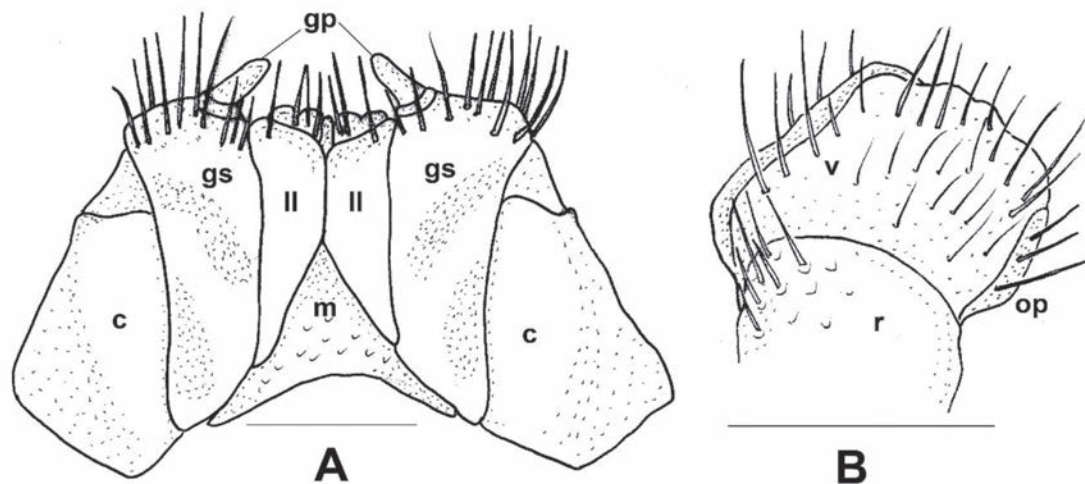


**Figure 13.** *Xystodesmus pallidus* (Verhoeff, 1937), comb. nov. **A** gnathochilarium of female paratype, ventral view **B** left vulva of female paratype, posterior view. Abbreviations: c = cardo, gp = gnathochilarial palps, gs = gnathochilarial stipites, ll = lingual lobes, m = mentum, op = operculum, r = receptacle, v = valve. Scale bars: 0.5 mm.

***Xystodesmus amoenus* (Takakuwa, 1942), comb. nov.**

Fig. 15A

*Koreoaria amoena* Takakuwa, 1942b: Daegu, South Korea (Takakuwa 1942b: 362–363, fig. 5)

*Koreoaria amoea* (sic!): Tanabe and Shinohara 1996: 1487: (“species possibly belonging to *Xystodesmus*”)

*Koreoaria amoea* (sic!): Marek et al. 2014: 71

**Descriptive notes** based on Takakuwa (1942b: 366). Body length 22 mm, width 4 mm. Male gonopod with two processes (Fig. 15A, redrawn from Takakuwa 1942b: 362, fig. 5), the femoral process continues in tibiotarsus (a) with a small tooth (b), taking the seminal groove all along to the end bending backwards (acropodite); whereas the other shorter and thinner process is the prefemoral process (“Prefemoralfortsatz”).

**Colouration.** Without the type material and fresh specimens, we can only rely on Takakuwa’s description (1942b: 366): “Rücken graulich, Kopf, Antennen und Bauch gelb, Bein proximal etwas graulich, distal gelb. Seitenflügel mit einem deutlich rötlichen Fleck.” [Back greyish, head, antennae, and belly yellow, legs proximally somewhat greyish, distally yellow. Paranota with a clearly reddish spot.] The important part is the last sentence, which is again in total agreement of *Xystodesmus* characters.

**Remarks.** Type material could not be studied since Takakuwa’s private collection, including type material of many species, is considered lost (Tanabe and Shinohara 1996; Chao and Chang 2008).

***Xystodesmus saltuosus* (Haga, 1968), comb. nov.**

Fig. 14A–C

*Rhysodesmus saltuosus* Haga, 1968: 8, fig. 11a–f: Mt Sarakura-yama, Kita-Kyushu City, 18 June 1961, leg. A. Haga

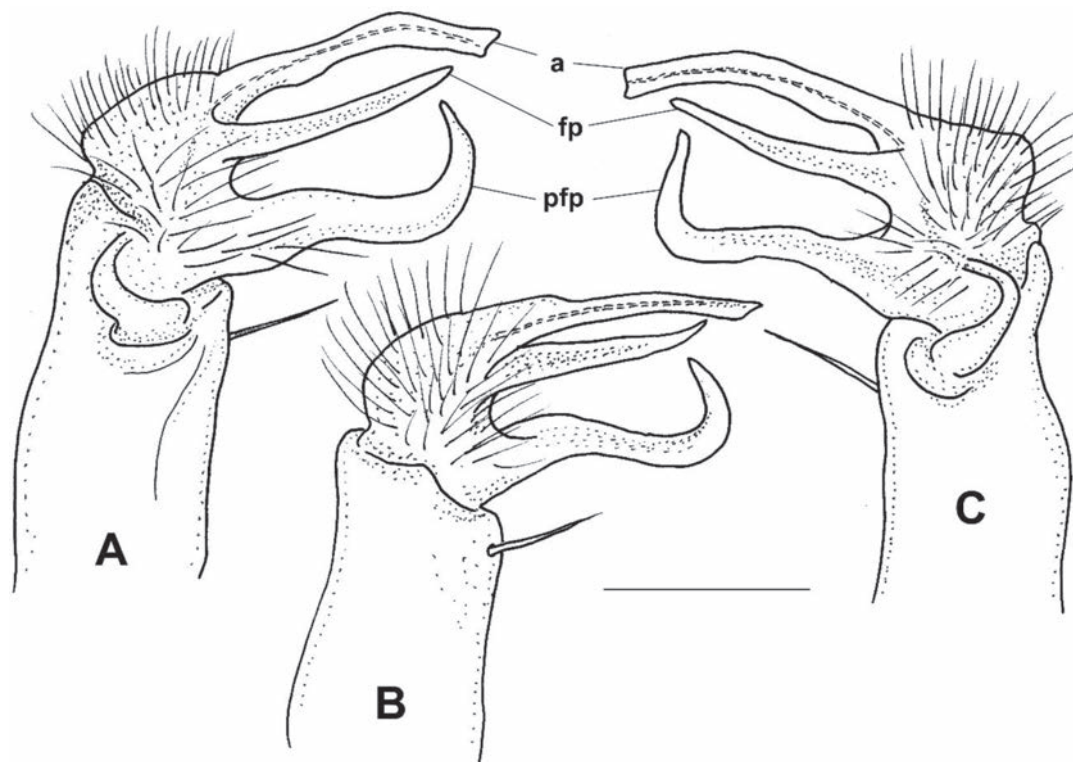


**Figure 14.** *Xystodesmus saltuosus* (Haga, 1968), comb. nov., holotype male from Kita-Kyushu (NSMT-My.162) **A** right gonopod mesal view **B, C** left gonopod lateral and mesal views, respectively. Abbreviations: a = acropodite, fp = femoral process, pfp = prefemoral process. Scale bar: 0.5 mm.

**Type material examined.** Holotype male (NSMT-My.162).

**Redescription.** Length not possible to measure (holotype is in 5 pieces), but apparently under 30 mm, midbody width with paraterga 4.8 mm, midbody metatergal length 1.2 mm, collum width 4 mm, median collum length 1.9 mm. Body sides between segments 7–14 subparallel.

Head smooth, with two frontal setae, epicranial suture distinct. Antennal articles slightly clavate, first article sub-globose, articles 2–6 subequal in length, article 7 small, as long as wide.

Collum in dorsal view subtrapezoidal, no traces of marginal ridges, lateral corners rounded, directed postero-ventrad, posterior margin slightly wavy. Pro- and metaterga smooth, transverse depression on metaterga hardly noticeable. Anterior edges of all paranota rounded, postero-lateral corners increasingly pointed caudad, from segment 5 onwards with a concave posterior excision. Lateral sides of paranota arched, those bearing pores depressed, pore formula normal.

Segments 15–19 gradually tapering, caudal corners increasingly pointed. Epiproct in dorsal view triangular, in lateral view slightly curved ventrad, with 2+2 apical and 4+4 lateral setae all on strong tubercles; paraprocts smooth, with two pairs of setae, upper ones on margins, lower ones on sides; hypoproct semicircular with 1+1 setae on small tubercles.

Bases of midbody leg pairs well separated by 1.0 mm, sterna smooth and wide, pro- and metasterna well separated. Coxa sub-globose; prefemur ~ 1.2× longer, with well-developed ventral spine on postgonopodal legs; femur incrassate, ~ 2× as long as wide; postfemur much shorter, approximately as long as wide, tibia and tarsus slender, subequal in length, ~ 2× as long as wide; claw large, flat, curved ventrad.

Colour of living specimens unknown; holotype completely faded due to preservation, currently yellow, and even pro- and metatergal differences cannot be traced.

**Male sexual characters.** Second leg pair with small coxal processes with a pair of strong setae (as in *X. rebekae* sp. nov., Fig. 7C), sterna of segments 4–6 and leg pairs 3 onwards without any modification. Gonopod (Fig. 14A–C) coxa long and slender, ~ 2× as long as wide, coxal apophysis completely lacking, apophyseal macroseta relatively small. Telopodite built of three subequal, subparallel processes: prefemoral process (*pdfp*) sits on short, densely setose prefemur; approximately as long as acropodite, curved distad at its end; solenomere has two processes, acropodite (*a*) subparallel-sided, flattened, tip rectangular as if cut off, prostatic groove runs along mesal side; and at its base, from the femoral part a third process (*fp*) starts, slightly shorter than acropodite, gradually tapering towards long, pointed tip.

Female unknown.

**Remarks.** *Rhysodesmus* is a Middle American genus, and the name was mistakenly used by early Japanese authors, mainly following the prominent Japanese myriapodologist Yoshioki Takakuwa (1873–1960). The situation was first explained in Japanese by Shinohara (1977), but also established by Hoffman (1980), Marek et al. (2014), and Huerta-de la Barrera et al. (2021). The species itself (*Rh. saltuosus*) was unfortunately overlooked by Shinohara (1977), Tanabe and Shinohara (1996), and Marek et al. (2014) since it was published in a private but widely available publication (Haga 1968). Huerta-de la Barrera et al. (2021) referred to Haga's publication, but did not specifically mention *Rh. saltuosus*. Since the holotype male was available for study we could establish its association with *Xystodesmus* and removed the species from *Rhysodesmus*.

### ***Xystodesmus martensii* (Peters, 1864)**

Fig. 17C, D

*Polydesmus* (*Fontaria*) *martensii* Peters, 1864: 531, no fig.

*Xystodesmus martensii*: Cook 1895: 5, no fig.

**Material examined.** • 4 males, 3 females, Japan, Honshu, Kanagawa Pref., Fujisawa City, Eno-shima Isl., Kodama Shrine, 35°18'03"N, 139°28'52"E, 20 m a.s.l., oak grove, 11 October 2010, leg. Z. Korsós and Y. Nakamura (HNHM diplo-04549); • 3 males, 4 females, Japan, Honshu, Kanagawa Pref., Isehara City, Mt. Oyama, Yabitsu Pass, 760 m a.s.l., 35°25'36"N, 139°14'05"E, *Cryptomeria japonica* forest, 11 October 2010, leg. Z. Korsós and Y. Nakamura (HNHM diplo-04550); 1 male, Japan, Honshu, Kanagawa Pref., Yamakita Town, Yuzuku, Myojin Pass, 12 October 2010, leg. Y. Nakamura (RUMF-ZD-00935)

**Descriptive notes.** Tanabe and Shinohara (1996) gave an extensive redescription of the species based on their new material and have shown great variation in the shape of male gonopods. The gonopods of the eight males we studied here fit within the range of variation described by Tanabe and Shinohara (1996). We also noticed the conspicuous metatergal tubercles, which are much more developed than in other *Xystodesmus* species.

**Colour of living specimens** (Fig. 17C, D). The Kanagawa samples represent two slightly different colour morphs: one pale greyish, the other one dark brown, but both have the typical and strong, reddish orange spots on paranota.

***Xystodesmus nikkoensis* (Chamberlin & Wang, 1953)**

Fig. 17E, F

*Nikkonus nikkoensis* Chamberlin & Wang, 1953: 9, fig. 3

*Xystodesmus nikkoensis*: Tanabe and Shinohara 1996: 1484, figs 3–7, 11J–K, 13A, 16A, 17L, M

**Material examined.** • 4 males, Japan, Northern Ryukyus, Kagoshima Pref., Osumi Group, Yaku-shima Isl., Anbo forest road, *Cryptomeria japonica* forest, 30°18'42.0"N, 130°37'54.0"E, 190 m a.s.l., 5 July 2010, leg. Z. Korsós (HNHM diplo-04551).

**Descriptive notes.** Tanabe and Shinohara (1996) gave a short redescription and showed relatively small variability in the male gonopod structure. Our specimens, collected exactly on the original type locality (“Anbo Rindo”, Yaku-shima Island) are in complete agreement. Tanabe and Shinohara (1996, p. 1484) also said *X. nikkoensis* is “the smallest species of xystodesmid in Japan”. This statement, however, in light of the present discovery of the new species *X. parvus* sp. nov. and *X. sesokoensis* sp. nov., is not true anymore.

**Colour of living specimens** (Fig. 17E, F). According to Tanabe and Shinohara (1996: 1484) Yaku-shima specimens have on “collum and metatergites with yellowish white paranotal spots”. Based on our freshly photographed animals also from Yaku-shima Isl., we can support this observation and can add that those paranotal spots are even more conspicuous next to the entirely dark brown body colour.

***Xystodesmus yamamiensis* Masuda, 2001**

Fig. 15B

**Material examined.** *Holotype* male (NSMT-My.294), and *paratype* male (NSMT-My. 295), Aichi Pref., Chita County, Minamichita Town, Yamami, 5 April 1998, leg. K. Masuda.

**Descriptive notes.** The original description and illustrations lack some important details, thus after the re-examination of the holotype, we present here an additional drawing of the male gonopod (Fig. 15B). Coxa stout, as wide as long, with a strong apophyseal process (*ca*) and a large macroseta (*ms*). Prefemur and acropodite slightly twisted, prefemoral process (*pfp*) ~ ¾ of length of acropodite, those of two gonopods crossing each other *in situ*. Prostatic groove runs along lateral side of acropodite (*a*) and ends on distal part of lower branch of bifurcated tip.

**Remarks.** Interestingly, the gonopods have a general similarity to *Riukiaria neptuna* (Pocock, 1895) (Korsós et al. 2011), as the end of acropodite is ramified: two branches in *X. yamamiensis*, three in *R. neptuna* (see Pocock 1895; Hoffman 1949). However, the body size (19–24 mm) and especially the colour of *X. yamamiensis* (“Keels have a red spot in roughly in the middle.” Masuda 2001: 635) clearly indicate that this is a species of *Xystodesmus*.

**Unidentified *Xystodesmus* female 1**

Fig. 16G

**Material examined.** • 6 females, Japan, Central Ryukyus, Okinawa Pref., Okinawa Group, Tokashiki-jima Isl., National Okinawa Youth Fellowship Center, mixed

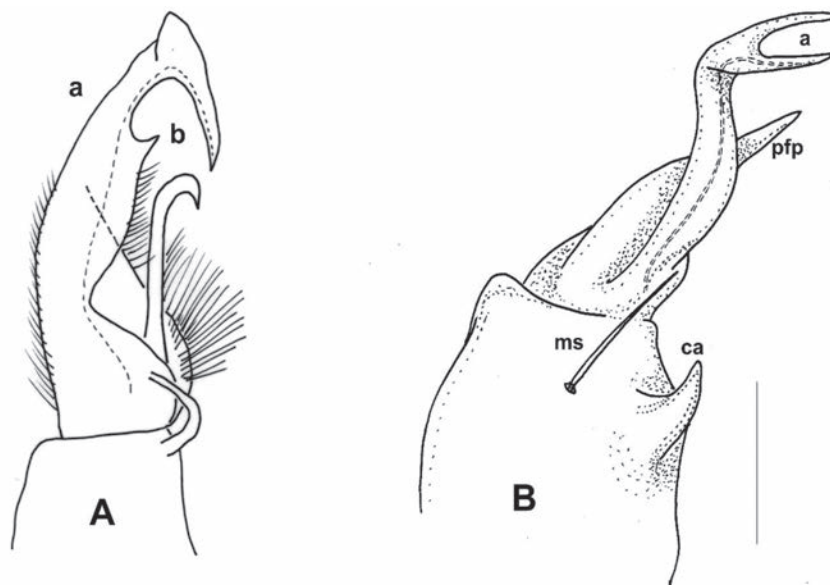


**Figure 15.** Male gonopods of *Xystodesmus* species. **A** *Xystodesmus amoenus* (Takakuwa, 1942), comb. nov., right gonopod of male type specimen from Daegu (= Taikyu), South Korea, redrawn from Takakuwa's original (1942b: 362, fig. 5), mesal view, not to scale. Abbreviations: "a = Tibiotarsus, b = Femurabschnitt mit kleiner Spitze" **B** *Xystodesmus yamamiensis* Masuda, 2001, left gonopod of holotype male from Yamami, Aichi Pref., Japan (NSMT-My.294), lateral view. Abbreviations: a = acropodite, ca = coxal apophysis, ms = macroseta, pfp = prefemoral process. Scale bar: 0.5 mm (**B**).

forest, 26°12'40.7"N, 127°21'46.4"E, 200 m, 9–10 April 2010, leg. Z. Korsós (No. 183) (RUMF); • 2 females, Japan, Central Ryukyus, Okinawa Pref., Okinawa Group, Tokashiki-jima Isl., Tokashiki, Otani forest road, mixed forest, 26°12'45.3"N, 127°21'26.3"E, 18 m, 10 April 2010, leg. Z. Korsós (HNHM diplo-04552); • 2 females, Japan, Central Ryukyus, Okinawa Pref., Okinawa Group, Tokashiki-jima Isl., National Okinawa Youth Fellowship Center, outside the fence, mixed forest, 26°12'44"N, 127°21'50"E, 215 m, 21 October 2010, leg. Z. Korsós (No. 266) (RUMF)

**Colour of living specimens** (Fig. 16G). Body uniformly dark brown, posterior edge of metaterga darker; paranota from 5<sup>th</sup> segment onward light, yellowish orange; head brown, antennae, legs, and underside whitish.

**Remark.** Probably the same species as the one occurring on Aka-jima Isl., i.e., *X. keramae* sp. nov. (Fig. 16B).

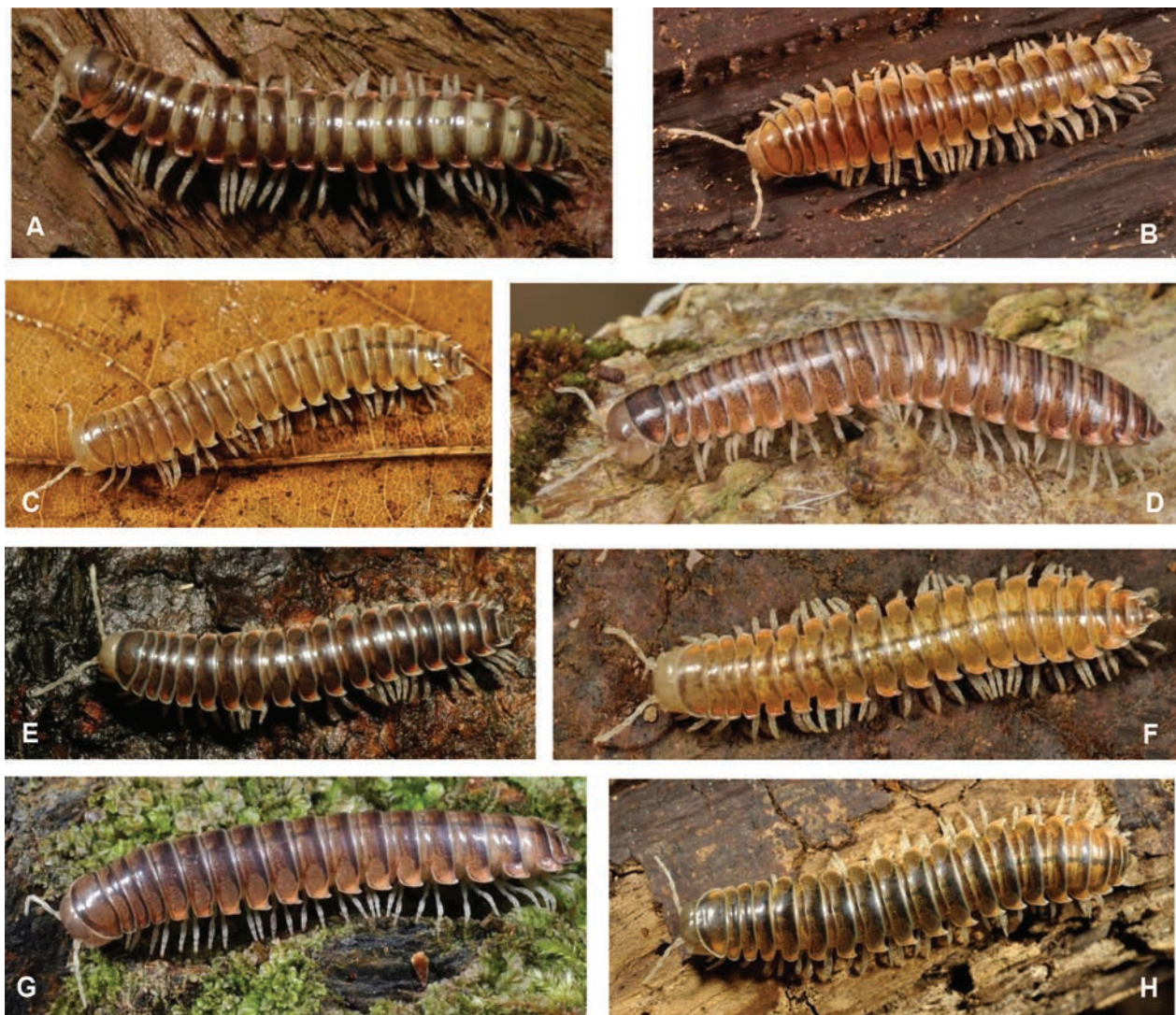
### Unidentified *Xystodesmus* female 2

Fig. 16H

**Material examined.** • 1 female, Japan, Central Ryukyus, Amami Group, Tokuno-shima Island, Kametsu, near the pass between Mt. Inokawa-dake and Mt. Hage-dake, 27°45'38.4"N, 128°58'53.7"E, *Castanopsis sieboldii* forest, 4 February 2012, leg. Y. Nakamura (HNHM diplo-04553)

**Colour of living specimens** (Fig. 16H). Body uniformly dark greyish brown, median and posterior part of metaterga darker; all paranota including collum with light, yellowish spots; head and epiproct greyish brown; antennae, legs, and underside whitish.

**Remark.** Up to now this is the only *Xystodesmus* specimen from Tokuno-shima Island and probably represent a different species. However, without knowing the male it would be premature to assign it to any category.



**Figure 16.** Live habitus of new *Xystodesmus* millipede species **A** *X. fasciatus* sp. nov., male paratype, Fukiage, Kagoshima Pref. **B** *X. keramae* sp. nov., male paratype, Aka-jima Isl., Okinawa Pref. **C** *X. kumeensis* sp. nov., male paratype, Kume-jima Isl., Okinawa Pref. **D** *X. parvus* sp. nov., male paratype, Okinoerabu-jima Isl., Kagoshima Pref. **E** *X. rebekae* sp. nov., male paratype, Mt. Yae-dake, Okinawa-jima Isl., Okinawa Pref. **F** *X. sesokoensis* sp. nov., male holotype, Sesoko-jima Isl., Okinawa Pref. **G** unidentified female, Tokashiki-jima Isl., Okinawa Pref. **H** unidentified female, Tokuno-shima Isl., Kagoshima Pref. Not to scale.

### Key to the species of *Xystodesmus*

Tanabe and Shinohara (1996) already provided a tentative key to the six species of *Xystodesmus* which they accepted as valid at that time (*X. shirozui*, *X. marten-sii*, *X. gracilipes*, *X. nikkoensis*, *X. serrulatus*, and *X. tokaiensis*). Since then, one new species, *X. yamamiensis* was described in 2001, so including the four new combinations and seven new species presented in this paper, we have now 18 *Xystodesmus* species for which to construct a complete key. This is a difficult task, and we agree with Tanabe and Shinohara (1996) that because of the significant variation in gonopodal morphology, a comparison of the illustrations and reference to the distribution will sometimes be more efficient. The key below starts with the countries (Korea and Japan, see also the maps in Fig. 18A, B), then body size (total length and maximum midbody width), but later only male gonopodal characters, and sometimes colouration, were used to separate the species.

- 1 Species from the Korean Peninsula ..... **2**  
 – Species from the Japanese islands ..... **3**  
 2 Male gonopod with 2 simple, forceps-like processes; acropodite with curved, thin solenomere, prefemoral process parallel-sided (Figs 11B, C, 12A, B); 4<sup>th</sup> and 5<sup>th</sup> legs with small, triangular coxal processes (Korean Peninsula) ..... ***X. pallidus* (Verhoeff, 1937), comb. nov.**  
 – Male gonopod with strong, thick acropodite, solenomere bending at right angle, prefemoral process thin and curved at the end (Fig. 15A); no triangular coxal processes on 4<sup>th</sup> and 5<sup>th</sup> legs (Korean Peninsula) ..... ***X. amoenus* (Takakuwa, 1942), comb. nov.**  
 3 Body length < 25–27 mm, midbody width < 5.0–5.2 mm ..... **4**  
 – Body length ~ 30 mm, midbody width > 5.2, often above 6.0 mm ..... **7**  
 4 Male gonopod with strong coxal apophysis. End of acropodite bifurcated (Aichi Pref., Honshu) ..... ***X. yamamiensis* Masuda, 2001**  
 – Male gonopod without coxal apophysis, or only with 1 small bump ..... **5**  
 5 Male gonopod stout, with strong, tongue-like prefemoral process; acropodite with strong femoral process and 1 small tooth under its tip (Fig. 3A–C). (Kumamoto and Oita Pref., Kyushu) ..... ***X. kumamotoensis* sp. nov.**  
 – Male gonopod is different; prefemoral process slender, acropodite is simple, without additional processes ..... **6**  
 6 Coxa of male gonopod with 1 small bump (but not apophysis!); prefemoral process slender with 2 small branches at tip; acropodite long, bending, apex is thicker with 1 small tooth (Fig. 8A–C). Body colour yellowish brown with pale orange paranotal spots (Fig. 16F). (Sesoko-jima Island, Okinawa Pref.) ..... ***X. sesokoensis* sp. nov.**  
 – Coxa of male gonopod with no modifications; prefemoral process and acropodite similar in size, spiralling around each other, tip of solenomere leaf-like (Fig. 6A–C). Body colour pale brownish with pale orange paranotal spots (Fig. 16D). (Okinoerabu-jima Island, Kagoshima Pref.) ..... ***X. parvus* sp. nov.**  
 7 Male gonopods with coxal apophysis ..... **8**  
 – Male gonopods without coxal apophysis ..... **13**  
 8 Coxal apophysis of male gonopod very strong, almost hook-like; prefemoral process flat and wide, curving backwards; acropodite with 3 small teeth at tip (Fig. 1A, B). Colour pattern fasciated with grey prozona and dark brown metazona, paranotal spots strong reddish (Fig. 16A). (Kagoshima Pref., Kyushu) ..... ***X. fasciatus* sp. nov.**  
 – Coxal apophysis weaker, not hook-like; gonopod structure less complicated, usually with only 2 subequal processes ..... **9**  
 9 Gonopods with a cup-shaped acropodite process (see Tanabe and Shinohara 1996: figs 12A, B, 14). Colouration greyish to dark brown, with strong red spots on paranota (Fig. 17C, D). Metaterga with 2 or 3 rows of conspicuous tubercles. (Ibaraki, Tochigi, Gunma, Saitama, Chiba, Tokyo, Kanagawa, Yamanashi and Shizuoka Pref., Honshu) ... ***X. martensii* (Peters, 1864)**  
 – Gonopods different, without cup-shaped process; paranotal spots not so strong. Metaterga without strong tubercles ..... **10**  
 10 Coxal apophysis well developed; gonopods with 2 simple, parallel, subequal processes ..... **11**  
 – Coxal apophysis weak, only slightly larger than a bump; gonopod processes always with some toothed or leaf-like extensions ..... **12**

- 11 Gonopod acropodite and prefemoral process subequal in length, very slender, entirely straight (see Tanabe and Shinohara 1996: figs 12D, 15D-I). (Aichi, Gifu, Nara, Mie, and Shizuoka Pref., Honshu, and Tokushima Pref., Shikoku) ..... ***X. serrulatus* (Miyosi, 1952)**
- Prefemoral process little longer than acropodite and curved backwards (Fig. 2A–C). Colouration pale brown, paranotal spots pale yellowish (Fig. 16B). (Aka-jima Island and Tokashiki-jima Isl., Okinawa Pref.) ... ***X. keramae* sp. nov.**
- 12 Prefemoral process shorter or subequal to acropodite; ventrally at mid-length with a small triangular process (see Tanabe and Shinohara 1996: figs 13A, 16A). Colouration dark brown, with bright yellow paranotal edges (Fig. 17E, F). (Yaku-shima Isl., Kagoshima Pref.) ..... ***X. nikkoensis* (Chamberlin & Wang, 1953)**
- Prefemoral process longer than acropodite, twisted at the end, and with a tooth with wide base at its midlength; acropodite with a small lamella at tip (Figs 5A–C). Colouration pale yellowish, paranotal spots almost invisible (Fig. 16C). (Kume-jima Isl., Okinawa Pref.) ..... ***X. kumeensis* sp. nov.**
- 13 Male gonopod with 3 processes (prefemoral, femoral, and acropodite) **14**
- Male gonopod with only 2 processes (prefemoral and acropodite) ..... **15**
- 14 Prefemoral process long, straight, and slender, with pointed tip; femoral process close to acropodite, latter with median flange (see Tanabe and Shinohara 1996: figs 13C, D, 16C, D). Tsushima Isl., Iki Isl., and Danjo Isl. (Oshima and Meshima) (Nagasaki Pref., Kyushu) ..... ***X. shirozui* (Takakuwa, 1942)**
- Prefemoral process curved, acropodite blunt, with a third femoral process arising near the base (Fig. 14A–C). (Fukuoka Pref., Kyushu) ..... ***X. saltuosus* (Haga, 1968), comb. nov.**
- 15 Prefemoral process of gonopod much shorter than acropodite; the latter with long, needle-like median branch (see Tanabe and Shinohara 1996: fig. 13B) (Ehime Pref., Shikoku) ..... ***X. gracilipes* (Takakuwa, 1943)**
- Prefemoral process and acropodite subequal in length ..... **16**
- 16 Acropodite and prefemoral process very close to each other, parallel, wide, and sickle-shaped, strongly curved medially; latter sometimes with lateral or median branch (see Tanabe and Shinohara 1996: figs 12C, 15A-C). (Shizuoka Pref., Honshu) ..... ***X. tokaiensis* Tanabe & Shinohara, 1996**
- Prefemoral process and acropodite stand widely separated, without any branches, slender, straight, or only slightly curved ..... **17**
- 17 Prefemoral process large, bending away from shorter acropodite; both slender and gradually tapering toward tip (Fig. 7A–C). Body colour dark brown, with strong reddish orange paranotal spots (Fig. 16E) (Okinawa-jima Isl., Okinawa Pref.) ..... ***X. rebekae* sp. nov.**
- Both prefemoral process and acropodite sickle-shaped in mesal view; end of acropodite widening into a lobe (Fig. 9A–C). Body colour grey or dark brown, with strong reddish orange paranotal spots (Fig. 17A, B) (Okinawa-jima Isl. and Kouri-jima Isl., Okinawa Pref.) ..... ***X. variatus* (Pocock, 1895), comb. nov.**

## Discussion

We present a review of all the species of the genus *Xystodesmus* in East Asia. Based on the smaller body size, the characteristic colour pattern with orange paranotal spots of living specimens, and the gonopod conformation



**Figure 17.** Live habitus of *Xystodesmus millipedes* **A**, **B** *X. variatus* (Pocock, 1895) males, Kouri-jima Isl., Okinawa Pref. **C**, **D** *X. martensii* (Peters, 1864) males **C** Eno-shima Isl., Kanagawa Pref. **D** Mt. Oyama, Kanagawa Pref. **E**, **F** *X. nikkoensis* (Chamberlin & Wang, 1953) males, Yaku-shima Isl., Kagoshima Pref. Not to scale.

with additional branches as compared to the simple forceps-like gonopods of *Riukiaria*, we describe seven new species from the southern part of Japan, and move two species into the genus *Xystodesmus* (from *Fontaria* and *Rhysodesmus*). The new species from the Ryukyu Archipelago considerably extend the distribution range of the genus to the south. The Korean genus *Koreoaria* with its two species is also synonymised here with *Xystodesmus* on the same morphological basis, and they now represent the first members of the genus on the Asian continent. All the presently known 18 species of *Xystodesmus* are re-evaluated and redescribed. Most of them are illustrated with colour habitus photographs taken of live specimens, to facilitate field identification.

When examining fresh material and literature data, it is clear that, based on gonopodal morphology and molecular phylogenetics, the closest East Asian genus to *Xystodesmus* Cook, 1895 is *Riukiaria* Attems, 1938. Our study, in agreement with Tanabe and Shinohara (1996), showed that in addition to gonopodal characters, live colouration is also important in the separation of the two genera (Korsós 2017). As opposed to the simple, bifurcated, forceps-like gonopod shape observed in most species of *Riukiaria*, *Xystodesmus* species usually have a slightly more complicated forceps-like gonopod with additional branches and appendages. In addition, there is a tendency in body size differences between the two genera as well as other morphological differences, like the presence or absence of metatergal tubercles, and rounded or acute posterolateral corners of parantata. However, variability is high in the two closely related genera, and assignment of already preserved specimens to the appropriate genus based purely on these

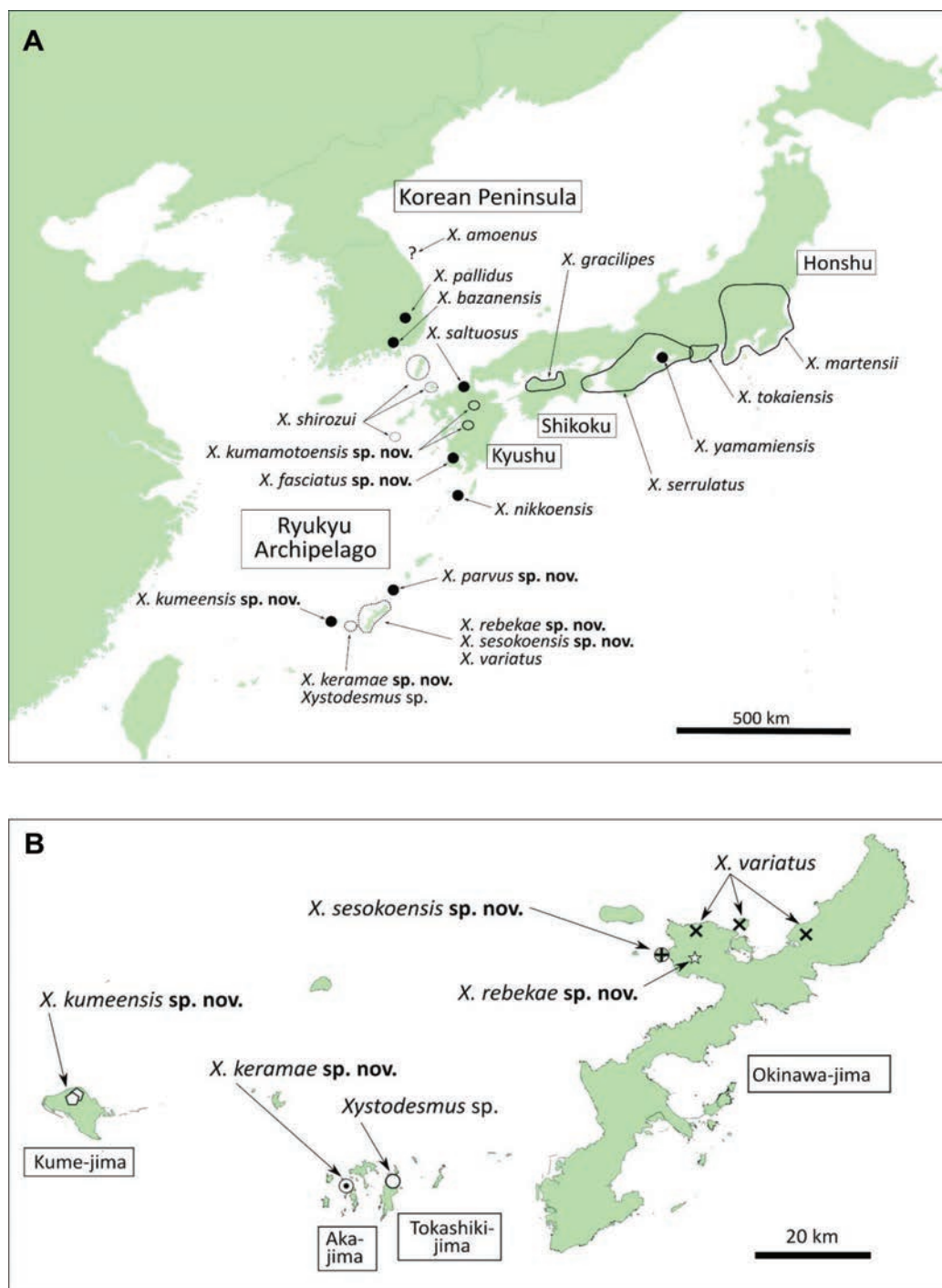


**Figure 18.** Distribution maps of *Xystodesmus* species dealt in this paper **A** map of Japan (Honshu, Shikoku, Kyushu, the Ryukyu Archipelago) and the Korean Peninsula, where species of *Xystodesmus* occur **B** map of the Okinawa Island Group with the occurrence of five *Xystodesmus* species.

traits is often remarkably difficult. With a long-standing experience of making field observations of hundreds of live specimens of East Asian xystodesmids, we noted a set of colour characters which seem quite stable and correspond to the generic assignments. The species of the genus *Xystodesmus* usually present uniformly brownish, greyish, or yellowish tergal colouration and lighter parano-ta, always with bright orange, yellow or pale whitish spots on them, and white legs and antennae whereas *Riukiaria* species are bright orange, yellow, or dark

metallic greenish tergal colouration often with dark spots or transverse bands, coloured or dark legs and antennae, and paranotal spots never orange. Recording and carefully describing the live colour patterns of East Asian xystodesmid species whenever possible might add valuable information to their taxonomy.

In the last part of the taxonomic section of their paper, Tanabe and Shinohara (1996) listed seven species which in their opinion possibly belong in *Xystodesmus*. These are *Rhysodesmus spinosissimus* Miyosi, 1952, *Riukiaria geniculata* (Takakuwa, 1941), *R. spiralipes* (Takakuwa, 1942), *R. variata* (Pocock, 1895), *Koreoaria pallida*, *K. amoena*, and *Pachydesmus bazanensis* Takakuwa, 1942. In the present study, *Riukiaria variata* and the two *Koreoaria* species are now assigned to *Xystodesmus*, but we have little to say about the remaining species. One exception, however, is *R. spiralipes* from Kume-jima Isl. which, according to freshly collected specimens, both in body size, colouration, and gonopod morphology agrees well with the generic characters of *Riukiaria* (and not *Xystodesmus*) as they are considered at the moment. The type material of the Takakuwa's and the Miyosi's species being supposedly lost, their exact status could only be settled with the investigation of new, topotypic specimens. *Pachydesmus bazanensis* was transferred to the newly erected genus *Nikkonus* by Chamberlin and Wang (1953), but without type material Tanabe and Shinohara (1996) maintained the combination, albeit *Pachydesmus* Cook, 1895 was excluded as it is a North American xystodesmid genus. Marek et al. (2014) already noticed that because of the body shape and colour described, and the type locality (Masan or Bazan, South Korea), it could be a member of *Xystodesmus*, most probably similar to *X. amoenus* comb. nov., also from the Korean Peninsula.

With respect to the phylogenetic relationship of *Xystodesmus* based on molecular genetic studies, only a few attempts were made. Nakamura and Korsós (2011) presented a maximum likelihood tree with 1063 base pairs of mitochondrial 16S rRNA (part), tRNA-Val, and 12S rRNA (part) genes, and found that *Riukiaria* (15 species) and *Xystodesmus* (9 species) are separated at 85% and 77% confidence levels (1000 bootstrap replicates). Only one species of *Riukiaria* (cf. *bifida* Takakuwa, 1942), and one of *Xystodesmus* (*fasciatus* sp. nov. in the present paper) were misplaced into the other generic group according to this research (Nakamura and Korsós 2011). In the phylogenetic study of Means et al. (2021b), based on four mitochondrial and two nuclear gene fragments, *Riukiaria* (11 species) and *Xystodesmus* (3 species) were shown to be sister taxa, and also separated from each other and other genera under the tribe Xystodesmini, subfamily Xystodesminae (Means et al. 2021b: fig. 2).

The Ryukyu Archipelago is a subtropical biodiversity hotspot, with many endemic life forms confined to a single or closely connected islands (Otsuka et al. 2000; Government of Japan 2019). The current geographical pattern of terrestrial vertebrates, especially amphibians and reptiles, indicates a strong influence of the formation in geohistory of the archipelago, dividing it into several well-separated island groups (Ota 2000). Millipedes of the family Xystodesmidae are blind soil-dwelling arthropods with limited dispersal ability, thus providing a good potential for historical biogeographical studies. An attempt was already made to consider the geographical distribution of North American xystodesmids (90 species of 20 genera) as an accurate predictor of their evolutionary history (Means and Marek 2017). Their hypothesis was that "geographical proximity may instead be a better predictor of evolutionary relationship than

morphology, especially since gonopodal anatomy is extremely divergent and similarities may be masked by evolutionary convergence” (Means and Marek 2017). Their results showed a high degree of morphological convergence in male gonopod shape, and although Euclidean geographical distance was not found to be a better predictor of evolutionary relationship using molecular topology, they concluded that gonopod characters should be viewed critically. When comparing North American to East Asian xystodesmid species, especially to *Xystodesmus* and *Riukiaria*, the similarities in both body shape, colour, and gonopod conformations are striking. One without knowledge of the origins of the samples could easily erroneously assign specimens into the opposite genera, as happened in the past with *Rhysodesmus* and *Pachydesmus*, both now being exclusively New World genera. However, recent molecular genetic studies show, with increasing confidence, that these morphological similarities are clearly the result of homoplasy (Means et al. 2021a, 2021b). A detailed investigation based on a wide taxon sampling in East Asia would certainly be worthwhile to clarify the evolutionary history of the species in the genera *Xystodesmus* and *Riukiaria* with respect to their narrow geographical distribution.

## Acknowledgements

We would like to express our sincere gratitude to Prof. H. Ota (Institute of Natural and Environmental Sciences, University of Hyogo, and the Museum of Nature and Human Activities) and M. Toda (Tropical Biosphere Research Center, University of the Ryukyus, Okinawa) for accelerating taxonomical studies on millipedes in the Ryukyus by inviting ZK for a research period. T. Tanabe (Kumamoto University, Japan) continuously followed our study with attention, and greatly helped with the preparation of manuscript. He also provided the specimens for one of the new species. E. Lazányi (HNHM) helped with the literature and registration codes for her museum; J. Beccaloni (NHMUK) and S. Friedrich (ZSMC) kindly arranged the loan of the holotypes of *Fontaria variata* and *Koreoaria pallida*, respectively. H. Ono (NSMT) provided comparative xystodesmine material from the collection under his care. We are indebted to M. Nakano (Kumamoto City), T. Menda (Culture Promotion Division of Kumamoto Prefectural Government), and T. Iihoshi (Kumamoto City) for collecting *X. kumamotoensis* specimens, and to K. Yahata (University of Tsukuba) for sending additional material of *X. variatus*. We would like to thank W. A. Shear (Hampden-Sydney, USA), and the late R. L. Hoffman (Radford, USA) and R. M. Shelley (NCSM, Raleigh, USA) who gave helpful comments to an earlier version of the manuscript. We are grateful to J. Means (VMNH) for his linguistic corrections and useful comments on the manuscript, and the reviewer P. Marek (Virginia Tech, xxx). N. Akkari (Natural History Museum Vienna) as subject editor of ZooKeys also provided many useful suggestions to improve the manuscript.

## Additional information

### Conflict of interest

The authors have declared that no competing interests exist.

### Ethical statement

No ethical statement was reported.

## Funding

ZK's study was supported by the Hungarian Research Fund (OTKA No. 69235).

## Author contributions

Conceptualization: ZK. Data curation: YN. Formal analysis: YN, ZK. Investigation: ZK. Methodology: ZK. Project administration: ZK. Validation: ZK.

## Author ORCIDs

Zoltán Korsós  <https://orcid.org/0000-0003-1545-5086>

## Data availability

All of the data that support the findings of this study are available in the main text.

## References

- Attems C (1938) Polydesmoidea II. Fam. Leptodesmidae, Platytrachidae, Oxydesmidae, Gomphodesmidae. In: Das Tierreich. Lief. 69, Walter de Gruyter and Co., Berlin and Leipzig, 487 pp.
- Chamberlin RV, Wang YM. (1953) Records of millipeds (Diplopoda) from Japan and other oriental areas, with descriptions of new genera and species. American Museum Novitates 1621: 1–13.
- Chao J-L, Chang H-W (2008) Neotype designation for two centipedes, *Scolopocryptops curtus* (Takakuwa, 1939) and *Cryptops nigropictus* Takakuwa, 1936, and a review of species of Scolopendromorpha (Chilopoda) in Taiwan. Collection and Research 21: 1–15. <https://libknowledge.nmns.edu.tw/nmns/upload/bulletin/000000177/209000c/200812-1.pdf>
- Cook OF (1895) The Crapedosomatidae of North America. Annals New York Academy of Science 9: 1–180. <https://doi.org/10.1111/j.1749-6632.1896.tb55430.x>
- Government of Japan (2019) Nomination of Amami-Oshima Island, Tokunoshima Island, Northern Part of Okinawa Island, and Iriomote Island for inscription on the World Heritage List. Government of Japan, Tokyo, 382 pp. <https://kyushu.env.go.jp/okinawa/amami-okinawa/en/world-natural-heritage/plan/pdf/a-1-e.pdf>
- Haga A (1968) [Japanese Millipedes]. Private publication, 11 pp. [in Japanese]
- Hoffman RL (1949) A new genus of xystodesmid millipeds from the Riu Kiu Archipelago with note on related Oriental genera. Natural History Miscellanea 45: 1–6.
- Hoffman RL (1956) Studies on some Oriental xystodesmine millipeds. Proceedings of the Entomological Society of Wasington 58(2): 95–104.
- Hoffman RL (1958) Revision of the millipede genus *Pachydesmus* (Polydesmida: Xystodesmidae). Proceedings of the United States National Museum 108(3399): 181–218. <https://doi.org/10.5479/si.00963801.108-3399.181>
- Hoffman RL (1980) Classification of the Diplopoda. Museum d'Histoire Naturelle, Geneve, 237 pp.
- Huerta-de la Barrera IE, Bueno-Villegas J, Means JC, Cupul-Magaña, FG (2021) Redescription of *Rhysodesmus dasypus* (Gervais, 1847), the type species of the genus (Polydesmida: Xystodesmidae). Zootaxa 5040(1): 66–76. <https://doi.org/10.11646/zootaxa.5040.1.3>
- Ikehara S, Shimojana M (1971) The terrestrial animals of the Senkaku Islands. In: Ikehara S (Ed.) Survey Report on the Senkaku Islands. University of the Ryukyus, Naha, 85–114. [in Japanese with English summary]

- Korsós Z (2017) Does colouration matter? Taxonomical comparison of *Xystodesmus* and *Riukiaria* millipede species (Diplopoda: Xystodesmidae). In: Abstract, 17<sup>th</sup> International Congress of Myriapodology, 23–26 July 2017, Maritime Park and Spa Resort, Krabi, Thailand, Tropical Natural History 5(Supplement): 5.
- Korsós Z, Nakamura Y, Tanabe T (2011) Two new millipede species of the genus *Riukiaria* (Diplopoda, Polydesmida, Xystodesmidae) endemic to the Ryukyu Archipelago, Japan. *Zootaxa* 2877: 55–68. <https://doi.org/10.11646/zootaxa.2877.1.3>
- Kurita K, Ota H, Hikida T (2017) A new species of *Plestiodon* (Squamata: Scincidae) from the Senkaku Group, Ryukyu Archipelago, Japan. *Zootaxa* 4254(5): 520–536. <https://doi.org/10.11646/zootaxa.4254.5.2>
- Marek PE, Tanabe T, Sierwald P (2014) A species catalog of the millipede family Xystodesmidae (Diplopoda: Polydesmida). Virginia Museum Natural History Publications 17: 1–117. [https://www.vmnh.net/content/vmnh/uploads/PDFs/research\\_and\\_collections/special\\_publications/vmnhspecialpub17.pdf](https://www.vmnh.net/content/vmnh/uploads/PDFs/research_and_collections/special_publications/vmnhspecialpub17.pdf)
- Masuda K (2001) A new xystodesmid millipeds of the genus *Xystodesmus* from Japan. Kumo, [Bulletin of] Chubu Spider Study Group 34: 635–636.
- Means JC, Marek PE (2017) Is geography an accurate predictor of evolutionary history in the millipede family Xystodesmidae? *PeerJ* 5: e3854 <https://doi.org/10.7717/peerj.3854>
- Means JC, Hennen DA, Marek PE (2021a) A revision of the minor species group in the millipede genus *Nannaria* Chamberlin, 1918 (Diplopoda, Polydesmida, Xystodesmidae). *ZooKeys* 1030: 1–180. <https://doi.org/10.3897/zookeys.1030.62544>
- Means JC, Hennen DA, Tanabe T., Marek PE (2021b) Phylogenetic systematics of the millipede family Xystodesmidae. *Insect Systematics and Diversity* 5(2): 1–26. <https://doi.org/10.1093/isd/ixab003>
- Minato H (1973) Myriapods of the Danjo Islands. In: Nagasaki Biological Society (Ed.) Fauna and flora of the Danjo Islands (Reports of the Nagasaki Biological Society Expedition to the Danjo Islands). Nagasaki Biological Society, Nagasaki, 127–128. [in Japanese]
- Miyosi Y (1952) Beiträge zur Kenntnis japanischer Myriopoden. 4. Aufsatz: Ueber eine neue Art und eine neue Unterart von Diplopoda. *Zoological Magazine* 61(9): 281–282. [in Japanese with German summary]
- Miyosi Y (1959) Über japanische Diplopoden. *Arachnological Society of East Asia, Spec. Number*, Osaka, 233 pp. [in Japanese, with German summary]
- Murakami Y (1965) Postembryonic development of the common Myriapoda of Japan XX. On new species of *Phruodesmus* (Diplopoda; Leptodesmidae) and *Lithobius* (Chilopoda; Lithobiidae). *Zoological Magazine* 74: 165–169. [in Japanese with English summary] <https://doi.org/10.34435/zm004214>
- Nakamura Y, Korsós Z (2010) Distribution and diversity of millipedes of the Ryukyu Archipelago, with the Senkaku and Daito Island Groups: A literature review (Arthropoda: Diplopoda). *Acta Arachnologica* 59(2): 73–86. <https://doi.org/10.2476/asjaa.59.73>
- Nakamura Y, Korsós Z (2011) [Phylogenetic relationships among *Riukiaria* and its sister genera *Yaetakaria* and *Xystodesmus* (Diplopoda: Polydesmida: Xystodesmidae) based on mtDNA sequences, and their taxonomical revision.] In: Naruse T, Fujita Y (Eds) Abstracts of the 47<sup>th</sup> Annual Meeting of the Japanese Society of Systematic Zoology, University of the Ryukyus, Okinawa, Japan, 57 pp. [in Japanese]
- Ota H (1998) Geographic patterns of endemism and speciation in amphibians and reptiles of the Ryukyu Archipelago, Japan, with special reference to their paleogeog-

- graphic implications. *Researches on Population Ecology* 40(2): 189–204. <https://doi.org/10.1007/BF02763404>
- Ota H (2000) The current geographic faunal pattern of reptiles and amphibians of the Ryukyu Archipelago and adjacent regions. *Tropics* 10(1): 51–62. <https://doi.org/10.3759/tropics.10.51>
- Otsuka H, Ota H, Hotta M (2000) International Symposium. The Ryukyu Islands. The arena of adaptive radiation and extinction of island fauna. *Tropics* 10(1): 1–242.
- Peters W (1864) Übersicht der im Königl. zoologischen Museum befindlichen Myriopoden aus der Familie der Polydesmi, so wie Beschreibungen einer neuen Gattung, *Trachyjulus*, der Juli, und neuer Arten der Gattung Siphonophora. *Monatsberichte der Königlichen Preussischen Akademie der Wissenschaften zu Berlin*, 529–551.
- Pocock RI (1895) Report upon the Chilopoda and Diplopoda obtained by P. W. Bassett-Smith, Esq., Surgeon R. N., and J. J. Walker, Esq., R. N., during the cruise in the Chinese Seas of H. M. S. 'Penguin', Commander W. U. Moore commanding. *Annals and Magazine of Natural History Ser. 6*, 15: 346–372. <https://doi.org/10.1080/00222939508677895>
- Shelley RM, Smith JM (2018) Expanded concept and revised taxonomy of the milliped family Xystodesmidae Cook 1895 (Polydesmida: Leptodesmidea: Xystodesmoidea): Incorporations of Euryuridae Pocock 1909 and Eurymerodesmidae Causey 1951, taxon revivals/proposals/transferrals, and a distributional update. *Insecta Mundi* 0660: 1–41.
- Shinohara K (1977) [Revaluation on Riukiaria Diplopoda]. *Acta Arachnologica* 27: 115–119. [in Japanese with English synopsis] [https://doi.org/10.2476/asjaa.27.Specialnumber\\_115](https://doi.org/10.2476/asjaa.27.Specialnumber_115)
- Sierwald P, Reft AJ (2004) The millipede collections of the world. *Fieldiana: Zoology (N.S.)* 103: 1–100.
- Takakuwa Y (1942a) Einige neue Arten von Diplopoda aus Nippon. *Zoological Magazine, Tokyo* 54(6): 237–239.
- Takakuwa Y (1942b) Die Myriopoden von Formosa, Philippinien, u. s. w. *Transactions of the Natural History Society of Formosa* 32(231): 359–367.
- Takakuwa Y (1943) Die drei neue Diplopoden aus Taiwan und Westnippon. *Transactions of the Natural History Society of Formosa* 33(242–243): 603–607.
- Takakuwa Y (1954) [Diplopoden aus Japan und ihn angrenzenden Gebieten]. *Japan Society for the Promotion of Science, Tokyo*, 241 pp. [in Japanese]
- Tanabe T (1994) The milliped genus *Levizonus* (Polydesmida, Xystodesmidae) in Japan. *Japanese Journal of Entomology* 62(1): 101–113. <https://dl.ndl.go.jp/pid/10654646/1/1>
- Tanabe T, Shinohara K (1996) Revision of the millipede genus *Xystodesmus*, with reference to the status of the tribe Xystodesmini (Diplopoda: Xystodesmidae). *Journal of Natural History* 30(10): 1459–1494. <https://doi.org/10.1080/00222939600770831>
- Verhoeff KW (1937) Zur Kenntnis ostasiatischer Diplopoden. *Zoologischer Anzeiger* 117(11/12): 309–321.

# Three new species of torrent treefrogs (Anura, Hylidae) of the *Hyloscirtus bogotensis* group from the eastern Andean slopes and the biogeographic history of the genus

Andrea Varela-Jaramillo<sup>1,2,3</sup>, Jeffrey W. Streicher<sup>4</sup>, Pablo J. Venegas<sup>1,5,6</sup>, Santiago R. Ron<sup>1</sup>

1 Museo de Zoología, Escuela de Biología, Facultad de Ciencias Exactas, Naturales y Ambientales, Pontificia Universidad Católica del Ecuador, Av. 12 de Octubre y Roca, Aptdo. 17-01-2184, Quito, Ecuador

2 3Diversity, Santo Domingo Oe5-71 y Cuba, Quito, Ecuador

3 Institute of Biology, Molecular Evolution and Systematics of Animals, University of Leipzig, Talstrasse 33, 04103 Leipzig, Germany

4 Herpetology, Natural History Museum, Cromwell Road, London, SW7 5BD, United Kingdom

5 Rainforest Partnership, 4005 Guadalupe St., Austin, TX 78751, USA

6 Instituto Peruano de Herpetología (IPH), Augusto Salazar Bondy 136, Urb. Higuiereta, Surco, Lima, Peru

Corresponding author: Santiago R. Ron ([santiago.r.ron@gmail.com](mailto:santiago.r.ron@gmail.com))



Academic editor: Fedor Konstantinov

Received: 8 April 2024

Accepted: 12 January 2025

Published: 13 March 2025

ZooBank: <https://zoobank.org/DAE3FB4E-155F-4529-856D-12732CB58D1D>

**Citation:** Varela-Jaramillo A, Streicher JW, Venegas PJ, Ron SR (2025) Three new species of torrent treefrogs (Anura, Hylidae) of the *Hyloscirtus bogotensis* group from the eastern Andean slopes and the biogeographic history of the genus. ZooKeys 1231: 233–292. <https://doi.org/10.3897/zookeys.1231.124926>

**Copyright:** © Andrea Varela-Jaramillo et al.  
This is an open access article distributed under terms of the Creative Commons Attribution License (Attribution 4.0 International – CC BY 4.0).

## Abstract

The *Hyloscirtus bogotensis* group contains 17 species of treefrogs from the tropical Andes and Central America. A taxonomic review of the Amazonian clades of this group is presented based on DNA sequences of nuclear and mitochondrial DNA and a preliminary phylogenomic analysis of ultraconserved elements, as well as morphological, bioacoustic, and environmental characters. Additionally, the role of the Andes in the diversification of the genus *Hyloscirtus* is explored by reconstructing their ancestral basin (Amazon, Pacific, Caribbean). Our integrative analysis indicates the existence of eight undescribed candidate species within the group. Three of those species are described, previously masked within *H. albopunctulatus*, *H. phyllognathus*, and *H. torrenticola*. A lectotype is also designated for *Hyla albopunctulata*. The new evidence suggests that neither *Hyloscirtus phyllognathus* nor *H. torrenticola* occur in Ecuador. The new species, *H. elbakyanae* **sp. nov.**, *H. dispersus* **sp. nov.**, and *Hyloscirtus maycu* **sp. nov.** differ from other members of the group in bioacoustics and external morphology. The most useful diagnostic characters among species were advertisement calls. In contrast, skin coloration is highly variable intraspecifically and, as a result, of low diagnostic value. High variation in color is partly a result of phenotypic plasticity. Our biogeographic reconstructions indicate that the Andean barrier influenced the diversification of *Hyloscirtus*. Since the early Oligocene, there have been only four colonization events across the Andes, between the Pacific and Amazon basins. Two of those events occurred more than 14 Mya, when most of the tropical Andes were below 3000 m. Species in the highland *H. larinopygion* group are younger, suggesting recent diversification as high montane forests and paramo habitats emerged.

**Key words:** Amazon Basin, Andes, biogeography, Chocó, Peru, phenotypic plasticity, phylogenomics, phylogeny, speciation, ultra-conserved elements

## Introduction

There are more than 8800 amphibian species in the world (AmphibiaWeb 2024); however, many of them remain undescribed, especially in the tropics. Andean and Amazonian frog biodiversity remains severely underestimated due to cryptic diversity, where morphologically similar individuals actually represent multiple species (Funk et al. 2012). Several DNA-based studies using mitochondrial, nuclear, and genomic data have provided evidence that cryptic diversity is common in the Andes and Amazon region (Caminer et al. 2017; Nascimento et al. 2019; Páez and Ron 2019; Chasiluisa et al. 2020; Guillory et al. 2020) – proof that sustain scientists' perseverance to unveil their real biodiversity.

The Andean genus *Hyloscirtus* Peters, 1882 (Hylidae, tribe Cophomantini) originated ~ 30–40 Ma (Wiens et al. 2006; Duellman et al. 2016; Feng et al. 2017) and is distributed in the Andes of Venezuela, Colombia, Ecuador, Peru, and Bolivia with a few species reaching lowland rainforests in Central America, the Chocó region, and the Amazon basin (Rojas-Runjaic et al. 2018; Yáñez-Muñoz et al. 2021). Within *Hyloscirtus*, the *H. bogotensis* group currently contains 17 species that live associated with streams and riverine habitats, between 100–3600 m (Frost 2023; IUCN 2023). The monophyly of the group is mainly supported by molecular data, with 95 transformations in nuclear and mitochondrial proteins and ribosomal genes (Faivovich et al. 2005; Wiens et al. 2010). A mental gland, proposed to be involved in chemical communication during reproduction, is present in this group (Duellman 1972; Duellman et al. 1997); however, it is convergent in species of the *Hyloscirtus armatus* species group and other species of the tribe Cophomantini (Brunetti et al. 2015).

Amazonian members of the *Hyloscirtus bogotensis* species group have several unresolved taxonomic issues (Almendáriz et al. 2014; Villacampa-Ortega et al. 2017). Within this group, *Hyloscirtus phyllognathus* Melin, 1941, *H. albopunctulatus* Boulenger, 1882 and *H. torrenticola* Duellman & Altig, 1978 occur in the Amazon basin of Colombia, Ecuador, and Peru, between 410–2190 m (Frost 2023; Suppl. material 1: fig. S1). *Hyloscirtus phyllognathus* inhabits from the northern Amazonian slopes of Cordillera Oriental of Colombia, continuing throughout the eastern Andes of Ecuador towards the southeast Andes of Peru. The type material was collected in Roque, San Martín Department, northern Peru (Melin 1941; Duellman 1972; Mueses-Cisneros 2005; Villacampa-Ortega et al. 2017). *Hyloscirtus albopunctulatus* occurs in the Amazon region of Ecuador and Peru towards the southeastern tip of the Amazon in Colombia. The type material was collected in Sarayacu, Provincia Pastaza, Ecuador (Boulenger 1882; Lynch 2005). *Hyloscirtus torrenticola* is distributed in the southeastern slopes of the Oriental Andes of Colombia and the northeastern slopes of the Andes of Ecuador. The type material was collected near El Pepino, Putumayo Department, Colombia (Duellman and Altig 1978; Yáñez-Muñoz and Reyes Puig 2008; Rivera-Correa 2016).

Many species of the *H. bogotensis* group have overlapping distribution ranges and are morphologically similar. As a result, their identification, based on morphological diagnosis from the literature, is problematic. For example, prior to Faivovich et al. (2006) taxonomic review, *H. albopunctulatus* was usually misidentified as *Boana nympha* (e.g., Duellman and Mendelson 1995). The scarce information available for *H. torrenticola* mentions few morphological differences to *H. phyllognathus* and is based mainly on tadpole morphology.

However, their songs are markedly different (Duellman and Altig 1978). Moreover, the phylogenetic affinities of these species are unknown, except for *H. phyllognathus* (Pyron and Wiens 2011; Almendáriz et al. 2014; Guayasamin et al. 2015; Duellman et al. 2016; Yáñez-Muñoz et al. 2021). Almendáriz et al. (2014), based on genetic data, report that Peruvian and Ecuadorian populations of *H. phyllognathus* are likely separate species (see also Rivera-Correa 2016). Additionally, Villacampa-Ortega et al. (2017) suggest that populations from the south of Peru are a different species. Guayasamin et al. (2015) highlight the genetic separation between populations from northern and southern Ecuador, all identified as *H. phyllognathus*. Therefore, given the taxonomic problems among Amazonian members of the *H. bogotensis* group, a large-scale population sampling and an integrative approach are needed to determine their true species limits, phylogenetic relationships, and geographic distribution.

Most species in the *Hyloscirtus bogotensis* species group inhabit the northern Andes, one of the most species-rich regions on earth (Rahbek et al. 2019). The causes for the high species richness of the northern Andes, and tropical mountains in general, are still enigmatic, a knowledge gap known as Humboldt's enigma (Rahbek et al. 2019). Biogeographic studies of densely sampled clades within Neotropical amphibians are scant (Crawford and Smith 2005; Wiens et al. 2006; Santos et al. 2009; Gonzalez-Voyer et al. 2011; Castroviejo-Fisher et al. 2014). Therefore, examining the diversification and biogeography of Andean clades, like *Hyloscirtus*, can help to understand why tropical mountains harbor so many species. Until now, the role of the Andes, as a barrier, in the diversification of *Hyloscirtus* has not been examined. In this paper, we investigate the phylogenetic relationships of treefrogs of the genus *Hyloscirtus* with emphasis on the Amazonian species of the *Hyloscirtus bogotensis* group. By using an integrative approach, we describe three new species and redefine the population content of *Hyloscirtus phyllognathus* and *H. albopunctulatus*. Additionally, we explore the ancestral geographic distribution and diversification history of the genus.

## Materials and methods

### Ethical statement

The procedures for handling specimens were conducted in full compliance with the guidelines for the management of live amphibians and reptiles in field and laboratory research (Beaupre et al. 2004; Esselstyn et al. 2008). Our research was conducted under collecting permits 001-11 IC-FAU-DNB/MA, 002-16 IC-FAU-DNB/MA, 003-17 IC-FAU-DNB/MA, 005-14 IC-FAU-DNB/MA, 005-2009-INVESTIGACIÓN-B-DPMS/MAE, 008-09 IC-FAU-DNB/MA, 011-2018-IC-FAU-DNB/MA, and 018-2016-IC-FLO-FAU-DPZCH-UPN-VS/M issued by the Ecuadorian Ministry of Environment.

### Molecular analyses

We extracted DNA from 93 samples of amphibian tissue (deposited at the QCAZ Museum at the Pontificia Universidad Católica del Ecuador) following standard phenol-chloroform extraction protocols (Sambrook et al. 1989). These samples belonged to individuals previously identified as *H. albopunctulatus* and

*H. phyllognathus*, mainly based on geographic location and some coloration patterns (e.g., specimens with large white spots in the dorsum and thick white tarsal folds were identified as *H. albopunctulatus*). However, these identifications were considered tentative as it was clear that the published diagnostic characters to differentiate *H. phyllognathus* from *H. albopunctulatus* were unreliable among Ecuadorian populations (SRR pers. obs.)

For Sanger sequencing, we used a standard polymerase chain reaction (PCR) to amplify three mitochondrial genes (12S ribosomal subunit gene, 16S ribosomal subunit gene [final ~ 320 bp], and NADH dehydrogenase 1 [ND1] + adjacent tRNAs) and two nuclear genes (proto-oncogene cellular myelocytomatosis [c-myc] and recombination activating gene 1 [RAG-1]), using primers listed in Goebel et al. (1999), Faivovich et al. (2005), Wiens et al. (2005), Wiens and Moen (2008), and Zhang et al. (2013). We followed amplification protocols from Goebel et al. (1999). Amplicons were sequenced by the MacroGen® sequencing team (Seoul, Korea).

We assembled forward and reverse sequences and visually inspected the trimmed and edited sequences with Geneious 9.1.2 software (Gene Matters Corp; Kearse et al. 2012). 321 newly generated sequences, from 93 individuals from Ecuador and Perú (one individual from nearby the *H. phyllognathus* type locality), are available in GenBank under accession numbers shown in Suppl. material 1: table S1. Additionally, we included 51 GenBank sequences, belonging to 47 individuals (available at <https://www.ncbi.nlm.nih.gov>), from Panamá, Venezuela, Colombia, Ecuador, Peru, and Bolivia. These sequences corresponded to all species of *Hyloscirtus* and were published by Faivovich et al. (2004); Darst and Cannatella (2004); Faivovich et al. (2005); Wiens et al. (2005, 2006); Elmer and Cannatella (2008); Coloma et al. (2012); Almendáriz et al. (2014); Guayasamin et al. (2015), and Rojas-Runjaic et al. (2018). As outgroup, we used species of *Boana* and *Dendropsophus* (Caminer and Ron 2014; Caminer et al. 2017) (see Suppl. material 1: table S1).

A total of 137 individuals were included in the study. We aligned the sequences using MAFFT Multiple Alignment with the algorithm LINS-i (Kato et al. 2002). We imported the alignments into Mesquite version 3.31 (Maddison and Maddison 2018) for final adjustments by hand. The final matrix had 3417 characters and 137 terminals and is available in Zenodo.org under DOI: 10.5281/zenodo.10733261.

We chose Maximum likelihood and Bayesian inference as optimality criteria because, unlike maximum parsimony, they allow the specification of models of substitution that capture well-known processes of DNA evolution (e.g., unequal rates among sites; Yang 2014). We used the software Partition Finder v. 2.1.1 (Lanfear et al. 2012) to identify the best partition strategy and best-fit model of nucleotide evolution for the dataset. The analysis was performed using the corrected Akaike Information Criterion (AICc). We also explored ModelFinder from IQ-Tree analysis. The preferred partitions found with their best substitution models for both searches are listed in Suppl. material 1: table S2.

We conducted Bayesian phylogenetic analyses in MrBayes 3.2.6 (Ronquist et al. 2012). The analysis involved four parallel runs of the Metropolis-coupled Monte Carlo Markov for 20 million generations. Each run had five chains with a temperature of 0.1 and was sampled every 1000 generations. Evolution models and partition strategies were applied according to the results from Partition Finder (see above). We used Tracer v. 1.6 (Rambaut et al. 2007) to

measure the convergence of independent runs and considered reached when the average standard deviation of split frequencies was  $< 0.05$  between runs and ESS values were higher than 200 for all parameters. For the consensus tree, we discarded 10% of the first trees as burn-in. We assessed the support in Bayesian trees using posterior probabilities derived from the final tree set. We carried out the Bayesian analyses at Cipres Science Gateway (available at <https://www.phylo.org>; Miller et al. 2010). We performed Maximum Likelihood analyses in IQ-Tree v. 1.6.8 (Nguyen et al. 2015; Trifinopoulos et al. 2016) using the partition schemes and best evolution models found by ModelFinder (see above) as implemented in IQ-Tree (TESTMERGE command; Kalyaanamoorthy et al. 2017) under the AICc criterion. A total of ten independent searches were run, looking for the best tree. Likelihood values of the searches were within 0.1 likelihood units, indicating convergence. We assessed the support using 100 bootstrap pseudoreplicates (-b 100 command).

We calculated genetic distances (uncorrected  $p$ -distances) using MEGA 5 (Tamura et al. 2011) for the 12S gene matrix; however, as the most widely used gene for species limits is 16S, we amplified 16S gene complete sequences (1388 kb) for the candidate species (see Suppl. material 1: table S3; Fouquet et al. 2007b).

Additionally, we sequenced nuclear ultra-conserved elements (UCEs) from a subset of 48 individuals (Suppl. material 1: table S1) to compare to the smaller (in terms of number of loci) mitochondrial and nuclear datasets. We followed a similar sequence capture protocol for anurans developed by Streicher et al. (2018), which uses the tetrapod probes of Faircloth et al. (2012) targeting 5060 UCE loci. We started with 200 ng/ $\mu$ L of double-stranded DNA (dsDNA) and built genomic shotgun libraries using New England Biolabs (NEB) reagents, including an initial fragmentation step with dsDNA fragmentase (NEB, M0348). Cleaning between all library construction steps (end-repair, a-tailing, ligation, size-selection, and enrichment) was performed with Serapure magnetic beads (Rohland and Reich 2012). We used the same custom adapters for the ligation step as Streicher et al. (2018). Size-selection of fragments between 200 and 500 base pairs was conducted using Blue Pippin (Sage Science) electrophoresis. The final PCR enrichment step included 12 cycles and libraries were amplified using TruSeq primers TS1 (5'-AGA TCG GAA GAG CAC ACG TCT GAA CTC CAG TCA C\*AT CTC GTA TGC CGTC TTC TGC TTG-3') and TS2 (5'-AGA TCG GAA GAG CGT CGT GTA GGG AAA GAG TGT AGA TCT CGG TGG TCG CCG TAT CATT-3') and a Phusion enzyme master mix (NEB, M0531). We conducted the final enrichment PCR as 15 equal replicates that were later pooled to avoid PCR biases. We confirmed successful genomic library construction with a 2200 Agilent Tape Station.

After genomic library construction, we used the MYbaits protocol (now Arbor Biosciences) for targeted sequence capture. To hybridize UCE probes with targeted *Hyloscirtus* DNA, we used a temperature of 65 C for 24 hours. We used Dynabeads (M-270 Streptavidin, Life Technologies) to isolate the biotinylated UCE probes. A post-capture enrichment PCR of 18 cycles was performed prior to sequencing using the same reagents as in the shotgun library construction. We confirmed a successful capture library construction with a 2200 Agilent Tape Station. Sequencing of the final UCE capture library was conducted using an Illumina NextSeq 500 and a paired end 2  $\times$  150 medium output kit at the NHMUK sequencing facility (London, UK).

We processed the UCE-capture data using the bioinformatics suite Phyluce v. 1.5.0 (Faircloth 2016). Briefly, this involved the removal of adapter contamination and low-quality bases with trimmomatic (Bolger et al. 2014), de novo assembly of contigs using Velvet 1.2.10 (Zerbino and Birney 2008), matching to UCE probe sequenced in Phyluce, and exportation of a concatenated alignment for phylogenomic analysis. We included previously generated UCE data (Streichler et al. 2018) for nine outgroup taxa, *Lepidobatrachus*, *Ceratophrys*, *Agalychnis*, *Phyllomedusa*, *Litoria*, *Boana*, *Dendropsophus*, *Hyla*, and *Scinax* (Suppl. material 1: table S1). To conduct phylogenomic analyses, we used RAxML 8.2.10 (Stamatakis 2014) using settings as described in Streicher et al. (2016). Given that allowing for missing data can improve phylogenetic support with UCEs (Streichler et al. 2016; Barrientos et al. 2021), we used a relatively high threshold for missing data (up to 80% missing data per taxon). We also ran a sensitivity test of missing data by inferring phylogenies for those samples with (1) > 200 UCEs enriched and (2) > 300 UCEs enriched. All bioinformatic analyses were conducted using the HPC server at NHMUK. The two phylogenomic data matrices generated are available on Zenodo.org under DOI: 10.5281/zenodo.14503491.

### Species limits and haplotype network

We used two criteria to determine the most likely number of species within the taxa of the *Hyloscirtus bogotensis* species group examined here, focusing on individuals assigned to *H. albopunctulatus* and *H. phyllognathus*, as described in Caminer and Ron (2020): (1) we applied a Poisson Tree Processes (PTP) model (Zhang et al. 2013) as implemented in the bPTP server (<http://species.h-its.org/ptp/>), and (2) we applied the Automatic Barcode Gap Discovery (ABGD) method (available at <https://bioinfo.mnhn.fr/abi/public/abgd>; Puillandre et al. 2012) using default parameters and the Kimura two-parameter distances. For both criteria, we used the available sequences for 12S. These analyses were also made for the 16S sequences to confirm the differentiation of our target species, but the results are based on the 12S matrix. To decrease the probability of committing a Type I error (i.e., incorrectly rejecting the null hypothesis of a group of individuals belonging to a single species), we chose the most conservative result between criteria 1 and 2; therefore, we adopted the result that found the lowest number of candidate species.

We also built a median joining network for the gene C-myc using the R package “pegas” (Paradis 2010). We interpreted the lack of haplotype sharing among candidate species as consistent with the hypothesis of their evolutionary independence. The aligned matrix for the haplotype network analysis is available in Zenodo.org under DOI 10.5281/zenodo.14935905

### Divergence times and ancestral area estimation

We used the software BEAST 2.6.6 (Bouckaert et al. 2019) to infer a time tree for *Hyloscirtus*. We analyzed the Sanger sequences matrix used for the ML phylogenetic searches, simplified into one terminal per species. The matrix was divided into five partitions under the models specified by PartitionFinder (see Results). We applied the relaxed exponential clock among branches and the rate for each branch was drawn independently from an underlying lognormal distribution with a Yule tree prior to speciation. Clock models and trees were linked among all

partitions. We used two secondary calibrations based on node ages estimated by Hime et al. (2021). The first node was the most recent common ancestor of *Boana* and *Hyloscirtus* at 33.3 My (node 494 in Hime et al. 2021: fig. S2), and the most recent common ancestor of *Hyloscirtus* and *Dendropsophus* at 50.0 My (node 481). The primary calibration points used by Hime et al. (2021) fall outside Hylidae. Therefore, our estimates should be interpreted with caution. The calibration points had a lognormal distribution prior with a  $\pm 1$  standard deviation. Because the ML analysis does not estimate branch divergence dates, it is less parameterized and should provide a better estimate of tree topology. Therefore, we enforced two topological constraints in BEAST to match the topology of the ML tree. The topological constraints were: (1) the monophyly of the *Hyloscirtus larinopygion* group, and (2) the monophyly of the *H. larinopygion* + *H. armatus* + *H. charazani* groups.

We conducted an ancestral area estimation aimed to explore the potential effect of the Andes as a vicariant barrier in the diversification of *Hyloscirtus*. The Andes separates two hydrographic basins, Amazon (east of the Andes) and Pacific (west of the Andes). We reconstructed the ancestral basin to determine the number of colonization events between basins. If the Andes are, in fact, a significant barrier, we expected a low number of events given that most species occur below 2000 m and, in the northern Andes, both basins have been separated by mountain passes higher than 2000 m for at least 20 Mya (Boschman 2021). Five species occurring in basins emptying in the Caribbean Sea were coded as “Caribbean” (*H. callipeza*, *H. jahni*, *H. japreria*, *H. lascinius*, and *H. platydactylus*). Ancestral basins were reconstructed as a discrete character with three states: (1) Pacific, (2) Amazon, and (3) Caribbean. For the reconstructions, we used “phytools” 2.0 R package (Revell 2024) under stochastic character mapping with three models: (1) Equal Rates, (2) Symmetric transition, and (3) All Rates Different (Harmon 2019). Central American species were coded as part of “Pacific” given the well-known biogeographic affinity between the Chocó and Central American amphibian communities (e.g., Lynch 1997; Ron 2000). Species distribution data was obtained from Anfíbios del Ecuador (Ron et al. 2022), AmphibiaWeb (2023), and the IUCN Red List website (IUCN 2023).

## Morphology

We examined 87 alcohol-preserved specimens of the Amazonian species of the *Hyloscirtus bogotensis* group available from Museo de Zoología (QCAZ) at Pontificia Universidad Católica del Ecuador and División de Herpetología at Centro de Ornitología y Biodiversidad (CORBIDI) in Peru. We also examined four syntypes of *Hyla albopunctulata* (syntypes BMNH 1880.12.5.159–162, 1880.12.5.230) deposited at the Natural History Museum, London (NHMUK). All type material of the new species is deposited at the QCAZ collection. Measured specimens are listed as Suppl. material 1: table S4 and belong to *H. albopunctulatus*, *H. phyllognathus* and the three new species described in this paper. We analyzed quantitative and qualitative morphological characters following the methodology and terminology described in Duellman (1970) and Duellman (2001). We measured ten characters using digital calipers ( $\pm 0.01$  mm): (1) snout-vent length (SVL); (2) head length (HL); (3) head width (HW); (4) eye diameter (ED); (5) tympanum diameter (TD); (6) tibia length (TL); (7) femur length (FEL); (8) foot length (FL); (9) interorbital distance (IOD); and (10) internarial distance (InD). The webbing

formula of hand and foot follows Savage and Heyer (1967) with modifications by Myers and Duellman (1982). Sex was determined by inspection of secondary sexual characters (e.g., mental gland, vocal slits, and vocal sac), and when in doubt, by gonadal inspection (presence of testes and ovaries/eggs). Raw morphometric data is available in Zenodo.org under doi: 10.5281/zenodo.14940291.

We also assessed 12 qualitative characters on preserved specimens, unless otherwise mentioned: (1) dorsal and ventral skin texture (smooth, finely granular or granular); (2) dorsal, ventral, and flank coloration; (3) snout (truncated to rounded) in dorsal and lateral views; (4) tympanum (conspicuous or inconspicuous); (5) mental gland (present or absent); (6) nuptial pads and projecting prepollex (present or absent); (7) ulnar, tarsal, and cloacal folds (conspicuous or inconspicuous); (8) calcar tubercle (absent or present), (9) pericloacal spots (ill-defined or well-defined); (10) ulnar and tarsal tubercles (present or absent); (11) subarticular and supernumerary tubercles (conspicuous or inconspicuous); and (12) webbing coloration in life. Coloration in life was obtained from digital photographs; for color terminology, we used the tool Name that Color (available in <https://chir.ag/projects/name-that-color/>).

We carried out a Principal Components Analysis (PCA) to quantitatively assess morphometric differences among species. To remove the effect of body size, the PCA was applied to the residuals of the linear regression between the SVL and the other morphometric variables. We applied a multivariate analysis of variance (MANOVA) to the residuals to test for morphometric differences between sexes for each species. Because we did not find significant differences, except for tibia length in *H. albopunctulatus*, we excluded this character and conducted the PCA combining data of both sexes – which benefited the analysis since our sample for females compared to males was small. We also excluded tympanum diameter because it was inconspicuous or difficult to measure in many specimens. We retained only components with eigenvalues > 1. Additionally, we ran pairwise comparisons of SVL measurements between species using Student t-tests. We used R statistical software for the analyses (RStudio Team 2023).

## Bioacoustics

Calls were recorded in the field with a Sennheiser K6 ME-67 directional microphone and an Olympus™ LS10 digital recorder. Calls are deposited in the audio archive of the Museo de Zoología QCAZ and are available through the Anfibios del Ecuador website (<https://bioweb.bio/>). We also analyzed calls available at The Cornell Lab of Ornithology website (<https://www.macaulaylibrary.org/>) of *Hyloscirtus phyllognathus* (eastern Ecuador) and *H. torrenticola* (type locality, southeastern Colombia: Putumayo Department, El Pepino, 1974), recorded by W. E. Duellman, M.S. Foster and R.W. McDiarmid. Additionally, we analyzed two calls of *Hyloscirtus phyllognathus* from Peru, CORBIDI 9590 from the Province of San Martín (geographically close to the type locality of the species) and CORBIDI 9976 (tissue QCAZ 60025) from the Province of Picota, recorded by PJV. The calls recorded by PJV were taken at 48 kHz, 24-bit, WAV format with a digital recorder Marantz PMD661MK2 and a unidirectional microphone Sennheiser ME64. We used the software Raven 1.5 (Charif et al. 2010) to analyze the calls. We obtained the measurements of spectral variables using a Fast Fourier Transformation (FFT) of 1024 points, a frequency resolution of 43.1 Hz, window type

Hann and filter bandwidth of 248 Hz. We measured the temporal variables on the oscillogram and spectral variables on the power spectrum. We followed the call-centered approach (uninterrupted units as calls whenever they are separated by longer silence intervals) and terminology for call parameters described in Köhler et al. (2017). Measured call variables were: (1) call duration: time from the beginning to the end of the call; (2) rise time of the call: time from the beginning of the call to the point of its maximum amplitude; (3) inter-call interval: time between the end of one call and the beginning of the next call; (4) dominant frequency of the call: frequency with the most energy, measured along the entire call; (5) fundamental frequency of the call: frequency with the most energy of the first harmonic of the call; and (6) frequency bandwidth of the call: the higher frequency at any point of the call minus the lowest frequency at any point of the call. If available, up to five calls were analyzed per individual to calculate an individual average. We conducted a Principal Components Analysis (PCA) to assess call differentiation among species. We included all acoustic variables measured in the analysis. For the PCA, we retained only components with eigenvalues > 1. We ran pairwise comparisons using Student t-tests to compare call durations and dominant frequencies between species. We used R statistical software for the analyses (RStudio Team 2023). Raw call data is available in Zenodo.org under doi: 10.5281/zenodo.14940291.

### Environmental data and conservation assessments

We characterized environmental conditions for known localities of each species by measuring eight bioclimatic variables at each locality using layers obtained from WorldClim (30s resolution; Hijmans et al. 2005). The choice of the eight bioclimatic variables was based on Menéndez-Guerrero and Graham (2013): (1) annual mean temperature – BIO1; (2) mean diurnal range (Mean of monthly (max temp – min temp)) – BIO2; (3) temperature seasonality – BIO4; (4) maximum temperature of warmest month – BIO5; (5) minimum temperature of the coldest month – BIO6; (6) annual precipitation – BIO12; (7) precipitation of warmest quarter – BIO18, and (8) precipitation of coldest quarter – BIO19. We obtained locality data from the QCAZ collection database. We also included the type locality for *Hyloscirtus torrenticola* (10.3 km west, by road, of El Pepino, Departamento Putumayo, Colombia, 1,440 m, 01°11'N, 76°41'W; Duellman and Altig 1978) and for its Ecuadorian record (2 km SSW, by road, of the Río Reventador, Provincia Napo, Ecuador, 1490 m, 00°11'S, 77°39'W; Duellman and Altig 1978); the type locality for *H. albopunctulatus* (based on our lectotype designation: Sarayacu, Provincia Pastaza, Ecuador, 1243 m, 01°43'48"S, 77°29'24"W; Ron et al. 2022) and the type locality of *H. phyllognathus* (17 km NE Tarapoto, Departamento San Martín, Perú, 850 m, 06°21'16.56"S, 76°14'4"W, Wiens et al. 2006). Two localities close to *H. phyllognathus* type locality were included (Catarata Ahuashiyacu, Departamento San Martín, Perú, 730 m, 06°30'0"S, 76°20'4.81"W and 35 km, road Tarapoto-Yurimaguas, Departamento San Martín, 594 m, Perú, 2°25'46.16"S, 76°16'3.65"W; CORBIDI). Additionally, we added another record of *H. phyllognathus* from Perú (Puesto de Control 15, Quebrada Mishquiyacu, Picota, Perú, 959 m, 6°56'26.81"S, 76°3'49.97"W; CORBIDI). We conducted a Principal Component Analysis

(PCA) for all the variables and retained only components with eigenvalues > 1. We ran pairwise comparisons using Student t-tests to compare habitat preferences between species. We used R statistical software for the analyses (RStudio Team 2023). Raw bioclimatic data is available in Zenodo.org under doi: 10.5281/zenodo.14940291.

We also assessed the Red List status of each species according to the IUCN Red List criteria (IUCN 2001). Geographic ranges were estimated using minimum convex polygons in QGIS software version 3.12.

## Results

### Phylogenetic analyses and biogeographic history

Maximum likelihood and Bayesian inference analyses resulted in similar topologies with incongruences only in clades with low support (Fig. 1). *Hyloscirtus* has two basally diverging clades, the *H. bogotensis* group and a clade including the *H. larinopygion*, *H. armatus*, and *H. jahni* species groups. Each species group had strong support in both analyses but weak support for relationships between groups, as previously reported (Coloma et al. 2012; Almendáriz et al. 2014; Guayasamin et al. 2015; Rojas-Runjaic et al. 2018; Ron et al. 2018). Amazonian members of the *Hyloscirtus bogotensis* group are part of two clades. One of them is composed predominantly by species from the Pacific basin and Central America, with a single Amazonian species (*H. albopunctulatus*). The other clade is composed predominantly by Amazonian species (Figs 1, 2), except for the basally diverging *H. lascinius* and *H. palmeri* (Caribbean, Pacific basin, and Central America).

Compared to previous phylogenomic studies, the sequence capture obtained a low coverage of UCEs among *Hyloscirtus* samples with the number of UCEs captured ranging from 9 to 1773 and an average of 585 UCEs captured per individual (Table 1). This low coverage may be explained by laboratory issues during the capture step; however, due to funding constraints we were unable to repeat the sequencing experiment to determine the exact cause. Nonetheless, the average available UCE data still number in the hundreds per individual making them relevant to species delimitation. It is important to note that because we did not have complete sample overlap with the concatenated matrix from Sanger sequencing, some of the clades predicted by the species delimitation could not be evaluated. Eleven of the samples had fewer than 200 UCEs captured, so they were excluded from the phylogenomic analysis (Table 1). The > 200 UCEs per taxon dataset contained 37 ingroup taxa, 2125 UCEs and had a concatenated length of 479755 base pairs. The > 300 UCEs per taxon dataset contained 31 ingroup taxa, 2230 UCEs and a concatenated length of 515965. The maximum likelihood trees for these analyses are presented as Fig. 3 and Suppl. material 1: fig. S2. In both phylogenies, four taxa had unexpected phylogenetic placements when compared to the concatenated Sanger dataset (Fig. 1), including QCAZ 55766 (*H. dispersus* sp. nov.), QCAZ 55526 (*H. palmeri*), QCAZ 40606 (*H. alytolylax*), and QCAZ 51332 (*H. alytolylax*). These unexpected placements were all associated with poorly supported branches (< 64 bootstrap support in the > 200 UCEs analysis; < 75 bootstrap support in the > 300 UCEs analysis, Suppl. material 1: figs S3, S4). As such, we removed these four taxa and re-ran the

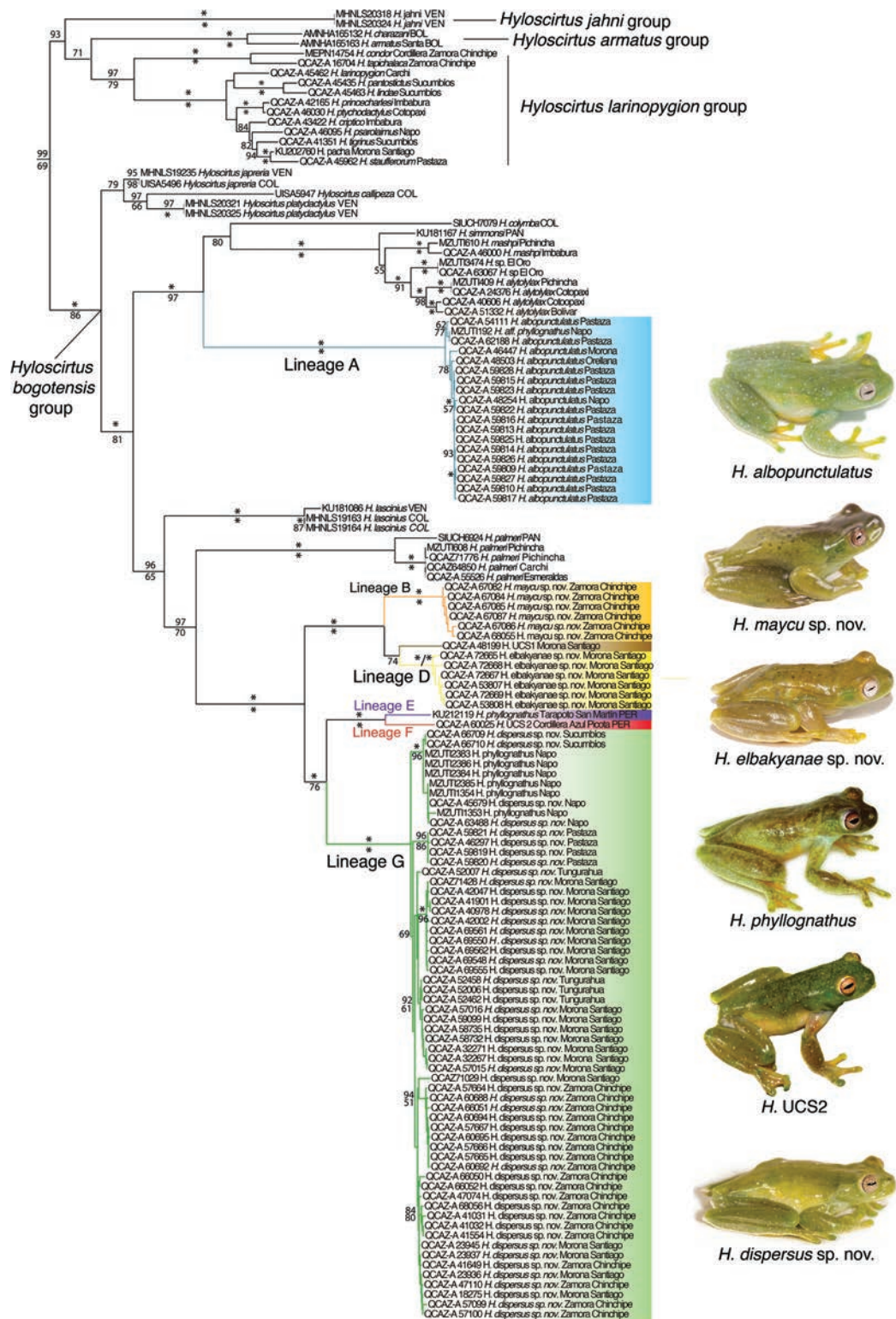


**Figure 1.** Maximum likelihood phylogram of *Hyloscirtus* for DNA sequences of mitochondrial (12S rRNA, 16S rRNA, ND1 and adjacent tRNAs) and nuclear genes (RAG1 and c-myc). Bayesian posterior probabilities (pp × 100) are shown above branches and bootstrap values below. Asterisks represent values of 100%. Missing values indicate posterior probabilities and bootstrap < 50. Amazonian species of the *H. bogotensis* group are shown with colored boxes. Outgroup species are not shown and include two species of *Boana* and two of *Dendropsophus* (Suppl. material 1: table S1). Voucher museum numbers are shown before the species name. For Ecuadorian populations, the province is provided after the species name. Abbreviations for other countries at the end of terminals: BOL (Bolivia), COL (Colombia), PAN (Panamá), PER (Perú), and VEN (Venezuela). UCS: unconfirmed candidate species. For locality data see Suppl. material 1: table S1.

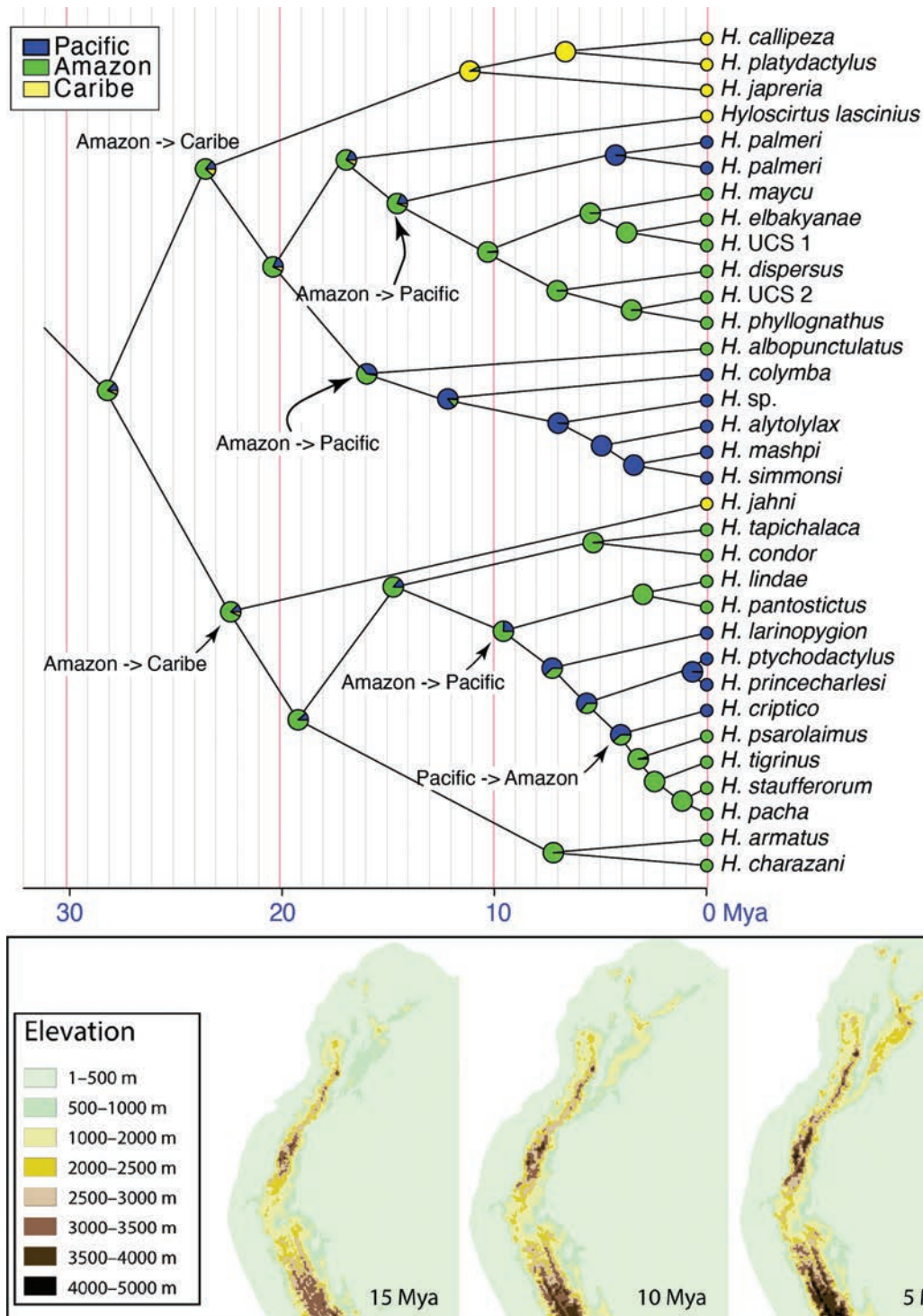


**Figure 2.** Time tree of *Hyloscirtus* species. Phylogeny based on Bayesian inferences with divergence time estimated in millions of years. One terminal per species is shown. Circles represent relative probabilities of ancestral distributions based on stochastic character mapping. Putative colonization events are shown with arrows. The maps below show an estimate of the elevation of the Andes, at the approximate times when trans-Andean colonizations took place (from Boschman 2021).

likelihood analyses in RAxML. The revised datasets contained 2207 and 2327 UCEs, for the > 200 and > 300 sets, respectively. The revised phylogenies from these datasets are presented as Fig. 3 (> 200 UCEs per taxon) and Suppl. material 1: fig. S2 (> 300 UCEs per taxon). Removing the four taxa improved branch support deep in the tree (but not for all shallow branches). When compared

**Table 1.** Quality metrics for *Hyloscirtus* UCE samples in this study include number of contigs, number of UCEs enriched, and its coverage per sample. See Suppl. material 1: table S1 for the locations of the *Hyloscirtus* species. The first 10 rows belong to the outgroup used for this analysis. The asterisks (\*) represent the samples included in the 200 UCEs phylogeny reconstructions after filtering for missing data. The sum symbol (+) are samples removed to reconstruct the phylogeny in Fig. 3 since they were problematic (see Results).

Species	Museum number	Contigs	UCEs	UCEs coverage (%)
<i>Dendropsophus leali</i>	SAMN 05559892	8555	1996	23.33
<i>Boana lanciformis</i>	SAMN 05559916	4949	1057	21.35
<i>Agalychnis callidryas</i>	SAMN 05559871	3105	1373	44.21
<i>Hyla cinerea</i>	SAMN 05559910	764	126	16.49
<i>Phyllomedusa tomopterna</i>	SAMN 05559926	564	134	23.75
<i>Litoria caerulea</i>	SAMN 05559920	30,118	1898	6.30
<i>Scinax catharinae</i>	SAMN 05559930	3413	1273	37.29
<i>Lepidobatrachus laevis</i>	SAMN 05559917	5814	2226	38.28
<i>Ceratophrys cornuta</i>	SAMN 05559887	40,359	1967	4.87
<i>Boana fasciata</i>	QCAZ48583	63434	137	0.22
<i>H. alytolylax</i>	QCAZ40606+	2885	326	11.30
<i>H. alytolylax</i>	QCAZ51332*	10309	609	5.91
<i>H. criptico</i>	QCAZ43422	2101	157	7.47
<i>H. staufferorum</i>	QCAZ45962*	3180	231	7.26
<i>H. palmeri</i>	QCAZ55526+	7208	487	6.76
<i>H. albopunctulatus</i>	QCAZ46447*	34921	403	1.15
<i>H. albopunctulatus</i>	QCAZ48254	763	86	11.27
<i>H. albopunctulatus</i>	QCAZ48503*	2814	213	7.57
<i>H. albopunctulatus</i>	QCAZ59813*	10318	687	6.66
<i>H. albopunctulatus</i>	QCAZ59814*	3215	310	9.64
<i>H. albopunctulatus</i>	QCAZ59815*	11085	581	5.24
<i>H. albopunctulatus</i>	QCAZ59816	147	22	14.97
<i>H. albopunctulatus</i>	QCAZ59817*	7194	423	5.88
<i>H. albopunctulatus</i>	QCAZ59822*	28247	998	3.53
<i>H. albopunctulatus</i>	QCAZ59823*	3182	237	7.45
<i>H. albopunctulatus</i>	QCAZ59826*	5216	322	6.17
<i>H. albopunctulatus</i>	QCAZ59827	105	9	8.57
<i>H. albopunctulatus</i>	QCAZ59828*	20251	957	4.73
<i>H. elbakyanae</i> sp. nov.	QCAZ53807*	63934	1699	2.66
<i>H. elbakyanae</i> sp. nov.	QCAZ53808*	7758	500	6.44
<i>H. dispersus</i> sp. nov.	QCAZ18275*	10234	893	8.73
<i>H. dispersus</i> sp. nov.	QCAZ23937	140	17	12.14
<i>H. dispersus</i> sp. nov.	QCAZ23945	189	26	13.76
<i>H. dispersus</i> sp. nov.	QCAZ40978*	22659	1016	4.48
<i>H. dispersus</i> sp. nov.	QCAZ41032*	7430	542	7.29
<i>H. dispersus</i> sp. nov.	QCAZ41649*	22281	1058	4.75
<i>H. dispersus</i> sp. nov.	QCAZ41901*	73651	1773	2.41
<i>H. dispersus</i> sp. nov.	QCAZ41951	128	17	13.28
<i>H. dispersus</i> sp. nov.	QCAZ42047*	3407	289	8.48
<i>H. dispersus</i> sp. nov.	QCAZ45679*	11175	711	6.36
<i>H. dispersus</i> sp. nov.	QCAZ47110*	4643	553	11.91
<i>H. dispersus</i> sp. nov.	QCAZ52006*	54758	1619	2.96

Species	Museum number	Contigs	UCEs	UCEs coverage (%)
<i>H. dispersus</i> sp. nov.	QCAZ52007	4	0	0
<i>H. dispersus</i> sp. nov.	QCAZ52458	1199	169	14.10
<i>H. dispersus</i> sp. nov.	QCAZ52462*	17787	936	5.26
<i>H. dispersus</i> sp. nov.	QCAZ57016*	17434	942	5.40
<i>H. dispersus</i> sp. nov.	QCAZ57099*	24843	968	3.90
<i>H. dispersus</i> sp. nov.	QCAZ57665*	7640	521	6.82
<i>H. dispersus</i> sp. nov.	QCAZ57666*	31536	1261	4.00
<i>H. dispersus</i> sp. nov.	QCAZ58735	253	43	17.00
<i>H. dispersus</i> sp. nov.	QCAZ59099*	4831	462	9.56
<i>H. dispersus</i> sp. nov.	QCAZ59819*	14063	281	2.00
<i>H. dispersus</i> sp. nov.	QCAZ59820*	2433	211	8.67
<i>H. dispersus</i> sp. nov.	QCAZ60692*	9358	621	6.64
<i>H. dispersus</i> sp. nov.	QCAZ60694*	49801	1554	3.12
<i>H. dispersus</i> sp. nov.	QCAZ60695*	22767	296	5.69
<i>H. UCS 2</i>	QCAZ60025*	17136	913	5.33

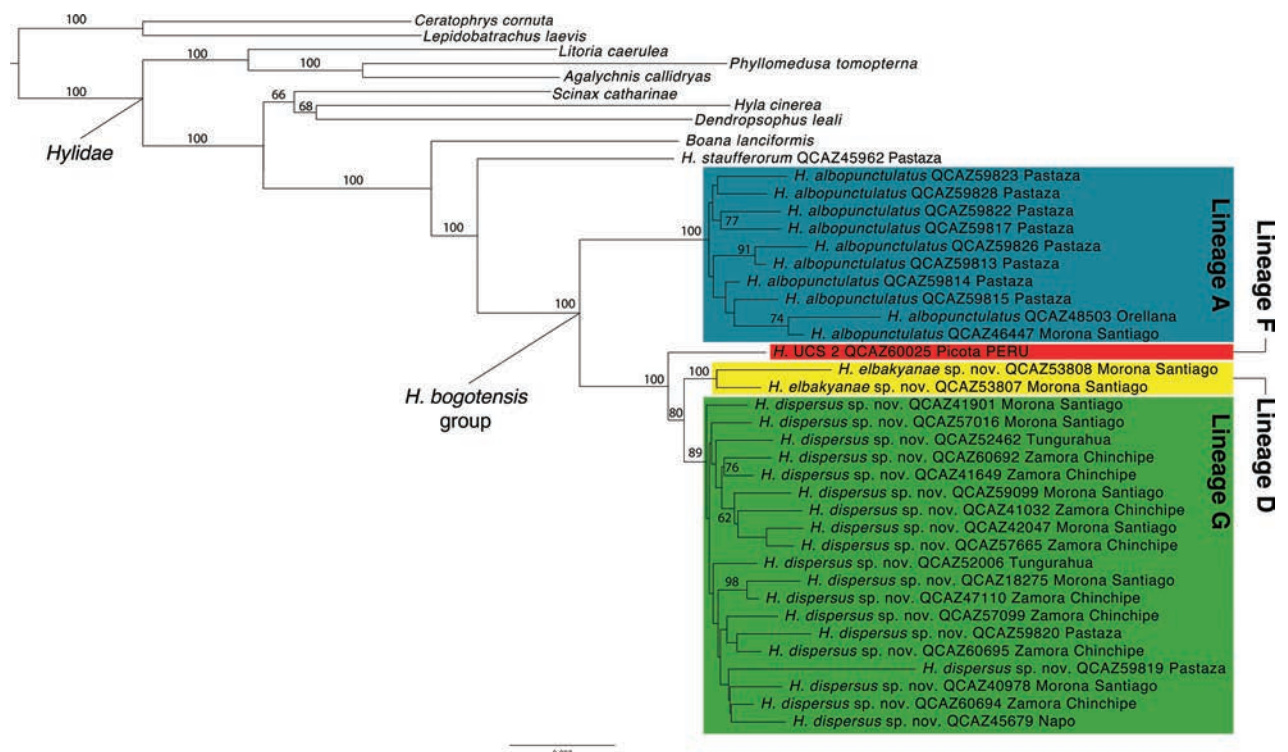


**Figure 3.** Best tree obtained under Maximum likelihood criterion when using taxa with more than 200 UCE loci enriched. Museum number of each individual is indicated. Numbers over the branches represent bootstrap values. Missing values indicate branch's support below 60. All samples within the *H. bogotensis* group belong to Ecuador except for QCAZ 60025 (clade F) from Perú.

to the Sanger mtDNA + nucDNA analysis (Fig. 1), the UCE-based phylogeny is broadly similar with strong support for the monophyly of *H. dispersus* sp. nov. (Lineage G), *H. elbakyanae* sp. nov. (Lineage D), and *H. albopunctulatus* (Lineage A), and the distinctiveness of Lineage F. *Hyloscirtus maycu* sp. nov. (Lineage B) was not part of this analysis because the specimens and tissues were collected a year after the UCE sequencing was completed.

Ancestral area estimation shows that the genus *Hyloscirtus* originated in the Amazon basin (Fig. 2). Divergence between the *H. bogotensis* group and its sister clade took place 28.5 Mya (high posterior density interval [95% HPD] = 21.6–35.0), in the early Oligocene (Fig. 2, Table 2). Diversification within the *H. bogotensis* species group started 23.8 Mya (95% HDP = 16.6–30.8). Overall, species from the highland clade, the *H. larinopygion* species group, are younger than those of the mid-elevation-lowland clade, the *H. bogotensis* species group (Fig. 2). While in the *H. larinopygion* group,  $\frac{3}{4}$  of the species are younger than 5 million years, in the *H. bogotensis* group, only  $\frac{1}{3}$  are. Two species pairs of the *H. larinopygion* group had recent speciation events, *H. pacha*-*H. staufferorum* (1.3 Mya) and *H. princecharlesi*-*H. ptychodactylus* (1.2 Mya). Within the *H. bogotensis* species group, the youngest species pair is *H. simmonsii*-*H. mashpi* (3.6 Mya).

Colonization events across the Andes, between the Pacific and Amazon basin, were infrequent in *Hyloscirtus*. During the 28 My of history of the *H. bogotensis* species group, there were only two events. Both events took place within a short period in the Miocene (14.8 and 16.2 Mya) and both were from the Amazon to the Pacific (Fig. 2). The other colonization events occurred in the higher elevation *H. larinopygion* species group. One event took place nearly 10 Mya from the Amazon to the Pacific basin. The other event is the most recent, at 4.2 Mya, and is the only event from the Pacific to the Amazon. Two events from the Amazon to the Caribbean basin are the most ancient in *Hyloscirtus* and took place ~ 20 Mya. There were no colonization events from the Caribbean to other basins. Interestingly, *H. palmeri* populations from Ecuador and Panama diverged 4.5 Mya, prior to the closure of the Panama isthmus. The favored model for ancestral reconstruction was Equal Rates (AIC = 56.7) followed by Symmetric Transition (58.8) and All Rates Different (61.9). Genetic distance analysis found divergences ranging from 3.7–14.8% for 12S and 5.0–14.8% for 16S (Table 3).

### Species limits

The species limits analyses support 19 candidate species within the *Hyloscirtus bogotensis* group according to the ABGD criteria and 21 candidate species according to the bPTP criteria (Suppl. material 1: figs S5, S6). Following our conservative rule, we propose 19 species for this group. Of these, 11 are named and eight are undescribed, representing a 72.7% increase in the number of species.

The available names for target candidate species are *Hyloscirtus albopunctulatus* (Boulenger, 1882), *Hyloscirtus phyllognathus* (Melin, 1941), and *Hyloscirtus torrenticola* (Duellman & Altig, 1978). Based on geographic location, species description, examination of the type material (Fig. 4A), and bioacoustic characteristics (e.g., differences in the rise time of the call and dominant frequency; see Table 4), we assign *Hyloscirtus albopunctulatus* sensu stricto to Lineage A (Fig. 1). We redescribe it and redefine its distribution range based on the new evidence.

Based on genetic, morphological (e.g., differences in head width and tibia length), bioacoustic (e.g., differences in call duration, distance between calls and dominant frequency), and geographic data (e.g., considering the distance of Peruvian populations) (see Table 4 and Suppl. material 1: table S5), we

**Table 2.** Node crown ages of representative *Hyloscirtus* clades in millions of years. For each node we show the estimated age with the 95% high posterior density interval (HDP).

Group/Clade/Species	Node age	95% HDP
	Age	
<i>H. armatus</i> group	7.45	1.44–14.97
<i>H. larinopygion</i> group	14.79	8.52–21.45
<i>H. bogotensis</i> group	23.84	16.64–30.80
( <i>H. colymba</i> + <i>H. alytolylax</i> + <i>H. mashpi</i> + <i>H. simmonsii</i> ) + <i>H. albopunctulatus</i>	16.22	9.81–22.5
( <i>H. maycu</i> sp. nov. + <i>H. elbakyanae</i> sp. nov. + <i>H. phyllognathus</i> + <i>H. dispersus</i> sp. nov.) + <i>H. palmeri</i>	14.79	9.14–20.80
( <i>H. callipeza</i> + <i>H. platydactylus</i> + <i>H. japreria</i> )	11.61	2.67–22.17
<i>H. phyllognathus</i> + <i>H. dispersus</i> sp. nov.	7.12	3.05–11.99
<i>H. alytolylax</i> + <i>H. mashpi</i> + <i>H. simmonsii</i>	4.99	1.77–8.70
<i>H. palmeri</i>	4.63	0.7–10.01
<i>H. phyllognathus</i>	3.6	0.77–7.11

**Table 3.** Pairwise genetic distances (uncorrected-p) between our target lineages of *Hyloscirtus*. *Hyloscirtus albopunctulatus* (Lineage A), *H. maycu* sp. nov. (Lineage B), *H. UCS 1* (Lineage C), *H. elbakyanae* sp. nov. (Lineage D), *H. phyllognathus* sensu stricto (Lineage E), *H. UCS 2* (Lineage F), and *H. dispersus* sp. nov. (Lineage G), based on sequences of 12S (below the diagonal) and 16S (above the diagonal). Mean and ± standard deviations are given with range in parentheses. Sequences of 16S were not available for Lineage E.

Lineage	A	B	C	D	E	F	G
<b>A</b>	–	0.131	0.160	0.131	–	0.127	0.153 ± 0.001 (0.151–0.155)
<b>B</b>	0.143 ± 0.002 (0.138–0.146)	–	0.147	0.051	–	0.117	0.128 ± 0.001 (0.123–0.129)
<b>C</b>	0.139 ± 0.001 (0.136–0.14)	0.046 ± 0.002 (0.043–0.049)	–	0.050	–	0.110	0.101 ± 0.002 (0.100–0.106)
<b>D</b>	0.129 ± 0.001 (0.125–0.131)	0.037 ± 0.001 (0.035–0.041)	0.039 ± 0.001 (0.037–0.041)	–	–	0.100	0.099 ± 0.009 (0.097–0.105)
<b>E</b>	0.127 ± 0.001 (0.127–0.131)	0.082 ± 0.001 (0.078–0.082)	0.074	0.069 ± 0.001 (0.127–0.131)	–	–	–
<b>F</b>	0.138 ± 0.002 (0.136–0.140)	0.074 ± 0.001 (0.072–0.076)	0.076	0.062 ± 0.001 (0.062–0.064)	0.039	–	0.089 ± 0.001 (0.086–0.090)
<b>G</b>	0.141 ± 0.002 (0.131–0.148)	0.099 ± 0.003 (0.092–0.109)	0.086 ± 0.001 (0.082–0.092)	0.083 ± 0.002 (0.078–0.094)	0.091 ± 0.002 (0.088–0.097)	0.084 ± 0.002 (0.082–0.090)	0.006 ± 0.004 (0.00–0.018)

conclude that *Hyloscirtus phyllognathus* sensu stricto is not distributed in Ecuador (see also Almendáriz et al. 2014). The ABGD and bPTP analyses indicate that Peruvian populations of “*Hyloscirtus phyllognathus*” represent two species (Lineages E and F). We tentatively assign *Hyloscirtus phyllognathus* sensu stricto to Lineage E as it is the closest to the type locality of the species (~ 50 km in a straight-line SSE of Roque, in San Martín, Perú). Advertisement calls of both lineages differ in dominant frequency and duration (Table 4). We could not make statistical comparisons as we only had one call per population. Likewise, morphological measurements of the individual of Lineage F overlap with the morphological space of individuals of Lineage E. More data is needed to confirm the assignment of Lineage E to *H. phyllognathus* and the status of Lineage F.

**Table 4.** Acoustic parameters comparing calls of *Hyloscirtus albopunctulatus* (Lineage A), *H. maycu* sp. nov. (Lineage B), *H. elbakayanae* sp. nov. (Lineage D), *H. phyllognathus* sensu stricto (Lineage E), *H. UCS 2* (Lineage F), *H. dispersus* sp. nov. (Lineage G) and *H. torrenticola* from type locality. Mean  $\pm$  SD is given with range in parentheses. Five calls were analyzed per individual.

Parameter	<i>H. albopunctulatus</i> (n = 7)	<i>H. maycu</i> sp. nov. (n = 1)	<i>H. elbakayanae</i> sp. nov. (n = 2)	<i>H.</i> <i>phyllognathus</i> sensu stricto (n = 1)	UCS 2 (n = 1)	<i>H. dispersus</i> sp. nov. (n = 13)	<i>H. torrenticola</i> sensu stricto (n = 2)
Series of calls	2 - > 70	10-13	4-13	3-4	3	1-8	3-4
Rise time of the call (s)	2.28 $\pm$ 0.80 (1.43-3.69)	0.832	0.57 $\pm$ 0.05 (0.53-0.60)	0.28	0.17	0.61 $\pm$ 0.50 (0.053-2.01)	0.16 $\pm$ 0.017 (0.148-0.173)
Call duration (s)	0.051 $\pm$ 0.005 (0.045-0.058)	0.053	0.06 $\pm$ 0.001 (0.055-0.057)	0.04	0.05	0.11 $\pm$ 0.015 (0.082-0.130)	0.03 $\pm$ 0.001 (0.026-0.028)
Inter-call duration (s)	0.30 $\pm$ 0.06 (0.17-0.35)	0.09	0.12 $\pm$ 0.007 (0.11-0.12)	0.06	0.05	0.33 $\pm$ 0.044 (0.270-0.440)	0.07 $\pm$ 0.007 (0.060-0.070)
Dominant frequency (Hz)	2149.84 $\pm$ 137.36 (1903.42-2309.0)	2343.8	2321.29 $\pm$ 127.86 (2230.88-2411.7)	2177.0	1851.9	2795.41 $\pm$ 138.68 (2573.05-3014.60)	2743.79 $\pm$ 48.22 (2709.60-2777.80)
Fundamental frequency (Hz)	1214.12 $\pm$ 184.71 (1068.72-1571.90)	1171.90	1184.35 $\pm$ 30.48 (1162.8-1205.9)	1974.6	1851.9	2700.63 $\pm$ 195.66 (2210.80-2924.20)	2743.75 $\pm$ 48.16 (2709.70-2777.80)
Bandwidth of the call (Hz)	378.51 $\pm$ 24.98 (344.5-421.9)	515.6	581.4 $\pm$ 91.36 (516.8-646)	372.5	416.3	359.06 $\pm$ 12.71 (343.1-383.85)	459.0 $\pm$ 36.06 (433.50-484.50)

The species description of *H. torrenticola* (Duellman and Altig 1978) and photographs of its type material (Fig. 4B) are inconclusive to enable differentiation of this species from other Amazonian group members. However, advertisement calls from its type locality indicate that it represents a species distinct from the other Amazonian lineages (e.g., differences in call duration and dominant frequency; see Table 4). Therefore, we do not assign *Hyloscirtus torrenticola* to any of the Amazonian lineages (A-G) included in our phylogeny.

Based on the assignments of the available binomials, we conclude that there are three new species that we describe below: Lineage B (*Hyloscirtus maycu* sp. nov.), Lineage D (*Hyloscirtus elbakayanae* sp. nov.) and Lineage G (*Hyloscirtus dispersus* sp. nov.). Lineage C is left undescribed because its single specimen, QCAZ 48199, is a juvenile. See Fig. 5 for the new species' geographic distribution. The haplotype network for the nuclear gene C-myc is consistent with the recognition of the three species as it shows that they lack shared haplotypes (Suppl. material 1: fig. S7).

### Morphological variation

Morphological variables from adult males and females are summarized in Suppl. material 1: table S5 and compared in Fig. 6. The morphometric PCA of 74 males and 17 females resulted in three principal components with an eigenvalue > 1, accounting for 63.3% of total variation. PC I was positively correlated with eye diameter and head width, PC II with foot length and internarial distance, and PC III with internarial distance and femur length (see Suppl. material 1: table S6). The morphometric space shows high overlap among all species, except for *H. phyllognathus* sensu stricto, between PC1 and PC2. Moreover, paired comparisons for SVL showed intra and interspecific differentiation (Fig. 7). There is sexual dimorphism as females are larger than males in *H. albopunctulatus* ( $t = 14.15$ ,  $df = 15$ ,  $p$ -value < 0.01), *H. dispersus* sp. nov. ( $t = 7.23$ ,

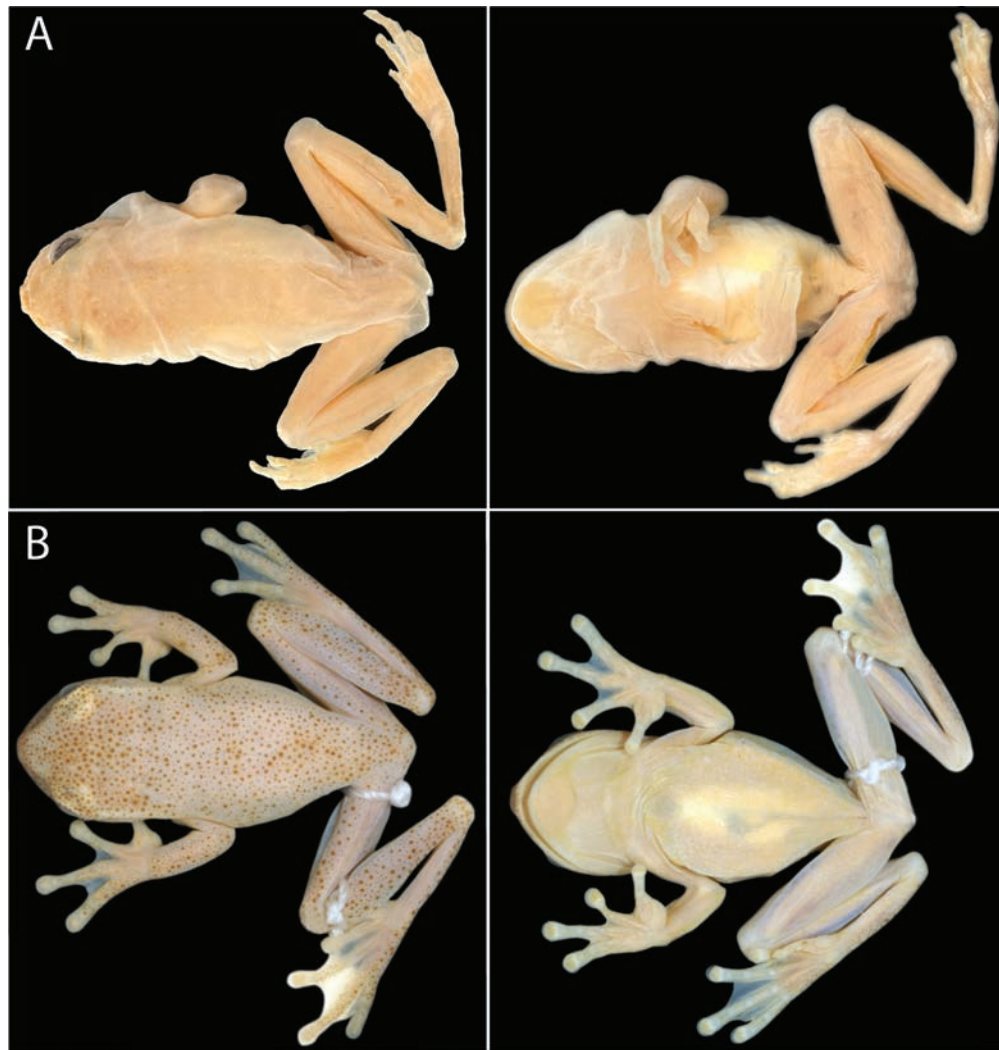


**Figure 4.** Photographs of the type material of *Hyloscirtus albopunctulatus* and *H. torrenticola* species **A** dorsal and ventral views of the lectotype of *H. albopunctulatus* BMNH 1880.12.5.230 **B** dorsal and ventral views of the holotype of *H. torrenticola* KU 16957. Photographs by JWS (**A**) and Martín R. Bustamante (BIOWEB archive) (**B**).

df = 11,  $p$ -value < 0.01) and *H. maycu* sp. nov. ( $t = 7.78$ , df = 2,  $p$ -value = 0.01); females of *H. elbakyanae* sp. nov. and *H. phyllognathus* are unknown. Among species, females of *H. albopunctulatus* are smaller than those of *H. dispersus* sp. nov. ( $t = -4.27$ , df = 11,  $p$ -value = 0.001). Males of *H. elbakyanae* sp. nov. are larger than males of *H. albopunctulatus*, *H. maycu* sp. nov. and *H. dispersus* sp. nov. ( $t = -7.81$ , df = 18,  $p$ -value < 0.001;  $t = -3.57$ , df = 4,  $p$ -value = 0.03;  $t = 4.04$ , df = 20,  $p$ -value < 0.001). Males of *H. phyllognathus* are also larger than *H. albopunctulatus*; *H. maycu* sp. nov. and *H. dispersus* sp. nov. ( $t = 7.42$ , df = 11,  $p$ -value < 0.001;  $t = 4.05$ , df = 4,  $p$ -value = 0.01;  $t = 4.39$ , df = 12,  $p$ -value < 0.001).

### Advertisement calls

Bioacoustic variables are summarized in Table 4 and call variation is shown in Fig. 8. The advertisement calls of all analyzed species are emitted in a series of 1 to 13 calls. The PCA of calls from 27 individuals resulted in two principal components with eigenvalues > 1. The two PCs accounted for 78.4% of the total variance. PC I was positively correlated with dominant and fundamental

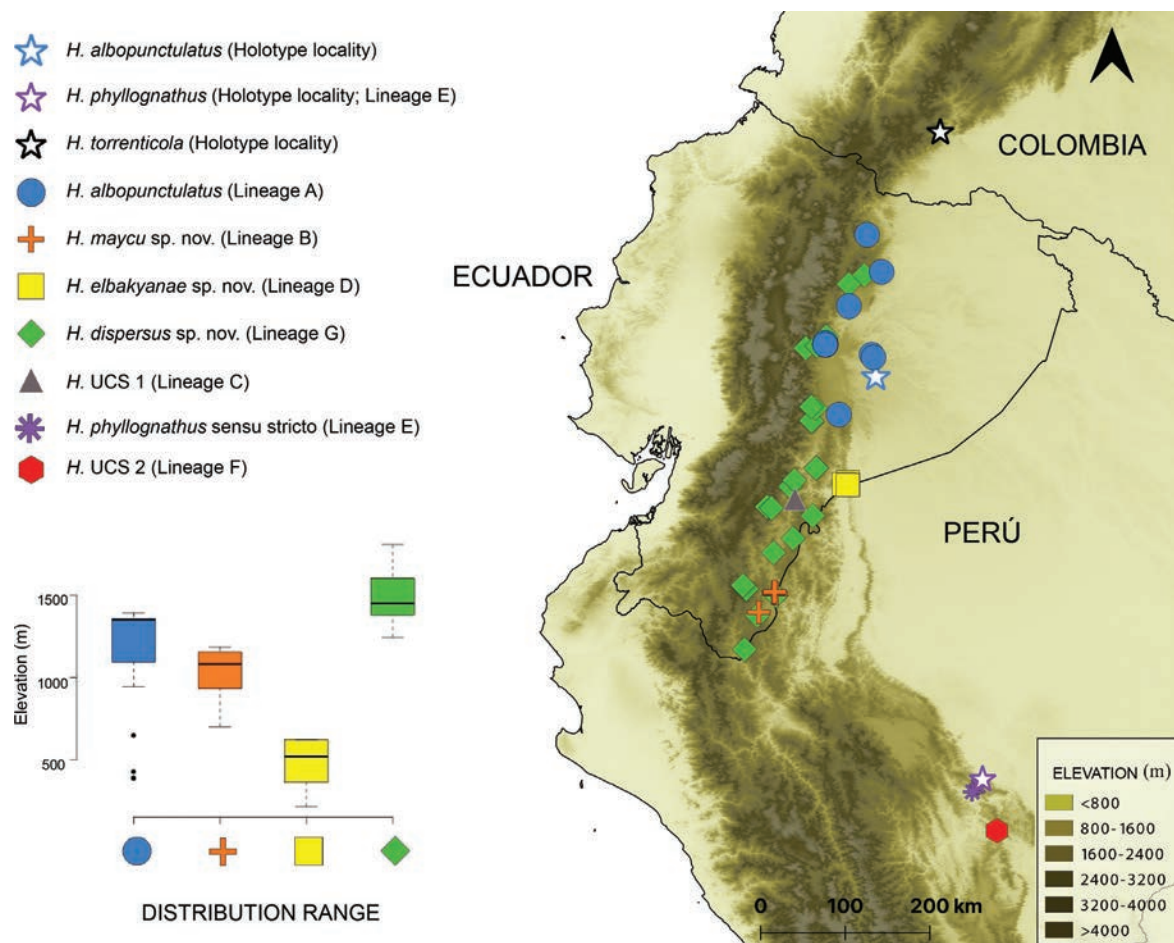


**Figure 5.** Geographic distribution of Amazonian species of the *Hyloscirtus bogotensis* group. Stars represent the type locality of *H. albopunctulatus*, *H. phyllognathus* and *H. torrenticola*. Symbol colors in the map match those of the lineages in the phylogeny. Boxplot comparing the elevational ranges are shown, which excludes *H. phyllognathus* and *H. torrenticola* due to the small sample.

frequency and call duration. PC II was positively correlated with rise time of the call and intercall interval (see Suppl. material 1: table S7). The acoustic space shows clear differentiation for *H. albopunctulatus*, *H. dispersus* sp. nov., and *H. torrenticola* (Fig. 8). In contrast, the calls from *H. maycu* sp. nov. and *H. elbakyanae* sp. nov. overlap. Pairwise comparisons showed significant differences. *Hyloscirtus dispersus* sp. nov., has a significantly longer call ( $t = -11.46$ ,  $df = 16.807$ ,  $p\text{-value} < 0.001$ ) with a higher dominant frequency ( $t = -8.227$ ,  $df = 19$ ,  $p\text{-value} < 0.001$ ) than the sympatric *H. albopunctulatus*. *Hyloscirtus torrenticola* sensu stricto has a significantly shorter call ( $t = 17.46$ ,  $df = 13.897$ ,  $p\text{-value} < 0.001$ ) than *H. dispersus* sp. nov., and a higher dominant frequency ( $t = -10.128$ ,  $df = 5.5338$ ,  $p\text{-value} < 0.001$ ) than *H. albopunctulatus* – the two geographically closest lineages. We could not statistically compare the calls of *H. phyllognathus sensu lato* from Peru as we only had one call per lineage. However, the spatial segregation in the PC is obvious in relation to *H. dispersus* sp. nov. (mainly regarding the rise time of the call, call duration and intercall duration, see Table 4) – its geographically and genetically closest species. Consequently, we did not assign *H. torrenticola* and *H. phyllognathus* to any of our Ecuadorian lineages (Fig. 5). Call differences are also noticeable in the spectrograms (Fig. 9).

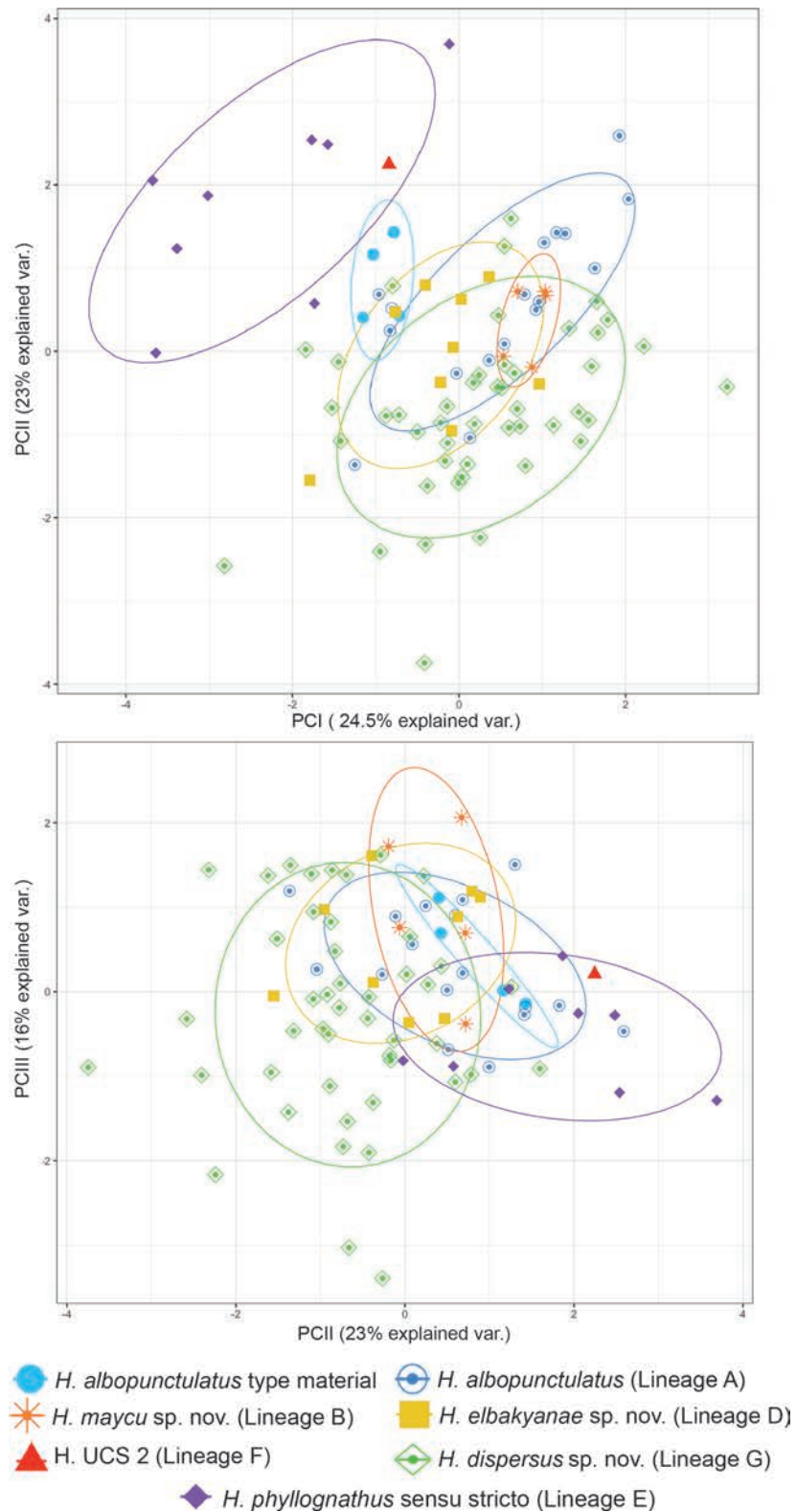


**Figure 6.** Principal components (PC) of the morphometric analysis. Seven size-corrected morphological variables were analyzed for adult females and males of *Hyloscirtus albopunctulatus* (including paralectotypes), *H. maycu* sp. nov., *H. elbakyanae* sp. nov., *H. dispersus* sp. nov., *H. phyllognathus* sensu stricto, and one individual of Lineage F (UCS 2). Normal data ellipses are shown by group. The contribution of each principal component to explain total variation is shown in parenthesis. Results of the PC analysis are shown in Suppl. material 1: table S6.

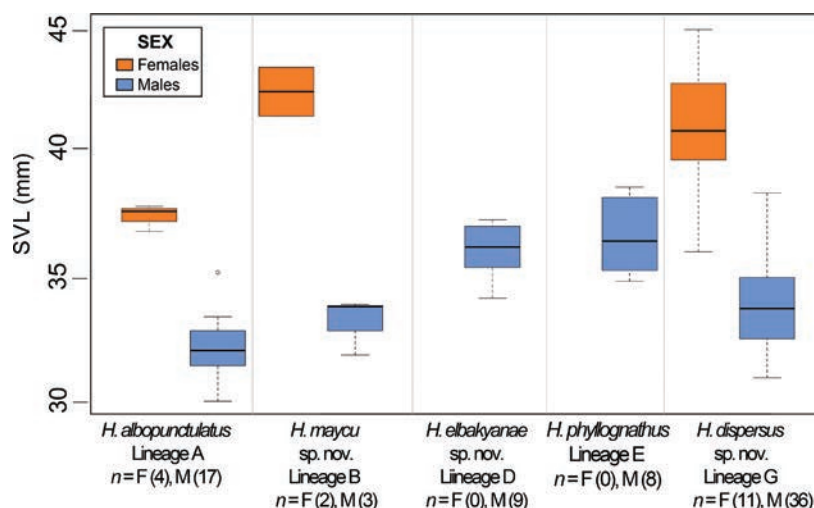


**Figure 7.** Boxplot of the snout-vent length (SVL) comparison analysis. SVL measurements of adult males and females of *Hyloscirtus albopunctulatus*, *H. maycu* sp. nov., *H. elbakyanae* sp. nov., *H. dispersus* sp. nov., and *H. phyllognathus*. The line in the middle of the box represents the median and the upper and lower ends of the box are the 75% and 25% quartiles, respectively.

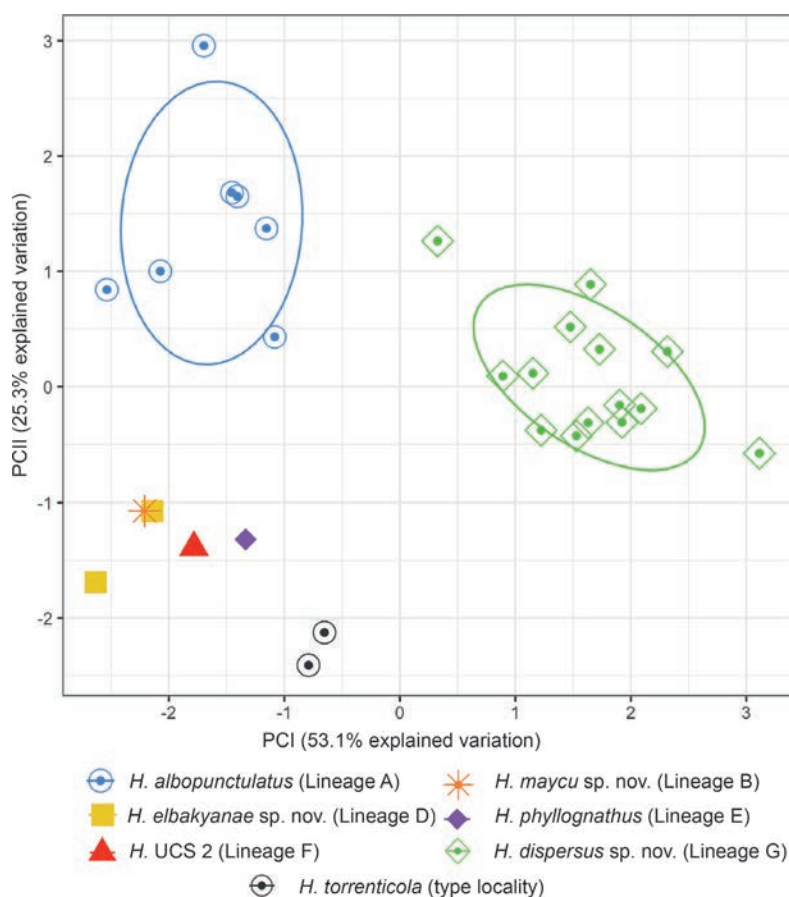


**Figure 8.** Principal components (PC) of the bioacoustic analysis. Six acoustic variables of advertisement calls were analyzed of *Hyloscirtus albopunctulatus*, *H. maycu* sp. nov., *H. elbakyanae* sp. nov., *H. dispersus* sp. nov., *H. phyllognathus* sensu stricto, *H. UCS 2* (Lineage F) and *H. torrenticola* sensu stricto. Normal data ellipses are shown by group. The contribution of each principal component to explain total variation is shown in parenthesis. Results of the PC analysis are shown in Suppl. material 1: table S7.

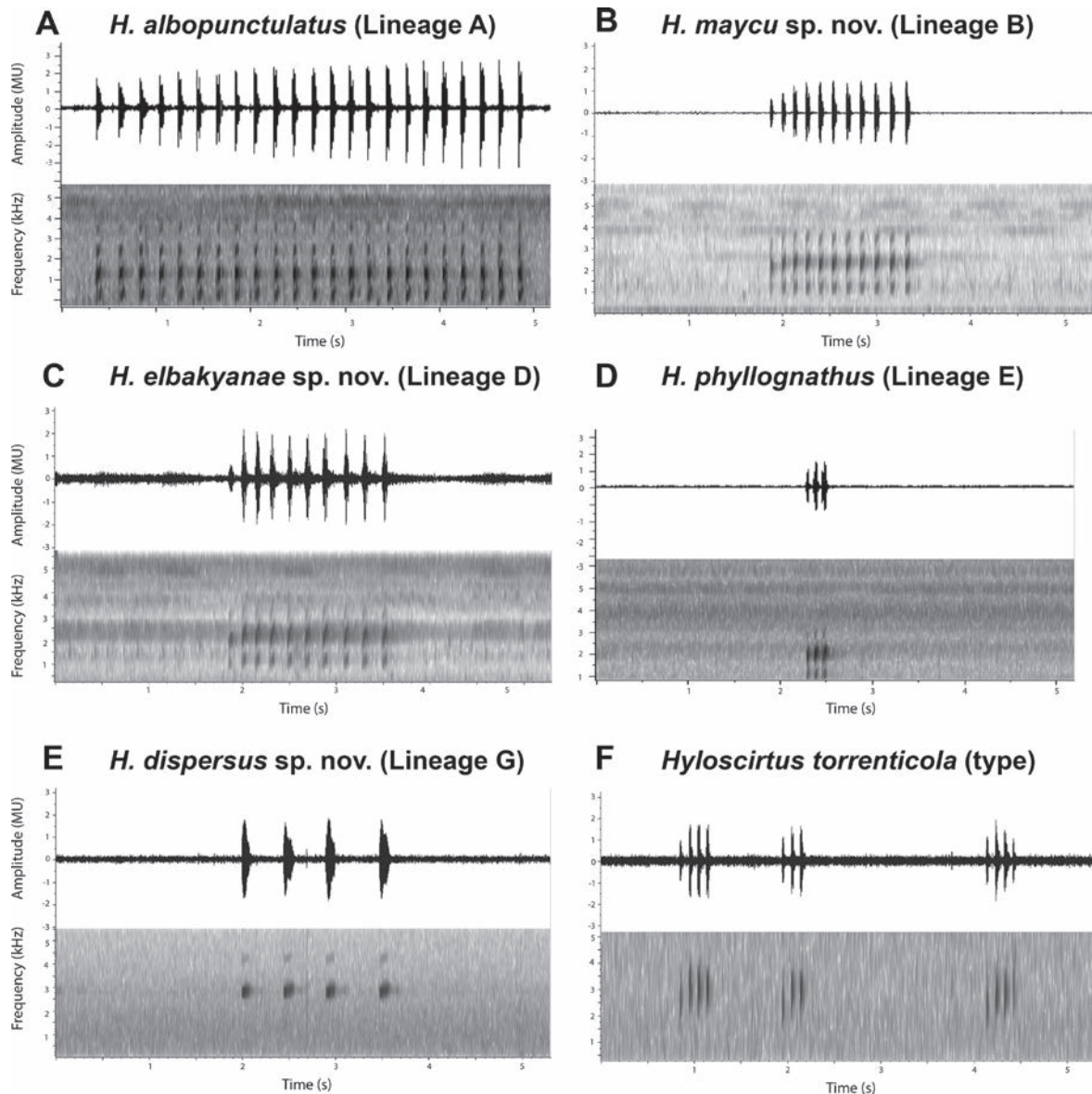


**Figure 9.** Advertisement calls of Amazonian species of the *Hyloscirtus bogotensis* species group. Oscillograms above with their corresponding spectrograms below are shown for each species.

### Environmental characteristics

The PCA analysis of 67 localities summarized environmental variables in two principal components (with eigenvalues > 1). They accounted for 91.8% of the total variance (Fig. 10). PC I was negatively correlated with precipitation variables while PC II was positively correlated with temperature diurnal range, temperature of the warmest month, and annual temperature (see Suppl. material 1: table S8). The environmental space PC I vs. PC II shows that *H. elbakyanae* sp. nov. occurs in wetter environments relative to *H. dispersus* sp. nov. ( $t = -13.97$ ,  $df = 41.95$ ,  $p$ -value < 0.001) and warmer environments relative to *H. albopunctulatus* ( $t = -8.95$ ,  $df = 10.99$ ,  $p$ -value < 0.001). The three Peruvian localities of *H. phyllognathus* are warmer than those of *H. albopunctulatus* and *H. elbakyanae* sp. nov. ( $t = -9.197$ ,  $df = 3.63$ ,  $p$ -value = 0.001 and  $t = -5.15$ ,  $df = 2.08$ ,  $p$ -value = 0.033). *Hyloscirtus maycu* sp. nov. occurs on dryer environments than *H. albopunctulatus* ( $t = -5.83$ ,  $df = 13.08$ ,  $p$ -value < 0.001). *Hyloscirtus torrenticola* has a low sample size, however, it appears

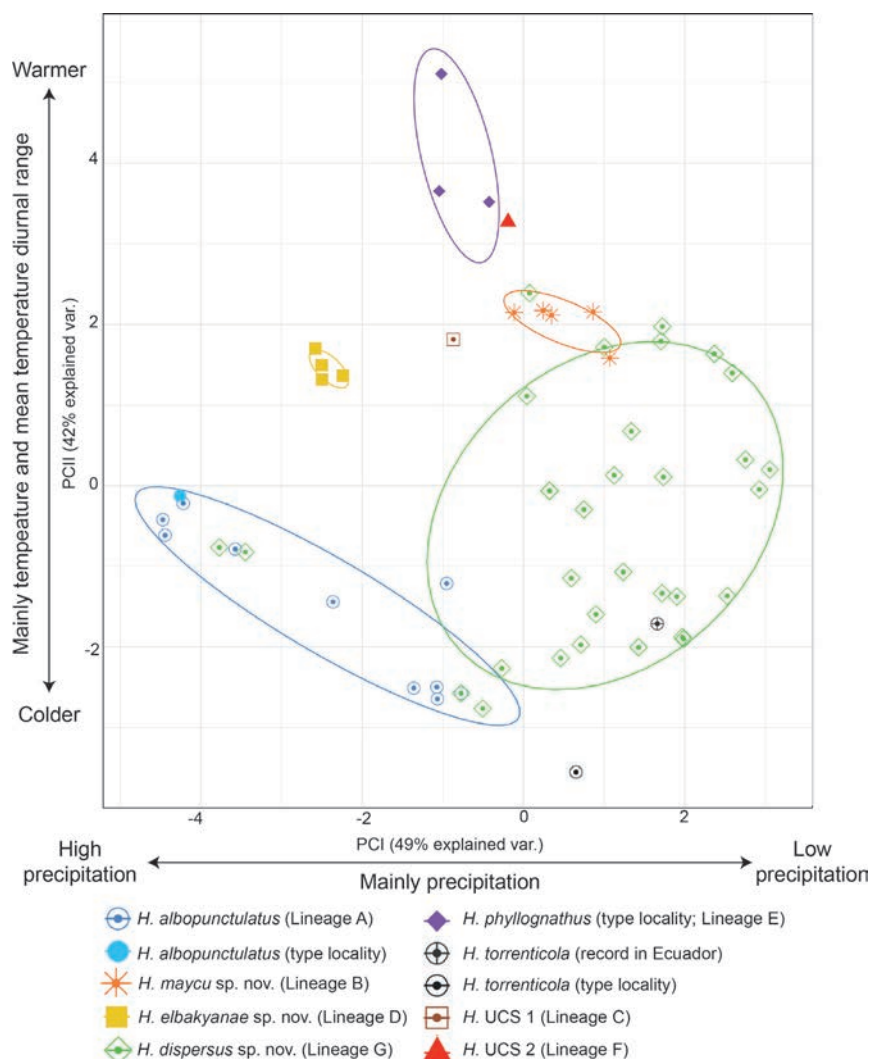


**Figure 10.** Principal components (PC) of the environmental envelope analysis. Eight environmental variables were analyzed of localities of *Hyloscirtus albopunctulatus*, *H. maycu* sp. nov., *H. elbakyanae* sp. nov., *H. dispersus* sp. nov., *H. phyllognathus* sensu stricto, *H. UCS 1* an individual from Lineage F (UCS 2), and *H. torrenticola* sensu stricto. Normal data ellipses are shown by group. The contribution of each principal component to explain total variation is shown in parentheses. The results of the PC analysis are shown in Suppl. material 1: table S8.

different from *H. maycu* sp. nov., *H. elbakyanae* sp. nov., and the individuals from Peru (*H. phyllognathus* sensu stricto + Lineage F) as it seems to occur under colder conditions. Regarding altitudinal ranges, *H. elbakyanae* sp. nov. has been registered at lower elevations (214–622 m) and does not overlap with the elevation range of *H. maycu* sp. nov. (882–1183) and *H. dispersus* sp. nov. (1262–1807 m) (Fig. 5).

### Systematic accounts

The taxonomic status of *Hyla albopunctulata* Boulenger, 1882

The description of *Hyla albopunctulata* was based on five syntypes, all adult males: BMNH 1880.12.5.159–162 from “Ecuador” and 1880.12.5.230 from “Sarayacu, Ecuador” (= Sarayacu, Provincia Pastaza, Ecuador). In accordance with amended Article 74.7.3 of the Code (ICZN 2003) we designate

the adult male BMNH 1880.12.5.230 as lectotype of *Hyla albopunctulata* Boulenger, 1882 in order to clarify its precise type locality and by consequence the application of the name, with specimens BMNH 1880.12.5.159–162 becoming paralectotypes. The lectotype BMNH 1880.12.5.230 (formerly 80.12.5.230; Fig. 4A), is the only type with precise locality information (see the Taxonomy). Therefore, the type locality for *Hyla albopunctulata* becomes “Sarayacu, Ecuador”.

We assign the binomial *Hyloscirtus albopunctulatus* to Lineage A (Fig. 1) based on morphological and acoustic evidence and the location of the type locality, which overlaps with the distribution range of Lineage A exclusively (Fig. 5). In addition, localities from Lineage A are at lower elevations (389–1391 m) than *H. dispersus* sp. nov. (1262–1807 m), the closest species to the type locality. The description of the species is consistent with the morphology of Lineage A. Shared characters include vomerine teeth in a scarcely interrupted series, snout in males rounded, canthus rostralis distinct, tympanum very small and indistinct, subarticular tubercles indistinct and SVL = 33 mm in males (Boulenger 1882). Based on this evidence, we conclude that *H. albopunctulatus* corresponds to Lineage A in our phylogeny.

### ***Hyloscirtus albopunctulatus* (Boulenger, 1882)**

Figs 4, 5, 7, 9, 11, 13–15

Common name: Standard English name: White-speckled tree frog

Standard Spanish name: Rana de torrente de puntos blancos (Frank and Ramus 1996)

*Hyla albopunctulata* Boulenger, 1882: 385, fig. 4. Type locality: Sarayacu, Ecuador.

**Type material.** Designated **lectotype** (Fig. 4A): BMNH 1880.12.5.230, adult male, from “Sarayacu, Ecuador”. **Paralectotypes:** BMNH 1880.12.5.159–162 adult males from “Ecuador”

**Definition.** In this section, coloration and characters refer to preserved specimens unless otherwise mentioned, based on four adult females and 17 adult males, including the paralectotypes. *Hyloscirtus albopunctulatus* can be diagnosed by the combination of the following characters: (1) mean SVL 32.3 mm in adult males (range 30.3–35.5;  $n = 17$ ) and mean SVL 37.8 mm in adult females (range 37.1–38.1;  $n = 4$ ) (Suppl. material 1: table S5, Fig. 7); (2) white supralabial stripe present; (3) tympanum round, inconspicuous in males and distinct in females, supratympanic fold present and unpigmented; (4) white ulnar and tarsal folds present and thick; (5) subarticular tubercles varying from small to inconspicuous in hands and feet; (6) supernumerary tubercles inconspicuous in hands and feet; (7) calcar tubercle absent; (8) pericloacal spots well-defined; (9) all surfaces plain cream with a combination of black and white spots in the dorsum; (10) in life, dorsal surfaces and flanks olive green to yellowish green, covered with white spots and with or without sparse or clumped black spots; axillar and inguinal regions yellowish or blueish; venter and anterior and posterior surfaces of thighs yellow; other ventral surfaces silver, brownish or greenish; yellow pericloacal spots; webbing yellow orange; iris clam shell with black or sand dune reticulations; (11) the advertisement

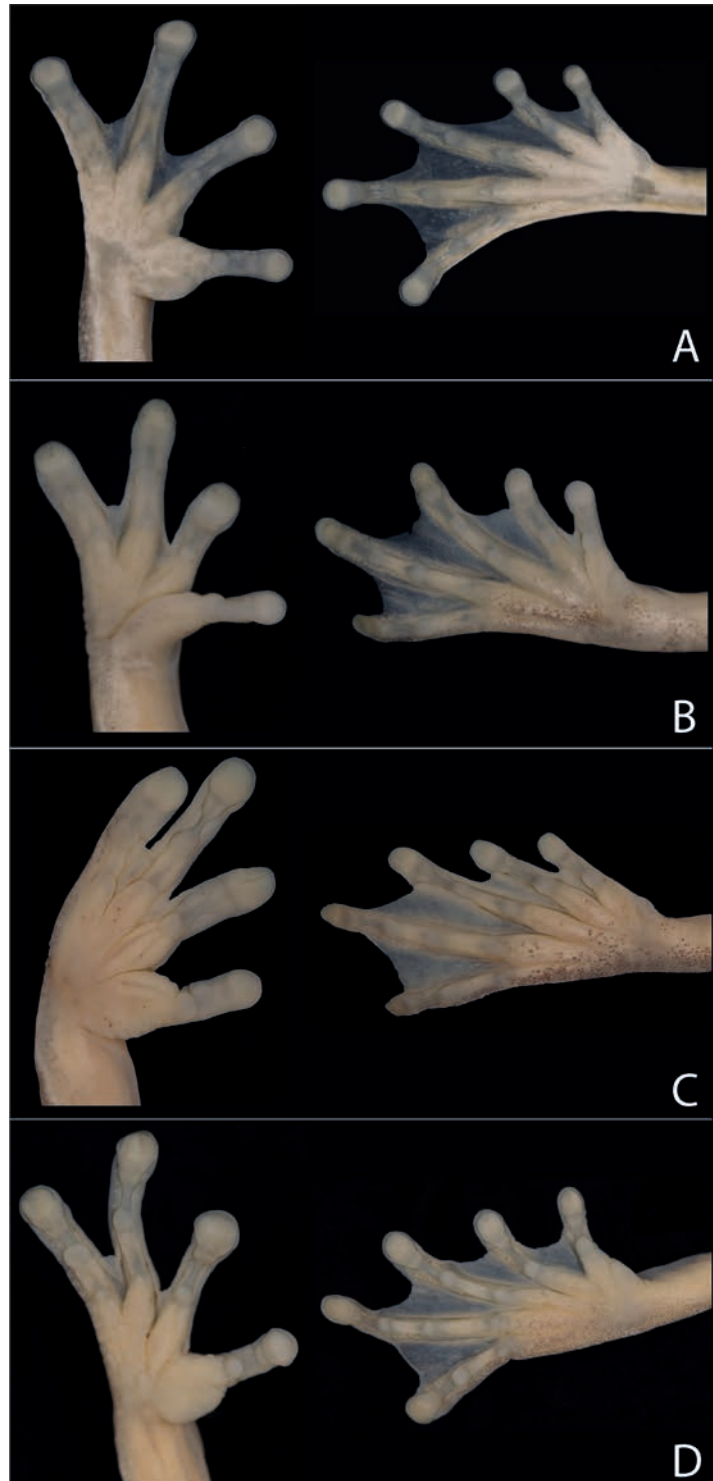


**Figure 11.** Ventral views of right hands and feet of the species **A** *H. albopunctulatus*, QCAZ 59825, SVL: 37.9 mm, female **B** *H. maycu* sp. nov., QCAZ 67087, SVL: 34.1 mm, male **C** *H. elbakyanae* sp. nov., QCAZ 53808, SVL: 36.1 mm, male **D** *H. dispersus* sp. nov., QCAZ 52006, SVL: 32.6 mm, male.

call consist of a single note, with a mean duration of  $0.051 \pm 0.005$  s, a mean dominant frequency of  $2147.84 \pm 137.36$  Hz and a fundamental frequency of  $1214.12 \pm 184.71$  Hz. The call can be repeated consecutively for an indefinite number of times (2 – > 70) in a series of calls.

**Diagnosis.** Characters in this section pertain to preserved specimens unless otherwise noticed. Coloration refers to live specimens. The most similar species to *Hyloscirtus albopunctulatus* living in the Amazon basin are *H. maycu* sp. nov., *H. elbakayanae* sp. nov., *H. dispersus* sp. nov., *H. phyllognathus*, and *H. torrenticola*. *Hyloscirtus albopunctulatus* differs by having a white supralabial stripe (absent in *H. elbakayanae* sp. nov.), a supratympanic fold (absent in all species except in *H. dispersus* sp. nov.), a thick tarsal fold (rudimentary in *H. maycu* sp. nov., *H. elbakayanae* sp. nov., and *H. phyllognathus*), small to inconspicuous subarticular tubercles in hands and feet (conspicuous in hands and feet in *H. maycu* sp. nov., *H. elbakayanae* sp. nov., and *H. dispersus* sp. nov.; Fig. 11), inconspicuous supernumerary tubercles in hands and feet (conspicuous in hands in *H. dispersus* sp. nov.), an absent calcar tubercle (present in *H. dispersus* sp. nov. and *H. phyllognathus*), well-defined pericloacal spots (ill-defined or absent in *H. maycu* sp. nov., *H. elbakayanae* sp. nov., and *H. torrenticola*), and a clam shell iris with black or sand dune reticulations (a clam shell iris with dark pinkish or leather reticulations in *H. maycu* sp. nov. and *H. elbakayanae* sp. nov., pearl or pinkish iris with leather reticulations in *H. dispersus* sp. nov. and bronze iris in *H. torrenticola*, Fig. 12).

The advertisement call of *H. albopunctulatus* has a rise time of  $2.28 \pm 0.80$  s (shorter in *H. maycu* sp. nov. with 0.832 s and in *H. elbakayanae* sp. nov. with  $0.57 \pm 0.05$  s), a dominant frequency of  $2149.84 \pm 137.36$  Hz and a fundamental frequency of  $1214.12 \pm 184.71$  Hz (higher dominant frequency of  $2795.41 \pm 138.68$  Hz and fundamental frequency of 2210.8–2924.2 Hz in *Hyloscirtus dispersus* sp. nov.). *Hyloscirtus torrenticola* also has a higher dominant frequency of  $2743.79 \pm 48.22$  Hz and a fundamental frequency of  $2743.75 \pm 48.16$  Hz. *Hyloscirtus albopunctulatus* has a call duration of  $0.051 \pm 0.005$  s (longer in *H. dispersus* sp. nov. with  $0.11 \pm 0.015$  s). *Hyloscirtus albopunctulatus* has an intercall duration of  $0.30 \pm 0.06$  s (shorter in *H. phyllognathus* with 0.05 s and in *H. torrenticola* with  $0.07 \pm 0.007$  s) (Table 4, Fig. 9; Melin 1941; Duellman and Altig 1978; Rivera-Correa 2016). Moreover, all males of *H. albopunctulatus* were registered calling from under rocks next to streams ( $n = 5$ ; Pontificia Universidad Católica del Ecuador 2024), while all males of *H. dispersus* sp. nov. have been found calling while perching in vegetation over streams ( $n = 14$ ; Pontificia Universidad Católica del Ecuador 2024).

**Variation.** Dorsal and ventral variation of adult preserved specimens is illustrated on Fig. 13. In preservative, dorsum varies from cream with white spots distributed throughout the body and limbs and thick black spots scattered across the body (e.g., QCAZ 59825) and limbs (e.g., QCAZ 59823), with minute black spots scattered in the entire body (e.g., QCAZ 59817) or accumulated in the head (e.g., QCAZ 59824), with dark flecks in body and limbs (e.g., QCAZ 59809), with barely visible minute black spots (e.g., QCAZ 62188) or absent black spots (e.g., QCAZ 59827), to cream with barely visible white spots and minute and thick black spots covering almost the entire dorsum (e.g., QCAZ 59814). We found evidence of conspicuous intraindividual phenotypic plasticity in color. Photos of QCAZ 59825 taken within 14 days of each other show variation in the presence of black spots on the dorsum, head, and snout. Similarly, QCAZ 59822, after 17 days, gained abundant black spots on the dorsum and head and increased the conspicuousness of the dark reticulations on the iris (Fig. 14A, B). We did not find phenotypic plasticity in ventral coloration. Ventral surfaces vary from cream (e.g., QCAZ 59825) to darker cream (e.g., QCAZ 59817). Mental gland in males varies from whitish cream (e.g., QCAZ 59814) to darker cream (e.g., QCAZ 59827).



**Figure 12.** Photographs of individuals of *Hyloscirtus phyllognathus* and *H. torrenticola* species in life **A** dorsolateral and ventral views of a male of *H. phyllognathus* sensu stricto (CORBIDI 9590, Catarata Ahuashiyacu, San Martín, Perú) **B** dorsolateral view of a female of *H. torrenticola* (MAR 1938, Departamento de Caquetá, Colombia) **C** dorsolateral view of a male of *H. torrenticola* (MAR 1974, same locality as B). Photographs by Alessandro Catenazzi (**A**) and Marco Rada (**B, C**).

In life (Fig. 15), the dorsum varies from light green with white spots scattered throughout the body and limbs, and few spread black marks (e.g., QCAZ 59825) or without black spots or marks (e.g., QCAZ 59811), yellowish green with white spots covering the entire body and limbs and spread black marks, accumulated in the anterior part of the body (e.g., QCAZ 59824) or minute and thick black spots across the body (e.g., QCAZ 59823) to brownish green with white spots in all the body and limbs and few black marks randomly dispersed (e.g., QCAZ 59808). Venter and posterior surfaces of thighs vary from yellow (e.g., QCAZ 59811) to greenish yellow (e.g., QCAZ 59808). Other ventral surfaces vary from whitish (e.g., QCAZ 59823) to brownish green (e.g., QCAZ 59824). Iris varies from clam shell with thin (e.g., QCAZ 59825) to thick black or sand dune reticulations (e.g., QCAZ 59823). Examined specimens are listed in Suppl. material 1: tables S1, S9.

**Distribution and natural history.** *Hyloscirtus albopunctulatus* is known from seven localities, from North to Central eastern Ecuador at elevations between 389 and 1391 m (Fig. 5). Biogeographic regions are Amazon Humid Tropical Forest, Eastern Foothill Forest, and Eastern Montane Forest (Ron et al. 2022). They are nocturnal and associated with streams near ravines.

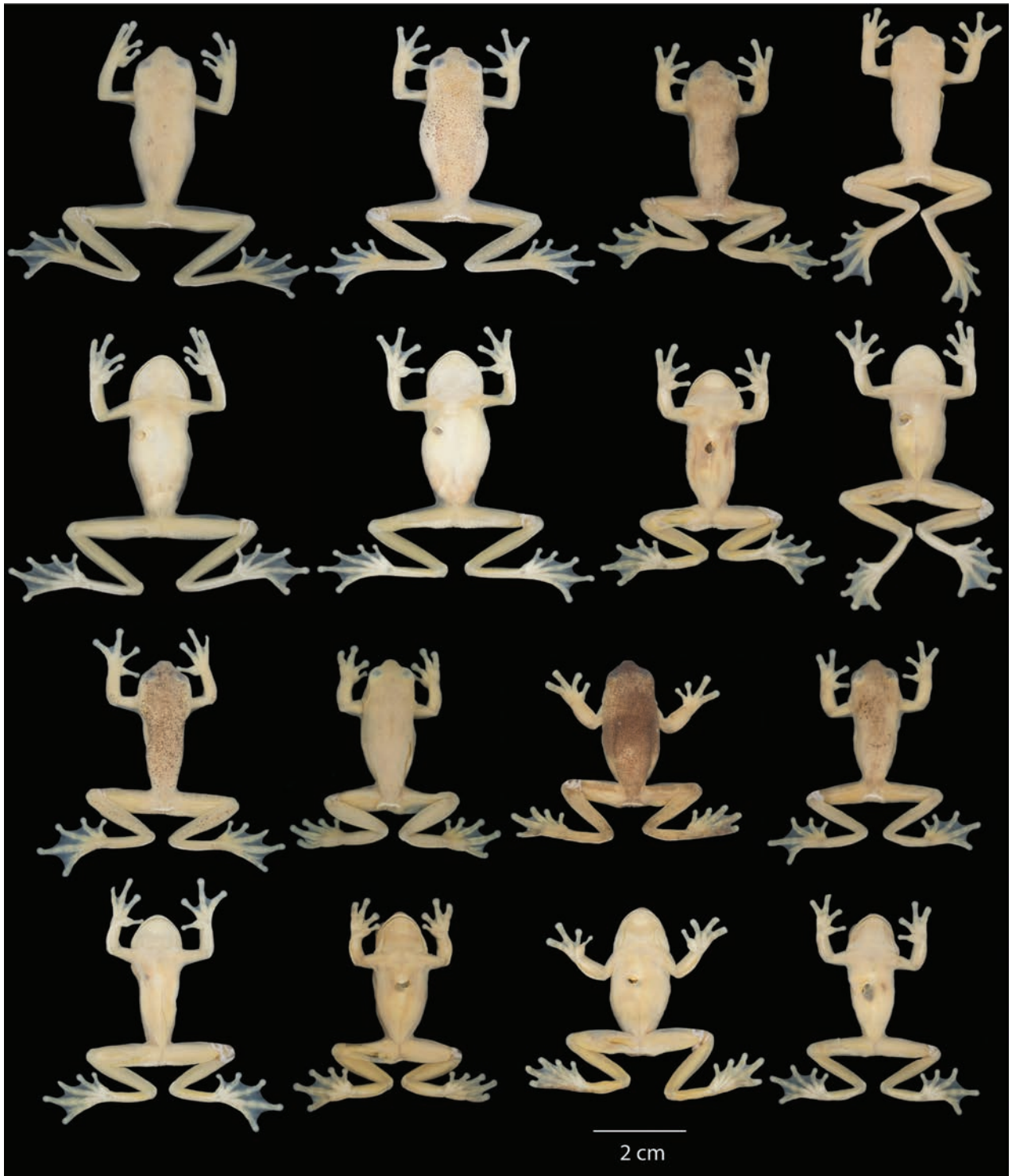


**Figure 13.** Variation of preserved specimens of *Hyloscirtus albopunctulatus*. Dorsal and ventral views. From left to right, first and second rows: QCAZ 62188, 59825 (adult females), QCAZ 59817, 54111 (adult males); third and fourth rows: QCAZ 59823, 59827, 59814 (adult males), QCAZ 59809 (subadult female). See Suppl. material 1: table S1 for locality information. All specimens are shown at the same scale.

Males call under rocks in ravines, leaf litter, streams, small creeks, caves, or cracks. Several individuals have been found perching on vegetation up to 2.5 m but have not been found calling there. The species occurs in sympatry with *Hyloscirtus dispersus* sp. nov.

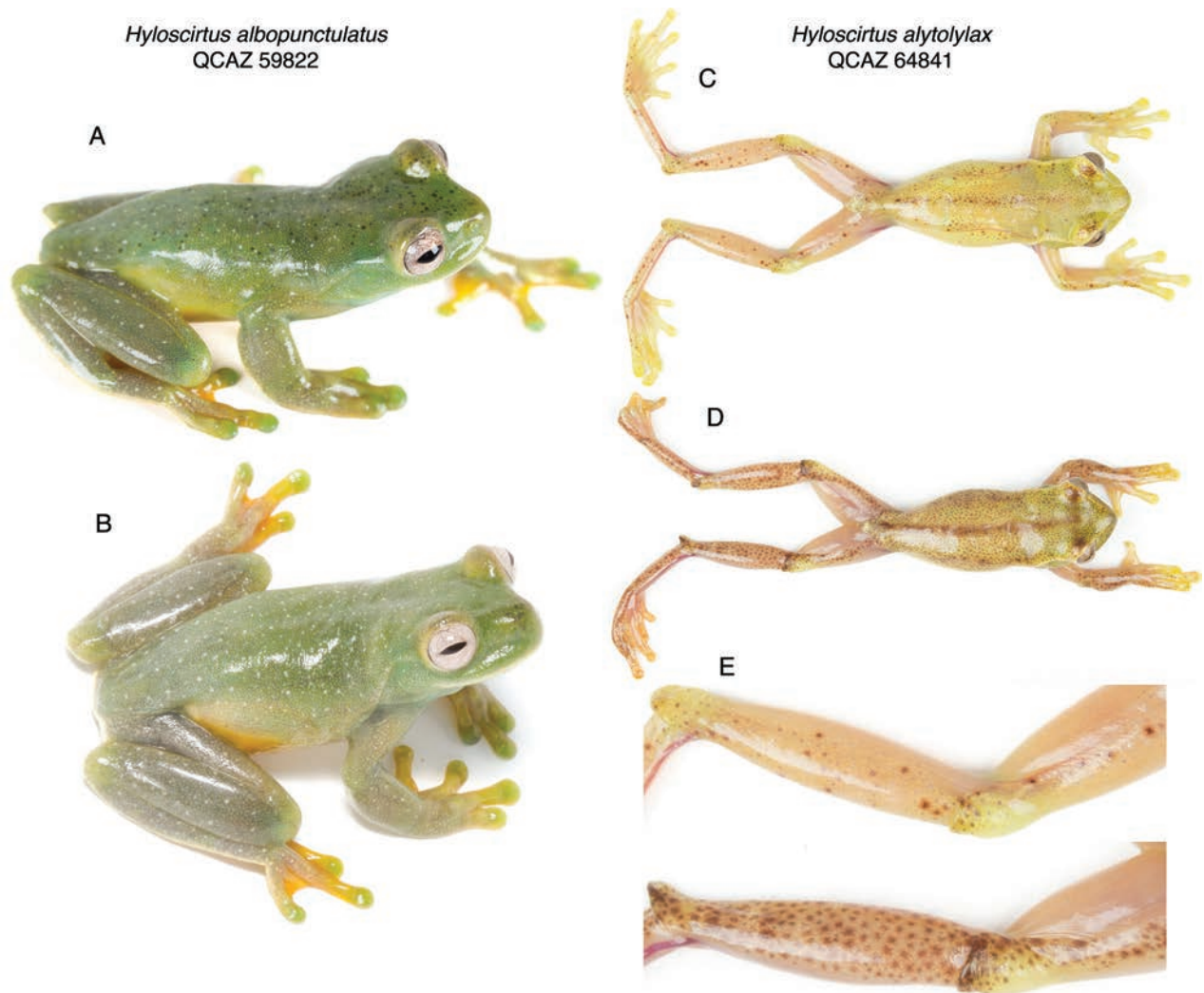


**Figure 14.** Phenotypic plasticity in dorsal color of *Hyloscirtus*. Left column: *H. albopunctulatus*, QCAZ 59822, adult male. Right column: *Hyloscirtus alytolylax*, QCAZ 64841, adult male. Photos in **A**, **B** were taken within 17 days of each other; photos in **C**, **D** within 16 minutes **E** Inset of the hindleg of QCAZ 64841 showing chromatophore change.

**Advertisement call.** We analyzed 26 calls from seven individuals. Six males (QCAZ 59813, 59815, 59817 and three non-collected males) from Comunidad Zarentza, Llanganates National Park, Provincia Pastaza, on 17–24 February 2017, air temperature 19–21 °C, recorded by D. Velalcázar and D. Rivadeneira. One individual (QCAZ 48503) from Reserva Río Bigal, Provincia Orellana, recorded by M. Read, on 22 May 2010. The advertisement call consists of a single tonal note, repeated a highly variable number of times in a series of calls (Fig. 9A). We found from two to more than 70 consecutive calls before long silence periods. One male (QCAZ 59815) called with short pauses during 4.08 s, broadcasting 926 calls. The average call duration is  $0.051 \pm 0.005$  s with an average inter-call interval of  $0.30 \pm 0.06$  s. The average dominant frequency of the call is  $2149.8 \pm 137.36$  Hz. Other call parameters are listed in Table 4.

**Conservation status.** The distribution polygon of *Hyloscirtus albopunctulatus* is 7921 km<sup>2</sup>. Habitat destruction for agriculture and cattle is rising within its distribution range (Ministerio del Ambiente 2013). However, they also inhabit undisturbed and protected areas like Parque Nacional Llanganates. Its tolerance to



**Figure 15.** Variation in life of *Hyloscirtus albopunctulatus*. Dorsolateral and ventral views. From left to right, first and second rows: QCAZ 59825, 59811, 59824 (adult females); third and fourth rows: QCAZ 59808, 59823 (adult males).

disturbed forests is unknown. Given its distribution range being less than 20000 km<sup>2</sup> and by having less than 10 known localities, we propose that *H. albopunctulatus* remains assigned to the Red List category Vulnerable (B1abiii).

***Hyloscirtus maycu* sp. nov.**

<https://zoobank.org/2E9E3BAC-DE92-4DB2-80C2-FCFBDDDB7065E>

Figs 5, 7, 9–11, 16, 17

Common name: Proposed standard English name: Maycu stream frog

Proposed standard Spanish name: Rana de torrente de Maycu

**Type material. Holotype.** • QCAZ 67087 (Figs 16, 17), field no. SC 56707, adult male from Ecuador, Provincia Zamora Chinchipe, Reserva Natural Maycu, plateau (4.2067°S, 78.6326°W), 882 m above sea level, collected by D. Almeida,

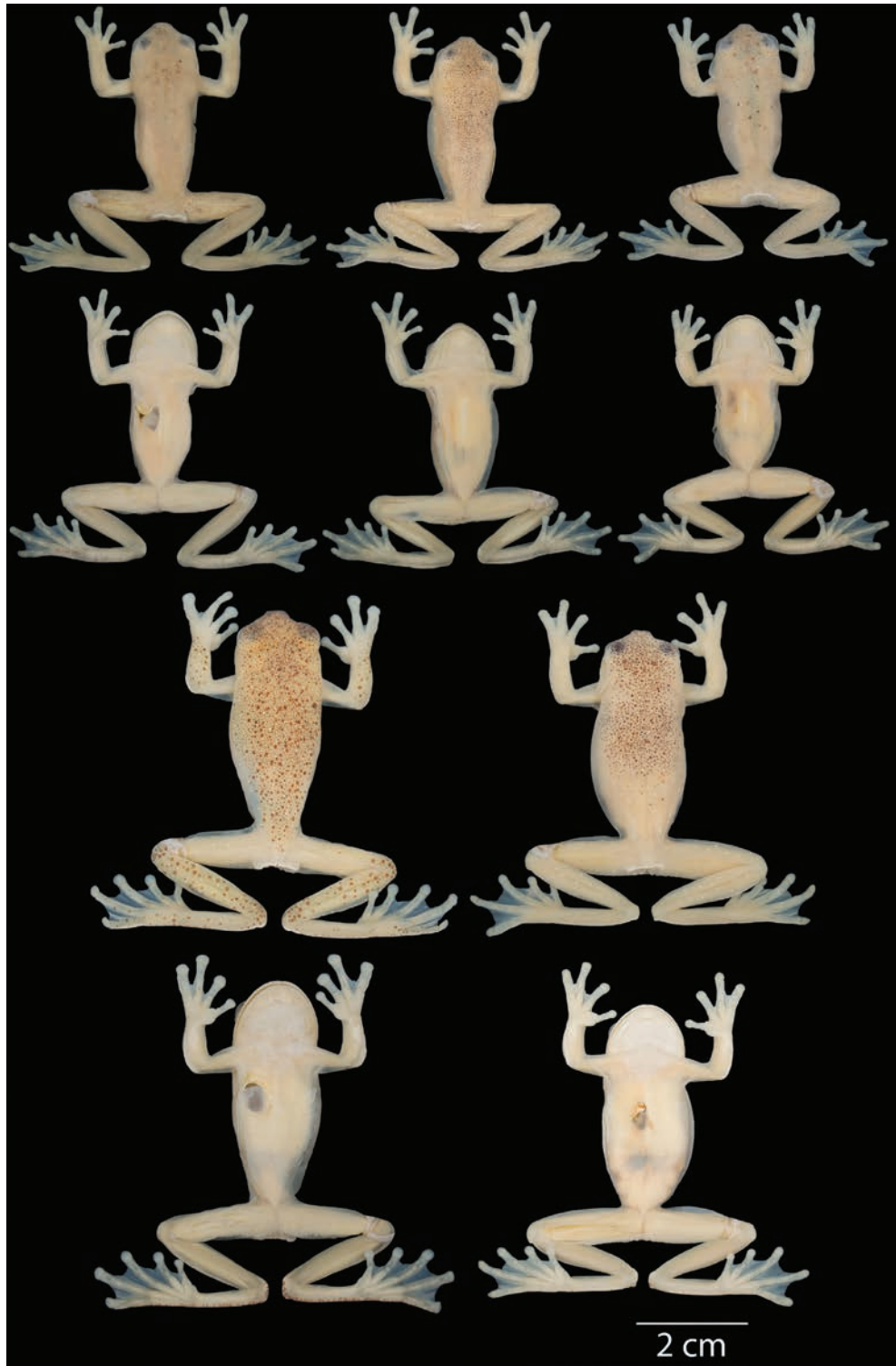


**Figure 16.** Variation of preserved specimens of *Hyloscirtus maycu* sp. nov. Dorsal and ventral views. From left to right, first and second rows: QCAZ 67087 (holotype, adult male), QCAZ 67082, 68055 (adult males); third and fourth rows: QCAZ 67081, 67086 (adult females). See Suppl. material 1: table S1 for locality information. All specimens are shown at the same scale.

K. Nusirquia, D. Núñez, D. Paucar, F. Hervas, J. Ortega, A. Achig, S. Pillajo, R. Gavilanez, and J. Mora on 27 February 2017. A 3D model of the holotype is available at the Sketchfab platform (<https://skfb.ly/oSqqr>). **Paratypes.** • All from Ecuador, Provincia Zamora Chinchipe. Collected with the holotype, QCAZ

67081, 67086 adult females, QCAZ 67082 adult male, QCAZ 67084, 67085 juveniles, QCAZ 67083 tadpole, 959–1219 m of elevation, collected on 23 and 25 February 2017 and 01 March 2017. Nuevo Paraíso, camp near Río Nangaritzza, Cordillera del Oso (4.4442°S, 78.8134°W), 1127 m, QCAZ 68055 adult male, collected on 16 May 2017 by K. Nusirquia, Darwin Núñez, Andrea Calispa

**Definition.** In this section, coloration and characters refer to preserved specimens unless otherwise mentioned. The definition and diagnosis are based on two adult females and three adult males. *Hyloscirtus maycu* sp. nov. can be diagnosed by the combination of the following characters: (1) mean SVL 33.4 mm in adult males (range 31.9–34.2;  $n = 3$ ) and mean SVL 42.7 mm in adult females (range 41.7–43.7;  $n = 2$ ; Suppl. material 1: table S5; Fig. 7); (2) white supralabial stripe present or absent; (3) tympanum round, inconspicuous in males and distinct in females; supratympanic fold inconspicuous and unpigmented; (4) white ulnar and tarsal folds inconspicuous or conspicuous; (5) subarticular tubercles conspicuous, round and single, in hands and feet; (6) supernumerary tubercles inconspicuous in hands and feet; (7) calcar tubercle absent; (8) pericloacal spots well-defined; (9) all surfaces plain cream with a combination of black and white spots in the dorsum; (10) in life, dorsal surfaces and flanks olive green to crete with white spots and minute or thick black spots scattered over the body; axillar and inguinal regions blueish or mongoose; venter and posterior surfaces of thighs yellow; other ventral surfaces silver or greenish; bones and articulations blue; unpigmented pericloacal spots; webbing yellow orange; iris clam shell with thick dark pinkish to leather reticulations; (11) the advertisement call consists of a single note, with duration of 0.053 s ( $n = 1$ ) and a dominant frequency of 2343.8 Hz and fundamental frequency of 1171.90 Hz. The call can be repeated consecutively from 10–13 times in a series of calls.

**Diagnosis.** Characters in this section pertain to preserved specimens unless otherwise noticed. Coloration refers to life specimens. The most similar species to *H. maycu* sp. nov. living in the Amazon basin are *Hyloscirtus albopunctulatus*, *H. elbakyanae* sp. nov., *H. dispersus* sp. nov., *H. phyllognathus*, and *H. torrenticola*. *Hyloscirtus maycu* sp. nov. differs by the absence of a supratympanic fold (present in *H. albopunctulatus* and *H. dispersus* sp. nov.), an inconspicuous tarsal fold (present and thick in *H. albopunctulatus*, *H. phyllognathus*, and *H. torrenticola*), conspicuous subarticular tubercles in hands and feet (small to inconspicuous in hands and feet in *H. albopunctulatus*; Fig. 11), inconspicuous supernumerary tubercles in hands and feet (conspicuous in hands in *H. dispersus* sp. nov.), pericloacal spots ill-defined or absent (well-defined in *H. albopunctulatus* and *H. phyllognathus*), an absent calcar tubercle (present in *H. dispersus* sp. nov. and *H. phyllognathus*), and a clam iris with dark pinkish or leather reticulations (a clam shell iris with black or sand dune reticulations in *H. albopunctulatus* and a bronze iris in *H. torrenticola*, Fig. 12). Although our sample size is small, the available evidence indicates that *H. maycu* sp. nov. differs from *H. elbakyanae* sp. nov. by its smaller size (Fig. 7).

The advertisement call of *H. maycu* sp. nov. has a rise time of 0.8 s (longer in *H. albopunctulatus* with  $2.28 \pm 0.80$  s and shorter in *H. elbakyanae* sp. nov. with  $0.57 \pm 0.05$  s and in *H. torrenticola* with  $0.16 \pm 0.017$  s), a dominant frequency of 2343.8 Hz and a fundamental frequency of 1171.9 Hz (higher dominant frequency in *H. dispersus* sp. nov. of  $2795.41 \pm 138.68$  Hz and fundamental frequency of  $2700.63 \pm 195.66$  Hz). *Hyloscirtus torrenticola* also has a higher dominant frequency of  $2743.79 \pm 48.22$  Hz and a fundamental frequency of



**Figure 17.** Variation in life of *Hyloscirtus maycu* sp. nov. Dorsolateral, lateral, and ventral views. From top to bottom: QCAZ 67081 (adult female), QCAZ 67082 (adult male), QCAZ 67087 (holotype, adult male), QCAZ 67086 (adult female).

$2743.75 \pm 48.16$  Hz. *Hyloscirtus maycu* sp. nov. has a call duration of  $0.053$  s (longer in *H. dispersus* sp. nov. of  $0.11 \pm 0.015$  s) (Table 4, Fig. 9; Melin 1941; Duellman and Altig 1978; Rivera-Correa 2016).

Additionally, *H. maycu* sp. nov. inhabits elevations between 882 and 1183 m, while *H. elbakyanae* sp. nov. lives lower between 214 and 622 m and in wetter and warmer environments (Figs 5, 10).

**Description of the holotype.** Description of characters based on the preserved specimen. Adult male (Figs 16, 17). Measurements (in mm): SVL 34.1; foot length 13.9, head length 9.7, head width 10.2, eye diameter 3.0, tympanum diameter 2.0, tibia length 17.2, femur length 17.2, internarial distance 3.1, inter-orbital distance 4.9. Head wider than long; body slender; snout rounded in dorsal and lateral view; distance from nostril to eye same as diameter of eye; canthus rostralis distinct; loreal region convex; internarial region slightly curved; top of the head slightly concave; nostrils not protuberant, round, directed anterolaterally; lips rounded, not flared; interorbital area slightly concave, longer than upper eyelid; tympanum and tympanic fold inconspicuous; tympanic annulus absent; tympanic membrane absent; mental gland present, diamond-shaped, well defined, extending  $\sim 1/3$  the size of the head; dentigerous processes of vomers slightly curved, transversal and posterior to ovoid choanae, each process narrowly separated from each other and bearing five teeth each; tongue cordiform, widely attached to mouth floor; vocal slits and subgular vocal sac present.

Forearms slender; axillary membrane absent; fingers bearing dermal fringes and rounded discs; relative lengths of fingers  $I < II < IV < III$ ; webbing formula  $I \text{ basal } II \text{ } 2^- \text{--} 3^- \text{ III } 2^+ \text{--} 2^- \text{ IV}$ ; subarticular tubercles prominent, round, single; supernumerary tubercles small; thenar tubercle absent; palmar tubercle small; prepollex present, not modified as a spine; nuptial pads absent; ulnar tubercles absent; outer ulnar fold present. Hindlimbs slender; toes bearing dermal fringes and rounded discs; relative length of toes  $I < II < III < V < IV$ ; extensive toe webbing, formula  $I \text{ } 1^- \text{--} 2^- \text{ II } 1^+ \text{--} 2^- \text{ III } 1^+ \text{--} 2^- \text{ IV } 2^- \text{--} 1^+ \text{ V}$ ; outer tarsal fold present; tarsal tubercles absent; calcar tubercle absent; subarticular tubercles conspicuous, round and single; supernumerary tubercles inconspicuous; inner metatarsal tubercle present and round, outer absent. Skin on dorsum, flanks, dorsal and ventral surfaces of limbs, thighs, and venter smooth; cloacal opening directed posteriorly at upper level of thighs; cloacal fold thick.

**Color of holotype in preservative** (Fig. 16). Dorsal surfaces of the head, dorsum, flanks, and limbs cream with few minute black and white spots scattered through the body. Venter, throat, and ventral surfaces of limbs plain cream. Mental gland pale cream. White supralabial stripe absent. Ulnar, tarsal, and cloacal folds white. Webbing cream. Other details are shown in Fig. 16.

**Color of holotype in life** (Fig. 17). Based on digital photographs. Dorsal surfaces and flanks olive green with white spots and minute black spots and a few dispersed black marks. Head darker brown, probably because of the high accumulation of minute black spots. Venter and posterior surface of thighs yellow. Axillar and inguinal regions and other ventral surfaces greenish white. Yellowish mental gland. Ulnar, tarsal, and cloacal folds white. Webbing yellow orange. Iris clam shell with leather reticulations.

**Variation.** Dorsal and ventral variation of adult specimens is illustrated on Fig. 16 (in preservative) and Fig. 17 (in life). In preservative, dorsum varies from cream with white spots scattered throughout the body and limbs with minute and thick darker brownish black spots scattered across the entire body and limbs (e.g., QCAZ 67081) or accumulated in the anterior part of the body (e.g., QCAZ 67086) to darker cream with scattered spots dispersed in the body and limbs and minute black spots covering the dorsum (e.g., QCAZ 67082) or barely visible minute black spots and a few black marks in

the anterior part of the body (e.g., QCAZ 68055). Venter varies from paler (e.g., QCAZ 67086) to darker cream (e.g., QCAZ 68055). White supralabial stripe varies from absent (e.g., QCAZ 67082), ill-defined (e.g., QCAZ 67081) to well-defined (e.g., QCAZ 67086).

In life (Fig. 17), dorsum varies from olive green with scattered white spots throughout the body and limbs with thick black spots in the body and limbs (e.g., QCAZ 67081) or few black marks in the body (e.g., QCAZ 67082) to paler olive green with spread white marks covering the entire body and limbs and few black marks in the mid part of the body (e.g., QCAZ 67086). Axillar and inguinal regions vary from blue (e.g., QCAZ 67081) to whitish. Ventral surfaces besides venter and posterior thighs vary from greenish (e.g., QCAZ 67081) to whitish (e.g., QCAZ 67082). A white supralabial stripe is present (e.g., QCAZ 67086) or absent (e.g., QCAZ 67082). Iris varies from clam shell with thin leather reticulations (e.g., QCAZ 67086), thick pinkish reticulations (e.g., QCAZ 67081) or thick leather reticulations (e.g., QCAZ 67082).

**Distribution and natural history.** *Hyloscirtus maycu* sp. nov. is known only from its type locality in Provincia Morona Santiago and one locality in Provincia Zamora Chinchipe (airline distance 32 km), at elevations between 882 and 1183 m, on the foothills of Cordillera del Cóndor, in Ecuador (Fig. 5). Biogeographic region is Eastern Lower Montane Forest (Ron et al. 2022). This species lives in primary and secondary forests. They are nocturnal and associated with ravines and streams. Males call from vegetation up to 2 m high, on the edge of the streams. One individual was recorded calling under a rock, and another on a rock in a ravine with low flow. A metamorph was found (in March) on an island of rock in the middle of a stream, suggesting that its tadpoles develop in streams, like other *Hyloscirtus*. A tadpole (QCAZ 67083) was found on a pool next to a stream in February.

**Advertisement call.** We analyzed five calls from one individual (QCAZ 67087) from Reserva Natural Maycu, Provincia Zamora Chinchipe, 27 February 2017, recorded by J. Ortega. The advertisement call consists of a single tonal note, repeated 10–13 times in a series of calls (Fig. 9B). Average call duration is 0.053 s with an average inter-call interval of 0.09 s. The average dominant frequency of the call is 2343.8 Hz. Other call parameters are listed in Table 4.

**Conservation status.** The distribution polygon of *H. maycu* sp. nov. is 54.8 km<sup>2</sup> (based on two localities). Its distribution range is small but overlaps with a protected area, Reserva Natural Maycu; however, it is also found in Cordillera del Cóndor, an area severely fragmented by deforestation due to agriculture, cattle raising, and threatened mining activities. In response to its distribution range being less than 20000 km<sup>2</sup> and by having less than 10 known localities, we propose assigning *H. maycu* sp. nov. to the Red List category Vulnerable c (VU B1a).

**Etymology.** The specific epithet *maycu* is used as a noun in apposition and refers to the type locality of the species, a protected area in Ecuador named Reserva Natural Maycu, managed by the NGO Naturaleza y Cultura Internacional. “Maycu” seems to be a derivation of the Shuar word “Maycua” or “Maycuwa”, which the Shuar people use to refer to some species of small trees of the genus *Brugmansia* (angel’s trumpet). The southern border of the Reserve has been invaded by illegal miners and provides an additional example of the threat that mining represents for biodiversity conservation (F. Serrano, in litt.).

***Hyloscirtus elbakyanae* sp. nov.**

<https://zoobank.org/6F4B822B-79BD-44CB-A810-B9531CAE982D>

Figs 5, 7, 9, 11, 18, 19

Common name: Proposed standard English name: Elbakyan stream frog

Proposed standard Spanish name: Rana de Torrente de Elbakyan

**Type material. Holotype.** • QCAZ 53808 (Figs 18, 19), field no. SC 39260, adult male from Ecuador, Provincia Morona Santiago, Comunidad Shaime, near Mirador de la Virgen (2.975540°S, 77.80346°W), 622 m above sea level, collected by SRR, A. Merino, F. Ayala, T. Camacho, and M. Cohen on 23 July 2012. A 3D model of the holotype is available at Sketchfab platform (<https://skfb.ly/oS-XSH>). **Paratypes.** • All collected in Ecuador, Provincia Morona Santiago. Same locality and collection data as the holotype, QCAZ 53807, 53831 adult males. Surroundings of Río Shaime (2.9409°S, 77.8012°W), 511 m, QCAZ 72665–66 adult males, collected on 6 June 2018; • Tiwintza-Shaime road (2.9750°S, 77.7957°W), 211 m, QCAZ 72667, collected on 8 June 2018; • Mirador de la Virgen, Tiwintza-Shaime road (2.9756°S, 77.8015°W), 529 m, QCAZ 72668 adult male, collected on 8 June 2018; • Peñas-Shaime road (2.9663°S, 77.8468°W), 363 m, QCAZ 72669, collected on 9 June 2018; • Peñas-Shaime road, 2.8 km E Río Yaupi (2.9663°S, 77.8468°W), 363 m, QCAZ 73709 adult male. F. Ayala, D. Núñez, K. Nusirquia and A. Carvajal collected all specimens from 2018.

**Definition.** In this section, coloration and characters refer to preserved specimens unless otherwise mentioned. The Definition and Diagnosis are based on eight adult males, females are unknown. *Hyloscirtus elbakyanae* sp. nov. can be diagnosed by the combination of the following characters: (1) male mean SVL 36.3 mm (range 34.5–37.6;  $n = 9$ ; Suppl. material 1: table S5, Fig. 7); (2) white supralabial stripe absent; (3) tympanum round, inconspicuous; supratympanic fold inconspicuous and unpigmented; (4) white ulnar and cloacal folds present; white tarsal fold present, inconspicuous to conspicuous; (5) subarticular tubercles conspicuous in hands and feet; (6) supernumerary tubercles inconspicuous; (7) calcar tubercle absent; (8) pericloacal spots well-defined; (9) all surface plain cream with inconspicuous or absent white spots and minute or thick black spots or flecks in the dorsum; (10) in life, dorsal surfaces and flanks olive green, brownish green or greyish green with or without white flecks and with minute or thick black spots or flecks; axillar and inguinal regions silver or brownish; venter and posterior surfaces of tights yellow; other ventral surfaces silver or brownish; pericloacal spots ill-defined, unpigmented; webbing yellow orange; iris pearl to clam shell with pinkish brown or leather reticulations; (11) the advertisement call consists of a single note, with a mean duration of  $0.056 \pm 0.001$  s and a dominant frequency of  $2321.29 \pm 127.86$  Hz and fundamental frequency of  $1184.35 \pm 30.48$  Hz. The call can be repeated in a series of 4–13 calls.

**Diagnosis.** Characters in this section pertain to preserved specimens unless otherwise noticed. Coloration refers to live specimens. The most similar species to *Hyloscirtus elbakyanae* sp. nov. in the Amazon basin are *Hyloscirtus albopunctulatus*, *H. maycu* sp. nov., *H. dispersus* sp. nov., *H. phyllognathus*, and *H. torrenticola*. *Hyloscirtus elbakyanae* sp. nov. differs by the absence of a white supralabial stripe (present in *H. albopunctulatus*, *H. phyllognathus* and *H. torrenticola*), an absent supratympanic fold (present in *H. albopunctulatus* and *H. dispersus* sp. nov.), an inconspicuous tarsal fold (conspicuous in *H. albopunctulatus*,



**Figure 18.** Variation of preserved specimens of *Hyloscirtus elbakyanae* sp. nov. Dorsal and ventral views. From left to right, first and second rows: QCAZ 72666, 73669, 72668 (adult males); third and fourth rows: QCAZ 53808 (holotype, adult male), QCAZ 72665, 73709 (adult males). See Suppl. material 1: table S1 for locality information. All specimens are shown at the same scale.

*H. phyllognathus*, and *H. torrenticola*), conspicuous subarticular tubercles in hands and feet (inconspicuous in hands and feet in *H. albopunctulatus*, Fig. 11), inconspicuous supernumerary tubercles in hands and feet (conspicuous in hands in *H. dispersus* sp. nov.), absent pericloacal spots (present in *H. albopunctulatus* and *H. phyllognathus*), absent calcar tubercle (present in *H. dispersus* sp. nov. and *H. phyllognathus*), and a clam shell or pearl iris (clam shell with black or sand dune reticulations in *H. albopunctulatus* and a bronze iris in *H. torrenticola*, Fig. 12).

The advertisement call of *Hyloscirtus elbakyanae* sp. nov. has a rise time of  $0.57 \pm 0.05$  s (longer in *H. albopunctulatus* with  $2.28 \pm 0.80$  s and in *H. torrenticola* with  $0.16 \pm 0.017$  s), a dominant frequency of  $2321.29 \pm 127.86$  Hz and a fundamental frequency of  $1184.35 \pm 30.48$  Hz (higher dominant frequency of  $2795.41 \pm 138.68$  Hz and fundamental frequency of  $2700.63 \pm 195.66$  Hz in *H. dispersus* sp. nov.). *Hyloscirtus torrenticola* also has a higher dominant frequency of  $2743.79 \pm 48.22$  Hz and a fundamental frequency of  $2743.75 \pm 48.16$  Hz. *Hyloscirtus elbakyanae* sp. nov. has a call duration of  $0.06 \pm 0.001$  s (longer in *H. dispersus* sp. nov. with  $0.11 \pm 0.015$  s) and an intercall duration of  $0.12 \pm 0.007$  s (shorter in *H. torrenticola* with  $0.07 \pm 0.007$  and longer in *H. albopunctulatus* with  $0.30 \pm 0.06$  s and in *H. dispersus* sp. nov. of  $0.33 \pm 0.044$  s) (Table 4, Fig. 9; Melin 1941; Duellman and Altig 1978; Rivera-Correa 2016).

Moreover, *H. elbakyanae* sp. nov. inhabits elevations between 214 and 622 m, while *H. maycu* sp. nov. lives higher between 882 and 1183 m, in colder and dryer environments (Figs. 5 and 10). The available evidence indicates that *H. elbakyanae* sp. nov. is larger than *H. maycu* sp. nov. (Fig. 7).

**Description of the holotype.** Description of characters based on preserved specimen. Adult male (Figs 18, 19). Measurements (in mm): SVL 36.1; foot length 14.3, head length 10.5, head width 11.7, eye diameter 3.4, tympanum diameter 1.6, tibia length 16.9, femur length 16.7, internarial distance 3.0, interorbital distance 5.5. Head wider than long; body slender; snout rounded in dorsal and lateral views; distance from nostril to eye shorter than diameter of eye; canthus rostralis distinct; loreal region concave; internarial region nearly flat; top of the head flat; nostrils not protuberant, round, directed anterolaterally; lips rounded, not flared; interorbital area slightly concave, longer than upper eyelid; tympanum inconspicuous, with upper and posterior margins barely covered by a curved and thin inconspicuous supratympanic fold reaching anterior margin of insertion of arm; tympanic annulus absent; tympanic membrane absent; mental gland present, oval-shaped, very distinct, extending  $\sim 1/2$  the length of the head; dentigerous processes of vomers straight, in transverse row posterior to level of choanae, which is round, each process narrowly separated from each other and bearing 4 teeth; tongue slightly cordiform, widely attached to mouth floor; vocal slits and vocal sac present.

Forearms slender; axillary membrane absent; fingers bearing dermal fringes and rounded discs; relative lengths of fingers  $I < II < IV < III$ ; webbing formula I basal II  $2^- - 3^-$  III  $2^+ - 2^-$  IV; subarticular tubercles prominent, round, single; supernumerary tubercles inconspicuous; thenar and palmar tubercles absent; small prepollex, not modified as a spine; nuptial pads absent; ulnar tubercles absent; outer ulnar fold present. Hindlimbs moderately robust; toes bearing rounded discs; relative length of toes  $I < II < III < V < IV$ ; extensive toe webbing, formula I  $1^- - 1^{3/4}$  II  $1^- - 2^-$  III  $1^+ - 1^-$  IV  $1^- - 1^-$  V; outer tarsal fold present; tarsal tubercles absent; calcar tubercle absent; subarticular tubercles round and single; supernumerary tubercles not distinctive; inner metatarsal tubercle present and ovoid, outer absent. Skin on dorsal surfaces and flanks smooth and ventral surfaces granular; cloacal opening directed posteriorly at upper level of thighs, rounded tubercles below; cloacal fold thick.

**Color of holotype in preservative** (Fig. 18). Dorsal surfaces of the dorsum, flanks and limbs cream covered with minute black spots, more abundant in the head. Very few white spots barely visible dispersed on the posterior dorsum and dorsal surfaces of the hindlimbs. Venter, throat, and ventral surfaces of

limbs plain cream. Mental gland cream with small black spots. White supralabial stripe absent. Ulnar, tarsal, and cloacal folds white. Webbing cream.

**Color of holotype in life** (Fig. 19). Based on digital photographs. Dorsal surfaces and flanks dark brownish green with minute black spots, more abundant on the anterior part of the head and limbs, as if those areas were dark brown. Few barely visible white flecks spread on the hindlimbs. Venter and posterior surfaces of thighs yellow, other ventral surfaces whitish. Throat greenish white. Tympanum pale green. Mental gland calico. Ulnar, tarsal, and cloacal folds white. Webbing yellow. Iris pearl with pinkish-brown reticulations.

**Variation.** Dorsal and ventral variation of adult specimens is illustrated on Figs 18, 19. In preservative, dorsum varies from cream with scattered white spots through the body and limbs and minute and thick black spots scattered across the body and limbs (e.g., QCAZ 73669) or barely visible black spots or marks (e.g., QCAZ 72666), without white spots and brownish black flecks dispersed in the body and limbs, more accumulated in the anterior part of the body (e.g., QCAZ 72668) or spots covering the entire body and limbs (e.g., QCAZ 72665) to paler cream without white spots and few black marks in the anterior part of the body (e.g., QCAZ 73709). Ventral surfaces vary from darker cream (e.g., QCAZ 72666) to paler cream (e.g., QCAZ 73709). Mental gland varies from cream (e.g., QCAZ 73669) to whitish (e.g., QCAZ 72665). White supralabial stripe varies from inconspicuous (e.g., QCAZ 72665) to absent (e.g., QCAZ 73709).

In life (Fig. 19), dorsum varies from pale olive green, olive green, brownish green, darker brownish green to greyish green with barely visible white spots scattered throughout the body and few black marks in the anterior part of the body (e.g., QCAZ 53831) or without black marks or spots (e.g., QCAZ 53807), to absent white or black spots (QCAZ 72665, 72667, 72669 and 73709). Ventral surfaces, besides venter and posterior thighs, vary from silver (e.g., QCAZ 53807) to whitish (e.g., QCAZ 73709). Iris varies from clam shell with thin reticulations (e.g., QCAZ 73709) to pearl with thicker reticulations (e.g., QCAZ 72667). White supralabial stripe varies from present (e.g., QCAZ 72665) to absent (e.g., QCAZ 72667).

**Distribution and natural history.** *Hyloscirtus elbakyanae* sp. nov. is known from seven localities, nearby the type locality, Comunidad Shaime, Provincia Morona Santiago, Ecuador, at elevations between 214–622 m (Fig. 5). Biogeographic regions are Amazon Humid Tropical Forest and Eastern Lower Montane Forest (Ron et al. 2022). This species lives in hillside forest, with varying levels of anthropogenic disturbance. The habitat is dominated by palms (*Iriartea deltoidea*) and trees up to 20–30 m high (collectors' observations). They are nocturnal and have been found on ravines with shrub vegetation on the edge of torrent rivers and streams. *Hyloscirtus elbakyanae* sp. nov. calls from under rocks in streams with little water and cracks. There are no records of individuals perching on riparian vegetation.

**Advertisement call.** We analyzed ten calls from two individuals. Both calls (QCAZ 53807–08) from Comunidad Shaime, Provincia Morona Santiago, recorded on 23 July 2012 by SRR and T. Camacho, water temperature 20–21 °C. The advertisement call consists of a single tonal note, repeated in series of 4–13 calls (Fig. 9C). Average call duration is  $0.06 \pm 0.05$  s with an average inter-call interval of  $0.12 \pm 0.007$  s. The average dominant frequency is  $2321.29 \pm 127.86$ . Other call parameters are listed in Table 4.

**Conservation status.** The distribution polygon of *H. elbakyanae* sp. nov. is 11 km<sup>2</sup>. There is evidence of deforestation due to logging and it is not known



**Figure 19.** Variation in life of *Hyloscirtus elbakyanae* sp. nov. Dorsolateral and ventral views. From left to right, first and second rows: QCAZ 53808 (holotype, adult male), QCAZ 53807, 53831 (adult males); third and fourth rows: QCAZ 72667, 72665 (adult males); fifth and sixth rows: QCAZ 73709, 72669 (adult males).

to occur in protected areas. There might be undiscovered populations because the region where it occurs has not been thoroughly sampled. However, in response to its distribution range being less than 20000 km<sup>2</sup> and having fewer than ten known localities, we propose assigning *H. elbakyanae* sp. nov. to the Red List category Vulnerable (VUB1abiii).

**Etymology.** The specific name *elbakyanae* sp. nov. is a noun in the genitive case and is a patronym for Alexandra Elbakyan. She is a computer programmer and creator of Sci-Hub, a website which provides free access to scientific articles. Sci-Hub allows scientists worldwide to access articles that, otherwise, are behind paywalls and unaffordable in low- and middle-income countries. Our research has greatly benefited from access to relevant literature using Sci-Hub through the years.

***Hyloscirtus dispersus* sp. nov.**

<https://zoobank.org/69BCDDF6-E41A-40E2-A389-44566337EC4C>

Figs 5, 7, 9–11, 20–22

Common name: Proposed standard English name: Dispersed stream frog

Proposed standard Spanish name: Rana de Torrente dispersa

**Type material. Holotype.** • QCAZ 52006 (Figs 20–22), field no. SC 38765, adult male from Ecuador, Provincia Tungurahua, Caserío Machay, 3 km E of Río Verde on the road to Puyo, (1.3923°S, 78.2801°W), 1349 m above sea level, collected by SRR, F. Ayala, T. Camacho, M. Yáñez, D. Rivadeneira, S. Aldás and D. Pareja on 19 September 2011. A 3D model of the holotype is available at Sketchfab platform (<https://skfb.ly/oSqqI>). **Paratypes.** • All collected in Ecuador. Provincia Sucumbíos: Río Azuela, Hostería El Reventador (0.0752°S, 77.5921°W), 1680 m, QCAZ 66709–10, adult males, collected by G. Vaca, M. Mejía and D. Escobar on 26 February 2017; • Provincia Napo: Cocodrilos, on Baeza–Archidona road (0.6710°S, 77.7928°W), 1575 m, QCAZ 63488, adult male, collected by SRR, S. Guamán, M.J. Navarrete, B. Proaño and A. Achig on 23 June 2016; • Provincia Tungurahua: same locality, date, and collectors as for the holotype, (1.4002°S, 78.2807°W), 1244 m, QCAZ 52007, adult male; • Reserva Río Zuñac (1.3765°S, 78.1540°W), 1594 m, QCAZ 52458, 52462, adult males, collected by F. Ayala, D. Paucar, Y. Sagredo, J.P. Reyes, F. Recalde, L. Recalde and S. Recalde on 16 January 2011; • Provincia Pastaza: Reserva Comunitaria Ankaku, on Puyo–Tena road (1.2676°S, 78.0479°W), 1668 m, QCAZ 46297, adult male, collected by E. Tapia on 15 October 2009; • Parque Nacional Llanganates, Comunidad Zarentza (0.3524°S, 78.072°W), 1419 m, QCAZ 59819–21, adult males, collected by D. Rivadeneira, F. Mora, J.C. Sánchez, D. Velalcázar, D. Núñez and J. Pinto; • Provincia Morona Santiago: Chiguinda (3.2278°S, 78.7200°W), 1741, QCAZ 18275, collected by Í. Tapia and G. Onore on 27 December 2001; • 16 km N El Ideal, on the road to Cuenca from Gualaquiza (3.2425°S, 78.6725°W), 1600 m, QCAZ 23936, metamorph, QCAZ 23937, 23945, adult males, collected by SRR and G. Romero on 09 April 2003; • 8.6 km E 9 de Octubre, Guamote–Macas road (2.24774°S, 78.2069°W), 1671 m, QCAZ 32267, adult male, collected by M. Bustamante, J. Guayasamin, E. Bonaccorso and J. F. Freile on 19 July 2006; • 4 km from Limón (Leonidas Plaza Gutiérrez), on the road to Plan de Milagro (2.9969°S, 78.4550°W), 1373–1409 m, QCAZ 40878, adult male, collected by I. Tapia, D. Salazar, L. Coloma and SRR on 07 June 2008, QCAZ 41901 adult female, collected by D. Salazar, E. Lemmon and A. Lemmon on 06 August 2008; • Limón (Leonidas Plaza Gutiérrez), Río Napinaza (2.9230°S, 78.4080°W), 1430 m, QCAZ 42002, adult male, collected by D. Salazar, E. Lemmon and A. Lemmon on 13 August 2008, QCAZ 42047, adult male, collected by D. Salazar and N. Peñafiel on 28 February 2008; • Bosque Protector Abanico (2.2448°S, 78.2053°W), 1646, QCAZ 49032, adult male, collected by Y. Sagredo and R. Jarín on 26 July 2010; • 9 de Octubre–Macas road (2.2351°S, 78.2167°W), 1683 m, QCAZ 57014–16, adult males, collected by F. Ayala, Y. Sagredo, S. Arroyo, S. Valverde and L. Cedeño on 02 March 2014; • Parque Nacional Sangay, Sardinayacu (2.0928°S, 78.1687°W), 1475–1735 m, QCAZ 58732–3, 58735, adult males, collected by D. Rivadeneira, D. Velalcázar, J. Pinto, F. Mora, D. Núñez, J.C. Sanchez and A. Correa between 16 January 2015 and 26 January 2015, QCAZ 59099, adult female, collected by SRR, D. Paucar, PJV, P. Baldeón, M. Caminer

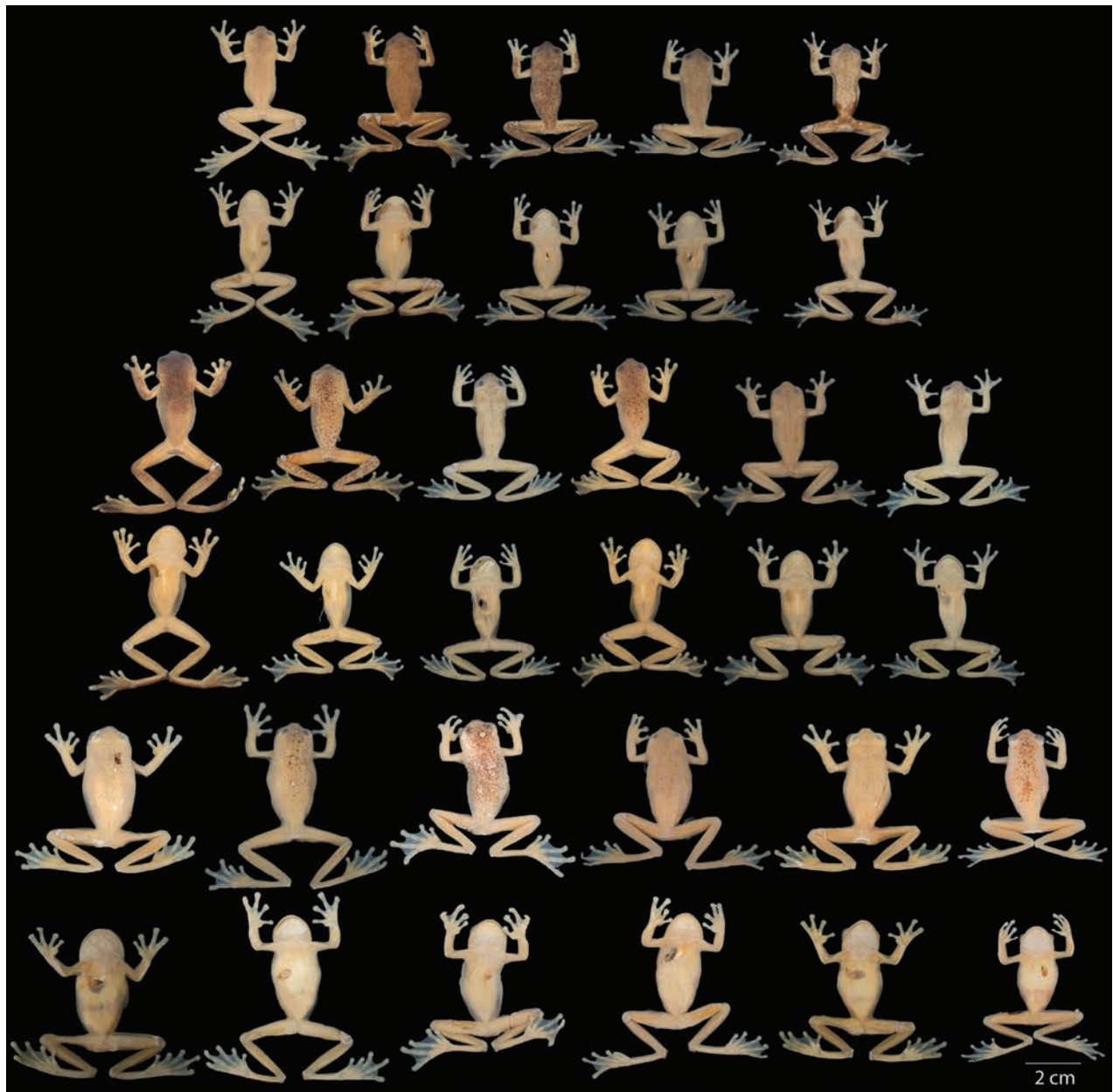


**Figure 20.** Variation of preserved specimens of *Hyloscirtus dispersus* sp. nov. Dorsal and ventral views. From left to right, first and second rows: QCAZ 52006 (holotype, adult male), QCAZ 41554, 69548, 69561, 66709 (adult males); third and fourth rows: QCAZ 66051, 52458, 66710, 66052, 69550, 63488 (adult males); fifth and six rows: QCAZ 60694, 57100, 41649, 41901, 60695, 41031 (adult females). See Suppl. material 1: table S1 for locality information. All specimens are shown at the same scale.

and K. Nusirquia on 28 February 2015; • Puchimi (2.7774°S, 78.1595°W), 1365–1450 m, QCAZ 69548, 69550, 69555, 69561–63, adult males, collected by D. Almeida, D. Núñez, K. Nusirquia and J. Mora on 09 July 2017; • Comunidad Shuar Kunkuk, base of Cordillera del Cóndor mountain range (3.3302°S, 78.1972°W), 1521 m, QCAZ 71029, adult female, collected by D. Almeida, D. Núñez, K. Nusirquia and R. Gavilanes on 01 March 2018; • Cordillera de Cutucú, Carlos Hurtado’s house surroundings (2.7818°S, 78.1604°W), 1380 m, QCAZ 71428, adult male, collected by D. Almeida, D. Paucar, D. Núñez, K. Nusirquia and R. Gavilanes on 29 January 2018; • Provincia Zamora Chinchipe: Miazí Alto (4.2502°S, 78.6174°W), 1250 m, QCAZ 41031, adult female, 41032, male,

collected by E. Tapia and J. Guayasamín on 12 April 2009, QCAZ 41554, adult male, collected by J. Guayasamín, E. Tapia and H. Braun on 07 April 2009, QCAZ 41649, adult female, collected by S. Aldás, J. Guayasamín and E. Tapia on 12 April 2009; • Los Encuentros (3.7568°S, 78.6457°W), QCAZ 47074, juvenile, 47110 female, collected by A. Almendáriz on 23 June 2009; Nuevo Paraíso, 700 m NO on the road to Las Tres Aguas (4.8710°S, 78.9757°W), 1742 m, QCAZ 57099–100, adult females, collected by D. Paucar, D. Almeida, G. Galarza and D. Pareja on 10 April 2014; • Reserva Numbami, 18 km on Zamora-Romerillos road (4.1760°S, 78.9561°W), 1434–1583 m, QCAZ 57664, 57667, adult males, 57665–66, adult females, collected by SRR, D. Paucar, PJV, D. Almeida, D. Velalcázar, M. J. Navarrete, S. Arroyo, N. Páez and Z. Lange on 11 July 2014; • Parque Nacional Podocarpus, Bombuscaro (4.1344°S, 78.9938°W), 1443 m, QCAZ 60688, 60692, adult males, 60694–95, adult females, collected by D. Rivadeneira, F. Mora, J. C. Sánchez, D. Velalcázar, D. Núñez, J. Pinto, K. Cruz and L. Tipantiza on 24 March 2015; • Concesión Mirador ECSA, Río Wawayme basin, towards Canales (3.59145°S, 78.4212°W), 1637 m, QCAZ 66050–52, adult males, collected by R. Betancourt, M. Cajamarca and L. Pandiguana on 23 November 2016; • Nuevo Paraíso, Ciudad Perdida (4.4803°S, 78.8294°W), 1334 m, QCAZ 68056, adult female, collected by F. Ayala, K. Nusirquia, D. Núñez and A. Calispa on 13 May 2017.

**Definition.** In this section, coloration and characters refer to preserved specimens unless otherwise mentioned. The Definition and Diagnosis are based on 11 adult females and 36 adult males. *Hyloscirtus dispersus* sp. nov. can be diagnosed by the combination of the following characters: (1) mean SVL 34.1 mm in adult males (range 31.3–38.7;  $n = 36$ ) and mean SVL 41.1 mm in adult females (range 35.4–45.2;  $n = 11$ ; Suppl. material 1: table S5, Fig. 7); (2) white supralabial stripe present or absent; (3) tympanum rounded, inconspicuous to conspicuous in males and conspicuous in females; supratympanic fold present and unpigmented; (4) white ulnar and tarsal folds; (5) subarticular tubercles conspicuous in hands and feet; (6) supernumerary tubercles inconspicuous in feet and conspicuous in hands; (7) calcar tubercle present; (8) pericloacal spots well-defined; (9) all surfaces plain cream with a combination of scattered large or minute black spots and with white spots or flecks varying from ill-defined to large on the dorsum; (10) in life, dorsal surfaces and flanks yellowish green, olive green, dull green, brownish green or greyish green, with barely visible to thick white spots and minute or thick black spots or flecks, scattered throughout the body; venter yellow, gold, whitish, brownish green, grayish green, or dark pinkish; axillar and inguinal regions and ventral surfaces yellow, blueish, greenish, silver, brownish green or dark pinkish; pericloacal spots yellow, white or unpigmented; webbing yellow, yellow orange, whitish or dark pinkish; iris pearl or pinkish with leather reticulations; (11) the advertisement call consist of a single note, with a mean duration of  $0.11 \pm 0.015$  s and a mean dominant frequency of  $2795.4 \pm 138.68$  Hz and a fundamental frequency of  $2700.63 \pm 195.66$  Hz. The call can be repeated in a series of 1 to 8 calls.

**Diagnosis.** Characters in this section pertain to preserved specimens unless otherwise noticed. Coloration refers to life specimens. The most similar species to *Hyloscirtus dispersus* sp. nov. living in the Amazon basin are *Hyloscirtus albopunctulatus* (sympatrically distributed, Fig. 5), *H. maycu* sp. nov., *H. elbakayanae* sp. nov., *H. phyllognathus*, and *H. torrenticola*. *Hyloscirtus dispersus*

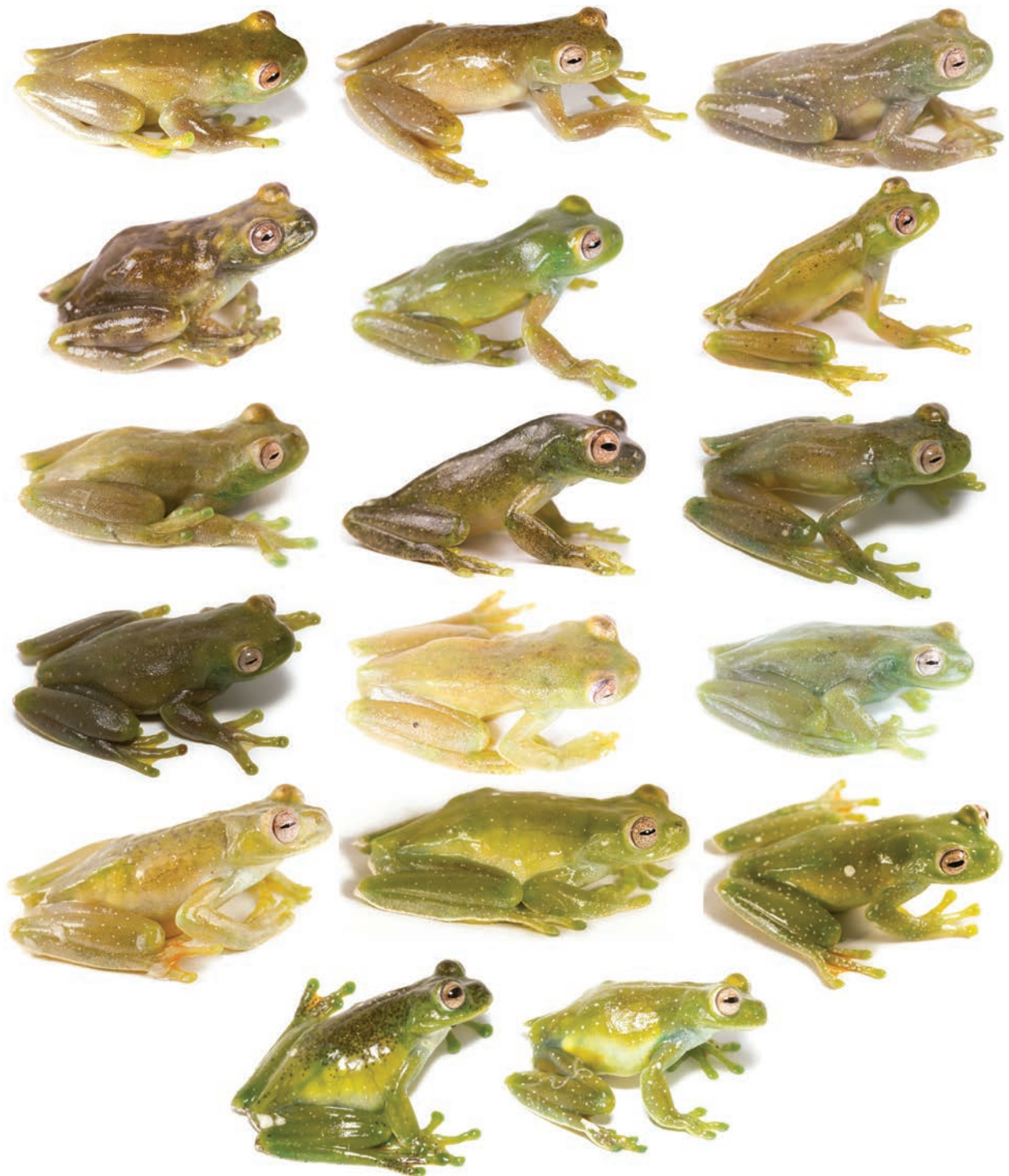


**Figure 21.** Variation in life of *Hyloscirtus dispersus* sp. nov. Dorsolateral view. From left to right, first row: QCAZ 52006 (holotype, adult male), 52463, 69562 (adult males); second row: QCAZ 66709, 59821, 66710 (adult males); third row: QCAZ 49032, 69563, 58732 (adult males); fourth row: QCAZ 58733, 63488, 69546 (adult males); fifth row: QCAZ 41031, 57100, 57666 (adult females); sixth row: QCAZ 60694, 60695 (adult females).

sp. nov. differs by having a supratympanic fold (absent in *H. maycu* sp. nov., *H. elbakyanae* sp. nov., *H. phyllognathus*, and *H. torrenticola*), an inconspicuous tarsal fold (thick in *H. albopunctulatus*, *H. phyllognathus*, and *H. torrenticola*), conspicuous subarticular tubercles in hands and feet (inconspicuous in hands and feet in *H. albopunctulatus*, Fig. 11), conspicuous supernumerary tubercles

in hands (inconspicuous in hands and feet in *H. albopunctulatus*, *H. maycu* sp. nov., and *H. elbakyanae* sp. nov.), well-defined pericloacal spots (ill-defined or absent in *H. maycu* sp. nov. and *H. elbakyanae* sp. nov.), a calcar tubercle present (absent in all species except for *H. phyllognathus*), and an iris pearl or pinkish with leather-colored reticulations (clam shell with black or sand dune reticulations in *H. albopunctulatus* and a bronze iris in *H. torrenticola*, Fig. 12).

The advertisement call of *Hyloscirtus dispersus* sp. nov. differs by having a call duration of  $0.11 \pm 0.015$  s (shorter in *H. albopunctulatus* with  $0.051 \pm 0.005$  s and in *H. torrenticola* with  $0.03 \pm 0.001$  s), a dominant frequency of  $2743.79 \pm 48.22$  Hz (lower in *H. albopunctulatus* with  $2149.84 \pm 137.36$  Hz and in *H. elbakyanae* sp. nov. with  $2321.29 \pm 127.86$  Hz) and a fundamental frequency of  $2700.63 \pm 195.66$  Hz (lower in *H. albopunctulatus* with  $1214.12 \pm 184.71$  Hz and in *H. elbakyanae* sp. nov. with  $1184.35 \pm 30.48$  Hz). *Hyloscirtus dispersus* sp. nov. has an intercall duration of  $0.33 \pm 0.044$  s (shorter in *H. phyllognathus* with 0.06 s and in *H. torrenticola* with  $0.07 \pm 0.007$  s) (Table 4, Fig. 9; Melin 1941; Duellman and Altig 1978; Rivera-Correa 2016). Moreover, all males of *H. dispersus* sp. nov. have been found calling while perching on vegetation over streams ( $n = 14$ ; Pontificia Universidad Católica del Ecuador 2024), while all males of *H. albopunctulatus* were registered calling from under the rocks next to streams ( $n = 5$ ; Pontificia Universidad Católica del Ecuador 2024).

Finally, *H. dispersus* sp. nov. inhabits elevations between 879 and 1807 m, while *Hyloscirtus elbakyanae* sp. nov. lives lower between 214 and 622 m and in warmer and wetter environments (Figs 5, 10).

**Description of the holotype.** Description of characters based on preserved specimen. Adult male (Figs 20–22). Measurements (in mm): SVL 32.7; foot length 13.6, head length 9.6, head width 9.5, eye diameter 2.9, tympanum diameter 1.5, tibia length 15.8, femur length 14.3, internarial distance 2.7, interorbital distance 4.8. Head slightly longer than wide; body slender; snout rounded in dorsal view and slightly truncated in lateral view; distance from nostril to eye shorter than diameter of eye; canthus rostralis distinct, slightly convex; loreal region slightly concave; internarial region and top of the head flat; nostrils not protuberant, round, directed anterolaterally; lips rounded, not flared; interorbital area flat, longer than upper eyelid; tympanum round, with upper and posterior margins covered by a curved unpigmented supratympanic fold, reaching anterior margin of insertion of arm; tympanic annulus absent; tympanic membrane absent; mental gland present, oval-shaped, barely defined, extending  $\sim 1/3$  the length of head; dentigerous processes of vomers straight, between round choanae, narrowly separated from each other, with five (right) and four (left) teeth; tongue slightly cordiform, widely attached to mouth floor; vocal slits and vocal sac present.

Forearms slender; axillary membrane absent; fingers bearing dermal fringes and rounded discs; relative lengths of fingers  $I < II < IV < III$ ; webbing formula I basal II 2–3<sup>+</sup> III 2<sup>1/2</sup>–2<sup>+</sup> IV; subarticular tubercles prominent, round, single; supernumerary tubercles small; thenar tubercle absent, palmar tubercle small; prepollex present, not modified as a spine; nuptial pads absent; ulnar tubercles absent; outer ulnar fold present. Hindlimbs slender; toes bearing dermal fringes and rounded discs; relative length of toes  $I < II < III < V < IV$ ; extensive toe webbing, formula I 2<sup>-</sup>–1<sup>+</sup> II 1<sup>+</sup>–2<sup>-</sup> III 1<sup>+</sup>–2<sup>+</sup> IV 2<sup>+</sup>–1<sup>-</sup> V; outer tarsal fold present; tarsal tubercles absent; calcar tubercle small, pinkish white; subarticular tubercles conspicuous, round and single; supernumerary tubercles inconspicuous in feet and conspicuous in



**Figure 22.** Variation in life of *Hyloscirtus dispersus* sp. nov. Ventral view. From left to right, first row: QCAZ 52006 (holotype, adult male), 52463, 69562 (adult males); second row: QCAZ 49032, 69563, 66709 (adult males); third row: QCAZ 59821, 66710, 58732 (adult males); fourth row: QCAZ 58733, 63408, 69456 (adult males); fifth row: QCAZ 69550, 59820 (adult males), QCAZ 41031 (adult female); sixth row: QCAZ 57099, 57666, 59099, 57100 (adult females).

hand; inner metatarsal tubercle present and ovoid, outer absent. Skin on dorsal surfaces and flanks smooth; venter finely granular; cloacal opening directed posteriorly at upper level of thighs, round tubercles below; cloacal fold present, thick.

**Color of holotype in preservative** (Fig. 20). Dorsal surfaces of the head, body, limbs, and flanks cream densely covered with minute black spots, bigger black spots dispersed on the head and anterior part of the body. Very few, barely visible, white spots scattered on the posterior dorsum and hindlimbs. Venter, throat, and ventral surfaces of limbs cream. Mental gland cream. White supralabial stripe. White ulnar fold. Pinkish white cloacal and tarsal folds with black spots. Webbing cream.

**Color of holotype in life** (Figs 21, 22). Based on digital photographs. Dorsal surfaces and flanks pale brownish green with minute black spots in the anterior part of the body and arms and white spots scattered throughout the body and limbs. Belly and other ventral surfaces are reddish brown. Tympanum and throat greenish. Mental gland yellowish green. Webbing reddish brown. Iris pinkish with leather reticulations.

**Variation.** Dorsal and ventral variation of adult specimens is illustrated on Figs 20–22. In preservative (Fig. 20), dorsal background coloration varies from darker and brownish cream to pale cream. Background coloration has a variable pattern of white spots distributed throughout the body and limbs with minute black spots scattered in the body (e.g., QCAZ 41901), minute and thick brownish black spots (e.g., QCAZ 57100), few black marks scattered in the dorsum (e.g., QCAZ 60695) or without black spots (e.g., QCAZ 69550), to barely visible white spots in the body with minute black spots dispersed in the body (e.g., QCAZ 66710), minute and thick black or brownish black spots covering half the body or the entire body and limbs (e.g., QCAZ 41554, 69548), covering half the body (e.g., QCAZ 66052, 66709), with dark marks and flecks across the body and limbs (e.g., QCAZ 66051, 52458) and big white marks with thick brownish spots in the body (e.g., QCAZ 41649) and barely visible black spots (e.g., QCAZ 60694). Ventral surfaces vary from pale cream (e.g., QCAZ 57100) to cream (e.g., QCAZ 66051), without any pattern. Throat cream or whitish cream, with or without minute black spots (e.g., 66709). Mental gland varies from cream (e.g., QCAZ 69548) to whitish cream (e.g., QCAZ 41554). Cloacal fold varies from white (e.g., QCAZ 60695), pinkish white (e.g., QCAZ 69550), to pinkish white with black spots (e.g., QCAZ 69561). White supralabial stripe varies from absent (e.g., QCAZ 69548), inconspicuous (e.g., QCAZ 66051) to conspicuous (e.g., QCAZ 66710).

In life, dorsal background coloration varies from yellowish green, pale olive green, olive green, brownish green, darker brownish green, greyish green to lemon grass (Figs 21, 22). Background coloration has a variable pattern of white spots scattered throughout the body and limbs with minute and thick black spots or marks scattered across the body (e.g., QCAZ 52463, 58732), accumulated in the anterior part (e.g., QCAZ 60694), accumulated in the entire body (e.g., QCAZ 69563), with black flecks (e.g., QCAZ 41031) or without black spots or any marks (e.g., QCAZ 57100, 69546) to barely visible or absent white spots without any dark spots or marks (e.g., QCAZ 49032, 66710). Additionally, the dorsum can be covered by thick white marks (e.g., QCAZ 57666, 60694). Venter and posterior tights vary from yellow (e.g., QCAZ 41031, 57666 – less common), greenish (e.g., QCAZ 57099, 59099), lemon grass (e.g., QCAZ 58732), brownish (e.g., QCAZ 52463, 69550), silver (e.g., QCAZ 59821) or white (e.g., QCAZ 69546). Ventral axillar and inguinal surfaces vary from yellow (e.g., QCAZ 41031) to green (e.g., QCAZ 59099) or white (e.g., QCAZ 69456). Throat white (e.g., QCAZ 41031), green (e.g., QCAZ 63488), or brownish (e.g., QCAZ 52463). White supralabial stripe varies from present (e.g., QCAZ 57100) to absent (e.g., QCAZ 66710). Iris varies from pearl with barely visible reticulations (e.g., QCAZ 69546) or leather reticulations (e.g., QCAZ 59821) to pinkish with leather reticulations (e.g., QCAZ 69563). Webbing matches ventral coloration.

**Distribution and natural history.** *Hyloscirtus dispersus* sp. nov. is known from more than 25 localities from northern to southern Ecuador in the eastern Andean slopes, at elevations between 879–1807 m (Fig. 5). From the species

analyzed in this study, this is the most widespread and its biogeographic regions are Eastern Lower Montane Forest and Eastern Montane Forest (Ron et al. 2022). This species lives in hillside forests, frequently found in secondary forest and artificial open areas. They are nocturnal and associated with streams of running water and ravines. Males call perched on riparian vegetation up to 2.5 m above the ground. It also occurs close to lagoons and small waterfalls. Perching sites include plants of Araceae, bromeliads, cedars, and ferns (Pontificia Universidad Católica del Ecuador 2024). This species has not been found living or calling under rocks. It is known to live in sympatry with *Hyloscirtus albopunctulatus* and potentially with *H. maycu* sp. nov.

**Advertisement call.** We analyzed 60 calls from 14 individuals. QCAZ 52006 from Caserío Machay, Provincia Tungurahua, 19 September 2011, recorded by SRR. QCAZ 59820 from Comunidad Zarentza, Llanganates National Park, Provincia Pastaza, 23 February 2015, air temperature 18 °C recorded by D. Rivadeneira. QCAZ 63488 from Cocodrilos, Provincia Napo, 23 June 2016, recorded by SRR. KU 164338 and one unvouchered specimen from 2 km SW of Río Reventador, Provincia Napo, 19 March 1975, temperature 18 °C, recorded by W. E. Duellman. USNM 286338, Río Reventador, Provincia Napo, recorded by R. McDiarmid. USNM 286349 from Baeza–Lago Agrio Road, Provincia Napo, 22 February 1985, recorded by R. McDiarmid. USNM 284316 from Cascada San Rafael, Provincia Napo, recorded by M. Foster. Two unvouchered specimens from San Rafael, Provincia Napo, recorded by R. McDiarmid. One unvouchered specimen from Sangay National Park, Provincia Morona Santiago, recorded by D. Batalas. Two unvouchered specimens from Río Azuela, Provincia Napo, 23 October 1971, temperature 18–19 °C, and one from Cordillera del Dué, Provincia Sucumbíos, recorded by W. Duellman. The advertisement call consists of a single note, repeated in series of 1–8 calls (Fig. 9E). Average call duration is  $0.11 \pm 0.015$  s with an average inter-call interval of  $0.33 \pm 0.044$  s. Mean dominant frequency is  $2795.41 \pm 138.68$  Hz. Other call parameters are listed in Table 4.

**Conservation status.** The distribution polygon of *H. dispersus* sp. nov. is 26,296 km<sup>2</sup>. Its distribution range overlaps with many protected areas. Its presence in secondary forests and artificial open areas indicates that it can withstand anthropogenic habitat change. Therefore, we propose assigning *H. dispersus* sp. nov. to the Red List category Least Concern.

**Etymology.** The specific epithet comes from the Latin word *dispersus* in reference to the wide distribution range of this species, extending from north to south of the eastern Andes of Ecuador and probably with a wider unknown distribution that includes neighboring countries, Colombia, and Peru.

## Discussion

### Cryptic diversity

Our review of Amazonian species of the *Hyloscirtus bogotensis* species group, based on an integrative approach, resulted in the discovery of three new cryptic species. Prior to our review, the group only had three formally described Amazonian species. Therefore, the species described here represent a 100% increase in species content. The new species are visually cryptic as a result of shared patterns of highly variable dorsal coloration. However, some diagnostic

morphological characters, genetic and bioacoustic data, and environmental conditions demonstrate that they represent evolutionary independent lineages.

Color is highly variable within the described species making morphology-based identification of closely related species challenging (see also Guayasamin et al. 2015). Our observations suggest that high variability is the result, in part, of phenotypic plasticity in coloration. Phenotypic plasticity refers to changes in the phenotype by a single genotype in different environments. We found two species of the *H. bogotensis* group with drastic coloration changes during short periods. One individual of *H. alytolylax*, for example, changed its dorsal coloration from greenish brown to greenish yellow, with scattered brown spots, within 16 minutes (Fig. 14C–E). We also found significant changes in *H. albopunctulatus* within periods of less than 20 days. Changes may have been faster, but we lacked photographs for shorter intervals. At least in *H. alytolylax*, color changes were likely physiological because they occurred within minutes. Physiological color plasticity is mediated by hormonal changes triggering intracellular mobilization of pigments (Duellman and Trueb 1994). A pending task is the assessment of the taxonomic extent of plastic color variation in *Hyloscirtus* and Hylidae, in general. Nevertheless, extensive intraspecific and intraindividual variation in dorsal coloration reinforce the notion of the unreliability of dorsal skin coloration in interspecies diagnosis.

As seen in other systematic reviews of Neotropical hylids (e.g., Funk et al. 2012; Rivadeneira et al. 2018), bioacoustic characters were one of the most useful phenotype components to diagnose closely related species. The most divergent calls were those of *H. dispersus* sp. nov. and *H. albopunctulatus* (sympatric species). The advertisement call of these species can be distinguished by ear and the parameters duration of the call and inter-call interval seem to play an important role. These differences, plus their preferred calling site, could help identify them in the field. Regarding morphology, some characters like iris coloration, tubercles and cloacal ornamentation can be useful for separating *H. albopunctulatus* from *H. dispersus* sp. nov. Other than size, we did not document morphological differences between *H. maycu* sp. nov. and *H. elbakyanae* sp. nov. However, they occur at different elevations and environments (drier and colder for *H. maycu* sp. nov.) In addition to their high genetic distances (5.1% for gene 16S; Table 3), the haplotype network for the nuclear gene *c-myc* also supports their distinctiveness as they do not have shared haplotypes (Suppl. material 1: fig. S7). Our time tree indicates that they diverged over 5 Mya (Fig. 2).

*Hyloscirtus torrenticola* was not included in the phylogenetic or morphological analyses; however, the bioacoustic analysis, with calls from its type locality (Fig. 9F), show that this species is distinct from the geographically closer *H. albopunctulatus* and *H. dispersus* sp. nov. Because all known populations of the *H. bogotensis* group from northeastern Ecuador belong to either *H. albopunctulatus* or *H. dispersus* sp. nov., we propose that *H. torrenticola* is absent in Ecuador, at least until documented records become available. The report of *H. torrenticola* by Duellman and Altig (1978) from SW Río Reventador, Ecuador, likely corresponds to *H. dispersus* sp. nov. On the other hand, *Hyloscirtus phyllognathus* sensu stricto (Lineage E) occurs in Peru and is genetically divergent from the Ecuadorian species (see also Almendáriz et al. 2014).

Geographically, the Peruvian populations of *Hyloscirtus phyllognathus* sensu stricto are greatly distant (345 km) from southernmost Ecuadorian populations, and their bioacoustic and morphological space differ (Figs 5, 8, 9D). Based on this

evidence, and the numerous Ecuadorian populations included in this study, we propose that *H. phyllognathus* sensu stricto does not occur in Ecuador and remains restricted to the Amazon basin of Peru. We do not know its actual distribution range, but excluding Ecuadorian populations greatly reduces its previous known range; however, extended sampling of northern Peruvian populations will provide better conclusions. Among all Amazonian species of the *Hyloscirtus bogotensis* group, only *H. dispersus* sp. nov., and *H. palmeri* maintain a large distribution range.

### Phylogenetic relationships and biogeographic history

*Hyloscirtus* monophyly is strongly supported, and four monophyletic species groups were recovered as previously reported (Rojas-Runjaic et al. 2018; Ron et al. 2018; Lyra et al. 2020). The phylogeny included 26 of the 40 described species of *Hyloscirtus*, one of the most comprehensive to date. Within the *Hyloscirtus bogotensis* species group, our results agreed with the latest phylogenies except for weakly supported nodes (Almendáriz et al. 2014; Guayasamin et al. 2015; Ron et al. 2018; Lyra et al. 2020). It should be noted that in all previous phylogenies of *Hyloscirtus* the identity of “*H. phyllognathus*” was mistaken and actually corresponds to *H. dispersus* sp. nov. – except for the individual KU212119, from Peru, which corresponds to *H. phyllognathus* sensu stricto (Lineage E, Fig. 1). The individual MZUTI192 identified as “*H. aff. phyllognathus*” by Guayasamin et al. (2015) actually corresponds to *H. albopunctulatus*.

While there were several limitations of our phylogenomic data generation and analyses (i.e., lower than expected UCE capture success, and four taxa with unexpected placements), the results of our preliminary analyses (Fig. 3, Suppl. material 1: figs S2–S4) are broadly consistent with the smaller molecular dataset. This includes strong support for the monophyly of *H. dispersus* sp. nov., *H. elbakyanae* sp. nov., and *H. albopunctulatus*, and the distinctiveness of one of the Peruvian lineages. Future scrutiny of this dataset is needed to clarify the four enigmatic taxa and issues associated with low-capture success. However, we interpret the general agreement with the smaller molecular dataset as evidence that many of the inferred phylogenetic relationships within the *Hyloscirtus bogotensis* species group are supported by widely distributed signal across the nuclear genome.

The lowest uncorrected *p*-genetic distance between species was 5.0% for the gene 16S (*H. maycu* sp. nov. and *H. elbakyanae* sp. nov.) and up to 15% (*Hyloscirtus albopunctulatus* relative to the other Amazonian lineages). It has been suggested that distances > 3.0% for the gene 16S are indicative of separate species (e.g., Fouquet et al. 2007a). That threshold supports the description of the new species presented here, a result that is reinforced by our genomic, bioacoustic, and morphological datasets. Almendáriz et al. (2014) suggested that populations of *H. phyllognathus* of Ecuador and Peru represented separate species and we confirmed that hypothesis with our results. Moreover, we found 4% of genetic differentiation within Peruvian populations, suggesting the existence of one undescribed species. Guayasamin et al. (2015) mentioned a divergence of *H. phyllognathus* in Ecuador between north and south populations. However, according to our analysis, this divergence is < 1.8%, and we consider it intraspecific genetic variation. Overall, genetic distances should be interpreted with caution as a wide range of divergences have been observed both within and between species.

Our time tree agrees with the divergence time estimates by Portik et al. (2023), the most comprehensive time tree of Anura published to date. For example, Portik et al. (2023) estimate the divergence between the *H. bogotensis* group and its sister clade at 32.9 My, near our estimate of 28.5 My and within our 95% HPD, 21.6–35.0 My. Similarly, diversification within the *H. bogotensis* started at 27.9 My in Portik et al. (2023) vs. 23.8 My in our time tree and within our 5% HPD (16.64–30.80 My).

Our biogeographic analyses indicate that the barrier imposed by the high elevations of the Andes has played a crucial role in shaping the diversification of *Hyloscirtus*. Despite the ancient origin of the group (early Oligocene) we only found four trans-Andean colonization events between the Amazon and Pacific basins: three from east to west (Amazon to Pacific) and one from the Pacific to the Amazon. Therefore, communities of *Hyloscirtus* have evolved independently on opposite sides of the Andes since the mid-Miocene. The oldest colonization events for the genus (two events > 20 Mya) took place from the Amazon to the Caribbean basin. They occurred when most of the tropical Andes were below 3000 m (Fig. 2) and the hydrographic systems in South America were markedly different.

Species of the highland *Hyloscirtus larinopygion* group were younger (average = 3.3 My) than those from lower elevations, the *Hyloscirtus bogotensis* group (7.8 My). This difference could be the result of the more recent origin of highland habitats as a result of Andean uplift during the last 5 My. A younger age for Andean species from higher elevations have been previously documented in plants (e.g., Hughes and Eastwood 2006). The most recent trans-Andean colonization event (~ 4 Mya) took place within the *H. larinopygion* group, a result consistent with its expected higher tolerance for cold climates relative to the lower elevation *H. bogotensis* species group. This scenario is supported by data on minimal critical temperature data ( $CT_{min}$ ) for both groups showing that tadpoles of the *H. larinopygion* group have  $CT_{min} \sim 4.5$  °C lower than those of the *H. bogotensis* group (*H. alytolylax*  $CT_{min} = 6.3$  °C; *H. cf. albopunctulatus*  $CT_{min} = 5.7$  °C; vs. 1.5 in *H. lindae*; Pintanel et al. 2022). Thus, the timing of the colonization events across the Andes is consistent with the current elevation range and thermal tolerance of each group. Our biogeographic reconstructions are the first step in studying the genus's origin and diversification history. Future studies can focus, for example, on the effects of barriers to gene flow or demographic modelling. This would allow for a more in-depth exploration of the biogeographic history and even comparisons with co-distributed genera.

Our environmental envelope analyses suggest the existence of environmental niche differences between closely related species of the *H. bogotensis* group. For example, *H. dispersus* sp. nov. occurs in drier environments relative to *H. elbakyanae* sp. nov. while *H. maycu* sp. nov. occurs in warmer environments than *H. albopunctulatus* (Fig. 10). Our analyses, however, are limited by the low number of known localities available for some species. We hope that the description of the new species will facilitate documenting new localities for the group and more comprehensive future analyses.

## Conclusions

Our results confirm that integrative approaches can help to assess the species boundaries of morphologically cryptic groups. Genetic and acoustic evidence played an important role in distinguishing species among the

*Hyloscirtus bogotensis* group, letting us describe three new species of torrent frogs for the Amazon basin. Two of the new species are threatened with extinction, highlighting the need to protect Andean cloud forests. Our ancestral distribution analysis provides additional insights to understand the effect of geographic barriers in amphibian diversification in the Neotropics.

## Acknowledgements

We thank Gabriela Castillo and Marcel Caminer for their guidance during the lab work for Sanger-based sequencing. Marcel Caminer and María José Navarrete gave advice for phylogenetic reconstructions and Alberto García Ayachi took morphological measurements of specimens at the CORBIDI museum. We thank the personnel of the Museo de Zoología QCAZ, especially Diego Paucar and Fernando Ayala, for assistance with specimen access. Gustavo Pazmiño provided good-quality photographs of live specimens. We thank Andrés Mármol, Micaela Stacey and Gustavo Pazmiño, from 3Diversity SAS, for making the 3D models of the holotypes of the new species. For specimen collection, we thank A. Achig, S. Aldás, D. Almeida, A. Almendáriz, S. Arroyo, F. Ayala, P. Baldeón, R. Betancourt, E. Bonaccorso, H. Braun, M. Bustamante, M. Cajamarca, A. Calispa, T. Camacho, M. Caminer, A. Carvajal, L. Cedeño, M. Cohen, K. Cruz, L. Coloma, A. Correa, V. Duran, E. Escobar, J. F. Freile, G. Galarza, R. Gavilanes, S. Guamán, J. Guayasamin, F. Hervas, R. Jarrín, Z. Lange, E. Lemmon, A. Lemmon, M. Mejía, A. Merino, F. Mora, J. Mora, M. J. Navarrete, D. Núñez, E. Nurisquia, G. Onore, J. Ortega, N. Páez, L. Pandiguana, D. Pareja, D. Paucar, N. Peñafiel, S. Pillajo, J. Pinto, B. Proaño, F. Recalde, L. Recalde, S. Recalde, J. P. Reyes, D. Rivadeneira, K. Roelants, G. Romero, Y. Sagredo, d. Salazar, J. C. Sánchez, L. Schulte, E. Tapia, I. Tapia, L. Tipantiza, E. Twomey, G. Vaca, S. Valverde, M. Yáñez-Muñoz. We also thank D. Batallas, W. Duellman, M. Foster, R. McDiarmid, J. Ortega, M. Read, D. Rivadeneira, and D. Velalcázar for call recordings. F. Serrano, Naturaleza y Cultura Internacional NGO, provided information about the Maycu reserve.

## Additional information

### Conflict of interest

The authors have declared that no competing interests exist.

### Ethical statement

No ethical statement was reported.

### Funding

Field and laboratory work in Ecuador were funded by Secretaría Nacional de Educación Superior, Ciencia, Tecnología e Innovación del Ecuador SENESCYT (Arca de Noé initiative; SRR and Omar Torres principal investigators) and a grant from Pontificia Universidad Católica del Ecuador, Dirección General Académica. The phylogenomic analysis was in part supported by NERC funds awarded to JWS (NE/R002150/1). Data generation and analyses conducted at the Natural History Museum, London were supported by the Genomics and Evolution of Life research themes.

## Author contributions

Conceptualization: AVJ, SRR. Data curation: SRR, AVJ, PJV. Formal analysis: SRR, AVJ. Funding acquisition: SRR, JWS. Methodology: AVJ, JWS, SRR. Project administration: SRR. Resources: SRR. Writing - original draft: AVJ, SRR. Writing - review and editing: AVJ, PJV, SRR, JWS.

## Author ORCIDs

Andrea Varela-Jaramillo  <https://orcid.org/0000-0002-0092-9915>

Jeffrey W. Streicher  <https://orcid.org/0000-0002-3738-4162>

Pablo J. Venegas  <https://orcid.org/0000-0002-6501-4492>

Santiago R. Ron  <https://orcid.org/0000-0001-6300-9350>

## Data availability

All of the data that support the findings of this study are available in the main text, Supplementary Information, and the repository Zenodo.org.

## References

- Almendáriz A, Brito J, Batallas D, Ron S (2014) Una especie nueva de rana arbórea del género *Hyloscirtus* (Amphibia: Anura: Hylidae) de la Cordillera del Cóndor. *Papéis Avulsos de Zoologia* (São Paulo) 54: 33–49. <https://doi.org/10.1590/0031-1049.2014.54.04>
- AmphibiaWeb (2024) University of California, Berkeley, CA, USA. <https://amphibiaweb.org/about/index.html> [accessed 19 February 2024]
- AmphibiaWeb (2023) University of California, Berkeley, CA, USA. <https://amphibiaweb.org/search/index.html> [accessed 17 March 2023]
- Barrientos LS, Streicher JW, Miller EC, Pie MR, Wiens JJ, Crawford AJ (2021) Phylogeny of terraranan frogs based on 2,665 loci and impacts of missing data on phylogenomic analyses. *Systematics and Biodiversity* 19: 818–833. <https://doi.org/10.1080/14772000.2021.1933249>
- Beaupre SJ, Jacobson ER, Lillywhite HB, Zamudio K (2004) Guidelines for use of live amphibians and reptiles in field and laboratory research (2<sup>nd</sup> edn.) The American Society of Ichthyologists and Herpetologists, USA, 43 pp.
- Bolger AM, Lohse M, Usadel B (2014) Trimmomatic: a flexible trimmer for Illumina sequence data. *Bioinformatics* 30: 2114–2120. <https://doi.org/10.1093/bioinformatics/btu170>
- Boschman LM (2021) Andean mountain building since the Late Cretaceous: A paleoelevation reconstruction. *Earth-Science Reviews* 220:103640. <https://doi.org/10.1016/j.earscirev.2021.103640>
- Bouckaert R, Vaughan TG, Barido-Sottani J, Duchêne S, Fourment M, Gavryushkina A, Heled J, Jones G, Kühnert D, De Maio N, Matschiner M, Mendes FK, Müller NF, Ogilvie HA, du Plessis L, Poppinga A, Rambaut A, Rasmussen D, Siveroni I, Suchard MA, Wu C-H, Xie D, Zhang C, Stadler T, Drummond AJ (2019) BEAST 2.5: An advanced software platform for Bayesian evolutionary analysis. *PLOS Computational Biology* 15: e1006650. <https://doi.org/10.1371/journal.pcbi.1006650>
- Boulenger GA (1882) Catalogue of the Batrachia Salientia s. Ecaudata in the collection of the British Museum (2<sup>nd</sup> edn.). Printed by order of the Trustees, London, 588 pp.
- Brunetti AE, Hermida GN, Luna MC, Barsotti AMG, Jared C, Antoniazzi MM, Rivera-Correa M, Berneck BVM, Faivovich J (2015) Diversity and evolution of sexually dimorphic

- mental and lateral glands in Cophomantini treefrogs (Anura: Hylidae: Hylinae). *Biological Journal of the Linnean Society* 114: 12–34. <https://doi.org/10.1111/bij.12406>
- Caminer M, Ron S (2014) Systematics of treefrogs of the *Hypsiboas calcaratus* and *Hypsiboas fasciatus* species complex (Anura, Hylidae) with the description of four new species. *ZooKeys* 370: 1–68. <https://doi.org/10.3897/zookeys.370.6291>
- Caminer MA, Ron SR (2020) Systematics of the *Boana semilineata* species group (Anura: Hylidae), with a description of two new species from Amazonian Ecuador. *Zoological Journal of the Linnean Society* 190: 1–32. <https://doi.org/10.1093/zoolin/zlaa002>
- Caminer MA, Milá B, Jansen M, Fouquet A, Venegas PJ, Chávez G, Loughheed SC, Ron SR (2017) Systematics of the *Dendropsophus leucophyllatus* species complex (Anura: Hylidae): Cryptic diversity and the description of two new species. *PLoS ONE* 12: 1–42. <https://doi.org/10.1371/journal.pone.0171785>
- Castroviejo-Fisher S, Guayasamin JM, Gonzalez-Voyer A, Vilà C (2014) Neotropical diversification seen through glassfrogs. *Journal of Biogeography* 41: 66–80. <https://doi.org/10.1111/jbi.12208>
- Charif RA, Stirckman LM, Waack AM (2010) Raven Pro 1.4 User's Manual. The Cornell Lab of Ornithology, Ithaca, NY, USA.
- Chasiluisa VD, Caminer MA, Varela-Jaramillo A, Ron SR (2020) Description and phylogenetic relationships of a new species of treefrog of the *Osteocephalus buckleyi* species group (Anura: Hylidae). *Neotropical Biodiversity* 6: 21–36. <https://doi.org/10.1080/23766808.2020.1729306>
- Coloma LA, Carvajal-Endara S, Dueñas JF, Paredes-Recalde A, Morales-Mite M, Almeida-Reinoso D, Tapia EE, Hutter CR, Toral E, Guayasamin JM (2012) Molecular phylogenetics of stream treefrogs of the *Hyloscirtus larinopygion* group (Anura: Hylidae), and description of two new species from Ecuador. *Zootaxa* 3364: 1–78. <https://doi.org/10.11646/zootaxa.3364.1.1>
- Crawford AJ, Smith EN (2005) Cenozoic biogeography and evolution in direct-developing frogs of Central America (Leptodactylidae: Eleutherodactylus) as inferred from a phylogenetic analysis of nuclear and mitochondrial genes. *Molecular Phylogenetics and Evolution* 35: 536–555. <https://doi.org/10.1016/j.ympev.2005.03.006>
- Darst CR, Cannatella DC (2004) Novel relationships among hyloid frogs inferred from 12S and 16S mitochondrial DNA sequences. *Molecular Phylogenetics and Evolution* 31: 462–475. <https://doi.org/10.1016/j.ympev.2003.09.003>
- Duellman WE (1970) The hylid frogs of Middle America. Vol. 1. Monograph of the Museum of Natural History, University of Kansas, 448 pp. <https://doi.org/10.1039/C4RA17109H>
- Duellman WE (1972) A review of the neotropical frogs of the *Hyla bogotensis* group. Occasional papers of the Museum of Natural History, the University of Kansas 11: 1–31. <https://doi.org/10.5962/bhl.part.15140>
- Duellman WE (2001) Hylid Frogs of Middle America. Society for the Study of Amphibians and Reptiles, Ithaca, New York. <https://www.nhbs.com/the-hylid-frogs-of-middle-america-2-volume-set-book> [accessed 3 March 2021]
- Duellman WE, Altig R (1978) New species of tree frogs (family Hylidae) from the Andes of Colombia and Ecuador. *Herpetologica* 34: 177–185.
- Duellman WE, Mendelson JR (1995) Amphibians and reptiles from northern Departamento Loreto, Peru: Taxonomy and biogeography. *The University of Kansas science bulletin*. 55: 329–376. <https://doi.org/10.5962/bhl.part.779>
- Duellman WE, Trueb L (1994) *Biology of Amphibians*. JHU Press, Baltimore, Maryland, 702 pp. <https://doi.org/10.56021/9780801847806>

- Duellman WE, De la Riva I, Wild E (1997) Frogs of the *Hyla armata* and *Hyla pulchella* group in the Andes of South America, with definitions and analyses of phylogenetic relationships of Andean group of *Hyla*. Scientific Papers. Natural History Museum, University of Kansas 3: 1–41. <https://doi.org/10.5962/bhl.title.48689>
- Duellman WE, Marion AB, Hedges SB (2016) Phylogenetics, classification, and biogeography of the treefrogs (Amphibia: Anura: Arboranae). *Zootaxa* 4104: 001–109. <https://doi.org/10.11646/zootaxa.4104.1.1>
- Elmer KR, Cannatella DC (2008) Three new species of leaf litter frogs from the upper Amazon forests : cryptic diversity within *Pristimantis "ockendeni"* (Anura: Strabomantidae) in Ecuador. *Zootaxa* 1784: 11–38. <https://doi.org/10.11646/zootaxa.1784.1.2>
- Esselstyn J, Garcia H, Saulog M, Heaney L (2008) A New Species of *Desmalopex* (Pteropodidae) from the Philippines, with a Phylogenetic Analysis of the Pteropodini. *Journal of Mammalogy* 89(4): 815–825. <https://doi.org/10.1644/07-MAMM-A-285.1>
- Faircloth BC (2016) PHYLUCES is a software package for the analysis of conserved genomic loci. *Bioinformatics* 32: 786–788. <https://doi.org/10.1093/bioinformatics/btv646>
- Faircloth BC, McCormack JE, Crawford NG, Harvey MG, Brumfield RT, Glenn TC (2012) Ultra-conserved elements anchor thousands of genetic markers spanning multiple evolutionary timescales. *Systematic Biology* 61: 717–726. <https://doi.org/10.1093/sysbio/sys004>
- Faivovich J, García PCA, Ananias F, Lanari L, Basso NG, Wheeler WC (2004) A molecular perspective on the phylogeny of the *Hyla pulchella* species group (Anura, Hylidae). *Molecular Phylogenetics and Evolution* 32: 938–950. <https://doi.org/10.1016/j.ympev.2004.03.008>
- Faivovich J, Haddad CFB, Garcia PCA, Frost DR, Campbell JA, Wheeler WC (2005) Systematic review of the frog family Hylidae, with special reference to Hylinae: phylogenetic analysis and taxonomic revision. *Bulletin of the AMNH* 294: 1. [https://doi.org/10.1206/0003-0090\(2005\)294\[0001:SR0TFF\]2.0.CO;2](https://doi.org/10.1206/0003-0090(2005)294[0001:SR0TFF]2.0.CO;2)
- Faivovich J, Moravec J, Cisneros-Heredia DF, Köhler J (2006) A new species of the *Hypsiboas benitezi* group from the Western Amazon Basin (Amphibia: Anura: Hylidae). *Herpetologica* 62: 96–108. <https://doi.org/10.1655/05-12.1>
- Feng Y-J, Blackburn DC, Liang D, Hillis DM, Wake DB, Cannatella DC, Zhang P (2017) Phylogenomics reveals rapid, simultaneous diversification of three major clades of Gondwanan frogs at the Cretaceous–Paleogene boundary. *Proceedings of the National Academy of Sciences* 114: 1–7. <https://doi.org/10.1073/pnas.1704632114>
- Fouquet A, Gilles A, Vences M, Marty C, Blanc M, Gemmell NJ (2007a) Underestimation of species richness in neotropical frogs revealed by mtDNA analyses. *PLOS Biology* 2: e1109. <https://doi.org/10.1371/journal.pone.0001109>
- Fouquet A, Vences M, Salducci M-D, Meyer A, Marty C, Blanc M, Gilles A (2007b) Revealing cryptic diversity using molecular phylogenetics and phylogeography in frogs of the *Scinax ruber* and *Rhinella margaritifera* species groups. *Molecular Phylogenetics and Evolution* 43: 567–582. <https://doi.org/10.1016/j.ympev.2006.12.006>
- Frank N, Ramus E (1996) Review of A Complete Guide to Scientific and Common Names of Reptiles and Amphibians of the World. *Copeia* 1996: 1066–1069. <https://doi.org/10.2307/1447688>
- Frost DR (2023) Amphibian Species of the World: an Online Reference. Version 6.1. Electronic Database. <https://amphibiansoftheworld.amnh.org/index.php>. American Museum of Natural History, New York, USA. <https://doi.org/10.5531/db.vz.0001> [accessed 17 March 2023]
- Funk WC, Caminer M, Ron SR, Chris Funk W, Caminer M, Ron SR (2012) High levels of cryptic species diversity uncovered in Amazonian frogs. *Proceedings. Biological Sciences* 279: 1806–1814. <https://doi.org/10.1098/rspb.2011.1653>

- Goebel AM, Donnelly JM, Atz ME (1999) PCR primers and amplification methods for 12S ribosomal DNA, the control region, cytochrome oxidase I, and cytochrome b in bufonids and other frogs, and an overview of PCR primers which have amplified DNA in amphibians successfully. *Molecular Phylogenetics and Evolution* 11: 163–199. <https://doi.org/10.1006/mpev.1998.0538>
- Gonzalez-Voyer A, Padial JM, Castroviejo-Fisher S, De La Riva I, Vilà C (2011) Correlates of species richness in the largest Neotropical amphibian radiation. *Journal of Evolutionary Biology* 24: 931–942. <https://doi.org/10.1111/j.1420-9101.2011.02243.x>
- Guayasamin JM, Rivera-Correa M, Arteaga A, Culebras J, Bustamante L, Pyron RA, Peñafiel N, Morochz C, Hutter CR (2015) Molecular phylogeny of stream treefrogs (Hylidae: *Hyloscirtus bogotensis* group), with a new species from the Andes of Ecuador. *Neotropical Biodiversity* 1: 2–21. <https://doi.org/10.1080/23766808.2015.1074407>
- Guillory WX, French CM, Twomey EM, Chávez G, Prates I, von May R, De la Riva I, Lötters S, Reichle S, Serrano-Rojas SJ, Whitworth A, Brown JL (2020) Phylogenetic relationships and systematics of the Amazonian poison frog genus *Ameerega* using ultra-conserved genomic elements. *Molecular Phylogenetics and Evolution* 142: 106638. <https://doi.org/10.1016/j.ympev.2019.106638>
- Harmon LJ (2019) Phylogenetic comparative methods: learning from trees. *Ecoevorxiv*, 234 pp. <https://doi.org/10.32942/OSF.IO/E3XNR>
- Hijmans RJ, Cameron SE, Parra JL, Jones PG, Jarvis A (2005) Very high resolution interpolated climate surfaces for global land areas. *International Journal of Climatology* 25: 1965–1978. <https://doi.org/10.1002/joc.1276>
- Hime PM, Lemmon AR, Lemmon ECM, Prendini E, Brown JM, Thomson RC, Kratochvil JD, Noonan BP, Pyron RA, Peloso PLV, Kortyna ML, Keogh JS, Donnellan SC, Mueller RL, Raxworthy CJ, Kunte K, Ron SR, Das S, Gaitonde N, Green DM, Labisko J, Che J, Weisrock DW (2021) Phylogenomics Reveals Ancient Gene Tree Discordance in the Amphibian Tree of Life. *Systematic Biology* 70: 49–66. <https://doi.org/10.1093/sysbio/syaa034>
- Hughes C, Eastwood R (2006) Island radiation on a continental scale: Exceptional rates of plant diversification after uplift of the Andes. *Proceedings of the National Academy of Sciences* 103: 10334–10339. <https://doi.org/10.1073/pnas.0601928103>
- ICZN (2003) Declaration 44. Amendment of Article 74.7.3. *The Bulletin of zoological nomenclature* 60: 263–263.
- IUCN (2001) Red List Categories and Criteria: Version 3.1. IUCN, Switzerland and Cambridge, U.K. <https://www.iucnredlist.org/species/55379/85897765#assessment-information> [accessed 31 January 2019]
- IUCN (2023) The IUCN Red List of Threatened Species. Version 2022-2. <http://www.iucnredlist.org/internal-pdf://0.0.1.74/search.html> [accessed 17 March 2023]
- Kalyaanamoorthy S, Minh BQ, Wong TKF, von Haeseler A, Jermiin LS (2017) ModelFinder: fast model selection for accurate phylogenetic estimates. *Nature Methods* 14: 587–589. <https://doi.org/10.1038/nmeth.4285>
- Katoh K, Misawa K, Kuma K, Miyata T (2002) MAFFT: a novel method for rapid multiple sequence alignment based on fast Fourier transform. *Nucleic Acids Research* 30: 3059–3066. <https://doi.org/10.1093/nar/gkf436>
- Kearse M, Moir R, Wilson A, Stones-Havas S, Cheung M, Sturrock S, Buxton S, Cooper A, Markowitz S, Duran C, Thierer T, Ashton B, Meintjes P, Drummond A (2012) Geneious Basic: an integrated and extendable desktop software platform for the organization and analysis of sequence data. *Bioinformatics (Oxford, England)* 28: 1647–1649. <https://doi.org/10.1093/bioinformatics/bts199>

- Köhler J, Jansen M, Rodríguez A, Kok PJR, Toledo LF, Emmrich M, Glaw F, Haddad CFB, Rödel M-O, Vences M (2017) The use of bioacoustics in anuran taxonomy: theory, terminology, methods and recommendations for best practice. *Zootaxa* 4251: 1–124. <https://doi.org/10.11646/zootaxa.4251.1.1>
- Lanfear R, Calcott B, Ho SYW, Guindon S (2012) Partitionfinder: combined selection of partitioning schemes and substitution models for phylogenetic analyses. *Molecular Biology and Evolution* 29: 1695–1701. <https://doi.org/10.1093/molbev/mss020>
- Lynch JD (1997) Biogeographic patterns of Colombian frogs and toads. *Revista de la Academia Colombiana de Ciencias* 21: 237–248. [https://doi.org/10.18257/raccefyn.21\(80\).1997.2973](https://doi.org/10.18257/raccefyn.21(80).1997.2973)
- Lynch J (2005) Discovery of the richest frog fauna in the world—an exploration of the forests to the north of Leticia. *Revista de la Academia Colombiana de Ciencias Exactas, Físicas y Naturales* 29: 581–588. [https://doi.org/10.18257/raccefyn.29\(113\).2005.2188](https://doi.org/10.18257/raccefyn.29(113).2005.2188)
- Lyra ML, Lourenço ACC, Pinheiro PDP, Pezzuti TL, Baêta D, Barlow A, Hofreiter M, Pombal JP JR, Haddad CFB, Faivovich J (2020) High-throughput DNA sequencing of museum specimens sheds light on the long-missing species of the *Bokermannohyla claresignata* group (Anura: Hylidae: Cophomantini). *Zoological Journal of the Linnean Society* 190: 1235–1255. <https://doi.org/10.1093/zoolinnean/zlaa033>
- Maddison WP, Maddison DR (2018) Mesquite: a modular system for evolutionary analysis. Version 3.31. <https://mesquiteproject.wikispaces.com/How+to+Cite+Mesquite> [accessed 05 May 2019]
- Melin D (1941) Contributions to the knowledge of the amphibia of south America. Gothenburg, Sweden, 71 pp.
- Menéndez-Guerrero PA, Graham CH (2013) Evaluating multiple causes of amphibian declines of Ecuador using geographical quantitative analyses. *Ecography* 36: 756–769. <https://doi.org/10.1111/j.1600-0587.2012.07877.x>
- Miller MA, Pfeiffer W, Schwartz T (2010) Creating the CIPRES Science Gateway for inference of large phylogenetic trees. In: 2010 Gateway Computing Environments Workshop (GCE): 1–8. <https://doi.org/10.1109/GCE.2010.5676129>
- Ministerio del Ambiente (2013) Sistema de clasificación de ecosistemas de Ecuador continental. Subsecretaría de Patrimonio Natural, Quito, Ecuador, 233 pp.
- Mueses-Cisneros J (2005) Fauna Anfibia Del Valle De Sibundoy, Putumayo-Colombia (The Amphibian Fauna of the Valle de Sibundoy, Putumayo Colombia). *Caldasia* 27: 229–242.
- Myers CW, Duellman WE (1982) A new species of *Hyla* from Cerro Colorado, and other tree frog records and geographical notes from western Panama. *American Museum Novitates* 2752: 1–32.
- Nascimento J, Lima JD, Suárez P, Baldo D, Andrade GV, Pierson TW, Fitzpatrick BM, Haddad CFB, Recco-Pimentel SM, Lourenço LB (2019) Extensive Cryptic Diversity Within the *Physalaemus cuvieri*–*Physalaemus ephippifer* Species Complex (Amphibia, Anura) Revealed by Cytogenetic, Mitochondrial, and Genomic Markers. *Frontiers in Genetics* 10. <https://doi.org/10.3389/fgene.2019.00719>
- Nguyen L-T, Schmidt HA, Von Haeseler A, Minh BQ (2015) IQ-TREE: A Fast and Effective Stochastic Algorithm for Estimating Maximum-Likelihood Phylogenies. *Molecular Biology and Evolution* 32: 268–274. <https://doi.org/10.1093/molbev/msu300>
- Páez NB, Ron SR (2019) Systematics of *Huicundomantis*, a new subgenus of *Pristimantis* (Anura, Strabomantidae) with extraordinary cryptic diversity and eleven new species. *ZooKeys* 2019: 1–112. <https://doi.org/10.3897/zookeys.868.26766>

- Paradis E (2010) pegas: an R package for population genetics with an integrated–modular approach. *Bioinformatics* 26: 419–420. <https://doi.org/10.1093/bioinformatics/btp696>
- Pintanel P, Tejedo M, Merino-Viteri A, Almeida-Reinoso F, Salinas-Ivanenko S, López-Rosero AC, Llorente GA, Gutiérrez-Pesquera LM (2022) Elevational and local climate variability predicts thermal breadth of mountain tropical tadpoles. *Ecography* 2022: e05906. <https://doi.org/10.1111/ecog.05906>
- Pontificia Universidad Católica del Ecuador (2024) Base de datos de la colección de anfibios del Museo de Zoología QCAZ. Versión 2024.0. <https://bioweb.bio/portal/> [accessed 11 March 2024]
- Portik DM, Streicher JW, Wiens JJ (2023) Frog phylogeny: A time-calibrated, species-level tree based on hundreds of loci and 5242 species. *Molecular Phylogenetics and Evolution* 188: 1–72. <https://doi.org/10.1016/j.ympev.2023.107907>
- Puillandre N, Lambert A, Brouillet S, Achaz G (2012) ABGD, Automatic Barcode Gap Discovery for primary species delimitation. *Molecular Ecology* 21: 1864–1877. <https://doi.org/10.1111/j.1365-294X.2011.05239.x>
- Pyron AR, Wiens JJ (2011) A large-scale phylogeny of Amphibia including over 2800 species, and a revised classification of extant frogs, salamanders, and caecilians. *Molecular Phylogenetics and Evolution* 61: 543–583. <https://doi.org/10.1016/j.ympev.2011.06.012>
- Rahbek C, Borregaard MK, Colwell RK, Dalgaard B, Holt BG, Morueta-Holme N, Nogues-Bravo D, Whittaker RJ, Fjeldså J (2019) Humboldt’s enigma: What causes global patterns of mountain biodiversity? *Science* 365: 1108–1113. <https://doi.org/10.1126/science.aax0149>
- Rambaut A, Suchard M, Drummond A (2007) Tracer v1.4. <http://tree.bio.ed.ac.uk/software/tracer/> [accessed 17 March 2024]
- Revell LJ (2024) phytools 2.0: an updated R ecosystem for phylogenetic comparative methods (and other things). *PeerJ* 12: e16505. <https://doi.org/10.7717/peerj.16505>
- Rivadeneira CD, Venegas PJ, Ron SR (2018) Species limits within the widespread amazonian treefrog *Dendropsophus parviceps* with descriptions of two new species (Anura, Hylidae). *ZooKeys* 2018: 25–77. <https://doi.org/10.3897/zookeys.726.13864>
- Rivera-Correa M (2016) Evolution of Andean Rivers *Hyloscirtus* (Anura: Hylidae): Phylogenetic relations, taxonomic review and delimitation of species. Pontificia Universidade Católica Do Rio Grande Do Sul. Faculdade de Biociencias. Tese de Doutorado. Porto Alegre, Brazil.
- Rohland N, Reich D (2012) Cost-effective, high-throughput DNA sequencing libraries for multiplexed target capture. *Genome Research* 22: 939–946. <https://doi.org/10.1101/gr.128124.111>
- Rojas-Runjaic FJM, Infante-Rivero EE, Salerno PE, Meza-Joya FL (2018) A new species of *Hyloscirtus* (Anura, Hylidae) from the Colombian and Venezuelan slopes of Sierra de Perijá, and the phylogenetic position of *Hyloscirtus jahni* (Rivero, 1961). *Zootaxa* 4382: 121–146. <https://doi.org/10.11646/zootaxa.4382.1.4>
- Ron SR (2000) Biogeographic area relationships of lowland Neotropical rainforest based on raw distributions of vertebrate groups. *Biological Journal of The Linnean Society* 71: 379–402. <https://doi.org/10.1111/j.1095-8312.2000.tb01265.x>
- Ron SR, Caminer MA, Varela-Jaramillo A, Almeida-Reinoso D (2018) A new treefrog from Cordillera del Cóndor with comments on the biogeographic affinity between Cordillera del Cóndor and the Guianan Tepuis (Anura, Hylidae, *Hyloscirtus*). *ZooKeys* 809: 97–124. <https://doi.org/10.3897/zookeys.809.25207>

- Ron SR, Merino-Viteri A, Ortiz DA (2022) Anfibios del Ecuador. Version 2022.0. Museo de Zoología, Pontificia Universidad Católica del Ecuador. <https://bioweb.bio/faunaweb/amphibiaweb> [accessed 21 March 2023]
- Ronquist F, Teslenko M, van der Mark P, Ayres DL, Darling A, Höhna S, Larget B, Liu L, Suchard MA, Huelsenbeck JP (2012) MrBayes 3.2: Efficient Bayesian Phylogenetic Inference and Model Choice Across a Large Model Space. *Systematic Biology* 61: 539–542. <https://doi.org/10.1093/sysbio/sys029>
- RStudio Team (2023) RStudio: Integrated Development for R. RStudio. <http://www.rstudio.com/> [accessed 17 March 2024]
- Sambrook J, Fritsch EF, Maniatis T (1989) *Molecular Cloning: a Laboratory Manual*. Cold Spring Harbor Laboratory Press, New York, USA. <https://trove.nla.gov.au/work/13615226>
- Santos JC, Coloma LA, Summers K, Caldwell JP, Ree R, Cannatella DC (2009) Amazonian amphibian diversity is primarily derived from late Miocene Andean lineages. *PLOS Biology* 7: 0448–0461. <https://doi.org/10.1371/journal.pbio.1000056>
- Savage JM, Heyer WR (1967) Variation and distribution in the tree-frog genus *Phyllomedusa* in Costa Rica, central America. *Beitrage zur Neotropischen Fauna* 5: 111–131. <https://doi.org/10.1080/01650526709360400>
- Stamatakis A (2014) RAxML version 8: a tool for phylogenetic analysis and post-analysis of large phylogenies. *Bioinformatics (Oxford, England)* 30: 1312–1313. <https://doi.org/10.1093/bioinformatics/btu033>
- Streicher JW, Schulte JA, Wiens JJ (2016) How Should Genes and Taxa be Sampled for Phylogenomic Analyses with Missing Data? An Empirical Study in Iguanuan Lizards. *Systematic Biology* 65: 128–145. <https://doi.org/10.1093/sysbio/syv058>
- Streicher JW, Miller EC, Guerrero PC, Correa C, Ortiz JC, Crawford AJ, Pie MR, Wiens JJ (2018) Evaluating methods for phylogenomic analyses, and a new phylogeny for a major frog clade (Hyoidea) based on 2214 loci. *Molecular Phylogenetics and Evolution* 119: 128–143. <https://doi.org/10.1016/j.ympev.2017.10.013>
- Tamura K, Peterson D, Peterson N, Stecher G, Nei M, Kumar S (2011) MEGA5: Molecular evolutionary genetics analysis using maximum likelihood, evolutionary distance, and maximum parsimony methods. *Molecular Biology and Evolution* 28: 2731–2739. <https://doi.org/10.1093/molbev/msr121>
- Trifinopoulos J, Nguyen L-T, von Haeseler A, Quang Minh B (2016) W-IQ-TREE: a fast online phylogenetic tool for maximum likelihood analysis. *Nucleic Acids Research* 44. <https://doi.org/10.1093/nar/gkw256>
- Villacampa-Ortega J, Serrano-Rojas SJ, Whitworth A (2017) *Amphibians of the Manu Learning Centre and Other Areas of the Manu Region*. The Crees Foundation, Cusco, Peru, 283 pp.
- Wiens JJ, Moen DS (2008) Missing data and the accuracy of Bayesian phylogenetics. *Journal of Systematics and Evolution* 46: 307–314.
- Wiens JJ, Fetzner JW, Parkinson CL, Reeder TW (2005) Hylid frog phylogeny and sampling strategies for speciose clades. *Systematic Biology* 54: 778–807. <https://doi.org/10.1080/10635150500234625>
- Wiens JJ, Graham CH, Moen DS, Smith SA, Reeder TW (2006) Evolutionary and ecological causes of the latitudinal diversity gradient in hylid frogs: treefrog trees unearth the roots of high tropical diversity. *The American Naturalist* 168: 579–596. <https://doi.org/10.1086/507882>
- Wiens JJ, Kuczynski CA, Hua X, Moen DS (2010) An expanded phylogeny of treefrogs (Hylidae) based on nuclear and mitochondrial sequence data. *Molecular Phylogenetics and Evolution* 55: 871–882. <https://doi.org/10.1016/j.ympev.2010.03.013>

- Yáñez-Muñoz M, Reyes Puig JP (2008) Evaluación de la Herpetofauna de las Reservas Biológicas de la Fundación Ecominga. Cuenca Alta del Río Pastaza. Ecuador. División de Herpetología Museo Ecuatoriano de Ciencias Naturales. Informe Técnico No. 25.
- Yáñez-Muñoz MH, Reyes-Puig JP, Batallas-Revelo D, Broaddus C, Urgilés-Merchán M, Cisneros-Heredia DF, Guayasamin JM (2021) A new Andean treefrog (Amphibia: *Hyloscirtus bogotensis* group) from Ecuador: an example of community involvement for conservation. PeerJ 9: e11914. <https://doi.org/10.7717/peerj.11914>
- Yang Z. (2014) Molecular Evolution: a Statistical Approach. Oxford University Press, Oxford, UK, 512 pp.
- Zerbino DR, Birney E (2008) Velvet: algorithms for de novo short read assembly using de Bruijn graphs. Genome Research 18: 821–829. <https://doi.org/10.1101/gr.074492.107>
- Zhang P, Liang D, Mao R-L, Hillis DM, Wake DB, Cannatella DC (2013) Efficient sequencing of Anuran mtDNAs and a mitogenomic exploration of the phylogeny and evolution of frogs. Molecular Biology and Evolution 30:1899–1915. <https://doi.org/10.1093/molbev/mst091>

## Supplementary material 1

### Additional information

Authors: Andrea Varela-Jaramillo, Jeffrey W. Streicher, Pablo J. Venegas, Santiago R. Ron  
Data type: doc

Explanation note: **table S1**. Taxon, voucher number, locality and GenBank data of the species included in the Sanger-based phylogenetic analysis. **table S2**. Details of the preferred partitions found with their best substitution models under Partition Finder and Model Find searches. **table S3**. Sequences for complete gene 16S, obtained from GenBank and amplified in this study. **table S4**. Examined specimens for the morphological analysis include the voucher number, sex of the specimen and the hosting museum. **table S5**. Measurements (in mm) of specimens of *Hyloscirtus*. **table S6**. Character loadings and eigenvalues for Principal Components (PC I, II and III) of the morphology analysis. **table S7**. Character loadings and eigenvalues for Principal Components (PC I–II) of the acoustic analysis. **table S8**. Character loadings and eigenvalues for Principal Components (PC I–II) of the environmental analysis. **table S9**. Additional specimens examined. **fig. S1**. Map showing the current distribution range known for *H. albopunctulatus*, *H. phyllognathus* and *H. torrenticola* before this study. **fig. S2**. Consensus tree obtained under Maximum likelihood criterion when using taxa with more than 300 UCE loci enriched. **fig. S3**. Consensus tree obtained under Maximum likelihood criterion when using taxa with more than 200 UCE loci enriched. **fig. S4**. Consensus tree obtained under Maximum likelihood criterion when using taxa with more than 300 UCE loci enriched. **fig. S5**. Species delimitation tree based on the Poisson Tree Process (PTP) criteria, using the 12S mitochondrial gene. **fig. S6**. Plot depicting the number of species recovered by the ABGD criteria as a function of the prior for intraspecific genetic divergences. **fig. S7**. Haplotype network for DNA sequences of 59 individuals for the nuclear gene C-myc.

Copyright notice: This dataset is made available under the Open Database License (<http://opendatacommons.org/licenses/odbl/1.0/>). The Open Database License (ODbL) is a license agreement intended to allow users to freely share, modify, and use this Dataset while maintaining this same freedom for others, provided that the original source and author(s) are credited.

Link: <https://doi.org/10.3897/zookeys.1231.124926.suppl1>

# Comparison of complete mitochondrial genome sequences in the *Aporrectodea caliginosa* species group (Annelida, Crassiclitellata, Lumbricidae)

Csaba Csuzdi<sup>1\*</sup>, Jachoon Koo<sup>2\*</sup>, Yong Hong<sup>3</sup>

<sup>1</sup> Kenderesi str. 39, Piliscsaba, Hungary

<sup>2</sup> Division of Science Education and Institute of Fusion Science, College of Education, Jeonbuk National University, Jeonju 54896, Republic of Korea

<sup>3</sup> Department of Agricultural Biology, College of Agriculture & Life Science, Jeonbuk National University, Jeonju 54896, Republic of Korea

Corresponding author: Yong Hong ([yonghong@jbnu.ac.kr](mailto:yonghong@jbnu.ac.kr))

## Abstract

We present for the first time the complete mitochondrial genomes (mt genomes) of the earthworms *Aporrectodea caliginosa* and *Ap. trapezoides* (Clitellata, Megadrili) collected in Hungary and Korea, respectively.

The complete mt genome of *Ap. trapezoides* comprised 15,014 base pairs. Lengths of the three complete *Ap. caliginosa* mt genomes varied between 15,090 and 15,123 bp. All four mt genomes contained 13 protein-coding genes (PCGs), two rRNA genes, 22 tRNA genes, and one major non-coding control region. These mt genome arrangements are identical to those observed in the mt genomes of most earthworms, and all the 37 genes are transcribed from the same directional strand. All 13 PCGs had the same ATG start codon. Most of the PCGs end with TAA or TAG, whereas the remaining end with an incomplete stop codon, T. Stop codons were consistent in the PCGs throughout the mt genomes, except *Ap. caliginosa* 5, which contains a TAG stop codon in ND5 instead of the TAA found in the other samples. Both species' genomes showed biased base composition, with 63.5% AT and 36.4% GC content in *Ap. trapezoides* and 62.8% and 37.2% in *Ap. caliginosa*. Phylogenetic analysis of the mt genomes corroborated the monophyly of the family Lumbricidae and the close relationship between *Ap. trapezoides* and *Ap. caliginosa* species pairs. The available *Ap. tuberculata* sequences were embedded between the *Ap. caliginosa* samples, thereby supporting the synonymy of the two names.

**Key words:** *Aporrectodea caliginosa*, *Aporrectodea trapezoides*, Lumbricidae, mitochondrial genome, phylogeny

## Introduction

*Aporrectodea caliginosa* was described as *Enterion caliginosum* Savigny, 1826 and placed in Savigny's "Tribu" No. 1 (Savigny 1826: 179). The "Tribu" No. 1 is defined as follows: "Les soies sont rapprochées par paires. La ceinture a de chaque côté deux pores qui correspondent chacun à un seul segment, et qui, si l'on compte celui qui les sépare, comprennent les trois pénultièmes" [The setae paired. The girdle (clitellum) has two pores (tubercles) on each side, each of



Academic editor: Samuel James

Received: 16 December 2024

Accepted: 6 February 2025

Published: 13 March 2025

ZooBank: <https://zoobank.org/BEFE7D67-93C1-4608-97C2-A74E260B6080>

Citation: Csuzdi C, Koo J, Hong Y (2025) Comparison of complete mitochondrial genome sequences in the *Aporrectodea caliginosa* species group (Annelida, Crassiclitellata, Lumbricidae). ZooKeys 1231: 293–310. <https://doi.org/10.3897/zookeys.1231.144623>

Copyright: © Csaba Csuzdi et al.  
This is an open access article distributed under terms of the Creative Commons Attribution License (Attribution 4.0 International – CC BY 4.0).

\* These authors contributed equally.

which corresponds to a single segment, and which, if the one between them is counted, comprise the three penultimate segments]. The species *caliginosum* was defined as “La ceinture, de huit segmens, finit avec le trente-quatrième du corps” [The clitellum, of eight segments, ending with the thirty-fourth of the body]. The diagnosis of *E. caliginosum* in modern terms according to Cain (1955: 482–483) is as follows: “Male pores with conspicuous lips, apertures on segment 15; setae paired; clitellum on 27–34; tubercula pubertatis on 31 and 33, two pairs of spermathecae opening on the ventral surface; four pairs of seminal vesicles; coelomic fluid not colored.”

The identity of *Enterion caliginosum* has provoked a long and continuing debate (Blakemore 2008). Gates (1972a, 1972b) and other North American authors (e.g. Reynolds 1977, 2022) regarded Savigny’s definition as inadequate and used the junior synonym name *Allolobophora turgida* Eisen, 1873 because Tétry (1937) erroneously cited the position of the tubercles as being on segment 31, 32 when revising Savigny’s material housed in the Muséum national d’Histoire naturelle in Paris. However, Tétry (1937) did not find the type material of *E. caliginosum* and Savigny (1826) never wrote of this (Cain 1955). As *E. caliginosum* is published according to ICZN Article 11 and its diagnosis satisfies Article 13, it is an available and valid senior name for this taxon.

Later, several synonyms (e.g. *Lumbricus lividus* Templeton, 1836; *Allolobophora similis* Friend, 1910 (see Blakemore 2008: 526 for a complete synonym list) and closely related taxa were described, such as *Lumbricus trapezoides* Dugés, 1828; *Allolobophora nocturna* Evans, 1946; *Allolobophora turgida* var. *tuberculata* (Eisen 1874). In addition, the latter three taxa, which together with *Ap. caliginosa*, form the *Ap. caliginosa* species group (Blakemore 2002), have been treated differently by different authors. For instance, Pop (1949), Zicsi (1982), and Csuzdi and Zicsi (2003) regarded all three species names as synonyms of *Ap. caliginosa*. Gates (1972a) and Reynolds (1977, 2022) considered *Ap. trapezoides*, *Ap. tuberculata*, and *Ap. nocturna* independent taxa from *Ap. caliginosa* (syn. *Ap. turgida*). Mršić (1991) considered *Ap. tuberculata* as a synonym for *Ap. caliginosa*, *Ap. trapezoides* as a subspecies of *Ap. caliginosa*, and *Ap. nocturna* as a valid species. Briones (1996) reviewed the *Ap. caliginosa* species group and concluded that there were only two valid taxa, *Ap. caliginosa* and *Ap. trapezoides*. However, the author did not comment on the status of *Ap. nocturna* owing to a lack of sufficient material.

To further complicate this issue, Bouché (1972) distinguished three subspecies within *Ap. caliginosa*, along with several invalid infrasubspecific taxa (varieties), that he placed in his genus *Nicodrillus* Bouché, 1972, a junior synonym of *Aporrectodea* Örley, 1885 (Sims and Gerard 1985).

The *Ap. caliginosa* species group is one of the most molecularly studied earthworm taxa. Early multigene phylogenetic analyses (Pérez-Losada et al. 2009; Fernández et al. 2011, 2012, 2013; Briard et al. 2012) revealed high genetic variability in the species group and the presence of several highly divergent cryptic lineages in different constituent taxa. *Aporrectodea tuberculata* with *Ap. caliginosa* form a well-separated clade from the other taxa in this complex. However, *Ap. caliginosa* was paraphyletic without *Ap. tuberculata*, and *Ap. trapezoides* comprised two highly separated clades and appeared to be polyphyletic, as clade I is more closely related to the clade comprising *Ap. nocturna*, *Ap. giardi*

(valid name *Ap. terrestris*), and *Ap. longa*. Later studies either corroborated these results (Shekhovtsov et al. 2017; Marchán et al. 2020) or found *Ap. caliginosa* polyphyletic (Shekhovtsov et al. 2016; Latif et al. 2020).

Over the past few years increasing number of complete mitochondrial genomes (mt genomes) have been published, facilitating the differentiation of closely related species (Zhang et al. 2016; Shekhovtsov et al. 2020; Csuzdi et al. 2022). Recently, Zhao et al. (2022) reported several nearly complete lumbricid mt genomes, including one *Ap. trapezoides* and six *Ap. tuberculata* sequences. Interestingly, one of the reported *Ap. tuberculata* sequences is registered as *Ap. caliginosa* in the GenBank (sample 420Ra, accession number NC\_066400).

Herein, we report the complete mt genomes of the Korean *Ap. trapezoides* and three Hungarian *Ap. caliginosa* specimens, as well as compare these data to the published complete or nearly complete mt genomes of the *Ap. caliginosa* species group to help solve this continuing taxonomic issue.

## Material and methods

### Sample preparation and DNA extraction

Adult *Ap. trapezoides* were collected from a farm in Seongsu-myeon, Imsil-gun, Jeollabuk-do, Korea (33°41'23.80"N, 126°38'33.67"E; 40 m a.s.l.) on March 28, 2021 and preserved in 99% ethanol until DNA extraction. *Ap. caliginosa* specimens were collected in a deciduous forest patch near Szendehely, Hungary (47°52'32.7"N, 19°6'16.6"E) on May 4, 2021, and preserved in 96% ethanol until DNA extraction. Voucher specimens of each species were deposited at Jeonbuk National University, Jeonju City, Korea. Total genomic DNA was prepared from a small portion of the body segments of a single adult earthworm using a QIAamp DNA Mini Kit (Qiagen, Hilden, Germany). The remaining tissue was preserved at -20 °C in 90% ethanol.

### TruSeq DNA library construction

The sequencing library was prepared by random fragmentation of genomic DNA, followed by 5' and 3' adapter ligations using the Illumina TruSeq DNA Nano Library Prep Kit according to the manufacturer's instructions (Illumina Inc., San Diego, CA, USA). The resulting libraries were quantified through a qPCR-based assay using the KAPA Library Quantification Kit for Illumina sequencing platforms, according to the manufacturer's instructions (Kapa Biosystems, Woburn, MA, USA). Libraries were qualified using the Agilent Technologies 2200 TapeStation (Agilent Technologies, Santa Clara, CA, USA).

### DNA sequencing, assembly, and annotation

Paired-end (2×150 base pairs [bp]) sequencing was performed using the Illumina HiSeq-X platform (Illumina Inc.) at Macrogen Inc. (Seoul, Korea). To reduce bias in the analysis, adapter trimming and quality filtering were performed using Trimmomatic v. 0.36 (Bolger et al. 2014). *De novo* assembly of raw sequencing reads was performed using various *k*-mer lengths in SPAdes

v. 3.13.0 (Bankevich et al. 2012). Mitochondrial contigs were assembled into a single contig using BLASTN alignment (<https://blast.ncbi.nlm.nih.gov/Blast.cgi>) against the *Lumbricus terrestris* mitogenome (GenBank accession number NC\_001673) as the reference sequence. Annotation and visualization of mt genomes were performed using the online MITOS software (Donath et al. 2019), and manual curation was performed using BLAST searches in the NCBI database for various earthworm mt genomes (Table 1). A comparative map of the mt genomes was created using Geneious Prime 2024 software. The *cox1* sequence was used as an anchor for the linearized mt genome maps. The annotated complete genome sequences were registered in GenBank under the accession numbers PQ572750–PQ572753.

### Phylogenetic analyses

To check the identity of the morphologically identified specimens, the *cox1* barcoding regions were analyzed with barcodes selected and downloaded from the BOLD v. 4 database (Ratnasingham and Hebert 2013) using the IQ-tree web server with default settings and suggested TPM2u+F+I+G4 substitution model.

To clarify the phylogenetic positions of the two taxa, complete or nearly complete mitogenomes were obtained from GenBank, comprising 26 species of Megascolecidae and 12 species of Lumbricidae. *Pontoscolex corethrus* (Müller, 1857) from the Rhinodrilidae family and *Drawida japonica* (Michaelsen, 1892) from the exquisiclitellate family Moniligastridae were used as outgroups. Phylogenetic analysis was conducted based on two datasets, a complete set of 37 mitochondrial genes and subset comprising only 13 protein-coding genes (PCGs), using maximum likelihood (ML) and Bayesian (BI) methods. Sequences for each gene from the 40 earthworm species (Table 1) were individually aligned using MAFFT v. 7 (Katoh and Standley 2013) and trimmed using TrimAl v. 1.2 (Capella-Gutiérrez et al. 2009). The trimmed sequences were concatenated into a single multi-gene alignment. The best-fit substitution model for each dataset was selected using ModelFinder (Kalyaanamoorthy et al. 2017) integrated within the IQ-TREE (Nguyen et al. 2014) based on the Bayesian Information Criterion (Schwarz 1978). The ML phylogenetic trees were constructed using IQ-TREE for both datasets by applying the selected GTR+F+I+R5 model. In addition, a partitioned ML analysis was also performed on the 13 PCG dataset using the best-fit models TIM2+F+R7 for *atp6+atp8+nd2+nd6* genes, GTR+F+I+G4 for *cox1+cox2+cox3+cytb* genes and TIM2+F+R10 for *nd1+nd3+nd4+nd4L+nd5* genes. Branch support was assessed using 5,000 ultrafast bootstrap replicates (Hoang et al. 2018). Bayesian analysis was performed using MrBayes v. 3.2.7 (Ronquist et al. 2012) with two independent runs set to 10 million generations each and sampling every 1000<sup>th</sup> generation (10,000 trees). Twenty-five percent of the trees were discarded as burn-in, and the remaining trees were combined and summarized into a 50% majority-rule consensus tree.

Estimation of the evolutionary divergences between the analyzed *Ap. caliginosa* group sequences were conducted in MEGA X (Kumar et al. 2018) using the uncorrected *p*-distance. The analyzed matrix was 14,681 bp long and contained only coding regions.

**Table 1.** List of Megadrili mitogenomes used in this study.

Family	Taxa	Genbank No.	Total length (bp)	Reference
Megascolecidae	<i>Amyntas aspergillus</i>	KJ830749	15,115	Zhang et al. 2016
	<i>Amyntas carnosus</i>	KT429008	15,160	Zhang et al. 2016
	<i>Amyntas corticis</i>	KM199290	15,126	Zhang et al. 2015
	<i>Amyntas cucullatus</i>	KT429012	15,122	Zhang et al. 2016
	<i>Amyntas gracilis</i>	KP688582	15,161	Zhang et al. 2015
	<i>Amyntas hupeiensis</i>	KT429009	15,069	Zhang et al. 2016
	<i>Amyntas jiriensis</i>	KT783537	15,151	Hong et al. 2017
	<i>Amyntas longisiphonus</i>	KM199289	15,176	Zhang et al. 2015
	<i>Amyntas moniliatus</i>	KT429020	15,133	Zhang et al. 2016
	<i>Amyntas morrissi</i>	KT429011	15,026	Zhang et al. 2016
	<i>Amyntas pectiniferus</i>	KT429018	15,188	Zhang et al. 2016
	<i>Amyntas robustus</i>	KT429019	15,013	Zhang et al. 2016
	<i>Amyntas seungpanensis</i>	OL321943	15,085	Kim and Hong 2022
	<i>Amyntas</i> sp. 1	KT429010	15,131	unpublished
	<i>Amyntas</i> sp. 2 JS-2012	KT429007	15,159	unpublished
	<i>Amyntas</i> sp. 2	KT429014	15,086	unpublished
	<i>Amyntas</i> sp. 3	KT429013	15,152	unpublished
	<i>Amyntas triastriatus</i>	KT429016	15,160	Zhang et al. 2016
	<i>Amyntas yunoshimensis</i>	LC573969	15,109	Seto et al. 2021
	<i>Duplodocodrilus schmardae</i>	KT429015	15,156	Zhang et al. 2016
	<i>Metaphire californica</i>	KP688581	15,147	Zhang et al. 2015
	<i>Metaphire guillelmi</i>	KT429017	15,174	Zhang et al. 2016
	<i>Metaphire hilgendorfi</i>	LC573968	15,186	Seto et al. 2021
	<i>Metaphire vulgaris</i>	KJ137279	15,061	Zhang et al. 2014
<i>Perionyx excavatus</i>	EF494507	15,083	unpublished	
<i>Tonoscolex birmanicus</i>	KF425518	15,170	Wang et al. 2015	
Lumbricidae	<i>Aporrectodea rosea</i>	MK573632	15,086	Shekhovtsov and Peltek 2019
	<i>Aporrectodea caliginosa</i>	<b>PQ572750</b>	<b>15,090</b>	<b>this study</b>
		<b>PQ572751</b>	<b>15111</b>	<b>this study</b>
		<b>PQ572752</b>	<b>15123</b>	<b>this study</b>
		CM035405	15,120	unpublished
		NC_066400	15,089	Zhao et al. 2022
	<i>Aporrectodea trapezoides</i>	<b>PQ572753</b>	<b>15,014</b>	<b>this study</b>
		OM687882	14,998	Zhao et al. 2022
	<i>Aporrectodea tuberculata</i>	OL840317	15,058	Zhao et al. 2022
		OM687883	15,125	Zhao et al. 2022
		OM687884	15,126	Zhao et al. 2022
		OM687885	15,129	Zhao et al. 2022
		OM687886	15,116	Zhao et al. 2022
	<i>Bimastus parvus</i>	MZ857199	15,194	Liu et al. 2021
	<i>Dendrobaena octaedra</i>	MZ857197	15,715	Liu et al. 2021
	<i>Eisenia andrei</i>	OK513069	15,714	Csuzdi et al. 2022
	<i>Eisenia fetida</i>	OK513070	16,560	Csuzdi et al. 2022
	<i>Eisenia nordenskioldi</i>	MZ857200	15,152	Liu et al. 2021
		OM687887	16,114	Zhao et al. 2022
		OL840314	15,290	Zhao et al. 2022
	<i>Lumbricus rubellus</i>	MN102127	15,464	Zhang et al. 2019
	<i>Lumbricus terrestris</i>	U24570	14,998	Boore and Brown 1995
	<i>Octolasion tyrtaeum</i>	MZ857201	14,977	Liu et al. 2021
Moniligastridae	<i>Drawida japonica</i>	KM199288	14,648	Zhang et al. 2016
Rhinodrilidae	<i>Pontoscolex corethrurus</i>	KT988053	14,835	Conrado et al. 2017

## Results

Based on the analysis of the barcoding region of *cox1* gene, our newly sequenced *Ap. trapezoides* specimen belongs to the widely distributed lineage 2 (Fernández et al. 2011). The *Ap. caliginosa* specimens analyzed were nested among the *caliginosa* lineage 2 specimens (Porco et al. 2013; Shekhovtsov et al. 2016), together with all *Ap. tuberculata* and *Ap. caliginosa* samples reported in the recent study by Zhao et al. (2022) (Fig. 1).

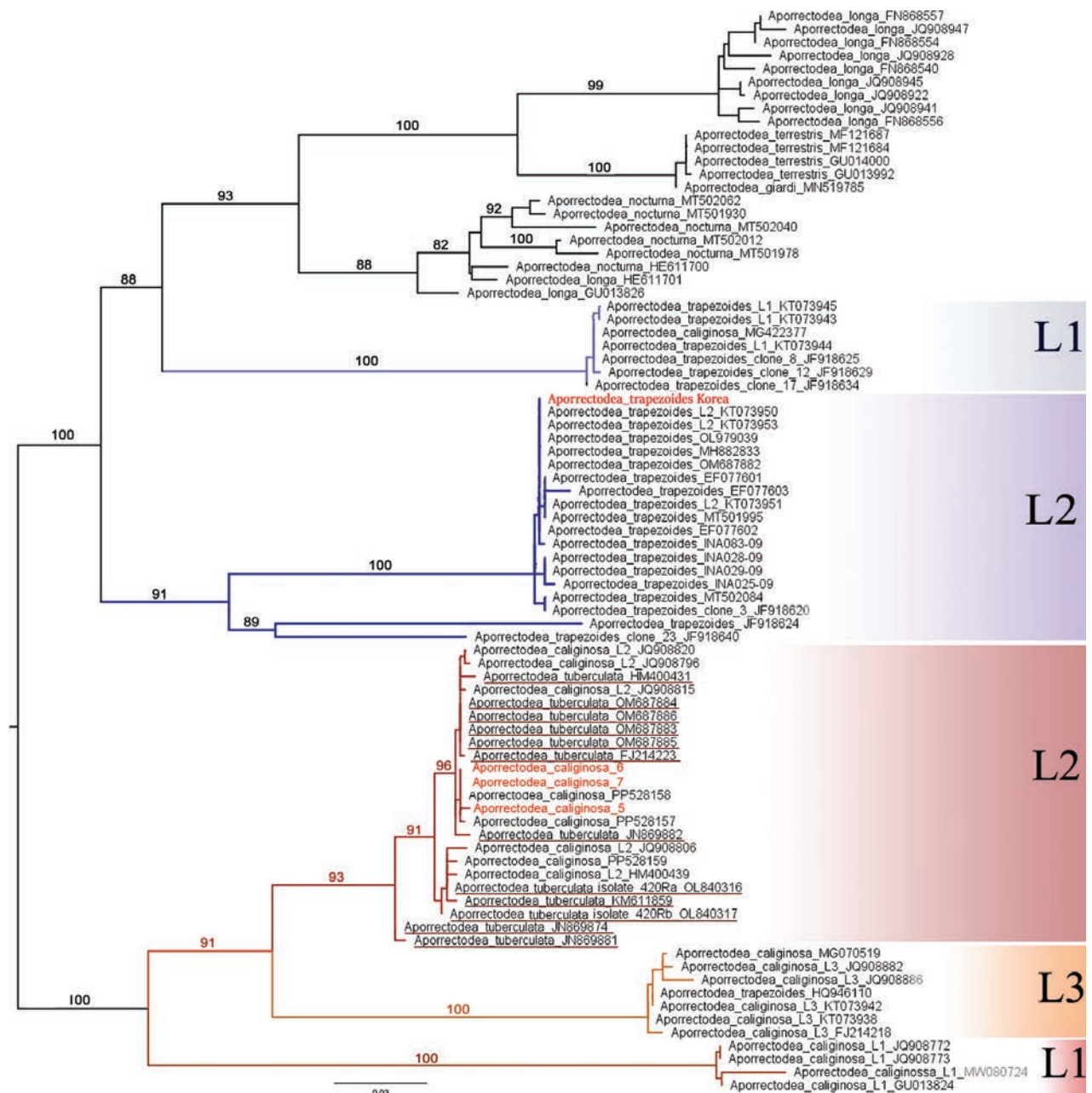


**Figure 1.** Maximum-likelihood (ML) tree based on the *cox1* gene fragments with bootstrap values of selected *Aporrectodea caliginosa* group specimens. Red names represent new sequences. L1, L2, and L3 refer to different lineages. *Ap. tuberculata* sequences are underlined.

The complete mt genome of *Ap. trapezoides* comprises 15,014 bp. The length of the three *Ap. caliginosa* mt genomes analyzed in this study varied between 15,090 and 15,123 bp. The mitogenome setup of both species followed the typical bauplan of the earthworm mitogenome assembly, consisting of 13 PCGs, 22 transfer RNAs, two ribosomal RNA genes, and a control region (Fig. 2; Table 2).

All genes were encoded on the heavy DNA strand, and both genomes showed biased base composition, with 63.5% AT and 36.4% GC content in *Ap. trapezoides* and 62.8% and 37.2% in *Ap. caliginosa*.

Overall mitogenome sequence similarity between the two species (*Ap. trapezoides* and *Ap. caliginosa* no. 5) was 80.8% and it increased to 85.8% when the control region was excluded. The 13 PCGs showed 71.2–85.9% similarity (Table 2). Among the PCGs, *cox2* showed the highest similarity (85.9%) and *atp8* the lowest (71.2%). The average similarity of the 13 PCGs between the two species was 84%. However, the deduced amino acid sequences of the 13 PCGs showed 92.7% similarity on average across species; *cox1* was the most similar (99.4%), and *atp8* the most dissimilar (66.04%; Table 3). The sequence variation between the two species was lower at the amino acid level than at the DNA level. In particular, *cox1* showed 82.47–84.41% similarity at the DNA level, but >99% similarity at the amino acid level (Table 4).

Phylogenetic reconstruction of the available complete or nearly complete lumbricid mitogenomes and use of the 13 PCGs strongly supported the family Lumbricidae (100% bootstrap support). In addition, the genera *Eisenia* and *Lumbricus* were resolved as monophyletic, and the close relationship between *Ap. trapezoides/caliginosa* species pairs was confirmed (Figs 3–5). Consequently, the genus *Aporrectodea* was found to be polyphyletic, as *Ap. rosea* did not form a clade with the other analyzed *Aporrectodea* species.

The uncorrected *p*-distances of the mitogenomes (excluding the non-coding region) between *Ap. caliginosa/tuberculata* and *Ap. trapezoides* ranged from 16.1% to 16.4% (Table 5). The two *Ap. trapezoides* (from China and Korea) did not exhibit any genetic distance (0.00%).

The maximum genetic distance within *Ap. caliginosa* was 11.1% between a Hungarian specimen (Apc-5) and CM035405 (Azores Island, Portugal); however, between the L2 specimens identified as *Ap. tuberculata* and *Ap. caliginosa* it was only 2.1% (between Apc-5 and OL840317).

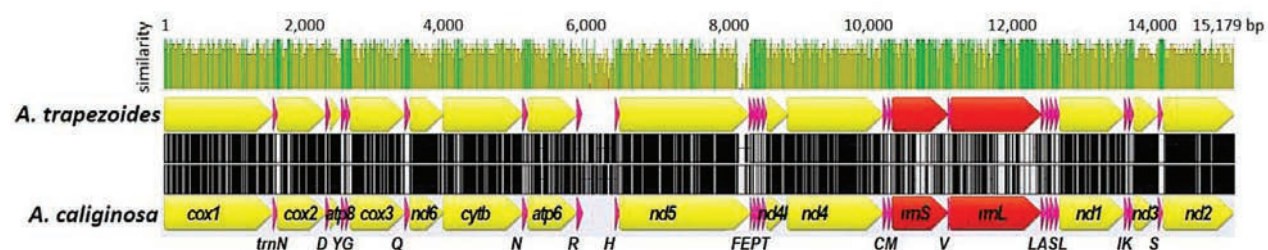


**Figure 2.** Comparison of the mitogenomes of *Aporrectodea trapezoides* and *Ap. caliginosa* (sample no. 5). Map was constructed based on sequence similarity using Geneious Prime 2021 software. Sequence similarity is represented by green (100%), brown (30–99%), and red (<30%). Yellow, pink, and red arrows indicate PCGs, tRNAs, and rRNAs, respectively. Organization of mitochondrial genes is described in Table 2. Non-coding (nc) region is defined between *trnR* and *trnH*.

**Table 2.** Comparative analysis of gene organization of *Aporrectodea trapezoides* and *Ap. caliginosa* mitogenomes.

Gene	<i>Ap. caliginosa</i> (CM035405)		<i>Ap. caliginosa</i> (NC_066400)		<i>Ap. tuberculata</i> (OL840317)		<i>Ap. trapezoides</i> (OM687882)		<i>Ap. trapezoides</i> (this study)		<i>Ap. caliginosa</i> 5 (this study)		Similarity (%)*
	Size (bp)	start/stop codon	Size (bp)	start/stop codon	Size (bp)	start/stop codon	Size (bp)	start/stop codon	Size (bp)	start/stop codon	Size (bp)	start/stop codon	
<i>cox1</i>	1540	ATG/T	1540	ATG/T	1540	ATG/T	1540	ATG/T	1540	ATG/T	1540	ATG/T	84.50%
<i>trnN</i>	61	–	61	–	61	–	61	–	61	–	61	–	88.9
<i>cox2</i>	687	ATG/TAG	687	ATG/TAG	687	ATG/TAG	687	ATG/TAG	687	ATG/TAG	687	ATG/TAG	85.9
<i>trnD</i>	61	–	61	–	61	–	61	–	61	–	61	–	90.2
<i>atp8</i>	160	ATG/T	160	ATG/T	160	ATG/T	160	ATG/T	160	ATG/T	160	ATG/T	71.2
<i>trnY</i>	63	–	63	–	63	–	62	–	62	–	63	–	95.2
<i>trnG</i>	63	–	63	–	63	–	63	–	63	–	63	–	93.7
<i>cox3</i>	778	ATG/T	778	ATG/T	778	ATG/T	778	ATG/T	778	ATG/T	778	ATG/T	83.8
<i>trnQ</i>	69	–	69	–	69	–	69	–	69	–	69	–	100
<i>nad6</i>	468	ATG/TAA	468	ATG/TAA	468	ATG/TAA	468	ATG/TAA	468	ATG/TAA	468	ATG/TAA	77.8
<i>cytb</i>	1140	ATG/TAA	1140	ATG/TAA	1140	ATG/TAA	1140	ATG/TAA	1140	ATG/TAA	1140	ATG/TAA	83
<i>trnW</i>	64	–	64	–	65	–	62	–	62	–	65	–	89.2
<i>atp6</i>	696	ATG/TAA	696	ATG/TAA	696	ATG/TAA	696	ATG/TAA	696	ATG/TAA	696	ATG/TAA	80.4
<i>trnR</i>	63	–	63	–	63	–	65	–	65	–	63	–	80.6
#NC	437	–	407	–	374	–	440	–	456	–	409	–	61
<i>trnH</i>	62	–	62	–	62	–	62	–	62	–	62	–	82.8
<i>nad5</i>	1722	ATG/TAA	1722	ATG/TAA	1722	ATG/TAA	1722	ATG/TAA	1722	ATG/TAA	1722	ATG/TAG	79.6
<i>trnF</i>	61	–	61	–	61	–	61	–	61	–	61	–	91.8
<i>trnE</i>	63	–	63	–	63	–	63	–	63	–	63	–	92.3
<i>trnP</i>	64	–	64	–	64	–	64	–	64	–	64	–	90.8
<i>trnT</i>	63	–	63	–	64	–	63	–	63	–	63	–	93.7
<i>nad4L</i>	297	ATG/TAA	297	ATG/TAA	297	ATG/TAA	297	ATG/TAA	297	ATG/TAA	297	ATG/TAA	79.9
<i>nad4</i>	1359	ATG/TAG	1359	ATG/TAG	1359	ATG/TAG	1359	ATG/TAG	1359	ATG/TAG	1359	ATG/TAG	80.8
<i>trnC</i>	65	–	65	–	65	–	65	–	65	–	65	–	90.9
<i>trnM</i>	63	–	63	–	63	–	63	–	63	–	63	–	96.8
<i>rrnS</i>	788	–	788	–	788	–	789	–	795	–	794	–	89
<i>trnV</i>	63	–	63	–	63	–	63	–	63	–	63	–	93.8
<i>rrnL</i>	1257	–	1256	–	1256	–	1256	–	1275	–	1295	–	86
<i>trnL</i>	62	–	62	–	62	–	62	–	62	–	62	–	93.7
<i>trnA</i>	62	–	62	–	62	–	62	–	62	–	62	–	88.7
<i>trnS</i>	67	–	67	–	67	–	67	–	67	–	67	–	94.1
<i>trnL</i>	62	–	62	–	62	–	62	–	62	–	62	–	98.4
<i>nad1</i>	922	ATG/T	922	ATG/T	922	ATG/T	922	ATG/T	922	ATG/T	922	ATG/T	83.6
<i>trnI</i>	66	–	66	–	66	–	64	–	64	–	66	–	90.9
<i>trnK</i>	63	–	63	–	63	–	64	–	64	–	63	–	92.3
<i>nad3</i>	354	ATG/TAG	354	ATG/TAG	354	ATG/TAG	354	ATG/TAG	354	ATG/TAG	354	ATG/TAG	74.6
<i>trnS</i>	64	–	64	–	64	–	64	–	64	–	64	–	100
<i>nad2</i>	1006	ATG/T	1006	ATG/T	1006	ATG/T	1006	ATG/T	1006	ATG/T	1006	ATG/T	79.1

\*Putative non-coding region between *trnR* and *trnH*.\* indicates the similarity of nucleotide sequence between *Ap. trapezoides* and *Ap. caliginosa* (*Apc-5*).

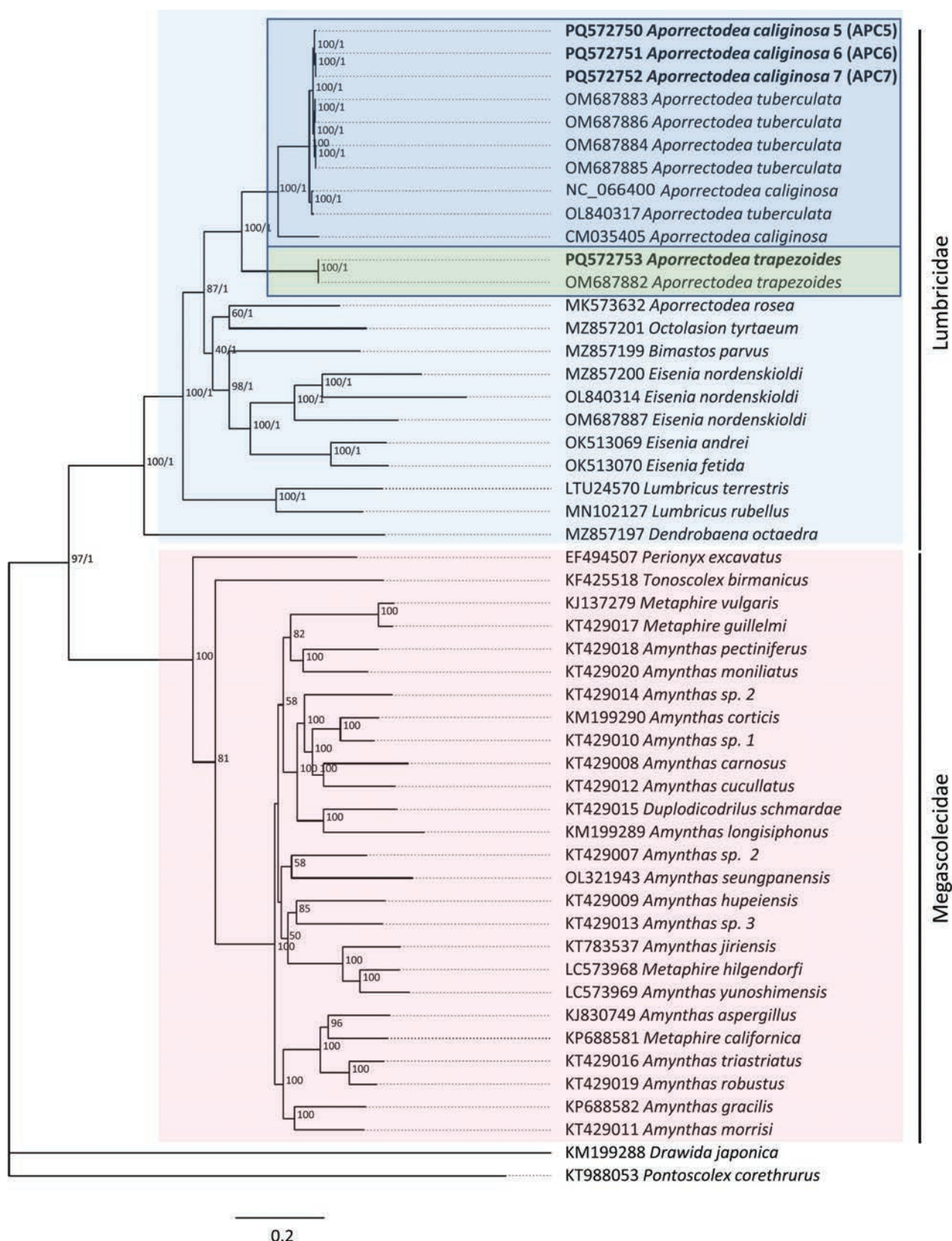


**Figure 3.** Phylogenetic analysis of 40 Megadrili group spp., including *Aporrectodea trapezoides* and *Ap. caliginosa*, based on sequences of 37 mitochondrial genes. Numbers beside nodes are ML bootstrap values and BI posterior probabilities. *Drawida japonica* and *Pontoscolex corethrus* were included as outgroups.

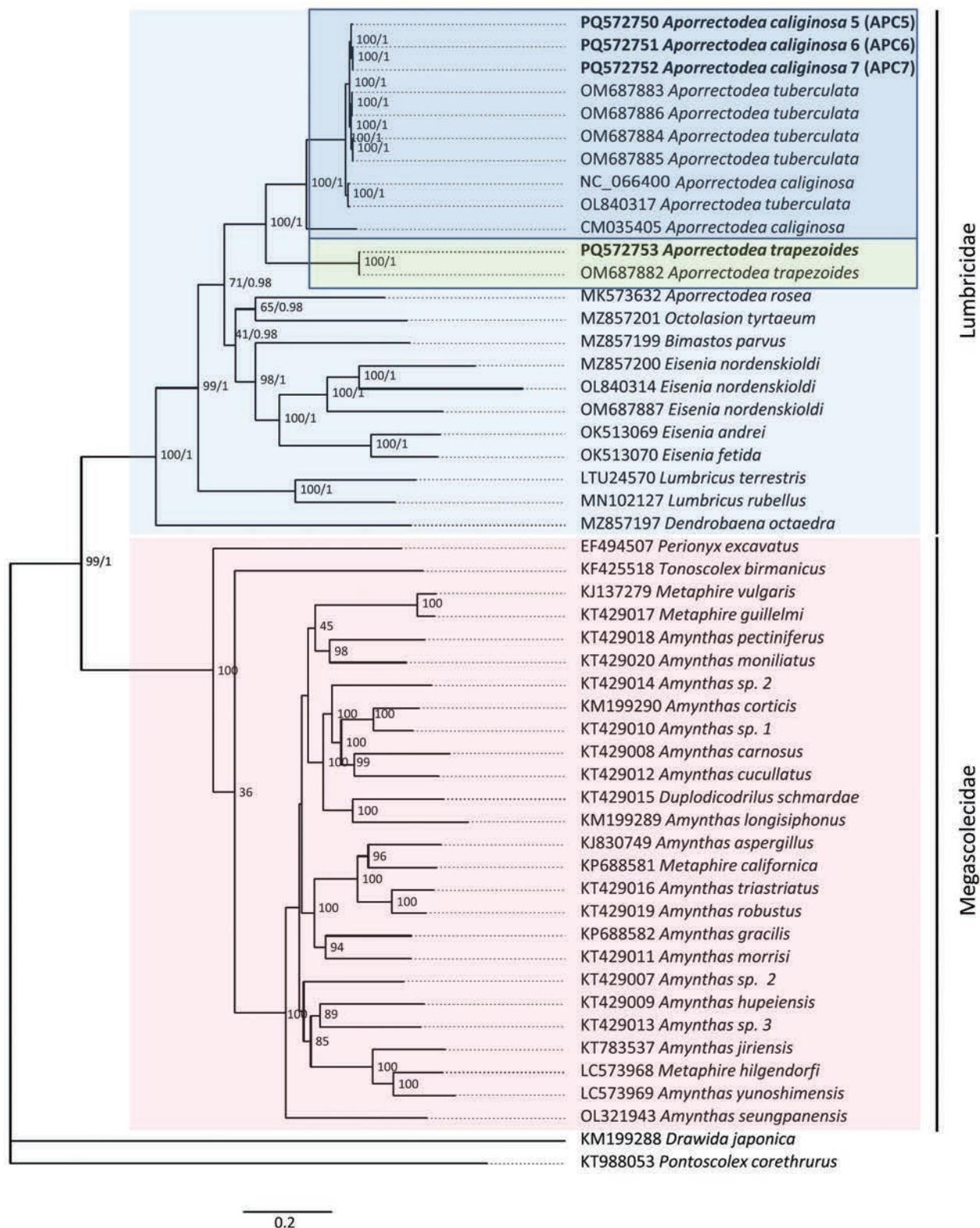


**Figure 4.** Phylogenetic analysis of 40 Megadrili group spp. using 13 PCGs, including *Aporrectodea trapezoides* and *Ap. caliginosa*. Numbers beside nodes are ML bootstrap values and BI posterior probabilities. *Drawida japonica* and *Pontoscolex corethrus* were included as outgroups.

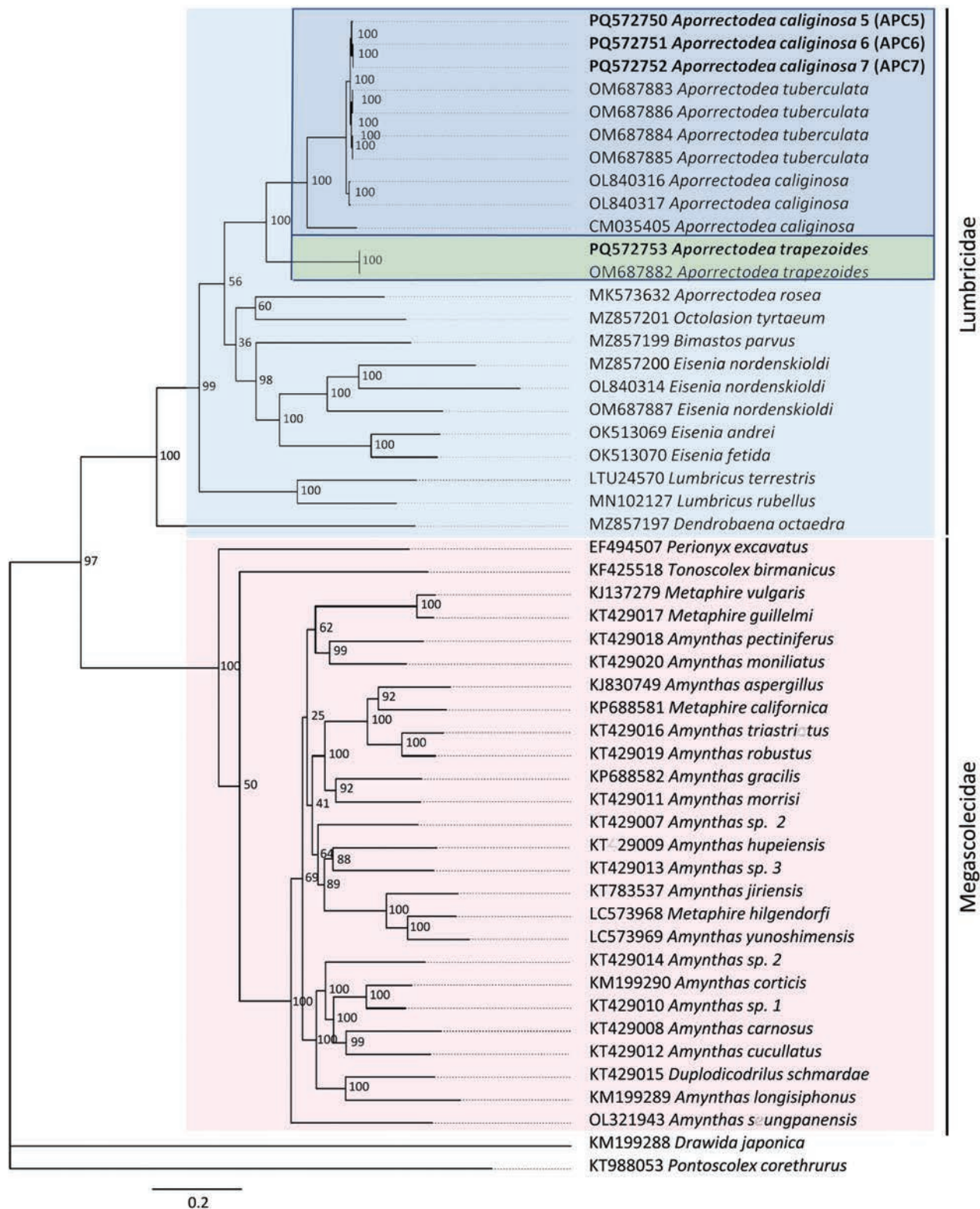


Figure 5. Partitioned phylogenetic analysis of 40 Megadrili group spp. using 13 PCGs, including *Aporrectodea trapezoides* and *Ap. caliginosa*. Numbers beside nodes are ML bootstrap values.

**Table 3.** Comparison of deduced amino acid composition of 13 PCGs in the *Aporrectodea caliginosa* species group.

Protein	aa size	<i>Ap. trapezoides</i> this study vs.	<i>Ap. trapezoides</i> this study vs.	<i>Ap. trapezoides</i> this study vs.	<i>Ap. caliginosa</i> (CM035405) vs.	<i>Ap. caliginosa</i> (Apc-5) vs.
		<i>A. caliginosa</i> (CM035405)	<i>A. caliginosa</i> (NC_066400)	<i>A. caliginosa</i> (Apc-5)	<i>A. caliginosa</i> (Apc-5)	<i>A. tuberculata</i> (OM687883)
COX1	513	99.40%	99.40%	99.40%	100%	100%
COX2	228	97.20%	96.73%	96.73%	99.53%	100%
ATP8	53	66.04%	66.04%	67.92%	86.79%	96.23%
COX3	259	96.00%	95.60%	95.60%	98.00%	99.60%
NAD6	156	86.71%	88.59%	86.58%	95.10%	97.99%
CYTB	379	97.35%	94.99%	95.78%	97.88%	99.74%
ATP6	231	89.96%	89.52%	89.52%	95.20%	99.13%
NAD5	573	91.94%	91.97%	91.97%	97.55%	99.30%
NAD4L	98	97.50%	91.84%	92.86%	92.86%	100%
NAD4	452	90.78%	91.57%	91.59%	97.00%	99.12%
NAD1	307	93.20%	94.77%	95.11%	95.58%	99.67%
NAD3	117	92.71%	88.79%	86.32%	94.79%	96.58%
NAD2	335	89.55%	87.74%	88.42%	95.82%	99.04%

\* All 13 mitochondrial proteins from mitogenome showed same size across the species.

**Table 4.** Comparison of the nucleotide sequences of the 13 PCGs between *Ap. trapezoides* and *Ap. caliginosa*.

Protein	<i>Ap. trapezoides</i> this study vs.	<i>Ap. trapezoides</i> this study vs.	<i>Ap. trapezoides</i> this study vs.	<i>A. caliginosa</i> (CM035405) vs.	<i>A. caliginosa</i> 5 this study vs.
	<i>A. caliginosa</i> (CM035405)	<i>A. caliginosa</i> (NC_066400)	<i>A. caliginosa</i> 5 this study	<i>A. caliginosa</i> 5 this study	<i>A. tuberculata</i> (OM687883)
COX1	82.47%	84.93%	84.41%	88.05%	99.03%
COX2	85.20%	85.96%	85.82%	89.88%	99.12%
ATP8	74.36%	73.58%	72.33%	84.62%	98.74%
COX3	83.20%	84.04%	83.53%	88.53%	99.49%
NAD6	79.87%	78.49%	77.63%	84.12%	98.49%
CYTB	82.94%	83.03%	82.76%	86.74%	99.03%
ATP6	80.06%	79.80%	80.23%	86.03%	98.70%
NAD5	79.04%	79.76%	79.64%	87.10%	98.78%
NAD4L	78.75%	79.93%	79.59%	82.50%	100%
NAD4	91.56%	80.68%	80.68%	86.28%	98.67%
NAD1	82.16%	84.69%	83.93%	86.73%	98.59%
NAD3	77.78%	76.92%	76.07%	84.05%	97.72%
NAD2	78.92%	78.81%	79.20%	85.64%	99.10%

## Discussion

Here, we report the first complete mitogenomes of *Ap. caliginosa* and *Ap. trapezoides*. The newly analyzed mt genomes showed an arrangement and base composition typical of earthworms (Shekhovtsov et al. 2020; Csuzdi et al. 2022) and fit into the size distribution of previously known complete earthworm mitogenomes (14,648–16,560) (Csuzdi et al. 2022; Zhao et al. 2022). Our data are in agreement with the published incomplete *Ap. caliginosa/tuberculata* mitogenomes (15,058–15,129 vs 15,090–15,123) which demonstrates that the

**Table 5.** Genetic *p*-distances of selected Lumbricidae mitogenomes using the complete mitogenome sequences excluding the non-coding region.

<i>Ap. rosea</i> MK573632												
<i>Ap. trapezoides</i> OM687882	0.203											
<i>Ap. trapezoides</i> this study	0.203	0.000										
<i>Ap. caliginosa</i> CM035405	0.202	0.164	0.163									
<i>Ap. caliginosa</i> NC_066400	0.201	0.161	0.161	0.110								
<i>Ap. caliginosa</i> (Apc-5)	0.200	0.164	0.164	0.111	0.021							
<i>Ap. caliginosa</i> (Apc-6)	0.201	0.164	0.164	0.110	0.020	0.004						
<i>Ap. caliginosa</i> (Apc-7)	0.201	0.164	0.164	0.110	0.020	0.004	0.000					
<i>Ap. tuberculata</i> OL840317	0.200	0.161	0.161	0.109	0.006	0.021	0.020	0.020				
<i>Ap. tuberculata</i> OM687884	0.201	0.163	0.163	0.109	0.020	0.011	0.010	0.010	0.020			
<i>Ap. tuberculata</i> OM687885	0.201	0.163	0.163	0.109	0.020	0.011	0.010	0.010	0.020	0.000		
<i>Ap. tuberculata</i> OM687883	0.201	0.163	0.163	0.109	0.020	0.010	0.009	0.009	0.020	0.005	0.005	
<i>Ap. tuberculata</i> OM687886	0.201	0.163	0.163	0.109	0.020	0.010	0.009	0.009	0.020	0.005	0.005	0.000

data from Zhao et al. (2022) are nearly complete, and only a few bp may be missing for circularity. For *Ap. trapezoides* (14,998 vs 15,014), this difference was also negligible.

Amino acid and base pair compositions across the 13 PCGs in *Ap. caliginosa* L2 and *Ap. tuberculata* species pairs were highly similar, showing 96–100% similarity across different genes. We obtained slightly lower similarity data when we compared *Ap. caliginosa* L2, and the sequence belonged to L3 (CM035405), indicating that the *Ap. tuberculata* sequences reported by Zhao et al. (2022) belong to *Ap. caliginosa*. This was clearly depicted in the phylogenetic reconstructions using the *cox1*, 13 PCGs, and complete mt genomes (Figs 1, 3, 4), corroborating the earlier findings of Briard et al. (2012) and Fernández et al. (2012) that *Ap. tuberculata* auct. (Eisen, 1874) is a synonym for *Ap. caliginosa* (Savigny, 1826). However, this was not observed for *Ap. trapezoides*, corroborating with previous results (Pérez-Losada et al. 2009; Fernández et al. 2011, 2012) and suggesting that *Ap. trapezoides* is distant from *Ap. caliginosa*, as it showed only 72.33%–91.56% nucleotide sequence similarity and 86.32%–99.4% amino acid composition similarity (lowest for *nad3* and highest for *cox1*; Tables 3, 4). This result was also reflected in the phylogenetic trees (Figs 1, 3, 4).

Phylogenetic analysis of the complete mt genomes (excluding the control region) and 13 PCGs strongly supported the monophyletic family Lumbricidae; however, the genus *Aporrectodea* proved to be polyphyletic. The species *Ap. rosea* does not form a clade with *Ap. caliginosa/trapezoides* sequences, reinforcing findings of previous studies' (Domínguez et al. 2015; Marchán et al. 2022, 2023), and restricting *Aporrectodea* Örley, 1885 to the *Ap. caliginosa/trapezoides* complex and other closely related Franco-Iberian species (Marchán et al. 2023).

## Acknowledgements

We would like to thank Editage ([www.editage.co.kr](http://www.editage.co.kr)) for English language editing. We thank Jovana Seculic, Parin Jirapatrasilp and an anonymous reviewer for their valuable comments on the manuscript.

## Additional information

### Conflict of interest

The authors have declared that no competing interests exist.

### Ethical statement

The samples used in this study are earthworms that are not included in the list of protected animals, and hence, the ethical statement is not applicable.

### Funding

This study was supported by the National Research Foundation of Korea (NRF) funded by the Ministry of Education under Grant number RS-2024-00338212.

### Author contributions

Conceptualization: YH. Data curation: JK. Formal analysis: CC, JK. Funding acquisition: YH. Methodology: JK. Writing – original draft: CC. Writing – review and editing: YH.

### Author ORCIDs

Csaba Csuzdi  <https://orcid.org/0000-0002-0319-7836>

Jachoon Koo  <https://orcid.org/0000-0002-3559-326X>

Yong Hong  <https://orcid.org/0000-0002-8093-9717>

### Data availability

The genome sequence data supporting the results of this study are openly available in GenBank of NCBI under the accession no. PQ572750–PQ572753.

## References

- Bankevich A, Nurk S, Antipov D, Gurevich AA, Dvorkin M, Kulikov AS, Lesin VM, Nikolenko SI, Pham S, Pribelski AD, Pyshkin AV, Sirotkin AV, Vyahhi N, Tesler G, Alekseyev MA, Pevzner PA (2012) Spades: A new genome assembly algorithm and its applications to single-cell sequencing. *Journal of Computational Biology* 19: 455–477. <https://doi.org/10.1089/cmb.2012.0021>
- Blakemore RJ (2002) *Cosmopolitan earthworms – an ecotaxonomic guide to the peregrine species of the world*, VermEcology Kippax ACT Australia, 506 pp.
- Blakemore RJ (2008) *Cosmopolitan earthworms – an eco-taxonomic guide to the species*. 3<sup>rd</sup> edition. VermEcology Yokohama, 757 pp.
- Bolger AM, Lohse M, Usade, B (2014) Trimmomatic – a flexible trimmer for Illumina sequence data. *Bioinformatics* 30(15): 2114–2120. <https://doi.org/10.1093/bioinformatics/btu170>
- Boore JL, Brown WM (1995) Complete sequence of the mitochondrial DNA of the annelid worm *Lumbricus terrestris*. *Genetics* 141(1): 305–319. <https://doi.org/10.1093/genetics/141.1.305>
- Bouché BM (1972) *Lombriciens de France Écologie et Systématique*. Institut National de la Recherche Agronomique. *Annales de Zoologie Ecologie Animale*. Numéro hors-série, Paris, 671 pp.
- Briard C, Qiu J-P, Zhao Q, Guernion M, Cluzeau D (2012) Phylogenetic study of some *Aporrectodea* species based on molecular markers. *Zoology in the Middle East* 58(Supplementum 4): 23–30. <https://doi.org/10.1080/09397140.2012.10648982>

- Briones MJ (1996) A taxonomic revision of the *Allolobophora caliginosa* complex (Oligochaeta, Lumbricidae): a preliminary study. *Canadian Journal of Zoology* 74(2): 240–244. <https://doi.org/10.1139/z96-030>
- Cain AJ (1955) The taxonomic statues of *Allolobophora iowana* Evans, 1948 (Oligochaeta, Lumbricidae). *Annals and Magazine of Natural History (Series 12)* 8(91): 481–497. <https://doi.org/10.1080/00222935508655659>
- Capella-Gutiérrez S, Silla-Martínez JM, Gabaldón T (2009) trimAl: a tool for automated alignment trimming in large-scale phylogenetic analyses. *Bioinformatics* 25(15): 1972–1973. <https://doi.org/10.1093/bioinformatics/btp348>
- Conrado AC, Arruda H, Stanton DWG, James SW, Kille P, Brown G, Silva E, Dupont L, Taheri S, Morgan AJ, Simões N, Rodrigues A, Montiel R, Cunha L (2017) The complete mitochondrial DNA sequence of the pantropical earthworm *Pontoscolex corethrurus* (Rhinodrilidae, Clitellata): mitogenome characterization and phylogenetic positioning. *ZooKeys* 688: 1–13. <https://doi.org/10.3897/zookeys.688.13721>
- Csuzdi Cs, Zicsi A (2003) Earthworms of Hungary (Annelida: Oligochaeta, Lumbricidae). Hungarian Natural History Museum, Budapest, 273 pp. <https://doi.org/10.5281/zenodo.4309820>
- Csuzdi Cs, Koo J, Hong Y (2022) The complete mitochondrial DNA sequences of two sibling species of lumbricid earthworms, *Eisenia fetida* (Savigny, 1826) and *Eisenia andrei* (Bouché, 1972) (Annelida, Crassicitellata): comparison of mitogenomes and phylogenetic positioning. *ZooKeys* 1097: 167–181. <https://doi.org/10.3897/zookeys.1097.80216>
- Domínguez J, Aira M, Breinholt JW, Stojanovic M, James SW, Pérez-Losada M (2015) Underground evolution: new roots for the old tree of lumbricid earthworms. *Molecular Phylogenetics and Evolution* 83: 7–19. <https://doi.org/10.1016/j.ympev.2014.10.024>
- Donath A, Jühling F, Al-Arab M, Bernhar, SH, Reinhardt F, Stadler PF, Middendorf M, Berrnt M (2019) Improved annotation of protein-coding genes boundaries in metazoan mitochondrial genomes. *Nucleic Acids Research* 47(20): 10543–10552. <https://doi.org/10.1093/nar/gkz833>
- Dugès A (1828) Recherches sur la circulation, la respiration et la reproduction des anelides abranches. *Annales des Sciences Naturelles* 15: 284–337.
- Eisen G (1873) Om Skandinaviens Lumbricier. Ofversigt af Kongliga Vetenskaps-Akademiens Forhandlingar 1873(8): 43–56. <https://archive.org/details/biostor-135527>
- Eisen G (1874) Bidrag till kännedomen om New Englands och Canadas Lumbricider. Ofversigt af Kongliga Vetenskaps-Akademiens Forhandlingar 1874(2): 41–50.
- Fernández R, Almodóvar A, Novo M, Gutiérrez M, Díaz Cosín DJ (2011) A vagrant clone in a peregrine species: phylogeography, high clonal diversity and geographical distribution in the earthworm *Aporrectodea trapezoides* (Dugès, 1828). *Soil Biology and Biochemistry* 43(10): 2085–2093. <https://doi.org/10.1016/j.soilbio.2011.06.007>
- Fernández R, Almodóvar A, Novo M, Simancas B, Díaz Cosín DJ (2012) Adding complexity to the complex: new insights into the phylogeny, diversification and origin of parthenogenesis in the *Aporrectodea caliginosa* species complex (Oligochaeta, Lumbricidae). *Molecular Phylogenetics and Evolution* 64(2): 368–379. <https://doi.org/10.1016/j.ympev.2012.04.011>
- Fernández R, Almodóvar A, Novo M, Gutiérrez M, Díaz Cosín DJ (2013) Earthworms, good indicators for palaeogeographical studies? Testing the genetic structure and demographic history in the peregrine earthworm *Aporrectodea trapezoides* (Dugès, 1828) in southern Europe. *Soil Biology and Biochemistry* 58: 127–135. <https://doi.org/10.1016/j.soilbio.2012.10.021>
- Friend H (1910) New garden worms. *Gardener's chronicle* 48: 98–99.

- Gates GE (1972a) Burmese earthworms. An introduction to the systematics of megadrile oligochaetes with special references to Southeast Asia. *Transactions of the American Philosophical Society* 62: 1–326. <https://doi.org/10.2307/1006214>
- Gates GE (1972b) Toward a revision of the earthworm family Lumbricidae. IV. The *trapezoides* species group. *Bulletin of the Tall Timbers Research Station* 12: 1–146 pp.
- Hoang, DT, Chernomor O, von Haeseler A, Minh BQ, Vinh LS (2018) UFBBoot2: Improving the ultrafast bootstrap approximation. *Molecular Biology and Evolution* 35: 518–522. <https://doi.org/10.1093/molbev/msx281>
- Hong Y, Kim MJ, Wang AR, Kim I (2017) Complete mitochondrial genome of the earthworm, *Amyntas jiriensis* (Clitellata: Megascolecidae). *Mitochondrial DNA A. DNA Mapping, Sequencing, and Analysis* 28(2):163–164. <https://doi.org/10.3109/19401736.2015.1115491>
- Kalyaanamoorthy S, Minh BQ, Wong TKF, von Haesele, A, Jermiin LS (2017) ModelFinder: fast model selection for accurate phylogenetic estimates. *Nature Methods* 14(6): 587–589. <https://doi.org/10.1038/nmeth.4285>
- Katoh K, Standley DM (2013) MAFFT multiple sequence alignment software version 7: Improvements in performance and usability. *Molecular Biology and Evolution* 30(4): 772–780. <https://doi.org/10.1093/molbev/mst010>
- Kim MJ, Hong Y (2022) Complete mitochondrial genome of the earthworm *Amyntas seungpanensis* (Clitellata: Megascolecidae). *Mitochondrial DNA B Resources* 7(6): 989–991. <https://doi.org/10.1080/23802359.2022.2080604>
- Kumar S, Stecher G, Li M, Knyaz C, Tamura K (2018) MEGA X: Molecular Evolutionary Genetics Analysis across computing platforms. *Molecular Biology and Evolution* 35(6): 1547–1549. <https://doi.org/10.1093/molbev/msy096>
- Latif R, Malek M, Aminjan AR, Pasantes JJ, Briones MJI, Csuzdi CS (2020) Integrative taxonomy of some Iranian peregrine earthworm species using morphology and barcoding (Annelida: Megadrili). *Zootaxa* 4877(1): 163–173. <https://doi.org/10.11646/zootaxa.4877.1.7>
- Liu H, Zhang Y, Xu W, Fang Y, Ruan H (2021) Characterization of five new earthworm mitogenomes (Oligochaeta: Lumbricidae): mitochondrial phylogeny of Lumbricidae. *Diversity* 13(11): 580. <https://doi.org/10.3390/d13110580>
- Marchán DF, Hedde M, Lapied E, Maggia ME, Novo M, Domínguez J, Decaëns T (2020) Contrasting phylogeographic patterns of earthworms (Crassiclitellata, Lumbricidae) on near-shore mediterranean islands. *European Journal of Soil Biology* 101: 103242. <https://doi.org/10.1016/j.ejsobi.2020.103242>
- Marchán DF, James SW, Lemmon AR, Moriarty Lemon E, Novo M, Domínguez J, Diaz-Cosin DJ, Trigo D (2022) A strong backbone for an invertebrate group: anchored phylogenomics improves the resolution of genus-level relationships within the Lumbricidae (Annelida, Crassiclitellata). *Organisms Diversity & Evolution* 22: 915–924. <https://doi.org/10.1007/s13127-022-00570-y>
- Marchán DF, Navarro AM, Pinadero SJ, Gerard S, Hedde M, Domínguez J, Decaëns T, Novo M (2023) Understanding the diversification and functional radiation of *Aporrectodea* (Crassiclitellata, Lumbricidae) through molecular phylogenetics of its endemic species. *European Journal of Soil Biology* 119: 103559. <https://doi.org/10.1016/j.ejsobi.2023.103559>
- Michaelsen W (1892) Terricolen der Berliner Zoologischen Sammlung, II. *Archiv für Naturgeschichte* 58: 209–261. <https://doi.org/10.5962/bhl.part.8321>
- Mršić N (1991) Monograph on earthworms (Lumbricidae) of the Balkans I–II. Slovenska Akademija Znanosti in Umetnosti, Razred za Naravoslovne Vede, Opera, 31, Ljubljana, 757 pp.

- Nguyen L-T, Schmidt HA, von Haeseler A, Minh BQ (2014) IQ-TREE: a fast and effective stochastic algorithm for Estimating maximum-likelihood phylogenies. *Molecular Biology and Evolution* 32(1): 268–274. <https://doi.org/10.1093/molbev/msu300>
- Örley L (1885) A palaearktikus övben élő terrikoláknak revíziója és elterjedése. *Értekezések a Természettudományok Köréből* 15: 1–34.
- Pérez-Losada, M, Ricoy M, Marshall JC, Domínguez J (2009) Phylogenetic assessment of the earthworm *Aporrectodea caliginosa* species complex (Oligochaeta: Lumbricidae) based on mitochondrial and nuclear DNA sequences. *Molecular Phylogenetics and Evolution* 52(2): 293–302. <https://doi.org/10.1016/j.ympev.2009.04.003>
- Pop V (1949) Lumbricidele din România. *Analele Academiei Republicii Populare Române* 1(9): 383– 505.
- Porco D, Decaëns T, Deharveng L, James SW, Skarżyński D, Erséus C, Butt KR, Richard B, Hebert PDN (2013) Biological invasions in soil: DNA barcoding as a monitoring tool in a multiple taxa survey targeting European earthworms and springtails in North America. *Biological Invasions* 15(4): 899–910. <https://doi.org/10.1007/s10530-012-0338-2>
- Ratnasingham S, Hebert PDN (2013) A DNA-based registry for all animal species: the Barcode Index Number (BIN) System. *PLoS ONE* 8(8): e66213. <https://doi.org/10.1371/journal.pone.0066213>
- Reynolds JW (1977) The earthworms (Lumbricidae and Sparganophilidae) of Ontario. Royal Ontario Museum Toronto, 141 pp. <https://doi.org/10.5962/bhl.title.60740>
- Reynolds JW (2022) The Earthworms (Lumbricidae, Megascolecidae and Sparganophilidae) in Canada. Canadian Food Inspection Agency Ottawa, 179 pp.
- Ronquist F, Teslenko M, van der Mark P, Ayres DL, Darling A, Höhna S, Larget B, Liu L, Suchard MA, Huelsenbeck JP (2012) MRBAYES 3.2: efficient Bayesian phylogenetic inference and model selection across a large model space. *Systematic Biology* 61: 539–542. <https://doi.org/10.1093/sysbio/sys029>
- Savigny JC (1826) Analyse d'un memoire sur les Lombrics par Cuvier. *Mémoires de l'Académie des sciences de l'Institut de France* 5: 176–184.
- Schwarz G (1978) Estimating the dimension of a model. *The Annals of Statistics* 6(2): 461–464. <https://doi.org/10.1214/aos/1176344136>
- Seto A, Endo H, Minamiya Y, Matsuda M (2021) The complete mitochondrial genome sequences of Japanese earthworms *Metaphire hilgendorfi* and *Amyntas yunoshimensis* (Clitellata: Megascolecidae). *Mitochondrial DNA B Resources* 6(3): 965–967. <https://doi.org/10.1080/23802359.2020.1830728>
- Shekhovtsov SV, Peltek SE (2019) The complete mitochondrial genome of *Aporrectodea rosea* (Annelida: Lumbricidae). *Mitochondrial DNA Part B, Resources* 4(1): 1752–1753. <https://doi.org/10.1080/23802359.2019.1610091>
- Shekhovtsov SV, Golovanova EV, Peltek SE (2016) Different dispersal histories of lineages of the earthworm *Aporrectodea caliginosa* (Lumbricidae, Annelida) in the Palearctic. *Biological Invasions* 18(3): 751–761. <https://doi.org/10.1007/s10530-015-1045-6>
- Shekhovtsov SV, Golovanova EV, Bazarova NE, Belova YN, Berman DI, Derzhinsky EA, Shashkov MP, Peltek SE (2017) Genetic diversity of the *Aporrectodea caliginosa* complex in Russia. *Vavilov Journal of Genetics and Breeding* 21(3): 374–379. <https://doi.org/10.18699/VJ17.255>
- Shekhovtsov SV, Golovanova EV, Ershov NI, Poluboyarova TV, Berman DI, Bulakhova NA, Szederjesi T, Peltek SE (2020) Phylogeny of the *Eisenia nordenskioldi* complex based on mitochondrial genomes. *European Journal of Soil Biology* 96: 103137. <https://doi.org/10.1016/j.ejsobi.2019.103137>

- Sims RW, Gerard BM (1985) Earthworms. Keys and notes to the identification and study of the Species. Synopsis of the British Fauna (New Series) E.J. Brill Leiden, 171 pp. <https://doi.org/10.1163/9789004611405>
- Templeton R (1836) A catalogue of the species of annulose animals, and of rayed ones, found in Ireland, as selected from the papers of the late J. Templeton, Esq., of Cranmore, with localities, description and illustration. Magazine of Natural History and Journal of Zoology, Botany, Mineralogy, Geology and Meteorology 9: 233–240.
- Tétry A (1937) Revision des lombriciens de la collection de Savigny. Bulletin du Muséum national d'Histoire naturelle 2(1): 72–81.
- Wang AR, Hong Y, Win TM, Kim I (2015) Complete mitochondrial genome of the Burmese giant earthworm, *Tonoscolex birmanicus* (Clitellata: Megascolecidae). Mitochondrial DNA. The Journal of DNA Mapping, Sequencing, and Analysis 26(3): 467–468. <https://doi.org/10.3109/19401736.2013.830300>
- Zhang L, Sechi P, Yuan M, Jiang J, Dong Y, Qiu J (2016) Fifteen new earthworm mitogenomes shed new light on phylogeny within the *Pheretima* complex. Scientific Reports 6: 20096. <https://doi.org/10.1038/srep20096>
- Zhao H, Fan S, Aspe NM, Feng L, Zhang (2022) Characterization of 15 earthworm mitogenomes from northeast China and its phylogenetic implication (Oligochaeta: Lumbricidae, Moniligastridae). Diversity 14(9): 714. <https://doi.org/10.3390/d14090714>
- Zicsi A (1982) Verzeichnis der bis 1971 beschriebenen und revidierten Taxa der Familie Lumbricidae (Oligochaeta). Acta zoologica hungarica 28: 421–454.

# Two new snake eels (Anguilliformes, Ophichthidae, *Ophichthus*) from Viet Nam, with redescriptions of *O. macrochir* (Bleeker) and *O. rutidoderma* (Bleeker)

Quang Van Vo<sup>1</sup>, Yusuke Hibino<sup>2</sup>, Hsuan-Ching Ho<sup>3,4</sup>, Thao Thu Thi Le<sup>1</sup>, Ying Giat Seah<sup>5</sup>

1 Institute of Oceanography, Vietnam Academy of Science and Technology, No. 01 Cau Da, Nha Trang City, Khanh Hoa, Vietnam

2 Kitakyushu Museum of Natural History and Human History, Kitakyushu, Fukuoka, Japan

3 Graduate Institute and Department of Aquaculture, National Kaohsiung University of Science and Technology, Kaohsiung, Taiwan

4 Australia Museum, Sydney, Australia

5 Faculty of Fisheries and Food Science, Universiti Malaysia Terengganu, Kuala Nerus, Terengganu 21030, Malaysia

Corresponding author: Hsuan-Ching Ho ([ogcoho@gmail.com](mailto:ogcoho@gmail.com))

## Abstract

Two new extremely elongate snake eel of the genus *Ophichthus* are described based on specimens collected from Vietnamese waters. *Ophichthus cuulongensis* Vo, Hibino & Ho, **sp. nov.** is distinguished from its congeners by having the dorsal-fin origin slightly behind the pectoral-fin tip, mean vertebral formula 14-63-202, range 12–17/60–64/199–207; teeth on jaws biserial to triserial; dorsal body dark brown, ventral body pale, anal fin initially white but changing to darker towards its tip. *Ophichthus nguyenorum* Vo, Hibino & Ho, **sp. nov.** is distinguished by having a snout rather pointed but the occipital convex (duck-shaped); body with numerous longitudinal wrinkles, weak on posterior abdomen; dorsal-fin origin slightly behind the pectoral-fin tip; one row of teeth on the maxilla anteriorly but increasing posteriorly; two rows on the lower jaw; all teeth small; body dark, usually including abdomen; dorsal fin darker with dark margin; anal fin initially pale but changing to darker towards tip; mean vertebral formula: 15-62-192, range 13–17/61–64/190–196. Descriptions of two related species, *O. macrochir* (Bleeker, 1852) and *O. rutidoderma* (Bleeker, 1852), are provided with updated morphological data.

**Key words:** Biodiversity, Elopomorpha, ichthyology, Mekong, Ophichthinae, *Ophichthus cuulongensis* sp. nov., *Ophichthus nguyenorum* sp. nov., taxonomy



Academic editor: Maria Elina Bichuette

Received: 18 September 2024

Accepted: 3 January 2025

Published: 13 March 2025

ZooBank: <https://zoobank.org/6C61817B-3D99-4A61-865C-BDDF332D4769>

**Citation:** Vo QV, Hibino Y, Ho H-C, Le TTT, Seah YG (2025) Two new snake eels (Anguilliformes, Ophichthidae, *Ophichthus*) from Viet Nam, with redescriptions of *O. macrochir* (Bleeker) and *O. rutidoderma* (Bleeker). ZooKeys 1231: 311–329. <https://doi.org/10.3897/zookeys.1231.137323>

Copyright: © Quang Van Vo et al.  
This is an open access article distributed under terms of the Creative Commons Attribution License (Attribution 4.0 International – CC BY 4.0).

## Introduction

The family Ophichthidae has the highest number of species among the anguilliform families, including more than 300 species distributed among 62 genera (Fricke et al. 2024). Many new species belonging to the snake eel genus *Ophichthus* have been described in recent decades (McCosker 2010; McCosker et al. 2012; McCosker and Ho 2015; McCosker and Psomadakis 2018; Hibino et al. 2019a, b; McCosker et al. 2020; Vo and Ho 2021; Ho et al. 2022; Kodeeswaran et al. 2024a, b; Behera et al. 2024; Hibino et al. 2024). The genus *Ophichthus* (Ahl, 1789) is a diverse genus of the family Ophichthidae with more than 100 valid species (Fricke et al. 2024). The genus *Ophichthus* can be separated into

two groups based on body shape: one group with the body stout to moderately elongate, its depth behind gill openings < 40 in TL and the second group with body shape elongate to extremely elongate, its depth behind gill openings > 40 in TL (McCosker et al. 2020).

The genus *Ophichthus* comprises 17 species in Vietnam with some new species and records reported recently (Vo et al. 2024). Historically, only three species with elongated to extremely elongated bodies, *Ophichthus macrochir* (Bleeker, 1852), *O. microcephalus* Day, 1878, and *O. rutidoderma* (Bleeker, 1852), were found in Viet Nam (Nguyen 1993; Nguyen and Nguyen 1994; Nguyen 2001; Vo et al. 2024). However, *O. microcephalus* is a questionable record due to the lack of firm evidence. In the Mekong estuary region, several elongate snake eels were identified as *O. rutidoderma* (and its synonym) or *Pisodonophis boro* (Hamilton, 1822) by previous authors (Mai et al. 1992; Rainboth 1996; Rainboth et al. 2012; Tran et al. 2013; Nagao Natural Environment Foundation 2021). However, we could not confirm those records based on only the brief information or photographs.

Recently (2023–2024), surveys of the family Ophichthidae in the Mekong estuary water were conducted and many specimens were collected. The morphological characteristics revealed that two new species in the genus *Ophichthus* are distinct from its congeners. Moreover, two other extremely elongated congeners, *O. macrochir* and *O. rutidoderma*, both lacking sufficient morphological data, are redescribed based on the types and additional specimens collected from various localities.

## Materials and methods

All methods for counts and measurements follow McCosker (2010), with further explanation below. Measurements for total and tail lengths are taken by 600- or 1000-mm rulers and others by digital caliper to the nearest 0.1 mm. Vertebral counts were made from radiograph films or digital radiograph photographs follow Böhlke (1982). Mean vertebral formula (**MVF**) is expressed as the average of predorsal, preanal and total vertebrae and vertebral formula (**VF**) are the solo number of each. The vertebral count includes the hypural. Terminology of head structures around lips and head pore system follow Hibino et al. (2019a, b), and are abbreviated as **SO** (supraorbital pores), **IO** (infraorbital pores), **POM** (preoperculomandibular pores), and **ST** (supratemporal pores). Lateral-line pores: head pores (**HLL**), pores before dorsal-fin origin (**PDLL**), pores before anal-fin origin (**PALL**) and total pores (**TLL**). Dorsal-fin origin (**DFO**) and anal-fin origin (**AFO**) are abbreviated. Total and head lengths are abbreviated as **TL** and **HL**, respectively.

Alcian blue was used to stain the skins of most specimens in order to make the precise counts of pores. Radiographs were made by a digital x-ray machine set up at the National Museum of Marine Biology & Aquarium, Taiwan, with pins inserted at origins of dorsal and anal fins. Specimens were deposited at the Natural History Museum, London, UK (**BMNH**); Pisces collection of National Museum of Marine Biology & Aquarium, Pingtung, Taiwan (**NMMB-P**); Kagoshima University Museum, Kagoshima, Japan (**KAUM-I**); Kitakyushu Museum of Natural History and Human History, Kitakyushu, Fukuoka, Japan (**KMNH VR**); and Institute of Oceanography, Nha Trang, Vietnam (**OIM-E**), Vietnam. Data used for comparison were either taken from specimens examined by the authors and various publications as indicated.

## Taxonomic account

### Family Ophichthidae

### Genus *Ophichthus* Ahl, 1789

#### *Ophichthus cuulongensis* Vo, Hibino & Ho, sp. nov.

<https://zoobank.org/8E3B8CBF-A165-4153-89CA-D656639B159A>

Figs 1, 2, Tables 1, 2

English name: Mekong's Estuary Snake Eel

Vietnamese name: Cá lịch mỡ

**Type material. Holotype:** • OIM-E. 55819, 904 mm TL, ripe female, field no. Q.01020, ca 12°19'N, 109°20'E, Đồng Hòa, Cần Giờ, Hồ Chí Minh city, south-east coast of Vietnam, South China Sea, bottom trawl, ca 10–20 m, 28 Aug. 2023. **Paratypes:** • Fifty seven specimens, 475–998 mm TL, all collected from some sites, including Đồng Hòa port fishing (10°22'57.45"N, 106°53'0.91"E), Cần Giờ district, Hồ Chí Minh city and Tân Bình market (ca 10°0'14.77"N, 106°37'23.73"E) and the old Ba Tri market (ca 10°2'25.96"N, 106°35'38.87"E), Ba Tri district and the Khâu Bông market (ca 9°49'33.35"N, 106°36'3.37"E), Thạnh Phú district, Bến Tre province: NMMB-P41234, 14 specimens, 640–831 mm TL, collected in 2020, 2023 & 2024 • OIM-E.55812, 945 mm TL, 13 Nov. 2013 • OIM-E.55813, 475 mm TL, 16 Sep. 2014 • OIM-E.55814, 783 mm TL, 13 Nov. 2014 • OIM-E.55815, 586 mm TL, 16 Sep. 2014 • OIM-E.55816, 880 mm TL, 10 Sep. 2016 • OIM-E.55817, 7 specimens, 640–872 mm TL, 06 & 08 Sep. 2020 • OIM-E.55818, 2 specimens, 710–725 mm TL, 22 Jun. 2023 • OIM-E.55820, 2 specimens, 696–781 mm TL, 20 Sep. 2023 • OIM-E.55821, 8 specimens, 732–878 mm TL, 23 Sep. 2023 • OIM-E.55822, 673 mm TL, 12 Oct. 2023 • OIM-E.55823, 2 specimens, 640–688 mm TL, 15 Oct. 2023 • OIM-E.55824, 10 specimens, 544–994 mm TL, 10 & 12 Nov. 2023 • OIM-E.55825, 2 specimens, 784–810 mm TL, 19 Jan. 2024. KMNH VR 100622, 4 specimens, 625–830 mm TL, collected in 2020 & 2023.

**Diagnosis.** An extremely elongate snake eel species of the genus *Ophichthus* with the following combination of characters: occipital not convex prominently, dorsal of snout with median shallow groove, reaching to interorbital pore; three or more shallow wrinkles (usually 3) on posterior part of eye; body with numerous longitudinal wrinkles, also prominent on abdomen; head length 5.2–6.2% TL; tail length 65.4–68.8% TL; two protrusions along upper lip from each side (some paratypes 1 on one side); dorsal-fin origin slightly behind pectoral-fin tip; SO 1 + 3, POM 5 (or rarely 6) + 2; teeth small (but larger in intermaxillary and anterior vomer); body dark brown, abdomen generally paler; dorsal fin with dark margin entirely, anal fin initially pale but in posterior part with faded dark margin, the area more than two head length; total vertebrae 199–207, MVF 14-62-202.

**Description.** Counts and measurements of the holotype (in mm). Total length 904, head 52.7, trunk 246.3, tail 605, predorsal length 73.1, pectoral-fin length 13.6; body depth at gill opening 16.2; body width at gill opening 13.0; body depth at anus 16.5; body width at anus 16.3; snout 7.2; upper jaw 13.6; snout overhang beyond tip of lower jaw 3.0; eye diameter 3.6; interorbital width 6.7; gill opening height 6.9; isthmus width 10.2.

Body extremely elongate (Fig. 1a), subcircular to posterior portion of tail, then becoming slightly compressed, its depth at gill openings 62 (55–69) in TL. Bran-

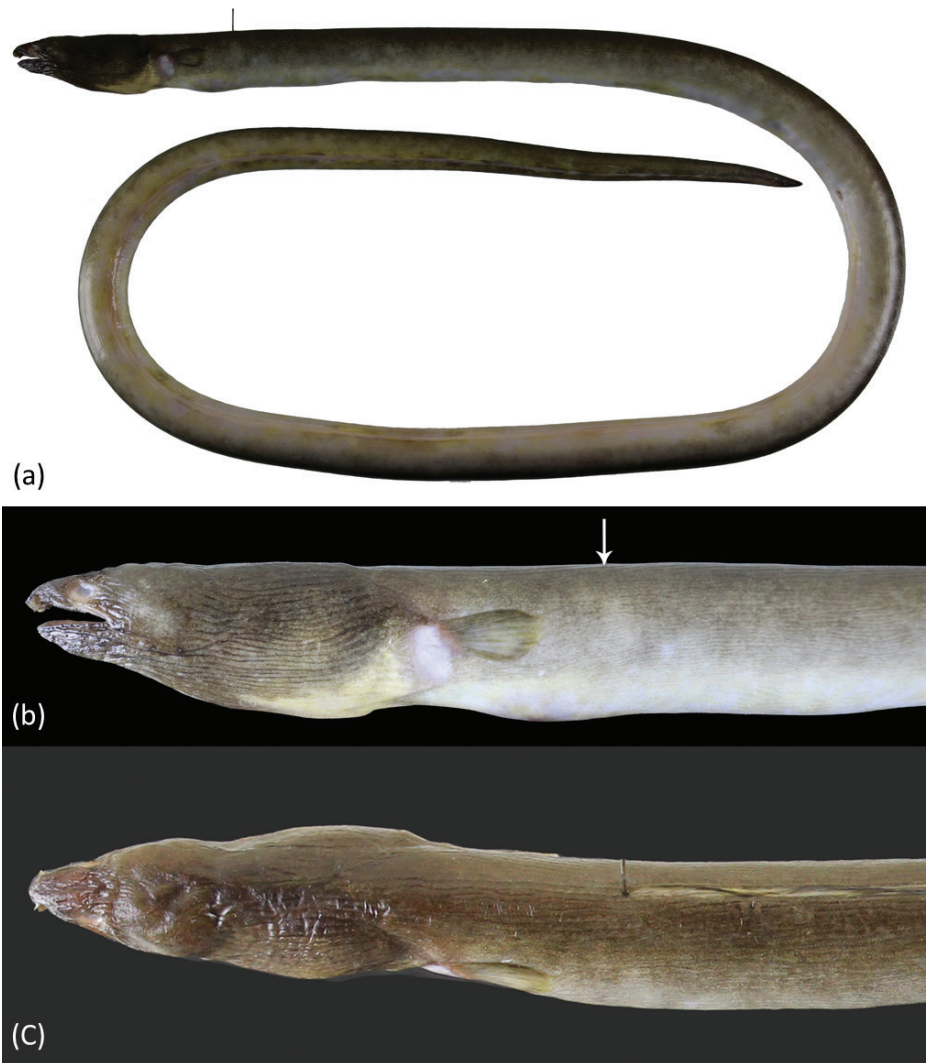


**Figure 1.** *Ophichthus cuulongensis* sp. nov., holotype, OIM-E. 55819, 904 mm TL **a** fresh specimen, arrows point to the DFO and AFO, respectively **b** close-up of head view from lateral side, arrow points to the DFO **c** close-up of head view from dorsal.

chial basket slightly expanded and deeper than trunk. Skin slightly wrinkled behind eye, nape, and body with numerous longitudinal wrinkles, also prominent on abdomen. Head short 17.6 (16.1–19.2) in TL and tail elongate 1.5 in TL. Snout short 7.0 (6.4–8.0), tip broadly conical at dorsal view, and bisected by a median shallow groove; lower jaw included, its tip extending slightly beyond posterior margin of anterior nostril tube; its length 4.6 (4.3–5.3) in HL. Upper jaw moderately long, rictus well behind posterior margin of eye; its length 4.0 (3.8–4.3) in HL.

Eye moderate, at mid of upper jaw, its diameter 3.2 (2.8–3.8) in upper-jaw length and 14.8 (13.1–16.8) in HL. Anterior nostril tubular, extending ventrolaterally from snout, reaching below upper lip and chin when directed downward. Posterior nostril a hole above upper lip, covered by a large flap that extends well below edge of mouth gape. Two barbels on upper lip (rarely 1 on one side). Dorsal-fin origin behind head, less than one pectoral-fin length behind fin tip and 1.4 (1.2–1.6) HL behind head. Median fins low but obvious, ending approximately one snout length before broadly pointed tail tip. Pectoral fin with narrow base, its length less than three times its base width, broad at middle, the longest rays at mid-fin.

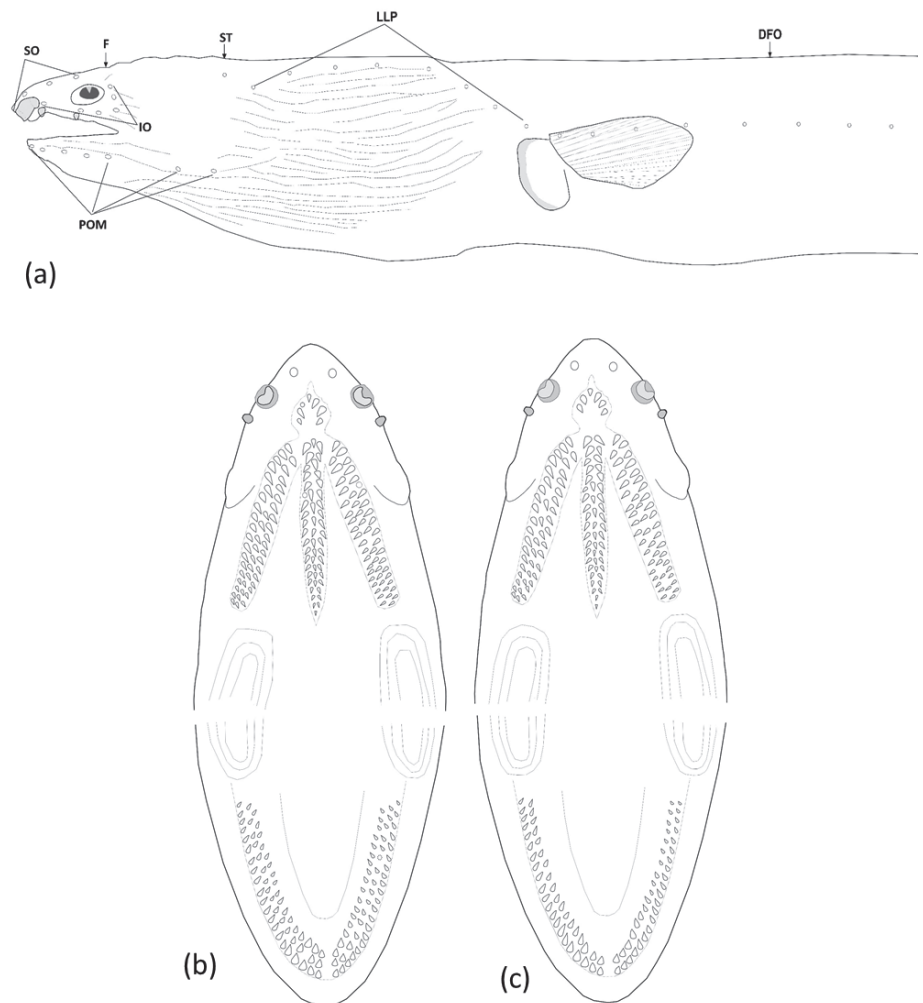


**Figure 2.** Drawing demonstrating the head pores (a) and teeth on both jaw (b, c) of *Ophichthus cuulongensis* sp. nov. a, b from the holotype c from OIM-E.55824, paratype, 808 mm TL.

Head pores small but apparent (Fig. 2a). SO 1 (ethmoid) + 3 on dorsal surface of snout and interorbital space; IO 3 + 3, one between nostrils, two below eye, and three behind eye; M 5 (1 paratype with 6 on left side), the last pore slightly before rictus; POP 2, F 1, ST 3. Indistinct minute sensory papillae present along nape, anterior margin of orbit, and around base of anterior nostril. Lateral-line pores apparent; HLL 9 (8–10), in an arching sequence, PDLL 15 (13–17; PALL 63 (62–65); TLL 198 (195–202), the last at approximately an upper-jaw length in front of tail tip.

Teeth (Figs 2b, c) moderately large, conical, and variable sizes. Intermaxillary with 4–6 teeth large and robust, arranged in two rows (some paratypes with a one at center), followed by 19 (17–20) teeth on vomer, biserial rows (some paratypes with 3 irregular rows and uniserial posteriorly), which decrease slightly in size posteriorly. Maxilla with 18–21 (right side) or 17–22 (left side) teeth mostly triserial (some paratypes biserial at anterior portion). Mandible with 17–24 teeth on right side or 18–25 teeth on left side; teeth arranged in two or three well-separated rows anteriorly, gradually becoming two rows at middle then three rows posteriorly, outer row slightly larger and more robust than the inner row (Fig. 2c).

**Table 1.** Morphometric and meristic data of four elongate *Ophichthus* species.

	<i>O. cuulongensis</i> sp. nov.			<i>O. nguyenorum</i> sp. nov.			<i>O. macrochir</i>		<i>O. rutidoderma</i>	
	Holotype	All types	SD	Holotype	All types	SD	Non-types		All types	
Total length (mm)	904	547–998 (n = 58)		887	697–967 (n = 18)		324–823 (n = 8)		415–867 (n = 11)	
<b>Proportions</b>		Mean (Range)	SD		Mean (Range)	SD	Mean (Range, n)		Mean (Range, n)	
As % of TL										
Head length	5.8	5.7 (5.2–6.2)	0.3	5.4	5.7 (5.4–6.2)	0.3	5.9 (5.6–6.7, 7)		6.3 (5.7–7.2, 8)	
Preanal length	33.1	32.7 (31.3–34.6)	0.8	32.0	32.8 (31.4–33.5)	0.6	35.5 (31.0–37.4, 7)		33.1 (32.2–34.1, 8)	
Trunk length	27.2	27.0 (25.3–28.5)	0.8	26.6	27.1 (25.9–28.0)	0.5	29.6 (25.2–31.7, 7)		26.8 (26.2–27.8, 8)	
Tail length	66.9	67.3 (65.4–68.8)	0.8	68.0	67.2 (66.5–68.6)	0.6	64.5 (62.5–69.3, 7)		66.8 (65.7–67.5, 8)	
Predorsal length	8.1	8.2 (7.1–9.5)	0.5	7.6	8.3 (7.6–8.7)	0.4	7.3 (6.7–7.9, 7)		8.7 (8.0–9.4, 8)	
Body depth at gill opening	1.8	1.6 (1.5–1.8)	0.1	1.6	1.6 (1.6–1.7)	0.1	1.6 (1.5–1.8, 6)		1.9 (1.5–2.1, 8)	
Body width at gill opening	1.4	1.5 (1.4–1.7)	0.1	1.5	1.5 (1.5–1.6)	0.0	1.4 (1.4–1.5, 3)		1.8 (1.6–2.3, 6)	
Body depth at mid-anus	1.8	1.8 (1.6–2.0)	0.1	1.5	1.5 (1.5–1.6)	0.1	1.6 (1.3–1.8, 6)		2.2 (1.8–2.6, 8)	
Body width at mid-anus	1.8	1.8 (1.6–2.0)	0.1	1.4	1.4 (1.4–1.5)	0.0	1.6 (1.5–1.9, 3)		2.2 (1.9–2.5, 6)	
As % of HL										
Snout length	13.7	14.3 (12.9–15.3)	0.7	15.3	15.7 (14.6–16.4)	0.5	17.0 (13.8–19.8, 7)		15.0 (12.4–16.9, 8)	
Eye diameter	6.8	6.8 (6.3–7.3)	0.3	5.9	6.2 (5.8–6.6)	0.2	7.1 (5.1–9.3, 7)		5.7 (4.0–7.1, 8)	
Upper-jaw length	25.8	25.1 (23.3–26.4)	1.0	29.5	29.6 (28.1–31.1)	0.8	33.0 (28.1–41.9, 7)		27.4 (22.6–29.7, 8)	
Low-jaw length	22.6	21.6 (19.0–23.1)	0.9	24.7	25.3 (24.7–26.3)	0.6	24.4 (24.2–24.9, 6)		24.2 (22.5–25.8, 2)	
Gill-opening length	13.1	13.9 (12.5–15.9)	0.9	17.6	17.3 (16.5–18.0)	0.5	11.5 (7.4–17.4, 7)		15.1 (8.1–20.2, 8)	
Interorbital width	12.7	13.3 (12.1–14.3)	0.6	13.00	13.2 (12.5–14.0)	0.4	13.2 (9.9–15.9, 7)		13.4 (11.8–16.1, 8)	
Isthmus width	19.4	17.9 (15.8–19.9)	0.9	15.3	15.0 (14.1–16.0)	0.6	18.5 (16.6–20.7, 6)		16.8 (14.6–19.0, 2)	
Pectoral-fin length	25.8	29.2 (22.9–34.1)	2.5	31.2	31.0 (28.4–33.6)	1.7	29.3 (27.0–32.9, 7)		30.3 (28.1–32.9, 7)	
<b>Counts</b>	–	n = 46	–	–	n = 18	–	n = 3		n = 9	
PALL	62	63 (62–65)	–	62	62 (61–64)	–	71 (70–73)		63 (59–67)	
Predorsal vertebrae	15	14 (12–17)	–	15	15 (13–17)	–	11 (11–12)		16 (14–16)	
Preanal vertebrae	63	62 (60–64)	–	63	62 (61–64)	–	70 (69–71)		63 (60–68)	
Total vertebrae	201	202 (199–207)	–	192	192 (190–196)	–	217 (214–221)		195 (191–199)	

**Coloration.** When fresh (Fig. 1a) body dark brown; pale white ventrally; dorsal fin dark margin; anal fin initially pale but in posterior part with faded dark margin, the area longer than two times head length; tail tip darker; pectoral fin pale to light yellow. After preservation, body uniformly dark brown dorsally and pale brown ventrally. Snout relatively darker than other skin; branchial basket and chest darker. Dorsal fin dark with dark margin; anal fin pale anteriorly and slightly blackish toward tail tip. Pectoral fin mostly pale with scattered dark grayish pigment on base. Mouth cavity pale with gray peppered dots. Peritoneum pale with gray peppered dots on upper half; stomach and intestine pale.

**Size.** The two largest specimens (998, 945 mm TL) are both ripe females with loose eggs.

**Etymology.** The specific name is derived from the Mekong River’s estuary. In Vietnamese, the name “cửu long” means nine dragons, which is the dragon’s mouth that waters flow from to the southern sea of Viet Nam.

**Table 2.** Selected morphological and meristic characteristics of eight elongate *Ophichthus* species. Data source: 1. This study; 2. Mishra et al. 2019; 3. Kodeeswaran et al. 2023; 4. McCosker 2010; 5. Lee and Asano 1997.

	<i>O. cuulongensis</i> sp. nov.	<i>O. nguyenorum</i> sp. nov.	<i>O. chilkensis</i>	<i>O. congroides</i>	<i>O. macrochir</i>	<i>O. microcephalus</i>	<i>O. rutidoderma</i>	<i>O. rotundus</i>
<b>Proportions</b>								
HL (%TL)	5.2–6.2	5.4–6.2	4.9–5.5	8.3–8.4	5.6–6.7	4.8	5.7–7.2	5.4–6.9
Trunk (%TL)	25.3–28.5	25.9–28.0	28.1–31.3	–	25.2–31.7	31.5	26.2–27.8	30.9–31.4
Tail (%TL)	65.4–68.8	66.5–68.6	63.5–70.7	60–63	62.5–69.3	63.8	65.7–67.5	60.7–66.7
<b>Ratios</b>								
TL/BD	48.9–63.8	61.8–68.8	50.0–90.9	–	54.9–74.5	71.4	39.2–56.2	37.0–43.5
PDL/HL	1.2–1.6	1.4–1.6	1.3–1.5	1.6–1.7	1.1–1.2	1.4	1.2–1.6	–
Trunk/HL	4.2–5.4	4.3–5.0	5.5–6.1	3.5–3.8	4.4–5.5	6.5	3.7–4.7	–
Trunk/PDL	2.7–3.8	3.0–3.5	4.1–4.6	2.1–2.3	3.2–4.5	4.6	2.9–3.3	–
HL/SNL	6.5–7.8	6.1–6.8	5.4–6.1	4.9–5.1	5.1–7.3	6.9	5.9–8.0	5.8–7.2
HL/UJL	3.8–4.3	3.2–3.6	3.2–3.8	2.3	2.4–3.6	4.0	3.4–4.4	–
<b>Meristics</b>								
SO	1 + 3	1 + 3	1 + 4	1 + 4	1 + 4	–	1 + 3	1 + 3
POM	5 (rarely 6) + 2	5 or 6 + 2	5 + 2	6 + 2	4–5 + 2	–	4–6 + 2	5 + 2
PDLL	13–17	13–16	13–14*	–	11–14	–	14–17	–
PALL	62–65	61–64	69–71	78	69–71	–	59–64	65–66
Protrusion number	2 (rarely 1)	1 (rarely 2)	1	0	2	1	2 (rarely 1)	2
MVF(VF)	14-62-202	15-62-192	11-69-210	21–76–206	11–70–217	13–72–214	15–63–197	14–64–182
TV	199–207	190–196	206–214	204–208	214–221	214	195–199	178–184
<b>Morphology</b>								
Skin condition	wrinkled	wrinkled	wrinkled	smooth	wrinkled	–	wrinkled	smooth
Body coloration	brown, bicolored	dark gray	dark olive brown	dark gray	black to dark brown	–	brown, bicolored	brown
Data sources	1	1	2, 3*	1, 4	1	2	1	1, 5

**Distribution.** Only known from the type series collected in Mekong’s estuary waters, southeast coast of Viet Nam, catching by bottom trawls and scoop net (push net); they are common in the waters. The depth range is estimated to be 8–20 m.

**Comparisons.** *Ophichthus cuulongensis* sp. nov. is similar to several of its congeners in their extremely elongated bodies. The selected characters for comparing these species are listed in Table 2. Compared to those species, *O. cuulongensis* sp. nov. has distinct vertebrae count ranging 199–207 in total. It readily differs from *O. nguyenorum* sp. nov. (190–196), *O. microcephalus* (214), and *O. rotundus* (178–184). Moreover, the new species differs from *O. congroides*, *O. chilkensis*, and *O. macrochir* in having fewer supraorbital pores (4 = 1 + 3, vs 5 = 1 + 4) and body coloration.

*Ophichthus cuulongensis* sp. nov. is most similar to *O. rutidoderma*, both sharing a short head, relatively long tail, body depth at anus and pores on head and lateral line. However, it can be distinguished from *O. rutidoderma* by its MVF 14-62-202 (vs 15-63-197), a higher total vertebral count (199–207, vs 195–199), maxillary teeth (mostly biserial or more vs uniserial anteriorly and biserial posteriorly), and mandible teeth (biserial to triserial vs biserial anteriorly and uniserial posteriorly).

*Ophichthus cuulongensis* sp. nov. is also similar to *O. chilensis* and *O. macrochir*, sharing a short head, a relatively long tail, an anus situated at the front of the total length, preopercuomandibular pores, and numerous longitudinal wrinkles on the body. However, it can be separated by its MVF 14-62-202 (vs 11-69-210 and 12-69-214, respectively), fewer total vertebrae (199–207, vs 206–214 and 207–221, respectively), and a shorter upper-jaw length (3.8–4.3 in HL, vs 3.2–3.8 and 2.4–3.6 in HL, respectively).

Although *Ophichthus cuulongensis* sp. nov. shares similar vertebral counts and preopercuomandibular pores with *O. congroides*, the former can be separated from the latter by having fewer lateral-line pores before anus (62–65 vs 78) and a shorter head length (5.2–6.2% TL, vs 8.3–8.4% TL) and a shorter snout length (6.5–7.8 in HL, vs 4.9–5.1 in HL) and a shorter upper-jaw length (3.8–4.3 in HL, vs 2.3 in HL) and different MVF (14-62-202 vs 21-76-206).

**Remarks.** *Ophichthus cuulongensis* sp. nov. has some characteristics, such as tooth arrangement and the shape of protrusions, which may be caused by ontogenetic changes. The jaws are arranged in biserial and triserial rows; vomerine teeth also show variability in arrangement among materials we examined. The teeth are large and robust to fat, becoming subequal anteriorly, similar to the teeth form of *Pisodonophis* in the larger specimens. The protrusions usually number two, but the one can degenerate or become very small on the side lip.

***Ophichthus nguyenorum* Vo, Hibino & Ho, sp. nov.**

<https://zoobank.org/9EF1D046-B202-461C-9DF7-4EDF7E149913>

Figs 3, 4; Tables 1, 2

English name: Darked Long-body Snake Eel

Vietnamese name: Cá lịch dài lưng đen

**Type material. Holotype** • OIM-E.55827, 887 mm TL, field no. Q.01095-3, ca 12°19'N, 109°20'E, Đông Hòa, Cần Giờ district, Hồ Chí Minh City, southeast coast of Vietnam, South China Sea, bottom trawl, ca 10–20 m, 10 Nov. 2023.

**Paratypes:** Seventeen specimens, 680–976 mm TL • NMMB-P41235, 5 specimens, 703–908 mm TL • KMNH VR 100623, 3 specimens, 740–848 mm TL • OIM-E.55826, 4 specimens, 784–976 mm TL, all collected with the holotype • OIM-E. 55828, 4 specimens, 697–852 mm TL • same location with holotype, bottom trawl, ca 10–20 m, 20 Jan. 2023; OIM-E. 55829, 680 mm TL • bottom trawl, ca 10–20 m, 20 Sep. 2023.

**Diagnosis.** An extremely elongate *Ophichthus* with the following combination of characters: snout rather pointed but occipital strongly convex (duck-shaped); body with numerous longitudinal wrinkles, weak on posterior abdomen; head 5.4–6.2% TL; preanal length 31.4–33.5% TL; tail 66.5–68.6% TL; snout length 14.6–16.4% HL; one protrusion along upper lip (rarely 2 on one side); dorsal-fin origin slightly behind pectoral-fin tip; SO 1 + 3, POM 5 or 6 + 2; all teeth small and sharp; teeth on maxilla in one row anteriorly but increasing posteriorly; teeth on mandible biserial; body dark, usually including abdomen; dorsal fin darker with dark margin; anal fin initially pale but darkening towards tip; total vertebrae 190–196, MVF 15-62-192.

**Description.** Counts and measurements of the holotype (in mm): total length 887, head 47.8, trunk 236.2, tail 601.4, predorsal length 67.4, pectoral-fin length

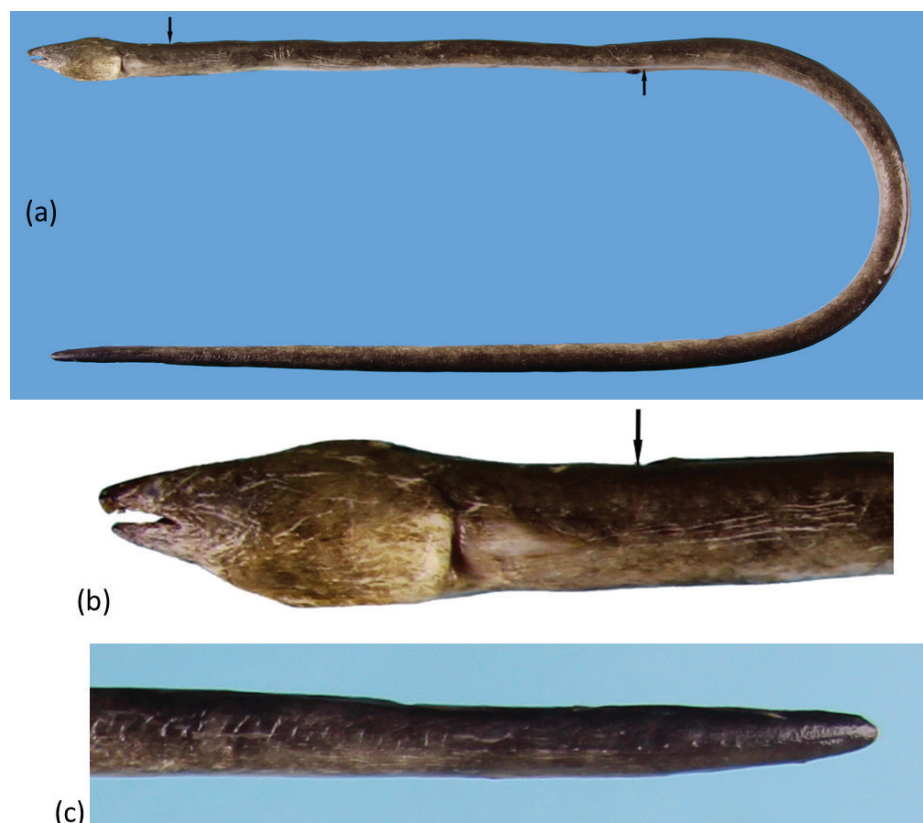


**Figure 3.** *Ophichthus nguyenorum* sp. nov. **a, b** fresh specimen of the holotype, OIM-E. 55827, 887mm TL, arrows point to the DFO and AFO, respectively **c** close-up of head view from lateral side of the paratype, OIM-E. 55827, 703 mm TL, arrow points to the DFO **d** close-up of tail view from ventral side of the holotype.

14.9; body depth at gill opening 14.4; body width at gill opening 13.7; body depth at anus 13.5; body width at anus 12.5; snout 7.3; upper jaw 14.1; snout overhang beyond tip of lower jaw 3.5; eye diameter 2.8; interorbital width 6.2; gill opening height 8.4; isthmus width 7.3.

An extremely elongate snake eel (Fig. 3a), subcircular to posterior portion of tail, then becoming slightly compressed, tail tip pointed and strong, its depth at gill openings 60.9 (57.6–64.2) in TL, Branchial basket slightly expanded and deeper than trunk. The skin slightly longitudinally wrinkled on body; skin folds not deep dorsally on body and weaker on posterior abdomen. Anus situated approximately in the anterior part of total length, head, and trunk 3.2 (3.0–3.2) in TL, head short 17.5 (16.1–18.6) in TL, and tail elongate 1.5 in TL. Snout short 6.4 (6.1–7.0) in HL, tip narrowly conical at dorsal view, underside of snout not bisected by a groove. Lower jaw short, its tip not extending beyond anterior margin of nostril tube; its length 4.1 (3.8–4.4) in HL. Upper jaw moderately long, rictus well behind posterior margin of eye; its length 3.4 (3.2–3.6) in HL.

Eye moderate in size, positioned above upper jaw, its diameter 4.8 (4.5–5.1) in upper jaw and 16.3 (15.1–17.3) in HL. Anterior nostril tubular, extending ventrolaterally from snout, reaching below upper lip and chin when directed downward. Posterior nostril is a hole above upper lip, covered by a broad flap that extends well below edge of upper lip. One protrusion on upper lip, positioned just behind anterior-nostril tube, rarely another one present below eye but extremely tiny and only on one side. Dorsal-fin origin behind head, by less than one pecto-

ral-fin length behind pectoral-fin tip and 1.5 (1.4–1.6) times head length behind head. Median fins low but obvious, ending approximately one upper-jaw length before the broadly pointed tail tip. Pectoral fin wedge-shaped with a narrow base, its length less than three times its base width, broad at middle and the longest rays at mid-fin.

Head pores small but apparent (Fig. 4a). SO 1 (ethmoid) + 3 on dorsal surface of snout and interorbital space; IO 3 + 3, 1 between nostrils, two below eye and three behind eye; POM 5 or 6 + 2 (5 + 2 in holotype), the last pore slightly before rictus; F 1, ST 3. Indistinct minute sensory papillae present along nape, anterior margin of orbit, and around base of anterior nostril. Lateral-line pores apparent; HLL 8 (8–9), in an arching sequence, PDLL 15 (13–16); PALL 62 (61–64); TLL 187 (185–190), the last at approximately one jaw length in front of tail tip.

Teeth (Fig. 4b, c) small, conical, sharp. Intermaxillary with 4–6 teeth arranged in two rows (some paratypes with one row with 3 or 4 teeth) followed by 22 (18–25) teeth on vomer, with biserial rows anteriorly (some paratypes with triserial irregular rows in middle) and uniserial posteriorly, which decrease slightly in size posteriorly. Maxilla with 22 (right side) (20–24) or 23 (left side) (21–25) teeth, mostly uniserial anteriorly and becoming biserial at posterior portion with irregular rows. Mandible with 27 (right side) (24–31) or 29 (left side) (27–34) teeth arrange in one irregular row anteriorly, gradually becoming two irregular rows posteriorly, some paratypes with additional teeth anteriorly forming two irregular rows and gradually becoming one row at middle and then two irregular rows posteriorly (Fig. 4c). Predorsal vertebrae 15 (13–17), pre-anal vertebrae 63 (61–64), and total vertebrae 192 (190–196) (one paratype specimen with a broken tail, total vertebrae only 185).

Coloration. When fresh (Fig. 3a) body uniformly dark; pectoral fin pale brown with peppered dots; anal fin pale anterior and change to darker toward the ending in approximately three times head length before the tail tip. After preservation, body uniformly dark dorsally and pale brown ventrally. Dorsal fin dark with dark margin; anal fin pale white anteriorly with slightly blackish pigment toward end of tail tip. Pectoral fin mostly dark grayish with scattered pigments. Mouth cavity dark except pale tooth ridges. Peritoneum pale with gray peppered dots on upper half; stomach and intestine pale. Tail tip blackish.

**Size.** The two largest specimens (976, 908 mm TL) are both ripe females with loose eggs.

**Etymology.** The specific name of the new species is derived to honor three doctors with the last name Nguyen: Dr. Phung Huu Nguyen, Huong Khac Nguyen, and Thi Nhat Nguyen for their contributions to marine fish taxonomy in Viet Nam.

**Distribution.** Only known from the type series collected from Mekong coastal region, southeast coast of Vietnam by bottom trawls. The depth range is estimated to be 10–20 m.

**Comparisons.** *Ophichthus nguyenorum* sp. nov. is different from most congeners belonging to the species group with elongate and extremely elongate bodies. Selected characters for comparing these species are listed in Table 2. Compared to those species, it has a distinct total vertebral count range 190–196, which differs from *Ophichthus cuulongensis* sp. nov. (199–207), *O. congroides* (204–208), *O. microcephalus* (214), *O. rotundus* (178–184). Moreover, the new species differs from *O. congroides*, *O. chilkensis*, and *O. macrochir* in having fewer supraorbital pores ( $4 = 1 + 3$ , vs  $5 = 1 + 4$ ).

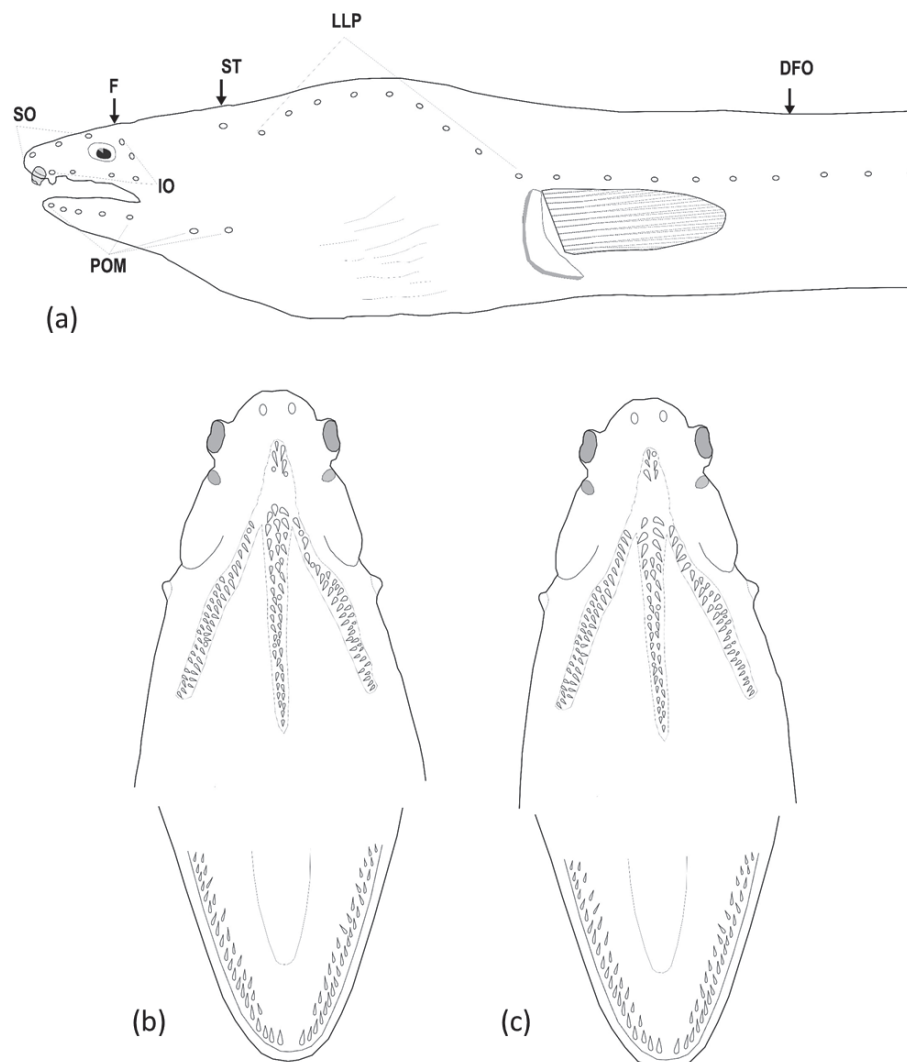


**Figure 4.** Drawing demonstrating the head pores (a) and teeth on both jaws (b, c) of *Ophichthus nguyenorum* sp. nov. a, b from the holotype c from OIM-E.55828, paratype, 708 mm TL.

Although *Ophichthus nguyenorum* sp. nov. is most similar to *O. rutidoderma*, both sharing a short head, relatively long tail, body depth at anus, and pores on head and lateral line; it can be distinguished from the latter species by its body uniformly dark and less body depth (61.8–68.8 in TL, vs 39.2–56.2 in TL), count of protrusions (generally 1 vs 2) and fewer total vertebrae (190–196 vs 195–199).

*Ophichthus nguyenorum* sp. nov. is also similar to *O. chilkinsis* and *O. macrochir*, sharing a short head, relatively long tail, and its anus situated at the front of total length, preopercular mandibular pores and numerous longitudinal wrinkles on the body, but it can be separated from the two species by its MVF 15-62-192 (vs 11-69-210 and 12-69-214, respectively), fewer total vertebrae (190–196, vs 206–214 and 207–221, respectively), shorter upper-jaw length (3.8–4.3 in HL, vs 3.2–3.8 and 2.4–3.6 in HL, respectively), and DFO behind the pectoral-fin tip (vs above tip of the fin). *Ophichthus nguyenorum* sp. nov. also can be separated from *O. congroides* in having fewer lateral-line pores before anus (62–64 vs 78) and a shorter head length (5.4–6.2% TL vs 8.3–8.4% TL), a shorter snout length (6.1–6.8 in HL, vs 4.9–5.1 in HL), a shorter upper-jaw length (3.2–3.6 in HL, vs 2.3 in HL), and different MVF (15-62-192 vs 21-76-206).

**Remarks.** *Ophichthus nguyenorum* sp. nov. has some characteristics, such as body coloration, tooth arrangement, and the shape of protrusions, which may be caused by ontogenetical changes. In small sizes, the body is dark grey dorsally and pale brown ventrally; the anal fin is pale brown anteriorly in a larger paratype. The vomerine teeth are arranged in biserial rows, and the upper jaw also has biserial rows posteriorly in some specimens. The protrusions are usually two; however, the posterior one can degenerate or become very small on the side lip.

***Ophichthus macrochir* (Bleeker, 1852)**

Fig. 5, Tables 1, 2

English name: Bigfin Snake Eel

Chinese name: 大鳍蛇鳗

*Ophisurus macrochir* Bleeker, 1852: 26 (type locality: Jakarta, Java, Indonesia).  
*Ophisurus woosuitingi* Chen, 1929: 22, pl. 2 (type locality: Ying Khou, Kwangtung, China).

**Material examined.** Eight specimens, 324–824 mm TL: BMNH 1867.11.28.262 (Bleeker specimen), 501 mm TL, Jakarta, Java, Indonesia; CAS 52580, 324 mm TL, Dumaguete, Negros, Philippines • CAS 233838, 631 mm TL, Lagoon of Aputit Island, northern Palawan, Philippines • KMNH VR 100261, 659 mm TL, Donggang, Taiwan • NMMB-P23577, 646 mm TL, Ke-tzu-liao, Kaohsiung, Taiwan • NMMB-P24692, 356 mm TL, Donggang, Taiwan • NMMB-P36831, 626 mm TL, Ke-tzu-liao, Kaohsiung, Taiwan • OIM-E.55830, 544 mm TL, Kỳ Hà market (ca 15°28'20"N, 108°41'01"E), Tam Kỳ, Quảng Nam, Vietnam; OIM-E.55831, ~ 824 mm TL (tail is broken), Đồng Hòa, Cần Giỏi, Hồ Chí Minh city, Vietnam.

**Diagnosis.** An elongate *Ophichthus* with the following combination of characters: body strongly wrinkled; head length 5.0–6.7% TL; tail length 62.5–69.3% TL; two protrusions along upper lip; dorsal-fin origin at approximately same vertical through pectoral-fin tip; SO 1 + 4, POM 4–5 (usually 5) + 2; teeth on maxilla mostly uniserial, on mandible biserial; teeth on vomer bi- or triserial; body uniformly black to dark brown; dorsal and anal fins dark gray to black; total vertebrae 214–221, MVF 11-70-217.

**Distribution.** Thailand (Gulf of Thailand), Indonesia (Java and Sumatra), Vietnam, Philippines, southern China, Taiwan, and Japan (larva only in Japan). Usually occurring in shallow water above 25 m, but specimens from Taiwan were possibly collected deeper than 100 m.

**Remarks.** We have not examined the holotype (RMNH.PISC.7174) directly; however, McCosker (2022) noted the MVF of that holotype *O. macrochir* is 11/70/221, the only available data for the holotype. McCosker and Ho (2015) provided the range of the total number of vertebrae of the species as 207–218 in the key based on specimens collected from Taiwan. *Ophichthus macrochir* has been recorded from several regions with morphological information (cf. Allen and Erdmann 2012; Hibino 2019; McCosker 2022), but diagnostic characters were uncertain. In addition, some elongate species have been described or redescribed as valid species in recent years (e.g., Mishra et al. 2019; this study). Based on only our examination and vertebral information of the holotype, a new diagnosis is provided herein.



**Figure 5.** *Ophichthus macrochir* (Bleeker, 1852), NMMB-P23577, 646 mm TL; preserved specimen **a** whole fish. Close-ups of head view from lateral side (**b**), view from dorsal (**c**) and view from ventral (**d**).

*Ophisurus woosuitingi* Chen, 1929 was originally described based on a single specimen collected from Kwangtung, southern China. We could not access the holotype of *O. woosuitingi*, but the description includes detailed

information on its morphological features, with good illustrations of the head and anterior trunk. According to Chen (1929), the species has the following morphological features: strongly wrinkled body; head 6.0% TL; body depth 1.4% TL (70.8 in TL); eye 6.2% HL; snout 18.7% HL; pectoral-fin length ~ 20% HL; dorsal-fin origin slightly behind the tip of the pectoral fin; SO ?1 (ethmoid not obvious) + 4, POM 5 + 2; preanal lateral-line pores 68; teeth on maxilla mostly uniserial, on mandible biserial; teeth on vomer bi- or triserial; body color uniformly blackish. It is evident that *O. woosuitingi* is a junior synonym of *O. macrochir*, although Tang and Zhang (2004) considered this name to be valid and separated it from *O. macrochir*.

Based on our extensive examination of *O. macrochir*, including specimens from various localities in the northwestern Pacific, we were unable to differentiate it from the Indian species *O. chilensis* based on the counts and measurements except for the protrusions on the upper lip (1 vs 2; Table 2). According to the redescription by Mishra et al. (2019), differences in fin coloration can distinguish *O. chilensis* from *O. macrochir* (dark gray to black vs dull white with posterior 1/3 of anal fin dark). Our investigation shows that the distribution of *O. macrochir* is restricted to the western Pacific, and the Indian records of *O. macrochir* might have been misidentifications of *O. chilensis*.

### ***Ophichthus rutidoderma* (Bleeker, 1852)**

Fig. 6, Tables 1, 2

English name: Olive Snake Eel

*Ophisurus rutidoderma* Bleeker, 1852: 30 (type locality: Jakarta, Java, Indonesia); Günther 1870:63 (as *Ophichthys rhytidoderma*, unjustified emendation).

*Ophisurus rutidodermatoides* Bleeker, 1852: 31 (type locality: Jakarta, Java, Indonesia); Günther 1870:62 (as *Ophichthys rhytidodermatoides*, unjustified emendation).

*Ophisurus lumbricoides* Bleeker, 1852: 32 (type locality unknown).

*Ophisurus maccllellandi* Bleeker, 1852: 33 (type locality: Jakarta, Java, Indonesia).

**Type material. Holotype** • BMNH 1867.11.28.226, 945 mm TL, Jakarta, Java, Indonesia (only vertebral examination).

**Other material examined.** 10 specimens, 415–867 mm TL: BMNH 1867.11.28.278, 569 mm TL, Jakarta, Java, Indonesia (Bleeker specimen of *O. maccllellandi*) • BMNH 1867.11.28.292, 610 mm TL, Jakarta, Java, Indonesia (holotype of *O. rutidodermatoides*; only vertebral examination) • BMNH 1867.11.28.300, 415 mm TL (holotype of *Ophisurus lumbricoides*; only vertebral examination), Jakarta, Java, Indonesia • KAUM–I. 39446, 867 mm TL, off Tanjung Sepat, Selangor, Malaysia • KMNH VR 100624–627, 4 specimens, 569–748 mm TL, purchased at Bagan Datuk, collected off mouth of Perak River, Perak, Malaysia • OIM-E.55787, 278 mm TL, Càn Giò fishing grounded, Hồ Chí Minh city, 15–17 m, Vietnam • OIM-E.55832, 590 mm TL, Bình Đại food market (ca 10°11'15"N, 106°41'40"E), Bình Đại District, Bến Tre province, Vietnam • OIM-E.55833, 700 mm TL, Đồng Hòa, Càn Giò District, Hồ Chí Minh City, Vietnam.

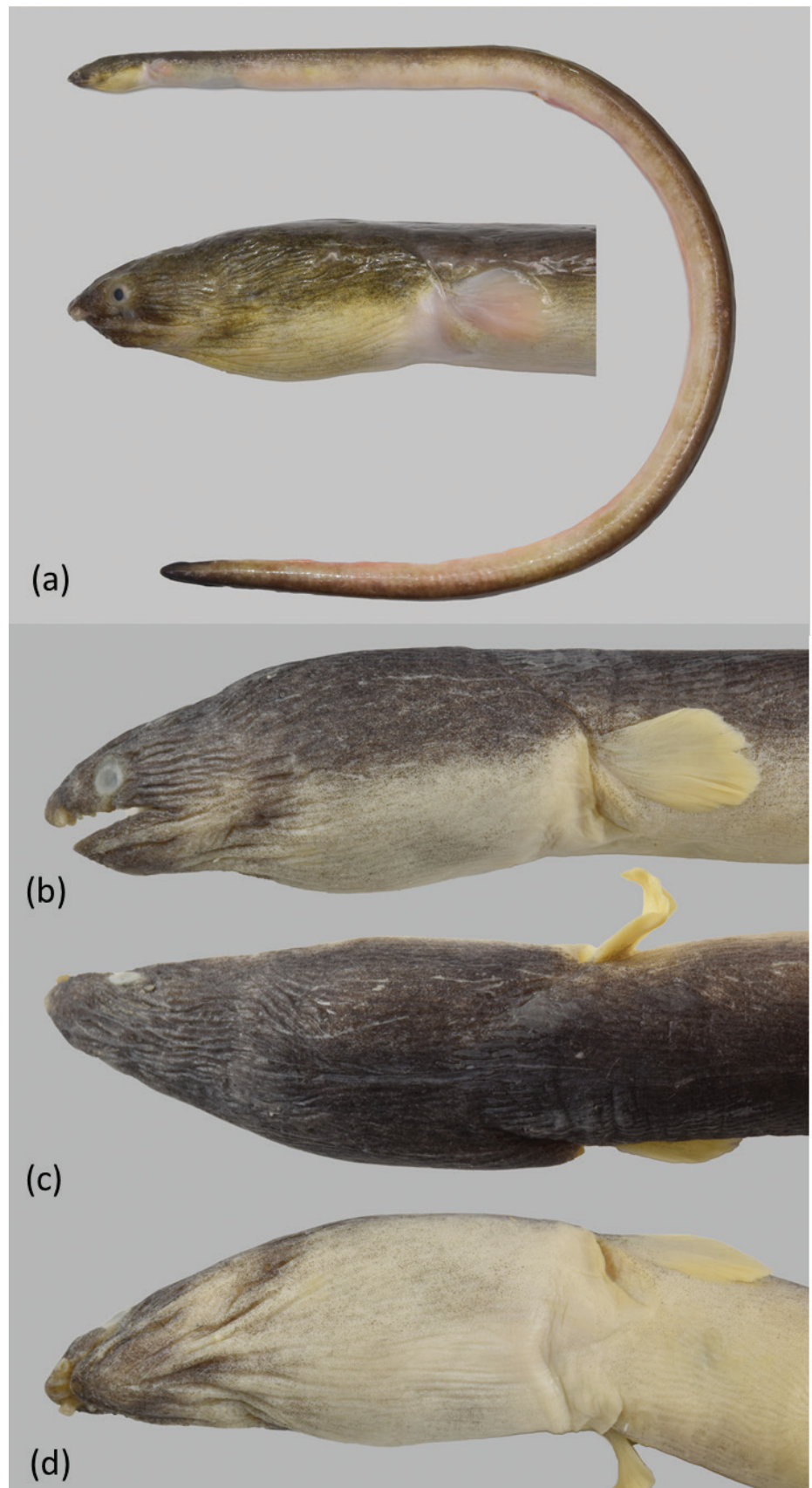


**Figure 6.** *Ophichthus rutidoderma* (Bleeker, 1852), KMNH VR 100624, 748 mm TL **a** fresh specimen, whole fish and close-up of head. Close-ups of head view from lateral side (**b**), view from dorsal (**c**), and view from ventral (**d**).

**Diagnosis.** An elongate *Ophichthus* with the following combination of characters: body with numerous longitudinal wrinkles, more than five longitudinal wrinkles on posterior part of eye; head length 5.7–7.2% TL; tail length 65.7–67.5% TL; two protrusions along upper lip (rarely 1 on one side); dorsal-fin origin behind pectoral-fin tip by less than one pectoral-fin length; SO 1 + 3; POM 4–6 (usually 5) + 2; teeth on maxilla uniserial initially, becoming biserial posteriorly; vomerine and dentary teeth biserial anteriorly, uniserial posteriorly; body bicolored; dorsal fin dark with narrow margin entirely, anal fin pale except ending; total vertebrae 195–199, MVF 15-63-197 ( $n = 9$ ).

**Distribution.** Southern Vietnam, Java, Indonesia, and Malay Peninsula of Malaysia. It is a shallow water species, collected adjacent to a river mouth. Collecting depth is estimated to be 5–20 m in Vietnam and Malaysia.

**Remarks.** *Ophichthus rutidoderma* has been recorded only from the South China Sea and western Australia; however, there are no detailed descriptions (usually only the name in list) except the original descriptions including several synonyms and a young specimen record by Vo et al. (2019) from Ho Chi Minh City, southern Vietnam. In Vo et al. (2019), the young Vietnamese specimen (278 mm TL) was reported as the first record from Vietnam, accompanied by a detailed morphological description. Although they described the specimen as having SO 1 + 4 and maxillary teeth arranged in a single row, the correct characteristics are SO 1 + 3 and a maxilla with primarily one row of teeth, except at the posterior end, whereas an additional row of four teeth is present. McCosker (2007) noted the vertebral information of several types, but he did not mention other characters. The record from Western Australia is based on the original description of *Ophichthus derbyensis* (holotype: 258 mm TL) by Whitley (1941). While its VF closely matches that of *O. rutidoderma*, the locality of *O. derbyensis* is significantly distant from the South China Sea. Moreover, *O. derbyensis* differs in dental morphology, with a completely single row of vomerine teeth (vs 2 anteriorly and 1 posteriorly in *O. rutidoderma*), and maxillary teeth that are biserial in the anterior-middle region but uniserial posteriorly (vs uniserial anteriorly and biserial posteriorly in *O. rutidoderma*). As such, we tentatively exclude *O. derbyensis* from synonymy with *O. rutidoderma*. Actually, *O. rutidoderma* appears to be a unique species restricted to the southwestern part of the South China Sea extending to the western coast of the Malay Peninsula. Future studies to determine the validity of *O. derbyensis* are required.

## Acknowledgements

We are grateful to James Maclaine (BMNH), David Catania (CAS), Hiroyuki Motomura (KAUM), Po-Na Lee, Ming-Hua Chiang (NMMB-P) for curatorial assistance, and to John E. McCosker (CAS) for the information on type specimens. This study is supported in part by the Vietnam Academy of Science and Technology (VAST) for QVV (grant VAST06.05/23-24), a Grant-in-Aid from the Japan Society for the Promotion of Science for JSPS Fellows to YH (DC2/PD: JP15J02820), a JSPS Grant-in-Aid for Early-Career Scientists KAKENHI (JP20K15593) to YH, and the Aquatic Biology Research Fund of the California Academy of Sciences to YH, and by the National Kaohsiung University of Science and Technology to YH and HCH. The National Museum of Marine Biology & Aquarium, Taiwan, supported the radiography facilities.

## Additional information

### Conflict of interest

The authors have declared that no competing interests exist.

### Ethical statement

All specimens were collected from the fish landing ground and dead before being collected.

### Funding

This study is supported in part by the Vietnam Academy of Science and Technology (VAST) for QVV (grant VAST06.05/23-24), a Grant-in-Aid from the Japan Society for the Promotion of Science for JSPS Fellows to YH (DC2/PD: JP15J02820), a JSPS Grant-in-Aid for Early-Career Scientists KAKENHI (JP20K15593) to YH, and the Aquatic Biology Research Fund of the California Academy of Sciences to YH, and by the National Kaohsiung University of Science and Technology to YH and HCH.

### Author contributions

QVV conducted the research and collected specimens; QVV and YH developed the draft; YH provided data of two nominal species; HCH provided facilities; TTTL, YGS provided information; all authors read the manuscript.

### Author ORCIDs

Quang Van Vo  <https://orcid.org/0000-0002-9680-6898>

Yusuke Hibino  <https://orcid.org/0000-0002-5670-3851>

Hsuan-Ching Ho  <https://orcid.org/0000-0003-1154-601X>

Thao Thu Thi Le  <https://orcid.org/0000-0002-9985-4668>

Ying Giat Seah  <https://orcid.org/0000-0002-2976-4448>

### Data availability

All of the data that support the findings of this study are available in the main text.

## References

- Allen GR, Erdmann MV (2012) Reef fishes of the East Indies. Volumes I. Tropical Reef Research, Perth Australia, x + 424 pp. <https://doi.org/10.1896/054.064.0104>
- Behera RK, Acharya S, Misra SS, Mohapatra A (2024) Morphological and molecular evidences confirm a new species in *Ophichthus* (Anguilliformes: Ophichthidae) from the east coast of India. *Bulletin of Marine Science* 100: 1–10. <https://doi.org/10.5343/bms.2023.0084> [online 13 June 2024]
- Bleeker P (1852) Bijdrage tot de kennis der Muraenoïden en Symbrancoïden van den Indischen Archipel. *Verhandelingen van het Bataviaasch Genootschap van Kunsten en Wetenschappen* 25: 1–62. [preprint part]
- Böhlke EB (1982) Vertebral formulae of type specimens of eels (Pisces: Anguilliformes). *Proceedings of the Academy of Natural Sciences of Philadelphia* 134: 31–49.
- Chen JTF (1929) A review of the Apodal fishes of Kwangtung. *Bulletin of the Biology Department, Science College, Sun Yatsen University* 1: 1–46. [pls 1–3]
- Fricke R, Eschmeyer WN, Fong JD (2024) Eschmeyer's catalog of fishes: genera/species by family/subfamily. <http://researcharchive.calacademy.org/research/ichthyology/catalog/SpeciesByFamily.asp> [accessed 02 May 2024]

- Günther A (1870) Catalogue of the fishes in the British Museum. Catalogue of the Physostomi, containing the families Gymnotidae, Symbranchidae, Muraenidae, Pegasidae, and of the Lophobranchii, Plectognathi, Dipnoi, Ganoidei, Chondropterygii, Cyclostomata, Leptocardi, in the British Museum. British Museum of Natural History, London, xxv + 549 pp.
- Hamilton F (1822) An account of the fishes found in the river Ganges and its branches. Archibald Constable, Edinburgh, 405 pp. [pls 1–39] <https://doi.org/10.5962/bhl.title.59540>
- Hibino Y (2019) Ophichthidae. In: Koeda K, Ho H-C (Eds) Fishes of Southern Taiwan. National Museum of Marine Biology & Aquarium, Pingtung, 118–154.
- Hibino Y, McCosker JE, Tashiro F (2019a) Four new deepwater *Ophichthus* (Anguilliformes: Ophichthidae) from Japan with a redescription of *Ophichthus pallens* (Richardson 1848). *Ichthyological Research* 66: 289–306. <https://doi.org/10.1007/s10228-018-00677-3>
- Hibino Y, Chiu Y-C, Chen H-M, Shao K-T (2019b) Two new species of the genus *Ophichthus* from the western central Pacific Ocean, with a redescription of *Ophichthus megalops* Asano, 1987 (Anguilliformes: Ophichthidae). *Zootaxa* 4702: 140–154. <https://doi.org/10.11646/zootaxa.4702.1.17>
- Hibino Y, Ho H-C, Huang J-F (2024) Descriptions of two new dark-body snake eels of the genus *Ophichthus* (Anguilliformes, Ophichthidae) from Taiwan. *ZooKeys* 1220: 63–78. <https://doi.org/10.3897/zookeys.1220.126337>
- Ho H-C, Ng S-L, Lin T-Y (2022) Description of a new *Ophichthus* eel from Dongsha Atoll, South China Sea, and a range extension of *Ophichthus kusanagi* Hibino, McCosker & Tashiro, 2019. *Raffles Bulletin of Zoology* 70: 312–319. <https://doi.org/10.26107/RBZ-2022-0015>
- Kodeeswaran P, Kathirvelpandian A, Mohapatra A, Kumar TTPA, Sarkar UK (2024a) A new snake eel species of the genus *Ophichthus* (Anguilliformes: Ophichthidae) from the southeast coast of India, Bay of Bengal, with the taxonomic account of *Ophichthus chilkensis*. *Journal of Fish Biology* 104(3): 737–745. <https://doi.org/10.1111/jfb.15617>
- Kodeeswaran P, Mohapatra A, Kumar TTPA (2024b) A new species of deep-water snake eel, *Ophichthus nigroventralis* (Anguilliformes: Ophichthidae) from the Arabian Sea, southwest coast of India. *Ichthyological Research* 71: 268–275. <https://doi.org/10.1007/s10228-023-00927-z>
- Lee C-L, Asano H (1997) A new ophichthid eel, *Ophichthus rotundus* (Ophichthidae, Anguilliformes) from Korea. *Korean Journal of Biological Sciences* 1: 549–552.
- Mai DY, Nguyen VT, Nguyen VT, Le HY, Hua BL (1992) Identification of freshwater fish species, Southern region, Viet Nam (Định loại các loài cá nước ngọt Nam bộ). Science and Technics Publishing House, Ha Noi, 351 pp. [in Vietnamese]
- McCosker JE (2007) *Luthulenchelys heemstraorum*, a new genus and species of snake eel (Anguilliformes: Ophichthidae) from KwaZulu-Natal, with comments on *Ophichthus rutidoderma* (Bleeker, 1853) and its synonyms. *Smithiana Bulletin* 7: 3–7. [https://doi.org/10.1643/0045-8511\(2007\)7\[783:ANDSOT\]2.0.CO;2](https://doi.org/10.1643/0045-8511(2007)7[783:ANDSOT]2.0.CO;2)
- McCosker JE (2010) Deepwater Indo-Pacific species of the snake-eel genus *Ophichthus* (Anguilliformes: Ophichthidae), with the description of nine new species. *Zootaxa* 2505: 1–39. <https://doi.org/10.11646/zootaxa.2505.1.1>
- McCosker JE (2022) Family Ophichthidae, Snake-eels, sand-eels and worm-eels. In: Heemstra PC, Heemstra E, Ebert DA, Holleman W, Randall JE (Eds) Coastal Fishes of the Western Indian Ocean. Vol. 2. South African Institute for Aquatic Biodiversity, Makhanda, 101–137.
- McCosker JE, Ho H-C (2015) New species of the snake eels *Echelus* and *Ophichthus* (Anguilliformes: Ophichthidae) from Taiwan. *Zootaxa* 4060: 71–85. <https://doi.org/10.11646/zootaxa.4060.1.11>

- McCosker JE, Psomadakis PN (2018) Snake eels of the genus *Ophichthus* (Anguilliformes: Ophichthidae) from Myanma (Indian Ocean) with the description of two new species. *Zootaxa* 4526: 71–83. <https://doi.org/10.11646/zootaxa.4526.1.5>
- McCosker JE, Ide S, Endo H (2012) Three new species of ophichthid eels (Anguilliformes: Ophichthidae) from Japan. *Bulletin of the National Museum of Nature and Science, Series A, Supplement 6*: 1–16.
- McCosker, JE, Bogorodsky SV, Mal AO, Alpermann TJ (2020) Description of a new snake eel *Ophichthus olivaceus* (Teleostei: Anguilliformes, Ophichthidae) from the Red Sea. *Zootaxa* 4750: 31–48. <https://doi.org/10.11646/zootaxa.4750.1.2>
- Mishra SS, Mohapatra A, Ray D, Mohanty SR, Tudu PC (2019) *Ophichthus chilkinsis* Chaudhuri, 1916 (Anguilliformes: Ophichthidae) – resurrection as a valid species from India, with re-description. *Zootaxa* 4586: 194–200. <https://doi.org/10.11646/zootaxa.4586.1.13>
- Nagao Natural Environment Foundation (2021) *Fishes of the Indochinese Mekong*. Nagao Natural Environment Foundation, Tokyo, xii + 546 pp.
- Nguyen KH (1993) *Marine Fishes of Vietnam*. Vol. 2, part 2. (Anguillomorpha, Cyprinomorpha, Atherinomorpha) (Cá biển Việt Nam: Anguillomorpha, Cyprinomorpha, Atherinomorpha. Tập 2, quyển 2). Science & Technology Publishers, Ha Noi and Ho Chi Minh City, 176 pp. [In Vietnamese]
- Nguyen HP (2001) *Fauna of Vietnam: Elopiformes, Anguilliformes, Clupeiformes, Gonorynchiformes*. Vol. 10 (Động vật chí Việt Nam: Cá biển – Bộ Cá chấu biển Elopiformes, Bộ Cá Chình Anguilliformes, Bộ Cá trích Clupeiformes, Bộ Cá sứa Gonorynchiformes. Tập 10). Science and Technics publishing House, Ha Noi, 330 pp. [in Vietnamese]
- Nguyen HP, Nguyen NT (1994) Checklist of marine fishes in Vietnam. Elopiformes to Mugiliformes (Vol. II. Osteichthyes) (Danh mục cá biển Việt Nam. Tập II: Lớp Cá Xương (Osteichthyes), từ bộ Cá Chấu biển (Elopiformes) đến bộ Cá Đối (Mugiliformes). Science and Technics Publishing House, Ha Noi, 269 pp. [in Vietnamese and English]
- Rainboth WJ (1996) *Fishes of the Cambodian Mekong*. Food Agriculture Organization of the United Nations. Mekong River Commission, DANIDA, 265 pp.
- Rainboth WJ, Vidthayanon C, Mai DY (2012) *Fishes of the greater Mekong ecosystem with species list and photographic atlas*. Miscellaneous Publications, Museum of Zoology, University of Michigan 201: 173 pp. [31 figs, 121 pls]
- Tang W-Q, Zhang C-G (2004) A taxonomic study on snake eel family Ophichthidae in China with the review of Ophichthidae (Pisces, Anguilliformes). *Journal of the Shanghai Ocean University* 13: 16–22. [In Chinese with English abstract]
- Tran DD, Shibukawa K, Nguyen PT, Ha HP, Tran LX, Mai HV, Utsugi K (2013) *Fishes of the Mekong Delta, Vietnam*. Can Tho University Publishing House, Can Tho, 174 pp. [in Vietnamese and English]
- Vo QV, Ho H-C (2021) A new species of the snake eel genus *Ophichthus* from Vietnam, with a new record of *Echelus polyspondylus* McCosker & Ho, 2015. *Raffles Bulletin of Zoology* 69: 71–79. <https://doi.org/10.26107/RBZ-2021-0006>
- Vo QV, Hibino Y, Ho H-C (2019) A new species of the snake eel genus *Ophichthus*, with additional records from Vietnam (Anguilliformes: Ophichthidae). *Zoological Studies* 58: 43. <https://doi.org/10.6620/ZS.2019.58-43>
- Vo QV, Ho H-C, Hibino Y, Le TTT, Tran HHT, Tran TC (2024) Records of species of the snake eels genus *Ophichthus* (family Ophichthidae) from Vietnam. *Vietnam Journal of Marine Science and Technology* 24: 55–68. <https://doi.org/10.15625/1859-3097/18415>
- Whitley GP (1941) Ichthyological notes and illustrations. *Australian Zoologist* 10: 1–50. [pls 1, 2]



# Description of a new species of *Stauropathes* (Anthozoa, Antipatharia, Schizopathidae) from Puerto Rico

Jeremy Horowitz<sup>1</sup>, Mina Barajas<sup>2</sup>, Luke J. McCartin<sup>3,4</sup>, Samuel A. Vohsen<sup>3,4</sup>, Santiago Herrera<sup>1,3,4</sup>

<sup>1</sup> Department of Invertebrate Zoology, Smithsonian Institution, National Museum of Natural History, Washington, DC, USA

<sup>2</sup> Department of Zoology, California State Polytechnic University, Humboldt, Arcata, CA, USA

<sup>3</sup> Department of Biological Sciences, Lehigh University, Bethlehem, PA, USA

<sup>4</sup> Lehigh Oceans Research Center, Lehigh University, Bethlehem, PA, USA

Corresponding author: Jeremy Horowitz ([Jerhorowitz@gmail.com](mailto:Jerhorowitz@gmail.com))

## Abstract

A new species of black coral, *Stauropathes monopinnata* **sp. nov.**, represented by two specimens collected 738 m and 1604 m deep off Puerto Rico and Hawaii, respectively, is recognized in the family Schizopathidae. The new species is characterized by a monopodial, unbranched corallum; simple, suboppositely arranged pinnules in two anterolateral rows along the stem with nearly 90° distal angles, spaced 12–17 mm apart in a row, and with smooth and triangular spines 0.05–0.08 mm tall; and polyps 4–9 mm in transverse diameter. A phylogeny composed of 90 taxa representing species in Schizopathidae and Cladopathidae (rooted in Cladopathidae) was reconstructed from 794 nuclear loci to show their systematic relationships. Herein, we provide morphological and molecular evidence to show that this new species is distinct from other species in the genus *Stauropathes*.

**Key words:** Black coral, genome skimming, molecular phylogenetics, morphology, targeted capture, taxonomy, ultra-conserved elements



Academic editor: James Reimer

Received: 12 September 2024

Accepted: 20 January 2025

Published: 13 March 2025

ZooBank: <https://zoobank.org/4ECF017A-A679-4DAE-89BE-6606835C0F44>

**Citation:** Horowitz J, Barajas M, McCartin LJ, Vohsen SA, Herrera S (2025) Description of a new species of *Stauropathes* (Anthozoa, Antipatharia, Schizopathidae) from Puerto Rico. ZooKeys 1231: 331–346. <https://doi.org/10.3897/zookeys.1231.136967>

Copyright: © Jeremy Horowitz et al.  
This is an open access article distributed under terms of the Creative Commons Attribution License (Attribution 4.0 International – CC BY 4.0).

## Introduction

Black corals are a group of hexacorals that occur in all oceans (except northern Arctic Ocean and hydrothermal vents) and depths from just below the surface to 8600 m. The taxonomy of black corals is undergoing an order-wide taxonomic review with novel data like next-generation sequencing techniques, which are providing greater phylogenetic resolution than single locus or even full mitochondrial genomes (Horowitz et al. 2020; Quattrini et al. 2024).

During the Schmidt Ocean Institute expedition FKt230417, titled ‘Health Diagnostics of Deep-Sea Coral’, 74 black corals were collected from the deep waters off Puerto Rico. This collection recently led to the discovery of new species representing a novel genus and family (Horowitz et al. 2024). Upon further examination of this collection, we discovered a monopodial, unbranched colony characterized by simple suboppositely positioned pinnules, which is a common feature among species in *Bathypathes* Brook, 1889. However, it differed from *Bathypathes* species in that the distances between the members of each subopposite pair of pinnules were extremely small, almost opposite, the colony

had wide spaces between pinnules in a row, and the longest pinnules were also the lowermost ones on the stem, which are common among species of *Stauropathes* Opresko, 2002. A second specimen, collected from deep waters off Hawaii, during the National Oceanic and Atmospheric Administration expedition titled: ‘Hohonu Moana: Exploring Deep Waters off Hawai’i’ possesses these same morphological characteristics. Both specimens, containing *Stauropathes*-like characters with the exception that they were not branched, were sequenced using genome skimming. We bioinformatically extracted conserved element loci to build a phylogenetic tree and place the new species within the Schizopathidae Brook, 1889. This analysis revealed that these specimens are more closely related to each other than to any other currently sequenced species, both falling as sister to nominal *Stauropathes* species including the type specimen of the type species, *Stauropathes stauocrada* Opresko, 2002 (USNM 98846). Herein, we present morphological and molecular evidence to describe this new-to-science species.

## Material and methods

### Specimen collection and deposition

The holotype was collected at Whiting Bank, 25 km southeast of Puerto Rico, 738 m deep during the Schmidt Ocean Institute expedition FKt230417 entitled: ‘Health diagnostics of deep-sea coral’ (Fig. 1) onboard the R/V *Falkor (too)* in 2023. The complete colony was collected using a manipulator arm of the ROV *SuBastian*. The paratype was collected 250 km southeast of Midway Atoll, Hawaii at a depth of 1604 m during the National Oceanic and Atmospheric Administration expedition entitled: ‘Hohonu Moana: Exploring Deep Waters off Hawai’i’ onboard the R/V *Okeanos Explorer* in 2016. Both specimens are deposited in the collections of the National Museum of Natural History (NMNH), Smithsonian Institution, Washington DC.

### Morphological analyses

The morphological characters of the specimens representing the new species were compared with nominal and currently accepted species in the genera *Bathypathes* and *Stauropathes*.

The skeletal spines were examined by cutting small fragments of the skeleton and removing the tissue with bleach and a sonicator. The fragments were then mounted on stubs and coated with a 30–40 nm thick layer of 60% gold: 40% palladium and imaged using a Zeiss EVO MA 15 scanning electron microscope (SEM). SEM stub numbers are from a series established by the authors at the NMNH. Spine height was measured as the distance from the spine tip to the middle of the base of the spine. Polyp in transverse diameter was measured as the distance from the distal edge of the distal lateral tentacles to the proximal edge of the proximal lateral tentacles. Branch diameter was measured near the base of the branch. Distance between pinnules of the same pair was measured from the middle of the base of the lower pinnule to the middle of the base of the upper pinnule.

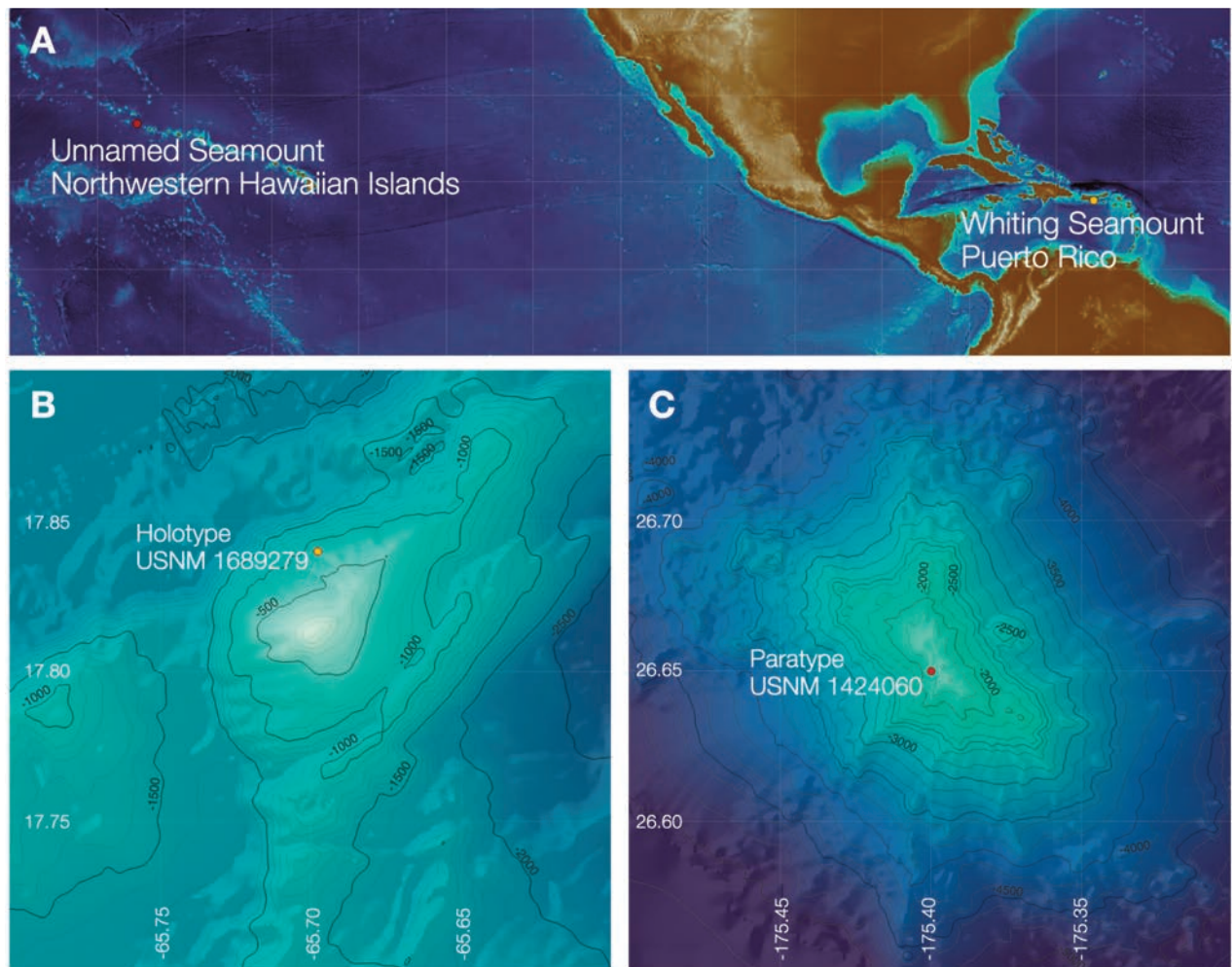
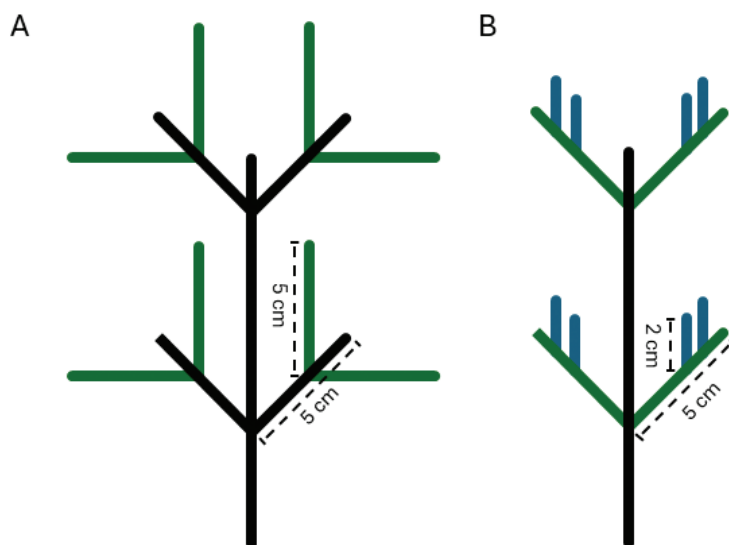


Figure 1. Locations where the holotype (yellow dot) and paratype (red dot) were collected.

We define the distinction between pinnule and pinnulated branch based on the similarity or dissimilarity of branching patterns at successive branch or ramification orders. If a ramification exhibits the same pinnulation pattern and length as its immediate lower-order ramification, it is a pinnulated branch, and its pinnules are first-order pinnules (Fig. 2A), as seen in *Telopathes* Maclsaac & Best, 2013 and *Stauropathes*. Conversely, if the pinnulation pattern changes at higher orders, each ramification represents a distinct pinnule order (Fig. 2B), as in *Myriopathes* Opresko, 2001.

### Molecular analyses

DNA was extracted from the holotype specimen USNM 1689279 alongside all specimens collected in Puerto Rico using the AutoGen GenePrep (AutoGen, Holliston, MA, USA) in the Laboratories of Analytical Biology (LAB) at the NMNH. GenePrep automatically extracts DNA using Phenol-Chloroform purification with high throughput. Extracted DNA was quantified using the QuantIT 1X dsDNA high-sensitivity kit (ThermoFisher Scientific, Waltham, MA, USA). Sequencing libraries were prepared in half reactions using the New England Biolabs (Ipswich, MA, USA) Next Ultra II FS DNA Library Prep kit with incubation times of either 7.5 or 8.5 mins for enzymatic shearing. Bead cleanups were per-



**Figure 2.** **A** example of a branching colony with a stem and pinnulated branches (black lines) and primary pinnules (green lines) **B** example of an unbranched colony with a stem (black line), primary pinnules (green lines), and secondary pinnules (blue lines).

formed using KAPA pure beads (Roche Diagnostics, Indianapolis, IN, USA) and an Opentrons robot with a bead ratio of 0.8X (Long Island City, NY, USA). Using Y-yoke adapter sequences, samples were indexed with unique combinations of iTru i5 and i7 barcode indices before pooling (Glenn et al. 2019). Library preparation for some samples failed, and libraries for these samples were re-prepared after further purifying the DNA extract using a Qiagen PowerClean Clean-up Pro kit following the manufacturer's instructions (Qiagen, Hilden, Germany).

For the paratype specimen from Hawaii (USNM 1424060) and all other specimens that were collected outside Puerto Rico waters, DNA was extracted with the DNeasy Blood and Tissue Kit (Qiagen, Germany), cleaned with the Qiagen Power Clean Pro kit, and concentrations were estimated using a High Sensitivity Qubit 4 Fluorometer (Invitrogen, US). High molecular weight DNA was sheared using a QSonica Inc Sonicator Q800R to a target size range of 400–800 bp and then checked via gel electrophoresis on a 1.5% agarose gel. Afterwards, DNA libraries were prepared with the Kappa Hyper Prep protocol using a ½ reaction with iTruSeq adapters and dual indexes (Glenn et al. 2019) following Quattrini et al. (2018).

For all specimens included in this study, DNA extraction and library preparation were conducted at LAB. Paired-end sequencing (150 bp) was performed on an Illumina - NovaSeq X Plus at the Oklahoma Medical Research Foundation Genomics Facility with other samples to obtain 10M paired-end (PE) reads (150 bp) per sample. Raw reads are deposited in the short read archive (SRA) of the National Center for Biotechnology Information (<https://www.ncbi.nlm.nih.gov/>).

### Phylogenetic analysis

The conserved loci were obtained from the high-throughput sequencing data. Raw reads were trimmed using Trimmomatic v. 0.35 (Bolger et al. 2014) and assembled using Spades v. 3.15 (Prjibelski et al. 2020). Ultra-conserved

elements (UCEs) and exon loci were extracted from the assembled data using the hexacoral-v2-baitset (Cowman et al. 2020), following the Phyluce pipeline (<https://phyluce.readthedocs.io/en/latest/tutorials/tutorial-1.html>) (Faircloth 2016) with modifications: minimum-identity and minimum-coverage thresholds set to 70%. These data were combined with loci that were determined to be conserved across black corals previously (see Horowitz et al. 2020, 2022, 2023a, 2023b, 2024). Loci were internally trimmed and aligned with MAFFT v. 7.130 (Katoh and Standley 2013). Then, `phyluce_align_get_only_loci_with_min_taxa` was used to obtain all loci with 50% taxon-occupancy, which were concatenated using `phyluce_align_concatenate_alignments`. 50% taxon-occupancy was chosen because it maximizes the number of loci incorporated into the phylogenetic reconstruction and, based on previous phylogenetic studies, yields high support values (Horowitz et al. 2023a, 2024). The phylogenomic inference was conducted on the concatenated dataset using maximum likelihood analysis in IQ-TREE v. 2.1 (Minh et al. 2020). A partitioned analysis (Chernomor et al. 2016) was conducted on the dataset using the best model for each locus [-m TESTMERGE (Kalyaanamoorthy et al. 2017)]. Ultrafast bootstrapping [-bb 1000 (Hoang et al. 2018)] and the Sh-like approximate likelihood ratio test [-alrt 1000 (Anisimova et al. 2011)] were also selected. All analyses were run on the Smithsonian's High-Performance Computing Cluster (<https://doi.org/10.25572/SIHPC>) housed at the Herndon Data Center, in Herndon VA, except for the phylogeny, which was built using FigTree v. 1.4.4 and R v. 4.4.1.

## Taxonomic results

### Family Schizopathidae Brook, 1889

### Genus *Stauropathes* Opresko, 2002

**Diagnosis (emended from Opresko 2002).** Corallum monopodial, unbranched or branched and pinnulate to the first order. Pinnules in two lateral or anterolateral rows and arranged in subopposite pairs. Spines smooth, triangular, and laterally compressed. Polyps 3–9 mm in transverse diameter.

**Type species.** *Stauropathes stauocrada* Opresko, 2002 (by original designation).

**Type locality.** North-central Pacific Ocean.

**Remarks.** This study demonstrates that the unbranched corallum with bilateral and subopposite pinnules is polyphyletic, occurring in the genera *Bathypathes* and *Stauropathes*, warranting emendation to the generic diagnosis for *Stauropathes*. Further, the two genera do not form monophyletic groups, where *Stauropathes* spp. (CMNI 2023-0258, USNM 1404493, and USNM 1424220) fall into the clade that consists of a majority of *Bathypathes*, while *Bathypathes alaskensis* Opresko & Molodtsova, 2021 (USNM 1013749) falls into the clade that consists of a majority of *Stauropathes*. Another finding of this study is that *Telopathes* is not polyphyletic, contradicting Cruz et al. (2024); however, additional sequence data from these three genera may suggest more complicated relationships, possibly fueled by hybridization and/or introgression, which has yet to be formally tested for any species in the order.

***Stauropathes monopinnata* Horowitz & Barajas, sp. nov.**

<https://zoobank.org/86C16844-9D66-42CF-9337-CF9CED4A8375>

Figs 1, 3–6, Table 1, Suppl. material 1

**Material examined. Holotype** • USNM 1689279, Whiting Bank, Puerto Rico, 17.8398°N, 65.6976°W, 738 m depth. Schmidt Ocean Institute R/V *Falkor (too)*, FKt230417, Health diagnostic of deep-sea coral, ROV *SuBastian* dive 518, April 29, 2023 (SEM stub No. 538). **Paratype** • USNM 1424060, 250 km southeast of Midway Atoll, Hawaii, 26.65°N, 175.4°W, 1604 m depth. NOAA (National Oceanic and Atmospheric Administration) R/V *Okeanos Explorer*, Cruise EX1603, Hohonu Moana: Exploring Deep Waters off Hawaii, ROV *Deep Discoverer* dive 5, March 5, 2016 (SEM stub 539).

**Type locality.** Whiting Bank, Puerto Rico, 738 m depth.

**Diagnosis.** Corallum monopodial, planar, unbranched, and pinnulate to the first order. Pinnules in two anterolateral rows and arranged in subopposite (almost opposite) pairs. Lowermost pinnules on stem 8 cm or more in length, decreasing in length towards apex of colony. Spines smooth and triangular with a rounded apex, 0.05–0.08 mm tall. Polyps 4–9 mm in transverse diameter, 2–3 mm interpolypar space, four to eight polyps counted per 5 cm.

**Description of holotype.** The holotype (USNM 1689279) is a 15 cm tall monopodial colony (Fig. 3A–C). The unpinnulated section is about 2 cm based on in situ imagery because the basal plate and lowermost section of unpinnulated stem were not collected (Fig. 3C). The pinnulated section is 13 cm in length. Pinnules are simple, arranged in two anterolateral rows and in subopposite pairs (Fig. 3A, B). The pinnules are curved towards the abpolypar side of the colony. The lowermost pinnules on the stem are 8.3 cm in length, pinnules midway up the pinnulated section of the stem are 8 cm in length, and the uppermost pinnules on the stem are 4.2 cm in length. Diameter of the lowermost pinnule near the base of the pinnule is ~1 mm. Distance between pinnules in one row ranges from 1.3 to 1.7 cm and distance between pinnules of the same pair (i.e., on opposite sides of the stem) is < 1 mm, in some cases nearly opposite (Fig. 3B). Eight pinnules can be counted per 5 cm including pinnules in both rows. The distal angle of pinnules is 80–90° except for the uppermost pinnules, which are about 45° (Fig. 3A–C), and the interior angle formed by the subopposite pinnules is 160–180° (Fig. 3A).

Polyps are arranged in a single row (Fig. 3C, D). Polyps are 8–9 mm in the transverse diameter with 0.2–0.3 mm interpolypar space, resulting in polypar density ranging from 4 to 5 per 5 cm (Fig. 3E). Based on in situ imagery, tentacles exceed 1 cm when fully extended and the tissue color is dark red, and when preserved is dark red to dark brown.

Spines (Fig. 4A–C) are smooth and triangular with a rounded apex (Fig. 4C) that is at right angles to the axis or slightly inclined distally, with long and sloping distal and proximal edges. Polypar and abpolypar spines are 0.03 to 0.05 mm tall. The spines on pinnules are arranged in longitudinal rows, six to seven of which can be seen in one view (Fig. 4A, B). Spines are spaced 0.12–0.33 mm apart in a row, with about four to five spines per mm (Fig. 4A, B).

**Description of the paratype.** The paratype (USNM 1424060) is a 14 cm tall colony (lowermost section of stem not collected) and the pinnulated section

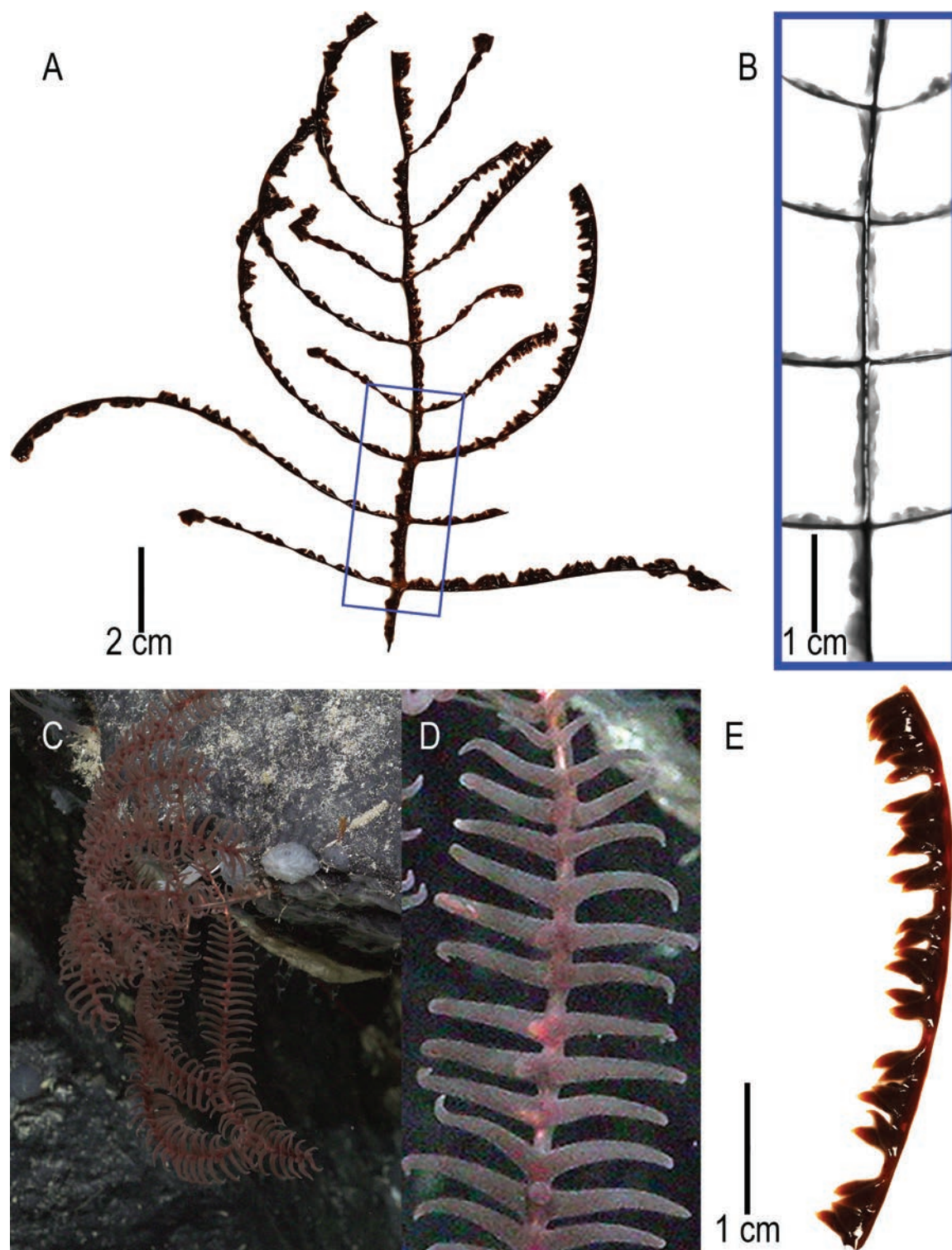


**Figure 3.** *Stauropathes monopinnata* sp. nov. holotype: USNM 1689279 **A** collected colony with **B** blue rectangle showing zoomed-in view of pinnule pattern **C** in situ image of colony **D** in situ image of colony showing zoomed-in view of polyp characteristics **E** section of pinnule showing polyp characteristics.

of stem is 12 cm (Fig. 5A). Based on in situ imagery (<https://data.oceannetworks.ca/SeaTube?resourceTypeid=1000&resourceId=23621&divId=3000&time=2016-03-06T00:56:55.000Z>), the whole colony was approximated to be ~25 cm in length and the unpinnulated section of stem was ~7 cm in length. Striatum is present and distinct from the lower broken-off end of the stem to the low-

ermost pair of pinnules. Pinnules are simple, arranged in anterolateral rows and in subopposite pairs (Fig. 5A). The lowermost pinnules are 2.5 and 3.0 cm long; however, based on in situ imagery (Fig. 5B) the lowermost pinnules were the longest on the colony prior to subsampling. Pinnules midway up the pinnulated section of the stem are 8.0 cm long and the most distal pinnules are 1.3 cm long (Fig. 5A). Diameter near the base of the pinnule is ~1 mm. Distance between pinnules in one row ranges from 1.2 to 1.4 cm and distance between members of the subopposite pairs is < 1 mm (Fig. 5A). In some cases, the members of a pair appear to be directly opposite to one another. Ten pinnules can be counted per 5 cm including pinnules in both rows (Fig. 5A). Distal angle of pinnules is 80–90° and the interior angle formed between pinnules of a subopposite pair is 160–180° (Fig. 5A).

Polyps are arranged in a single row and are 4–6 mm in transverse diameter with an interpolypar space of 2 mm. Polypar density ranges from seven to eight per 5 cm. Based on in situ imagery, the tissue is dark red, and when preserved, it is brown to dark brown (Fig. 5B).

Spines are smooth, laterally compressed, and triangular with a rounded apex (Fig. 5C–E). Spines are 0.03–0.06 mm tall. The spines on pinnules are arranged in longitudinal rows, seven to eight of which can be seen in one view (Fig. 5C, D). Spines are spaced 0.23–0.36 mm apart in a row with about three to four spines per mm (Fig. 5C, D).

**Intraspecific variation.** Both specimens possess simple pinnules with wide distal angles, arranged in slightly anterolateral rows, and in subopposite pairs that are almost opposite. Spacing between pinnules in one row is wide in both specimens:  $\leq 1.7$  cm in the holotype and  $\leq 1.4$  cm in the paratype, resulting in eight and ten pinnules per 5 cm. The spines on both specimens are short ( $\leq 0.06$  mm tall), smooth, triangular with a rounded apex, and arranged in longitudinal rows, seven to eight of which are visible in lateral view. Tissue color is similar for both specimens; dark red in situ and a dark red-to-brown when preserved.

A minor difference between the holotype and paratype is that based on in situ footage, the paratype pinnules are more rigid than the holotype. A major difference between the holotype and paratype is their polyp characteristics, where the holotype has polyps 8–9 mm in transverse diameter with 0.2–0.3 mm interpolypar space, resulting in a density of four to five polyps per 5 cm, while the paratype's smaller polyps are 4–6 mm in transverse diameter with 0.2 cm interpolypar space, resulting in a higher density of seven to eight per 5 cm. This is a notable difference that could be interpreted as the holotype and paratype representing different species. However, without additional specimens possessing similar morphological traits as these specimens with differing-sized polyps, it is premature to describe these two specimens as polyp size could vary within the species.

**Phylogenetic results.** A total of 63–1052 conserved element loci were obtained per specimen. Total number of contigs ranged from 234,560 to 439,048,041 base pairs (bp) (average lengths ranged from 109 to 953 bp). The 50% taxon-occupancy matrix included 794 loci that were concatenated into an alignment with a total length of 385,232 bp. A 75% taxon-occupancy matrix, including 465 loci, was also run to compare results, and the topology in the region of the trees, including the new species, did not change. Read and locus summary statistics are detailed in Suppl. material 1.

The two specimens representing the new species with 100% branch support fell sister to the clade containing *Stauropathes stauocrada* (USNM 98846 species-

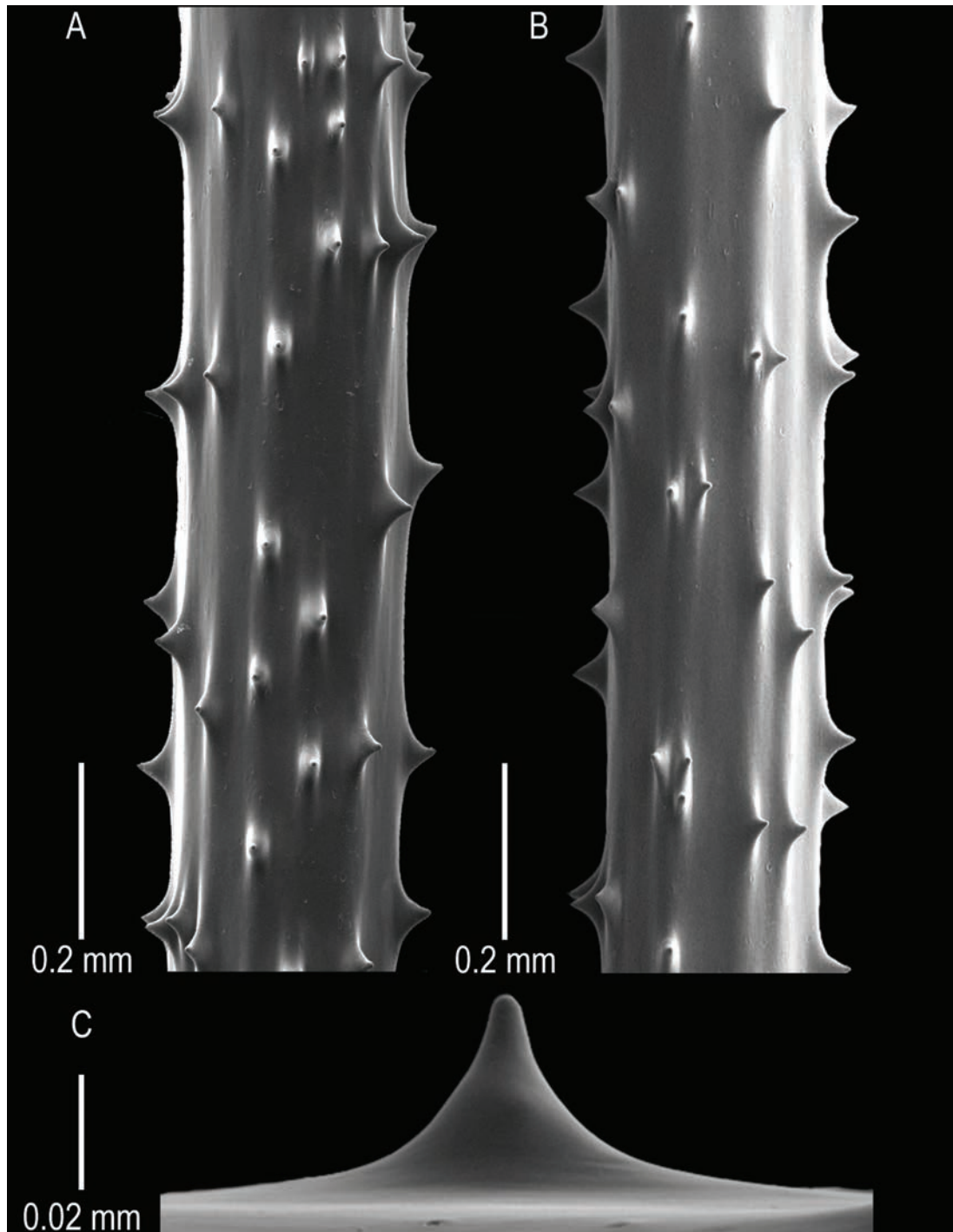


**Figure 4.** *Stauropathes monopinnata* sp. nov. holotype: USNM 1689279 **A, B** sections of pinnules showing skeletal spines **C** zoomed-in view of a singular skeletal spine.

and genus-level holotype specimen, and USNM 1071042) (Fig. 5), supporting our decision to place the new species in *Stauropathes*. This clade also contains *Stauropathes* cf. *punctata* (Roule, 1905) (USNM 1606527), *Stauropathes* cf. *stellata* Opresko, 2019 (USNM 1424179), and *Bathypathes alaskensis* (USNM 1013749).

**Comparative diagnosis.** *Stauropathes monopinnata* sp. nov. differs from the four other species in the genus morphologically. The most prominent difference is that the new species is unbranched whereas the other species are branched. The new species also has wider distances between pinnules in a row; reaching

1.7 cm in the holotype compared to a maximum of 1.2 cm in *S. staurocrada* and *S. arctica* (Lütken, 1871), and 0.8 cm in *S. stellata* and *S. punctata*. Four of the species in the genus possess small spine heights less than 0.07 mm (spine measurements were not reported for the type of *S. punctata*). The species however, differ in the number of rows of spines that can be seen in one lateral view of a pinnule. The number of rows for the new species (six to eight visible on a pinnule diameter of 0.25 mm) is greater than that for *S. staurocrada* (four to six on pinnule diameter of 0.28 mm) and *S. stellata* (three to four on pinnule diameter of 0.28 mm) and less than *S. arctica* (nine to ten on pinnule diameter of 0.34 mm). The new species also has polyps that are 4 to 9 mm in transverse diameter, equal to or larger than *S. staurocrada* (4 mm), and the range includes polyps of *S. stellata* (6 mm) and *S. arctica* (7 mm). The transverse diameter of the polyps was not reported for *S. punctata*. A complete comparison of the morphological features of *Stauropathes* species can be found in Table 1.

While the lack of branches and the two rows of subopposite pinnules in the new species is typical of *Bathypathes* species, it differs morphologically in several ways: the distances between the members of each subopposite pair are smaller, and in some cases, the pinnules are almost opposite; the colonies have wider spaces between pinnules in a row, and the longest pinnules are also the lowermost ones on the stem.

**Table 1.** Comparison of species in the genus *Stauropathes*.

Feature	<i>S. monopinnata</i> sp. nov. holotype <sup>a</sup>	<i>S. monopinnata</i> sp. nov. paratype <sup>b</sup>	<i>S. staurocrada</i> <sup>c</sup>	<i>S. stellata</i> <sup>d</sup>	<i>S. punctata</i> <sup>e</sup>	<i>S. arctica</i> <sup>f</sup>
Corallum	unbranched	unbranched	branched	branched	branched	branched
Stem length (cm) (pinnulated / unpinnulated)	13 / 2	12 / 2 (unpinnulated section incomplete)	13 / not collected	6.3 / 6.1	21 / not collected	20 / 5
Pinnule diameter near base (mm)	1	1	1	0.5	1	Not reported
Pinnular angle (distal / interior)	45–90° / 160–180°	80–90° / 160–180°	60–70° / 90–150°	80–90° / 160–180°	80–90° / 160–180°	80–90° / 160–180°
Distance between pinnules on one side (mm)	13–17	12–14	8–12	5–10	6–8	12
Max Pinnule length (cm):	8.3	8	2	5.5	1	3
Pinnule density per 5 cm (both rows)	8	10	5–6	8	Not reported	Not reported
Number of orders of pinnules	1	1	1	1	1	>1? <sup>g</sup>
Spine height (mm)	0.03–0.05	0.03–0.06	0.04–0.06	0.06–0.07	Not reported	0.02–0.06
Spine ornamentation	Smooth	Smooth	Smooth	Smooth	Not reported	Smooth
Number of spine rows per view	6–7	7–8	4–6	3–4	Not reported	9–10
Space between spines in one row (mm)	0.12–0.17	0.11–0.44	0.12–0.24	0.21–0.33	Not reported	0.06–0.12
Spine density per 1 mm	4–5	4	8	4–6	Not reported	5
Polyp transverse diameter (mm)	8–9	4–6	2–4	5–6	Not reported	3–7
Polyp density per 5 cm	4–5	7–8	10–11	6–7	Not reported	Not reported
Number of polyps between adjacent pinnules in the same row	2	2	2	Not reported	Not reported	Not reported
Striatum	Lowest section not collected	Striations present until first row of pinnules	Present	Present from 2 cm above basal plate and extends 4 cm	Not reported	Not reported

<sup>a</sup> *Stauropathes monopinnata* sp. nov. holotype (USNM 1689279) herein described. <sup>b</sup> *Stauropathes monopinnata* sp. nov. paratype (USNM 1424060) herein described. <sup>c</sup> *Stauropathes staurocrada* holotype (USNM 98846) in Opresko (2002). <sup>d</sup> *Stauropathes stellata* holotype (USNM 16059) in Opresko (2019). <sup>e</sup> *Stauropathes punctata* type series described in Roule (1905). <sup>f</sup> *Stauropathes arctica* Brook's (1889) translation of species described by Lütken (1871). <sup>g</sup> Unclear if ramification orders are pinnulated branches or pinnules.

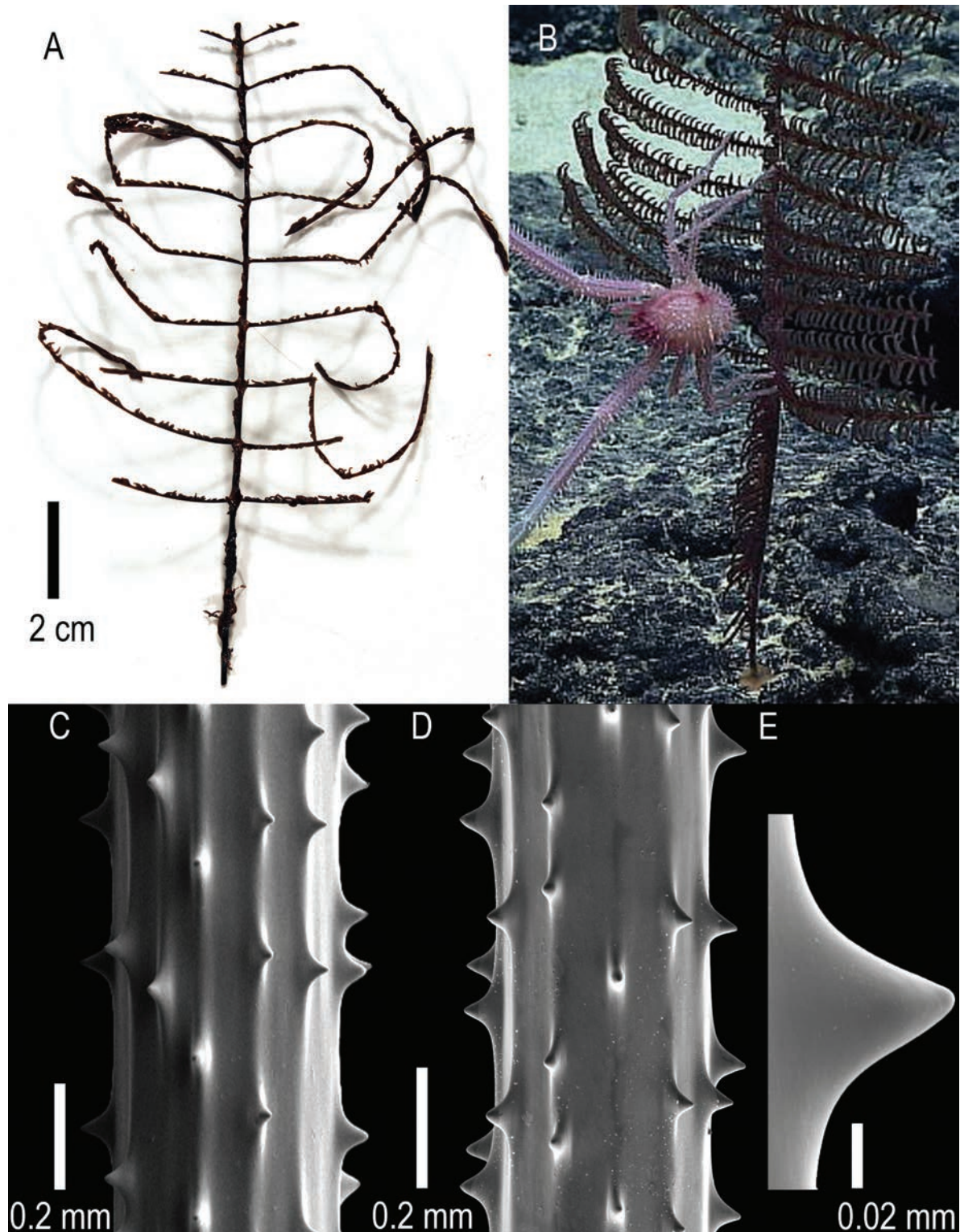
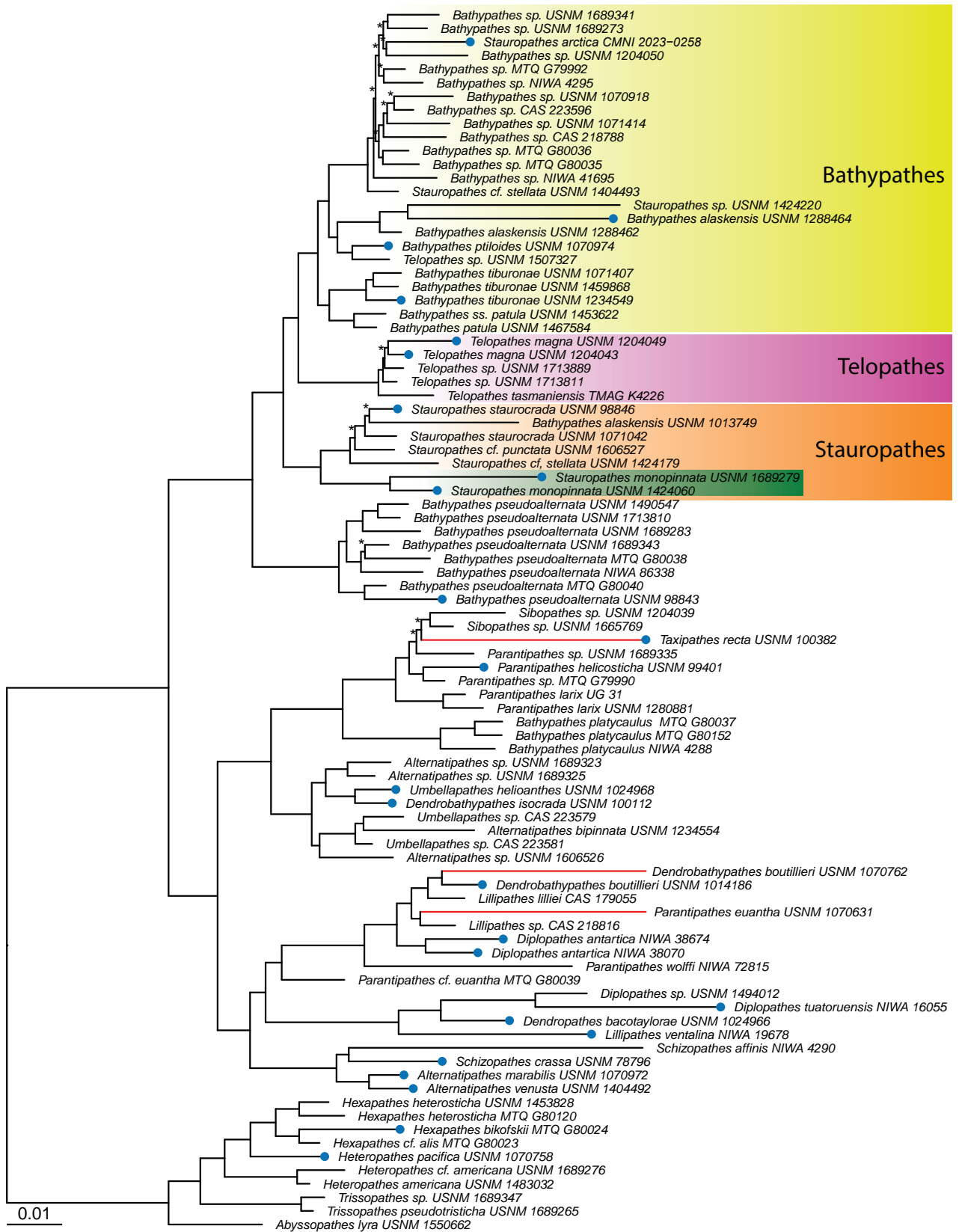


Figure 5. *Stauropathes monopinnata* sp. nov. paratype (USNM 1424060) A collected colony B in situ image of colony C, D sections of pinnules showing skeletal spines E zoomed-in view of a singular skeletal spine.

**Etymology.** The specific name derives from the Latin “mono” (one) and “pin-nata” (feathered) referring to the new species general appearance due to the distinctive lack of branches compared to the other species in the genus.

**Distribution.** Known from North Central Atlantic Ocean to North Pacific Ocean from 738 to 1604 m depth.



**Figure 6.** Maximum likelihood phylogeny of antipatharians of the families Schizopathidae and Cladopathidae based on a 50% complete matrix containing 794 loci. Taxa in green rectangle represent the holotype and paratype specimens of the new species. Ultrafast Bootstrap support values are 100% at all nodes unless noted with an asterisk (\*). Red branches were artificially shortened and do not represent true branch length. The phylogeny rooted to Cladopathidae.

**Discussion and conclusions.** This study presents morphological and molecular evidence to support the description of a new species within the genus *Stauropathes*. Furthermore, this study provides the most speciose molecular phylogeny of the family Schizopathidae to date, including specimens representing all 13 accepted schizopathid genera, holotypes or paratypes of 20 species, five of which also represent types at the genus level, and 12 species sequenced for the first time.

The new *Stauropathes* species, which lacks branches (like *Bathypathes*), required an emendation of the diagnosis of *Stauropathes* to include unbranched morphotypes. Additionally, the finding of one *Bathypathes* species in the *Stauropathes* clade and two *Stauropathes* species in the *Bathypathes* clade suggests they have a complicated evolutionary history, possibly driven by convergent evolution or hybridization.

Speciation is complex, and the phylogenetic models used in black coral studies have relied on maximum likelihood analyses with General Time Reversible substitution model, which does not account for processes like hybridization, recombination, or site-specific variation in substitution rates (Steenwyk et al. 2023). When dealing with complicated evolutionary histories, which seems to be the case for genera in Schizopathidae (see also ‘The Trigeneric Complex’ described in Bledsoe-Becerra et al. (2022)) a multispecies coalescent model should be used for estimating phylogenies while accounting for unresolved lineage sorting (Ramírez-Portilla and Quattrini 2023). This is an essential next step for resolving relationships at the species level for black corals.

## Acknowledgements

The authors wish to thank W. Keel, W. Moser, and K. Reed for their assistance during visits to the Museum Support Center at the NMNH. The photomicrographs were prepared in the NMNH SEM Laboratory with assistance from S. D. Whittaker. Laboratory work was conducted in and with the support of the L.A.B. facilities of the National Museum of Natural History. We also thank the Schmidt Ocean Institute R/V Falkor (too) crew and personnel for their assistance and support, as well as Colleen Hansel, chief scientist of cruise FKt230417. We acknowledge the following museums and universities that made their material available for study: California Academy of Sciences, Canadian Museum of Nature Invertebrates, Museum of Tropical Queensland, National Institute of Water and Atmospheric Research, Tasmanian Museum and Art Gallery, University of Geneva, and the National Museum of Natural History. Specimens were provided by the National Institute of Water and Atmospheric Research Invertebrate Collection from various research voyages including: KAH024, TAN0413 “Seamounts: their importance to fisheries and marine ecosystems”, undertaken by the NIWA and funded by the New Zealand Foundation for Research, Science and Technology (FRST) with additional funding from the Ministry of Fisheries (MFish) and NOAA Satellite Operations Facility); TAN0802 Ross Sea IPY-CAML Survey funded by the New Zealand Government under the New Zealand International Polar Year Census of Antarctic Marine Life Project with project governance provided by the MFish Science Team and the Ocean Survey 20/20 CAML Advisory Group (Land Information New Zealand (LINZ), MFish, Antarctica New Zealand, Ministry of Foreign Affairs and Trade, and NIWA); TAN1007 Kermadec Arc Minerals (KARMA) voyage, funded by FRST, in collaboration with Auckland University, Institute of Geological and Nuclear Science (GNS),

and Woods Hole Oceanographic Institute (WHOI); TAN1104 Ocean Survey 20/20 Mapping the Mineral Resources of the Kermadec Arc Project, funded by LINZ, GNS, NIWA, and WHOI; TAN1213 Nascent Inter-Ridge Volcanic And Neotectonic Activity (NIRVANA) voyage, funded by the Ministry for Primary Industries, in collaboration with Auckland University, GNS, and the University of New Hampshire, USA. SH was supported by NOAA award NA18OAR0110289 and the National Academies of Sciences, Engineering, and Medicine Gulf Research Program Early-Career Fellowship under award 2000013668. We thank Allana Christine Guliman for assistance with data management for this study. Research activities in Puerto Rico waters were coordinated with the Departamento de Recursos Naturales y Ambientales under permit # 2023-IC-019 (O-VS-PVSIS-SJ-01354-01022023).

## Additional information

### Conflict of interest

The authors have declared that no competing interests exist.

### Ethical statement

No ethical statement was reported.

### Funding

This project was funded in part by the Smithsonian Institution Barcode Network.

### Author contributions

Conceptualization: JH. Data curation: JH, LJM, SH. Formal analysis: JH, LJM. Funding acquisition: SH. Investigation: LJM, SAV, MB, JH. Methodology: LJM, SH, MB, JH. Project administration: JH. Supervision: JH, SH. Validation: LJM. Visualization: MB, SH. Writing – original draft: LJM, JH, SH, MB, SAV. Writing – review and editing: LJM, JH, SAV, MB.

### Author ORCIDs

Jeremy Horowitz  <https://orcid.org/0000-0002-2643-5200>

Luke J. McCartin  <https://orcid.org/0000-0001-5374-3148>

Samuel A. Vohsen  <https://orcid.org/0000-0003-1710-292X>

Santiago Herrera  <https://orcid.org/0000-0001-7204-9434>

### Data availability

Raw sequence reads were submitted to GenBank under BioProject # PRJNA1078781. Bioproject and biosample information for all specimens are listed in Suppl. material 1.

## References

- Anisimova M, Gil M, Dufayard J-F, Dessimoz C, Gascuel O (2011) Survey of branch support methods demonstrates accuracy, power, and robustness of fast likelihood-based approximation schemes. *Systematic Biology* 60: 685–699. <https://doi.org/10.1093/sysbio/syr041>
- Bledsoe-Becerra YM, Whittaker IS, Horowitz J, Naranjo KM, Johnson-Rosemond J, Mullins KH, Cunningham KM, Shetty S, Messinides SN, Behney MS, Fehsal JA, Watson AN, McKnight KE, Nasiadka TW, Popa H, Pettay DT, Appiah-Madson HJ, Distel DL, Brugler MR (2022) Mitogenomics reveals low variation within a trigenic complex of black

- corals from the North Pacific Ocean. *Organisms Diversity and Evolution* 22: 343–353. <https://doi.org/10.1007/s13127-021-00537-5>
- Bolger AM, Lohse M, Usadel B (2014) Trimmomatic: a flexible trimmer for Illumina sequence data. *Bioinformatics* 30: 2114–2120. <https://doi.org/10.1093/bioinformatics/btu170>
- Brook G (1889) Report on the Antipatharia. Report on the Scientific Results of the Voyage of H.M.S. Challenger. *Zoology* 32: 1–222.
- Chernomor O, von Haeseler A, Minh BQ (2016) Terrace aware data structure for phylogenomic inference from supermatrices. *Systematic Biology* 65: 997–1008. <https://doi.org/10.1093/sysbio/syw037>
- Cowman PF, Quattrini AM, Bridge TCL, Watkins-Colwell GJ, Fadli N, Grinblat M, Roberts TE, McFadden CS, Miller DJ, Baird AH (2020) An enhanced target-enrichment bait set for Hexacorallia provides phylogenomic resolution of the staghorn corals (Acroporidae) and close relatives. *Molecular Phylogenetics and Evolution* 153: 106944. <https://doi.org/10.1016/j.ympev.2020.106944>
- Cruz BA, Cappelmann A, Chutjian H, Roman JC, Reid MA, Wright J, Gonzalez AD, Keyman T, Griffith KM, Appiah-Madson HJ, Distel DL, Hayes VE, Drewery J, Pettay DT, Staton JL, Brugler MR (2024) Complete mitochondrial genomes of the black corals *Alternatipathes mirabilis* Opresko & Molodtsova, 2021 and *Parantipathes larix* (Esper, 1788) (Cnidaria, Anthozoa, Hexacorallia, Antipatharia, Schizopathidae). *ZooKeys* 2024: 79–93. <https://doi.org/10.3897/zookeys.1196.116837>
- Faircloth BC (2016) PHYLUCE is a software package for the analysis of conserved genomic loci. *Bioinformatics* 32: 786–788. <https://doi.org/10.1093/bioinformatics/btv646>
- Glenn TC, Pierson TW, Bayona-Vásquez NJ, Kieran TJ, Hoffberg SL, Thomas JC, Lefever DE, Finger JW, Gao B, Bian X, Louha S, Kolli RT, Bentley KE, Rushmore J, Wong K, Shaw TI, Rothrock MJ, McKee AM, Guo TL, Mauricio R, Molina M, Cummings BS, Lash LH, Lu K, Gilbert GS, Hubbell SP, Faircloth BC (2019) Adapterama II: Universal amplicon sequencing on Illumina platforms (TaggiMatrix). *PeerJ* 2019. <https://doi.org/10.7717/peerj.7786>
- Hoang DT, Chernomor O, von Haeseler A, Minh BQ, Vinh LS (2018) UFBoot2: Improving the Ultrafast Bootstrap Approximation. *Molecular Biology and Evolution* 35: 518–522. <https://doi.org/10.1093/molbev/msx281>
- Horowitz J, Brugler MR, Bridge TCL, Cowman PF (2020) Morphological and molecular description of a new genus and species of black coral (Cnidaria: Anthozoa: Hexacorallia: Antipatharia: Antipathidae: Blastopathes) from Papua New Guinea. *Zootaxa* 4821: zootaxa.4821.3.7. <https://doi.org/10.11646/zootaxa.4821.3.7>
- Horowitz J, Opresko D, Molodtsova TN, Beaman RJ, Cowman PF, Bridge TCL (2022) Five new species of black coral (Anthozoa; Antipatharia) from the Great Barrier Reef and Coral Sea, Australia. *Zootaxa* 5213: 1–35. <https://doi.org/10.11646/zootaxa.5213.1.1>
- Horowitz J, Opresko DM, González-García MDP, Quattrini AM (2023a) Description of a new species of black coral in the family Aphanipathidae (Anthozoa, Antipatharia) from Puerto Rico. *ZooKeys* 2023: 97–110. <https://doi.org/10.3897/zookeys.1173.104141>
- Horowitz J, Quattrini AM, Brugler MR, Miller DJ, Pahang K, Bridge TCL, Cowman PF (2023b) Bathymetric evolution of black corals through deep time. *Proceedings of the Royal Society B: Biological Sciences* 290. <https://doi.org/10.1098/rspb.2023.1107>
- Horowitz J, Opresko DM, Herrera S, Hansel CM, Quattrini AM (2024) Ameripathidae, a new family of antipatharian corals (Cnidaria, Anthozoa, Hexacorallia, Antipatharia). *ZooKeys* 2024: 355–375. <https://doi.org/10.3897/zookeys.1203.121411>
- Kalyaanamoorthy S, Minh BQ, Wong TKF, von Haeseler A, Jermini LS (2017) ModelFinder: fast model selection for accurate phylogenetic estimates. *Nature methods* 14: 587–589. <https://doi.org/10.1038/nmeth.4285>

- Katoh K, Standley DM (2013) MAFFT Multiple Sequence Alignment Software Version 7: Improvements in Performance and Usability. *Molecular Biology and Evolution* 30: 772–780. <https://doi.org/10.1093/molbev/mst010>
- Lütken C (1871) *Antipathes antarctica*, en ny Sortkoral fra Polarhavet. Oversigt over det Kongelige Danske videnskabernes selskabs forhandling. Oversigt over det Kongelige Danske videnskabernes selskabs forhandling 2: 18–26.
- Minh BQ, Hahn MW, Lanfear R (2020) New methods to calculate concordance factors for phylogenomic datasets [Rosenberg M (Ed.)]. *Molecular Biology and Evolution* 37: 2727–2733. <https://doi.org/10.1093/molbev/msaa106>
- Opresko DM (2002) Revision of the Antipatharia (Cnidaria: Anthozoa). Part II. Schizopathidae. *Zoologische Mededelingen* 76: 1–17.
- Opresko DM (2019) New species of black corals (Cnidaria: Anthozoa: Antipatharia) from the New Zealand region, part 2. *New Zealand Journal of Zoology* 47: 149–186. <https://doi.org/10.1080/03014223.2019.1650783>
- Prjibelski A, Antipov D, Meleshko D, Lapidus A, Korobeynikov A (2020) Using SPAdes De Novo Assembler. *Current Protocols in Bioinformatics* 70: e102. <https://doi.org/10.1002/cpbi.102>
- Quattrini AM, Faircloth BC, Dueñas LF, Bridge TCL, Brugler MR, Calixto-Botía IF, DeLeo DM, Forêt S, Herrera S, Lee SMY, Miller DJ, Prada C, Rádis-Baptista G, Ramírez-Portilla C, Sánchez JA, Rodríguez E, McFadden CS (2018) Universal target-enrichment baits for anthozoan (Cnidaria) phylogenomics: New approaches to long-standing problems. *Molecular Ecology Resources* 18: 281–295. <https://doi.org/10.1111/1755-0998.12736>
- Quattrini AM, McCartin LJ, Easton EE, Horowitz J, Bowers H, Mitchell K, Sei M, McFadden CS (2024) Skimming genomes for systematics and DNA barcodes of corals. *Ecology and Evolution* 14(5): e11254. <https://doi.org/10.1002/ece3.11254>
- Ramírez-Portilla C, Quattrini AM (2023) Perspectives on the Grey Zone of species delimitation with notes on invertebrates in the marine environment. *Bulletin of the Society of Systematic Biologists* 2. <https://doi.org/10.18061/bssb.v2i2.9255>
- Roule L (1905) Description des Antipathaires et Cerianthaires recueillis par S.A.S. le Prince de Monaco dans L'Atlantique nord. *Resultats des Campagnes Scientifiques accomplies sur son yacht par Albert ler Prince De Monaco* 30: 1–100. <https://doi.org/10.5962/bhl.title.59328>
- Steenwyk JL, Li Y, Zhou X, Shen XX, Rokas A (2023) Incongruence in the phylogenomics era. *Nature Reviews Genetics* 24: 834–850. <https://doi.org/10.1038/s41576-023-00620-x>

## Supplementary material 1

### Read and locus summary statistics for all specimens included in the study

Authors: Jeremy Horowitz, Mina Barajas, Luke J. McCartin, Samuel A. Vohsen, Santiago Herrera

Data type: xlsx

Copyright notice: This dataset is made available under the Open Database License (<http://opendatacommons.org/licenses/odbl/1.0/>). The Open Database License (ODbL) is a license agreement intended to allow users to freely share, modify, and use this Dataset while maintaining this same freedom for others, provided that the original source and author(s) are credited.

Link: <https://doi.org/10.3897/zookeys.1231.136967.suppl1>

# Description of four new synallactid species (Holothuroidea, Synallactida, Synallactidae) from the tropical Western Pacific Ocean

Yunlu Xiao<sup>1,2,3</sup> , Ning Xiao<sup>1,4,5</sup>

1 Department of Marine Organism Taxonomy and Phylogeny, Institute of Oceanology, Chinese Academy of Sciences, Qingdao 266071, China

2 Institute of Deep-sea Science and Engineering, Chinese Academy of Sciences, Sanya 572000, China

3 University of Chinese Academy of Sciences, Beijing 100049, China

4 Laboratory for Marine Biology and Biotechnology, Qingdao Marine Science and Technology Center, Qingdao, China

5 Shandong Province Key Laboratory of Experimental Marine Biology, Institute of Oceanology, Chinese Academy of Sciences, Qingdao 266071, China

Corresponding author: Ning Xiao ([xiaoning@qdio.ac.cn](mailto:xiaoning@qdio.ac.cn))

## Abstract

Four synallactid specimens were collected during four deep-water benthic fauna surveys (2013–2018) conducted at three seamounts ('Jiaolong', 'Y3', and 'M4') and the Ganquan Plateau in the South China Sea, tropical Western Pacific Ocean, at depths ranging from 344 to 3610 m. Morphological examination of these specimens revealed four new species belonging to three genera, which are described as *Synallactes tenuibrachius* sp. nov., *Bathyplores liaoi* sp. nov., *Bathyplores varicolumna* sp. nov., and *Amphigymnas ganquani* sp. nov. Notably, *Amphigymnas ganquani* sp. nov. represents the first report of an *Amphigymnas* species in the South China Sea. Detailed descriptions are provided for the morphological features, including the type locality, and geographic and bathymetric distributions of these species. These findings contribute to the understanding of seamount biodiversity and provide valuable insights for advancing research on seamount ecology, management, and conservation.



Academic editor:

Didier Vanden Spiegel

Received: 26 November 2024

Accepted: 17 January 2025

Published: 13 March 2025

ZooBank: <https://zoobank.org/3848521C-41B0-4D10-9130-2E4227A27484>

Citation: Xiao Y, Xiao N (2025)

Description of four new synallactid species (Holothuroidea, Synallactida, Synallactidae) from the tropical Western Pacific Ocean. ZooKeys 1231: 347–370. <https://doi.org/10.3897/zookeys.1231.142729>

Copyright: © Yunlu Xiao & Ning Xiao.

This is an open access article distributed under terms of the Creative Commons Attribution License (Attribution 4.0 International – CC BY 4.0).

**Key words:** *Amphigymnas*, *Bathyplores*, new species, ROV, seamounts, *Synallactes*, taxonomy

## Introduction

Holothuroids, commonly known as sea cucumbers, are echinoderms from the class Holothuroidea. They play a critical role in shaping benthic community structure and biogeochemical processes through feeding, fecal production, and locomotory activities (Roberts et al. 2001; Witbaard et al. 2001). Currently, more than 1800 accepted holothuroid species are recognized (WoRMS 2024a), distributed across various marine environments from shallow water to hadal zones (Iken et al. 2001; Jamieson et al. 2011; Lee et al. 2017). The majority of these species are found in the tropical Indo-West Pacific region (Conand 1990). The current classification system for the class Holothuroidea was established by Miller et al. (2017), who conducted extensive molecular phylogenetic analyses of representatives of most families and species-level taxa. Their findings supported the existence of seven orders: Apodida, Dendrochirotida, Elaspodida,

Holothuriida, Molpadida, Persiculida, and Synallactida. Within the order Synallactida, three families are recognized: the predominantly shallow-water Stichopodidae Haeckel, 1896, and the deep-water Synallactidae Ludwig, 1894, and Deimatidae Théel, 1882. The family Synallactidae is one of the least studied large taxa of deep-sea holothuroids (Solís-Marín 2005; Gebruk et al. 2012; Solís-Marín et al. 2024). It is almost exclusively found in deep-sea habitats (Solís-Marín 2003) and comprises more than 80 accepted species across ten genera (*Allopatides* Koehler & Vaney, 1905; *Amphigymnas* Walsh, 1891; *Bathyploetes* Östergren, 1896; *Capheira* Ludwig, 1893; *Dendrothuria* Koehler & Vaney, 1905; *Galatheathuria* Hansen & Madsen, 1956; *Paelopatides* Théel, 1886; *Pseudothuria* Koehler & Vaney, 1905; *Scotothuria* Hansen, 1978; *Synallactes* Ludwig, 1894). This variable family is characterized by the absence of tentacle ampullae, a paired gonad, and ossicles composed basically of tables and rods (Solís-Marín 2003, 2005; O’Loughlin and Ahearn 2005). Although new species have been frequently described in recent years, the family Synallactidae remains poorly understood (Thandar 2008; Massin and Hendrickx 2010; O’Loughlin et al. 2013; Samyn and Vandenspiegel 2016; Solís-Marín et al. 2024). This persistent deficiency in taxonomic research presents a significant obstacle to advancing our understanding of the diversity and ecological roles within this family.

Seamounts are unique deep-sea landforms that play an important role in shaping marine biodiversity patterns and processes (Boehlert and Genin 1987; Hannington et al. 1995). They are “diversity hotspots”, often hosting higher species richness than other coastal and oceanic areas (Worm et al. 2003; Samadi et al. 2006; Morato et al. 2008, 2010) and serving as important habitats for benthic invertebrates (Pitcher and Bulman 2007). The tropical Indo-West Pacific region, as the world marine biodiversity center, is one of the priority regions for future research on seamount ecosystems and biodiversity (Xu 2021). This region contains numerous seamounts such as the Yap (Y3), Mariana (M2), and Caroline (M4) seamounts. The South China Sea (**SCS**), a semi-enclosed marginal sea in the tropical Western Pacific Ocean, includes many seamounts scattered across its abyssal plain (Huang et al. 2023). Although seamounts are acknowledged as highly productive biodiversity hotspots (Clark et al. 2012; Wagner et al. 2020; Yesson et al. 2021), research on these ecosystems remains limited, and reports of Synallactidae from seamounts are particularly rare. To bridge the knowledge gap, the Institute of Oceanology, Chinese Academy of Sciences (**IOCAS**) conducted several scientific expeditions between 2013 and 2018. During these surveys, four synallactid specimens were collected from three seamounts (named ‘Jiaolong’, ‘Y3’, and ‘M4’) and the Ganquan Plateau in the SCS, at depths ranging from 344 to 3610 m, using the Remotely Operated Vehicle submersible (**ROV**) ‘Faxian’ (discovery in Chinese) and the manned submersible ‘Jiaolong’ and ‘Shenhaiyongshi’. Detailed examination of ossicles and external morphological features revealed that the four specimens belonged to three genera and represent four new species, which are described and illustrated in this work.

## Materials and methods

The Remotely Operated Vehicle submersible (**ROV**) ‘Faxian’, deployed from the research vessel R/V ‘Kexue’ (science in Chinese), along with the Human Occupied Vehicles (**HOVs**) ‘Jiaolong’ and ‘Shenhaiyongshi’, were used to collect four

synallactid specimens during four surveys conducted in the tropical Western Pacific (2013–2018) (Fig. 1). These specimens were photographed immediately on board prior to preservation. They were then fixed in 95% ethanol for morphological examination and subsequently stored in the Marine Biological Museum of Chinese Academy of Sciences (**MBMCAS**) at Qingdao, China. Due to the limited availability of molecular data for Synallactidae, identification of the four specimens relied solely on morphological characteristics.

Morphological observations were performed using a stereomicroscope (ZEISS Stemi 2000-C, Wetzlar, Germany). To prepare ossicles, soft tissues from the body wall, tentacles, papillae, and tube feet were digested in a solution of 15% sodium hypochlorite for 4–5 h. The digested samples were then rinsed with distilled water, air-dried, mounted on aluminum stubs, and coated with gold. The ossicle features of the four specimens were examined and photographed under a Nikon Eclipse Ni-U microscope (Tokyo, Japan) and a Hitachi S-3400N (Tokyo, Japan) scanning electron microscope (**SEM**).

Abbreviations used in the text: **ROV**, Remotely Operated Vehicle submersible; **HOV**, Human Occupied Vehicles; **IOCAS**, the Institute of Oceanology, Chinese Academy of Sciences; **MBM**, Marine Biological Museum of Chinese Academy of Sciences, Qingdao, China; **RN**, registration number; **CN**, collection number; **SCS**, South China Sea; **SEM**, scanning electron microscope.

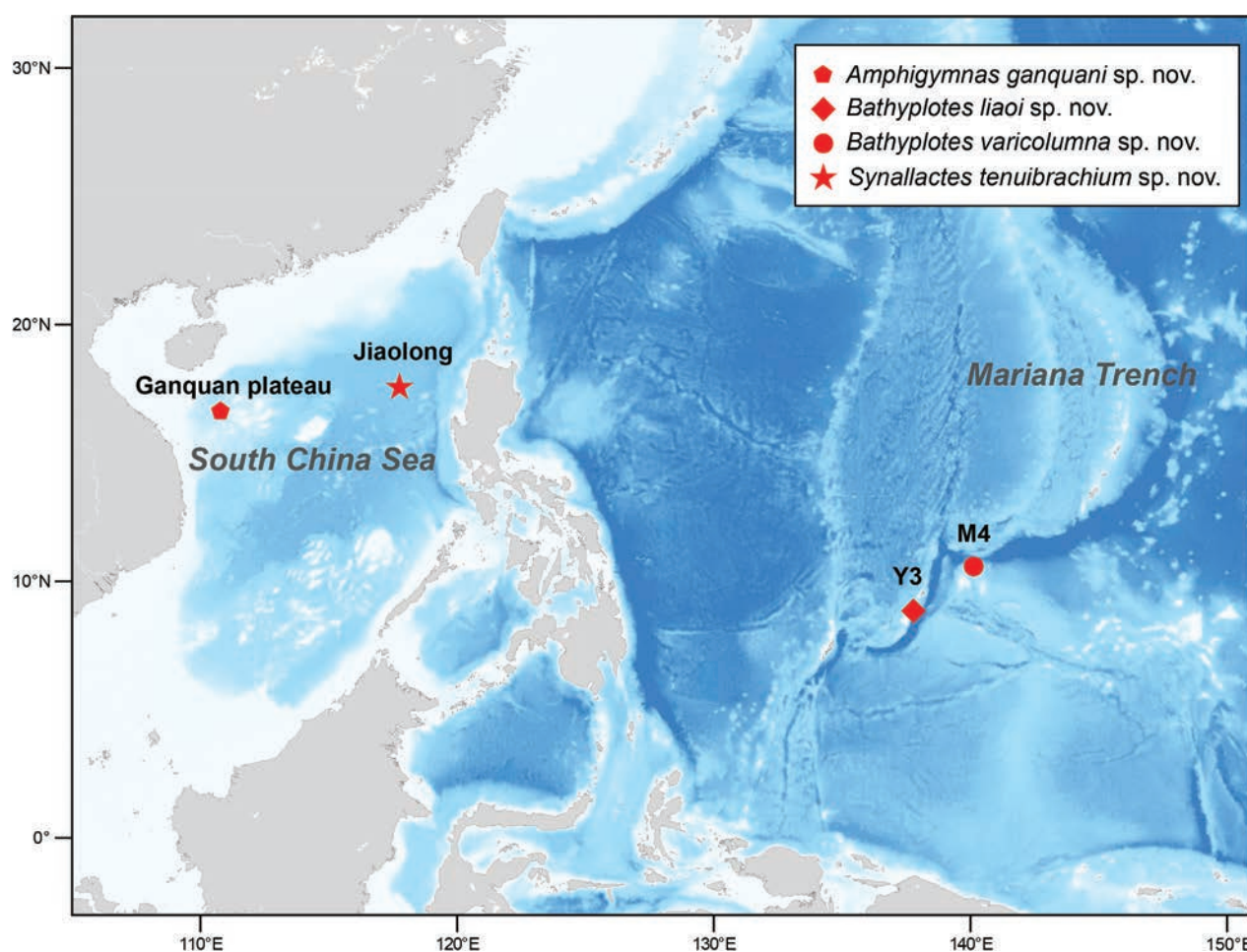


**Figure 1.** Sampling sites of the studied holothuroid species from tropical Western Pacific, showing the location of three seamounts.

## Systematics

**Order Synallactida Miller, Kerr, Paulay, Reich, Wilson, Carvajal & Rouse, 2017**  
**Family Synallactidae Ludwig, 1894**

**Genus *Synallactes* Ludwig, 1894**

**Diagnosis.** Body cylindrical or subcylindrical. Tentacles 18–20. Ventral surface flattened, without any marginal border. Ventral tube feet and dorsal papillae in longitudinal series, confined to ambulacra. Three zones of tube feet on ventral surface. Body wall with tri- or quadri-radiate tables, the distal ends of the arms with a larger or smaller number of perforations, often lateral processes forming a complex lattice-like network with similar processes of other arms. Spire consisting of a single pillar, terminally divided or perforated, or both [adapted from Solís-Marín 2005: 570–571].

**Type species.** *Synallactes alexandri* Ludwig, 1894.

**Type locality.** North Pacific Ocean, Azuero Peninsula, Gulf of Panama, depth 588 m (Solís-Marín 2003).

***Synallactes tenuibrachius* sp. nov.**

<https://zoobank.org/B4D25768-197C-41A8-8363-7D3EB2AB17FF>

Figs 2, 3

**Material examined. Holotype** • West Pacific, the Jiaolong Seamount in the SCS, depth 3610 m, 5 Jul. 2013, preserved in 95% ethanol, CN: III, RN: MBM286921.

**Diagnosis.** Body subcylindrical, convex dorsally, flattened ventrally. Mouth and anus terminal. Dorsal papillae conical, scattered on the bivium, with alternating large and small papillae. Ventrolateral papillae placed in a single row on each body side. Midventral radius with one or two small tube feet at the anterior and posterior ends. Ventrolateral tube feet arranged in double alternate rows. Dorsal body wall perforated plates and tables, tables with four or five slender arms. Papillae with tables, spires of tables higher than those of tables in the dorsal body wall. Ventral body wall tables with four or five arms. Tables with 4–6 arms in ventral tube feet, the distal ends of the arms enlarged, branched, rarely connected, and possessing a number of perforations.

**Description.** Body subcylindrical, slightly convex dorsally, flattened ventrally. Skin soft and gelatinous. Color red in life (Fig. 2A, B). After 95% ethanol fixation, color white, body length 9 cm and width 4 cm (Fig. 2C, D). Mouth and anus terminal. Tentacles, calcareous ring, and polian vesicles lost. Dorsal surface with numerous large and small papillae, scattered all over the bivium (Fig. 2A–C). Large papillae arranged in longitudinal rows along dorsal radii, ~ 10 in each row; small papillae mainly distributed in both dorsal interradii, ~ 20 on each body side (Fig. 2C). Ventrolateral papillae large, forming a simple row around the margin of the brim (Fig. 2A, B). Ventrolateral tube feet conical, arranged in a double alternate row, ~ 22 on each body side (Fig. 2D). Midventral tube feet radius with one or two small tube feet at the anterior and posterior ends of the body (Fig. 2D). **Ossicles.** Dorsal body wall tables with four or five arms (Fig. 3A1–A9), arms slightly broader at the tip with one or two perforations,

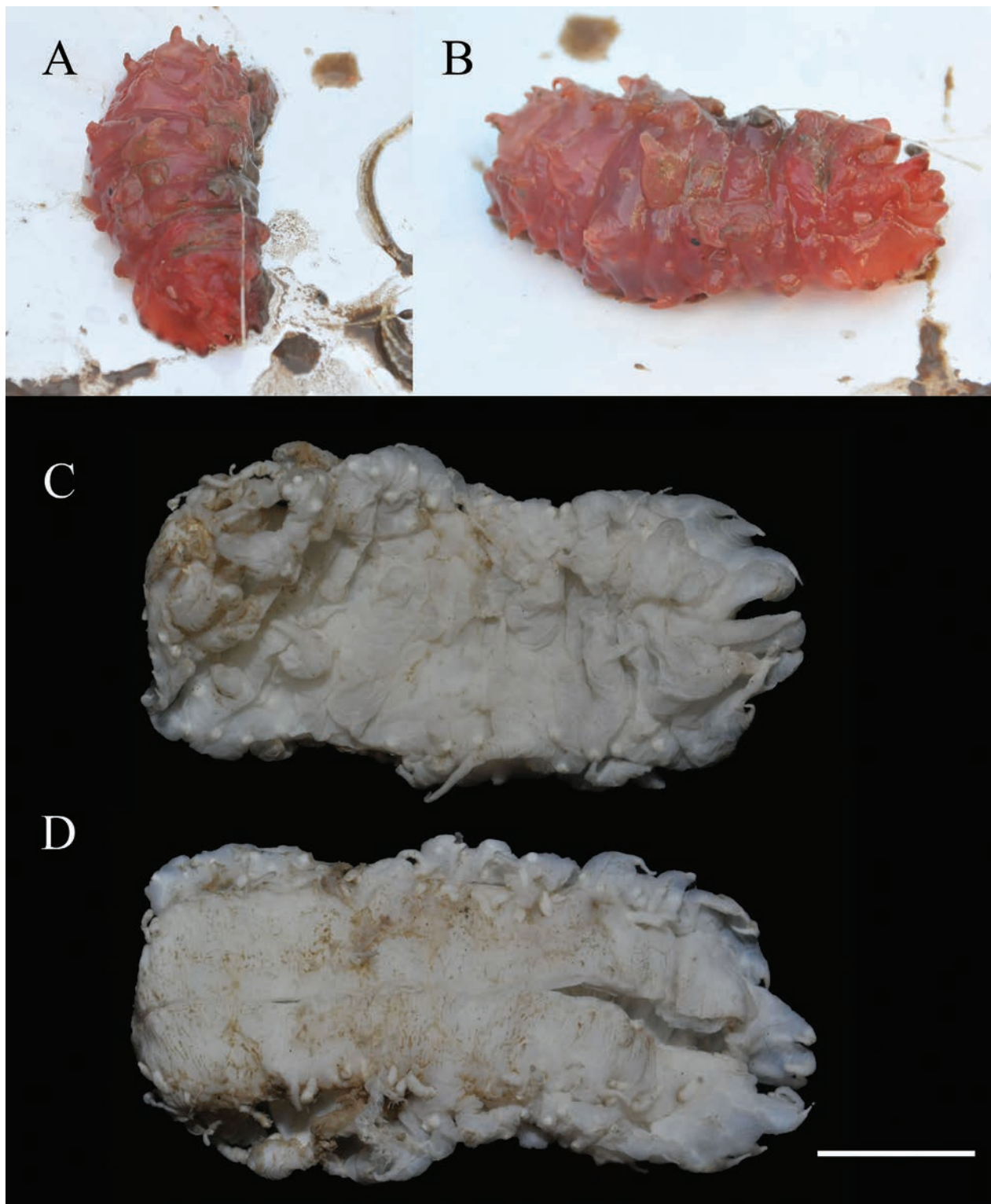


**Figure 2.** *Synallactes tenuibrachius* sp. nov. holotype: MBM286921 **A, B** living specimen **C, D** preserved specimen **C** dorsal view **D** ventral view. Scale bar: 2 cm.

50–70  $\mu\text{m}$  in length, spires with simple tips, often bearing several spines on the side, 82–100  $\mu\text{m}$  in height; simple concave perforated plates (Fig. 3A10), 75  $\mu\text{m}$  in diameter. Papillae with four-armed tables (Fig. 3B1, B2), the spires significantly higher than those in the dorsal body wall, 110–155  $\mu\text{m}$  in height. Ventral body wall with tables similar to those in the dorsal body wall (Fig. 3C1–C5),

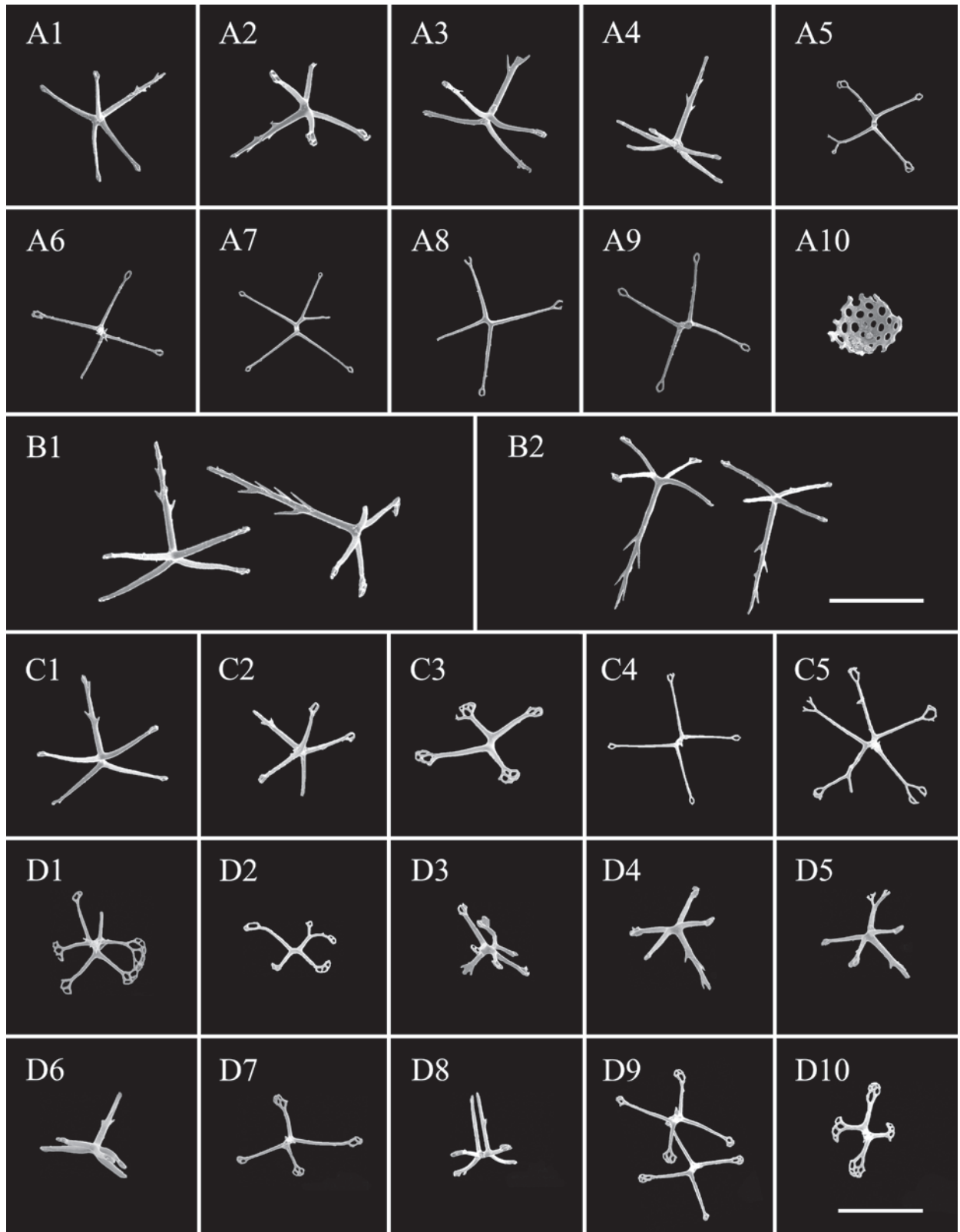


**Figure 3.** SEM images of *Synallactes tenuibrachius* sp. nov. holotype: MBM286921. Ossicles from **A1–A10** dorsal body wall **B1–B2** papillae **C1–C5** ventral body wall **D1–D10** ventral tube feet. Scale bars: 100  $\mu$ m.

except that the end of arms bifurcated or bearing more perforations (up to 5) in some tables. Tables with 4–6 arms in ventral tube feet (Fig. 3D1–D10), irregular in shape, the distal ends of the arms enlarged, branched, and possessing

several perforations, sometimes the enlarged ends of the arms connected with one another (Fig. 3D1); rarely a four-armed table with two parallel pillars (Fig. 3D8), ~ 68 µm in height, without transverse beam.

**Type locality.** The Jiaolong Seamount in the South China Sea, tropical Western Pacific, depth 3610 m.

**Etymology.** The name of the new species is a combination of the Latin words *tenuis* meaning 'slender' and *brachium* meaning 'arm'. It refers to the very slender arms of tables in the body wall.

**Distribution.** Only known from its type locality.

**Remarks.** The new species, *Synallactes tenuibrachius* sp. nov., is characterized by the tube feet arranged in a double alternate row along each ventrolateral radius and all tables possessing very slender arms. Among the five species of *Synallactes* with single-pillared tables featuring pointed tops (i.e., *S. aenigma*, *S. horridus*, *S. robertsoni*, *S. profundus*, and *S. laguardai*; Solís-Marín 2003; Solís-Marín 2005), the new species most resembles *S. aenigma* Ludwig, 1894, *S. horridus* Koehler & Vaney, 1905, and *S. profundus* (Koehler & Vaney, 1905) based on the ossicle features of the body wall. Specifically, all have single-pillared tables with pointed tops and four- or five-armed discs, with the distal ends of the arms exhibiting only a few perforations. However, there are some differences between them. Compared with *S. aenigma*: 1) In the new species, the midventral ambulacrum bears only one or two small tube feet at the anterior and posterior ends of the body. In contrast, Ludwig (1894) noted that *S. aenigma* possesses a few tube feet organized into two long rows on the midventral radius. 2) The anus in *S. tenuibrachius* sp. nov. is terminal, whereas in *S. aenigma*, it is dorsal. 3) The spires in *S. tenuibrachius* sp. nov., are generally unbranched at the end, with some arms having enlarged ends that may connect to each other, while in *S. aenigma*, the spires of tables are divided into 2–10 elongated tips at the end, and the arms of tables never seem to be connected. 4) *Synallactes tenuibrachius* sp. nov. differs from *S. aenigma* by the types of ossicles in the tube feet. The tube feet of *S. tenuibrachius* sp. nov. have only tables, whereas those of *S. aenigma* have spiny, curved support rods, and well-developed mesh-like discs in addition to tables.

Compared with *S. horridus*: 1) *S. tenuibrachius* sp. nov. exhibits numerous large and small papillae scattered on the dorsal surface and only one or two small tube feet placed on the midventral ambulacrum at the anterior and posterior ends of the body. By contrast, *S. horridus* has large conical papillae on all radii except midventral radius, and some tube feet are confined to the anterior region of midventral radius. 2) The body wall of *S. tenuibrachius* sp. nov. contains tables with cross-shaped discs and small perforated plates, but no rods, while the body wall of *S. horridus* has many cruciform bodies and rods, with perforated plates absent. 3) All the arms and spires of tables in the body wall of *S. tenuibrachius* sp. nov. are more slender and fragile, compared to the solid and high spires of the cruciform bodies in the body wall of *S. horridus*.

Compared with *S. profundus*: The new species differs from *S. profundus* by the arrangement and number of the ventral tube feet. The tube feet in *S. tenuibrachius* sp. nov. are arranged in a double alternate row on each ventrolateral radius, while the midventral radius is completely naked. In *S. profundus*, the tube feet are arranged in a single row on each ventrolateral radius, with the midventral radius hosting a few tube feet near the anterior and posterior ends.

## Genus *Bathyplores* Östergren, 1896

**Diagnosis.** Tentacles 15–20. Mouth ventral, anus dorsal, subdorsal or nearly terminal. Skin rather thick. Body with sole-like ventral side, usually with marginal appendages. Midventral ambulacrum with a few tube feet or naked. Ventrolateral tube feet arranged in a single row or multiple rows. Dorsal papillae more or less distinctly arranged in rows. Tables with cross-shaped disc and a spire formed by 1–5 pillars, usually with several transverse beams (rarely without transverse beams); C-shaped bodies may be present [adapted from Solís-Marín 2003: 124].

**Type species.** *Bathyplores natans* (Sars, 1868) by original designation.

**Type locality.** Lofoten, northern Norway, depth 366–549 m.

### *Bathyplores varicolumna* sp. nov.

<https://zoobank.org/7E4D63FA-EB18-4906-96BB-57E8B25315B8>

Figs 4, 5

**Material examined. Holotype** • West Pacific, the M4 Seamount located in the Caroline Ridge, Dive FX-Dive137 (10°35.04'N, 140°07.27'E), depth 1195 m, 21 Aug. 2017, preserved in 95% ethanol, CN: C144, RN: MBM286925.

**Diagnosis.** Body elongated, ventrally flattened. Mouth ventral, anus terminal. Peltate tentacles 16. Dorsal surface with scattered large papillae and laterally with a simple row of small papillae. The dorsal side irregularly arranged with several low 'fungiform' whitish warts. Ventral surface with scattered minute tube feet. Dorsal body wall lacking ossicles. Papillae cross-shaped tables and rods, tables with 4–7 arms, 3–5 pillars, and without transverse beams. Cross-shaped tables with single pillars in low whitish warts. Cross-shaped tables with single pillars, support rods, and irregular shaped ossicles in the ventral body wall. Cross-like discs of tables, perforated plates, and support rods in ventral tube feet. Rods, smaller tables, and irregular deposits in tentacles.

**Description.** Body elongated, ventrally flattened, body wall thin and pliable. Color pale pink in situ, and orange in life (Fig. 4A, B). Body 24 cm long and 6.5 cm wide in living specimen (Fig. 4C, D). Mouth ventral, anus terminal. Peltate tentacles 16. Circum-oral papillae present (Fig. 4B). Bivium with some scattered large papillae and laterally with a simple row of small papillae (Fig. 4A, C). A number of low whitish warts arranged along the two dorsal interradii (Fig. 4C). Trivium with some scattered minute tube feet (Fig. 4B, D). Ventral surface with three series (a middle series and one lateral series on each side) of tube feet (Fig. 4D), the middle series forming multiple rows, occupying a third of the ventral surface, other two series forming two or three rows on each side. Brim narrow and retracted, formed by ventrolateral papillae (Fig. 4A, B). **Ossicles.** Dorsal body wall lacking ossicles. Dorsal papillae with tables and rods (Fig. 5A), cross-shaped discs of tables 190–260 µm across, with 4–7 arms, each arm ~ 45–155 µm long, the ends of the arms enlarged and pierced with holes, the spires composed of 3–5 pillars, without transverse beams, the top of pillars fused, making the tip of spires spinous; rods curved, 280–315 µm long. Ventral body wall with tables, rods and irregularly shaped ossicles (Fig. 5B), cross-shaped discs of tables with four arms, and only one central pillar (often truncated); rods up to 95 µm. Cross-like discs of tables in ventral tube

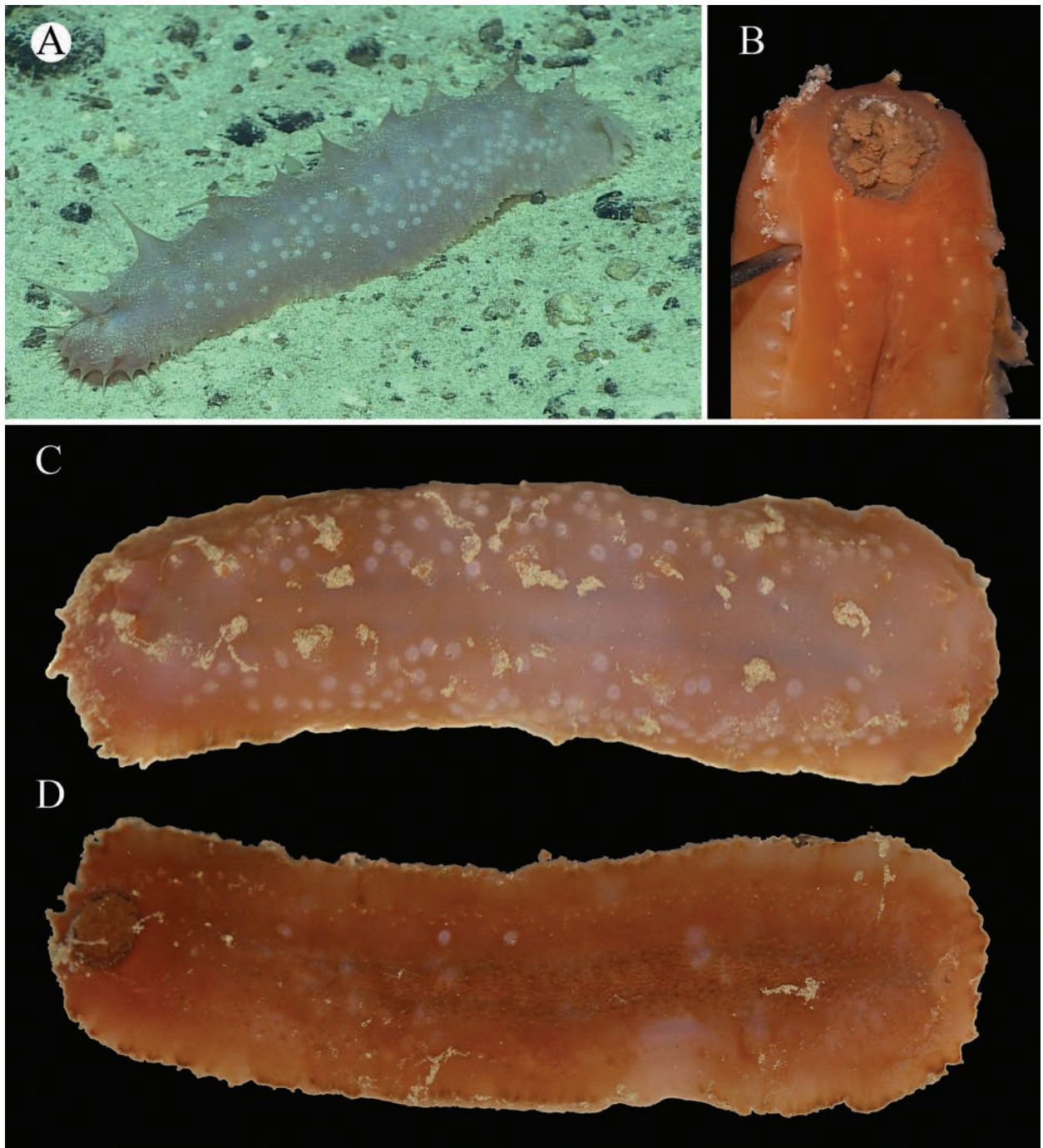
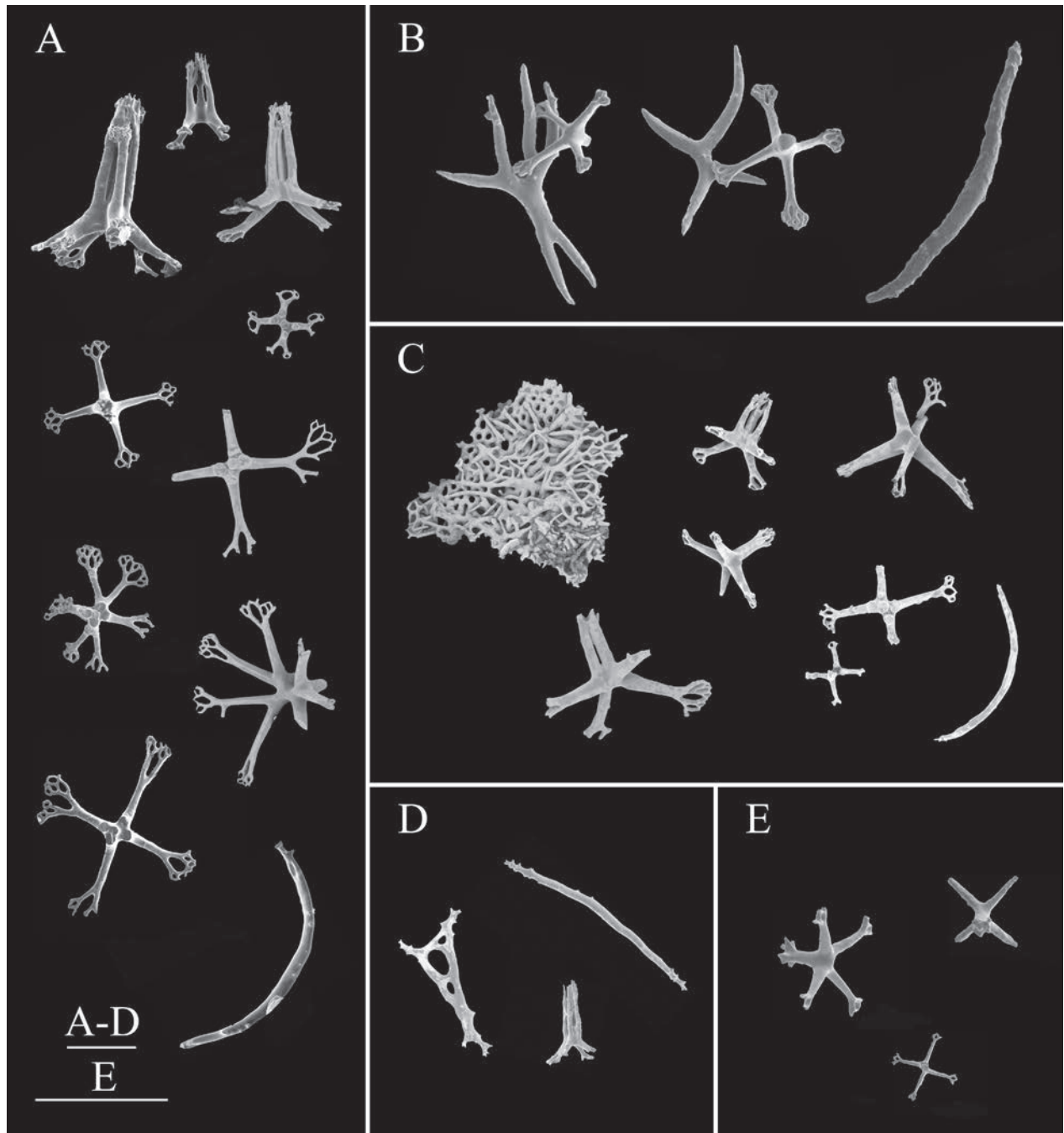


Figure 4. *Bathyplores varicolumnna* sp. nov. holotype: MBM286925 **A** in situ image **B** tentacles **C** dorsal view **D** ventral view. Scale bar: 3 cm.

feet 100–222  $\mu\text{m}$  across, with 1–4 pillars, without transverse beams, the top of pillars fused; terminal plates and rods also in tube feet (Fig. 5C). Rods, smaller tables, and irregular deposits in tentacles (Fig. 5D). Tables with four arms in low whitish warts similar to those in the ventral body wall, and possessing only one central pillar, the top of pillars often irregularly branched or truncated (Fig. 5E).

**Type locality.** The M4 Seamount located in the Caroline Ridge of the tropical Western Pacific, depth 1195 m.

**Etymology.** The Latin word *varicolumnna* means ‘various pillars’ and is used to describe tables characterized by different types of pillars.



**Figure 5.** SEM images of *Bathyploetes varicolumnna* sp. nov. holotype: MBM286925. Ossicles from **A** dorsal papillae **B** ventral body wall **C** ventral tube feet **D** tentacles **E** ‘fungiform’ whitish warts. Scale bars: 100  $\mu$ m.

**Distribution.** Only known in its type locality.

**Remarks.** The body of the new species, with a sole-like ventral side, and its tables featuring cross-shaped discs with typically three or four pillars, confirm its placement within the genus *Bathyploetes*. In most *Bathyploetes* species, tables generally possess four pillars, rarely three or five. However, in the new species, tables exhibit a broader variation, with 1–5 pillars, and 4–7 arms, an uncommon variation within this genus. Among the known species of *Bathyploetes*, the morphology of *Bathyploetes varicolumnna* sp. nov. most closely resembles that of *B. moseleyi*. Both species share tables with numerous arms and dorsal interradial bearing numerous low whitish warts.

Nonetheless, the new species can be distinguished from *B. moseleyi* by the following differences: 1) Both *B. moseleyi* and the new species possess three series of tube feet on the ventral surface: a middle series and one lateral series on each side. However, the middle tube feet in *B. moseleyi* are arranged in a thin double row, whereas the middle tube feet in *B. varicolumna* sp. nov. are scattered irregularly and broadly along the midventral radius. 2) In *B. moseleyi*, tables have discs with 4–8 arms, and their spires are formed by four pillars and one, rarely two transverse beams, or are often entirely devoid of transverse beams. In contrast, the tables in *B. varicolumna* sp. nov. have discs with 4–7 arms, and their spires consist of 1–5 pillars without transverse beams. 3) The tube feet of *B. moseleyi* contain support rods, whereas those of *B. varicolumna* sp. nov. possess tables and terminal plates in addition to rods. 4) In *B. moseleyi*, whitish warts contain only a few rods at their ends. In *B. varicolumna* sp. nov., however, the predominant ossicles are four-armed tables with cross-shaped discs, supported by a single central pillar that is often irregularly branched or truncated at the top.

***Bathyplotes liaoi* sp. nov.**

<https://zoobank.org/F8A68557-64F1-41B9-B1C4-8F536D013EDD>

Figs 6–8

**Material examined. Holotype** • West Pacific, the Y3 Seamount near the Yap Trench, Dive FX-Dive 21 (8°51'N, 137°47'E), depth 344 m, 24 Dec. 2014, preserved in 95% ethanol, CN: Y30165, RN: MBM286918.

**Diagnosis.** Body elongated, dorsally convex, ventrally flattened. Mouth ventral, anus dorsal. Tentacles 18. Dorsal papillae arranged in six longitudinal rows. Brim formed by small ventrolateral papillae. Tube feet irregularly scattered on the ventral surface. Dorsal body wall containing tables with cross-shaped discs, four (rarely five) pillars of tables bearing numerous large spines, and four to six transverse beams; small tables with annular discs; perforated plates. Dorsal papillae with perforated plates, tables with cross-shaped discs, and support rods. Ventral body wall ossicles similar to those in the dorsal body wall, except for some tables with much higher spires. Tube feet with perforated plates, irregularly shaped ossicles, and small tables with annular discs. Tentacles with spiny rods.

**Description.** Body elongated, slightly pointed at each extremity, dorsal slightly arched, ventral flattened (Fig. 6A–C). Color in life faint yellow, sub-transparent, dorsal papillae, tube feet, and tentacles darker (Fig. 6B, C). Body 15 cm long and 5 cm wide before fixation (Fig. 6B, C). Mouth ventral, anus dorsal and surrounded by numerous small papillae (Fig. 6B, C). Peltate tentacles 18. Dorsal surface densely covered with approximately equal conical papillae, arranged in six longitudinal rows, with ~ 14–18 papillae in each row (Fig. 6A, B). The jagged edges on both sides of the body formed by a single row of numerous smaller papillae. Tube feet irregularly arranged longitudinally throughout the ventral sole, ~ 86 in each row. **Ossicles.** Tables of two types in the dorsal body wall (Fig. 7A1–A7): 1) Cross-shaped discs (Fig. 7A1–A4) with four arms, each arm bearing small spines, 100–200 µm in length, with a number of perforations at the ends, four (rarely five) pillars bearing numerous large spines, four to six transverse beams, the spires measuring 108–200 µm in height, tips formed by fused pillars. 2) Annular discs (Fig. 7A5–A7) with four large holes formed by simple diagonal bars,

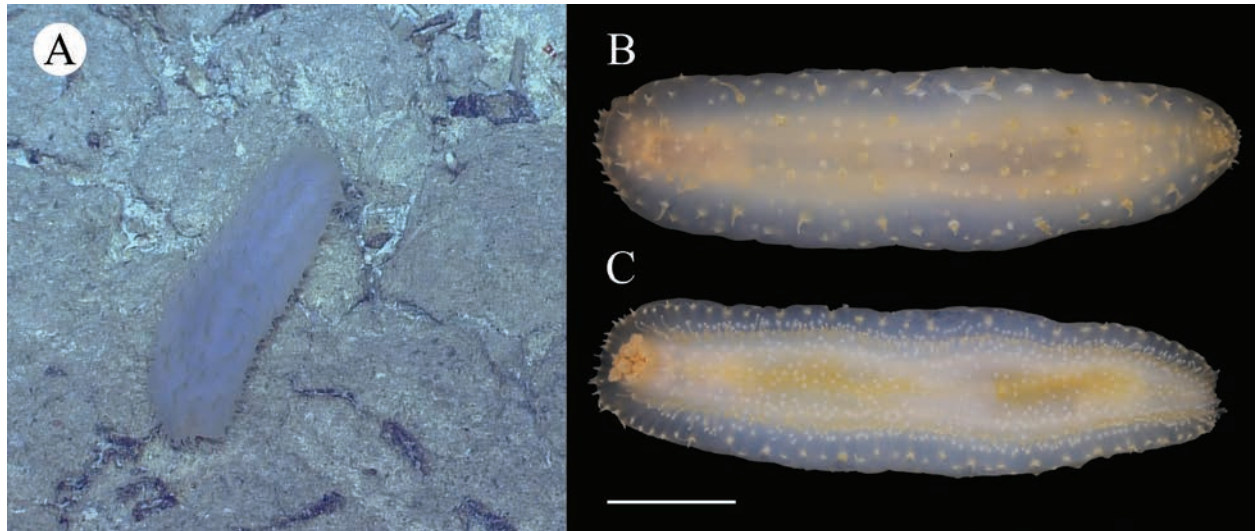


**Figure 6.** *Bathyplores liaoi* sp. nov. holotype: MBM286918 **A** in situ image **B** dorsal view **C** ventral view. Scale bar: 3 cm.

discs  $\sim 58 \mu\text{m}$  in diameter, the spires  $30\text{--}42 \mu\text{m}$  high, with one or two transverse beams. Dorsal papillae with most tables (Fig. 7B1–B4) similar to those of the dorsal body wall (first type), rarely smaller tables with four transverse beams (Fig. 7B4); perforated plates, measuring  $400 \mu\text{m}$  in diameter (Fig. 7B5); spinous rods up to  $366 \mu\text{m}$  in length (Fig. 7B4). Ventral body wall tables with four-armed discs, small tables with annular discs, and perforated plates (Fig. 7C1, C2 and Fig. 8), most ossicles of similar features to those in the dorsal body wall, except that a few tables with really high spire, measuring  $245 \mu\text{m}$  in height (Fig. 8A, B). In tentacles (Fig. 7D) rods  $70\text{--}500 \mu\text{m}$  long. Tube feet with four types of ossicles: 1) perforated plates (Fig. 7E1); 2) smaller tables with annular discs (Fig. 7E2–E7),  $\sim 88 \mu\text{m}$  in diameter, the spires of tables higher than those in the dorsal body wall (second type), measuring  $48\text{--}64 \mu\text{m}$  high, four spiny pillars with three transverse beams; 3) rods up to  $404 \mu\text{m}$  in length (Fig. 7E8).

**Type locality.** The Y3 Seamount near the Yap Trench, tropical Western Pacific,  $344 \text{ m}$  depth.

**Etymology.** The species is named after one of the pioneers in the study of holothuroid fauna in China, Professor Yulin Liao.

**Distribution.** Only known from its type locality.

**Remarks.** The predominance of four-pillared tables undoubtedly indicates that this species belongs to the *Bathyplores*. *Bathyplores liaoi* sp. nov. is mostly similar, in terms of ossicle types, to *Bathyplores patagiatus* Fisher, 1907, which has been regarded as a synonym of *Bathyplores natans*. Both species share the presence of ossicles that include four-armed crosses, small tables with annular discs, and spinous rods. However, the new species can be distinguished from *B. patagiatus* by the presence of tube feet on the midventral radius and differences in the shape of the spires of tables. In *Bathyplores liaoi* sp. nov., the tables typically have four, rarely five pillars, with their dilated ends of spires usually formed by these fused pillars, rather than expanding into a crown. In contrast, the tables in *B. patagiatus* are robust, with each table possessing four pillars and a broad thorny crown formed by the highly dilated spire ends, resembling a quadrilateral tower. Moreover, the pillar ends in *B. patagiatus* are often unfused. The new species also differs from *B. patagiatus* by the presence

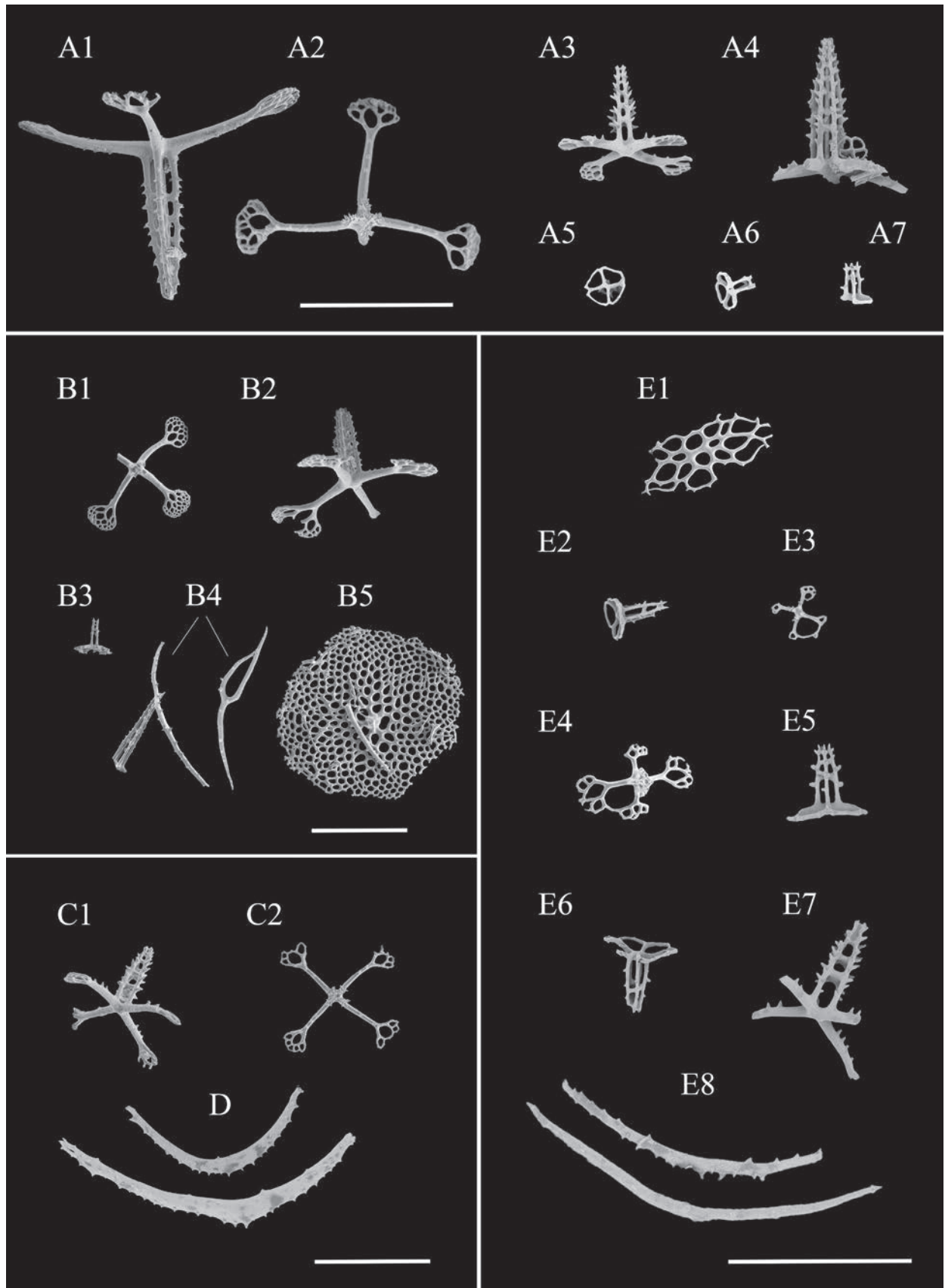
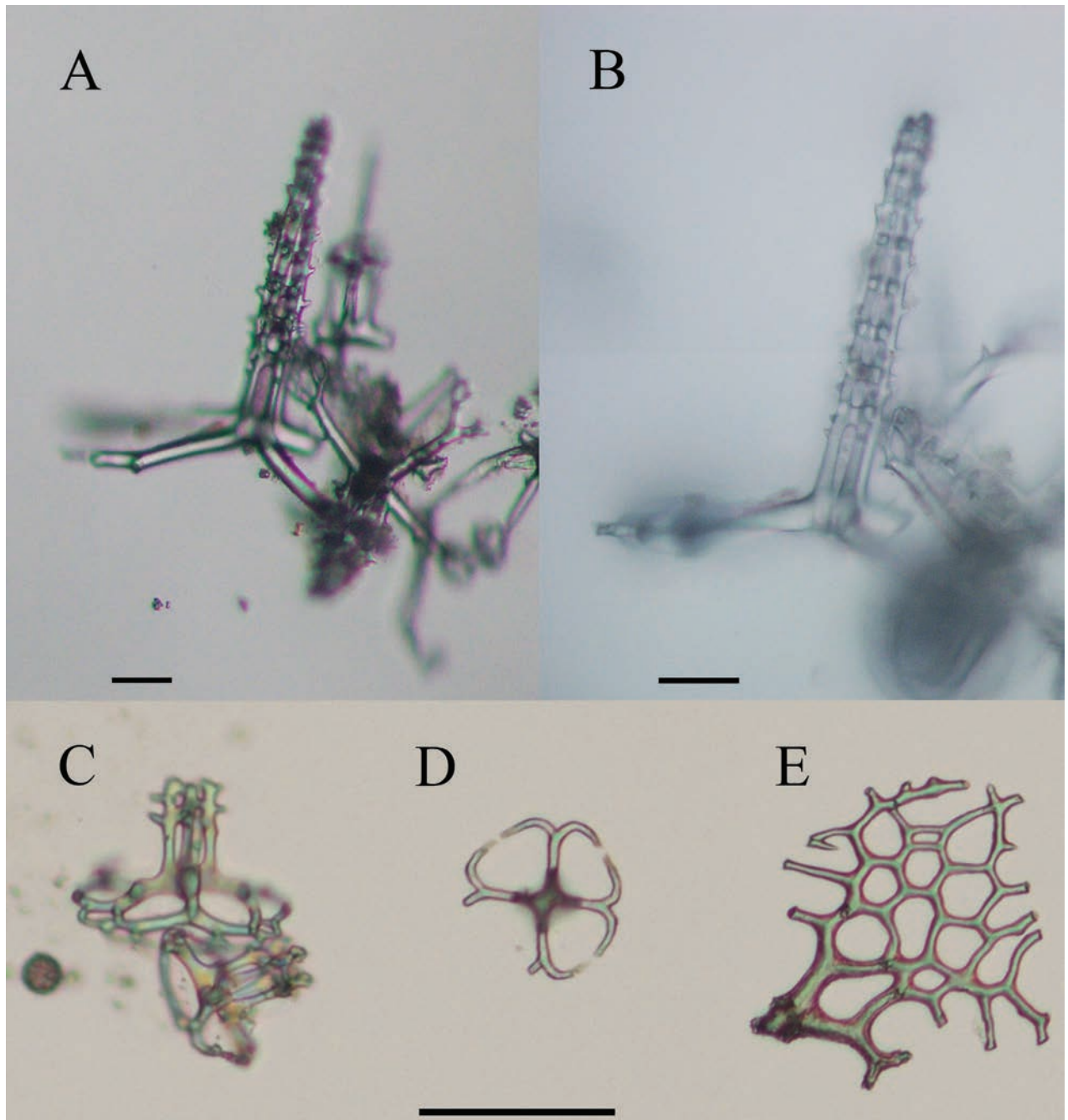


Figure 7. SEM images of *Bathyploetes liaoi* sp. nov. holotype: MBM286918. Ossicles from **A1–A7** dorsal body wall **B1–B5** dorsal papillae **C1, C2** ventral body wall **D** tentacles **E1–E8** tube feet. Scale bars: 200  $\mu$ m.



**Figure 8.** Optical microscope images of *Bathyploetes liaoi* sp. nov. holotype: MBM286918. Ossicles from ventral body wall **A, B** tables with very high spires and four-armed discs **C** small tables with annular discs **D** annular discs **E** perforated plates. Scale bars: 50  $\mu$ m.

of tables with annular discs and five-pillared crosses in the dorsal body wall, as well as perforated plates in the ventral body wall and papillae. In *B. liaoi* sp. nov., the arms of the crosses bear small spines, whereas those in *B. patagiatus* are smooth. The spines on the spires of tables in *B. liaoi* sp. nov. are distributed along the entire length of the pillars, while in *B. patagiatus*, the spines are confined to the upper half, even in tables with exceptionally long spires. In addition, *B. liaoi* sp. nov. lacks C-shaped ossicles present in *B. patagiatus*.

Both *Bathyploetes liaoi* sp. nov. and *B. phlegmaticus* have two types of tables in the body wall: 1) large tables of characteristic form, with cross-like discs and 2)

smaller tables with annular discs. The arms and pillars of both types of tables possess spines. However, the new species exhibits several key differences from *B. phlegmaticus*: 1) The number and arrangement of papillae are different. In *B. liaoi* sp. nov.: the dorsal surface was densely covered with conical papillae of approximately equal size, arranged in six longitudinal rows, with ~ 14–18 papillae each row. The jagged edges along both sides of the body were formed by a single row of numerous smaller papillae. In *B. phlegmaticus*, a delicate rim was formed by free papillae, with ~ 35 at the anterior part of the body and ~ 12 along the anterior and posterior lateral edges. Papillae on the ventral side are few, irregularly distributed, and not confined to the radii. 2) Tube feet in *B. phlegmaticus* have rods and a well-developed endplate. However, tube feet in *B. liaoi* sp. nov. include tables with annular discs, irregular large ossicles, rods, and a plate. 3) Tables have different numbers of transverse beams. In *B. phlegmaticus*, the spires of large tables possess 6–8 transverse beams, while smaller tables have 1–3 transverse beams. In *B. liaoi* sp. nov., the large tables have fewer transverse beams (4–6), and the smaller tables have only one or two transverse beams.

### Genus *Amphigymnas* Walsh, 1891

**Diagnosis.** Body wall calcareous, brittle, similar to that of the elasipodid family Deimatidae. Mouth ventral, peltate tentacles 20. Dorsal and lateral body with long conical calcareous papillae, including a ventrolateral series. Body flat ventrally, tube feet in ambulacral series or scattered. Anus subdorsal posterior. Ossicles in body wall large table discs with many perforations, discs variably with or lacking spires often comprising three or four pillars, sometimes with more fused pillars, without distal spines or teeth, spires sometimes reduced to short unconnected pillars [adapted from O’Loughlin et al. 2013: 38].

**Type species.** *Amphigymnas multipes* Walsh, 1891 accepted as *Amphigymnas woodmasoni* (Walsh, 1891).

**Type locality.** Indian Ocean, Andaman Sea, off Dyer Point and North Cinque Island, depth 343–402 m.

### *Amphigymnas ganquani* sp. nov.

<https://zoobank.org/B0A06953-CB2A-41AD-97D2-295D92330F52>

Figs 9–11

**Material examined. Holotype** • West Pacific, the Ganquan Plateau in the SCS, depth 1350 m, 12 May 2018, preserved in 95% ethanol, CN: GQHT-SY-066-12, RN: MBM286926.

**Diagnosis.** Body elongated, cylindrical, gradually tapering at both ends. Color yellowish white. Skin fragile, glass-like. Mouth ventral, oral disc with front-suspended dorsal papillae, anus terminal. Peltate tentacles 20. Dorsal papillae arranged in two rows along each dorsal ambulacrum. Ventrolateral papillae arranged in a single row. Ventrolateral tube feet arranged in a single row on each side. Midventral ambulacrum placed in alternate two rows. Dorsal body wall tables with short or high 4-pillared spires and 0–2 transverse beams. Papillae tables and widened midrods, tables with higher spires, four or more usually

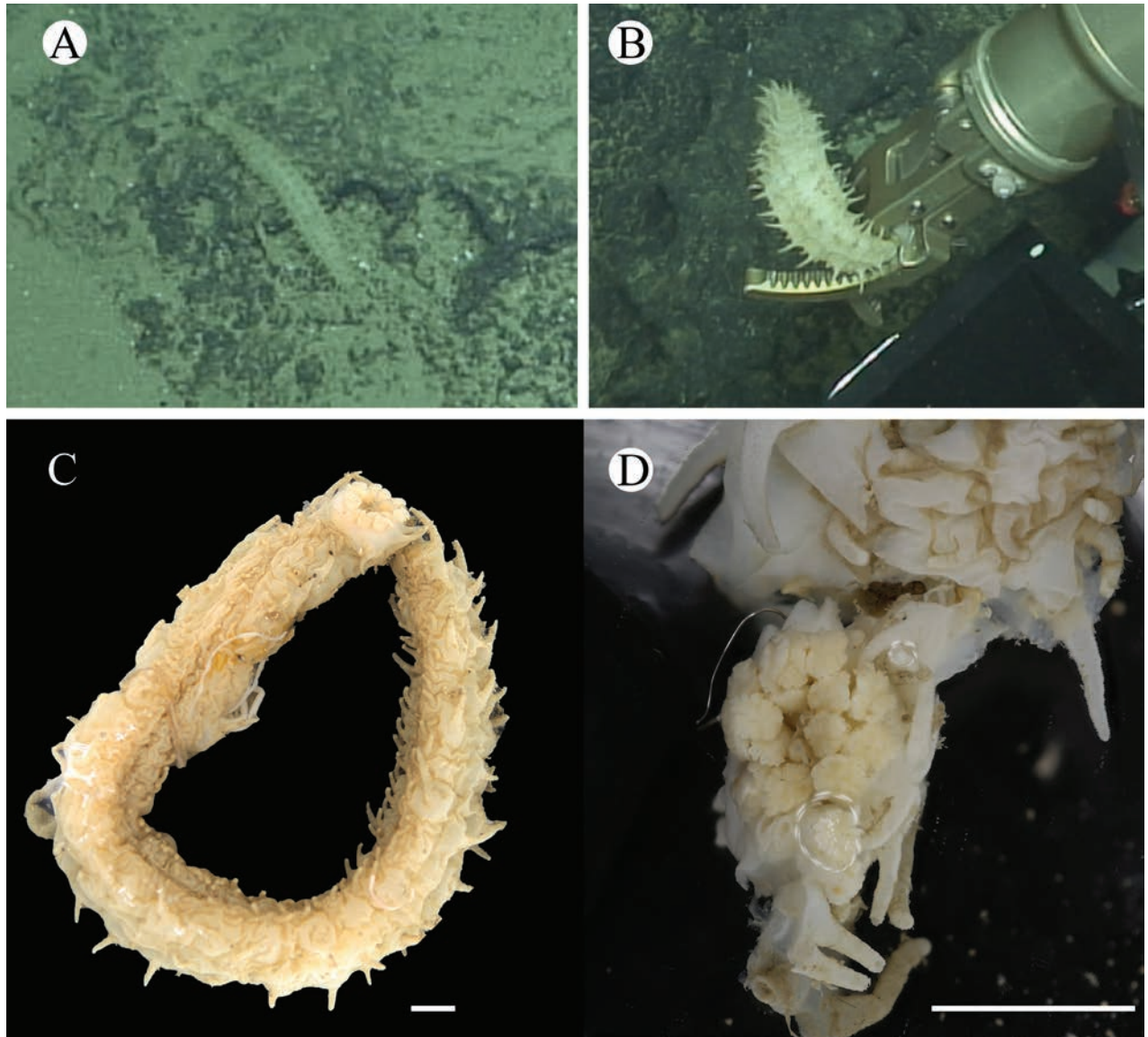


**Figure 9.** *Amphigymnas ganquani* sp. nov. holotype: MBM286926 **A, B** in situ images **C** holotype after fixation **D** tentacles. Scale bars: 1 cm.

fused pillars, and three or four transverse beams. Ventral body wall with smaller tables, spires truncate, without transverse beams. Tube feet tables with truncate and high pillars. Tentacles support rods.

**Description.** Body long and cylindrical, slightly slender at both ends (Fig. 9A, B), ventral flattened. Body 28 cm long, 2.5 cm wide mid-body before fixation (Fig. 9C). Color yellowish white, body wall thin, calcareous, and fragile. Mouth ventral, anteriorly overhung by a few dorsal papillae (Fig. 9C, D), anus terminal. Peltate tentacles 20, measuring 0.25–0.3 cm in diameter after fixation (Fig. 9D). Two paired conical papillae placed in a single series on each dorsal radius (four rows across dorsally), each up to 1 cm long after fixation. Ventrolateral papillae arranged in a single row, ~ 22 on each body side, up to 1.5 cm long after fixation. Irregular tube feet relatively large and placed in single rows on ventrolateral radii, ~ 60 in each row. Midventral tube feet small, placed in alternate two rows, ~ 80 in each row. Longitudinal muscles undivided, tentacle ampullae absent, and gonads arranged in clusters. **Ossicles.** Dorsal body wall tables (Fig. 10A–J),

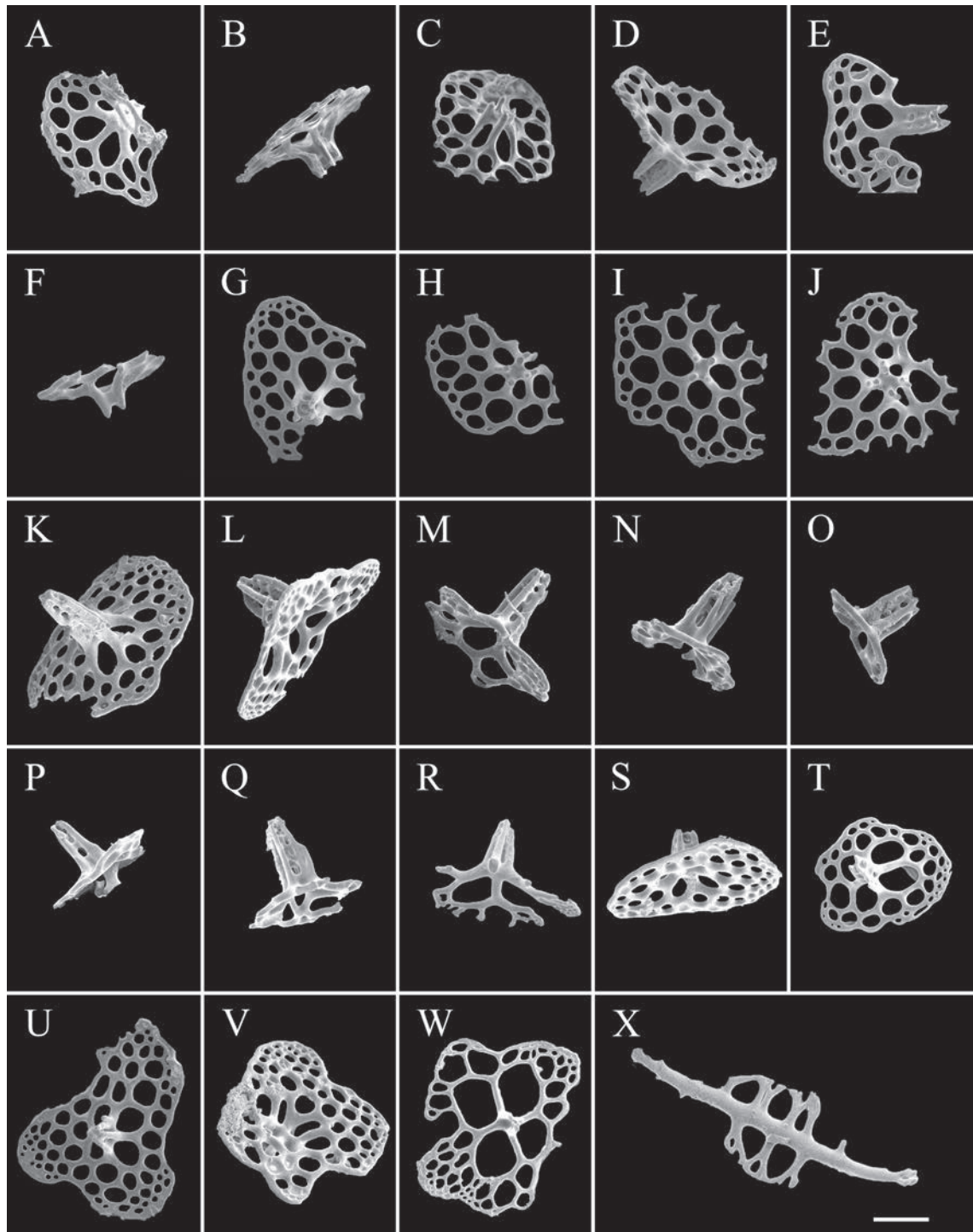
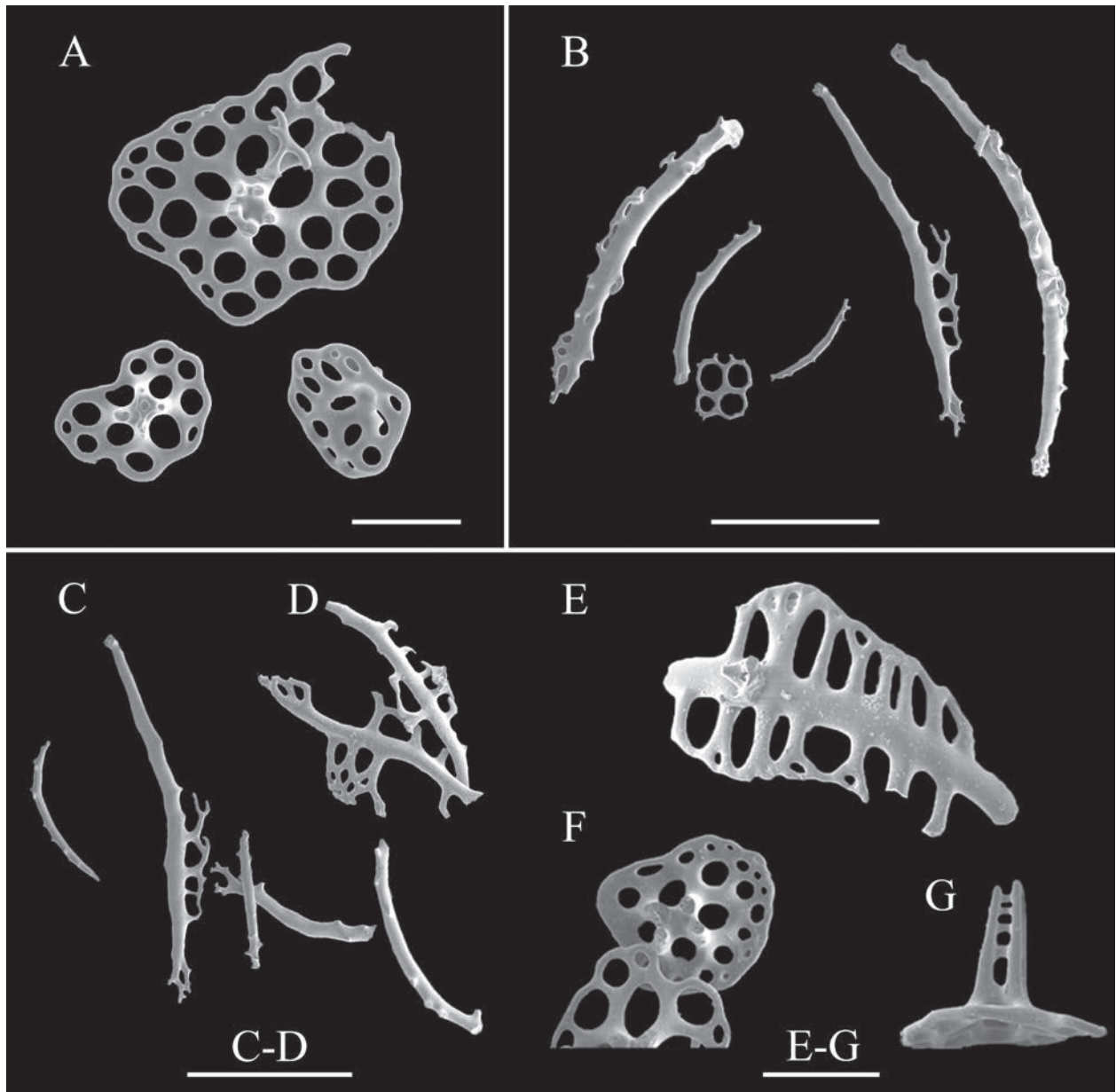


Figure 10. SEM images of *Amphigymnas ganquani* sp. nov. holotype: MBM286926. Ossicles from **A–J** dorsal body wall **K–X** dorsal and lateral papillae. Scale bar: 100  $\mu$ m.

discs perforated plates, edges usually incomplete, 220–370  $\mu$ m across, with numerous perforations of similar size, spires with four pillars (mainly) or more pillars (Fig. 10G, H, J), short or relatively high, lacking or possessing one (rarely) or two transverse beams. Short pillars lacking or with one beam, ~ 50–80  $\mu$ m in length (Fig. 10A–C, F–J), relatively high pillars with two beams, 100–120  $\mu$ m in length (Fig. 10D, E). Spires of tables in dorsal and lateral papillae possessing much higher and firmer spires (Fig. 10K–W) than those in dorsal body wall,



**Figure 11.** SEM images of *Amphigygnas ganquani* sp. nov. holotype: MBM286926. Ossicles from **A** ventral body wall **B** tentacles **C–G** tube feet. Scale bars: 100 µm (**A, E–G**); 300 µm (**B–D**).

discs up to 400 µm across, with four large central perforations and many small outer perforations, four or more pillars, up to 150 µm in length, usually fused, making the number of transverse beams uncertain, some spires of tables possibly possessing 3–4 transverse beams; widened midrods in papillae up to 600 µm long, with marginal projections (Fig. 10X). Ventral body wall with smaller tables (Fig. 11A), discs 144–267 µm across, edges more complete and smooth, spires truncate, without transverse beams. Tentacles predominantly rods, curved, bearing irregular marginal projections, up to 803 µm long (Fig. 11B). Tube feet support rods straight to curved, widened midrods bearing irregular marginal projections, some placing through the entire length (Fig. 11C–E); tables with truncate pillars (Fig. 11F), without transverse beams; tables with high pillars, possessing four beams (Fig. 11G).

**Type locality.** The Ganquan Plateau in the South China Sea, tropical Western Pacific, depth 1350 m.

**Etymology.** The specific name refers to the Ganquan Plateau, where the holotype was sampled.

**Distribution.** Currently known from the type locality.

**Remarks.** The new species belongs to *Amphigymnas* Walsh, 1891, characterized by the glass-like body wall formed by numerous large tables, large conical papillae on the dorsal and ventrolateral radii, and a midventral row of small tube feet filled with many support rods.

The new species differs from the *A. bahamensis* Deichmann, 1930 by the arrangement of ventral tube feet and the number of pillars of dorsal tables. Dorsal tables in the new species have at least four pillars, whereas those of *A. bahamensis* have rare 3-pillared truncate spires. Additionally, the ventral tube feet in the new species are arranged along both the ventrolateral and midventral radii, while those in *A. bahamensis* are restricted to the midventral radius. The external morphological differences between the new species and *Amphigymnas woodmasoni* are slight. However, the new species can be distinguished primarily by ossicle features: Tables in *A. woodmasoni* have four large central perforations surrounded by many smaller peripheral holes, and the spires of tables are usually rather primitive and reduced to four spines (without forming pillars) on the body walls and papillae. In contrast, the spires of tables on body walls and papillae in the new species are relatively high and often exhibit four or more pillars, rather than being reduced to spines. Notably, in the papillae they can reach heights of up to 150  $\mu\text{m}$ . In comparison to *Amphigymnas staplesi* O’Loughlin in O’Loughlin et al. 2013, the new species exhibits several distinguishing characteristics: The oral disc of *A. staplesi* is surrounded by a continuous series of papillae, whereas the new species has only front-suspended dorsal papillae. The new species is quite different from *A. staplesi* by the ossicle features: 1) In *A. staplesi*, the tables of dorsal body wall have discs with four large central perforations and many smaller outer perforations, and the spires have four pillars and two transverse beams. In the new species, the dorsal tables have discs with perforations of approximately equal diameters, and the spires have four or more pillars and 0–2 transverse beams; 2) The pillars of the new species are relatively higher, sturdier, and often irregularly fused, distinguishing them from those in *A. staplesi*; 3) Additionally, the new species possesses support rods, which are absent in *A. staplesi*; 4) The new species lacks endplates in its ventrolateral tube feet, whereas *A. staplesi* possesses endplates.

The genus *Amphigymnas* was newly recorded in the SCS, and the discovery of the new species expands the geographical distribution of this genus.

## Discussion

Until recently, a total of ten genera and 85 accepted species in the family Synallactidae (WoRMS 2024b). Using distribution data from published literature and findings from this study, we examined the geographical distribution and species diversity of synallactids across the world’s oceans, with a particular focus on the tropical Western Pacific. Table 1 presents a summary of the distribution of synallactid species in the Pacific Ocean, with a focus on the tropical Western Pacific.

**Table 1.** Overview of the distribution of synallactid species in the Pacific Ocean and tropical Western Pacific.

Genus	Number of accepted species	Number of species in the Pacific Ocean	Species in the tropical Western Pacific	
			Number	Species
<i>Allopatides</i>	2	1	1	<i>A. corrugatus</i>
<i>Capheira</i>	2	0	0	–
<i>Dendrothuria</i>	2	1	1	<i>D. megalopharynx</i>
<i>Galatheathuria</i>	1	1	1	<i>G. aspera</i>
<i>Paelopatides</i>	21	7	3	<i>P. appendiculata</i> , <i>P. illicitus</i> , and <i>P. ovalis</i>
<i>Pseudothuria</i>	1	0	0	–
<i>Scotothuria</i>	1	0	0	–
<i>Synallactes</i>	27	15	9	<i>S. chuni</i> , <i>S. discoidalis</i> , <i>S. gilberti</i> , <i>S. heteroculus</i> , <i>S. monoculus</i> , <i>S. multivesiculatus</i> , <i>S. nozawai</i> , <i>S. sagamiensis</i> , and <i>S. triradiata</i>
<i>Bathyplores</i>	25	13	9	<i>B. angustus</i> , <i>B. cinctus</i> , <i>B. crebrapapilla</i> , <i>B. dofleinii</i> , <i>B. imperfectus</i> , <i>B. moseleyi</i> , <i>B. natans</i> , <i>B. punctatus</i> , and <i>B. sulcatus</i>
<i>Amphigymnas</i>	3	1	1	<i>A. woodmasoni</i>
Total	85	39	25	–

In summary, more than half of the species within each genus described occur in the Pacific Ocean, with 29 synallactid species (including the four new species described here) identified in the deep water of the tropical Western Pacific. This represents over one-third of all species in the family Synallactidae, highlighting the higher synallactid species richness of this region. However, only three species (i.e., *Synallactes tenuibrachius* sp. nov., *Amphigymnas ganquani* sp. nov., and *Galatheathuria aspera*) have been reported in South China Sea. This underscores the need for further deep-sea biodiversity surveys in the SCS to better understand the diversity, distribution patterns, and ecological characteristics of holothuroid fauna in this underexplored region. Such studies will contribute to global marine biodiversity knowledge, support regional conservation strategies, and inform ecosystem-based management approaches for the tropical Western Pacific.

## Acknowledgments

We are grateful to the crews of R/V Kexue for their work in the collection of the specimens during the survey. We appreciate the scientists of the Department of Marine Organism Taxonomy & Phylogeny, Institute of Oceanology, Chinese Academy of Sciences (IOCAS) for their help in taking photographs of fresh specimens on board.

## Additional information

### Conflict of interest

The authors have declared that no competing interests exist.

### Ethical statement

No ethical statement was reported.

## Funding

This work was supported by the National Natural Science Foundation of China (No. 42376135 and No. 42176114), the National Science Foundation for Distinguished

Young Scholars (42025603), the NSFC Innovative Group Grant (No. 42221005) and the Senior User Project of RV KEXUE (KEXUE2020GZ01), the National Key Research and Development Program of China (2023YFC2809300).

### Author contributions

Yunlu Xiao conceived and designed this project, performed morphological examination and description, conducted molecular analyses, and wrote or reviewed drafts of the paper. Ning Xiao conceived and designed this project, reviewed and edited drafts of the paper and approved the final draft.

### Author ORCIDs

Yunlu Xiao  <https://orcid.org/0009-0005-9787-033X>

### Data availability

All of the data that support the findings of this study are available in the main text.

### References

- Boehlert GW, Genin A (1987) A review of the effects of seamounts on biological processes. In: Keating BH, Fryer P, Batzia R, Boehlert GW (Eds) Seamounts, Islands, and Atolls. American Geophysical Union, Washington DC, 319–334. <https://doi.org/10.1029/GM043p0319>
- Clark MR, Schlacher TA, Rowden AA, Stocks KI, Consalvey M (2012) Science priorities for Seamounts: Research links to conservation and management. PLoS ONE 7(1): e29232. <https://doi.org/10.1371/journal.pone.0029232>
- Conand C (1990) The Fishery Resources of Pacific Island Countries: Holothurians. Food & Agriculture Organization, Rome, 143 pp.
- Fisher WK (1907) The Holothurians of the Hawaiian Islands. United States National Museum, Smithsonian Institute Press, Washington D.C 32: 637–744. <https://doi.org/10.5479/si.00963801.32-1555.637>
- Gebrek AV, Solís-Marín FA, Billett DSM, Rogacheva AV, Tyler PA (2012) Review of the genus *Zygothuria* Perrier, 1898 and the Atlantic group of species of the genus *Mesothuria* Ludwig, 1894 (Synallactidae: Holothuroidea) with description of the new species *Mesothuria milleri* sp. nov. Journal of Natural History 46: 265–348. <https://doi.org/10.1080/00222933.2011.638423>
- Haeckel E (1896) Systematische Phylogenie der Echinodermen. pp. 348–504. In: Systematische Phylogenie der Wirbellosen Thiere (Invertebrata): Zweiter Teil des Entwurfs einer systematischen Stammengeschichte. Reimer, Berlin, 720 pp. <https://doi.org/10.1515/9783111443935>
- Hannington MD, Jonasson IR, Herzig PM, Petersen S (1995) Physical and chemical processes of seafloor mineralization at mid-ocean ridges. In: Humphris SE, Zierenberg RA, Mullineaux LS, Thomson RE (eds) Seafloor hydrothermal systems: physical, chemical, biological, and geological Interactions. Geophysical Monograph 91: 115–157. <https://doi.org/10.1029/GM091p0115>
- Hansen B (1978) *Scotothuria herringi*, a new genus and species of bathypelagic holothurians (Holothurioidea, Aspidochirota, Synallactidae). Steenstrupia 5(4): 33–39.
- Hansen B, Madsen FJ (1956) On two bathypelagic holothurians from the South China Sea, *Glatheathuria* n. g. *aspera* (Théel) and *Enypniastes globosa* n. sp. Galathea Reports 2: 55–60.

- Huang H, Xu S, Li S, Wang X, Guo K, Yan R, Xie W, Yin K (2023) Diversity and Distribution of Harmful Algal Bloom Species from. *Microbiology Spectrum* 11: 1–19. <https://doi.org/10.1128/spectrum.04169-22>
- Iken K, Brey T, Wand U, Voigt J, Junghans P (2001) Food web structure of the benthic community at the Porcupine Abyssal Plain (NE Atlantic): A stable isotope analysis. *Progress in Oceanography* 50: 383–405. [https://doi.org/10.1016/S0079-6611\(01\)00062-3](https://doi.org/10.1016/S0079-6611(01)00062-3)
- Jamieson AJ, Gebruk A, Fujii T, Solan M (2011) Functional effects of the hadal sea cucumber *Elpidia atakama* (Echinodermata: Holothuroidea, Elasipodida) reflect small-scale patterns of resource availability. *Marine Biology* 158: 2695–2703. <https://doi.org/10.1007/s00227-011-1767-7>
- Koehler R, Vaney C (1905) An Account of the Deep-Sea Holothuroidea Collected by the Royal Indian Marine Survey Ship Investigator. The Indian Museum, Calcutta, 1–170. <https://doi.org/10.5962/bhl.title.1730>
- Lee S, Ferse S, Ford A, Wild C, Mangubhai S (2017) Effect of sea cucumber density on the health of reef-flat sediments. Fiji's Sea Cucumber Fishery: Advances in Science for Improved Management. Wildlife Conservation Society.
- Ludwig H (1893) Vorläufiger Bericht über die erbeuteten Holothurien. In: Reports on the Dredging Operations off the West Coast of Central America to the Galapagos, etc., by the U. S. Fish Commission Steamer "Albatross". IV. Bulletin of the Museum of Comparative Zoology at Harvard College 24(4): 105–114.
- Ludwig H (1894) The Holothuroidea. In: Reports on an exploration off the west coasts of Mexico, Central and South America, and off the Galapagos Islands, in charge of Alexander Agassiz, by the U. S. Fish Commission Steamer "Albatross," during 1891, Lieut. Commander Z. L. Tanner, U. S. N., commanding. XII. Memoirs of the Museum of Comparative Zoology at Harvard College 17(3): 1–183.
- Massin C, Hendrickx ME (2010) A new species of deep-water Holothuroidea (Echinodermata) of the genus *Synallactes* from off western Mexico. *Scientia Marina* 74: 599–603. <https://doi.org/10.3989/scimar.2010.74n3599>
- Miller AK, Kerr AM, Paulay G, Reich M, Wilson NG, Carvajal JI, Rouse GW (2017) Molecular phylogeny of extant Holothuroidea (Echinodermata). *Molecular Phylogenetics and Evolution* 111: 110–131. <https://doi.org/10.1016/j.ympev.2017.02.014>
- Morato T, Varkey DA, Damaso C, Machete M, Santos M, Prieto R, Santos RS, Pitcher TJ (2008) Evidence of a seamount effect on aggregating visitors. *Marine Ecology Progress Series* 357: 23–32. <https://doi.org/10.3354/meps07269>
- Morato T, Hoyle SD, Allain V, Nicol SJ (2010) Seamounts are hotspots of pelagic biodiversity in the open ocean. *Proceedings of the National Academy of Sciences of the United States of America* 107(21): 9707–9711. <https://doi.org/10.1073/pnas.0910290107>
- O'Loughlin PM, Ahearn C (2005) A review of pygal-furrowed Synallactidae (Echinodermata: Holothuroidea), with new species from the Antarctic, Atlantic and Pacific oceans. *Memoirs of Museum Victoria* 62: 147–179. <https://doi.org/10.24199/j.mmv.2005.62.5>
- O'Loughlin PM, Mackenzie M, VandenSpiegel D (2013) New sea cucumber species from the seamounts on the Southwest Indian Ocean Ridge (Echinodermata: Holothuroidea: Aspidochirotida, Elasipodida, Dendrochirotida). *Memoirs of Museum Victoria* 70: 37–50. <https://doi.org/10.24199/j.mmv.2013.70.04>
- Östergren H (1896) Zur Kenntnis der Subfamilie Synallactinae unter den Aspidochiroten. *Festschrift für Lilljeborg*, 345–360.
- Pitcher TJ, Bulman C (2007) Raiding the larder: A quantitative evaluation framework and trophic signature for seamount food webs. In: Pitcher TJ, Morato T, Hart PJB, Clark

- MR, Haggan N, Santos RS (Eds) *Seamounts: Ecology, Fisheries, and Conservation*. Blackwell, Oxford, UK, 282–295. <https://doi.org/10.1002/9780470691953.ch14>
- Roberts D, Moore HM, Berges J, Patching JW, Carton MW, Eardly DF (2001) Sediment distribution, hydrolytic enzyme profiles and bacterial activities in the guts of *Oneirophanta mutabilis*, *Psychropotes longicauda* and *Pseudostichopus villosus*: what do they tell us about digestive strategies of abyssal holothurians? *Proceedings in Oceanography* 50: 443–458. [https://doi.org/10.1016/S0079-6611\(01\)00065-9](https://doi.org/10.1016/S0079-6611(01)00065-9)
- Samadi S, Bottan L, Macpherson E, De Forges BR, Boisselier MC (2006) Seamount endemism questioned by the geographic distribution and population genetic structure of marine invertebrates. *Marine Biology* 149: 1463–1475. <https://doi.org/10.1007/s00227-006-0306-4>
- Samyn Y, Vandenspiegel D (2016) Sublittoral and bathyal sea cucumbers (Echinodermata: Holothuroidea) from the Northern Mozambique Channel with description of six new species. *Zootaxa* 4196: 451–497. <https://doi.org/10.11646/zootaxa.4196.4.1>
- Sars M (1868) Om Afbildninger af nogle af hans son I forrige Aar ved Lofoten fundne Echinodermer og Coelenterater. *Forhandlinger Videnskabs Selskabet, Christiania*. 1867: 19–23.
- Solís-Marín FA (2003) *Molecular Phylogeny, Systematics and Biology of the Holothurian Family Synallactidae*. Ph.D. thesis, University of Southampton, 356 pp.
- Solís-Marín FA (2005) *Synallactes laguardai*, a new species of sea cucumber from South Africa (Echinodermata: Holothuroidea: Synallactidae). *Proceedings of the Biological Society of Washington* 118: 570–575. [https://doi.org/10.2988/0006-324X\(2005\)118\[570:SLANSO\]2.0.CO;2](https://doi.org/10.2988/0006-324X(2005)118[570:SLANSO]2.0.CO;2)
- Solís-Marín FA, Caballero Ochoa A, Conejeros-Vargas C (2024) *Synallactes mcdanieli* sp. nov., a new species of sea cucumber from British Columbia, Canada and the Gulf of Alaska, USA (Holothuroidea, Synallactida). *Biodiversity Data Journal* 12: e124603. <https://doi.org/10.3897/BDJ.12.e124603>
- Thandar AS (2008) Additions to the holothuroid fauna of the southern African temperate faunistic provinces, with descriptions of new species. *Zootaxa* 1697: 1–57. <https://doi.org/10.11646/zootaxa.1697.1.1>
- Théel H (1882) Report on the Holothuroidea dredged by H.M.S. 'Challenger' during the years 1873–76. Part I. Report on the Scientific Results of the Voyage of H.M.S. Challenger during the years 1873–1876. *Zoology* 4: 1–176.
- Théel H (1886) Report on the Holothuroidea collected by H.M.S. Challenger during the Years 1873–76. Part II. Report on the Scientific Results of the Voyage of H.M.S. Challenger during the years 1873–76. *Zoology* 14: 1–290.
- Wagner D, Friedlander AM, Pyle RL, Brooks CM, Gjerde KM, Wilhelm TA (2020) Coral reefs of the high seas: hidden biodiversity hotspots in need of protection. *Frontiers in Marine Science* 7: 2296–7745. <https://doi.org/10.3389/fmars.2020.567428>
- Walsh JHT (1891) List of deep-sea holothurians collected during seasons 1887 to 1891, with description of new species. *Natural History Notes from HM. Indian Survey Steamer INVESTIGATOR, Commander RF. Hoskyn, RN. commanding. No. 24. Journal of the Asiatic Society of Bengal* 60: 197–204.
- Witbaard R, Duineveld G, Kok A, Van der Weele J, Berghuis EM (2001) The response of *Oneirophanta mutabilis* (Holothuroidea) to the seasonal deposition of phytopigments at the Porcupine Abyssal Plain in the Northeast Atlantic. *Progress in oceanography* 50(1–4): 423–441. [https://doi.org/10.1016/S0079-6611\(01\)00064-7](https://doi.org/10.1016/S0079-6611(01)00064-7)
- Worm B, Lotze HK, Myers RA (2003) Predator diversity hotspots in the blue ocean. *Proceedings of the National Academy of Sciences* 100(17): 9884–9888. <https://doi.org/10.1073/pnas.1333941100>

- WoRMS (2024a) Holothuroidea. <https://www.marinespecies.org/aphia.php?p=taxdetails&id=123083> [accessed August 2024]
- WoRMS (2024b) Synallactidae Ludwig, 1894. <https://www.marinespecies.org/aphia.php?p=taxdetails&id=123185> [accessed September 2024]
- Xu K (2021) Exploring seamount ecosystems and biodiversity in the tropical Western Pacific Ocean. *Journal of Oceanology and Limnology* 39: 1585–1590. <https://doi.org/10.1007/s00343-021-1585-9>
- Yesson C, Letessier TB, Nimmo-Smith A, Hosegood P, Brierley AS, Hardouin M, Proud R (2021) Improved bathymetry leads to > 4000 new seamount predictions in the global ocean—but beware of phantom seamounts! *UCL Open Environment*, 4: 03. <https://doi.org/10.14324/111.444/ucloe.000030>

# The genus *Liocanthyrus* Guignot, 1957 (Coleoptera, Noteridae) in Argentina: new records and larval morphology

Juan I. Urcola<sup>1,2</sup>, Mario E. Toledo<sup>3</sup>, Stephen M. Baca<sup>4</sup>, Mariano C. Michat<sup>1,2</sup>

<sup>1</sup> Laboratory of Entomology, Department of Biodiversity and Experimental Biology, Faculty of Exact and Natural Sciences, University of Buenos Aires, Buenos Aires, Argentina

<sup>2</sup> Institute of Biodiversity and Experimental and Applied Biology (IBBEA), CONICET-University of Buenos Aires, Buenos Aires, Argentina

<sup>3</sup> Department of Sustainable Crop Production (DI.PRO.VE.S.), Università Cattolica del Sacro Cuore, Piacenza, Italy

<sup>4</sup> Department of Entomology, LSU Agricultural Center, 404 Life Sciences Building, Baton Rouge, Louisiana 70803, USA

Corresponding author: Mariano C. Michat ([marianoide@gmail.com](mailto:marianoide@gmail.com))

## Abstract

The genus *Liocanthyrus* Guignot, 1957 is formally reported from Argentina since its first mention in an unpublished work more than 40 years ago. A single species, *L. nanops* Baca et al., 2014, is recognised, with few records in the northeast part of the country, suggesting that these may represent the southern distributional limit for the genus. The habitat, a floodplain stream in the southern Atlantic Forest, is described, where both adults and larvae were collected, as well as co-occurring taxa. The first- and third-instar larvae of *L. nanops* are described for the first time. The first instar, which was unknown for the genus, gives the chance to document its primary chaetotaxy in detail. This species presents two posterodorsal projections on the abdominal segment VIII, which represent elongations of the membranous posterolateral areas of segment VIII, where setae AB8 and AB14 are usually inserted; these two setae accompany the elongation of these regions and are therefore inserted on the projections. The projections are shared with the previously described larvae of *L. clayae* (J. Balfour-Browne, 1969) but not with those of other noterid genera, and, thus, supports this unique feature as diagnostic of *Liocanthyrus*.

**Key words:** Burrowing water beetle, chaetotaxy, immatures, South America, taxonomy



Academic editor: Christopher Majka

Received: 17 December 2024

Accepted: 18 February 2025

Published: 13 March 2025

ZooBank: <https://zoobank.org/DAB12BD6-E9D1-4B57-89DB-2D8EC06A6ED2>

**Citation:** Urcola JI, Toledo ME, Baca SM, Michat MC (2025) The genus *Liocanthyrus* Guignot, 1957 (Coleoptera, Noteridae) in Argentina: new records and larval morphology. ZooKeys 1231: 371–384. <https://doi.org/10.3897/zookeys.1231.144746>

Copyright: © Juan I. Urcola et al.  
This is an open access article distributed under terms of the Creative Commons Attribution License (Attribution 4.0 International – CC BY 4.0).

## Introduction

The burrowing water beetle genus *Liocanthyrus* Guignot, 1957 currently comprises 11 medium-sized species (adult length 2.7–3.3 mm) widely distributed across the Neotropical Region, with records from Venezuela, Guyana, Suriname, French Guiana, Brazil, and Paraguay (Baca et al. 2014; Guimarães and Ferreira-Jr 2015; García et al. 2018). Unlike other noterid genera, *Liocanthyrus* occurs mainly in lotic habitats or those associated with moving water, such as pools near waterfalls (Baca et al. 2014). Morphologically, adults of this genus are characterized by the following combination of characters: (1) prosternal process very broad and truncate with a slight posteromedial projection, (2) anteroapical angle of metafemur with close, linear series of long setae, (3) pronotal margins smooth and pronotal bead broad, (4) posterior metatibial spur smooth,

not serrate, and (5) female genitalia bearing short laterotergites extending posteriorly beyond bases of gonocoxae (Baca et al. 2014). Recently, the larva of a species of *Liocanthydrus* (*L. clayae* (J. Balfour-Browne, 1969)) was described for the first time (Urcola et al. 2021), and it can be easily distinguished from other known noterid genera by the presence of two posterodorsal projections on the last abdominal segment, a unique and conspicuous characteristic that facilitates differentiation from other noterids from which the larvae are known: *Canthydrus* Sharp, 1882, *Hydrocanthus* Say, 1823, *Neohydrocoptus* Satô, 1972, *Noterus* Clairville, 1806, *Phreatodytes* Uéno, 1957, *Suphis* Aubé, 1836, *Suphisellus* Crotch, 1872, *Sternocanthus* (Guignot, 1948), and *Synchortus* Sharp, 1880 (e.g. Uéno 1957; Bertrand 1972; Watts 2002; Dettner 2016; Urcola et al. 2019, 2020; Urcola and Michat 2023). However, as the first instar was not available, primary chaetotaxy could not be described and remains unknown for the genus.

In Argentina, seven noterid genera have been reported: *Hydrocanthus*, *Prionothydrus* Gómez & Miller, 2013, *Mesonoterus* Sharp, 1882, *Notomicrus* Sharp, 1882, *Suphis*, *Suphisellus*, and *Liocanthydrus* (Urcola et al. 2024). The latter genus, however, was only mentioned in a doctoral thesis (Grosso 1979), where adult morphology of a single species was documented. In that study, Grosso reported the collection of 21 specimens in Formosa Province, and identified them as *Canthydrus octoguttatus* Zimmermann, 1921 (*Liocanthydrus*, by that time considered a subgenus within *Canthydrus*, was elevated to genus rank by Baca et al. 2014). Here, we report the presence of *L. nanops* Baca et al., 2014 in the country, and describe the larvae including primary chaetotaxy for the first time for the genus.

## Material and methods

### Material examined

One instar I and one instar III larvae of *L. nanops* were collected in association with adults at Iguazú National Park (Misiones Province, Argentina) in January 2024. The association of adults with juveniles is firmly established as no other *Liocanthydrus* species was present in the stream. *Suphisellus* and *Hydrocanthus*, the only other noterid genera found in that site, have the larvae described and can be easily ruled out by several characters (Urcola et al. 2020; Urcola and Michat 2023). Adults and larvae were collected from a stream floodplain using a dip net, preserved in 96% ethanol, and taken to the Laboratory of Entomology, Buenos Aires, Argentina (LEBA) for study. Additional adults from a previous collecting event in the same area (c. 1997) were found housed in LEBA and are here identified as *L. nanops*. All collected and examined material is deposited in LEBA.

### Adult morphology

As the presence of *L. octoguttatus* in Argentina is put into doubt in this paper (see below), and considering that this was the only known record of the genus in the country, we believe it prudent to provide some measurements and illustrate the habitus and male genitalia of the specimens we collected.

Male genitalia were dissected, cleared in lactic acid, mounted temporarily on slides with gel alcohol for observation, and then stored together with the

specimens. Terminology of male genitalia follows Miller and Nilsson (2003) and Toledo and Negri (2024).

Habitus photographs were taken using a Nikon D800e digital camera equipped with Nikon AFS VR Micro-NIKKOR 105 mm f/2.8G IF-ED and Raynox MSN-202 lenses. Photographs of male genitalia were generated with a Leica MZ6 stereomicroscope (with Leica DMC2900 camera attached) or with an Olympus CX41 microscope (with Olympus LC30 camera attached). Images were processed using Helicon Focus 6.7.1 Pro. Drawings of male genitalia were made by tracing over photographs using the image editing software Adobe Illustrator (CC 2019).

Measurements were taken using a Leica MZ6 stereomicroscope equipped with an ocular micrometer: total length (TL), greatest width (GW), greatest width of head (HW), distance between eyes (EW), anterior pronotal width, across anterolateral angles (PNWant), posterior pronotal width, across posterolateral angles (PNWpost), total length of prosternum plus noterid platform at midline (TLVP; prosternum, metaventricle, metacoxae). The ratios TL/GW, HW/EW and PNWpost/PNWant were also calculated.

### Larval morphology

Larvae were cleared in lactic acid, dissected, and mounted on glass slides with polyvinyl-lacto-glycerol. Observations (at magnifications up to 1000×) and drawings were made using an Olympus CX41 compound microscope equipped with a camera lucida. Drawings were scanned and digitally edited using Adobe Illustrator. The methods and terms used herein largely follow those employed in a previous study of the larval morphology and chaetotaxy of the genus *Suphis* (Urcola et al. 2019). The reader is referred to that work for a complete list and additional explanations of the terms used in the present study.

## Results

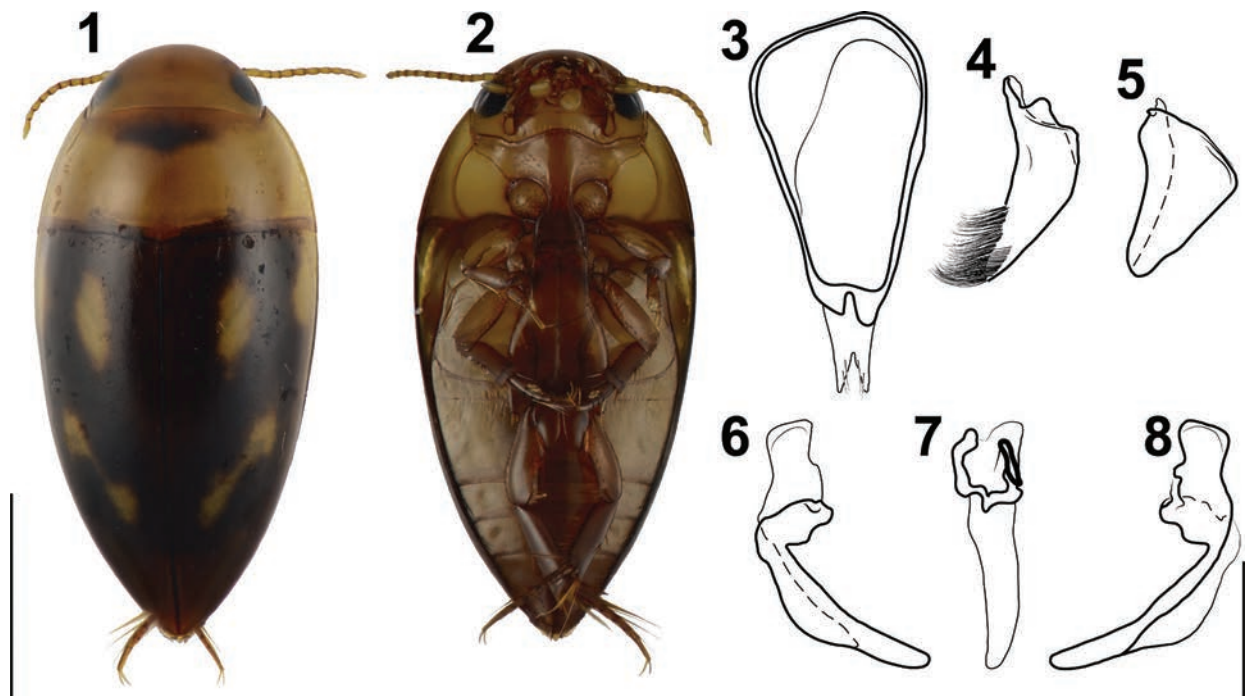
### *Liocanthyrus nanops* Baca et al., 2014

Figs 1–12, 16, 18–37, Tables 1, 2

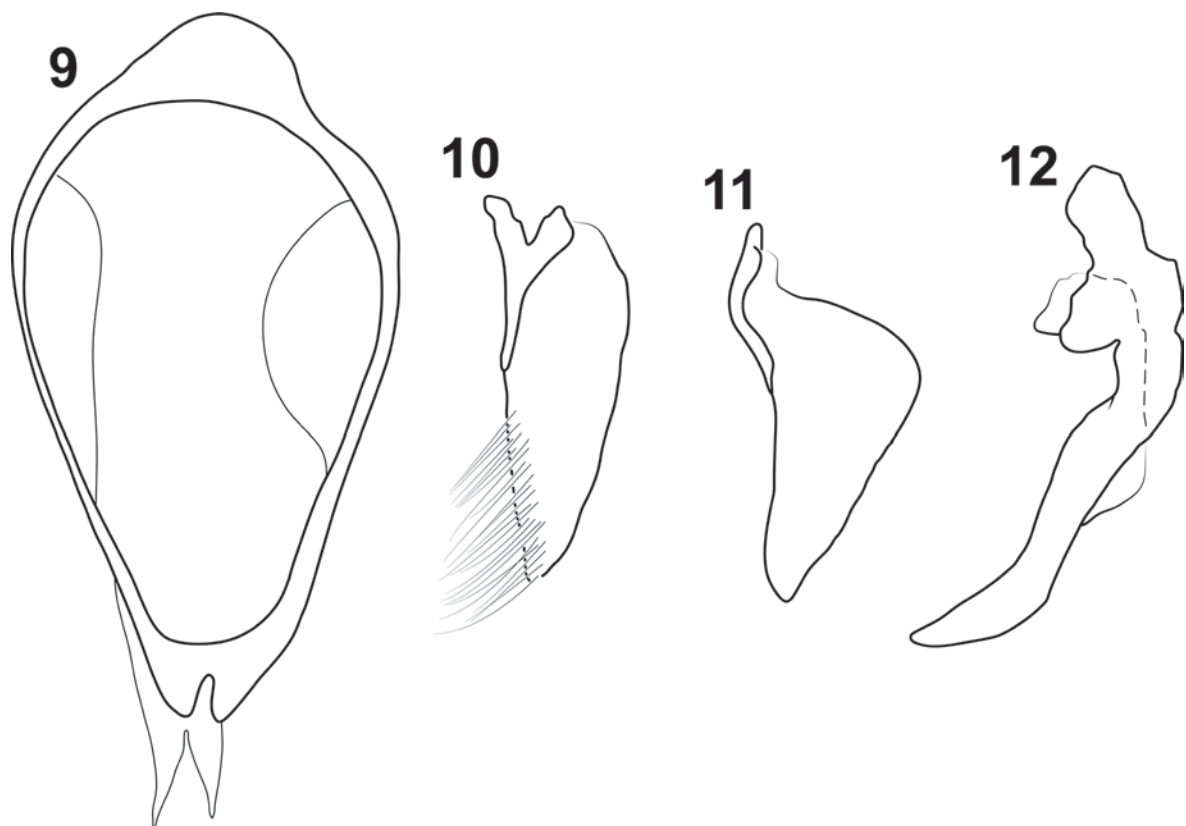
**Material examined.** ARGENTINA – Misiones Province: 2 ♂ and 4 ♀, Iguazú National Park, 25°40'S, 54°27'W, 27.IX.1997, López Ruf leg. (LEBA) • 1 larva of instar III and 19 adults, Iguazú National Park, Daniel "Pupi" Somay bird observatory, 25°42'54"S, 54°26'54"W, alt. 197 m a.s.l., 9.I.2024, Urcola leg. (LEBA) • 1 larva of instar I and 18 adults, same data except 10.I.2024 (LEBA).

**Measurements.** TL = 2.8–3.10 mm, mean = 2.95 mm; GW = 1.35–1.50 mm, mean = 1.4 mm; TL/GW = 2.0–2.2 mm, mean = 2.1 mm; HW = 0.85–0.95 mm, mean = 0.9 mm; EW = 0.5–0.65 mm, mean = 0.55 mm; HW/EW = 1.5–1.7 mm, mean = 1.55 mm; PNWant = 0.85–1.0 mm, mean = 0.95 mm; PNWpost = 1.3–1.5 mm, mean = 1.35 mm; PNWpost/PNWant = 1.4–1.5 mm, mean = 1.45 mm; TLVP = 1.15–1.3 mm, mean = 1.2 mm.

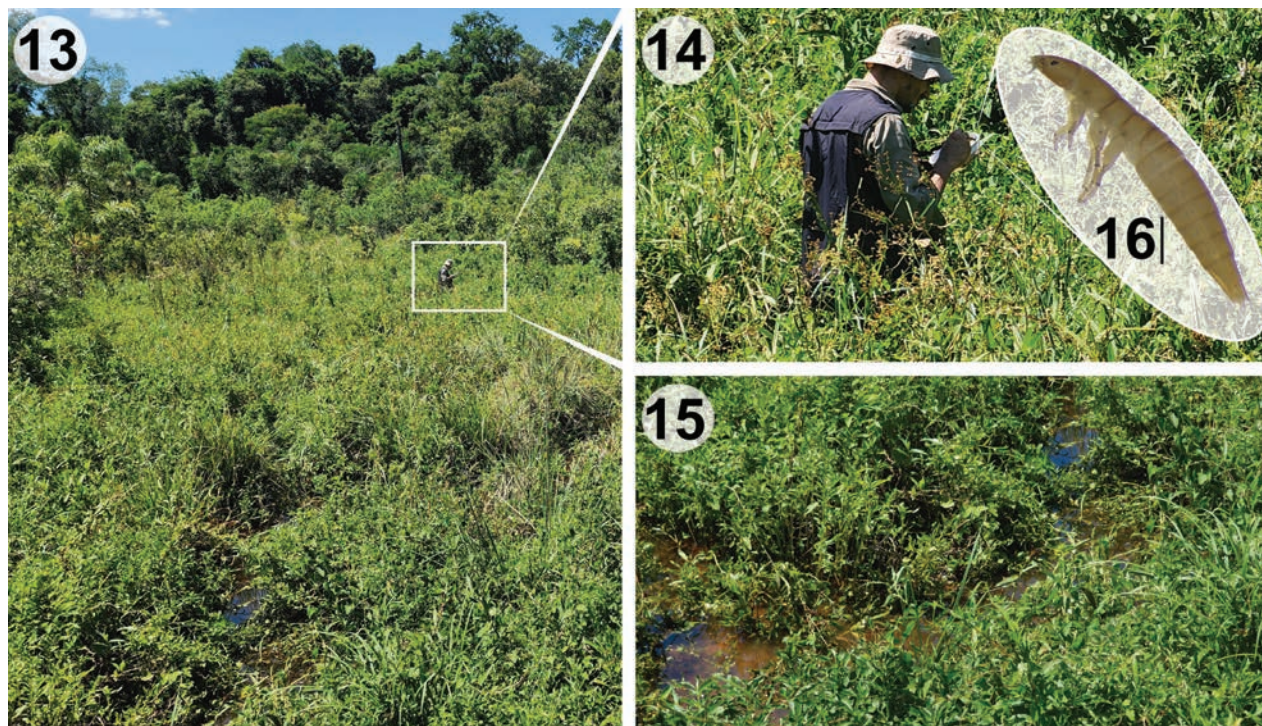
**Variation in adult morphology.** Similar to what was reported by Baca et al. (2014), the specimens examined here show considerable variation in color. Many of the specimens exhibit a yellow head and pronotum, whereas in others these parts are reddish brown. The dark macula on the anteromedial region



Figures 1–8. Habitus (1, 2) and genitalia (3–8) of *Liocanthyrus nanops* Baca et al., 2014, male from Argentina, Misiones Province (LEBA) 1 dorsal aspect 2 ventral aspect 3 segment IX, right lateral aspect 4 right lateral lobe, right lateral aspect 5 left lateral lobe, right lateral aspect 6 median lobe, left lateral aspect 7 median lobe, dorsal aspect 8 median lobe, right lateral aspect. Scale bars: 1.00 mm (1, 2); 0.25 mm (3–8).



Figures 9–12. Male genitalia of *Liocanthyrus nanops* Baca et al., 2014, modified from drawings in Grosso (1979) 9 segment IX, right lateral aspect 10 right lateral lobe, right lateral aspect 11 left lateral lobe, right lateral aspect 12 median lobe, right lateral aspect. Scale bar: 0.5 mm.



Figures 13–16. Habitat of *Liocanthyrus nanops* Baca et al., 2014, Iguazú NP, Misiones Province, Argentina **13** general view of the stream's flooding site **14** collecting of beetles **15** details of the stream **16** instar III larva of *L. nanops*. Scale bar: 0.5 mm.

of the pronotum (Fig. 1) is absent in some individuals. Most of the specimens have dark elytra with clearly visible yellow spots (Fig. 1), while in others the elytra are dark reddish brown and the spots are only slightly lighter. The specimens collected in 1997 have a reddish-brown head and pronotum, the latter lacking the dark anteromedial macula, and the elytra are slightly darker with the spots barely visible (similar in color to the head and pronotum). However, examination of the aedeagus revealed the same diagnostic characters as reported by Baca et al. (2014) and the other specimens collected here. Finally, the two males collected in 1997 have the anterodorsal margin of sternite IX widened, similar to that reported by Grosso (1979) for specimens identified as *L. octoguttatus*. However, we observed that this character is variable in the rest of the material examined, with this widening absent in most specimens (Fig. 3).

**Remarks.** Based on Grosso's (1979) redescription and drawings of the male genitalia of the specimens alleged to be *L. octoguttatus* (Figs 9–12, modified from original drawings), we can observe that the left lateral lobe has a well-projected distal angle (Fig. 11). The only known species of *Liocanthyrus* in which the left lateral lobe has this shape is *L. nanops* (Baca et al. 2014) (Fig. 5), which is also the only species distributed near the area where the specimens studied by Grosso were collected (Fig. 17). This evidence, summed to the shape of the apex of the median lobe in lateral view (Fig. 12) led us to conclude that the specimens studied by Grosso belong to *L. nanops*. It should be noted that, when Grosso identified his material, *L. nanops* had not yet been described. Grosso likely relied on Zimmermann's (1921) treatment of *L. octoguttatus*, which lacks a description of the male genitalia (a crucial feature to recognize that it belongs to a distinct species given the very similar external appearance of both species).

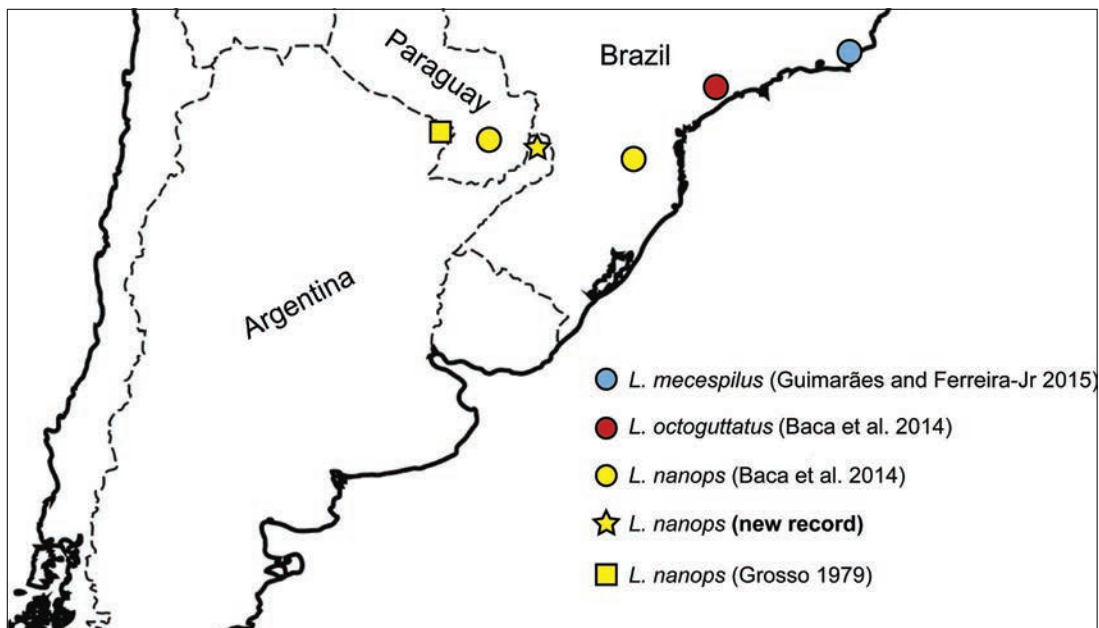
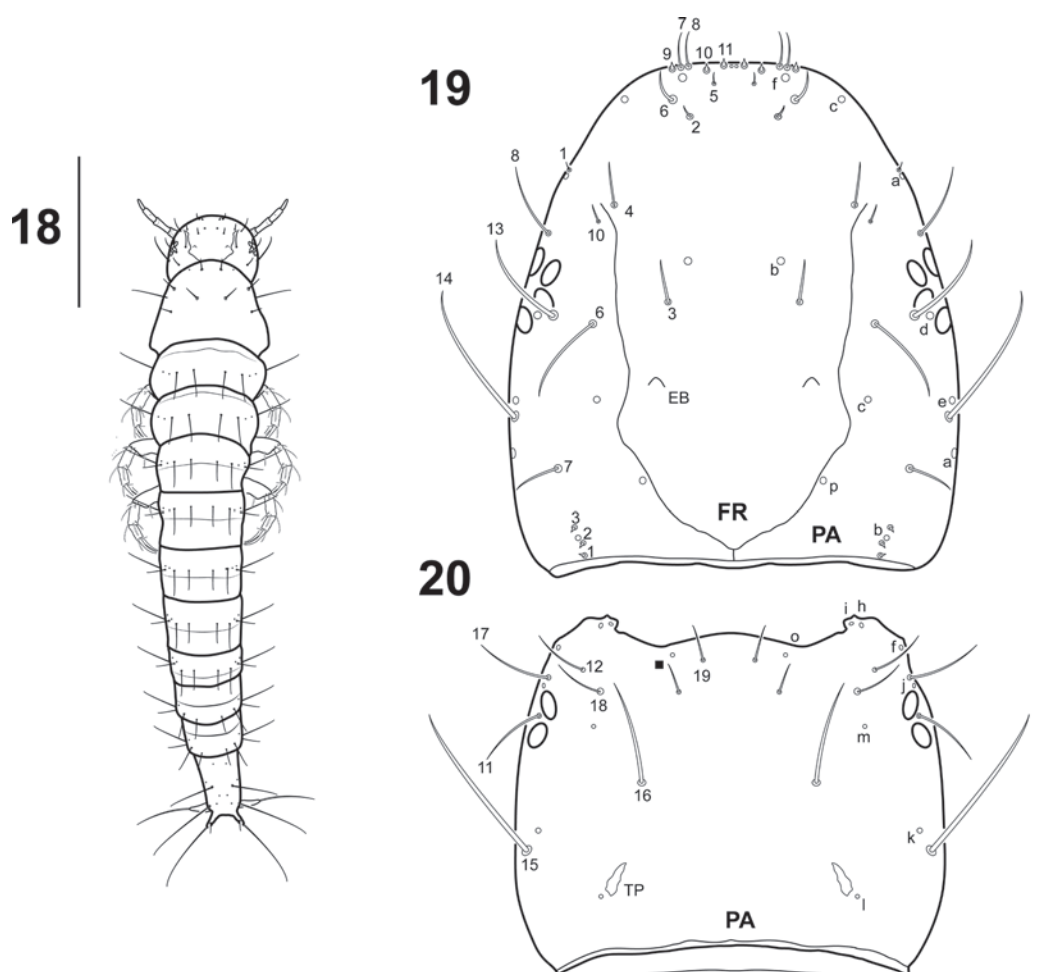
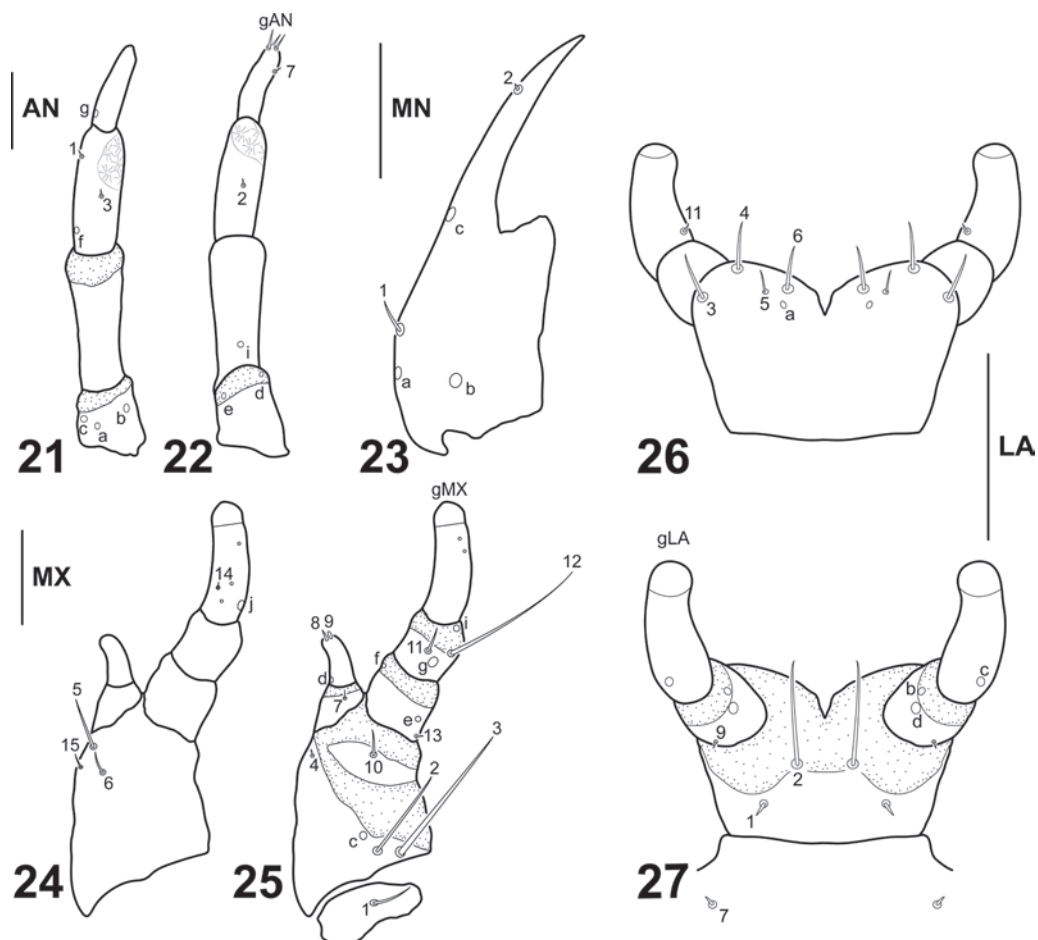


Figure 17. Known distributional data for the southernmost *Liocanthyrus* species with references of records.



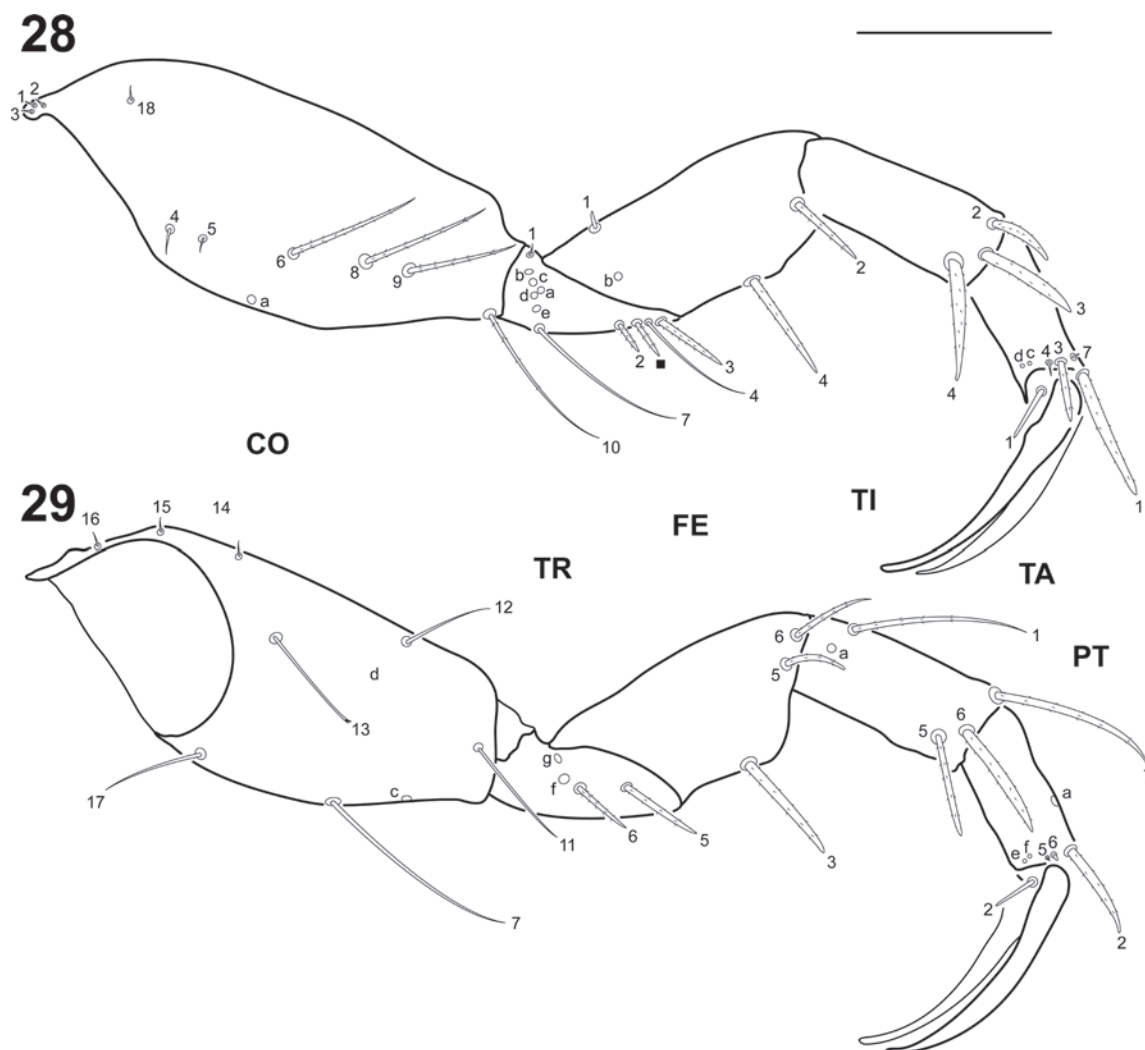
Figures 18–20. *Liocanthyrus nanops* Baca et al., 2014, instar I **18** habitus, dorsal aspect **19** cephalic capsule, dorsal aspect **20** cephalic capsule, ventral aspect. Numbers and lowercase letters indicate primary setae and pores, respectively. Solid square indicates additional seta. EB: egg burster, FR: frontoclypeus, PA: parietal, TP: tentorial pit. Scale bars: 0.50 mm (**18**); 0.10 mm (**19, 20**).



Figures 21–27. *Liocanthyrus nanops* Baca et al., 2014, instar I **21** left antenna, dorsal aspect **22** right antenna, ventral aspect **23** left mandible, dorsal aspect **24** right maxilla, dorsal aspect **25** left maxilla, ventral aspect **26** labium, dorsal aspect **27** labium, ventral aspect. Numbers and lowercase letters indicate primary setae and pores, respectively. AN: antenna, LA: labium, MN: mandible, MX: maxilla. Scale bars: 0.04 mm.

Table 1. Measurements and ratios for the larval instars of *Liocanthyrus nanops* Baca et al. 2014 ( $n = 1$ ).

Measure	Instar I	Instar III	Measure	Instar I	Instar III
TL (mm)	1.97	3.51	MP1/MP3	0.50	0.69
MW (mm)	0.38	0.63	MP2/MP3	0.60	0.62
HL (mm)	0.34	0.56	MP/LP	2.10	1.20
HW (mm)	0.31	0.56	LP1/LP2	0.67	0.67
FRL (mm)	0.34	0.54	L3 (mm)	0.74	1.27
OCW (mm)	0.25	0.51	L3/L1	1.25	1.27
HL/HW	1.10	1.00	L3/L2	1.09	1.10
HW/OCW	1.24	1.08	L3/HW	2.37	2.31
COL/HL	0.02	0.02	CO/FE (L3)	1.85	1.70
FRL/HL	0.99	0.98	TI/FE (L3)	0.72	0.63
A/HW	0.60	0.53	TA/FE (L3)	0.57	0.44
A1/A3	0.63	0.59	CL/TA (L3)	1.38	1.44
A2/A3	1.05	1.29	LAS (mm)	0.27	0.70
A4/A3	0.73	0.53	LAS/HW	0.87	1.26
MNL/MNW	3.25	2.53	U (mm)	0.13	0.17
MNL/HL	0.38	0.35	U/LAS	0.48	0.25
A/MP	1.79	1.93	U/HW	0.42	0.31
GA/MP1	1.20	1.00			



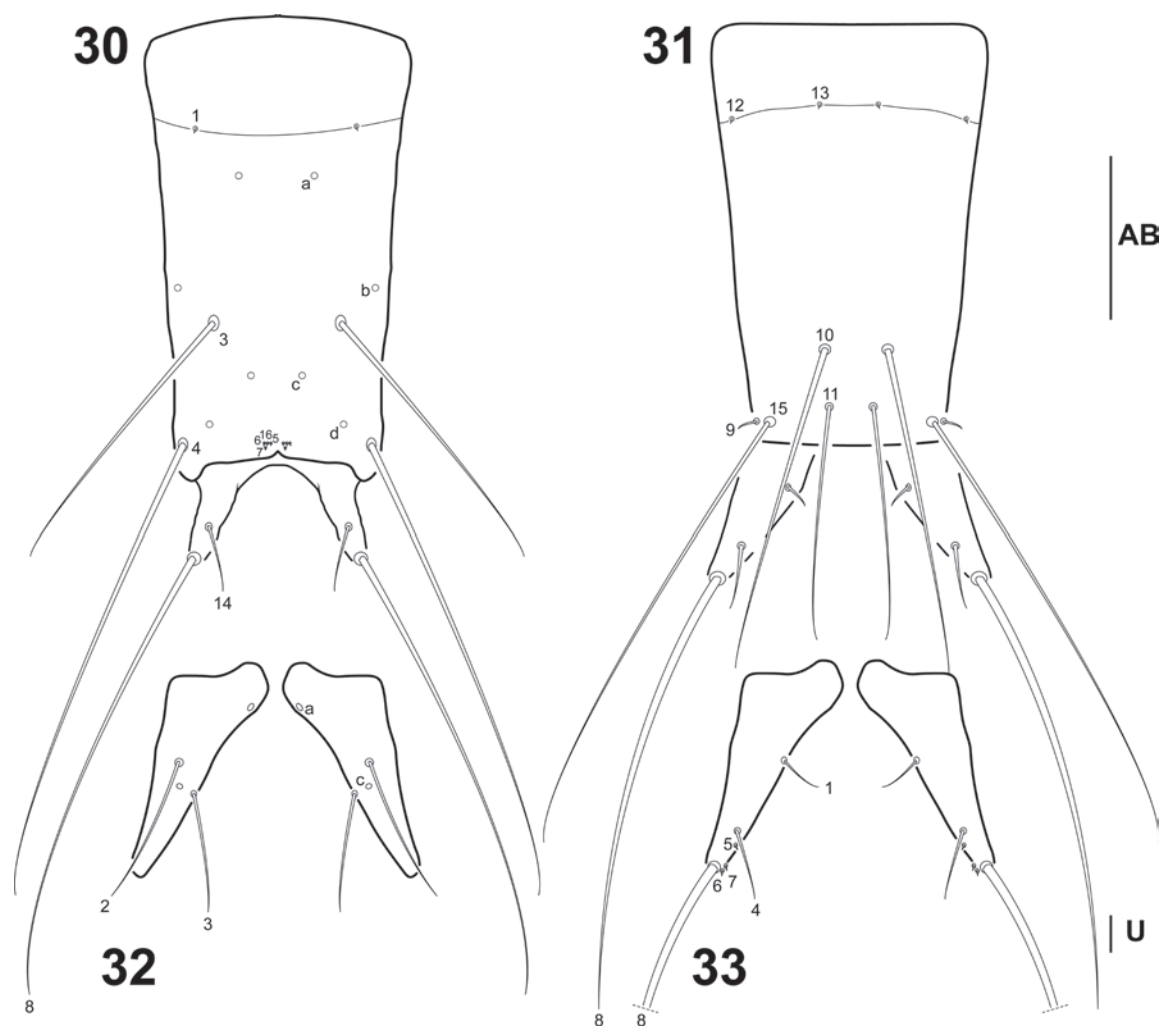
**Figures 28–29.** *Liocanthyrus nanops* Baca et al., 2014, instar I **28** left metathoracic leg, anterior aspect **29** right metathoracic leg, posterior aspect. Numbers and lowercase letters indicate primary setae and pores respectively. Solid square indicates additional seta. CO: coxa, FE: femur, PT: pretarsus, TA: tarsus, TI: tibia, TR: trochanter. Scale bar: 0.10 mm.

**Table 2.** Number and position of secondary setae on the legs of larvae of *Liocanthyrus nanops* Baca et al. 2014. Numbers between slash marks refer to pro-, meso-, and metathoracic leg, respectively. A = anterior, PD = posterodorsal, PV = posteroventral; Total = total number of secondary setae on the article (i.e., excluding primary setae) ( $n = 1$ ).

Article	Position	Instar III
Coxa	A	0 / 2 / 2
	PD	1 / 1 / 1
	PV	0 / 1 / 1
	Total	1 / 4 / 4

**Habitat and co-occurring taxa.** Adults and larvae of *L. nanops* were collected in a stream floodplain with other noterid species: *Hydrocanthus socius* Sahlberg, 1844, *Suphisellus balzani* (Régimbart, 1889), and *S. rufipes* (Sharp, 1882). The sampling site was mostly exposed to sunlight, had a muddy bottom, shallow depth, slow current, cool water, and abundant emergent vegetation (Figs 13–15).

**Distribution.** Argentina (Formosa, Misiones) (new record), Brazil, and Paraguay (Fig. 17).



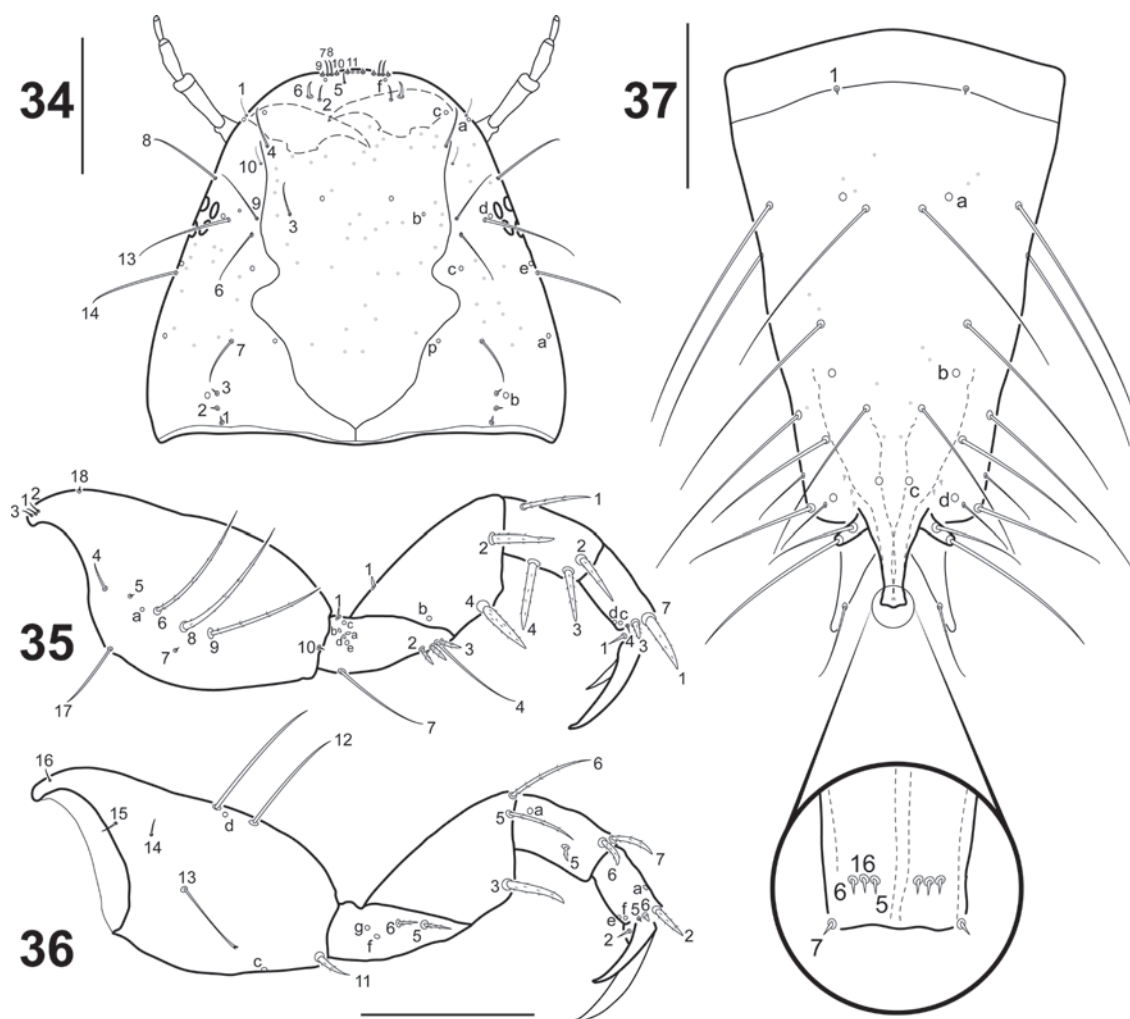
**Figures 30–33.** *Liocanthyrus nanops* Baca et al., 2014, instar I **30** abdominal segment VIII, dorsal aspect **31** abdominal segment VIII and urogomphi, ventral aspect **32** urogomphi, dorsal aspect **33** urogomphi, ventral aspect. Numbers and lowercase letters indicate primary setae and pores, respectively. AB: abdominal segment VIII, UR: urogomphus. Scale bars: 0.10 mm (**30, 31**); 0.02 mm (**32, 33**).

#### Description of larva. Instar I (Figs 18–33).

**Color.** Entirely testaceous.

**Body.** Elongate, nearly parallel sided (Fig. 18). Measurements and ratios that characterize the body shape are given in Table 1.

**Head.** Prognathous; cephalic capsule (Figs 19, 20) slightly longer than broad; maximum width posterior to stemmata; slightly narrowed posteriorly; occipital foramen large; coronal suture very short; ecdysial suture U-shaped; tentorial pits visible postero-ventrally, well separated from each other and from occipital foramen; six lateral stemmata arranged in two curved vertical rows at each side. Frontoclypeus elongate, roughly subovate, anterior margin rounded, with two spine-like egg bursters on basal third. **Antenna** (Figs 21, 22). Short, robust, shorter than maximum head width, composed of four antennomeres; A2 and A3 longest, subequal; A3 with a rugged area on distal portion; A4 approximately 3/4 length of A3; A1 shortest. **Mandible** (Fig. 23). Symmetrical, short, basal half broad, inner margin with strong subrectangular process, distal half slender, curved inwards, narrowing to pointed apex, inner margin smooth. **Maxilla** (Figs 24, 25). Cardo small, suboval;



**Figures 34–37.** *Liocanthyrus nanops* Baca et al., 2014, instar III **34** head, dorsal aspect **35** left prothoracic leg, anterior aspect **36** right prothoracic leg, posterior aspect **37** abdominal segment VIII, dorsal aspect. Numbers and lowercase letters indicate primary setae and pores, respectively (some setae on abdominal segment VIII could not be identified). Scale bars: 0.20 mm.

stipes well developed, subtrapezoidal, bearing a galea on distal inner margin and a palpus on distal outer margin; galea well developed, composed of two galeomeres, GA2 more slender and subequal in length to GA1; palpifer not clearly differentiated from stipes, more evident in ventral view; palpus short, robust, composed of three palpomeres, MP1 shortest, MP3 longest. **Labium** (Figs 26, 27). Prementum well developed, subrectangular, somewhat broader than long, anterior margin narrowly indented medially; palpus short, robust, composed of two palpomeres, LP2 longer than LP1.

**Thorax.** Terga fully sclerotised, convex (Fig. 18); pronotum about as long as meso- and metanotum combined, meso- and metanotum subequal in length, approximately as wide as pronotum; protergite subrectangular, lateral margins rounded, more developed than meso- and metatergite; meso- and metatergite with anterotransverse carina; ecdysial line absent. **Legs** (Figs 28, 29). Short, robust, composed of six articles, L1 shortest, L3 longest; coxa broad, elongate, trochanter lacking annulus, femur, tibia and tarsus short, subcylindrical, pretarsus with two long, slender, slightly curved claws, posterior claw slightly shorter than anterior claw.

**Abdomen.** Eight-segmented (Fig. 18); segments I–VIII completely sclerotised, ring-like, progressively narrowing to apex, with anterotransverse carina; segment VIII (Figs 30, 31) the longest and narrowest, with two terminal dorsal projections, lacking a U-shaped wavy membranous area ventrally, contiguous to urogomphi; siphon absent. **Urogomphi** (Figs 32, 33). Short, cylindrical, visible in dorsal view (Fig. 18), not fused to each other.

**Chaetotaxy.** Similar to that of *L. clayae* (see Urcola et al. 2021) except for the following features: seta FR1 very short (Fig. 19); seta PA9 absent (Fig. 19); seta AN1 inserted more distally (Fig. 21); seta MN1 short (Fig. 23); MP3 with several minute sensilla on surface (Figs 24, 25); pore URa located on dorsal surface (Fig. 32). Setae on abdominal segment VIII were not named in instar II of *L. clayae* due to the presence of secondary setae. Therefore, they are detailed here for *L. nanops*: dorsal surface of segment VIII with one seta (AB1) on basal region, one seta (AB3) on distal third and one long (AB4) and four minute (AB5, AB6, AB7, AB16) setae apically (Fig. 30); each terminal dorsal projection with one short medial seta (AB14) and one long apical seta (AB8); ventral surface of segment VIII with two setae (AB12, AB13) on basal region and four setae (AB9, AB10, AB11, B15) on distal region (Fig. 31).

**Instar III** (Figs 16, 34–37)

As for instar I except for the following features:

**Body.** Measurements and ratios that characterise body shape are shown in Table 1.

**Head.** Egg bursters absent; A2 longer than A3; A4 shortest, approximately 1/2 length of A3; mandible more robust, process less prominent (Fig. 34).

**Abdomen.** Siphon relatively long, slender, apex truncated (Fig. 37).

**Chaetotaxy.** Frontoclypeus with 14–21 minute secondary setae on anterior half and 3–4 minute secondary setae on posterior half; dorsal surface of parietal with seta PA9 present (inserted close to seta PA6), 0–4 minute secondary setae on anterior portion and 10–13 minute secondary setae on posterior portion (Fig. 34); ventral surface of parietal with 10–13 minute secondary setae on anterior half and 1–2 minute secondary setae on posterior half; secondary leg setation detailed in Table 2 and Figs 35, 36; abdominal segments I–VII with several secondary setae; dorsal surface of abdominal segment VIII (Fig. 37) with three elongate hair-like secondary setae and 2–3 minute secondary setae on anterior portion, 2–3 minute secondary setae on medial portion, and five hair like-like secondary seta and 4–5 minute secondary setae on posterior portion; ventral surface of abdominal segment VIII with two elongate hair-like secondary setae on anterior portion, one elongate hair-like secondary seta on medial portion, and one short and one long secondary setae on posterior portion.

**Remarks.** When comparing the first and third instars of *L. nanops* with the supposedly third instar of *L. clayae* (Urcola et al. 2021), we can conclude that the larva of this latter species is actually a second instar. This conclusion is based on the following evidence: the head of the larva of *L. clayae* (as expressed in the head width) exhibits an intermediate size between the first and third instars of *L. nanops*; the mandibles in *L. clayae* are not as robust as those of the third instar of *L. nanops*; and the siphon in *L. clayae* is more developed than that of the first instar of *L. nanops* but not as strongly developed as that of the third instar of this species. Regarding chaetotaxy, seta PA9 is absent on the parietal of the first instar of *L. nanops*. This conspicu-

ous sensillum, however, is present in the third instar of this species (Fig. 34), as well as in all noterid larvae known in detail (e.g. Urcola et al. 2019, 2020, 2021). Since we examined only a single specimen of each instar of *L. nanops*, we prefer not to consider the absence of PA9 in instar I as a diagnostic character for the species until more material can be studied.

## Discussion

In this study we document the finding of *L. nanops* in Argentina and thus formally report the presence of the genus *Liocanthyrus* in the country after its first mention in an unpublished work more than 40 years ago (Grosso 1979). We also postulate that the only series of specimens previously known from the country, identified as *L. octoguttatus* (Grosso 1979), is conspecific with *L. nanops*, thus excluding *L. octoguttatus* from the Argentine fauna. These findings significantly enhance our understanding of the distribution of this genus in the southern limit of its range. Additional samplings, however, may reveal the presence of this genus in other areas of northeastern Argentina and southern Brazil and Paraguay.

The larvae of *L. nanops* are described here for the first time, raising to two the number of species of *Liocanthyrus* with larvae known in detail. Even though only a single specimen of each instar I and III was examined, we compared both the morphometric and chaetotaxic features with those of the second instar of *L. clayae* (misidentified as third instar in Urcola et al. 2021). The larvae of both species share the following characteristics: (1) an elongated body, (2) the posterior tentorial pits not contiguous with the occipital foramen, (3) the seta AN7 inserted distally on antennomere 4, (4) the inner dorsal margin of the mandible not serrate, (5) the absence of a U-shaped wavy membranous area ventrally on abdominal segment VIII, (6) the presence of two posterodorsal projections on the abdominal segment VIII, and (7) the urogomphi not fused along inner margin. The posterodorsal projections of the abdominal segment VIII, first described in Urcola et al. (2021), are so far unique within Noteridae and represent posterior elongations of the membranous posterolateral areas of segment VIII, where the setae AB8 and AB14 are usually inserted (see for example their insertion in *Suphis* and *Hydrocanthus*, Urcola et al. 2019, 2020). Consequently, setae AB8 and AB14 accompany the elongation of these regions and are therefore part of the posterior projections that characterize *Liocanthyrus* larvae.

## Acknowledgements

We thank Konrad Dettner and Cesar Benetti for their valuable comments on the manuscript. Our thanks also to the Administración de Parque Nacionales (APN) for granting us authorization to carry out this project in Iguazú National Park, as well as to Eduardo Lestani and the park guards for their assistance in our fieldwork.

## Additional information

### Conflict of interest

The authors have declared that no competing interests exist.

## Ethical statement

No ethical statement was reported.

## Funding

The work of J.I.U. was supported by a postgraduate scholarship from CONICET. M.C.M. and J.I.U. were supported by Agencia Nacional de Promoción Científica y Tecnológica under Grant PICT-I-INVI-00460 and by Universidad de Buenos Aires under Grants UBA-CyT-20020190100240BA, UBACyT-20020220400253BA and FUNDACEN (+4i).

## Author contributions

All authors have contributed equally.

## Author ORCIDs

Juan I. Urcola  <https://orcid.org/0000-0002-5684-2464>

Mario E. Toledo  <https://orcid.org/0000-0001-9295-3711>

Stephen M. Baca  <https://orcid.org/0000-0002-0957-302X>

Mariano C. Michat  <https://orcid.org/0000-0002-1962-7976>

## Data availability

All of the data that support the findings of this study are available in the main text.

## References

- Baca SM, Gustafson GT, Toledo M, Miller KB (2014) Revision of the Neotropical burrowing water beetle genus *Liocanthyrus* Guignot (Coleoptera: Noteridae: Noterinae: Noterini) with the description of two new species. *Zootaxa* 3793: 231–246. <https://doi.org/10.11646/zootaxa.3793.2.3>
- Bertrand H (1972) Larves et Nymphes des Coléoptères Aquatiques du Globe. F. Paillart, Paris, 804 pp.
- Dettner K (2016) Noteridae Thomson, 1857. In: Beutel RG, Leschen RAB (Eds) *Handbook of Zoology, Vol. IV Arthropoda: Insecta. Part 38. Coleoptera, Vol. 1: Morphology and Systematics, 2<sup>nd</sup> edn.* (Archostemata, Adephaga, Myxophaga, Polyphaga (partim)). Walter De Gruyter, Berlin, 96–105.
- García M, Camacho J, Poleo N (2018) El género *Liocanthyrus* en Venezuela (Coleoptera: Noteridae) con descripción de dos nuevas especies. *UNED Research Journal* 10: 296–303. <https://doi.org/10.22458/urj.v10i2.2161>
- Grosso LE (1979) Contribución al conocimiento biológico y sistemático de las especies argentinas de Noteridae (Coleoptera, Adephaga). Doctoral thesis N° 374, Universidad Nacional de La Plata, La Plata, Argentina.
- Guimarães BA, Ferreira Jr N (2015) Two new species and new records of *Liocanthyrus* Guignot (Coleoptera: Noteridae) from Brazil. *Zootaxa* 3914: 591–596. <https://doi.org/10.11646/zootaxa.3914.5.8>
- Miller KB, Nilsson AN (2003) Homology and terminology: communicating information about rotated structures in water beetles. *Latissimus* 17: 1–4.
- Toledo ME, Negri I (2024) Taxonomic and faunistic notes on *Canthydrus* Sharp, 1882. II. Revision of the Oriental and East Palearctic species (Coleoptera: Noteridae) *Koleopterologische Rundschau* 94: 1–65.
- Uéno SI (1957) Blind aquatic beetles of Japan, with some accounts of the fauna of Japanese subterranean waters. *Archiv für Hydrobiologie* 53: 250–296.

- Urcola JI, Michat MC (2023) Description of the mature larva of *Suphisellus curtus* (Sharp, 1882) (Coleoptera: Noteridae) with chaetotaxy analysis. *Aquatic Insects* 44: 273–283. <https://doi.org/10.1080/01650424.2022.2162086>
- Urcola JI, Alarie Y, Benetti CJ, Rodriguez G, Michat MC (2019) Larval morphology and analysis of primary chaetotaxy in the genus *Suphis* Aubé, 1836 (Coleoptera: Noteridae). *Zootaxa* 4619: 121–138. <https://doi.org/10.11646/zootaxa.4619.1.5>
- Urcola JI, Alarie Y, Benetti CJ, Michat MC (2020) Description of the larval stages of *Hydrocanthus socius* Sahlberg, 1844 (Coleoptera: Noteridae) with chaetotaxy analysis. *Annales Zoologici* 70: 687–695. <https://doi.org/10.3161/00034541ANZ2020.70.4.012>
- Urcola JI, Benetti CJ, Alarie Y, Michat MC (2021) The unknown larva of the burrowing water beetle genus *Liocanthyrus* Guignot, 1957 (Coleoptera: Noteridae). *Journal of Natural History* 54: 2285–2296. <https://doi.org/10.1080/00222933.2020.1842931>
- Urcola JI, Baca S, Rodriguez G, Michat MC (2024) *Prionohydus cambyreta* sp. n. from Iberá wetlands—the first species of the genus from northern Argentina (Coleoptera: Noteridae). *Zootaxa* 5523: 483–493. <https://doi.org/10.11646/zootaxa.5523.4.7>
- Watts CHS (2002) Checklists and Guides to the Identification, to Genus, of Adult and Larval Australian Water Beetles of the Families Dytiscidae, Noteridae, Hygrobiidae, Halipilidae, Gyrinidae, Hydraenidae and the Superfamily Hydrophiloidea (Insecta - Coleoptera). Identification Guide No. 43. Cooperative Research Centre for Freshwater Ecology, Albury, New South Wales, 110 pp.
- Zimmermann A (1921) Beiträge zur Kenntnis der südamerikanischen Schwimmkäferfauna nebst 41 Neubeschreibungen. *Archiv für Naturgeschichte* 87: 181–206.